

MICROWAVE TRANSISTOR AMPLIFIERS

Analysis and Design



SECOND EDITION

Guillermo Gonzalez

MICROWAVE TRANSISTOR AMPLIFIERS

Analysis and Design

Second Edition

Guillermo Gonzalez



Prentice Hall
Upper Saddle River, New Jersey 07458

Library of Congress Cataloging-in-Publication Data

Gonzalez, Guillermo

Microwave transistor amplifiers : analysis and design / Guillermo Gonzalez. — 2nd ed.

p. cm.

Includes bibliographical references and index.

ISBN 0-13-254335-4

1. Transistor amplifiers. 2. Microwave amplifiers. I. Title.

TK7871.2.G59 1996

621.381'325—dc 20

96-9182

CIP

Acquisitions Editor: Eric Svendsen

Production Editor: Rose Kernan

Cover Designer: Wendy Alling Judy

Buyer: Julia Meehan

Editorial Assistant: Kathryn E. Cassino



© 1997, 1984 by Prentice-Hall, Inc.
Upper Saddle River, NJ 07458

All rights reserved. No part of this book may be reproduced, in any form or by any means, without permission in writing from the publisher.

The author and publisher of this book have used their best efforts in preparing this book. These efforts include the development, research, and testing of the theories and programs to determine their effectiveness. The author and publisher shall not be liable in any event for incidental or consequential damages with, or arising out of, the furnishing, performance, or use of these programs.

Printed in the United States of America

20 19 18 17 16 15 14 13 12 11

ISBN 0-13-254335-4

Prentice-Hall International (UK) Limited, *London*

Prentice-Hall of Australia Pty. Limited, *Sydney*

Prentice-Hall of Canada, Inc., *Toronto*

Prentice-Hall Hispanoamericana, S. A., *Mexico*

Prentice-Hall of India Private Limited, *New Delhi*

Prentice-Hall of Japan, Inc., *Tokyo*

Prentice-Hall Asia Pte. Ltd., *Singapore*

CONTENTS

PREFACE

vii

1 REPRESENTATIONS OF TWO-PORT NETWORKS

1

- 1.1 Introduction, 1
- 1.2 The Impedance, Admittance, Hybrid, and *ABCD* Matrices, 1
- 1.3 Transmission-Line Concepts, 4
 - The Lossy Transmission Line, 20*
- 1.4 The Scattering Matrix and the Chain Scattering Matrix, 22
- 1.5 Shifting Reference Planes, 26
- 1.6 Properties of Scattering Parameters, 28
 - Scattering Matrix of n -Port Networks, 42*
- 1.7 Power Waves and Generalized Scattering Parameters, 45
 - Generalized Scattering Matrix for n -Port Networks, 52*
- 1.8 Two-Port Network Parameters Conversions, 60
- 1.9 Measurement of Scattering Parameters, 61
- 1.10 Scattering Parameters of Transistors, 66
- 1.11 Characteristics of Microwave Transistors, 71
 - Bipolar Transistors, 71*

Field Effect Transistors, 79

Problems, 86

2 MATCHING NETWORKS AND SIGNAL FLOW GRAPHS 92

- 2.1 Introduction, 92
- 2.2 The Smith Chart, 93
- 2.3 The Normalized Impedance and Admittance Smith Chart, 105
- 2.4 Impedance Matching Networks, 112
- 2.5 Microstrip Matching Networks, 141
 - Microstrip Lines, 141*
 - Design of Matching Networks, 152*
- 2.6 Signal Flow Graphs and Applications, 175
 - Applications of Signal Flow Graphs, 180*
- 2.7 Power-Gain Expressions: Alternate Derivations, 185
 - Power-Gain Expressions in Terms of S_p parameters, 192*
- 2.8 VSWR Calculations, 194
 - Problems, 200

3 MICROWAVE TRANSISTOR AMPLIFIER DESIGN 212

- 3.1 Introduction, 212
- 3.2 Power Gain Equations, 213
- 3.3 Stability Considerations, 217
- 3.4 Constant-Gain Circles: Unilateral Case, 228
 - Unconditionally Stable Case, $|S_{ii}| < 1$, 231*
 - Potentially Unstable Case, $|S_{ii}| > 1$, 234*
- 3.5 Unilateral Figure of Merit, 238
- 3.6 Simultaneous Conjugate Match: Bilateral Case, 240
- 3.7 Operating and Available Power-Gain Circles, 247
 - Operating Power-Gain Circles, 247*
 - Unconditionally stable bilateral case, 247*
 - Potentially unstable bilateral case, 252*
 - Available Power-Gain Circles, 257*
 - Unconditionally stable bilateral case, 257*
 - Potentially unstable bilateral case, 260*
- 3.8 Constant VSWR Circles, 260
- 3.9 DC Bias Networks, 273
 - BJT Bias Networks, 273*
 - GaAs FET Bias Networks, 280*
- Problems, 283

4	NOISE, BROADBAND, AND HIGH-POWER DESIGN METHODS	294
4.1	Introduction,	294
4.2	Noise in Two-Port Networks,	295
4.3	Constant Noise Figure Circles,	299
4.4	Broadband Amplifier Design,	323
	<i>Balanced Amplifiers,</i>	327
	<i>Feedback Amplifiers,</i>	333
4.5	Amplifier Tuning,	348
4.6	Bandwidth Analysis,	348
4.7	High-Power Amplifier Design,	352
	<i>Class-A Operation,</i>	353
	<i>Class-B and Class-C Operation,</i>	356
	<i>Intermodulation Distortion,</i>	362
	<i>Power Combiners,</i>	364
	<i>Design Examples,</i>	365
4.8	Two-Stage Amplifier Design,	372
	Problems,	374
5	MICROWAVE TRANSISTOR OSCILLATOR DESIGN	384
5.1	Introduction,	384
5.2	Oscillation Conditions,	384
	<i>Feedback Oscillators,</i>	384
	<i>One-Port Negative-Resistance Oscillators,</i>	388
5.3	Two-Port Negative-Resistance Oscillators,	397
5.4	Oscillator Design Using Large-Signal Measurements,	404
5.5	Oscillator Configurations,	411
	<i>Dielectric Resonator Oscillators,</i>	414
	<i>YIG Oscillators,</i>	422
	<i>Varactor-Tuned Oscillators,</i>	425
	Problems,	428
	APPENDIX COMPUTER-AIDED DESIGNS	433
	APPENDIX A A.1. CIRCLE EQUATIONS: BILINEAR TRANSFORMATION	449
	A.2. DERIVATION OF THE INPUT AND OUTPUT STABILITY CIRCLES [EQUATIONS (3.3.5) AND (3.3.6)]	451
	APPENDIX B STABILITY CONDITIONS	453

APPENDIX C	UNCONDITIONAL STABILITY CONDITIONS: $K > 1$ and $B_1 > 0$,	462
APPENDIX D	DERIVATION OF THE UNILATERAL CONSTANT- GAIN CIRCLES [EQUATION (3.4.10)],	464
APPENDIX E	E.1. ANALYSIS OF (3.6.5) AND (3.6.6) FOR $\Gamma_{Ms} < 1$ AND $\Gamma_{ML} < 1$,	466
	E.2. CONDITION FOR A SIMULTANEOUS CONJUGATE MATCH,	467
APPENDIX F	DERIVATION OF $G_{T,max}$ [EQUATION (3.6.10)],	469
APPENDIX G	DERIVATION OF THE CONSTANT OPERATING POWER-GAIN CIRCLES,	472
APPENDIX H	EXPRESSIONS FOR Γ_{ML},	474
APPENDIX I	CONSTANT VSWR CIRCLES,	476
APPENDIX J	MAPPING OF CIRCLES IN THE Γ_s AND Γ_L PLANES,	478
APPENDIX K	NOISE CONCEPTS,	480
APPENDIX L	NOISE FIGURE OF AN AMPLIFIER,	485
APPENDIX M	CONDITIONS FOR A STABLE OSCILLATION,	493
	INDEX,	499

PREFACE

In this second edition, I have expanded considerably the material in the original book. New material has been included throughout the book to cover scattering parameter techniques in detail. Additional design procedures have been included for amplifiers and oscillators. At the suggestion of many readers, detailed derivations are included for several relations that were either referenced or included in the problems sections of the first edition. The revisions and additions make the text as self-contained as possible. Many new examples and problems have been added.

The main objective of this book has remained to present a unified treatment of the analysis and design of microwave transistor amplifiers using scattering parameters techniques. The term *microwave frequencies* is used to refer to those frequencies whose wavelengths are in the centimeter range (i.e., 1 to 100 cm). However, the design procedures and analysis presented in this book are not limited to the microwave frequencies. In fact, they can be used in any frequency range where the scattering parameters of a transistor are known.

This book is intended to be used in a senior-graduate-level course in microwave transistor amplifiers and oscillators, or by practicing microwave engineers. It is assumed that the reader has completed the undergraduate network theory, electronics, and electromagnetic courses, or equivalent courses. The transmission-line theory needed is fully covered in this book, especially the use of Smith charts as a design tool.

The main transistors used in microwave amplifiers and oscillators are the silicon bipolar junction transistor (BJT) and the gallium-arsenide metal-semiconductor field-effect transistor (GaAs MESFET). The high-electron

mobility transistor is also discussed (HEMT). The BJT performs very well up to approximately 4 GHz. In this frequency range the BJTs are reliable, low cost, have a high gain, and a low noise figure. The GaAs MESFET performance above approximately 4 GHz is superior to that of the BJT, as well as for very low-noise applications below 4 GHz.

Microwave transistors are conveniently represented by two-port networks and characterized by scattering parameters. The scattering parameters are popular because they are easy to measure with modern network analyzers, their use in microwave transistor amplifier design is conceptually simple, and they provide meaningful design information. Furthermore, flow graph theory is readily applicable.

Chapter 1 to 4 present the basic principles and techniques used in microwave transistor amplifier analysis and design. These chapters provide the foundation for a well-designed microwave transistor amplifier. Specifically, in Chapter 1 a detailed review of transmission-line concepts is given. The section on transmission lines provides a comprehensive presentation of transmission-line theory under a sinusoidal excitation. A new section dealing with power waves and generalized scattering parameters is included. The measurement of the scattering parameters is discussed. The section on the characteristics of microwave transistors has been updated.

Chapter 2 begins with a discussion of Smith charts. The design of matching networks in the Smith charts using lumped elements and microstrip transmission lines is discussed. Two- and three-lumped-elements matching networks are discussed in detail, as well as a variety of microstrip matching configurations. Signal flow graphs are used to derive the gain relations, and a section on the derivation of power relations directly from the incident and reflected waves is included. Power-gain expressions in terms of the power scattering parameters are given. Relations for the calculations of VSWRs and mismatch factors are discussed.

Chapter 3 deals with microwave transistor amplifier design. A detailed derivation of the stability conditions has been included. Design procedures are presented involving the transducer power gain, the operating power gain, and the available power gain. Constant-gain circles for unilateral and bilateral devices are derived. A section dealing with the trade-offs between VSWRs and gain has been included. The last part of the chapter discusses the selection and design of various dc bias networks.

Chapter 4 treats the topics of low-noise amplifiers and the trade-offs between low-noise performance, gain, and VSWRs. New material on the design of broadband amplifiers, balance amplifiers, couplers, and feedback amplifiers is included. The section of power amplifiers has been expanded significantly.

Chapter 5 discusses oscillators. Basically, an oscillator consists of an amplifier with the proper amount of feedback to make it oscillate. The negative-resistance approach to oscillator design is studied in detail. A variety of oscillators are designed using BJTs, GaAs FETs, dielectric resonators (DRs), and varactor diodes.

Several new appendixes that supplement the text material are included. For example, Appendix A discusses circles equations, the bilinear transformation, and transformation properties of circles. The derivation of the stability conditions is provided in Appendix B. Appendix I shows the derivation of the constant input and output VSWR circles. Appendix K discusses noise concepts, and Appendix L shows the derivation of the noise figure relation for a two-port network.

The number of problems has been increased significantly. The problems form an integral part of the text, and even if they are not solved, they should be read.

Many of the design calculations in this book can be conveniently made using a simple computer-aided design (CAD) program or a programmable calculator. In the first edition of the book, a listing of the program UM-MAAD (University of Miami Microwave Amplifiers Analysis and Design) was given. The latest version of UM-MAAD can be obtained from the author by sending him, at the address provided at the end of this Preface, a 3.5" disk and a stamped, self-addressed envelope. This CAD program, written in FORTRAN-77, is simple to use.

For completeness, some design examples using a large-scale CAD program are given in the Appendix titled "Computer-Aided Designs." The examples illustrate some of the simulations and optimizations that can be performed using a large-scale CAD program. It is only after the problem is fully understood that CAD techniques should be used. Otherwise, the natural human tendency to be erroneous and inefficient can substantially increase the cost of a design. The large-scale CAD program used in the Appendix titled "Computer-Aided Designs" is the Hewlett-Packard HP85150B Microwave and RF Design Systems (referred to as the HP MDS program). A copy of this program was donated by Hewlett-Packard to the University of Miami in 1990 for teaching and research purposes.

Many of my students and users of the first edition have provided input to this book. I wish to thank all of my former students for their helpful comments, especially the invaluable suggestions and constructive criticisms from Branko Avanic, William Sanfiel, Deniz Ergener, Ching Y. Kung, Claudio J. Traslavina, Levent Y. Erborra, Augusto E. Rodriguez, Edgar Duque, Sergio Bustamante, and William C. Pirkle.

This second edition was carefully reviewed by Orlando Sosa, Ramon Ponce, and Mahes M. Ekanayake. The contributions of Dr. Branko Avanic to the solutions of the problems were very helpful, as were his many inputs. Dr. Kamal Premaratne, a friend and colleague, has provided comments and inputs to both the first and second editions of this book, especially in the chapter on oscillators.

Over the years, I have also received support and encouragement from several colleagues—namely, Professors Tzay Young, Reuven Lask, Kamal Yacoub, Manuel A. Huerta, and James C. Nearing.

I also wish to give special thanks to Dr. Les Besser. In the 1970s, he first introduced me to CAD methods applied to microwave transistor amplifier

design. Over the years, he has motivated my thinking and influenced the way that I approach some design problems. Dr. Besser has also done a lot to promote education in the microwave electronics field. He teaches a variety of excellent courses (Besser Associates, 4600 El Camino Real #210, Los Altos, CA 94022) which are very well known and highly regarded in the microwave industry.

Finally, my deepest appreciation goes to my wife, Pat, my children, Donna and Alex, and my late parents, Ricardo and Raquel, for their love, encouragement, and patience.

*Guillermo Gonzalez, Ph.D.
University of Miami
Department of Electrical and Computer Engineering
Coral Gables, Florida 33124*

REPRESENTATIONS OF TWO-PORT NETWORKS

1.1 INTRODUCTION

In order to characterize the behavior of a two-port network, measured data of both its transfer and impedance functions must be obtained. At low frequencies, the z , y , h , or $ABCD$ parameters are examples of network functions used in the description of two-port networks. These parameters cannot be measured accurately at higher frequencies because the required short- and open-circuit tests are difficult to achieve over a broadband range of microwave frequencies.

A set of parameters that is very useful in the microwave range are the *scattering parameters* (S parameters). These parameters are defined in terms of traveling waves and completely characterize the behavior of two-port networks.

In the 1970s the popularity of S parameters increased because of the appearance of new network analyzers, which performed S -parameter measurements with ease. The S parameters are simple to use in analysis, and flow graph theory is directly applicable. Although the principal use of S parameters in this text is in the characterization of two-port networks, they can also be used in the characterization of n -port networks.

Power waves and the use of generalized scattering parameters (S_p parameters) in the analysis of two-port networks are also discussed.

1.2 THE IMPEDANCE, ADMITTANCE, HYBRID, AND $ABCD$ MATRICES

At low frequencies the two-port network shown in Fig. 1.2.1 can be represented in several ways. The most common representations are the impedance matrix (z parameters), the admittance matrix (y parameters), the hybrid matrix

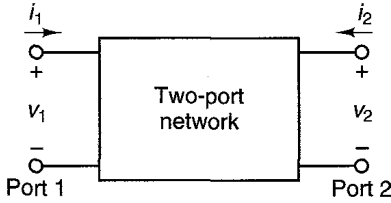


Figure 1.2.1 Two-port network representation.

(h parameters), and the chain or $ABCD$ matrix (chain or $ABCD$ parameters). These parameters are defined as follows:

z Parameters:

$$v_1 = z_{11}i_1 + z_{12}i_2$$

$$v_2 = z_{21}i_1 + z_{22}i_2$$

or in matrix form

$$\begin{bmatrix} v_1 \\ v_2 \end{bmatrix} = \begin{bmatrix} z_{11} & z_{12} \\ z_{21} & z_{22} \end{bmatrix} \begin{bmatrix} i_1 \\ i_2 \end{bmatrix}$$

y Parameters:

$$\begin{bmatrix} i_1 \\ i_2 \end{bmatrix} = \begin{bmatrix} y_{11} & y_{12} \\ y_{21} & y_{22} \end{bmatrix} \begin{bmatrix} v_1 \\ v_2 \end{bmatrix}$$

h Parameters:

$$\begin{bmatrix} v_1 \\ i_2 \end{bmatrix} = \begin{bmatrix} h_{11} & h_{12} \\ h_{21} & h_{22} \end{bmatrix} \begin{bmatrix} i_1 \\ v_2 \end{bmatrix}$$

$ABCD$ Parameters:

$$\begin{bmatrix} v_1 \\ i_1 \end{bmatrix} = \begin{bmatrix} A & B \\ C & D \end{bmatrix} \begin{bmatrix} v_2 \\ -i_2 \end{bmatrix}$$

The previous two-port representations are very useful at low frequencies because the parameters are readily measured using short- and open-circuit tests at the terminals of the two-port network. For example,

$$z_{11} = \left. \frac{v_1}{i_1} \right|_{i_2=0}$$

is measured with an ac open circuit at port 2 (i.e., $i_2 = 0$).

The z , y , and $ABCD$ parameters are also useful in the computer analysis of circuits. When two-port networks are connected in series, as shown in Fig. 1.2.2, we can find the overall z parameters by adding the individual z parameters, namely

$$\begin{bmatrix} v_1 \\ v_2 \end{bmatrix} = \begin{bmatrix} v_1^a + v_1^b \\ v_2^a + v_2^b \end{bmatrix} = \begin{bmatrix} z_{11}^a + z_{11}^b & z_{12}^a + z_{12}^b \\ z_{21}^a + z_{21}^b & z_{22}^a + z_{22}^b \end{bmatrix} \begin{bmatrix} i_1 \\ i_2 \end{bmatrix}$$

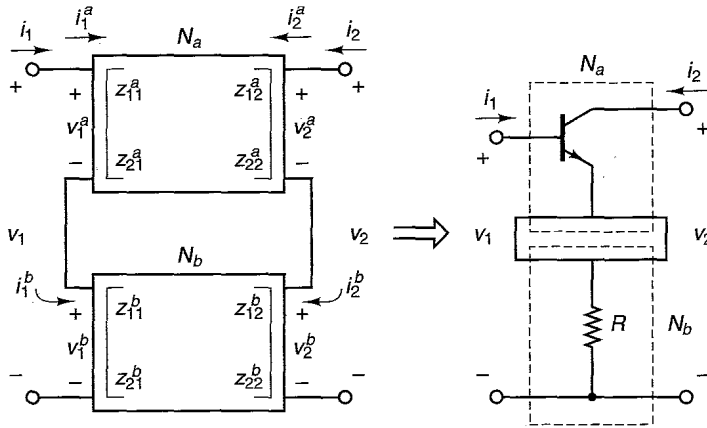


Figure 1.2.2 Series connection using z parameters and a typical application.

When two-port networks are connected in shunt, as shown in Fig. 1.2.3, we can find the overall y parameters by adding the individual y parameters, namely

$$\begin{bmatrix} i_1 \\ i_2 \end{bmatrix} = \begin{bmatrix} i_1^a + i_1^b \\ i_2^a + i_2^b \end{bmatrix} = \begin{bmatrix} y_{11}^a + y_{11}^b & y_{12}^a + y_{12}^b \\ y_{21}^a + y_{21}^b & y_{22}^a + y_{22}^b \end{bmatrix} \begin{bmatrix} v_1 \\ v_2 \end{bmatrix}$$

When cascading two-port networks the chain or $ABCD$ matrix can be used as follows (see Fig. 1.2.4):

$$\begin{bmatrix} v_1 \\ i_1 \end{bmatrix} = \begin{bmatrix} v_1^a \\ i_1^a \end{bmatrix} = \begin{bmatrix} A^a & B^a \\ C^a & D^a \end{bmatrix} \begin{bmatrix} v_2^a \\ -i_2^a \end{bmatrix} = \begin{bmatrix} A^a & B^a \\ C^a & D^a \end{bmatrix} \begin{bmatrix} A^b & B^b \\ C^b & D^b \end{bmatrix} \begin{bmatrix} v_2^b \\ -i_2^b \end{bmatrix} \quad (1.2.1)$$

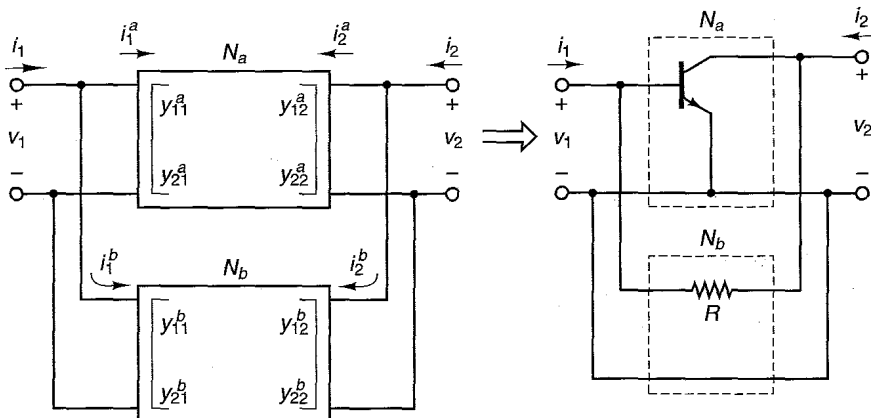


Figure 1.2.3 Shunt connection using y parameters and a typical application.

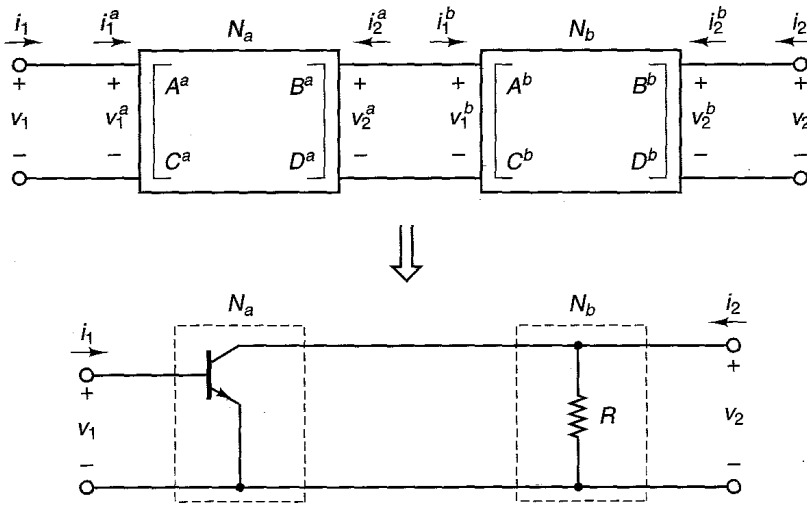


Figure 1.2.4 Cascade connection using $ABCD$ parameters and a typical application.

because $v_2^a = v_1^b$ and $-i_2^a = i_1^b$. The relation (1.2.1) shows that the overall $ABCD$ matrix is equal to the product (i.e., matrix multiplication) of the individual $ABCD$ matrices.

At microwave frequencies the z , y , h , or $ABCD$ parameters are very difficult (if not impossible) to measure. The reason is that short and open circuits to ac signals are difficult to implement over a broadband, at microwave frequencies. Also, an active two-port (e.g., a microwave transistor) might oscillate under short- or open-circuit conditions. Therefore, a new representation of the two-port network at microwave frequencies is needed. The appropriate representation is called the *scattering matrix* and the scattering parameters are defined in terms of traveling waves.

1.3 TRANSMISSION-LINE CONCEPTS

There are many varieties of transmission lines. Three common types of transmission lines are shown in Fig. 1.3.1: the two-wire transmission line, the coaxial transmission line, and the microstrip transmission line. The microstrip transmission line is the most appropriate for the construction of microwave amplifiers. The theory of operation of these transmission lines can be explained using a distributed circuit model for the transmission lines. Such a model provides practical results for the voltage and current along the transmission lines without having to resort to Maxwell's equations.

An electrical model for a transmission line is shown in Fig. 1.3.2a. Viewed as a two-port network, the transmission line receives power from the source at the input port (source end) and delivers power to the load at the output port (load end). The length l of the transmission line is divided into many identical

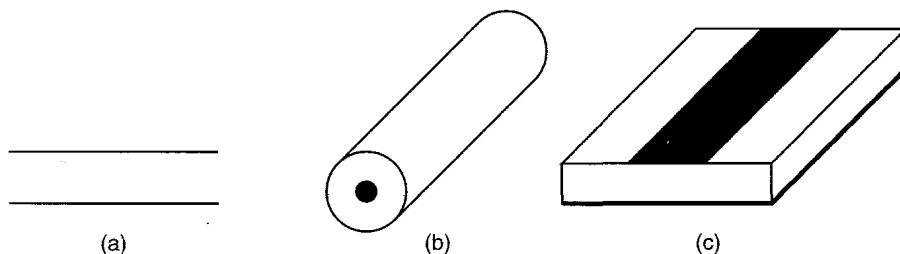


Figure 1.3.1 (a) Two-wire transmission line; (b) coaxial transmission line; (c) microstrip transmission line.

sections Δx . Each section Δx is modeled by a resistance R per unit length (R in Ω/m), an inductance L per unit length (L in H/m), a capacitance C per unit length (C in F/m); and a conductance G per unit length (G in S/m). These parameters are assumed to be constant along the transmission line (i.e., the transmission line is uniform).

Figure 1.3.2b shows a section Δx of the transmission line and the voltage and currents at the input and output ports of the section Δx of transmission line. Observe that the voltages and currents along the transmission line are functions of position and time. At the input of the section Δx the voltage and current are $v(x,t)$ and $i(x,t)$, while at the output the voltage and current are $v(x + \Delta x,t)$ and $i(x + \Delta x,t)$.

Applying Kirchhoff's voltage law to the model in Fig. 1.3.2b gives

$$v(x,t) - v(x + \Delta x,t) = R\Delta xi(x,t) + L\Delta x \frac{\partial i(x,t)}{\partial t}$$

Dividing by Δx we can write

$$\frac{v(x + \Delta x,t) - v(x,t)}{\Delta x} = -Ri(x,t) - L \frac{\partial i(x,t)}{\partial t}$$

As Δx approaches zero the left-hand side is recognized as the partial derivative of $v(x,t)$ with respect to x . Hence, taking the limit as $\Delta x \rightarrow 0$ we obtain

$$\frac{\partial v(x,t)}{\partial x} = -Ri(x,t) - L \frac{\partial i(x,t)}{\partial t} \tag{1.3.1}$$

Similarly, applying Kirchhoff's current law to the model in Fig. 1.3.2b gives

$$i(x,t) - i(x + \Delta x,t) = G\Delta xv(x + \Delta x,t) + C\Delta x \frac{\partial v(x + \Delta x,t)}{\partial t}$$

Dividing by Δx and taking the limit as $\Delta x \rightarrow 0$ results in

$$\frac{\partial i(x,t)}{\partial x} = -Gv(x,t) - C \frac{\partial v(x,t)}{\partial t} \tag{1.3.2}$$

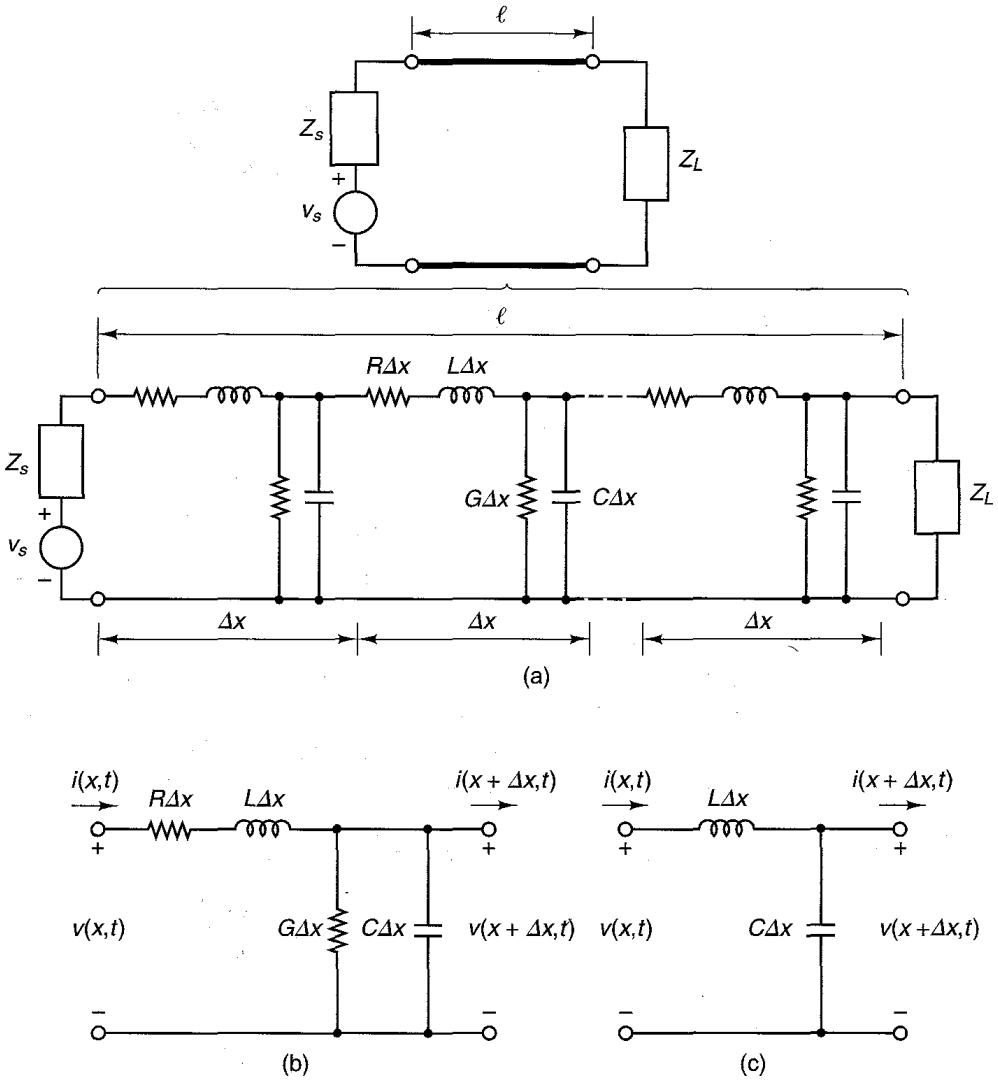


Figure 1.3.2 (a) A distributed circuit model for a transmission line; (b) a section Δx of the transmission line; (c) a section Δx in a lossless transmission line.

The partial differential equations (1.3.1) and (1.3.2) describe the voltages and currents along the transmission lines. Of particular practical interest in microwave electronics is the *lossless* transmission line—that is, a transmission line where R and G are negligible, or simply $R = G = 0$. A section Δx in a lossless transmission line is shown in Fig. 1.3.2c.

In a lossless transmission line, $R = G = 0$ and (1.3.1) and (1.3.2) reduce to

$$\frac{\partial v(x, t)}{\partial x} = -L \frac{\partial i(x, t)}{\partial t} \tag{1.3.3}$$

and

$$\frac{\partial i(x,t)}{\partial x} = -C \frac{\partial v(x,t)}{\partial t} \quad (1.3.4)$$

We are interested in the solution of (1.3.3) and (1.3.4) for a sinusoidal excitation of the line. Phasor analysis will be used to obtain the steady-state solution for $v(x,t)$ and $i(x,t)$.

For a sinusoidal excitation [i.e., for $v_s(t) = V_s \cos \omega t$] the steady-state voltages and currents along the transmission line are also sinusoidal functions of time whose dependence on position and time can be expressed in the general form

$$v(x,t) = f(x)\cos(\omega t + \varphi(x)) \quad (1.3.5)$$

and

$$i(x,t) = g(x)\cos(\omega t + \eta(x)) \quad (1.3.6)$$

where $f(x)$ and $g(x)$ are real functions of position and where $\varphi(x)$ and $\eta(x)$ describe the positional dependence of the phase.

Using Euler's formula, namely

$$e^{j\theta} = \cos \theta + j \sin \theta$$

where $\cos \theta$ is the real part of $e^{j\theta}$ (i.e., $\text{Re}[e^{j\theta}] = \cos \theta$) and $\sin \theta$ is the imaginary part of $e^{j\theta}$ (i.e., $\text{Im}[e^{j\theta}] = \sin \theta$), we can express (1.3.5) and (1.3.6) in the form

$$v(x,t) = f(x)\cos(\omega t + \varphi(x)) = f(x)\text{Re}[e^{j(\omega t + \varphi(x))}] = \text{Re}[f(x)e^{j\varphi(x)}e^{j\omega t}] \quad (1.3.7)$$

and

$$i(x,t) = g(x)\cos(\omega t + \eta(x)) = g(x)\text{Re}[e^{j(\omega t + \eta(x))}] = \text{Re}[g(x)e^{j\eta(x)}e^{j\omega t}] \quad (1.3.8)$$

In (1.3.7) and (1.3.8) we can define the phasor quantities

$$V(x) = f(x)e^{j\varphi(x)}$$

and

$$I(x) = g(x)e^{j\eta(x)}$$

and write (1.3.7) and (1.3.8) in the form

$$v(x,t) = \text{Re}[V(x)e^{j\omega t}] \quad (1.3.9)$$

and

$$i(x,t) = \text{Re}[I(x)e^{j\omega t}] \quad (1.3.10)$$

The phasors $V(x)$ and $I(x)$ are complex functions of position and express the variations of the voltage and current as a function of position along the transmission line.

Substituting (1.3.9) and (1.3.10) into (1.3.3) gives

$$\frac{\partial}{\partial x} \text{Re}[V(x)e^{j\omega t}] = -L \frac{\partial}{\partial t} \text{Re}[I(x)e^{j\omega t}] \quad (1.3.11)$$

Since the Re operator commutes with the $\partial/\partial x$ and $\partial/\partial t$ operators, we can write (1.3.11) in the form

$$\text{Re} \left[\frac{\partial V(x)}{\partial x} e^{j\omega t} \right] = -L \text{Re} \left[I(x) \frac{\partial e^{j\omega t}}{\partial t} \right] = -L \text{Re} [I(x)j\omega e^{j\omega t}] \quad (1.3.12)$$

Observing that $V(x)$ is only a function of position, it follows that

$$\frac{\partial V(x)}{\partial x} = \frac{dV(x)}{dx}$$

and (1.3.12) can be written as

$$\text{Re} \left[\left(\frac{dV(x)}{dx} + j\omega LI(x) \right) e^{j\omega t} \right] = 0 \quad (1.3.13)$$

Equation (1.3.13) must be satisfied for all times t . Therefore, the term in parentheses must be zero, namely

$$\frac{dV(x)}{dx} = -j\omega LI(x) \quad (1.3.14)$$

Actually, this last step might not be so obvious to the reader. It can be proved by observing that for $\omega t = 0$, $e^{j0} = 1$, and (1.3.13) gives

$$\text{Re} \left[\frac{dV(x)}{dx} + j\omega LI(x) \right] = 0 \quad (1.3.15)$$

and for $\omega t = \pi/2$, $e^{j\pi/2} = j$, and (1.3.13) gives

$$\text{Re} \left[\left(\frac{dV(x)}{dx} + j\omega LI(x) \right) j \right] = 0$$

which is equivalent to

$$\text{Im} \left[\frac{dV(x)}{dx} + j\omega LI(x) \right] = 0 \quad (1.3.16)$$

Equations (1.3.15) and (1.3.16) show that both the real and imaginary parts of $(dV(x)/dx) + j\omega LI(x)$ must be zero. Hence, (1.3.14) is verified.

A comparison of (1.3.3) and the corresponding phasor equation in (1.3.14) shows that (1.3.14) follows by simply replacing in (1.3.3) the $\partial/\partial t$ operator by $j\omega$, and $v(x,t)$ and $i(x,t)$ by the phasors $V(x)$ and $I(x)$, respectively. The use of phasors allows us to change the partial differential equation (1.3.3) into the ordinary differential equation (1.3.14).

Similarly, substituting (1.3.9) and (1.3.10) into (1.3.4) results in the following phasor equation:

$$\frac{dI(x)}{dx} = -j\omega CV(x) \quad (1.3.17)$$

Equations (1.3.14) and (1.3.17) are the differential equations satisfied by the phasors $V(x)$ and $I(x)$ along a lossless transmission line. These equations can be solved for $V(x)$ and $I(x)$ as follows. Differentiating (1.3.14) with respect to x gives

$$\frac{d^2V(x)}{dx^2} = -j\omega L \frac{dI(x)}{dx} \quad (1.3.18)$$

Substituting (1.3.17) into (1.3.18) gives

$$\frac{d^2V(x)}{dx^2} = -j\omega L(-j\omega C)V(x) = -\omega^2LCV(x)$$

or

$$\frac{d^2V(x)}{dx^2} + \beta^2V(x) = 0 \quad (1.3.19)$$

where

$$\beta = \omega\sqrt{LC} \quad (1.3.20)$$

The parameter β (in radians per meter) is known as the propagation constant.

The general solution to the second-order differential equation in (1.3.19) is

$$V(x) = Ae^{-j\beta x} + Be^{j\beta x} \quad (1.3.21)$$

where the constants A and B are, in general, complex constants. They can be evaluated using the boundary conditions at the input and output ports of the transmission line.

The general solution $I(x)$ can be obtained from (1.3.14) and (1.3.21). That is,

$$\begin{aligned} I(x) &= \frac{-1}{j\omega L} \frac{dV(x)}{dx} = \frac{-1}{j\omega L} \frac{d}{dx} [Ae^{-j\beta x} + Be^{j\beta x}] \\ &= \frac{\beta}{\omega L} [Ae^{-j\beta x} - Be^{j\beta x}] \end{aligned} \quad (1.3.22)$$

Defining the characteristic impedance of the transmission line as

$$Z_o = \frac{\omega L}{\beta} = \frac{\omega L}{\omega\sqrt{LC}} = \sqrt{\frac{L}{C}} \quad (1.3.23)$$

we can express (1.3.22) in the form

$$I(x) = \frac{A}{Z_o} e^{-j\beta x} - \frac{B}{Z_o} e^{j\beta x} \quad (1.3.24)$$

From (1.3.23) we observe that Z_o in a lossless transmission line is real.

The time-dependent form of the voltage and current along the transmission line follows from (1.3.9) and (1.3.10). That is,

$$v(x,t) = \text{Re}[V(x)e^{j\omega t}] = \text{Re}[Ae^{-j(\beta x - \omega t)} + Be^{j(\beta x + \omega t)}] \quad (1.3.25)$$

and

$$i(x,t) = \text{Re}[I(x)e^{j\omega t}] = \text{Re}\left[\frac{A}{Z_o} e^{-j(\beta x - \omega t)} - \frac{B}{Z_o} e^{j(\beta x + \omega t)}\right] \quad (1.3.26)$$

In the simple case that A and B are real, (1.3.25) and (1.3.26) can be expressed in the form

$$v(x,t) = A \cos(\omega t - \beta x) + B \cos(\omega t + \beta x) \quad (1.3.27)$$

and

$$i(x,t) = \frac{A}{Z_o} \cos(\omega t - \beta x) - \frac{B}{Z_o} \cos(\omega t + \beta x) \quad (1.3.28)$$

The functions $A \cos(\omega t - \beta x)$ and $B \cos(\omega t + \beta x)$ are known as wave functions. Let us examine the wave characteristics of these functions. Let $v_1(x,t) = A \cos(\omega t - \beta x)$. The function $v_1(x,t)$ can be analyzed by first fixing the position x and observing the behavior of $v_1(x,t)$ as a function of time. To this end we let $x = 0$ and plot $v_1(0,t) = A \cos \omega t$ in Fig. 1.3.3a. The function $v_1(0,t)$ is seen to vary sinusoidally as time increases. In Fig. 1.3.3a the time interval between two consecutive equal values of the periodic signal is defined as the period T . Hence, in Fig. 1.3.3a the period T is given by

$$\omega t|_{t=T} = 2\pi$$

or

$$T = \frac{2\pi}{\omega} = \frac{1}{f}$$

Next, we examine the behavior of $v_1(x,t)$ as a function of position. To this end we let $t = 0$ and plot $v_1(x,0) = A \cos \beta x$ in Fig. 1.3.3b. In Fig. 1.3.3b the distance between two consecutive equal values of the signal is defined as the wavelength. Hence, the wavelength is given by

$$\beta x|_{x=\lambda} = 2\pi$$

or

$$\lambda = \frac{2\pi}{\beta} \quad (1.3.29)$$

If we now look at two values of $v_1(x,t)$ as a function of time we can calculate the speed of propagation of the wave. For example, at times t_1 and t_2 (where $t_2 > t_1$) we have

$$v_1(x,t_1) = A \cos(\beta x - \omega t_1)$$

and

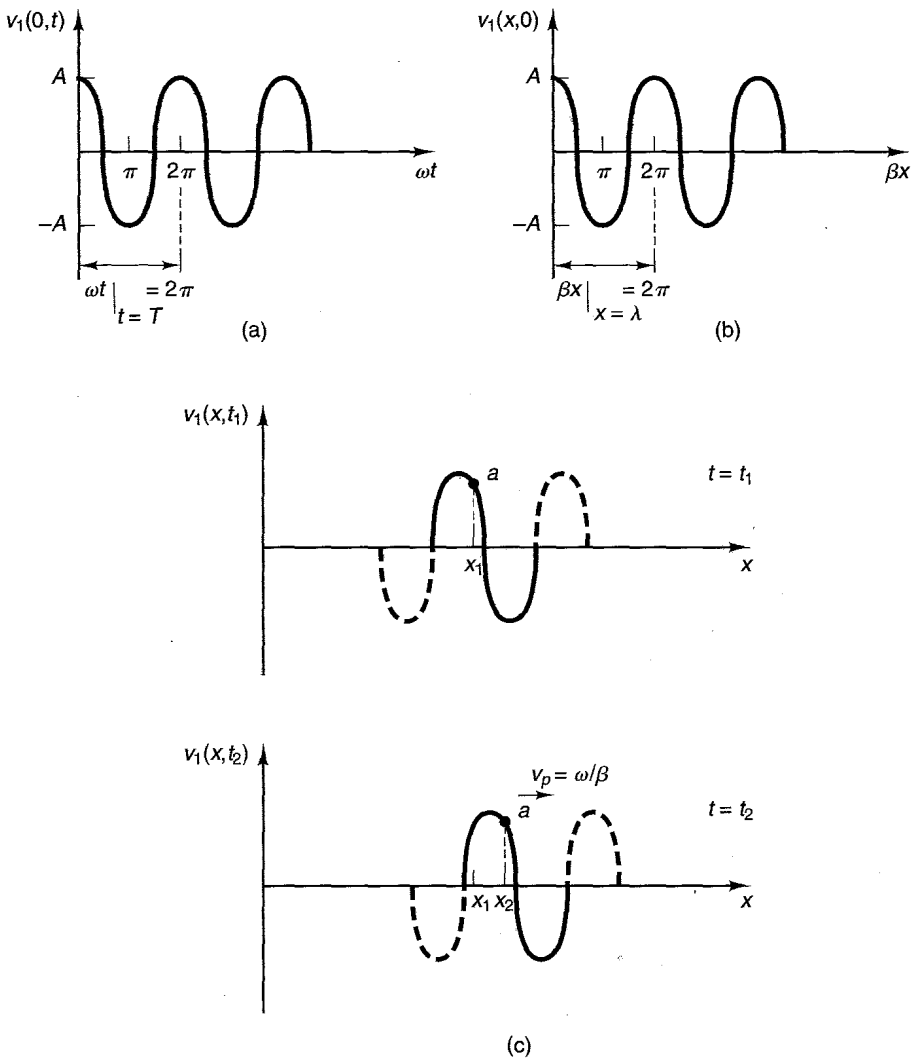


Figure 1.3.3 (a) Plot of $v_1(0,t) = A \cos \omega t$; (b) plot of $v_1(x,0) = A \cos \beta x$; (c) calculation of the phase velocity.

$$v_1(x,t_2) = A \cos(\beta x - \omega t_2)$$

A plot of $v_1(x,t_1)$ and $v_1(x,t_2)$ is shown in Fig. 1.3.3c. A point of constant phase a at $t = t_1$ and at $t = t_2$ is shown in the figure. Since at point a the phase of $v_1(x_1, t_1)$ is identical to the phase of $v_1(x_2, t_2)$ we can write

$$v_1(x_1, t_1) = v_1(x_2, t_2)$$

or

$$\cos(\beta x_1 - \omega t_1) = \cos(\beta x_2 - \omega t_2)$$

Hence,

$$\beta x_1 - \omega t_1 = \beta x_2 - \omega t_2$$

or

$$\frac{x_2 - x_1}{t_2 - t_1} = \frac{\omega}{\beta} \quad (1.3.30)$$

The quantity on the left is recognized as the speed of propagation of the point a , known as the phase velocity v_p . That is,

$$v_p = \frac{x_2 - x_1}{t_2 - t_1} = \frac{\omega}{\beta} = \frac{\omega}{\omega\sqrt{LC}} = \frac{1}{\sqrt{LC}} \quad (1.3.31)$$

Substituting (1.3.20) into (1.3.29) and using (1.3.31) we obtain

$$\lambda = \frac{2\pi}{\beta} = \frac{2\pi}{\omega\sqrt{LC}} = \frac{v_p}{f} = v_p T$$

In other words, the wavelength is the distance traveled by the wave in a time interval equal to one period.

Furthermore, from (1.3.30) since $t_2 > t_1$ and ω/β is a positive quantity, it follows that $x_2 - x_1$ must be positive or $x_2 > x_1$. This shows that the point of constant phase is moving toward the right in Fig. 1.3.3c (i.e., toward the load in a transmission line). In other words, the function $A \cos(\omega t - \beta x)$ represents a traveling wave moving at a velocity v_p toward the load. This wave is called an outgoing wave when viewed from the source, or an incident wave when viewed from the load.

The analysis of $B \cos(\omega t + \beta x)$ will show that this function represents a traveling wave moving at a velocity v_p toward the left (i.e., toward the source in a transmission line). This wave is called an incoming wave when viewed from the source, or a reflected wave when viewed from the load. The nomenclature *incident wave* and *reflected wave* is preferred in transmission-line work.

Since the wave $A \cos(\omega t - \beta x)$ is associated with the phasor $Ae^{-j\beta x}$, and $B \cos(\omega t + \beta x)$ with $Be^{j\beta x}$, we also refer to the phasor $Ae^{-j\beta x}$ as the incident wave (in phasor form) and $Be^{j\beta x}$ as the reflected wave (in phasor form). The quantity βx is known as the electrical length of the line. In general, the voltage and current in a transmission line are composed of an incident and a reflected wave.

A transmission line of characteristic impedance Z_o , length l , and terminated in a load Z_L is shown in Fig. 1.3.4a. The source end is located at $x = 0$ and the load end at $x = l$. The incident and reflected waves are also shown where the wavy arrow symbol is used to denote a wave.

It is convenient in some transmission-line problems to show the load end at a distance zero and the source end at a distance l from the load. Letting $x = l - d$ in (1.3.21) and (1.3.24) we can write (see Fig. 1.3.4b)

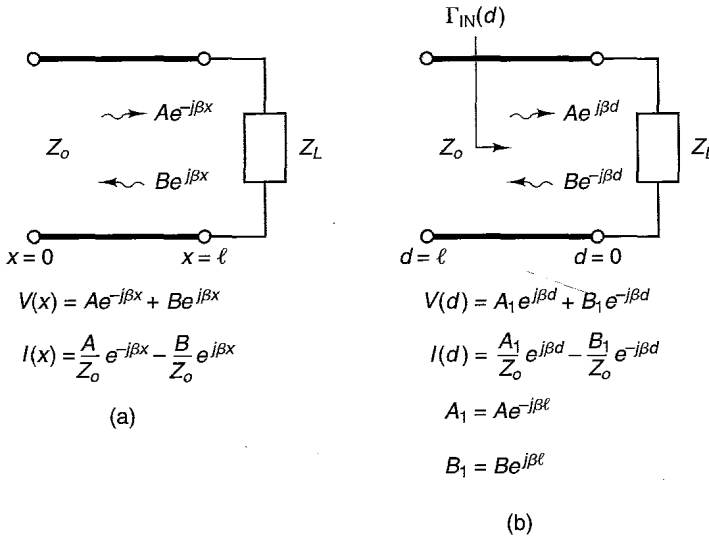


Figure 1.3.4 Transmission line with the source end at $x = 0$ and load end at $x = l$; (b) transmission line with the load end at $d = 0$ and source end at $d = l$.

$$V(d) = A_1 e^{j\beta d} + B_1 e^{-j\beta d} \tag{1.3.32}$$

and

$$I(d) = \frac{A_1}{Z_0} e^{j\beta d} - \frac{B_1}{Z_0} e^{-j\beta d} \tag{1.3.33}$$

where $A_1 = Ae^{-j\beta l}$ and $B_1 = Be^{j\beta l}$. The change $x = l - d$ (such that $d = l - x$) is done in some transmission-line problems in order to measure positive distances as one moves from the load (at $d = 0$) toward the source (at $d = l$). From (1.3.32) and (1.3.33) we observe that in terms of the variable d the phasor $A_1 e^{j\beta d}$ represents the incident wave and $B_1 e^{-j\beta d}$ the reflected wave (see Fig. 1.3.4b). Figure 1.3.4 summarizes the two nomenclatures commonly used in the analysis of transmission lines.

The reflection coefficient is defined as the ratio of the incident to the reflected wave along a transmission line. In Fig. 1.3.4b the reflection coefficient at any position d , denoted by $\Gamma_{IN}(d)$, is

$$\Gamma_{IN}(d) = \frac{B_1 e^{-j\beta d}}{A_1 e^{j\beta d}} = \frac{B_1}{A_1} e^{-2j\beta d} \tag{1.3.34}$$

The load reflection coefficient, denoted by Γ_0 , is the value of $\Gamma_{IN}(d)$ at $d = 0$. That is

$$\Gamma_0 = \Gamma_{IN}(0) = \frac{B_1}{A_1}$$

Hence, (1.3.34) can be expressed in the form

$$\Gamma_{IN}(d) = \Gamma_0 e^{-j2\beta d} \tag{1.3.35}$$

Also, (1.3.32) and (1.3.33) can be expressed in the forms

$$V(d) = A_1(e^{j\beta d} + \Gamma_0 e^{-j\beta d}) = A_1 e^{j\beta d}(1 + \Gamma_0 e^{-j2\beta d}) \tag{1.3.36}$$

and

$$I(d) = \frac{A_1}{Z_o}(e^{j\beta d} - \Gamma_0 e^{-j\beta d}) = \frac{A_1}{Z_o} e^{j\beta d}(1 - \Gamma_0 e^{-j2\beta d}) \tag{1.3.37}$$

The value of the complex constant A_1 is obtained by using a known value of $V(d)$ (i.e., a boundary condition), usually the value of $V(d)$ at the source end (i.e., at $d = l$). Of course, the value of $V(d)$ at $d = l$ depends on the source amplitude and phase and source impedance connected to the line at $d = l$. As we will show shortly [see (1.3.39)] the complex constant Γ_0 is simply evaluated in terms of Z_L and Z_o .

Referring to Fig. 1.3.5, the input impedance of the transmission line at any position d is defined as

$$Z_{IN}(d) = \frac{V(d)}{I(d)} = Z_o \frac{e^{j\beta d} + \Gamma_0 e^{-j\beta d}}{e^{j\beta d} - \Gamma_0 e^{-j\beta d}} \tag{1.3.38}$$

In (1.3.38) the constant Γ_0 can be evaluated using the boundary condition at the load, namely that the value of the input impedance at $d = 0$ must be equal to Z_L . That is,

$$Z_{IN}(0) = Z_L$$

Then, from (1.3.38)

$$Z_{IN}(0) = Z_L = Z_o \frac{1 + \Gamma_0}{1 - \Gamma_0}$$

or

$$\Gamma_0 = \frac{Z_L - Z_o}{Z_L + Z_o} \tag{1.3.39}$$

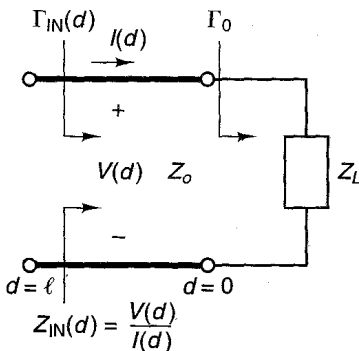


Figure 1.3.5 Input impedance of the transmission line at any position d .

Equation (1.3.39) shows that $\Gamma_0 = 0$ when $Z_L = Z_o$. That is, there is no reflection from the load when $Z_L = Z_o$. A line with $Z_L = Z_o$ is called a properly terminated or matched transmission line.

Substituting (1.3.39) into (1.3.38) gives

$$\begin{aligned} Z_{\text{IN}}(d) &= Z_o \frac{(Z_L + Z_o)e^{j\beta d} + (Z_L - Z_o)e^{-j\beta d}}{(Z_L + Z_o)e^{j\beta d} - (Z_L - Z_o)e^{-j\beta d}} \\ &= Z_o \frac{Z_L \cos \beta d + jZ_o \sin \beta d}{Z_o \cos \beta d + jZ_L \sin \beta d} \\ &= Z_o \frac{Z_L + jZ_o \tan \beta d}{Z_o + jZ_L \tan \beta d} \end{aligned} \quad (1.3.40)$$

Equation (1.3.40) gives the value of the input impedance at any location d along the transmission line. At $d = 0$, (1.3.40) reduces to $Z_{\text{IN}}(0) = Z_L$, as expected. At the input of the line the input impedance follows from (1.3.40) with $d = l$. A very important property of a transmission line, and one that is used extensively in the design of microwave amplifiers, is the ability of the transmission line to change a load impedance to another value of impedance at its input.

The addition of the two waves traveling in opposite directions in a transmission line produces a standing-wave pattern—that is, a sinusoidal function of time whose amplitude is a function of position.

From (1.3.36) the magnitude of the voltage along the line is given by

$$|V(d)| = |A_1| |1 + \Gamma_0 e^{-j2\beta d}| \quad (1.3.41)$$

From (1.3.41), it follows that the maximum value of $|V(d)|$ along the line has the value

$$|V(d)|_{\text{max}} = |A_1| (1 + |\Gamma_0|) \quad (1.3.42)$$

and the minimum value of $|V(d)|$ is

$$|V(d)|_{\text{min}} = |A_1| (1 - |\Gamma_0|) \quad (1.3.43)$$

These values are used to define the voltage standing-wave ratio (VSWR), namely

$$\text{VSWR} = \frac{|V(d)|_{\text{max}}}{|V(d)|_{\text{min}}} = \frac{1 + |\Gamma_0|}{1 - |\Gamma_0|} \quad (1.3.44)$$

We now analyze four important cases of transmission lines: the matched line, the short-circuited line, the open-circuited line, and the quarter-wave line.

In the properly terminated or matched transmission line shown in Fig. 1.3.6a, we obtain from (1.3.39), (1.3.40), and (1.3.44) that $\Gamma_0 = 0$, $Z_{\text{IN}}(d) = Z_L$, and $\text{VSWR} = 1$. In other words, there is no reflected wave (since $\Gamma_0 = 0$), the input impedance is Z_o at any location d , and the VSWR has its minimum value of one.

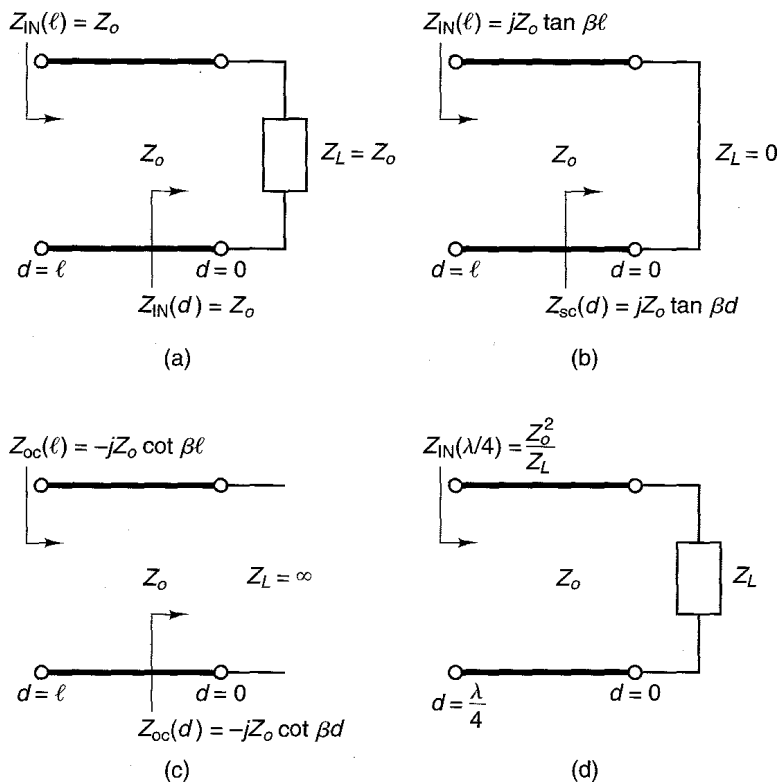


Figure 1.3.6 (a) The matched transmission line; (b) the short-circuited transmission line; (c) the open-circuited transmission line; (d) the quarter-wave transmission line.

In the short-circuited transmission line ($Z_L = 0$) shown in Fig. 1.3.6b, it follows that $\Gamma_0 = -1$, $VSWR = \infty$, and the input impedance at a distance d , called $Z_{sc}(d)$, is given by

$$Z_{sc}(d) = jZ_0 \tan \beta d \quad (1.3.45)$$

Observe that the amplitudes of the incident and reflected waves are the same since $|\Gamma_0| = 1$ (i.e., there is total reflection from the load), and consequently the VSWR attains its largest value of infinity.

In the open-circuited transmission line ($Z_L = \infty$) shown in Fig. 1.3.6c it follows that $\Gamma_0 = 1$, $VSWR = \infty$, and the input impedance at a distance d , called $Z_{oc}(d)$, is given by

$$Z_{oc}(d) = -jZ_0 \cot \beta d$$

Again, there is total reflection from the load since $|\Gamma_0| = 1$, and consequently the VSWR attains its largest value of infinity.

Another important transmission line is the quarter-wave transmission line (also known as the quarter-wave transformer) shown in Fig. 1.3.6d. With $d = \lambda/4$, (1.3.40) gives

$$Z_{IN}(\lambda/4) = \frac{Z_o^2}{Z_L} \tag{1.3.46}$$

Equation (1.3.46) shows that in order to transform a real impedance Z_L to another real impedance given by $Z_{IN}(\lambda/4)$, a quarter-wave line with real characteristic impedance of value

$$Z_o = \sqrt{Z_{IN}(\lambda/4)Z_L}$$

can be used.

Let us return to the short-circuited transmission line in Fig. 1.3.6b and calculate the voltage along the line. From (1.3.36) with $\Gamma_0 = -1$ the voltage $V(d)$ along the short-circuited line is

$$V(d) = A_1(e^{j\beta d} - e^{-j\beta d}) = j2A_1 \sin \beta d$$

Hence,

$$v(d,t) = \text{Re}[V(d)e^{j\omega t}] = \text{Re}[2A_1 \sin \beta d e^{j(\omega t + \pi/2)}]$$

In order to proceed we need to know the value of the complex constant A_1 . For simplicity let us assume that A_1 is real. Hence, we obtain

$$v(d,t) = 2A_1 \sin \beta d \cos(\omega t + \pi/2) \tag{1.3.47}$$

The plot of (1.3.47) is shown in Fig. 1.3.7a, and a plot of $|V(d)|$ is shown in Fig. 1.3.7b. These plots illustrate the standing-wave pattern along the transmission line.

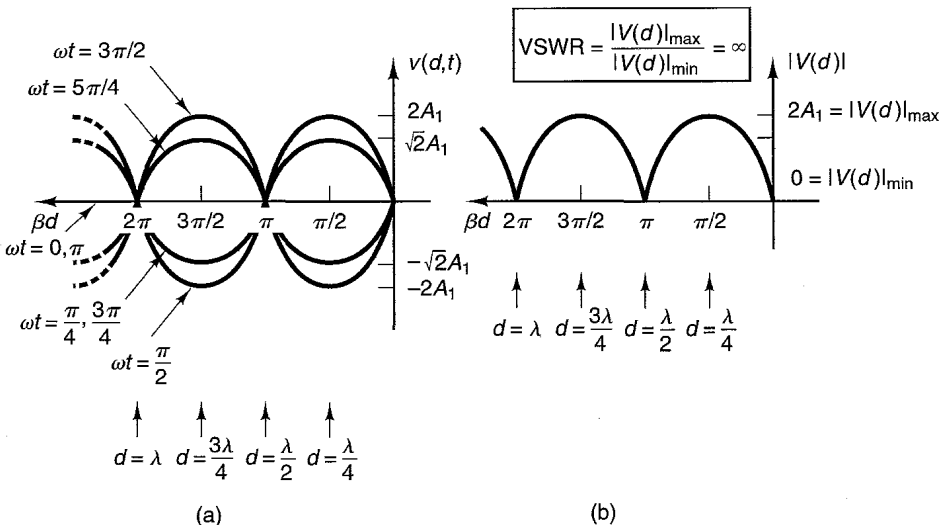


Figure 1.3.7 (a) Plots of $v(d,t)$ as a function of βd for $\omega t = 0, \pi/4, \pi/2, 3\pi/4, \pi, 5\pi/4,$ and $3\pi/2$ for a short-circuited line; (b) plot of $|V(d)|$ for a short-circuited line.

Example 1.3.1

(a) Find the load reflection coefficient, the input impedance, and the VSWR in the transmission line shown in Fig. 1.3.8a. The length of the transmission line is $\lambda/8$ and its characteristic impedance is 50Ω .

(b) Evaluate $V(\lambda/8)$, $I(\lambda/8)$, $P(\lambda/8)$, $V(0)$, $I(0)$ and $P(0)$.

(c) Find the length in centimeters of the $\lambda/8$ transmission line at $f = 1$ GHz.

Solution. (a) Since the length of the line is $l = \lambda/8$ it follows that the electrical length of the line is $\beta l = \pi/4$ (or 45°). From (1.3.39)

$$\Gamma_0 = \frac{Z_L - Z_o}{Z_L + Z_o} = \frac{(50 + j50) - 50}{(50 + j50) + 50} = 0.447 \angle 63.44^\circ$$

From (1.3.40), the input impedance at $d = \lambda/8$ is

$$Z_{IN}(\lambda/8) = 50 \left[\frac{(50 + j50) + j50 \tan 45^\circ}{50 + j(50 + j50) \tan 45^\circ} \right] = 100 - j50 \Omega$$

From (1.3.44) with $|\Gamma_0| = 0.447$ the VSWR is

$$\text{VSWR} = \frac{1 + 0.447}{1 - 0.447} = 2.62$$

This problem is revisited in Chapter 2 (see Example 2.2.4), where Γ_0 , $Z_{IN}(\lambda/8)$, and the VSWR are calculated using the Smith chart.

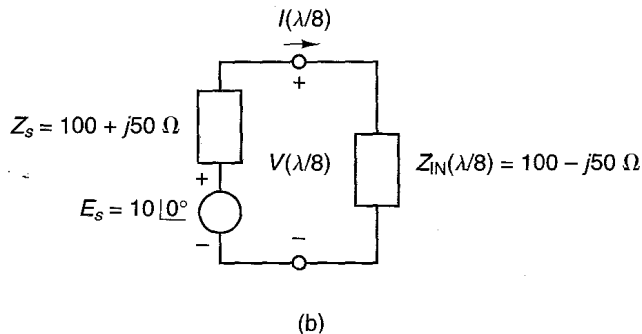
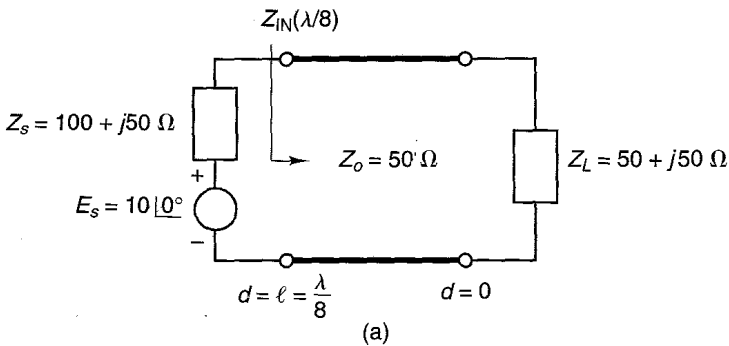


Figure 1.3.8 (a) Transmission line circuit for Example 1.3.1; (b) equivalent circuit at $d = \lambda/8$.

(b) The equivalent circuit at $d = \lambda/8$ is shown in Fig. 1.3.8b. For the given value of Z_s there is maximum power delivered to $Z_{\text{IN}}(\lambda/8)$ [since $Z_{\text{IN}}(\lambda/8) = Z_s^*$]. Also, since the line is lossless the power delivered to the input of the line is equal to the power delivered to the load.

From Fig. 1.3.8b the value of $V(\lambda/8)$ is

$$V(\lambda/8) = \frac{E_s Z_{\text{IN}}(\lambda/8)}{Z_{\text{IN}}(\lambda/8) + Z_s} = \frac{10 \angle 0^\circ (100 - j50)}{100 - j50 + 100 + j50} = 5.59 \angle -26.57^\circ \text{ V}$$

and $I(\lambda/8)$ is

$$I(\lambda/8) = \frac{E_s}{Z_{\text{IN}}(\lambda/8) + Z_s} = \frac{10 \angle 0^\circ}{200} = 0.05 \text{ A}$$

The input power $P(\lambda/8)$ can be calculated using

$$\begin{aligned} P(\lambda/8) &= \text{Re}[V_{\text{rms}}(\lambda/8) I_{\text{rms}}^*(\lambda/8)] = \frac{1}{2} \text{Re}[V(\lambda/8) I^*(\lambda/8)] \\ &= \frac{1}{2} \text{Re}[5.59 \angle -26.57^\circ (0.05)] = 0.125 \text{ W} \end{aligned}$$

where we used the fact that for sinusoidal signals the root mean square (rms) value of the phasor and its peak value are related by $\sqrt{2}$. That is,

$$V_{\text{rms}}(\lambda/8) = \frac{V(\lambda/8)}{\sqrt{2}}$$

and

$$I_{\text{rms}}(\lambda/8) = \frac{I(\lambda/8)}{\sqrt{2}}$$

In order to calculate the voltage and current at the load end, we need to evaluate $V(d)$. $V(d)$ is given by (1.3.36), where the complex constant A_1 can be evaluated from the boundary condition at $d = \lambda/8$.

$$V(\lambda/8) = 5.59 \angle -26.57^\circ = A_1 e^{j\pi/4} [1 + 0.447 \angle 63.44^\circ e^{-j\pi/2}]$$

which can be solved for A_1 , giving

$$A_1 = 3.95 \angle -63.44^\circ$$

Therefore,

$$\begin{aligned} V(d) &= 3.95 \angle -63.44^\circ e^{j\beta d} [1 + 0.447 \angle 63.44^\circ e^{-j2\beta d}] \\ &= 3.95 \angle -63.44^\circ e^{j\beta d} + 1.77 e^{-j\beta d} \end{aligned}$$

This expression gives the value of the voltage at any position along the transmission line. At the load end (i.e., at $d = 0$) we obtain

$$V(0) = 3.95 \angle -63.44^\circ + 1.77 = 5 \angle -45^\circ \text{ V}$$

The current at the load follows from

$$I(0) = \frac{V(0)}{Z_L} = \frac{5 \angle -45^\circ}{50 + j50} = 0.071 \angle -90^\circ \text{ A}$$

Finally, the power delivered to the load is

$$\begin{aligned} P(0) &= \operatorname{Re}[V_{\text{rms}}(0)I_{\text{rms}}^*(0)] = \frac{1}{2} \operatorname{Re}[V(0)I^*(0)] = \frac{1}{2} \operatorname{Re}[5 \angle -45^\circ (0.071 \angle 90^\circ)] \\ &= 0.125 \text{ W} \end{aligned}$$

which is identical to $P(\lambda/8)$ since the line is lossless.

(c) Assuming that the speed of propagation for the waves is the speed of light, the wavelength at 1 GHz is

$$\lambda = \frac{v_p}{f} = \frac{3 \times 10^{10}}{10^9} = 30 \text{ cm}$$

Therefore, the length of the transmission line is

$$l = \frac{\lambda}{8} = \frac{30}{8} = 3.75 \text{ cm}$$

Unless otherwise specified, all transmission lines in this book are assumed to be lossless and uniform.

The Lossy Transmission Line

For the lossy transmission line shown in Fig. 1.3.2b, the associated Kirchhoff's equations are (1.3.1) and (1.3.2). The phasor forms of (1.3.1) and (1.3.2) are

$$\frac{dV(x)}{dx} = -(R + j\omega L)I(x) \quad (1.3.48)$$

and

$$\frac{dI(x)}{dx} = -(G + j\omega C)V(x) \quad (1.3.49)$$

Solving (1.3.48) and (1.3.49), we obtain

$$\frac{d^2V(x)}{dx^2} - \gamma^2 V(x) = 0 \quad (1.3.50)$$

where the complex propagation constant γ is given by

$$\gamma = \alpha + j\beta = \sqrt{(R + j\omega L)(G + j\omega C)} \quad (1.3.51)$$

The attenuation constant α is given in nepers per meter and the propagation constant β in radians per meter. In lossy media the values of α and β can be evaluated using (1.3.51).

The general solution of (1.3.50) is

$$V(x) = Ae^{-\gamma x} + Be^{\gamma x} \quad (1.3.52)$$

and from (1.3.48) it follows that $I(x)$ can be expressed in the form

$$I(x) = \frac{A}{Z_o} e^{-\gamma x} - \frac{B}{Z_o} e^{\gamma x} \quad (1.3.53)$$

where

$$Z_o = \sqrt{\frac{R + j\omega L}{G + j\omega C}}$$

Z_o is known as the complex characteristic impedance of the transmission line.

Equations (1.3.52) and (1.3.53) represent the voltage and current along the transmission line as a pair of waves traveling in opposite directions, with phase velocity $v_p = \omega/\beta$ and decreasing in amplitude according to e^{-ax} or e^{ax} . The wave $e^{-\gamma x} = e^{-ax}e^{-j\beta x}$ is called the *incident wave* (outgoing wave) and the wave $e^{\gamma x} = e^{ax}e^{j\beta x}$ is called the *reflected wave* (incoming wave).

The time-dependent forms of $v(x,t)$ and $i(x,t)$ are

$$v(x,t) = \text{Re}[V(x)e^{j\omega t}] = \text{Re}[Ae^{-ax}e^{-j(\beta x - \omega t)} + Be^{ax}e^{j(\beta x + \omega t)}] \quad (1.3.54)$$

and

$$i(x,t) = \text{Re}[I(x)e^{j\omega t}] = \text{Re}\left[\frac{A}{Z_o} e^{-ax}e^{-j(\beta x - \omega t)} - \frac{B}{Z_o} e^{ax}e^{j(\beta x + \omega t)}\right] \quad (1.3.55)$$

For real values of A and B , and expressing Z_o as $Z_o = |Z_o| \angle \theta$ we can write (1.3.54) and (1.3.55) in the forms

$$v(x,t) = Ae^{-ax} \cos(\omega t - \beta x) + Be^{ax} \cos(\omega t + \beta x)$$

and

$$i(x,t) = \frac{A}{|Z_o|} e^{-ax} \cos(\omega t - \beta x - \theta) - \frac{B}{|Z_o|} e^{ax} \cos(\omega t + \beta x - \theta)$$

With $x = l - d$, (1.3.52) and (1.3.53) become

$$V(d) = A_1 e^{\gamma d} + B_1 e^{-\gamma d}$$

and

$$I(d) = \frac{A_1}{Z_o} e^{\gamma d} - \frac{B_1}{Z_o} e^{-\gamma d}$$

where $A_1 = Ae^{-\gamma l}$ and $B_1 = Be^{\gamma l}$. Then, it follows that the reflection coefficient is given by

$$\Gamma_{\text{IN}}(d) = \frac{B_1 e^{-\gamma d}}{A_1 e^{\gamma d}} = \Gamma_0 e^{-2\gamma d}$$

where

$$\Gamma_0 = \frac{B_1}{A_1} = \frac{Z_L - Z_o}{Z_L + Z_o}$$

and the input impedance is given by

$$Z_{\text{IN}}(d) = Z_o \frac{Z_L + Z_o \tanh \gamma d}{Z_o + Z_L \tanh \gamma d}$$

1.4 THE SCATTERING MATRIX AND THE CHAIN SCATTERING MATRIX

Introducing the notation

$$V^+(x) = Ae^{-j\beta x}$$

and

$$V^-(x) = Be^{j\beta x}$$

we can write (1.3.21) and (1.3.24) in the form

$$V(x) = V^+(x) + V^-(x) \quad (1.4.1)$$

and

$$I(x) = I^+(x) - I^-(x) = \frac{V^+(x)}{Z_o} - \frac{V^-(x)}{Z_o} \quad (1.4.2)$$

Also, the reflection coefficient between the incident and reflected wave can be written as

$$\Gamma(x) = \frac{V^-(x)}{V^+(x)} \quad (1.4.3)$$

Introducing the normalized notation

$$v(x) = \frac{V(x)}{\sqrt{Z_o}}$$

$$i(x) = \sqrt{Z_o} I(x)$$

$$a(x) = \frac{V^+(x)}{\sqrt{Z_o}}$$

and

$$b(x) = \frac{V^-(x)}{\sqrt{Z_o}}$$

we can write (1.4.1), (1.4.2), and (1.4.3) in the form

$$v(x) = a(x) + b(x) \quad (1.4.4)$$

$$i(x) = a(x) - b(x) \quad (1.4.5)$$

and

$$b(x) = \Gamma(x)a(x) \tag{1.4.6}$$

From (1.4.4) and (1.4.5) the normalized incident voltage wave $a(x)$ and the normalized reflected voltage wave $b(x)$ in terms of $V(x)$ and $I(x)$ are

$$a(x) = \frac{1}{2} [v(x) + i(x)] = \frac{1}{2\sqrt{Z_o}} [V(x) + Z_o I(x)] \tag{1.4.7}$$

and

$$b(x) = \frac{1}{2} [v(x) - i(x)] = \frac{1}{2\sqrt{Z_o}} [V(x) - Z_o I(x)] \tag{1.4.8}$$

If instead of a one-port transmission line we have the two-port network shown in Fig. 1.4.1 with incident wave $a_1(l_1)$ and reflected wave $b_1(l_1)$ at port 1 (which is located at $x_1 = l_1$), and incident wave $a_2(l_2)$ and reflected wave $b_2(l_2)$ at port 2 (which is located at $x_2 = l_2$), we can generalize (1.4.6) and write

$$b_1(l_1) = S_{11}a_1(l_1) + S_{12}a_2(l_2)$$

and

$$b_2(l_2) = S_{21}a_1(l_1) + S_{22}a_2(l_2)$$

or, in matrix form,

$$\begin{bmatrix} b_1(l_1) \\ b_2(l_2) \end{bmatrix} = \begin{bmatrix} S_{11} & S_{12} \\ S_{21} & S_{22} \end{bmatrix} \begin{bmatrix} a_1(l_1) \\ a_2(l_2) \end{bmatrix} \tag{1.4.9}$$

Observe that $a_1(l_1)$, $a_2(l_2)$, $b_1(l_1)$, and $b_2(l_2)$ are the values of the incident and reflected waves at the specific locations denoted as port 1 and port 2 in Fig. 1.4.1. The parameters S_{11} , S_{12} , S_{21} , and S_{22} , which represent reflection and transmission coefficients, are called the *scattering parameters* (S parameters) of the two-port network, measured at ports 1 and 2. The matrix

$$[S] = \begin{bmatrix} S_{11} & S_{12} \\ S_{21} & S_{22} \end{bmatrix}$$

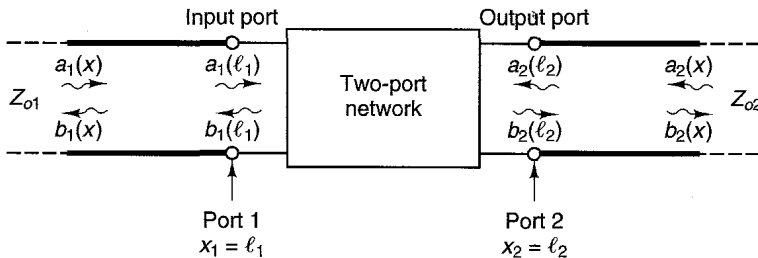


Figure 1.4.1 Incident and reflected waves in a two-port network.

is called the *scattering matrix*. The term $S_{11}a_1(l_1)$ represents the contribution to the reflected wave $b_1(l_1)$ due to the incident wave $a_1(l_1)$ at port 1. Similarly, $S_{12}a_2(l_2)$ represents the contribution to the reflected wave $b_1(l_1)$ due to the incident wave $a_2(l_2)$ at port 2, and so on.

The S parameters are seen to represent reflection or transmission coefficients. From (1.4.9), the S parameters measured at the specific locations shown as port 1 and port 2 in Fig. 1.4.1 are defined as follows:

$$\begin{aligned}
 S_{11} &= \left. \frac{b_1(l_1)}{a_1(l_1)} \right|_{a_2(l_2)=0} && \text{(input reflection coefficient with} \\
 &&& \text{output properly terminated)} \\
 S_{21} &= \left. \frac{b_2(l_2)}{a_1(l_1)} \right|_{a_2(l_2)=0} && \text{(forward transmission coefficient} \\
 &&& \text{with output properly terminated)} \\
 S_{22} &= \left. \frac{b_2(l_2)}{a_2(l_2)} \right|_{a_1(l_1)=0} && \text{(output reflection coefficient} \\
 &&& \text{with input properly terminated)} \\
 S_{12} &= \left. \frac{b_1(l_1)}{a_2(l_2)} \right|_{a_1(l_1)=0} && \text{(reverse transmission coefficient} \\
 &&& \text{with input properly terminated)}
 \end{aligned}$$

If the two-port network in Fig. 1.4.1 represents a transistor, the transistor must be properly biased. Hence, the transistor S parameters are measured at a given Q point, under *small-signal conditions*. In addition, the S parameters vary with frequency; therefore, their values as the frequency is varied are usually measured. Techniques for separating the traveling waves and measuring the S parameters are discussed in Section 1.9.

The advantage of using S parameters is clear from their definitions. They are measured using a matched termination [i.e., making $a_1(l_1) = 0$ or $a_2(l_2) = 0$]. For example, to measure S_{11} we measure the ratio $b_1(l_1)/a_1(l_1)$ at the input port with the output port properly terminated—that is, with $a_2(l_2) = 0$. Terminating the output port with an impedance equal to the characteristic impedance of the transmission line produces $a_2(l_2) = 0$, because a traveling wave incident on the load will be totally absorbed and no energy will be returned to the output port. This situation is illustrated in Fig. 1.4.2, where $a_2(l_2) = 0$ for $Z_2 = Z_{o2}$.

Observe that the network output impedance Z_{OUT} does not have to be matched to Z_{o2} . In fact, it is rare that $Z_{\text{OUT}} = Z_{o2}$, but with $Z_2 = Z_{o2}$ the condition $a_2(l_2) = 0$ is satisfied. Similar considerations apply to measurements at the input port. Also, the characteristic impedances of the transmission lines are usually identical (i.e., $Z_{o1} = Z_{o2}$), with 50Ω being the standard value.

Using matched resistive terminations to measure the S parameters of a transistor has the advantage that the transistor does not oscillate. In contrast, if we were to use a short- or open-circuit test, the transistor could become unstable.

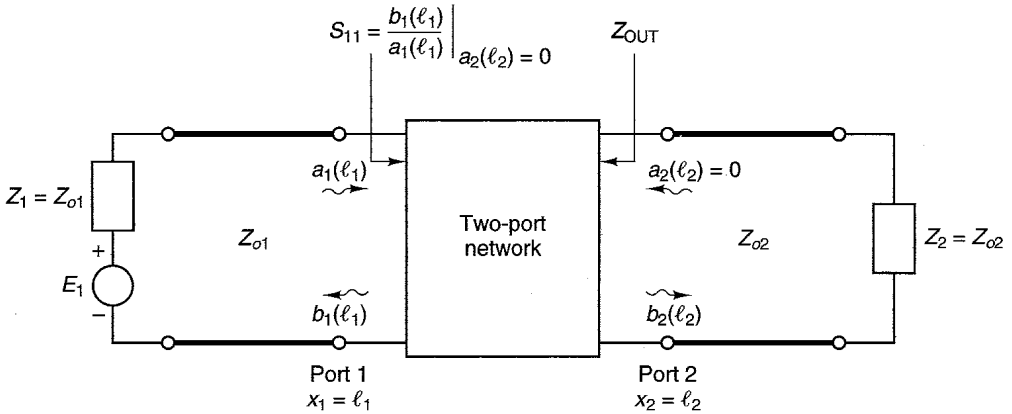


Figure 1.4.2 Procedure for measuring S_{11} . The characteristic impedances of the transmission lines are Z_{o1} and Z_{o2} .

The *chain scattering parameters*, also called the *scattering transfer parameters* or *T parameters*, are used when cascading networks. They are defined in such a way that the input waves $a_1(l_1)$ and $b_1(l_1)$ in Fig. 1.4.1 are the dependent variables and the output waves $a_2(l_2)$ and $b_2(l_2)$ are the independent variables. That is,

$$\begin{bmatrix} a_1(l_1) \\ b_1(l_1) \end{bmatrix} = \begin{bmatrix} T_{11} & T_{12} \\ T_{21} & T_{22} \end{bmatrix} \begin{bmatrix} b_2(l_2) \\ a_2(l_2) \end{bmatrix} \quad (1.4.10)$$

The relationship between the S and T parameters can be developed from (1.4.9) and (1.4.10). Namely,

$$\begin{bmatrix} T_{11} & T_{12} \\ T_{21} & T_{22} \end{bmatrix} = \begin{bmatrix} \frac{1}{S_{21}} & -\frac{S_{22}}{S_{21}} \\ \frac{S_{11}}{S_{21}} & S_{12} - \frac{S_{11}S_{22}}{S_{21}} \end{bmatrix} \quad (1.4.11)$$

and

$$\begin{bmatrix} S_{11} & S_{12} \\ S_{21} & S_{22} \end{bmatrix} = \begin{bmatrix} \frac{T_{21}}{T_{11}} & T_{22} - \frac{T_{21}T_{12}}{T_{11}} \\ \frac{1}{T_{11}} & -\frac{T_{12}}{T_{11}} \end{bmatrix} \quad (1.4.12)$$

The T parameters are useful in the analysis of cascade connections of two-port networks. Figure 1.4.3 shows that the output waves of the first network (N_x) are identical to the input waves of the second network (N_y), namely

$$\begin{bmatrix} b_{2x} \\ a_{2x} \end{bmatrix} = \begin{bmatrix} a_{1y} \\ b_{1y} \end{bmatrix}$$

Since

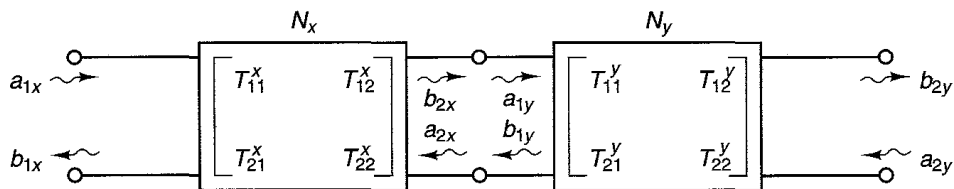


Figure 1.4.3 Cascade connection of two-port networks.

$$\begin{bmatrix} a_{1x} \\ b_{1x} \end{bmatrix} = \begin{bmatrix} T_{11}^x & T_{12}^x \\ T_{21}^x & T_{22}^x \end{bmatrix} \begin{bmatrix} b_{2x} \\ a_{2x} \end{bmatrix}$$

and

$$\begin{bmatrix} a_{1y} \\ b_{1y} \end{bmatrix} = \begin{bmatrix} T_{11}^y & T_{12}^y \\ T_{21}^y & T_{22}^y \end{bmatrix} \begin{bmatrix} b_{2y} \\ a_{2y} \end{bmatrix}$$

it follows that the chain scattering matrix of the cascade connection can be written in terms of the individual chain scattering matrix as follows:

$$\begin{bmatrix} a_{1x} \\ b_{1x} \end{bmatrix} = \begin{bmatrix} T_{11}^x & T_{12}^x \\ T_{21}^x & T_{22}^x \end{bmatrix} \begin{bmatrix} T_{11}^y & T_{12}^y \\ T_{21}^y & T_{22}^y \end{bmatrix} \begin{bmatrix} b_{2y} \\ a_{2y} \end{bmatrix} \quad (1.4.13)$$

Hence, the overall T matrix is obtained by multiplying $[T^x]$ and $[T^y]$. Equation (1.4.13) is useful in the analysis and design of microwave amplifiers using computer-aided design techniques.

1.5 SHIFTING REFERENCE PLANES

In practice we often need to attach transmission lines to the two-port network. Since the S parameters are measured using traveling waves, we need to specify the positions where the measurements are made. The positions are called *reference planes*. For example, in Fig. 1.5.1 we can measure the S parameters at the reference planes located at port 1' and port 2' and relate them to the S parameters at port 1 and port 2 of the two-port network.

At the reference planes at port 1 and port 2 in Fig. 1.5.1, we write the scattering matrix as

$$\begin{bmatrix} b_1(l_1) \\ b_2(l_2) \end{bmatrix} = \begin{bmatrix} S_{11} & S_{12} \\ S_{21} & S_{22} \end{bmatrix} \begin{bmatrix} a_1(l_1) \\ a_2(l_2) \end{bmatrix} \quad (1.5.1)$$

and at port 1' and port 2' as

$$\begin{bmatrix} b_1(0) \\ b_2(0) \end{bmatrix} = \begin{bmatrix} S'_{11} & S'_{12} \\ S'_{21} & S'_{22} \end{bmatrix} \begin{bmatrix} a_1(0) \\ a_2(0) \end{bmatrix} \quad (1.5.2)$$

In (1.5.1) the parameters, S_{11} , S_{12} , S_{21} , and S_{22} denote the S parameters at the unprimed reference planes (i.e., at $x_1 = l_1$ and $x_2 = l_2$); and in (1.5.2) the parame-

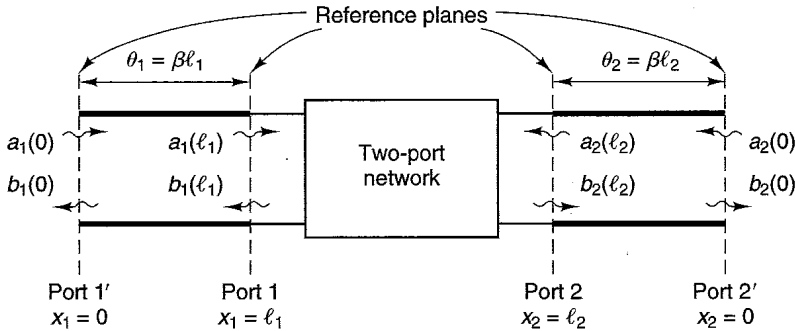


Figure 1.5.1 Model for shifting reference planes.

ters S'_{11} , S'_{12} , S'_{21} , and S'_{22} denote the S parameters at the primed reference planes (i.e., at $x_1 = 0$ and $x_2 = 0$).

The transmission lines and the two-port network in Fig. 1.5.1 when viewed from port 1' and port 2' constitute a new two-port network whose S parameters are defined by (1.5.2). The angles θ_1 and θ_2 are the electrical lengths of the transmission lines between the primed and unprimed reference planes.

From our knowledge of traveling waves on a lossless transmission line we can write

$$\begin{aligned} b_1(l_1) &= b_1(0)e^{j\theta_1} \\ a_1(l_1) &= a_1(0)e^{-j\theta_1} \\ b_2(l_2) &= b_2(0)e^{j\theta_2} \end{aligned}$$

and

$$a_2(l_2) = a_2(0)e^{-j\theta_2}$$

where the factor $e^{\pm j\theta}$ accounts for the phase difference of the waves at the different reference planes. Substituting the previous relations into (1.5.1) gives

$$\begin{bmatrix} b_1(0) \\ b_2(0) \end{bmatrix} = \begin{bmatrix} S_{11}e^{-j2\theta_1} & S_{12}e^{-j(\theta_1+\theta_2)} \\ S_{21}e^{-j(\theta_1+\theta_2)} & S_{22}e^{-j2\theta_2} \end{bmatrix} \begin{bmatrix} a_1(0) \\ a_2(0) \end{bmatrix} \quad (1.5.3)$$

Comparing (1.5.3) with (1.5.2) gives the relations

$$\begin{bmatrix} S'_{11} & S'_{12} \\ S'_{21} & S'_{22} \end{bmatrix} = \begin{bmatrix} S_{11}e^{-j2\theta_1} & S_{12}e^{-j(\theta_1+\theta_2)} \\ S_{21}e^{-j(\theta_1+\theta_2)} & S_{22}e^{-j2\theta_2} \end{bmatrix} \quad (1.5.4)$$

and

$$\begin{bmatrix} S_{11} & S_{12} \\ S_{21} & S_{22} \end{bmatrix} = \begin{bmatrix} S'_{11}e^{j2\theta_1} & S'_{12}e^{j(\theta_1+\theta_2)} \\ S'_{21}e^{j(\theta_1+\theta_2)} & S'_{22}e^{j2\theta_2} \end{bmatrix} \quad (1.5.5)$$

Equations (1.5.4) and (1.5.5) provide the relationship between S parameters at two sets of reference planes.

1.6 PROPERTIES OF SCATTERING PARAMETERS

Consider the two-port network shown in Fig. 1.6.1 where the transmission lines are assumed to be lossless and the characteristic impedances are *real*. This is the typical situation at microwave frequencies where 50-Ω transmission lines (i.e., $Z_{o1} = Z_{o2} = 50 \Omega$) and 50-Ω terminations are commonly used. From (1.4.1) and (1.4.2) the voltages and currents along the transmission lines can be written as

$$V_i(x_i) = V_i^+(x_i) + V_i^-(x_i) \tag{1.6.1}$$

and

$$I_i(x_i) = I_i^+(x_i) - I_i^-(x_i) = \frac{V_i^+(x_i)}{Z_{oi}} - \frac{V_i^-(x_i)}{Z_{oi}} \tag{1.6.2}$$

where $i = 1$ or 2 .

The phasor notation in (1.6.1) and (1.6.2) is used for peak values, and for root mean square (rms) scaled values the following rms phasor notation is used:

$$V_{i,rms}(x_i) = V_{i,rms}^+(x_i) + V_{i,rms}^-(x_i)$$

and

$$I_{i,rms}(x_i) = I_{i,rms}^+(x_i) - I_{i,rms}^-(x_i)$$

where for sinusoidal signals the rms value of the phasor and their peak value are related by $\sqrt{2}$. That is,

$$V_{i,rms}(x_i) = \frac{V_i(x_i)}{\sqrt{2}}$$

$$V_{i,rms}^+(x_i) = \frac{V_i^+(x_i)}{\sqrt{2}}$$

etc.

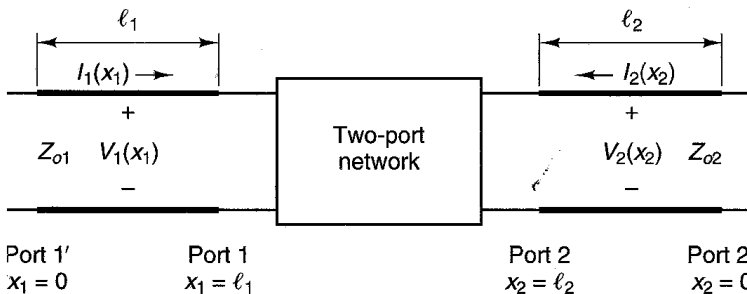


Figure 1.6.1 Two-port network.

[Note: In the first edition of this book it was assumed that the voltages and currents in (1.6.1) and (1.6.2) were scaled to rms values.]

Using the normalized notation (similar to the notation introduced in Section 1.4)

$$\begin{aligned} v_i(x_i) &= \frac{V_i(x_i)}{\sqrt{Z_{oi}}} \\ i_i(x_i) &= \sqrt{Z_{oi}} I_i(x_i) \\ a_i(x_i) &= \frac{V_i^+(x_i)}{\sqrt{Z_{oi}}} = \sqrt{Z_{oi}} I_i^+(x_i) \end{aligned}$$

and

$$b_i(x_i) = \frac{V_i^-(x_i)}{\sqrt{Z_{oi}}} = \sqrt{Z_{oi}} I_i^-(x_i)$$

we can express (1.6.1) and (1.6.2) in the form

$$v_i(x_i) = a_i(x_i) + b_i(x_i)$$

and

$$i_i(x_i) = a_i(x_i) - b_i(x_i)$$

It also follows that the normalized incident and reflected voltages at the i th port in terms of $V_i(x_i)$ and $I_i(x_i)$ are

$$a_i(x_i) = \frac{1}{2\sqrt{Z_{oi}}} [V_i(x_i) + Z_{oi} I_i(x_i)] \quad (1.6.3)$$

and

$$b_i(x_i) = \frac{1}{2\sqrt{Z_{oi}}} [V_i(x_i) - Z_{oi} I_i(x_i)] \quad (1.6.4)$$

Observe that in (1.6.3) and (1.6.4) the normalizing impedances Z_{o1} and Z_{o2} are the characteristic impedances of the transmission lines.

The average power associated with the incident wave on the primed i th port (i.e., at $x_1 = 0$ and $x_2 = 0$) can be expressed in several ways, namely

$$\begin{aligned} P_i^+(0) &= \text{Re}[V_{i,\text{rms}}^+(0) (I_{i,\text{rms}}^+(0))^*] = \frac{1}{2} \text{Re}[V_i^+(0) (I_i^+(0))^*] \\ &= \frac{1}{2} \text{Re} \left[V_i^+(0) \frac{(V_i^+(0))^*}{Z_{oi}} \right] = \frac{1}{2} \frac{|V_i^+(0)|^2}{Z_{oi}} \\ &= \frac{1}{2} |a_i(0)|^2 = |a_{i,\text{rms}}(0)|^2 \end{aligned} \quad (1.6.5)$$

Similarly, the average reflected power is

$$\begin{aligned}
 P_i^-(0) &= \text{Re}[V_{i,\text{rms}}^-(0) (I_{i,\text{rms}}^-(0))^*] = \frac{1}{2} \text{Re}[V_i^-(0) (I_i^-(0))^*] \\
 &= \frac{1}{2} \text{Re}\left[V_i^-(0) \frac{(V_i^-(0))^*}{Z_{oi}} \right] = \frac{1}{2} \frac{|V_i^-(0)|^2}{Z_{oi}} \\
 &= \frac{1}{2} |b_i(0)|^2 = |b_{i,\text{rms}}(0)|^2
 \end{aligned} \tag{1.6.6}$$

Since the line is lossless [i.e., $P_i^+(0) = P_i^+(\ell_i)$ and $P_i^-(0) = P_i^-(\ell_i)$], (1.6.5) and (1.6.6) show that the quantities $\frac{1}{2}|a_i(0)|^2 = \frac{1}{2}|a_i(x_i)|^2$ and $\frac{1}{2}|b_i(0)|^2 = \frac{1}{2}|b_i(x_i)|^2$ represent the power associated with the incident and reflected waves, respectively.

Now consider the network in Fig. 1.6.2, in which port 1' is excited by the sinusoidal voltage source represented by the phasor E_1 with source impedance $Z_1 = Z_{o1}$, and port 2' is matched (i.e., $Z_2 = Z_{o2}$). When the output port is matched we say that the network is terminated in its normalizing impedance. Again, we point out that in practice Z_{o1} and Z_{o2} are real (usually 50-Ω transmission lines) and Z_1 and Z_2 are pure resistors (usually 50 Ω). In Fig. 1.6.2 Z_{T1} is the input impedance of the two-port at $x_1 = \ell_1$. Since port 2 in Fig. 1.6.2 is terminated in its normalizing impedance, at $x_2 = 0$ we can write

$$V_2(0) = -Z_{o2}I_2(0) \tag{1.6.7}$$

and from (1.6.3) it follows that

$$a_2(0) = \frac{1}{2\sqrt{Z_{o2}}} [V_2(0) + Z_{o2} I_2(0)] = \frac{1}{2\sqrt{Z_{o2}}} [-Z_{o2} I_2(0) + Z_{o2} I_2(0)] = 0$$

Hence, there is no reflected wave from the load $Z_2 = Z_{o2}$.

At $x_1 = 0$, we have

$$V_1(0) = E_1 - Z_{o1} I_1(0) \tag{1.6.8}$$

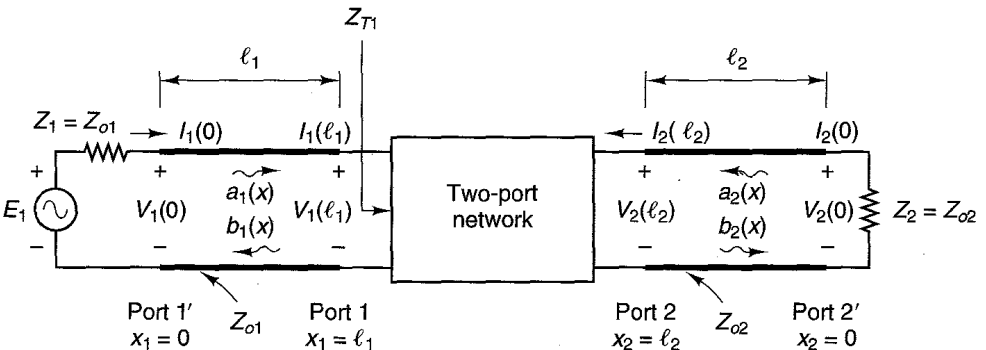


Figure 1.6.2 Two-port network excited by the sinusoidal voltage source represented by the phasor E_1 with source impedance $Z_1 = Z_{o1}$ and terminated in the impedance $Z_2 = Z_{o2}$.

Substituting (1.6.8) into (1.6.3) gives

$$a_1(0) = \frac{E_1}{2\sqrt{Z_{o1}}}$$

or

$$|a_1(0)|^2 = \frac{|E_1|^2}{4Z_{o1}}$$

Hence, from (1.6.5)

$$P_1^+(0) = \frac{1}{2} |a_1(0)|^2 = \frac{|E_1|^2}{8Z_{o1}} \quad (1.6.9)$$

Equation (1.6.9) shows that the power in the incident wave $\frac{1}{2}|a_1(0)|^2$ represents the power available from the source E_1 with internal resistance $Z_1 = Z_{o1}$. We call this quantity P_{AVS} [i.e., $P_{AVS} = P_1^+(0)$ when $Z_1 = Z_{o1}$]. Since the line is lossless [i.e., $\frac{1}{2}|a_1(0)|^2 = \frac{1}{2}|a_1(l_1)|^2$] the quantity $\frac{1}{2}|a_1(l_1)|^2$ represents the power available from the source at port 1. The power available from the source is independent of the input impedance Z_{T1} of the two-port network.

If Z_1 is not equal to Z_{o1} then (1.6.8) must be modified accordingly, and the resulting incident power [i.e., the value of $\frac{1}{2}|a_1(0)|^2$] will not be equal to the power available from the source.

Substituting (1.6.8) into (1.6.9) gives

$$\begin{aligned} \frac{1}{2}|a_1(0)|^2 &= \frac{E_1 E_1^*}{8Z_{o1}} = \frac{[V_1(0) + Z_{o1}I_1(0)][V_1(0) + Z_{o1}I_1(0)]^*}{8Z_{o1}} \\ &= \frac{1}{8Z_{o1}} [|V_1(0)|^2 + Z_{o1}I_1(0)V_1^*(0) + Z_{o1}V_1(0)I_1^*(0) + Z_{o1}^2|I_1(0)|^2] \end{aligned} \quad (1.6.10)$$

Similarly, from (1.6.4) we obtain

$$\begin{aligned} \frac{1}{2}|b_1(0)|^2 &= \frac{1}{8Z_{o1}} [|V_1(0)|^2 - Z_{o1}I_1(0)V_1^*(0) - Z_{o1}I_1^*(0)V_1(0) \\ &\quad + Z_{o1}^2|I_1(0)|^2] \end{aligned} \quad (1.6.11)$$

Subtracting (1.6.11) from (1.6.10) gives

$$\begin{aligned} \frac{1}{2}|a_1(0)|^2 - \frac{1}{2}|b_1(0)|^2 &= \frac{1}{4} [I_1(0)V_1^*(0) + I_1^*(0)V_1(0)] \\ &= \frac{1}{2} \operatorname{Re}[I_1(0)V_1^*(0)] \end{aligned}$$

which represents the power delivered to port 1', or to port 1 since the line is lossless. We call this quantity $P_1(0)$ [i.e., $P_1(0) = \frac{1}{2}|a_1(0)|^2 - \frac{1}{2}|b_1(0)|^2$]. Therefore, it follows that

$$\frac{1}{2} |b_1(0)|^2 = P_{\text{AVS}} - P_1(0) \quad (1.6.12)$$

The quantity $\frac{1}{2}|b_1(0)|^2$ represents the reflected power from port 1 or port 1'. Equation (1.6.12) can also be written as

$$\frac{1}{2} |b_1(l_1)|^2 = P_{\text{AVS}} - P_1(l_1)$$

Equation (1.6.12) shows that the generator sends the available power $P_{\text{AVS}} = \frac{1}{2}|a_1(0)|^2$ toward the input port 1. This power is independent of the input impedance Z_{T1} . If the input impedance Z_{T1} is matched to the transmission line (i.e., if $Z_{T1} = Z_{o1}$), then the reflected power is zero. However, if $Z_{T1} \neq Z_{o1}$, part of the incident power $\frac{1}{2}|a_1(0)|^2$ is reflected back to the generator. The reflected power is given by $\frac{1}{2}|b_1(0)|^2$ and the net power delivered to port 1 is

$$P_1(0) = P_1(l_1) = P_{\text{AVS}} - \frac{1}{2} |b_1(0)|^2$$

From (1.6.7) and (1.6.4) we obtain

$$\begin{aligned} b_2(0) &= \frac{1}{2\sqrt{Z_{o2}}} [V_2(0) - Z_{o2}I_2(0)] = \frac{1}{2\sqrt{Z_{o2}}} [-Z_{o2}I_2(0) - Z_{o2}I_2(0)] \\ &= -\sqrt{Z_{o2}} I_2(0) \end{aligned}$$

Therefore,

$$\frac{1}{2} |b_2(0)|^2 = \frac{1}{2} |I_2(0)|^2 Z_{o2}$$

represents the power delivered to the load $Z_2 = Z_{o2}$. We will denote the power delivered to the load Z_2 by $P_2(0)$ [i.e., $P_2(0) = \frac{1}{2}|b_2(0)|^2$].

In order to calculate the S parameters of the two-port network in Fig. 1.6.2 at the unprimed reference planes (i.e., at ports 1 and 2) we first observe that S_{11} at $x_1 = l_1$ is given by

$$S_{11} = \left. \frac{b_1(l_1)}{a_1(l_1)} \right|_{a_2(l_2)=0} = \left. \frac{V_1^-(l_1)}{V_1^+(l_1)} \right|_{V_2^+(l_2)=0} \quad (1.6.13)$$

which from (1.3.39) can be expressed as

$$S_{11} = \frac{Z_{T1} - Z_{o1}}{Z_{T1} + Z_{o1}} \quad (1.6.14)$$

Equation (1.6.13) or (1.6.14) shows that S_{11} is the reflection coefficient of port 1 with port 2 terminated in its normalizing impedance Z_{o2} (i.e., $a_2 = 0$).

The evaluation of S_{11} at $x_1 = 0$ (denoted by S'_{11}) can be done using (1.5.4) (i.e., $S'_{11} = S_{11}e^{-j2\beta l_1}$); or alternately we can calculate the input impedance at $x_1 = 0$, and its associated reflection coefficient would be S'_{11} .

If we consider the quantity $|S_{11}|^2$ we find from (1.6.9) and (1.6.12) that

$$|S_{11}|^2 = \left. \frac{|b_1(l_1)|^2}{|a_1(l_1)|^2} \right|_{a_2(l_2)=0} = \frac{P_{AVS} - P_1(l_1)}{P_{AVS}}$$

or

$$P_1(l_1) = P_1(0) = P_{AVS}(1 - |S_{11}|^2) \quad (1.6.15)$$

The previous relations show that $|S_{11}|^2$ represents the ratio of the power reflected from port 1 to the power available at port 1. If $|S_{11}| > 1$, the power reflected is larger than the power available at port 1. Therefore, in this case port 1 acts as a source of power and oscillations can occur.

The evaluation of S_{21} at the unprimed reference plane is as follows:

$$\begin{aligned} S_{21} &= \left. \frac{b_2(l_2)}{a_1(l_1)} \right|_{a_2(l_2)=0} = \left. \frac{\sqrt{Z_{o2}} I_2^-(l_2)}{\sqrt{Z_{o1}} I_1^+(l_1)} \right|_{I_2^+(l_2)=0} \\ &= \left. \frac{-\sqrt{Z_{o2}} I_2(l_2)}{\sqrt{Z_{o1}} I_1^+(l_1)} \right|_{I_2^+(l_2)=0} \end{aligned} \quad (1.6.16)$$

The last step in (1.6.16) follows because $I_2(l_2) = I_2^+(l_2) - I_2^-(l_2) = -I_2^-(l_2)$ [since $I_2^+(l_2) = 0$].

Equation (1.6.16) can be manipulated further to make the evaluation of S_{21} simpler. To this end we replace the network in Fig. 1.6.2 by the equivalent network shown in Fig. 1.6.3. The equivalent network was obtained by finding the Thévenin's equivalent at ports 1 and 2. At port 1 the Thévenin's voltage is called $E_{1,TH}$ and the Thévenin's resistance (obtained by setting $E_1 = 0$) is simply Z_{o1} . The Thévenin voltage (i.e., the open-circuit voltage at $x_1 = l_1$ in Fig. 1.6.2) can be shown to be $E_{1,TH} = E_1 e^{-j\beta l_1}$. At the matched port 2, the Thévenin's equivalent resistance is Z_{o2} .

From (1.6.3), $I_1^+(l_1)$ is given by

$$I_1^+(l_1) = \frac{a_1(l_1)}{\sqrt{Z_{o1}}} = \frac{1}{2Z_{o1}} [V_1(l_1) + Z_{o1} I_1(l_1)] \quad (1.6.17)$$

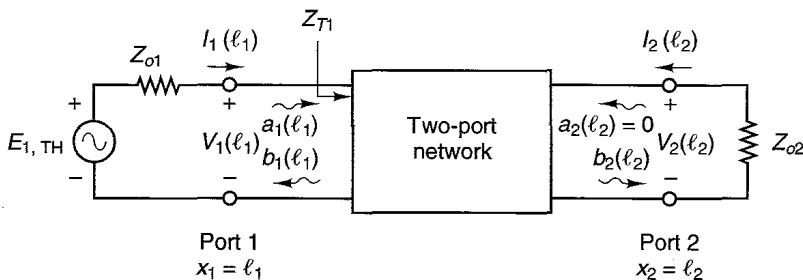


Figure 1.6.3 Two-port network with Thévenin's equivalent at ports 1 and 2.

where from Fig. 1.6.3, $V_1(l_1)$ is given by

$$V_1(l_1) = E_{1,\text{TH}} - Z_{o1}I_1(l_1) \quad (1.6.18)$$

Substituting (1.6.18) into (1.6.17) gives

$$I_1^+(l_1) = \frac{E_{1,\text{TH}}}{2Z_{o1}} \quad (1.6.19)$$

Also, at port 2 of Fig. 1.6.3 we have

$$-I_2(l_2) = \frac{V_2(l_2)}{Z_{o2}} \quad (1.6.20)$$

Substituting (1.6.19) and (1.6.20) into (1.6.16) results in the following practical expression for S_{21} :

$$S_{21} = \frac{2\sqrt{Z_{o1}}}{\sqrt{Z_{o2}}} \frac{V_2(l_2)}{E_{1,\text{TH}}} \quad (1.6.21)$$

Equation (1.6.21) shows that S_{21} represents a forward voltage transmission coefficient from port 1 to port 2. To evaluate S_{21} at the primed reference planes, one uses (1.5.4). From (1.6.21), $|S_{21}|^2$ can be expressed as

$$|S_{21}|^2 = \frac{\frac{1}{2} |V_2(l_2)|^2 / Z_{o2}}{|E_{1,\text{TH}}|^2 / 8Z_{o1}}$$

which shows that $|S_{21}|^2$ represents the ratio of the power delivered to the load Z_{o2} (i.e., P_L) to the power available from the source $E_{1,\text{TH}}$ (i.e., P_{AVS}). The ratio P_L/P_{AVS} is known as the *transducer power gain* G_T . Hence, the transducer power gain is given by

$$G_T = |S_{21}|^2 \quad (1.6.22)$$

If $Z_1 = Z_2 = Z_o$ it follows from (1.6.21) that

$$S_{21} = \frac{V_2}{\left(\frac{E_{1,\text{TH}}}{2}\right)}$$

and the transducer power gain is given by

$$G_T = |S_{21}|^2 = \left| \frac{V_2}{E_{1,\text{TH}}/2} \right|^2$$

If we analyze the network shown in Fig. 1.6.4 in which the sinusoidal excitation represented by the phasor E_2 with source impedance $Z_2 = Z_{o2}$ is placed

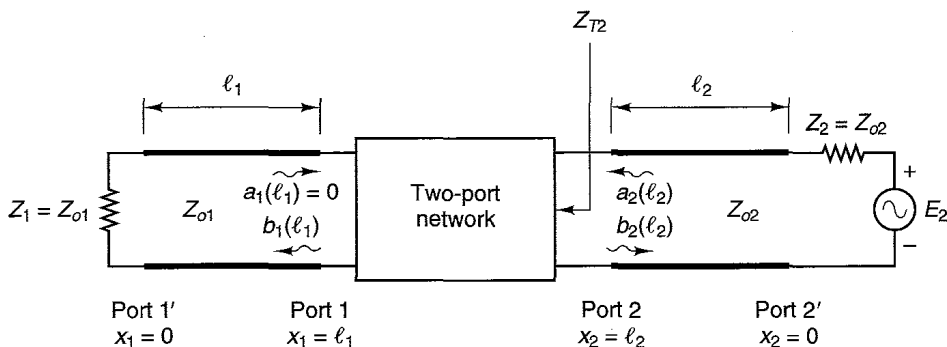


Figure 1.6.4 Two-port network excited by the voltage source E_2 with internal impedance $Z_2 = Z_{o2}$ and terminated in the impedance $Z_1 = Z_{o1}$.

at port 2' and port 1' is matched (i.e., $Z_1 = Z_{o1}$) we find that at the unprimed reference planes

$$S_{22} = \left. \frac{b_2(l_2)}{a_2(l_2)} \right|_{a_1(l_1)=0} = \frac{Z_{T2} - Z_{o2}}{Z_{T2} + Z_{o2}} \quad (1.6.23)$$

and

$$S_{12} = \left. \frac{b_1(l_1)}{a_2(l_2)} \right|_{a_1(l_1)=0} = \frac{2\sqrt{Z_{o2}} V_1(l_1)}{\sqrt{Z_{o1}} E_{2,TH}}$$

where $E_{2,TH}$ is the Thévenin's voltage at port 2. Equation (1.6.23) shows that S_{22} is the reflection coefficient of port 2 with port 1 terminated in its normalizing impedance $Z_1 = Z_{o1}$ [i.e., $a_1(l_1) = 0$], and S_{12} represents a reverse voltage transmission coefficient from port 2 to port 1. Equation (1.5.4) can be used to evaluate S'_{22} and S'_{12} at the primed reference planes.

The quantity $|S_{22}|^2$ represents the ratio of the power reflected from port 2 to the power available at port 2. If $|S_{22}| > 1$, the power reflected is larger than the power available at port 2 and oscillation can occur. The quantity $|S_{12}|^2$ represents a reverse transducer power gain. In fact,

$$|S_{12}|^2 = \frac{\frac{1}{2} |V_1(l_1)|^2 / Z_{o1}}{|E_{2,TH}|^2 / 8Z_{o2}}$$

The S parameters of a transistor are commonly measured with $Z_{o1} = Z_{o2} = Z_o$ and $Z_1 = Z_2 = Z_o$ in Fig. 1.6.2. These S parameters are said to be measured in a Z_o system. If this transistor is then used in the circuit of Fig. 1.6.2 with arbitrary terminations Z_1 and Z_2 the gain G_T is no longer given by (1.6.22). In Sections 2.6 [see (2.6.13)] we will show that for arbitrary values of Z_1 and Z_2

the gain G_T can be expressed in terms of Z_1 , Z_2 , and the S parameters of the transistor measured in a Z_o system.

Example 1.6.1

Evaluate the S parameters, in a Z_o system, of (a) a series impedance Z and (b) a shunt admittance Y .

Solution. (a) The two-port network of a series impedance is shown in Fig. 1.6.5a, and the network connected to transmission lines with characteristic impedances Z_o , excited by a source represented by the phasor E_1 with source impedance $Z_1 = Z_o$, and terminated in the normalizing impedance $Z_2 = Z_o$ is shown in Fig. 1.6.5b (i.e., in a Z_o system). The Thévenin's equivalent circuit is shown in Fig. 1.6.5c.

The S parameters are evaluated at the reference planes denoted by port 1 and port 2. From (1.6.14) we find that

$$S_{11} = \left. \frac{b_1(l_1)}{a_1(l_1)} \right|_{a_2(l_2)=0} = \frac{Z_{T1} - Z_o}{Z_{T1} + Z_o}$$

where from Fig. 1.6.5c $Z_{T1} = Z + Z_o$. Therefore,

$$S_{11} = \frac{Z}{Z + 2Z_o} \quad (1.6.24)$$

Since $V_2(l_2)$ is given by (see Fig. 1.6.5c)

$$V_2(l_2) = \frac{E_{1,TH}Z_o}{Z + 2Z_o}$$

we find from (1.6.21) (with $Z_{o1} = Z_{o2} = Z_o$) that

$$S_{21} = \frac{2V_2(l_2)}{E_{1,TH}} = \frac{2Z_o}{Z + 2Z_o} \quad (1.6.25)$$

From symmetry, we observe that $S_{22} = S_{11}$ and $S_{12} = S_{21}$.

If the two-port network consists of a series inductor with $Z = j100 \Omega$, then in a 50- Ω system (i.e., with $Z_o = 50 \Omega$) it follows that the S parameters of the series inductor from (1.6.24) and (1.6.25) are

$$[S] = \begin{bmatrix} 0.707 \angle 45^\circ & 0.707 \angle -45^\circ \\ 0.707 \angle -45^\circ & 0.707 \angle 45^\circ \end{bmatrix}$$

(b) The two-port network of a shunt admittance is shown in Fig. 1.6.6a, and the terminated network is shown in Fig. 1.6.6b. The Thévenin's equivalent circuit is shown in Fig. 1.6.6c. In this case

$$Z_{T1} = \frac{1}{Y} \parallel Z_o = \frac{Z_o}{1 + Z_o Y}$$

and from (1.6.14)

$$S_{11} = \frac{Z_{T1} - Z_o}{Z_{T1} + Z_o} = \frac{-Z_o Y}{2 + Z_o Y} \quad (1.6.26)$$

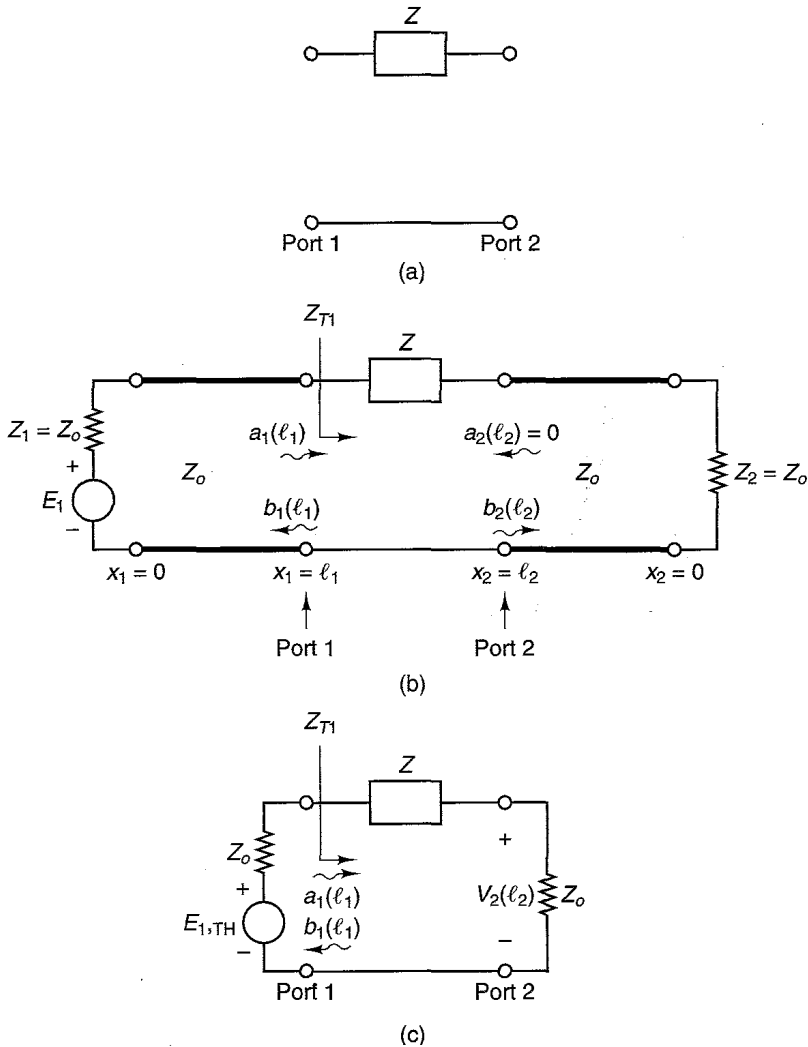


Figure 1.6.5 (a) A two-port network consisting of a series impedance Z ; (b) the two-port network excited by a source and terminated in the normalizing impedance $Z_2 = Z_o$; (c) a Thévenin's equivalent circuit.

Since from Fig. 1.6.6c

$$V_2(\ell_2) = \frac{E_{1,TH} Z_{T1}}{Z_{T1} + Z_o} = \frac{E_{1,TH}}{2 + Z_o Y}$$

we obtain from (1.6.21) that

$$S_{21} = \frac{2V_2(\ell_2)}{E_{1,TH}} = \frac{2}{2 + Z_o Y} \tag{1.6.27}$$

Again, from symmetry we observe that $S_{22} = S_{11}$ and $S_{12} = S_{21}$.

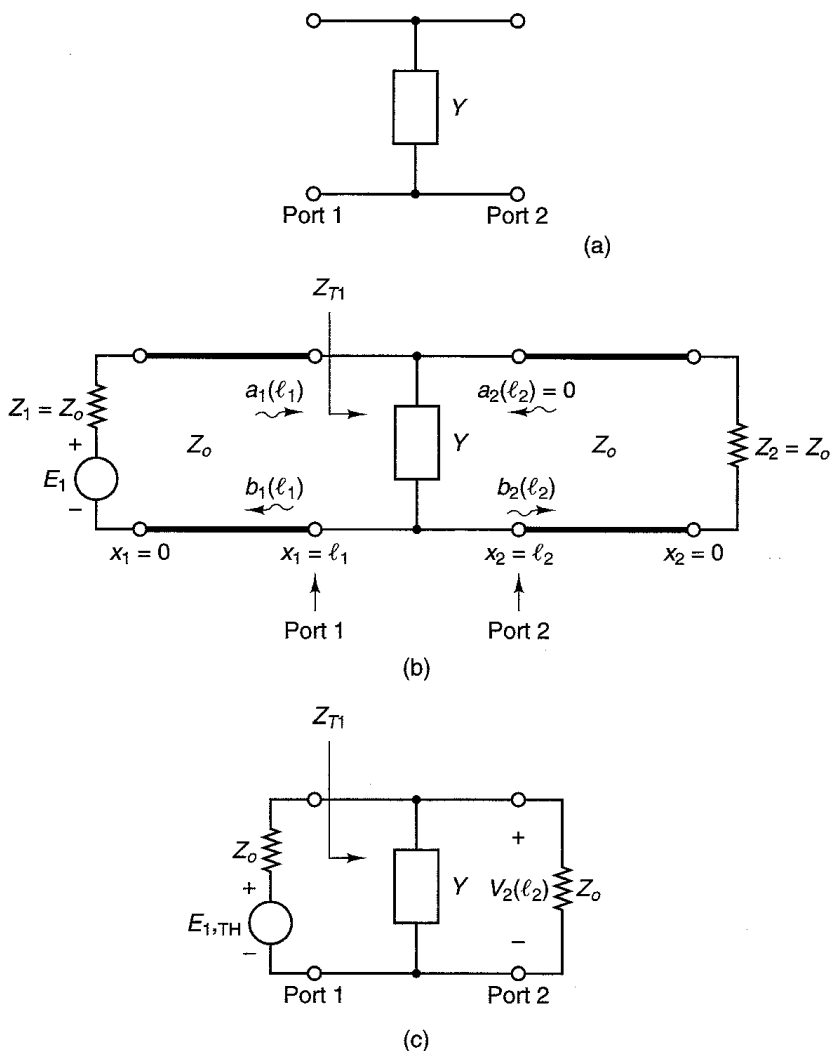


Figure 1.6.6 (a) A two-port network consisting of a shunt admittance Y ; (b) the two-port network excited by a source and terminated in the normalizing impedance $Z_2 = Z_o$; (c) A Thévenin's equivalent circuit.

If the two-port network consists of a shunt $100\text{-}\Omega$ resistor (i.e., $Y = 1/100 = 10\text{ mS}$), then in a $50\text{-}\Omega$ system it follows that the S parameters of the shunt resistor from (1.6.26) and (1.6.27) are

$$[S] = \begin{bmatrix} -1/5 & 4/5 \\ 4/5 & -1/5 \end{bmatrix}$$

Example 1.6.2

Evaluate the S parameters of the short-circuited shunt stub shown in Fig. 1.6.7a.

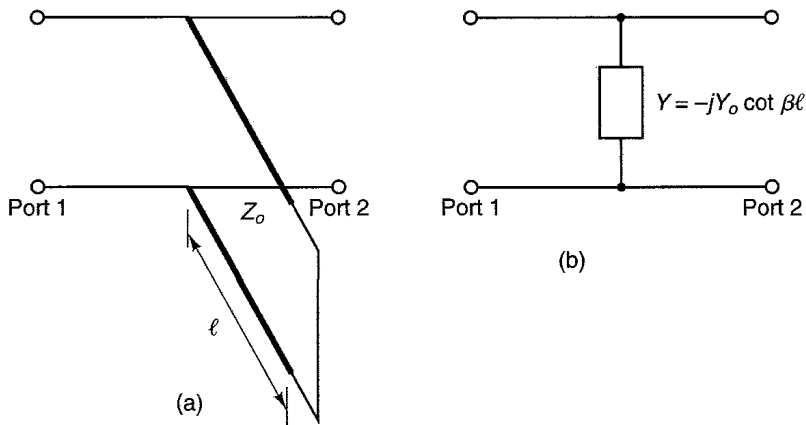


Figure 1.6.7 (a) A short-circuited shunt stub, (b) equivalent shunt admittance.

Solution: The input impedance of a short-circuited shunt stub of length l was derived in Section 1.3, namely $Z_{sc}(l) = jZ_o \tan \beta l$. Hence, its input admittance (denoted by Y) is

$$Y = \frac{1}{Z_{sc}} = -jY_o \cot \beta l$$

where $Y_o = 1/Z_o$.

The short-circuited shunt stub can be replaced by its equivalent shunt admittance Y as shown in Fig. 1.6.7b. Then, using the results of Example 1.6.1(b), the S parameters of the shunt admittance in Fig. 1.6.7b in a Z_o system are readily found. That is, from (1.6.26) we obtain

$$S_{11} = S_{22} = \frac{-Z_o Y}{2 + Z_o Y} = \frac{-1}{1 + j2 \tan \beta l}$$

and from (1.6.27)

$$S_{21} = S_{12} = \frac{2}{2 + Z_o Y} = \frac{2}{2 - j \cot \beta l}$$

Example 1.6.3

In the two-port network shown in Fig. 1.6.8:

- Find $Z_{IN}(0)$.
- Evaluate $a_1(0)$, $b_1(0)$, $a_1(\lambda/8)$, $b_1(\lambda/8)$, and $a_2(0)$.
- Evaluate $V_1(0)$, $V_1(\lambda/8)$, $I_1(0)$, and $I_1(\lambda/8)$.
- Evaluate the average input power at $x_1 = 0$ and at $x_1 = \lambda/8$.
- Evaluate S_{11} at $x_1 = 0$ and $x_1 = \lambda/8$.
- Evaluate the input VSWR and the output VSWR.

(g) If the scattering parameters of the two-port network measured at the $x_1 = x_2 = \lambda/8$ reference planes are $S_{11} = 0.447 \angle 63.4^\circ$, $S_{12} = 0.01 \angle 40^\circ$, $S_{21} = 5 \angle 135^\circ$, and $S_{22} = 0.6 \angle 40^\circ$, calculate the power delivered to the load Z_2 .

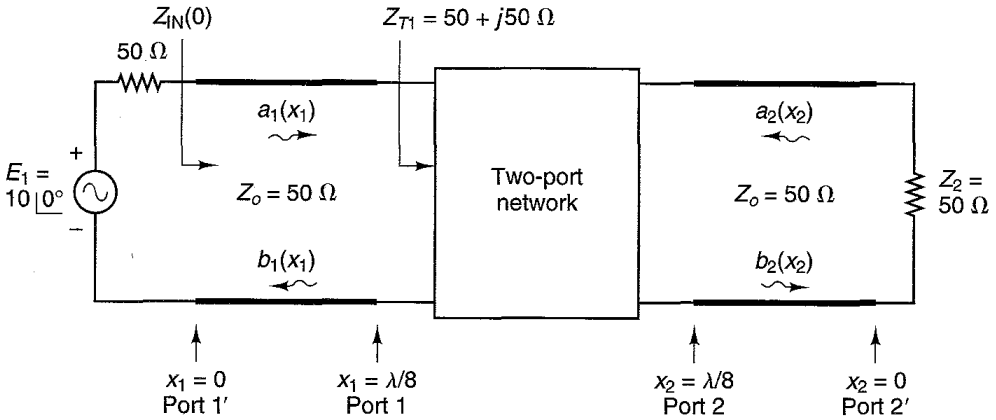


Figure 1.6.8 Circuit diagram for Example 1.6.3.

Solution: (a) Except for notational changes, the input impedance calculation is the same as that in Example 1.3.1. That is, substituting $Z_{T1} = 50 + j50 \Omega$ for Z_L in (1.3.40) the input impedance at $x_1 = 0$ [which corresponds to $d = \lambda/8$ in (1.3.40)] is

$$Z_{IN}(0) = Z_{IN}(d)|_{d=\lambda/8} = 50 \frac{(50 + j50) + j50 \tan 45^\circ}{50 + j(50 + j50) \tan 45^\circ} = 100 - j50 \Omega$$

(b) Since at $x_1 = 0$ the voltage $V_1(0)$ is $V_1(0) = 10 \angle 0^\circ - 50I_1(0)$, it follows from (1.6.3) that

$$a_1(0) = \frac{1}{2\sqrt{Z_o}} [V_1(0) + Z_o I_1(0)] = \frac{1}{2\sqrt{50}} [10 - 50I_1(0) + 50I_1(0)] = \frac{1}{\sqrt{2}}$$

Then, with $l_1 = \lambda/8$ it follows that $\theta_1 = \beta l_1 = \pi/4$ and

$$a_1(\lambda/8) = a_1(0)e^{-j\pi/4} = \frac{1}{\sqrt{2}} \angle -45^\circ$$

From (1.6.4),

$$b_1(0) = \frac{1}{2\sqrt{Z_o}} [V_1(0) - Z_o I_1(0)] = \frac{1}{2\sqrt{50}} [10 - 2(50)I_1(0)] \quad (1.6.28)$$

The current $I_1(0)$ is given by

$$I_1(0) = \frac{E_1}{50 + Z_{IN}(0)} = \frac{10}{50 + 100 - j50} = 0.063 \angle 18.435^\circ \text{ A} \quad (1.6.29)$$

Substituting (1.6.29) into (1.6.28) gives

$$b_1(0) = \frac{1}{2\sqrt{50}} [10 - 2(50)0.063 \angle 18.435^\circ] = 0.316 \angle -26.57^\circ$$

The value of the reflected wave $b_1(\lambda/8)$ follows from

$$b_1(\lambda/8) = b_1(0)e^{j\pi/4} = 0.316 \angle -26.57^\circ \angle 45^\circ = 0.316 \angle 18.43^\circ$$

At the output port the line is matched. Hence, $a_2(0) = 0$.

An alternative way of calculating the reflected wave $b_1(\lambda/8)$ is to calculate S_{11} at $x_1 = \lambda/8$ using (1.6.14), namely

$$S_{11} = \frac{Z_{T1} - 50}{Z_{T1} + 50} = \frac{(50 + j50) - 50}{(50 + j50) + 50} = 0.447 \angle 63.43^\circ \quad (1.6.30)$$

Then

$$b_1(\lambda/8) = S_{11}a_1(\lambda/8) = 0.447 \angle 63.43^\circ \left(\frac{1}{\sqrt{2}} \angle -45^\circ \right) = 0.316 \angle 18.43^\circ$$

(c) $V_1(0)$ can be evaluated in several ways. We can use a voltage divider equation at $x_1 = 0$ to obtain

$$V_1(0) = \frac{E_1 Z_{IN}(0)}{50 + Z_{IN}(0)} = \frac{10(100 - j50)}{50 + (100 - j50)} = 7.07 \angle -8.13^\circ \text{ V}$$

The current $I_1(0)$ was evaluated in (1.6.29). Hence, $V_1(0)$ can also be evaluated using $V_1(0) = I_1(0)Z_{IN}(0)$. Alternatively, $V_1(0)$ can be evaluated using the fact that

$$v_1(0) = \frac{V_1(0)}{\sqrt{Z_o}} = a_1(0) + b_1(0)$$

or

$$V_1(0) = \sqrt{Z_o} [a_1(0) + b_1(0)] = \sqrt{50} \left[\frac{1}{\sqrt{2}} + 0.316 \angle -26.57^\circ \right] = 7.07 \angle -8.13^\circ \text{ V}$$

The voltage $V_1(\lambda/8)$ is given by

$$\begin{aligned} V_1(\lambda/8) &= \sqrt{Z_o} [a_1(\lambda/8) + b_1(\lambda/8)] = \sqrt{50} \left[\frac{1}{\sqrt{2}} \angle -45^\circ + 0.316 \angle 18.43^\circ \right] \\ &= 6.32 \angle -26.57^\circ \text{ V} \end{aligned}$$

and

$$I_1(\lambda/8) = \frac{V_1(\lambda/8)}{Z_{T1}} = \frac{6.32 \angle -26.57^\circ}{50 + j50} = 0.089 \angle -71.57^\circ \text{ A}$$

(d) The input power at $x_1 = 0$ is

$$P_1(0) = \frac{1}{2} \text{Re}[V_1(0)I_1^*(0)] = \frac{1}{2} \text{Re}[7.07 \angle -8.13^\circ (0.063 \angle -18.43^\circ)] = 0.2 \text{ W}$$

and the power at $x_1 = \lambda/8$ is

$$P_1(\lambda/8) = \frac{1}{2} \text{Re}[V_1(\lambda/8)I_1^*(\lambda/8)] = \frac{1}{2} \text{Re}[6.32 \angle -26.57^\circ (0.089 \angle 71.57^\circ)] = 0.2 \text{ W}$$

As expected, $P_1(0) = P_1(\lambda/8)$ since the line is lossless.

Another way of calculating $P_1(0)$ and $P_1(\lambda/8)$ is to use (1.6.15). Since

$$P_{AVS} = \frac{1}{2} |a_1(0)|^2 = \frac{1}{2} \left(\frac{1}{\sqrt{2}} \right)^2 = 0.25 \text{ W}$$

it follows from (1.6.15) that

$$P_1(0) = P_1(\lambda/8) = P_{AVS}(1 - |S_{11}|^2) = 0.25(1 - (0.447)^2) = 0.2 \text{ W}$$

(e) S_{11} at $x_1 = \lambda/8$ was evaluated in (1.6.30). Similarly, at the input of the line $x_1 = 0$ (i.e., at the primed plane), denoting the value as S'_{11} , we obtain

$$S'_{11} = \frac{Z_{IN}(0) - Z_o}{Z_{IN}(0) + Z_o} = \frac{(100 - j50) - 50}{(100 - j50) + 50} = 0.447 \angle -26.57^\circ$$

Observe that S_{11} and S'_{11} are related by [see (1.5.5)]

$$S_{11} = S'_{11} e^{j2\beta\lambda/8} = S'_{11} e^{j\pi/2} = 0.447 \angle 63.43^\circ$$

(f) The output transmission line is matched (i.e., $Z_2 = Z_o = 50 \Omega$). Therefore, the load reflection coefficient associated with $Z_2 = 50 \Omega$ is zero, and the output VSWR is unity.

At the input, the reflection coefficient associated with Z_{T1} is S_{11} . Hence, using (1.3.44) with $|\Gamma_0|$ replaced by $|S_{11}|$ gives an input VSWR of

$$\text{VSWR} = \frac{1 + |S_{11}|}{1 - |S_{11}|} = \frac{1 + 0.447}{1 - 0.447} = 2.62$$

(g) Since the output is matched (i.e., $Z_2 = Z_{o2} = 50 \Omega$) it follows that $a_2(0) = a_2(\lambda/8) = 0$. Hence, from (1.6.16) we have that

$$b_2(\lambda/8) = S_{21} a_1(\lambda/8)$$

or

$$b_2(\lambda/8) = 5 \angle 135^\circ \left(\frac{1}{\sqrt{2}} \angle -45^\circ \right) = 3.54 \angle 90^\circ$$

Then

$$b_2(0) = b_2(\lambda/8) e^{-j\pi/4} = 3.54 \angle 45^\circ$$

The power delivered to Z_2 is

$$P_2(0) = \frac{1}{2} |b_2(0)|^2 = \frac{1}{2} (3.54)^2 = 6.27 \text{ W}$$

Scattering Matrix of n -Port Networks

The extension of the previous formulation to an n -port network is simple. Consider the n -port network shown in Fig. 1.6.9. The transmission lines are assumed to be lossless with characteristic impedance Z_{oi} ($i = 1$ to n). Then it follows that we can write the scattering matrix of the n port, at the unprimed reference planes, in the form

$$[b] = [S] [a] \quad (1.6.31)$$

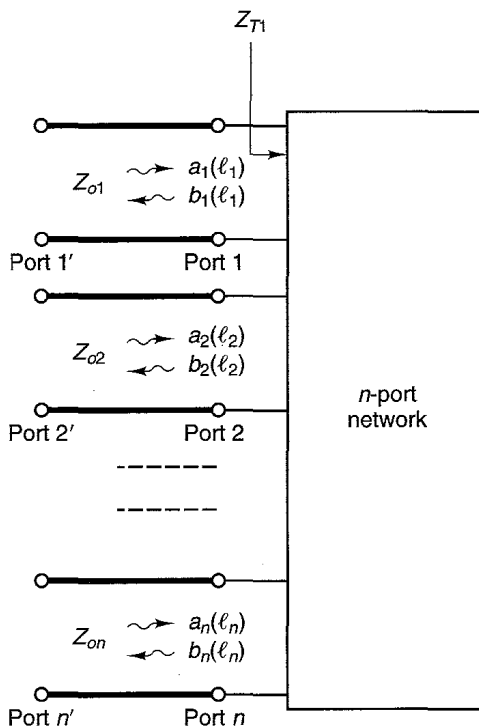


Figure 1.6.9 An n -port network.

where

$$[a] = \frac{1}{2} [Z_o^{-1/2}] ([V] + [Z_o] [I]) \tag{1.6.32}$$

$$[b] = \frac{1}{2} [Z_o^{-1/2}] ([V] - [Z_o] [I]) \tag{1.6.33}$$

$$[S] = \begin{bmatrix} S_{11} & S_{12} & \cdot & \cdot & S_{1n} \\ S_{21} & S_{22} & \cdot & \cdot & S_{2n} \\ \cdot & \cdot & \cdot & \cdot & \cdot \\ \cdot & \cdot & \cdot & \cdot & \cdot \\ S_{n1} & S_{n2} & \cdot & \cdot & S_{nn} \end{bmatrix}$$

and

$$[Z_o^{-1/2}] = \begin{bmatrix} Z_{o1}^{-1/2} & 0 & \dots & 0 \\ 0 & Z_{o2}^{-1/2} & \dots & 0 \\ \cdot & & \cdot & \cdot \\ \cdot & & \cdot & \cdot \\ \cdot & & \cdot & \cdot \\ 0 & \dots & & Z_{on}^{-1/2} \end{bmatrix}$$

The $[a]$, $[b]$, $[V]$, and $[I]$ are column matrices. That is,

$$[a] = \begin{bmatrix} a_1 \\ a_2 \\ \cdot \\ a_n \end{bmatrix} \quad [b] = \begin{bmatrix} b_1 \\ b_2 \\ \cdot \\ b_n \end{bmatrix} \quad [V] = \begin{bmatrix} V_1 \\ V_2 \\ \cdot \\ V_n \end{bmatrix} \quad [I] = \begin{bmatrix} I_1 \\ I_2 \\ \cdot \\ I_n \end{bmatrix}$$

The S parameters of the n -port networks are easily measured. For example, from (1.6.31) S_{11} at $x_1 = l_1$ is given by

$$S_{11} = \frac{b_1(l_1)}{a_1(l_1)} \Big|_{a_j=0 (j=2,3,\dots,n)} = \frac{Z_{T1} - Z_{o1}}{Z_{T1} + Z_{o1}}$$

where Z_{T1} is the impedance seen at port 1 with the other ports matched. In other words, S_{11} can be measured by connecting a voltage source E_1 with source impedance Z_{o1} to port 1' and terminating all other ports in their normalizing impedances (i.e., using matched terminations so that $a_j = 0$ for $j = 2, 3, \dots, n$).

A transistor can be considered to be a three-port device, as shown in Fig. 1.6.10. In this case the scattering matrix, also called the *indefinite scattering matrix*, is

$$\begin{bmatrix} b_1 \\ b_2 \\ b_3 \end{bmatrix} = \begin{bmatrix} S_{11} & S_{12} & S_{13} \\ S_{21} & S_{22} & S_{23} \\ S_{31} & S_{32} & S_{33} \end{bmatrix} \begin{bmatrix} a_1 \\ a_2 \\ a_3 \end{bmatrix} \quad (1.6.34)$$

The name "indefinite scattering matrix" is used because no definite choice is made to ground a particular port. For example, the meaning of S_{11} in (1.6.34) is

$$S_{11} = \frac{b_1}{a_1} \Big|_{a_2=0, a_3=0} \quad (1.6.35)$$

That is, to measure S_{11} , reference resistances of 50Ω are used at ports 2 and 3. In a two-port common-emitter configuration, S_{11} is measured with the emitter grounded. Therefore, the value of S_{11} in (1.6.35) will be different from the value of S_{11} in a two-port common-emitter configuration. Similarly, the parameters S_{12} , S_{21} , and S_{22} in (1.6.34) will be different from the S_{12} , S_{21} , and S_{22} in a two-port common-emitter configuration.

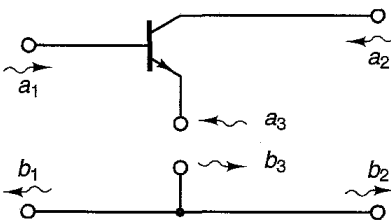


Figure 1.6.10 A transistor as a three-port network.

1.7 POWER WAVES AND GENERALIZED SCATTERING PARAMETERS

In the previous two sections we showed that in a transmission line it is quite natural to represent the voltage and currents in terms of traveling waves—that is, an incident wave $a(x)$ and a reflected wave $b(x)$. In this section we discuss the analysis of lumped circuits (from one-port to n -port lumped circuits) in terms of a new set of waves, called *power waves*.

We first consider the one-port circuit shown in Fig. 1.7.1a, where both the source and load impedances are, in general, complex. The normalized incident and reflected traveling waves defined in (1.4.4) and (1.4.5) do not appear suitable for the analysis of the circuit in Fig. 1.7.1a since there is no transmission line, and therefore the characteristic impedance is not defined. In addition, the concept of a load reflection coefficient according to (1.3.39) or (1.4.3) has no meaning. However, we can introduce a new set of waves, called the power waves. The power waves a_p and b_p are defined by a linear transformation analogous to (1.4.7) and (1.4.8). That is, let

$$a_p = \frac{1}{2\sqrt{R_s}}(V + Z_s I) \tag{1.7.1}$$

and

$$b_p = \frac{1}{2\sqrt{R_s}}(V - Z_s^* I) \tag{1.7.2}$$

where $R_s = \text{Re}[Z_s]$. The definitions in (1.7.1) and (1.7.2) are such that the quantity $\frac{1}{2}|a_p|^2$ is equal to the power available from the source, and the reflected power wave b_p is zero when the load impedance is conjugately matched to the source impedance (i.e., when $Z_L = Z_s^*$). In Fig. 1.7.1b a power-wave representation of the one-port network is shown.

Let us look further into the significance of these power waves. From Fig. 1.7.1a the relation between V and I is

$$V = E_s - Z_s I \tag{1.7.3}$$

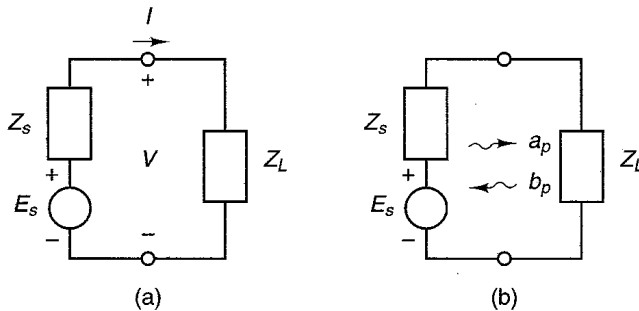


Figure 1.7.1 (a) A lumped one-port network, (b) power-waves representation.

Substituting (1.7.3) into (1.7.1) gives

$$a_p = \frac{1}{2\sqrt{R_s}} (E_s - Z_s I + Z_s I) = \frac{E_s}{2\sqrt{R_s}} \quad (1.7.4)$$

Hence,

$$|a_p|^2 = \frac{|E_s|^2}{4R_s}$$

or

$$\frac{1}{2} |a_p|^2 = |a_{p,\text{rms}}|^2 = \frac{|E_s|^2}{8R_s} \quad (1.7.5)$$

which is recognized as the power available from the source (i.e., $P_{\text{AVS}} = \frac{1}{2} |a_p|^2$). In the circuit of Fig. 1.7.1a maximum power is delivered to the load when $Z_L = Z_s^*$. In fact, the reader should recall that the power delivered to the load (P_L), where

$$P_L = \frac{1}{2} |I|^2 \text{Re}[Z_L] = \frac{1}{2} \left| \frac{E_s}{Z_s + Z_L} \right|^2 \text{Re}[Z_L]$$

attains its maximum value when $Z_L = Z_s^*$, and $P_{L,\text{max}}$ (or P_{AVS}) is given by

$$P_{L,\text{max}} = P_{\text{AVS}} = \frac{1}{8} \frac{|E_s|^2}{R_s}$$

which is identical to (1.7.5).

Since $\frac{1}{2} |a_p|^2$ represents the power available from the source, then $\frac{1}{2} |b_p|^2$ should represent the reflected power. In fact, from (1.7.1) and (1.7.2) we obtain

$$\begin{aligned} \frac{1}{2} |a_p|^2 - \frac{1}{2} |b_p|^2 &= \frac{1}{8R_s} (V + Z_s I) (V + Z_s I)^* - \frac{1}{8R_s} (V - Z_s^* I) (V - Z_s^* I)^* \\ &= \frac{1}{2} \text{Re}[V^* I] \end{aligned}$$

which is recognized as the power dissipated in Z_L (i.e., P_L). Therefore,

$$P_L = \frac{1}{2} |a_p|^2 - \frac{1}{2} |b_p|^2 \quad (1.7.6)$$

From (1.7.6), we can also write

$$\frac{1}{2} |b_p|^2 = P_{\text{AVS}} - P_L$$

Hence, the reflected power $\frac{1}{2} |b_p|^2$ is equal to the available power from the source minus the power dissipated in the load.

Under conjugate matched conditions the power available from the source is delivered to Z_L and the power reflected $\frac{1}{2} |b_p|^2$ is zero (a very important prop-

erty of the power waves). In fact, in the conjugate matched circuit shown in Fig. 1.7.2 we have

$$V = Z_s^* I$$

and from (1.7.2) the reflected power wave is

$$b_p = \frac{1}{2\sqrt{R_s}} (Z_s^* I - Z_s^* I) = 0 \quad (1.7.7)$$

as expected.

A power-wave reflection coefficient Γ_p (also called a generalized reflection coefficient) can be defined as the ratio of b_p to a_p . Hence, from (1.7.1) and (1.7.2) we obtain

$$\Gamma_p = \frac{b_p}{a_p} = \frac{V - Z_s^* I}{V + Z_s I} = \frac{\frac{V}{I} - Z_s^*}{\frac{V}{I} + Z_s} = \frac{Z_L - Z_s^*}{Z_L + Z_s} \quad (1.7.8)$$

Using (1.7.8) we can express (1.7.6) in the form

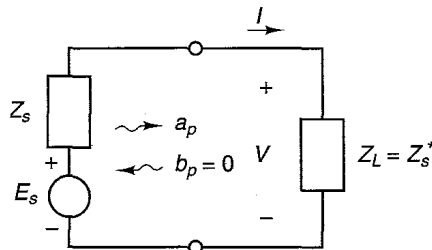
$$P_L = \frac{1}{2} |a_p|^2 (1 - |\Gamma_p|^2) = P_{AVS} (1 - |\Gamma_p|^2)$$

Solving (1.7.1) and (1.7.2) for V and I gives

$$V = \frac{1}{\sqrt{R_s}} (Z_s^* a_p + Z_s b_p) \quad (1.7.9)$$

and

$$I = \frac{1}{\sqrt{R_s}} (a_p - b_p) \quad (1.7.10)$$



$$a_p = \frac{E_s}{2\sqrt{R_s}}$$

$$V = V_p^+ = \frac{Z_s^*}{\sqrt{R_s}} a_p$$

$$V_p^- = 0$$

Figure 1.7.2 Conjugate matched network.

One should observe that the addition and subtraction of the incident and reflected traveling waves in (1.4.4) and (1.4.5) is equal to the normalized voltage and current along the transmission line, while from (1.7.9) and (1.7.10) the voltage and currents are not given by a simple addition or subtraction of the power waves.

From (1.7.9) and (1.7.10) we can also define incident and reflected voltages and currents (denoted by V_p^+ , V_p^- , I_p^+ , and I_p^-) and relate them to the power waves. That is, let

$$V = V_p^+ + V_p^- \quad (1.7.11)$$

and

$$I = I_p^+ - I_p^- \quad (1.7.12)$$

where

$$V_p^+ = \frac{Z_s^*}{\sqrt{R_s}} a_p \quad (1.7.13)$$

$$V_p^- = \frac{Z_s}{\sqrt{R_s}} b_p \quad (1.7.14)$$

$$I_p^+ = \frac{a_p}{\sqrt{R_s}} = \frac{V_p^+}{Z_s^*} \quad (1.7.15)$$

and

$$I_p^- = \frac{b_p}{\sqrt{R_s}} = \frac{V_p^-}{Z_s} \quad (1.7.16)$$

From (1.7.13) and (1.7.14) a voltage reflection coefficient Γ_V can be defined as

$$\Gamma_V = \frac{V_p^-}{V_p^+} = \frac{Z_s b_p}{Z_s^* a_p} = \frac{Z_s}{Z_s^*} \Gamma_p = \frac{Z_s}{Z_s^*} \frac{Z_L - Z_s^*}{Z_L + Z_s} \quad (1.7.17)$$

Furthermore, from (1.7.15) and (1.7.16) a current reflection coefficient Γ_I can be defined as

$$\Gamma_I = \frac{I_p^-}{I_p^+} = \frac{b_p}{a_p} = \Gamma_p$$

which is identical to the power-wave reflection coefficient.

An alternative way of introducing the power waves would be to define incident and reflected voltages (V_p^+ and V_p^-) in Fig. 1.7.1a and then define the power waves a_p and b_p in terms of V_p^+ and V_p^- . We will not go through this development of the power waves since it would be somewhat repetitious. However, a better understanding of the previous concepts is gained by calculating directly the incident and reflected voltages in Fig. 1.7.1a, and then verifying their relationship with the power waves [i.e., (1.7.13) and (1.7.14)].

In Fig. 1.7.1a the voltage V_p^+ , which is defined as the voltage V when $Z_L = Z_s^*$, is given by

$$V_p^+ = \frac{E_s Z_s^*}{Z_s + Z_s^*} = \frac{E_s Z_s^*}{2R_s} \quad (1.7.18)$$

Using (1.7.4), (1.7.18) can be expressed in the form

$$V_p^+ = \frac{Z_s^*}{\sqrt{R_s}} a_p$$

which is recognized as (1.7.13).

In Fig. 1.7.1a, V is given by

$$V = \frac{E_s Z_L}{Z_L + Z_s}$$

Since $V = V_p^+ + V_p^-$ and V_p^+ is given by (1.7.18), it follows that the reflected voltage is

$$V_p^- = V - V_p^+ = \frac{E_s Z_L}{Z_L + Z_s} - \frac{E_s Z_s^*}{2R_s} = \frac{E_s Z_s}{2R_s} \frac{Z_L - Z_s^*}{Z_L + Z_s} \quad (1.7.19)$$

Equation (1.7.19) can be expressed in several ways. Using (1.7.17) and (1.7.18), (1.7.19) can be expressed in the form

$$V_p^- = V_p^+ \Gamma_V$$

Using (1.7.13) and (1.7.17), V_p^- can be written as

$$V_p^- = \frac{Z_s^*}{\sqrt{R_s}} a_p \left(\frac{Z_s}{Z_s^*} \frac{b_p}{a_p} \right) = \frac{Z_s}{\sqrt{R_s}} b_p$$

which is recognized as (1.7.14).

In terms of incident and reflected voltages, the analysis of the circuit in Fig. 1.7.2, where $Z_L = Z_s^*$, produces: $V = V_p^+$ and $V_p^- = 0$ since there is no reflected wave.

It is simple to verify that in Fig. 1.7.1a the current I is

$$I = \frac{E_s}{Z_s + Z_L}$$

and the incident and reflected currents are

$$I_p^+ = \frac{E_s}{2R_s}$$

and

$$I_p^- = I_p^+ \Gamma_I$$

where Γ_I is the current reflection coefficient.

When the normalizing impedance Z_s is real and positive, the expressions for the power waves a_p and b_p are identical to the traveling waves $a(x)$ and $b(x)$. In fact, when Z_s is equal to a real and positive normalizing impedance Z_o , the relations derived for power waves are identical to those derived for traveling waves. Specifically, for Z_s real and equal to Z_o , (1.7.1) and (1.7.2) are identical to (1.4.7) and (1.4.8). Also, V and I in (1.7.11) and (1.7.12) are identical to $V(x)$ and $I(x)$ in (1.4.1) and (1.4.2). Finally, Γ_p , as well as Γ_V and Γ_I , are all equal to Γ_0 . That is, for $Z_s = Z_s^* = Z_o$,

$$\Gamma_0 = \Gamma_p = \Gamma_V = \Gamma_I = \frac{Z_L - Z_o}{Z_L + Z_o}$$

From a mathematical point of view the relations of $a(x)$ and $b(x)$ as functions of $V(x)$ and $I(x)$ are linear transformations such that $V(x)$ and $I(x)$ follow from the inverse transformation. Similarly, the relations for a_p and b_p as functions of V and I [i.e., (1.7.1) and (1.7.2)] are different linear transformations, where their inverse transformations in (1.7.9) and (1.7.10) give V and I in a one-port network.

In the case of a two-port network, as shown in Fig. 1.7.3, we can define generalized scattering parameters (S_p parameters), denoted by S_{p11} , S_{p12} , S_{p21} , and S_{p22} , in terms of power waves as follows:

$$b_{p1} = S_{p11}a_{p1} + S_{p12}a_{p2} \quad (1.7.20)$$

$$b_{p2} = S_{p21}a_{p1} + S_{p22}a_{p2} \quad (1.7.21)$$

where

$$a_{p1} = \frac{1}{2\sqrt{R_1}}(V_1 + Z_1 I_1) \quad (1.7.22)$$

$$a_{p2} = \frac{1}{2\sqrt{R_2}}(V_2 + Z_2 I_2) \quad (1.7.23)$$

$$b_{p1} = \frac{1}{2\sqrt{R_1}}(V_1 - Z_1^* I_1) \quad (1.7.24)$$

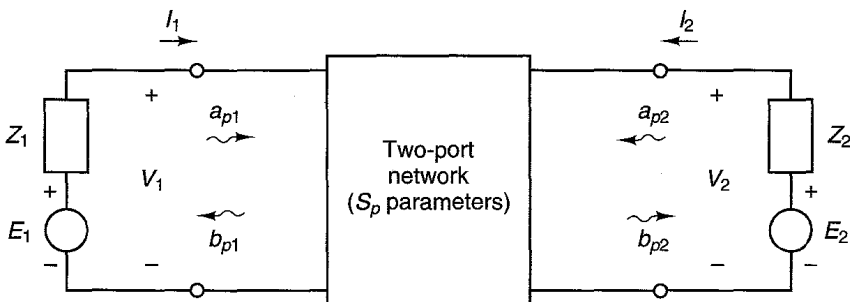


Figure 1.7.3 Two-port network representation in terms of generalized scattering parameters.

and

$$b_{p2} = \frac{1}{2\sqrt{R_2}} (V_2 - Z_2^* I_2) \quad (1.7.25)$$

The resistors R_1 and R_2 are $R_1 = \text{Re}[Z_1]$ and $R_2 = \text{Re}[Z_2]$. The values of the S_p parameters depend on the terminal impedances Z_1 and Z_2 . These impedances are called the reference impedances.

There is no way of directly measuring the generalized scattering parameters. For example, from (1.7.20)

$$S_{p11} = \left. \frac{b_{p1}}{a_{p1}} \right|_{a_{p2}=0}$$

Hence, S_{p11} can be determined if a_{p1} and b_{p1} can be measured with $a_{p2} = 0$. In Fig. 1.7.4 the circuit in Fig. 1.7.3 is shown with $E_2 = 0$, the output voltage is $V_2 = -I_2 Z_2$, and from (1.7.23) it follows that $a_{p2} = 0$. Unfortunately, a_{p1} and b_{p1} are not traveling waves and, therefore, cannot be separated and measured using a directional coupler.

The evaluation of S_{p11} in Fig. 1.7.4 follows from (1.7.8); that is,

$$S_{p11} = \frac{Z_{T1} - Z_1^*}{Z_{T1} + Z_1} \quad (1.7.26)$$

The input power to the two-port network can be expressed as

$$P_{\text{IN}} = \frac{1}{2} |a_{p1}|^2 - \frac{1}{2} |b_{p1}|^2 = P_{\text{AVS}}(1 - |S_{p11}|^2)$$

While the S_p parameters cannot be measured, the S parameters of the two-port in Fig. 1.7.3 can be easily measured and the S_p parameters can be calculated in terms of the S parameters. Recall that the S parameters in a Z_o system are measured by inserting transmission lines with characteristic impedances Z_o at both ports in Fig. 1.7.3, changing Z_1 and Z_2 to Z_o (usually $Z_o = 50 \Omega$), and taking the appropriate measurement of the traveling waves $a_1(x), a_2(x)$,

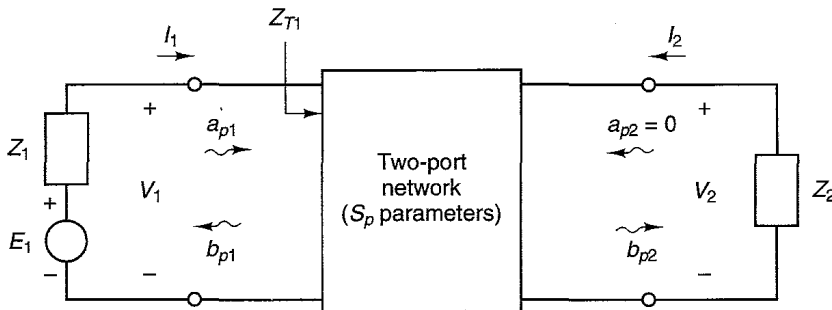


Figure 1.7.4 Two-port network with $E_2 = 0$.

$b_1(x)$, and $b_2(x)$. The relations between the S_p parameters and the S parameters are derived in Section 2.7.

Power-gain expressions for the network in Fig. 1.7.4 are easily written in terms of S_p parameters. For example, $a_{p2} = 0$ in Fig. 1.7.4, and the power delivered to the load Z_2 , denoted by P_L , is

$$P_L = \frac{1}{2} |b_{p2}|^2$$

Since from (1.7.21), when $a_{p2} = 0$, $b_{p2} = S_{21}a_{p1}$ we can express P_L in the form

$$P_L = \frac{1}{2} |S_{p21}|^2 |a_{p1}|^2$$

The power available from the source is $\frac{1}{2} |a_{p1}|^2$; therefore the transducer power gain for the network in Fig. 1.7.4 is given by

$$G_T = \frac{P_L}{P_{AVS}} = |S_{p21}|^2 \quad (1.7.27)$$

Equation (1.7.27) gives the transducer power gain of a two-port network with arbitrary terminations Z_s and Z_L . If in Fig. 1.7.4 we let $Z_1 = Z_2 = Z_o$ then it also follows from (1.6.22) that $G_T = |S_{21}|^2$, where S_{21} is measured using the normalizing impedance Z_o . In other words, for $Z_1 = Z_2 = Z_o$ it follows that

$$G_T = |S_{p21}|^2 = |S_{21}|^2 \quad (1.7.28)$$

Equation (1.7.28) expresses the fact that in a system where the S parameters are measured with $Z_1 = Z_2 = Z_o$ the transducer power gain is simply $|S_{21}|^2$. Since for $Z_1 = Z_2 = Z_o$ power waves and traveling waves give identical results, it follows that the transducer power gain is also given by $|S_{p21}|^2$. For source and load impedances such that $Z_1 \neq Z_o$ and $Z_2 \neq Z_o$ it follows that $|S_{p21}|^2 \neq |S_{21}|^2$.

In Sections 2.6 and 2.7 we will learn that the gain G_T in Fig. 1.7.4 (as well as other power expressions) can be conveniently expressed in terms of Z_1 , Z_2 , and the S parameters of the transistor measured in a Z_o system.

Generalized Scattering Matrix for n -Port Networks

In the n -port network shown in Fig. 1.7.5 the normalizing incident and reflected power waves are defined as

$$[a_p] = \frac{1}{2} [R^{-1/2}] ([V] + [Z][I]) \quad (1.7.29)$$

and

$$[b_p] = \frac{1}{2} [R^{-1/2}] ([V] - [Z^*][I]) \quad (1.7.30)$$

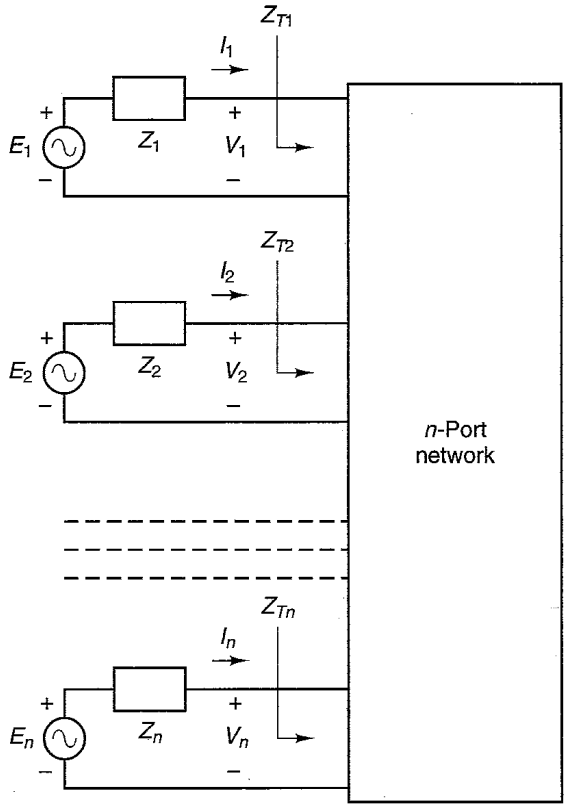


Figure 1.7.5 An n -port network.

where

$$[a_p] = \begin{bmatrix} a_{p1} \\ a_{p2} \\ \cdot \\ \cdot \\ a_{pn} \end{bmatrix} \quad [b_p] = \begin{bmatrix} b_{p1} \\ b_{p2} \\ \cdot \\ \cdot \\ b_{pn} \end{bmatrix} \quad [V] = \begin{bmatrix} V_1 \\ V_2 \\ \cdot \\ \cdot \\ V_n \end{bmatrix} \quad [I] = \begin{bmatrix} I_1 \\ I_2 \\ \cdot \\ \cdot \\ I_n \end{bmatrix}$$

$$[Z] = \begin{bmatrix} Z_1 & 0 & \dots & 0 \\ 0 & Z_2 & \dots & 0 \\ \cdot & & & \cdot \\ \cdot & & & \cdot \\ 0 & \dots & & Z_n \end{bmatrix}$$

and

$$[R^{-1/2}] = \begin{bmatrix} (\operatorname{Re} Z_1)^{-1/2} & 0 & \cdots & 0 \\ 0 & (\operatorname{Re} Z_2)^{-1/2} & \cdots & 0 \\ \cdot & & & \cdot \\ \cdot & & & \cdot \\ \cdot & & & \cdot \\ 0 & \cdots & & (\operatorname{Re} Z_n)^{-1/2} \end{bmatrix}$$

Observe that in the case of a one-port network, (1.7.29) and (1.7.30) reduce to (1.7.1) and (1.7.2), and for a two-port network the equations reduce to (1.7.22) to (1.7.25).

Solving (1.7.29) and (1.7.30) for $[V]$ and $[I]$ results in

$$\begin{aligned} [V] &= [V_p^+] + [V_p^-] \\ [I] &= [I_p^+] - [I_p^-] \end{aligned}$$

where

$$\begin{aligned} [V_p^+] &= [Z^*] [I_p^+] \\ [V_p^-] &= [Z] [I_p^-] \\ [a_p] &= [R^{1/2}] [I_p^+] \end{aligned}$$

and

$$[b_p] = [R^{1/2}] [I_p^-]$$

The generalized scattering matrix of the n -port network is defined as

$$[b_p] = [S_p] [a_p] \quad (1.7.31)$$

where

$$[S_p] = \begin{bmatrix} S_{p11} & S_{p12} & \cdots & S_{p1n} \\ S_{p21} & \cdots & \cdots & \cdots \\ \cdot & & & \cdot \\ \cdot & & & \cdot \\ \cdot & & & \cdot \\ S_{pn1} & \cdots & \cdots & S_{pnn} \end{bmatrix}$$

The definition in (1.7.31) shows that different reference impedances Z_i ($i = 1$ to n) produce different values of the generalized scattering parameters. Therefore, the generalized scattering parameters are defined in terms of specific reference impedances. If the reference impedances are pure resistances (denoted by $Z_i = Z_{oi}$), the formulation in (1.7.29), (1.7.30), and (1.7.31) is identical to (1.6.31) to (1.6.33).

The S_p parameters of the n -port network are defined by (1.7.31). For example, the parameter $S_{p\ddot{u}}$ is recognized as the input power reflection coefficient of port i , determined with all other ports terminated in their reference impedances (i.e., with $E_k = 0$ then $V_k = -Z_k I_k$ and $a_k = 0$, $k \neq i$, $k = 0, 1, 2, \dots, n$). Therefore,

$$S_{p\ddot{u}} = \left. \frac{b_{pi}}{a_{pi}} \right|_{a_k=0, k \neq i, k=0, 1, \dots, n} = \frac{V_i - Z_i^* I_i}{V_i + Z_i I_i} = \frac{Z_{Ti} - Z_i^*}{Z_{Ti} + Z_i}$$

The quantity $|S_{p\ddot{u}}|^2$ can be shown to be the transducer power gain from port i to port k .

Example 1.7.1

Calculate the power waves and the power delivered to the load in the circuit shown in Fig. 1.7.6.

Solution: In Fig. 1.7.6, the voltage V and the current I are given by

$$V = \frac{E_s Z_L}{Z_L + Z_s} = \frac{10(100 - j50)}{100 - j50 + 100 + j50} = 5.59 \angle -26.57^\circ \text{ V}$$

and

$$I = \frac{E_s}{Z_L + Z_s} = \frac{10}{200} = 0.05 \text{ A}$$

From (1.7.1) [see also (1.7.4)] with $R_s = \text{Re}[Z_s] = 100 \Omega$ and $V = E_s - IZ_s$ it follows that the power wave a_p is

$$a_p = \frac{1}{2\sqrt{R_s}} (V + Z_s I) = \frac{E_s}{2\sqrt{R_s}} = \frac{10}{2\sqrt{100}} = 0.5$$

Since a conjugate match condition exists in Fig. 1.7.6, the reflected power wave b_p is zero [see (1.7.7)]. Therefore, the power delivered to the load is equal to P_{AVS} and given by (1.7.5), namely

$$P_L = \frac{1}{2} |a_p|^2 = \frac{1}{2} (0.5)^2 = 0.125 \text{ W}$$

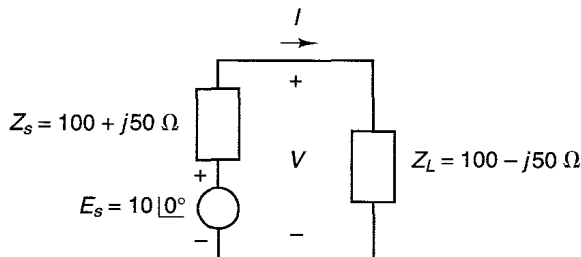


Figure 1.7.6 Circuit for Example 1.7.1.

The circuit in Fig. 1.7.6 is identical to the equivalent circuit in Example 1.3.1 (see Fig. 1.3.8b). Traveling waves were used in the solution of Example 1.3.1.

Example 1.7.2

Calculate the power delivered to the load in the circuit shown in Fig. 1.7.7a using (a) power waves and (b) traveling waves.

Solution: The transmission line in Fig. 1.7.7a is matched since $Z_L = Z_o$. Therefore, $\Gamma_0 = 0$ and the input impedance at $x = 0$ is $Z_{IN}(x = 0) = Z_{IN}(d = \lambda/4) = 50 \Omega$. The equivalent circuit at $x = 0$ is shown in Fig. 1.7.7b.

We can analyze the equivalent circuit at the input of the transmission line, shown in Fig. 1.7.7b, either in terms of power waves or traveling waves. For power-waves analysis we use the notation in Fig. 1.7.7b, and for traveling-waves analysis we use the notation in Fig. 1.7.7c.

(a) Power-Waves Analysis

The equivalent lumped one-port network in Fig. 1.7.6b can be analyzed in terms of power waves as follows. Since

$$V = \frac{30(50)}{50 + 100} = 10 \text{ V}$$

and

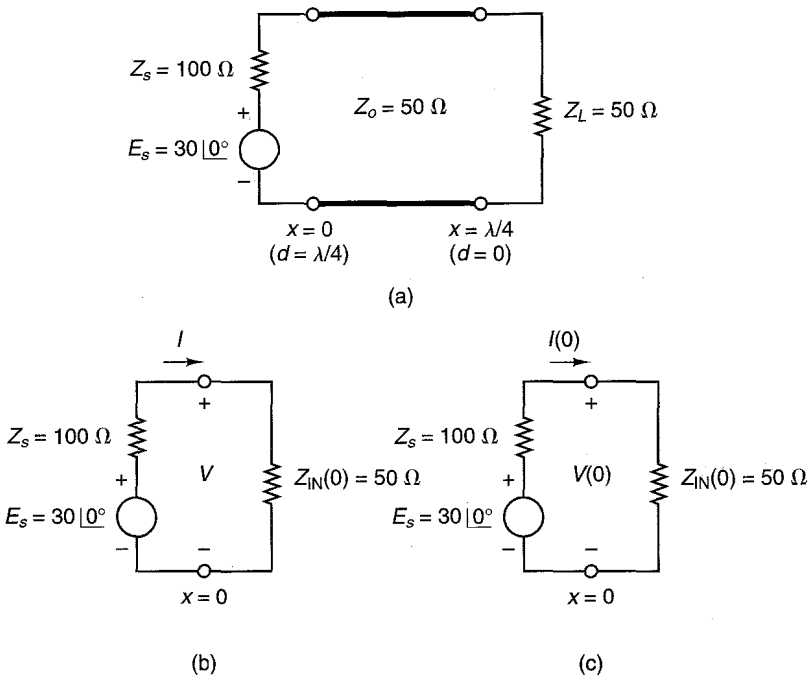


Figure 1.7.7 (a) Transmission-line circuit for Example 1.7.2; (b) the equivalent circuit at $x = 0$ for power-waves analysis; (c) the equivalent circuit at $x = 0$ for traveling-waves analysis.

$$I = \frac{30}{50 + 100} = 0.2 \text{ A}$$

from (1.7.1) and (1.7.2) with $R_s = \text{Re}[Z_s] = 100 \Omega$ we obtain

$$a_p = \frac{1}{2\sqrt{R_s}}(V + Z_s I) = \frac{1}{2\sqrt{100}}(10 + 100(0.2)) = 1.5$$

and

$$b_p = \frac{1}{2\sqrt{R_s}}(V - Z_s^* I) = \frac{1}{2\sqrt{100}}(10 - 100(0.2)) = -0.5$$

The power available from the source is

$$P_{\text{AVS}} = \frac{1}{2} |a_p|^2 = \frac{1}{2} (1.5)^2 = 1.125 \text{ W}$$

Observe that since $Z_{\text{IN}}(0) = 50 \Omega$ is not conjugate matched to the source Z_s , there is a reflected power wave b_p . The reflected power is $\frac{1}{2} |b_p|^2 = \frac{1}{2} (0.5)^2 = 0.125 \text{ W}$, and the power dissipated in $Z_{\text{IN}}(0)$ is

$$P_{\text{IN}} = \frac{1}{2} |a_p|^2 - \frac{1}{2} |b_p|^2 = 1.125 - 0.125 = 1 \text{ W}$$

Since the line is lossless, the power delivered to the load in Fig. 1.7.7a is 1 W.

The previous calculation for P_{IN} can also be made by observing that the power reflection coefficient is

$$\Gamma_p = \frac{b_p}{a_p} = -\frac{1}{3}$$

Therefore,

$$P_{\text{IN}} = P_{\text{AVS}}(1 - |\Gamma_p|^2) = 1.125 \left(1 - \left(\frac{1}{3}\right)^2\right) = 1 \text{ W}$$

As a check to the calculations of a_p and b_p , we can use (1.7.9) and (1.7.10) to verify the values of V and I . That is, with $Z_s = Z_s^* = 100 \Omega$, V and I in terms of a_p and b_p are

$$V = \frac{1}{\sqrt{100}} [100(1.5) + 100(-0.5)] = 10 \text{ V}$$

and

$$I = \frac{1}{\sqrt{100}} [1.5 - (-0.5)] = 0.2 \text{ A}$$

which, of course, are the correct values of V and I .

(b) Traveling-Wave Analysis

Referring to Fig. 1.7.7c, the voltage and currents at the input of the line are denoted by $V(0)$ and $I(0)$, respectively. Their values are $V(0) = 10 \text{ V}$ and $I(0) = 0.2 \text{ A}$.

From (1.4.7) and (1.4.8) with $Z_o = 50 \Omega$, it follows that

$$a(0) = \frac{1}{2\sqrt{Z_o}} [V(0) + Z_o I(0)] = \frac{1}{2\sqrt{50}} [10 + 50(0.2)] = \sqrt{2}$$

and

$$b(0) = \frac{1}{2\sqrt{Z_o}} [V(0) - Z_o I(0)] = \frac{1}{2\sqrt{50}} [10 - 50(0.2)] = 0$$

As expected, there is no reflected wave [i.e., $b(x) = 0$] in a matched transmission line. Observe that $\frac{1}{2}|a(0)|^2 = 1 \text{ W}$ is not equal to the power available from the source ($P_{AVS} = 1.125 \text{ W}$). In fact, only when $Z_s = Z_o$ is $\frac{1}{2}|a(0)|^2$ equal to P_{AVS} .

The power dissipated by $Z_{IN}(0)$ (and in the load since the line is lossless) is

$$P_{IN} = \frac{1}{2} |a(0)|^2 - \frac{1}{2} |b(0)|^2 = \frac{1}{2} (\sqrt{2})^2 = 1 \text{ W}$$

The previous calculation for P_{IN} can also be made by observing that $\Gamma_0 = 0$. Therefore,

$$P_{IN} = \frac{1}{2} |a(0)|^2 (1 - |\Gamma_0|^2) = \frac{1}{2} (\sqrt{2})^2 = 1 \text{ W}$$

The values of $V(0)$ and $I(0)$ can be verified using (1.4.4) and (1.4.5), namely

$$V(0) = \sqrt{Z_o} v_1(0) = \sqrt{50} [a(0) + b(0)] = \sqrt{50} [\sqrt{2}] = 10 \text{ V}$$

and

$$I(0) = \frac{i(0)}{\sqrt{Z_o}} = \frac{1}{\sqrt{50}} [a(0) - b(0)] = \frac{1}{\sqrt{50}} [\sqrt{2}] = 0.2 \text{ A}$$

which, of course, are the correct values of the voltage and current:

The incident wave along the line is given by

$$a(x) = a(0)e^{-j\beta x} = \sqrt{2}e^{-j\beta x}$$

and, since $b(x) = 0$, $V(x)$ is given by

$$V(x) = \sqrt{Z_o} a(x) = \sqrt{50} (\sqrt{2}e^{-j\beta x}) = 10e^{-j\beta x}$$

With $d = \lambda/4 - x$ we can write the voltage in terms of d as

$$V(d) = 10e^{-j\pi/2} e^{j\beta d}$$

Example 1.7.3

Calculate the generalized parameters S_{p11} and S_{p21} at 1 GHz in the lossless, reciprocal, two-port network shown in Fig. 1.7.8a. Then calculate S_{p22} and S_{p12} using Fig. 1.7.8b.

Solution: At 1 GHz the impedance of the inductor is $Z_L = j10 \Omega$, and it follows that $V_1 = 0.167 \angle 0^\circ E_1$, $I_1 = 0.0118 \angle -45^\circ E_1$, $V_2 = 0.118 \angle -45^\circ E_1$, and $I_2 = -0.0118 \angle -45^\circ E_1$. From (1.7.22) to (1.7.25) we obtain: $a_{p1} = 0.071 \angle 0^\circ E_1$, $b_{p1} =$

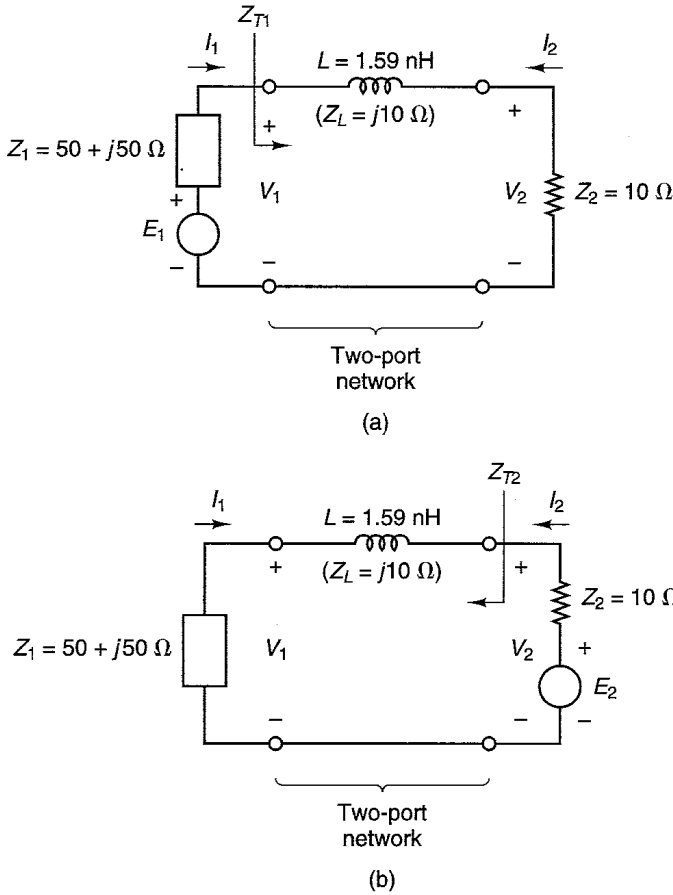


Figure 1.7.8 (a) A two-port network consisting of a series 1.59 nH inductor with reference impedances Z_1 and Z_2 and with the voltage E_1 at the input; (b) same network with the voltage E_2 at the output.

$0.061 \angle 78.69^\circ E_1$, $a_{p2} = 0$, and $b_{p2} = 0.037 \angle -45^\circ E_1$. Therefore, in Fig. 1.7.8a, $Z_{T1} = 10 + j10 \Omega$ and from (1.7.26)

$$S_{p11} = \left. \frac{b_{p1}}{a_{p1}} \right|_{a_{p2}=0} = \frac{Z_{T1} - Z_1^*}{Z_{T1} + Z_1} = \frac{10 + j10 - (50 - j50)}{10 + j10 + (50 + j50)} = 0.85 \angle 78.69^\circ \quad (1.7.32)$$

and

$$S_{p21} = \left. \frac{b_{p2}}{a_{p1}} \right|_{a_{p2}=0} = \frac{0.037 \angle -45^\circ}{0.071 \angle 0^\circ} = 0.525 \angle -45^\circ$$

From Fig. 1.7.8b we have $Z_{T2} = 50 + j60 \Omega$, and it follows that $V_1 = 0.833 \angle 0^\circ E_2$, $I_1 = -0.0118 \angle -45^\circ E_2$, $V_2 = 0.92 \angle 5.19^\circ E_2$, and $I_2 = 0.0118 \angle -45^\circ E_2$. From (1.7.22) to (1.7.25) we obtain: $a_{p1} = 0$, $b_{p1} = 0.083 \angle -45^\circ E_2$, $a_{p2} = 0.158 \angle 0^\circ E_2$, and $b_{p2} = 0.134 \angle 11.32^\circ E_2$. Therefore, it follows that

$$S_{p22} = \left. \frac{b_{p2}}{a_{p2}} \right|_{a_{p1}=0} = \frac{Z_{T2} - Z_2^*}{Z_{T2} + Z_2} = \frac{50 + j60 - 10}{50 + j60 + 10} = 0.85 \angle 11.3^\circ \quad (1.7.33)$$

and

$$S_{p12} = \left. \frac{b_{p1}}{a_{p2}} \right|_{a_{p1}=0} = \frac{0.083 \angle -45^\circ}{0.158 \angle 0^\circ} = 0.525 \angle -45^\circ$$

An important comment is that most CAD programs will calculate the generalized scattering parameters of two-port networks. For example, for the two-port network in Fig. 1.7.8a they will calculate the S_p parameters. If the S parameters of the 1.59-nH inductor in Fig. 1.7.8a are desired in a 50- Ω system, one lets $Z_1 = Z_2 = 50 \Omega$ in Fig. 1.7.8a, and the resulting S_p parameters calculated by the CAD program are the S parameters of the 1.59-nH inductor.

1.8 TWO-PORT NETWORK PARAMETERS CONVERSIONS

At a given frequency a two-port network can be described in terms of several parameters. Therefore, it is desirable to have relations to convert from one set of parameters to another. For example, the z parameters of a two-port network are defined by

$$[V] = [z] [I] \quad (1.8.1)$$

where

$$[V] = \begin{bmatrix} v_1 \\ v_2 \end{bmatrix}$$

$$[I] = \begin{bmatrix} i_1 \\ i_2 \end{bmatrix}$$

and

$$[z] = \begin{bmatrix} z_{11} & z_{12} \\ z_{21} & z_{22} \end{bmatrix}$$

In terms of incident and reflected waves, we obtain from (1.8.1)

$$[V^+] + [V^-] = [z] ([I^+] - [I^-])$$

or

$$([z] + [Z_o]) [I^-] = ([z] - [Z_o]) [I^+]$$

where Z_o is assumed to be real and

$$[Z_o] = \begin{bmatrix} Z_o & 0 \\ 0 & Z_o \end{bmatrix}$$

Therefore, the scattering matrix [i.e., (1.4.9)] in terms of z parameters is given by

$$[S] = \frac{[b]}{[a]} = \frac{[V^-]}{[V^+]} = \frac{[I^-]}{[I^+]} = ([z] + [Z_o])^{-1}([z] - [Z_o]) \quad (1.8.2)$$

and solving for $[z]$, we obtain

$$[z] = [Z_o] ([\mathbf{1}] + [S]) ([\mathbf{1}] - [S])^{-1} \quad (1.8.3)$$

where $[\mathbf{1}]$ is the unit diagonal matrix. Equations (1.8.2) and (1.8.3) give the conversion relations between the S and z parameters. These conversions, as well as others among the z , y , h , $ABCD$, and S parameters, are tabulated in Fig. 1.8.1.

1.9 MEASUREMENT OF SCATTERING PARAMETERS

Measurement of the S parameters of a transistor requires reflection and transmission measurement of traveling waves at both ports. The transistors must be properly biased at the desired Q point, and *small-signal conditions* must be maintained through the measurements. Two measurement systems that are used to measure S parameters are discussed in this section. The first measurement system uses a vector voltmeter, and the second system uses a network analyzer.

The measurement system using a vector voltmeter is illustrated in Fig. 1.9.1a. The vector voltmeter used is the HP8508A, which operates over the frequency range extending from 0.1 MHz to 1 GHz. The probes A and B from the vector voltmeter are inserted into two HP11536A TEEs to measure the incident voltage at A_1 and the reflected voltage at B_1 .

The set-up in Fig. 1.9.1a is used to measure S_{11} and S_{21} of a transistor in a 50- Ω system. The main components are a signal generator to produce a sinusoidal signal at the frequency where the S parameters of the device are measured, a vector voltmeter, two dual directional couplers, two dc bias circuits, a short-circuit calibration section, and a *through* calibration section. The vector voltmeter measures the magnitude of two voltages (in Volts rms) and the phase difference between them (in degrees). The dual directional couplers are used to separate and measure the incident and reflected voltages. The dc bias circuits consist of a coupling capacitor and a large inductor. This large inductor is commonly known as a radio frequency coil (RFC). The RFC presents a very high impedance to the ac signal and zero impedance to the dc signal. The transistor gets its base to emitter voltage through the dc bias circuit #1, and its collector to emitter voltage through the dc bias circuit #2. A dc bias circuit is shown in Fig. 1.9.1b. The voltage V_{BB} and resistor R_B will set the Q -point values of I_B and I_C , and V_{CC} sets the collector to emitter voltage. The voltage V_{BB} can be varied to obtain exactly the desired Q -point value of I_C .

A signal proportional to the incident voltage is read with probe A measuring the signal at position A_1 , and a signal proportional to the reflected voltage is read with probe B measuring the signal at position B_1 . If the constant of proportionality is the same for the incident and for the reflected voltages (i.e., if

S	z	y	h	ABCD
S ₁₁ S ₁₂ S ₂₁ S ₂₂	S ₁₁ = $\frac{(Z_{11}-1)(Z_{22}+1) - Z_{12}Z_{21}}{\Delta_1}$ S ₁₂ = $\frac{2Z_{12}}{\Delta_1}$ S ₂₁ = $\frac{2Z_{21}}{\Delta_1}$ S ₂₂ = $\frac{(Z_{11}+1)(Z_{22}-1) - Z_{12}Z_{21}}{\Delta_1}$	S ₁₁ = $\frac{(1-Y_{11})(1+Y_{22}) + Y_{12}Y_{21}}{\Delta_2}$ S ₁₂ = $\frac{-2Y_{12}}{\Delta_2}$ S ₂₁ = $\frac{-2Y_{21}}{\Delta_2}$ S ₂₂ = $\frac{(1+Y_{11})(1-Y_{22}) + Y_{12}Y_{21}}{\Delta_2}$	S ₁₁ = $\frac{(h_{11}-1)(h_{22}+1) - h_{12}h_{21}}{\Delta_3}$ S ₁₂ = $\frac{2h_{12}}{\Delta_3}$ S ₂₁ = $\frac{-2h_{21}}{\Delta_3}$ S ₂₂ = $\frac{(1+h_{11})(1-h_{22}) + h_{12}h_{21}}{\Delta_3}$	A + B - C - D $\frac{A+B-C-D}{\Delta_4}$ $\frac{2(A'D-B'C)}{\Delta_4}$
Z	Z ₁₁ Z ₁₂ Z ₂₁ Z ₂₂	Y ₁₂ $\frac{Y_{22}}{ Y }$ $\frac{Y_{21}}{ Y }$ $\frac{Y_{11}}{ Y }$ Y ₂₂	$\frac{ h }{h_{22}}$ $\frac{h_{12}}{h_{22}}$ $\frac{1}{h_{22}}$ $\frac{h_{12}}{h_{11}}$	$\frac{A}{C}$ $\frac{D}{C}$ $\frac{1}{C}$ $\frac{D}{B}$
Y	Y ₁₁ Y ₁₂ Y ₂₁ Y ₂₂	Y ₁₁ Y ₁₂ Y ₂₁ Y ₂₂	$\frac{1}{h_{11}}$ $\frac{h_{21}}{h_{11}}$ $\frac{ h }{h_{11}}$ $\frac{1}{h_{11}}$	$\frac{D}{B}$ $\frac{-\Delta_B}{B}$ $\frac{1}{B}$ $\frac{A}{B}$
h	h ₁₁ h ₁₂ h ₂₁ h ₂₂	$\frac{ z }{z_{22}}$ $\frac{z_{12}}{z_{22}}$ $\frac{1}{z_{22}}$ $\frac{z_{11}}{ z }$	h ₁₁ h ₁₂ h ₂₁ h ₂₂	$\frac{B}{D}$ $\frac{-\Delta_B}{D}$ $\frac{1}{D}$ $\frac{C}{D}$
ABCD	A B C D	$\frac{z_{11}}{z_{21}}$ $\frac{1}{z_{21}}$ $\frac{z_{22}}{z_{21}}$	$\frac{- h }{h_{21}}$ $\frac{-h_{22}}{h_{21}}$ $\frac{1}{h_{21}}$	A B C D

$Z_{11} = z_{11}/Z_0, Z_{12} = z_{12}/Z_0, Z_{21} = z_{21}/Z_0, Z_{22} = z_{22}/Z_0$
 $Y_{11} = y_{11}/Z_0, Y_{12} = y_{12}/Z_0, Y_{21} = y_{21}/Z_0, Y_{22} = y_{22}/Z_0$
 $h_{11} = h_{11}/Z_0, h_{12} = h_{12}/Z_0, h_{21} = h_{21}/Z_0, h_{22} = h_{22}/Z_0$
 $A' = A, B' = B, C' = C, D' = D$
 $|z| = z_{11}z_{22} - z_{12}z_{21}$
 $|y| = y_{11}y_{22} - y_{12}y_{21}$
 $|h| = h_{11}h_{22} - h_{12}h_{21}$

Conversion between Common-Base, Common-Emitter, and Common-Collector y Parameters

$$\begin{aligned}
 y_{11,e} &= y_{11,b} + y_{12,b} + y_{21,b} + y_{22,b} = y_{11,c} \\
 y_{12,e} &= -(y_{12,b} + y_{22,b}) = -(y_{11,c} + y_{12,c}) \\
 y_{21,e} &= -(y_{21,b} + y_{22,b}) = -(y_{11,c} + y_{21,c}) \\
 y_{22,e} &= y_{22,b} = y_{11,c} + y_{12,c} + y_{21,c} + y_{22,c} \\
 \\
 y_{11,b} &= y_{11,e} + y_{12,e} + y_{21,e} + y_{22,e} = y_{22,c} \\
 y_{12,b} &= -(y_{12,e} + y_{22,e}) = -(y_{21,c} + y_{22,c}) \\
 y_{21,b} &= -(y_{21,e} + y_{22,e}) = -(y_{12,c} + y_{22,c}) \\
 y_{22,b} &= y_{22,e} = y_{11,c} + y_{12,c} + y_{21,c} + y_{22,c} \\
 \\
 y_{11,c} &= y_{11,e} = y_{11,b} + y_{12,b} + y_{21,b} + y_{22,b} \\
 y_{12,c} &= -(y_{11,e} + y_{12,e}) = -(y_{11,b} + y_{21,b}) \\
 y_{21,c} &= -(y_{11,e} + y_{21,e}) = -(y_{11,b} + y_{12,b}) \\
 y_{22,c} &= y_{11,e} + y_{12,e} + y_{21,e} + y_{22,e} = y_{11,b}
 \end{aligned}$$

(b)

Figure 1.8.1 (a) Conversions among the z , y , h , $ABCD$, and S parameters; (b) conversions between y parameters.

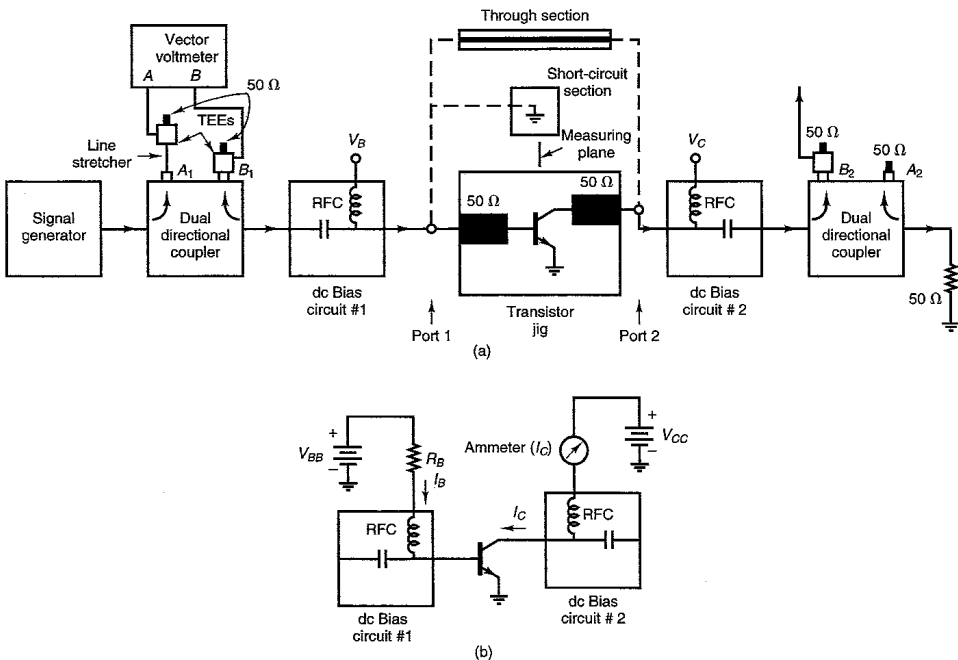


Figure 1.9.1 (a) Block diagram of an S -parameter measuring system using a vector voltmeter; (b) the dc bias arrangement.

the attenuation introduced by the directional coupler in the forward and reverse direction is the same), the vector voltmeter will measure the voltages at A_1 and B_1 , and therefore the voltage ratio between the B and the A probes, which is exactly $|S_{11}|$. To measure the phase of S_{11} , the system must be calibrated so that the electrical length traveled by the incident voltage and the reflected voltage is equal. This ensures a zero degree phase shift between the incident and reflected voltages at A and B . The short-circuited section shown in Fig. 1.9.1a is used to calibrate the phase between probe A and probe B . With the short-circuited section connected at the position of the transistor, the line stretcher is adjusted until the phase difference in the vector voltmeter reads 180° (which is the phase shift produced by a short circuit). When the transistor jig is connected (with the input port of the transistor at the same position as the short-circuited section), the vector voltmeter will read the phase difference between B and A , which is the angle of S_{11} . The measuring or reference plane is indicated in Fig. 1.9.1a.

The parameter S_{21} is also measured using the set-up in Fig. 1.9.1a. In this case the ratio used is that of the transmitted voltage measured at B_2 to the incident voltage measured at A_1 . The angle calibration for S_{21} is accomplished using the through calibration section shown in Fig. 1.9.1a. With the through section connected, the line stretcher is adjusted until a zero degree phase shift is read in the vector voltmeter. A little thought shows that if the short-circuited calibration section is made exactly half the length of the through calibration section, once the line stretcher is adjusted with the short-circuit section, the vector voltmeter will automatically produce a zero degree phase shift with the through section.

The parameters S_{22} and S_{12} are measured by reversing the transistor jig and the associated dc bias connections. This system provides a fairly inexpensive method for measuring S parameters. After the initial set-up of the system it is quite simple to measure the S parameters of a two-port network over a wide frequency range.

At a given Q point and frequency, the S parameters of the transistor will be constant for certain amplitude values of the incident voltage V_1^+ . As the amplitude of V_1^+ is increased, the transistor will be driven into its nonlinear region and the S parameters will vary as a function of the input signal amplitude.

The second method for measuring S parameters uses a network analyzer. Network analyzers generate a calibrated RF signal and have three input measuring channels (see Fig. 1.9.2). These channels are commonly called the R , the A , and the B channels. The R channel is used to measure the incident voltage, and the A and B channels measure reflected and transmitted voltages. The two measuring channels A and B allow the measuring of any two parameters with a single measurement set-up. The RF signal generator of the network analyzer provides the sinusoidal test signal, which can be either a single frequency sinusoid or a sweep-mode sinusoidal signal. The output of the RF signal generator is calibrated in dBm (using a $50\text{-}\Omega$ load).

Network analyzers can display a variety of rectangular and polar plots versus frequency of the signals applied to the R , A , and B inputs. The rectangu-

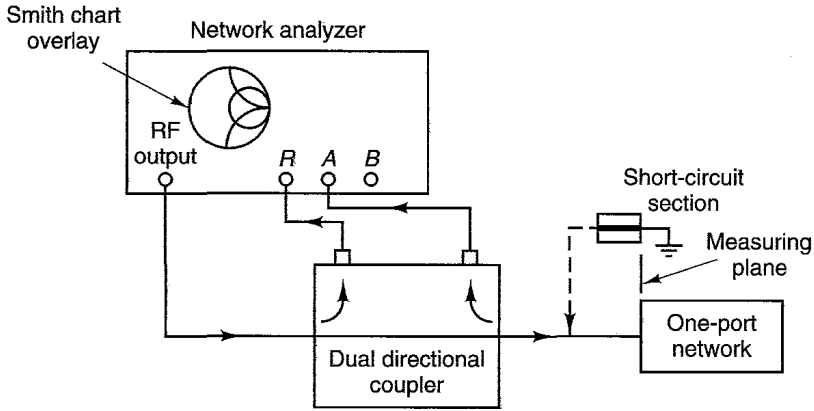


Figure 1.9.2 One-port measurements using a network analyzer.

lar measurements available in network analyzers are (a) power level at the R input (in dBm), (b) power level at the A input (in dBm), (c) power level at the B input (in dBm), (d) power ratio between the A and R inputs (A/R), (e) power ratio between the B and R inputs (B/R), (f) phase difference between the A and R inputs ($\angle A/R$) and (g) phase difference between the B and R inputs ($\angle B/R$). The network analyzer can also display in polar form the power ratio and phase of A/R and B/R . This XY -type of display provides magnitude and phase information. In fact, with proper calibration a Smith chart can be superimposed on the screen of the network analyzer and reflection coefficient data can be read directly from the screen.

Figure 1.9.2 illustrates a measurement set-up that can be used for one-port measurements, such as the input impedance or reflection coefficient of a one-port network. A short-circuited calibration section is used to calibrate the network analyzer display. Network analyzers contain internal circuitry for phase calibration; therefore, the phase difference between the channels can be calibrated by simply rotating a knob in the analyzer. For example, if a polar display of A/R is selected, the short-circuited section can be used to set the dot on the screen to the edge of the Smith chart at 180° . In other words, the reflection coefficient of the short circuit at the measuring plane is set at $1\angle 180^\circ$. Then, when the one-port is connected for measurements (at the indicated measuring plane), the dot will move to the proper value of reflection coefficient (or impedance) in the Smith chart.

Figure 1.9.3 shows a measurement set-up for S parameters. This set-up is similar to that shown in Fig. 1.9.1a. After the proper phase calibration with the R , A , and B channels connected in the position shown in Fig. 1.9.3, selection of A/R in polar form will display S_{11} , and B/R will display S_{21} . With the transistor jig reversed, the parameters S_{22} and S_{12} are measured.

Since one of the most important uses of the network analyzer is to measure S parameters, an S -parameter test set is usually a part of the network

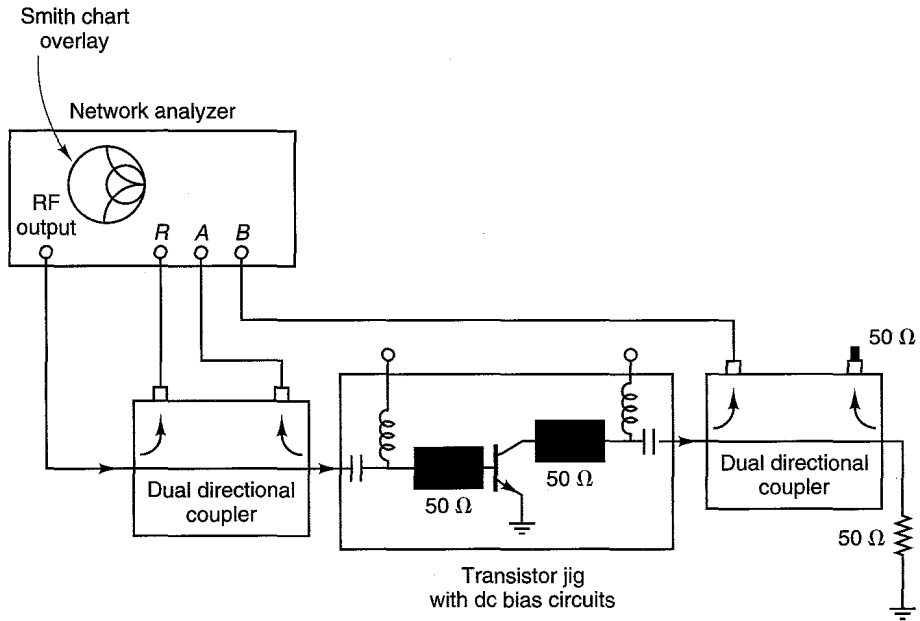


Figure 1.9.3 A measurement set-up for S parameters using a network analyzer.

analyzer, or an external S -parameter test set is interfaced with the network analyzer. An HP8753C network analyzer with an HP85047 S -parameter test set is shown in Fig. 1.9.4. Observe that the RF signal from the network analyzer is connected to the RF input of the S -parameter test set. The R , A and B channels of the network analyzer are connected to the corresponding R , A , and B channels of the S -parameter test set. The calibration of the measuring system in Fig. 1.9.4 is accomplished using a short-circuited section and a through section.

The S -parameter test set provides a convenient means for measuring S parameters. Basically, it replaces the two dual directional couplers shown in Fig. 1.9.3, provides two measuring ports (denoted by port 1 and port 2) to connect the device under test, and provides connections to apply the dc bias to ports 1 and 2. An electronic switch selects the S parameters to be measured such that the S -parameter test set applies the RF signal to the appropriate port, applies the appropriate $50\text{-}\Omega$ termination to the other port, and outputs the appropriate A/R and B/R signals to the network analyzer.

1.10 SCATTERING PARAMETERS OF TRANSISTORS

The S parameters of microwave transistors are usually available for the transistor in chip and packaged form. Transistors in chip form are used when the best performance in gain, bandwidth, and noise is desired. Packaged transistors

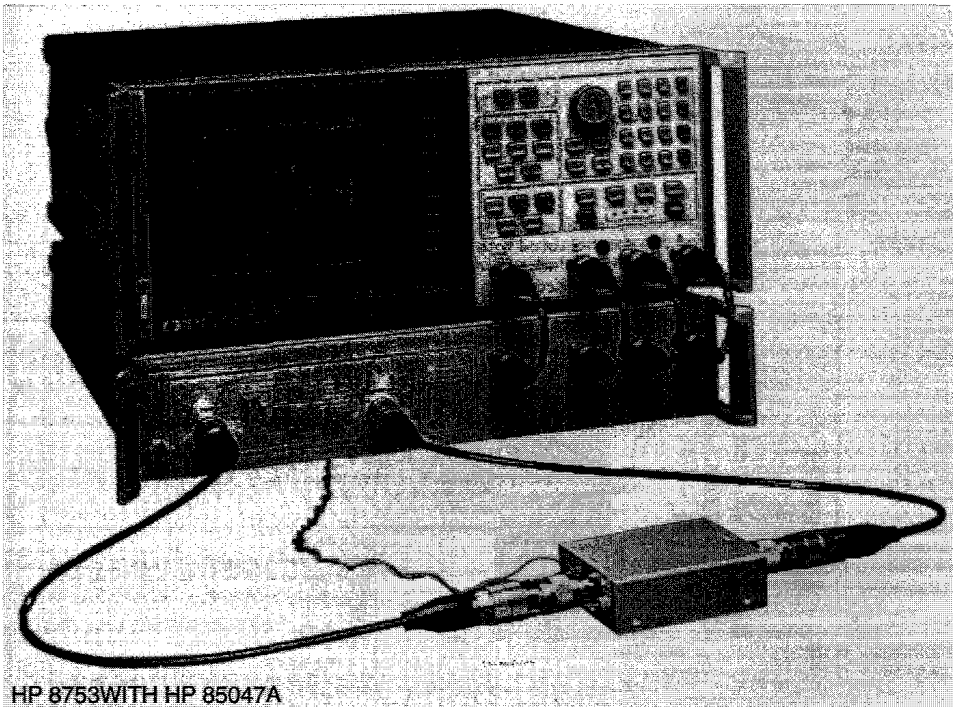


Figure 1.9.4 The HP8753C network analyzer with an HP85047A S -parameter test set. (From HP Test and Measurements Catalog, 1994; courtesy of Hewlett Packard)

are very popular because they come in sealed enclosures and are easy to work with. The parasitic elements introduced by the package produce a degradation in the transistor ac performance.

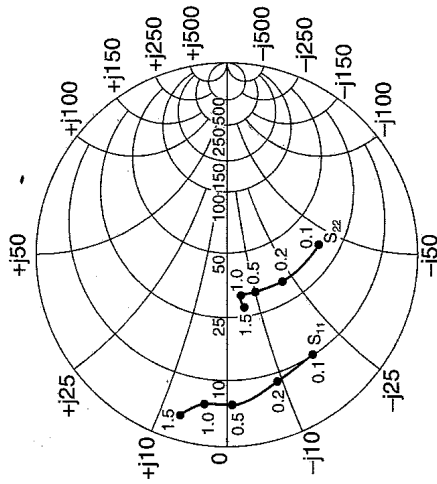
Manufacturers usually measure and provide common-emitter or common-source S parameters of transistors as a function of frequency at a given dc bias. Since the minimum noise figure, linear output power, and maximum gain require different dc bias settings, the manufacturers usually provide two or three sets of S parameters.

Conversions among S parameters or to other parameters can be done using the conversion relations in Fig. 1.8.1. For example, to convert from common-emitter to common-base S parameters, we first convert the common-emitter S parameters to common-emitter y parameters, then convert the common-emitter y parameters to common-base y parameters, and then convert the common-base y parameters to common-base S parameters.

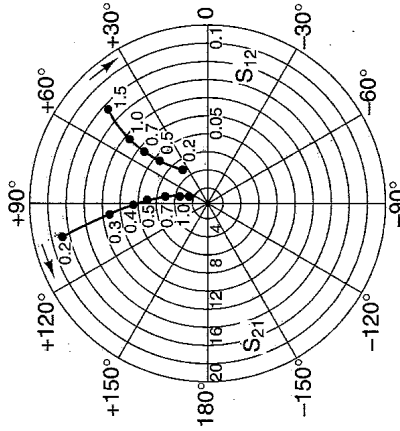
The common-emitter S parameters of a transistor are shown in Fig. 1.10.1. This figure illustrates some of the information typically provided by manufacturers. The values of the S parameters are explicitly given at various recommended Q points as a function of frequency. Figure 1.10.1 also shows that the values of S_{11} and S_{22} as a function of frequency are conveniently shown

MRF962 COMMON-EMITTER S-PARAMETERS

INPUT/OUTPUT REFLECTION
COEFFICIENTS versus FREQUENCY
($V_{CE} = 10V, I_c = 50 \text{ mA}$)



FORWARD/REVERSE TRANSMISSION
COEFFICIENTS versus FREQUENCY
($V_{CE} = 10V, I_c = 50 \text{ mA}$)



(a)

V _{CE} (Volts)	I _C (mA)	f (MHz)	S ₁₁		S ₂₁		S ₁₂		S ₂₂	
			S ₁₁	∠φ	S ₂₁	∠φ	S ₁₂	∠φ	S ₂₂	∠φ
5.0	10	100	0.70	-102	17.42	128	0.044	43	0.65	-57
		300	0.75	-156	7.11	98	0.058	24	0.32	-97
		500	0.78	-170	4.36	86	0.064	25	0.26	-110
		700	0.78	-176	3.16	77	0.071	26	0.23	-117
		1000	0.78	176	2.26	67	0.078	27	0.24	-126
	25	1500	0.79	167	1.51	54	0.092	29	0.31	-133
		100	0.69	-131	24.24	118	0.029	38	0.56	-87
		300	0.77	-167	8.76	95	0.039	32	0.35	-137
		500	0.79	-176	5.26	85	0.046	36	0.32	-160
		700	0.80	178	3.82	78	0.055	40	0.31	-158
	50	1000	0.79	173	2.72	70	0.067	42	0.32	-164
		1500	0.81	164	1.82	59	0.086	42	0.34	-167
		100	0.71	-147	27.72	113	0.021	37	0.53	-107
		300	0.78	-173	9.59	94	0.030	40	0.41	-152
		500	0.81	179	5.72	85	0.038	46	0.39	-163
10	10	700	0.81	176	4.09	78	0.048	50	0.38	-169
		1000	0.81	171	2.89	71	0.061	51	0.38	-175
		1500	0.82	163	1.96	62	0.082	49	0.40	-177
		100	0.71	-92	18.77	131	0.037	47	0.70	-44
		300	0.74	-150	8.09	100	0.051	28	0.34	-69
	25	500	0.75	-166	5.01	87	0.056	28	0.27	-75
		700	0.76	-174	3.62	78	0.064	28	0.24	-79
		1000	0.76	179	2.58	69	0.071	30	0.24	-88
		1500	0.77	168	1.72	55	0.085	31	0.31	-104
		100	0.67	-120	27.10	122	0.027	42	0.57	-68
	50	300	0.73	-163	10.27	97	0.035	36	0.27	-110
		500	0.76	-174	6.21	86	0.043	39	0.22	-124
		700	0.77	-179	4.48	78	0.051	41	0.20	-132
		1000	0.77	175	3.19	71	0.062	43	0.20	-139
		1500	0.78	166	2.13	59	0.080	42	0.25	-142
	50	100	0.68	-137	31.53	116	0.020	37	0.49	-85
		300	0.74	-169	11.17	95	0.028	40	0.27	-131
		500	0.77	-177	6.69	85	0.037	46	0.24	-144
		700	0.77	178	4.82	78	0.047	48	0.23	-152
		1000	0.77	173	3.42	71	0.059	50	0.23	-158
1500	0.79	165	2.30	61	0.078	47	0.27	-159		

(b)

Figure 1.10.1 S-parameter data for the Motorola MRF962 transistor. (From Motorola RF Data Manual, second edition; reproduced with permission of Motorola, Inc.)

in a Smith chart (the Smith chart is discussed in detail in Sections 2.2 and 2.3). For example, at $V_{CE} = 10$ V, $I_C = 50$ mA, and $f = 1500$ MHz, the value of S_{11} is listed as $0.79 \angle 165^\circ$. Using (1.6.14), the impedance associated with S_{11} in a $50\text{-}\Omega$ system is

$$Z_{T1} = Z_o \frac{1 + S_{11}}{1 - S_{11}} = 50 \frac{1 + 0.79 \angle 165^\circ}{1 - 0.79 \angle 165^\circ} = 5.97 + j6.5 \Omega$$

From the Smith chart plot it is seen that the impedance associated with S_{11} at $f = 1500$ MHz is approximately the value of Z_{T1} calculated in the preceding equation.

The forward and reverse transmission coefficients S_{21} and S_{12} are usually given in a polar plot, as shown in Fig. 1.10.1. Observe that the amplitude scale for S_{21} is different from the amplitude scale for S_{12} . For example, at $V_{CE} = 10$ V, $I_C = 50$ mA, and $f = 500$ MHz we read from the plots: $S_{21} = 7 \angle 80^\circ$ and $S_{12} = 0.036 \angle 45^\circ$. These readings closely agree with the listed values.

For many transistors, plots of S_{11} and S_{22} are given for the transistor in chip and packaged forms. Typical plots of S_{11} for a transistor in chip form and packaged form are shown in Fig. 1.10.2. We will learn in Chapter 2 that these plots can be used to develop equivalent circuits for the input and output impedances of the transistor.

A typical Bode plot of the behavior of $|S_{21}|$, $|S_{12}|$, and $|S_{21}S_{12}|$ is shown in Fig. 1.10.3. It is seen that the parameter $|S_{21}|$ is constant for frequencies below the beta cutoff frequency (i.e., f_β) and then decays at 6 dB/octave. The transducer cutoff frequency (f_s) is the frequency where $|S_{21}|$ is equal to 1 (0 dB). The parameter $|S_{12}|$ increases at approximately 6 dB/octave, levels off around f_s , and decays at higher frequencies.

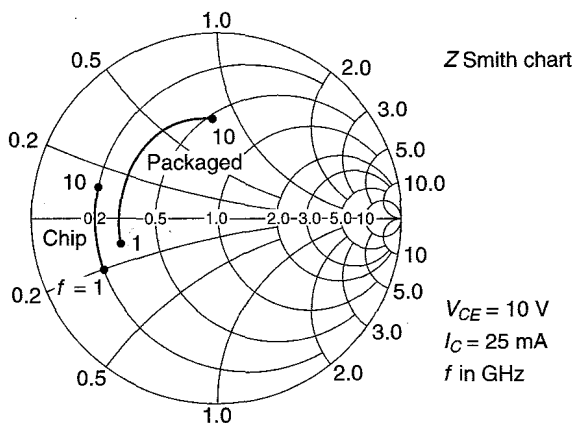


Figure 1.10.2. S_{11} of a common-emitter transistor in chip and packaged form.

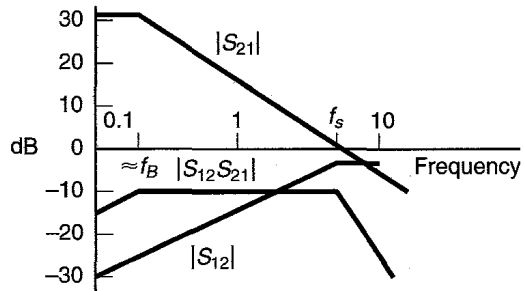


Figure 1.10.3 Frequency behavior of $|S_{21}|$, $|S_{12}|$, and $|S_{12}S_{21}|$. (From Ref. [1.1]; courtesy of Hewlett-Packard.)

1.11 CHARACTERISTICS OF MICROWAVE TRANSISTORS

Bipolar Transistors

Most microwave bipolar junction transistors (BJTs) are planar in form and made from silicon in the npn type. Below 4 GHz, silicon BJTs provide a reliable and low-cost solution to many electronic designs. The transistor dimensions are very small in order to permit operation at microwave frequencies. For example, typical emitter widths of $2 \mu\text{m}$ are found in general purpose microwave transistors, and emitter widths from $0.5 \mu\text{m}$ to $1 \mu\text{m}$ in low-noise microwave transistors. Base thickness of tenth of a micron are typical.

Four common applications where silicon BJTs are used at microwave frequencies are small-signal amplifiers, linear power amplifiers, low-noise amplifiers, and oscillators. Manufacturers usually provide a selection of transistors in chip and packaged forms specially made to suit one of the previous applications. Figure 1.11.1 lists typical power gains, output power, and noise figure performances for silicon BJTs in packaged form. For specific and up-to-date information, one should acquire the microwave catalog from several manufacturers. Also, *Microwave and RF* magazine publishes on a regular basis comprehensive performance characteristics of microwave transistors.

BJTs are manufactured using ion implantation and self-alignment techniques to obtain a multifinger emitter-base construction. A typical cross section of a silicon BJT is shown in Fig. 1.11.2a, and the top view of the structure is shown in Fig. 1.11.2b. This type of structure minimizes the electron transit time from the emitter to the collector while maintaining a large emitter area. An example of a packaged transistor is shown in Fig. 1.11.2c.

Power BJTs are also available. The increased power required for these transistors is obtained using an interdigitated construction, as shown in Fig. 1.11.2d.

The equivalent hybrid- π model of the intrinsic BJT is shown in Fig. 1.11.3. In the microwave range, the reactance of $C_{b'c}$ is very small in comparison to the resistance of $r_{b'c}$, and the resistor r_{ce} is very large. Also, the reactance of $C_{b'e}$ is usually smaller than the resistance $r_{b'e}$. Therefore, the simplified model shown in Fig. 1.11.4 follows.

	Frequency	Power Gain	Output Power	Minimum Noise Figure
Small-signal transistors (or general purpose transistors)	1 GHz	20 dB	20 dBm	1.8 dB
	2 GHz	18 dB	20 dBm	2.4 dB
	4 GHz	11 dB	18 dBm	3.5 dB
Linear power transistors	1 GHz	15 dB	29 dBm	—
	2 GHz	12 dB	29 dBm	—
	4 GHz	8 dB	27 dBm	—
Low-noise transistors	1 GHz	18 dB	18 dBm	1.2 dB
	2 GHz	13 dB	18 dBm	1.7 dB
	4 GHz	9 dB	18 dBm	2.8 dB
Oscillators	1 GHz	—	30 dBm	—
	2 GHz	—	30 dBm	—
	4 GHz	—	27 dBm	—

Figure 1.11.1 Typical performances for silicon BJTs in packaged form.

A more advanced hybrid- π model will include the distributed nature of $r_{bb'}$ and $C_{b'c}$, as shown in Fig. 1.11.5.

The following example illustrates in a simple manner how the S parameters depend on the model used for the transistor.

Example 1.11.1

(a) A transistor with $\beta = 100$ is biased at $V_{CE} = 10$ V and $I_C = 10$ mA, as shown in Fig. 1.11.6a. The small-signal behavior of the transistor at frequencies below 100 kHz can be represented by the hybrid model shown in Fig. 1.11.6b. Calculate, using Fig. 1.11.6b, the S parameters of the transistor at frequencies below 100 kHz.

(b) At 1 MHz the small-signal behavior of the transistor can be modeled using the hybrid- π model shown in Fig. 1.11.7a. Determine the S_{11} parameter of the transistor at 1 MHz.

Solution. (a) The capacitors C_1 and C_2 are coupling capacitors. Their values are large in order to behave like short circuits to the ac signal. The two radio frequency coils RFCs are large inductors. Their purpose is to behave like an open circuit to the ac signals and to present zero impedance to the dc signal. V_{CE} is equal to V_{CC} since the RFC at the collector is a short circuit at dc.

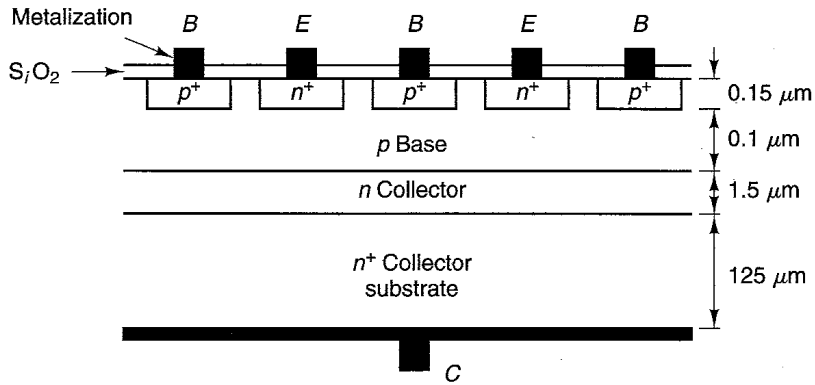
Since $\beta = 100$, the base current is

$$I_B = \frac{I_C}{\beta} = \frac{10 \times 10^{-3}}{100} = 100 \mu\text{A}$$

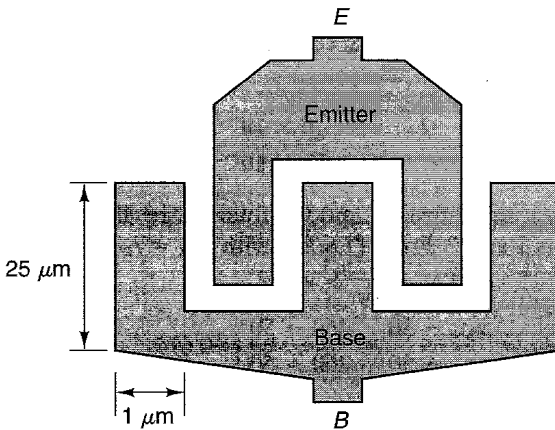
Then the value of R_B is

$$R_B = \frac{V_{BB} - 0.7}{I_B} = \frac{5 - 0.7}{100 \times 10^{-6}} = 43 \text{ k}\Omega$$

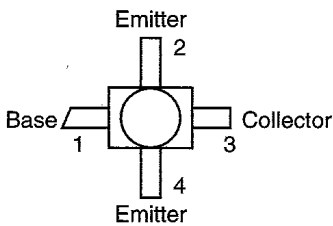
To set the Q point accurately, the value of V_{BB} is varied, around its nominal value of 5 V, until a current of 10 mA is read with an ammeter connected in series with the V_{CC} supply.



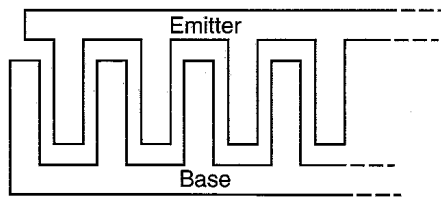
(a)



(b)



(c)



(d)

Figure 1.11.2 (a) Typical silicon BJT cross section; (b) top view; (c) packaged transistor; (d) top view of an interdigitated BJT.

The ac model shown in Fig. 1.11.6b is obtained by replacing C_1 and C_2 with short circuits, the RFCs by open circuits, and the transistor by its hybrid model for frequencies below 100 kHz. The value of $r_{b'e}$ in Fig. 1.11.6b is

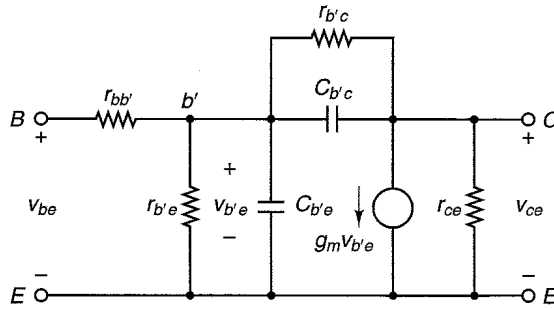


Figure 1.11.3 Hybrid- π model of a common-emitter BJT.

$$r_{b'e} = \beta \frac{26 \times 10^{-3}}{I_c} = 100 \frac{26 \times 10^{-3}}{10 \times 10^{-3}} = 260 \Omega$$

and the transconductance is

$$g_m = \frac{\beta}{r_{b'e}} = \frac{I_c}{26 \times 10^{-3}} = \frac{10 \times 10^{-3}}{26 \times 10^{-3}} = 385 \text{ mS}$$

Figure 1.11.6c shows an equivalent model obtained by finding the Thévenin's equivalent circuits at ports 1 and 2. From (1.6.14), with $Z_{T1} = r_{b'e}$, the value of S_{11} in a 50- Ω system is

$$S_{11} = \frac{r_{b'e} - 50}{r_{b'e} + 50} = \frac{260 - 50}{260 + 50} = 0.677$$

From Fig. 1.11.6c

$$v_{b'e} = \frac{E_{1,TH} r_{b'e}}{r_{b'e} + Z_o} = \frac{E_{1,TH}(260)}{260 + 50} = 0.839 E_{1,TH}$$

and

$$v_2 = -g_m v_{b'e} (r_{ce} \parallel 50) \approx -0.385 v_{b'e} (50) = -19.25 v_{b'e}$$

Therefore,

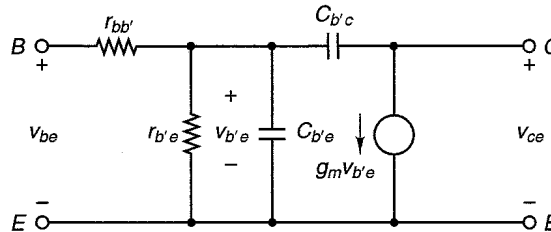


Figure 1.11.4 Simplified hybrid- π model of a microwave BJT in the common-emitter configuration.

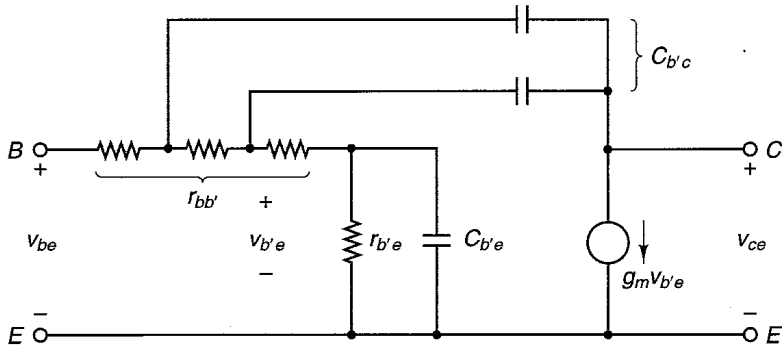


Figure 1.11.5 A hybrid- π model that includes the distributed nature of $r_{bb'}$ and $C_{b'c}$.

$$v_2 = -19.25(0.839)E_{1,TH} = -16.15E_{1,TH}$$

Then, using (1.6.21), we obtain

$$S_{21} = 2 \frac{V_2}{E_{1,TH}} = 2(-16.15) = -32.3 \text{ (or } 32.3 \angle 180^\circ)$$

From (1.6.23), with $Z_{T2} = r_{ce} = 100 \text{ k}\Omega$, the value of S_{22} is

$$S_{22} = \frac{r_{ce} - 50}{r_{ce} + 50} \approx 1$$

which shows that r_{ce} behaves like an open circuit in a 50- Ω system.

Since there is no transmission from the output to the input in the model in Fig. 1.11.6c, we obtain $S_{12} = 0$.

(b) At 1 MHz the high-frequency capacitances affect the frequency response of the amplifier and, therefore, the values of the S parameters. The use of Miller's theorem allows us to draw the equivalent input circuit shown in Fig. 1.11.7b, where C_M is the input Miller's capacitance, namely

$$C_M = C_{b'c}(1 - A_v) \approx C_{b'c}(1 + g_m(50)) = 1 \times 10^{-12}(1 + 19.25) = 20.25 \text{ pF}$$

Hence, the input capacitance is

$$C_{IN} = C_{b'e} + C_M = 10 \times 10^{-12} + 20.25 \times 10^{-12} = 30.25 \text{ pF}$$

The input impedance in Fig. 1.11.7b is

$$Z_{IN} = r_{b'e} \parallel \frac{1}{j\omega C_{IN}} = 260 \parallel \frac{1}{j2\pi 10^6(30.25 \times 10^{-12})} = 259.4 - j12.8 \Omega$$

Therefore,

$$S_{11} = \frac{Z_{IN} - 50}{Z_{IN} + 50} = \frac{(259.4 - j12.8) - 50}{(259.4 - j12.8) + 50} = 0.677 \angle -1.13^\circ$$

The other S parameters can be evaluated analytically, or using a CAD program. For the circuit in Fig. 1.11.7a, the other S parameters are $S_{12} = 0$, $S_{21} = 32.2 \angle 179.5^\circ$, and $S_{22} = 0.999 \angle -0.62^\circ$.

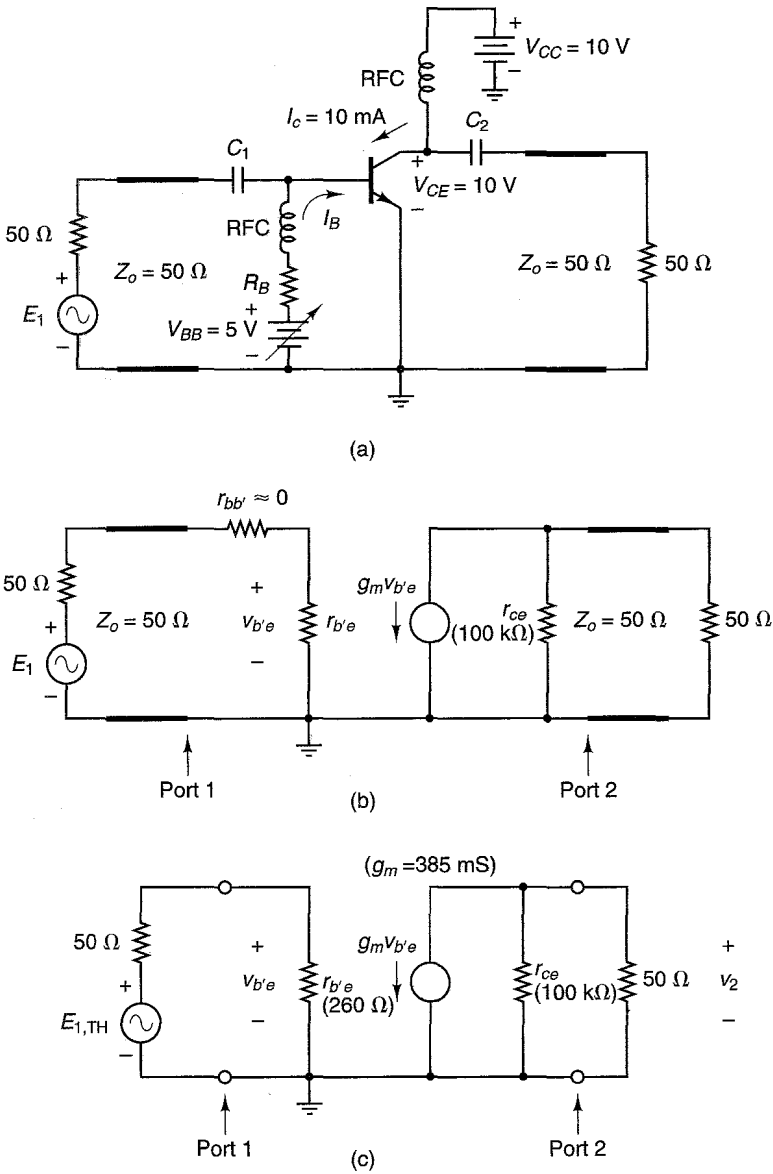


Figure 1.11.6 (a) Transistor circuit for Example 1.11.1; (b) the ac model for frequencies below 100 kHz; (c) equivalent ac model.

The equivalent circuit for the transistor in packaged form must include additional parasitic elements introduced by the package. One such model is shown in Fig. 1.11.8. The meaning of the extrinsic parasitic elements L_b , L_e , L_c , C_{be} , C_{bc} , and C_{ce} is self-explanatory. Typical values of the parasitic inductances

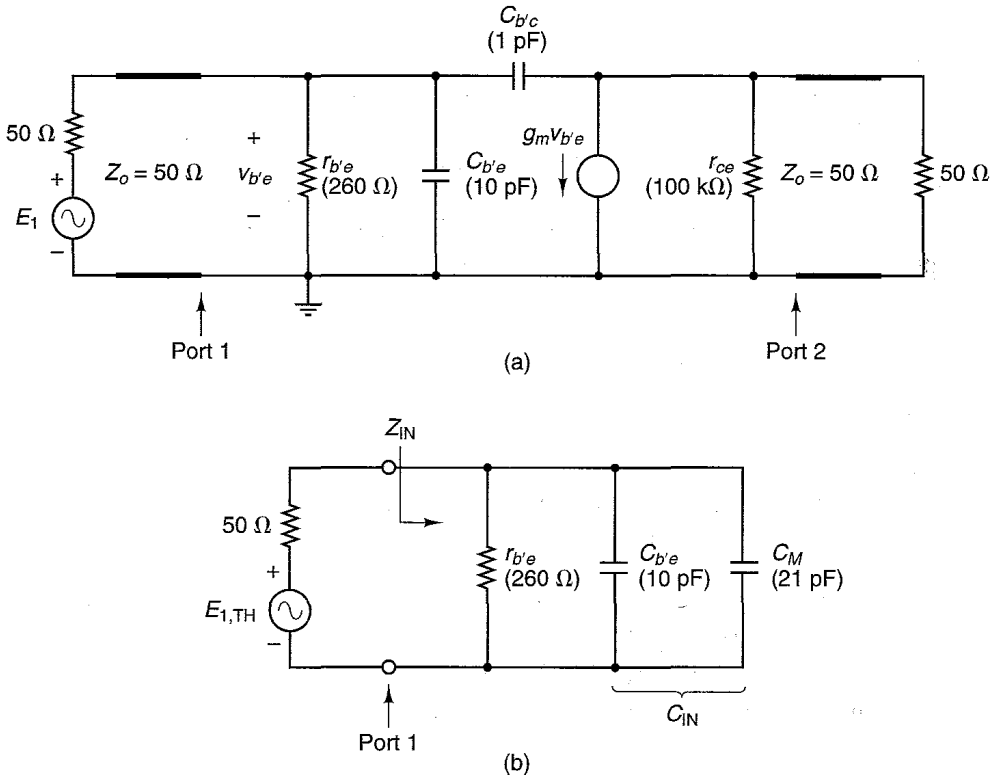


Figure 1.11.7 (a) The ac model at 1 MHz; (b) an equivalent input circuit for the model in (a).

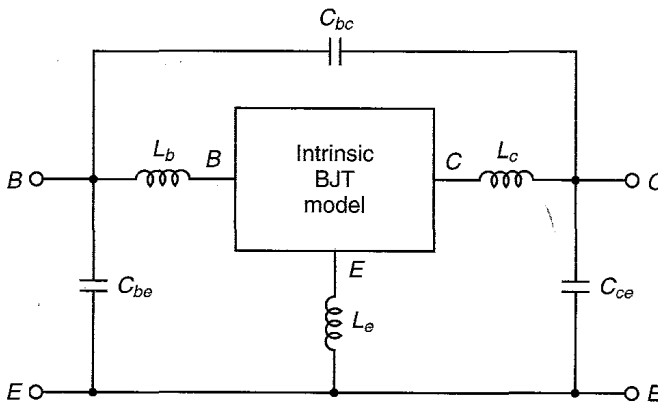


Figure 1.11.8 Modeling the parasitic elements introduced by the package.

are 0.2 nH to 1 nH, and of the parasitic capacitances they are 0.01 pF to 0.05 pF. More advanced packaged models include the addition of small resistances in series with the inductors L_b , L_e , and L_c , and the use of transmission lines to model the distributed nature of the parasitics associated with the package.

Small-signal models can also be obtained from the cross-section geometry of the transistor chip and a knowledge of its operation. The reader is referred to the article by Hsu and Snapp [1.2] for the equivalent circuit of the BJT chip shown in Fig. 1.11.9. Typical values for the HP HXTR-2001 transistor chip are given at 15 V and 15 mA. The equivalent circuit for the transistor in packaged form must include additional extrinsic parasitic elements, as illustrated in Fig. 1.11.8.

Some advanced CAD programs (such as the HP85150B Microwave Design System) allow designers to compare the measured S parameters of a transistor with those obtained from a given model and to optimize the model components in order to match the measured S parameters.

There are two figures of merit that are commonly used by manufacturers of microwave BJTs to describe the transistor performance:

1. f_T : the gain-bandwidth frequency. It is the frequency where the short-circuit gain $|h_{fe}(\omega)|$ approximates unity.
2. f_{\max} : the maximum frequency of oscillation. It is the frequency where the maximum available power gain of the transistor (called $G_{A,\max}$) is equal to 1.

$G_{A,\max}$ and f_{\max} can be measured by conjugately matching the source impedance to the transistor input impedance, and the load to the transistor output impedance. Of course, the transistor must be unconditionally stable (i.e., no oscillations). $G_{A,\max}$ is higher than the transducer gain $|S_{21}|^2$ because of the matching conditions. These concepts are discussed in detail in Chapter 3.

The frequency dependence of $h_{fe}(\omega)$ is given by

$$h_{fe}(\omega) = \frac{h_{fe}}{1 + j\omega/f_\beta}$$

where h_{fe} is the low-frequency short-circuit current gain and f_β is the beta cut-off frequency, namely

$$f_\beta = \frac{1}{2\pi r_{b'e}(C_{b'e} + C_{b'c})} \approx \frac{1}{2\pi r_{b'e}C_{b'e}}$$

The frequencies f_T and f_{\max} for the intrinsic BJT model, shown in Fig. 1.11.4, are given by

$$f_T \approx \frac{g_m}{2\pi C_{b'e}} \quad (1.11.1)$$

and

$$f_{\max} = \sqrt{\frac{f_T}{8\pi r_{b'e} C_{b'c}}} \quad (1.11.2)$$

Also, f_β and f_T are related by

$$f_\beta = \frac{f_T}{h_{fe}} \quad (1.11.3)$$

The frequency f_T can also be expressed in terms of the total signal time delay from emitter to collector as [1.3]

$$f_T = \frac{1}{2\pi\tau_{ec}}$$

where τ_{ec} is the emitter-to-collector time delay, namely

$$\tau_{ec} \approx \tau_b + \tau_c$$

The parameter τ_b represents the base delay time and τ_c the base-to-collector depletion-layer delay time.

Figure 1.11.10 illustrates the meaning of f_T , f_β , and f_{\max} . Observe the gain rolloff at the rate of 6 dB/octave.

Two sources of noise in a microwave BJT are thermal noise and shot noise. *Thermal noise* is caused by the thermal agitation of the carriers in the ohmic resistance of the emitter, base, and collector. *Shot noise* is a current-dependent effect caused by fluctuations in the electron and hole currents due to bias conditions.

Flicker noise (or $1/f$ noise) is not a problem in silicon BJTs at microwave frequencies since this noise is only significant at low frequencies (below 10 kHz to 50 kHz).

Above 4 GHz the performance of silicon BJTs diminishes significantly. For example, at 8 GHz a typical power gain is low (around 7 dB) with a high noise figure (greater than 5 dB).

BJTs using gallium arsenide (GaAs) semiconductors have been developed. These devices are called heterojunction bipolar transistors (HBJTs). The increased velocity of the electrons in the n -doped GaAs results in higher gains and better microwave performance. With HBJT, power gains of 20 dB with minimum noise figure of 4 dB can be obtained at 10 GHz.

Field Effect Transistors

The fabrication of gallium arsenide field-effect transistors (GaAs FETs) is made in the metal semiconductor field effect transistor structure (MESFET). That is, the gate terminal is constructed using a Schottky barrier gate. The microwave FETs are made with GaAs because the electron mobility is greater than that of silicon. The high electron mobility results in excellent frequency response and noise performance, especially above 4 GHz.

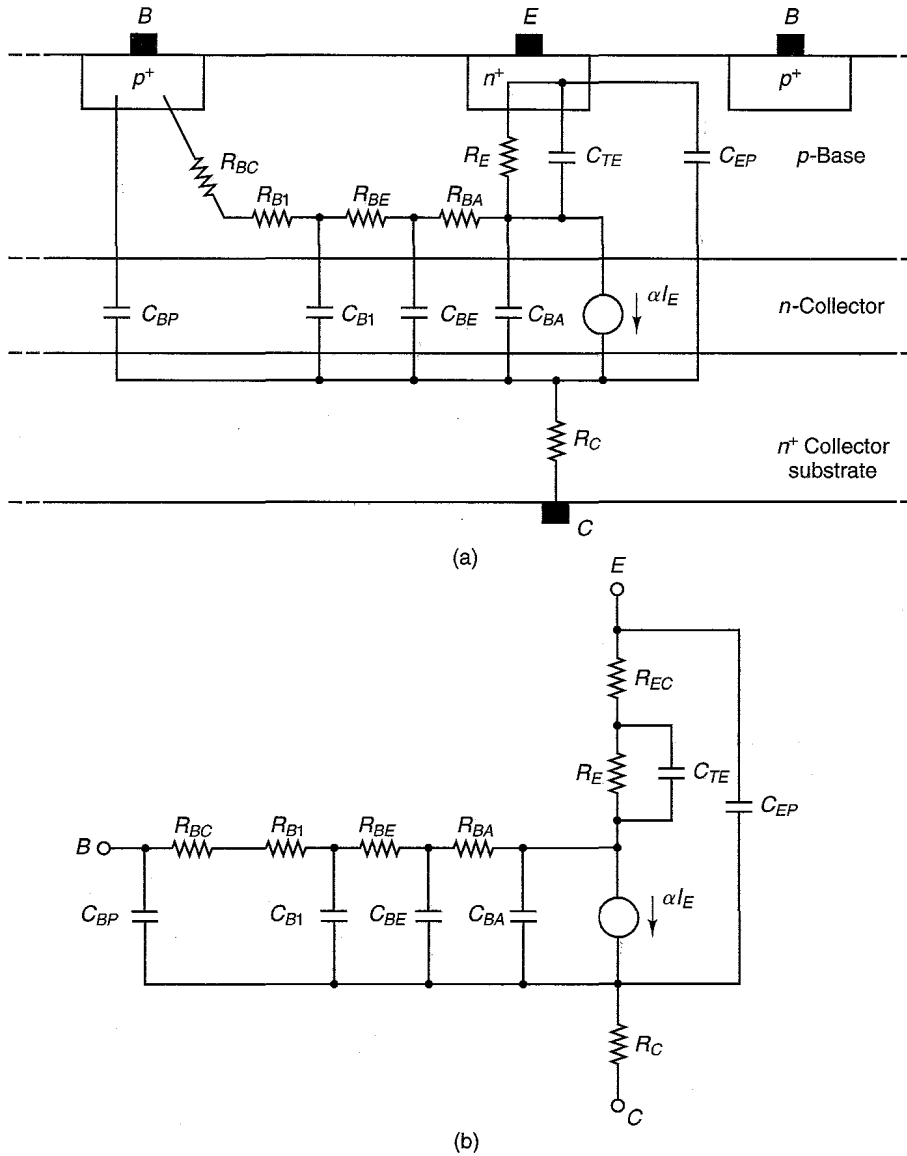


Figure 1.11.9 (a) The transistor cross-section geometry; (b) small-signal model developed from the cross-section geometry of a BJT.

In fact, GaAs MESFETs have become the transistor of choice above 4 GHz, and for a variety of very low noise applications below 4 GHz. Figure 1.11.11 shows typical power gains, output power, and noise figure performances for GaAs MESFETs in packaged form. Certainly, at frequencies above 4 GHz,

Values for the HXTR2001 at $V_{CE} = 15\text{ V}$ and $I_C = 15\text{ mA}$

- $C_{BP} = 0.066\text{ pF}$ —Base bond pad capacitance
- $C_{EP} = 0.06\text{ pF}$ —Emitter bond pad capacitance
- $C_{BI} = 0.07\text{ pF}$ —Collector to base distributed capacitor
- $C_{BE} = 0.056\text{ pF}$
- $C_{BA} = 0.032\text{ pF}$
- $C_{TE} = 4.8\text{ pF}$ —Base to emitter junction capacitance
- $R_{BC} = 0.2\ \Omega$ —Base contact resistance
- $R_{BI} = 0.2\ \Omega$ —Base distributed resistance
- $R_{EC} = 0.2\ \Omega$
- $R_{BE} = 3.5\ \Omega$
- $R_{BA} = 4.4\ \Omega$
- $R_C = 5\ \Omega$ —Collector resistance
- $R_E = 1.7\ \Omega$ —Emitter-base diode resistance
- $\alpha_o = 0.99$ —Low-frequency common-base current gain
- $f_b = 22.7\text{ GHz}$ —Base cutoff frequency
- $\tau = 10.8\text{ ps}$ —Collector delay time depletion region

$$\alpha = \frac{\alpha_o}{1 + j \frac{f}{f_b}} e^{-j\omega\tau}$$

Figure 1.11.9 Continued

GaAs MESFETs have higher power gains, lower noise figures, and higher output power capabilities than silicon BJTs.

Molecular-beam epitaxy is used in the construction of GaAs MESFETs. Figure 1.11.12a shows a typical crosssection of a GaAs MESFET chip. Power GaAs MESFETs are also available. Basically, these devices are constructed by connecting several low-power transistors in parallel—that is, using an interdigitated construction with a large gate width (to increase g_m) and with 8 to 12 source, gate, and drain fingers to obtain a large output power. The top view of an interdigitated chip is shown in Fig. 1.11.12b.

The high-frequency model of the intrinsic GaAs FET in a common-source configuration is shown in Fig. 1.11.13. The capacitor C_i represents the

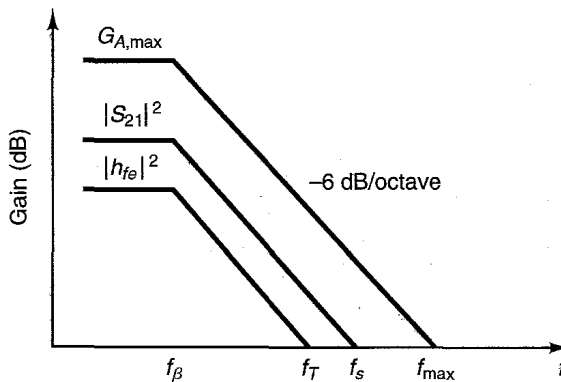
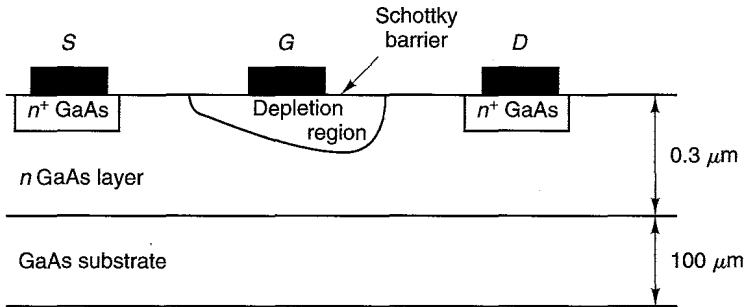


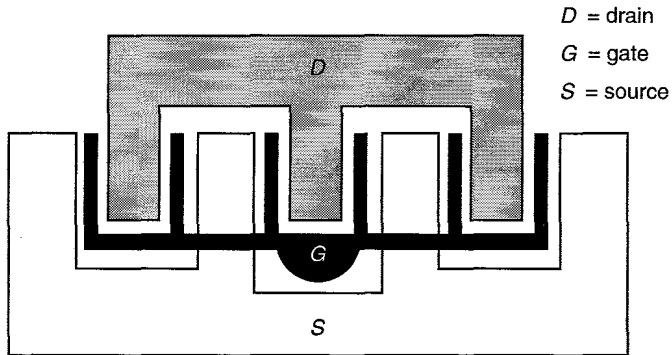
Figure 1.11.10 Frequency characteristics of $G_{A,max}$, $|S_{21}|^2$, and $|h_{fe}|^2$.

	Frequency	Power Gain	Output Power	Minimum Noise Figure
Small-signal transistors (or general purpose transistors)	4 GHz	14 dB	20 dBm	0.8 dB
	6 GHz	11 dB	20 dBm	1.0 dB
	12 GHz	9 dB	18 dBm	1.8 dB
Linear power transistors	4 GHz	8 dB	30 dBm	—
	6 GHz	4.5 dB	30 dBm	—
	12 GHz	4.5 dB	25 dBm	—
Low-noise transistors	4 GHz	15 dB	18 dBm	0.5 dB
	6 GHz	13 dB	18 dBm	0.65 dB
	12 GHz	9.5 dB	16.5 dBm	1.1 dB
Oscillators	4 GHz	—	10 dBm	—
	6 GHz	—	10 dBm	—
	12 GHz	—	10 dBm	—

Figure 1.11.11 Typical performances for GaAs MESFETs in packaged form.



(a)



(b)

Figure 1.11.12 (a) A typical cross section of a GaAs MESFET chip; (b) top view.

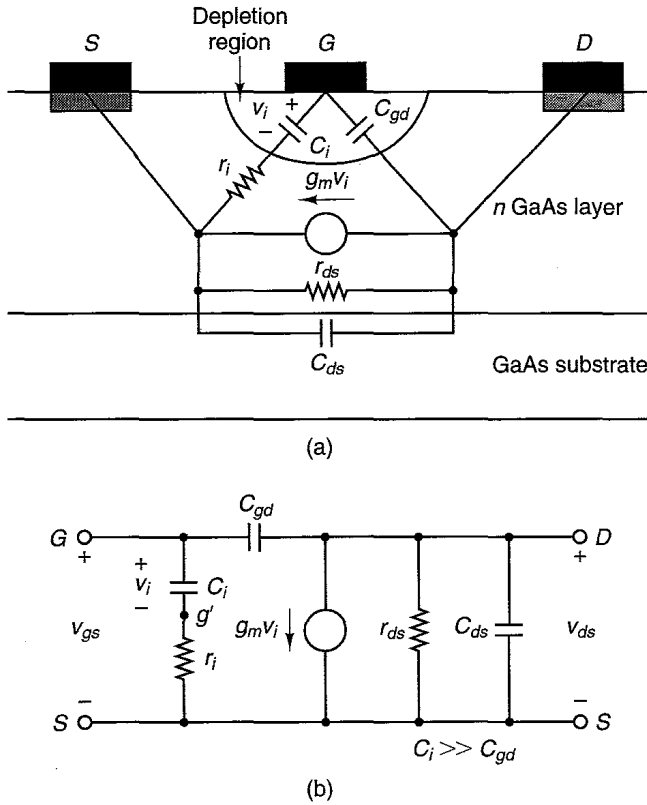


Figure 1.11.13 (a) Cross-sectional geometry of a GaAs FET; (b) GaAs FET high-frequency model for the common-source configuration.

gate-to-source capacitance, and the resistor r_i is the small gate-to-source channel resistance (i.e., the charging resistance of C_i). Typical values for the parameters in Fig. 1.11.13 for a GaAs MESFET having a gate length of $1 \mu\text{m}$ and a gate width of $250 \mu\text{m}$ are $C_i = 0.3 \text{ pF}$, $C_{gd} = 0.02 \text{ pF}$ (gate to drain capacitance), $C_{ds} = 0.05 \text{ pF}$ (drain to source capacitance), $r_{ds} = 600 \Omega$ (drain to source resistance), $g_m = 40 \text{ mS}$ (transconductance), and $r_i = 2.5 \Omega$.

The model for the transistor in packaged form is shown in Fig. 1.11.14. This model includes the extrinsic parasitic elements $R_g, L_g, R_s, L_s, R_d,$ and L_d . Typical values of parasitic inductances are 0.1 nH to 0.9 nH , and values of parasitic resistors are 0.2Ω to 0.1Ω .

When the GaAs FET feedback capacitance is very small and can be neglected, there is no reverse transmission from the output to the input port of the transistor and the transistor becomes unilateral (i.e., $S_{12} = 0$). The simplified unilateral high-frequency model for the intrinsic GaAs FET is shown in Fig. 1.11.15.

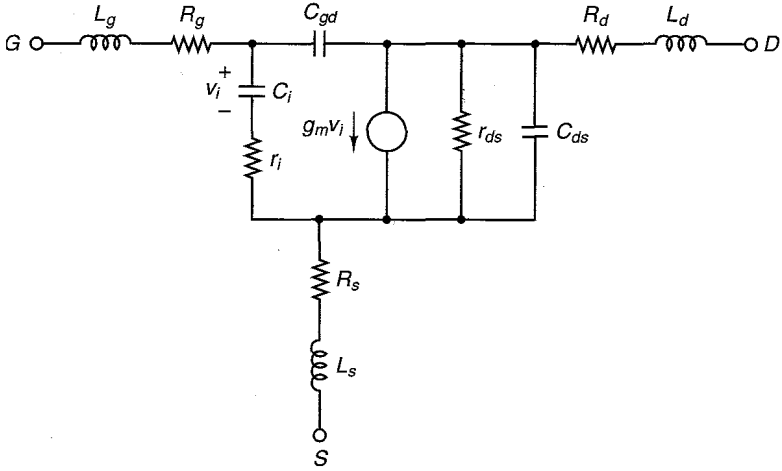


Figure 1.11.14 A microwave GaAs FET common-source model that includes parasitic elements.

The short length of the gate determines the frequency response of the GaAs FET. For the model shown in Fig. 1.11.15, the frequencies f_T and f_{max} are given by

$$f_T = \frac{g_m}{2\pi C_i} \tag{1.11.4}$$

and

$$f_{max} = \frac{f_T}{2} \sqrt{\frac{r_{ds}}{r_i}} \tag{1.11.5}$$

Since f_T is limited by the electron transit time (τ_c) through the channel, f_T can be expressed in the form [1.3]

$$f_T = \frac{1}{2\pi\tau_c} \tag{1.11.6}$$

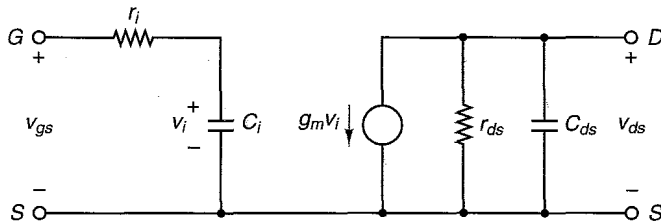


Figure 1.11.15 Simplified unilateral high-frequency model for a common-source GaAs FET.

where

$$\tau_c = \frac{L}{v_s}$$

Here L is the gate length and v_s is the electron saturation drift velocity.

Another expression for f_{\max} , found experimentally, is [1.3]

$$f_{\max} = \frac{33 \times 10^3}{L}$$

Equation (1.11.6) shows the importance of the short gate lengths required for operation at microwave frequencies. For example, with $L = 0.5 \mu\text{m}$ and $v_s = 1 \times 10^7 \text{ cm/s}$, it follows that $f_T = 31.8 \text{ GHz}$.

Further improvements in the performance of GaAs microwave transistors have been obtained using a heterojunction chip structure. A GaAs transistor fabricated using a heterojunction is known as a high-electron mobility transistor (HEMT) or as a modulation doped field effect transistor (MODFET). A typical heterojunction is formed at the interface of a layer of n -type GaAs and a layer of n -type AlGaAs. A typical cross section of a HEMT is shown in Fig. 1.11.16. The operation of HEMT devices is discussed in detail by Pengelly [1.4]. In the HEMT the electrons travel in the n^+ AlGaAs channel, resulting in a very high electron mobility. These devices operate at frequencies well above 30 GHz.

The intrinsic noise sources in a GaAs FET are the thermal-generated channel noise and the induced noise at the gate. The induced noise at the gate is produced by the channel noise voltage. There is no shot noise in the GaAs MESFET. However, the flicker noise ($1/f$ noise) is significant below 10 MHz to 50 MHz and therefore can affect the performance of some oscillators. The extrinsic noise sources (see Fig. 1.11.14) are associated with the resistances R_g and R_s and the gate bonding pad resistance.

Regardless of the transistor used, the S parameters of the device provide all the required information for design purposes. The small-signal model

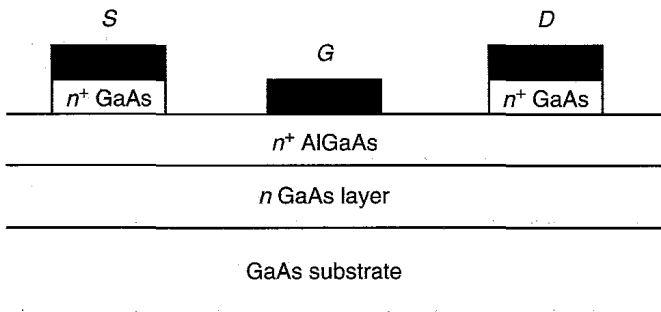


Figure 1.11.16 A cross section of a typical HEMT.

provides an inside to the operation of the transistor and is helpful for noise characterization of the device.

PROBLEMS

- 1.1** Show that the maximum and minimum values of $|V(d)|$ along a transmission line are given by (1.3.42) and (1.3.43), respectively.
- 1.2** In Example 1.3.1 write the expressions for $v(d,t)$ and $i(d,t)$ along the transmission line.
- 1.3** In the circuit shown in Fig. P1.3,
- (a) Calculate the load reflection coefficient, $Z_{IN}(\lambda/8)$, and the VSWR.
- (b) Evaluate $V(\lambda/8)$, $I(\lambda/8)$, $P(\lambda/8)$, $V(0)$, $I(0)$, and $P(0)$.

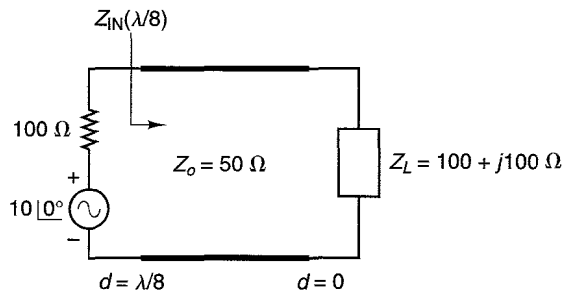


Figure P1.3

- 1.4** Show that for equal reference resistance ($Z_{o1} = Z_{o2}$), the scattering matrix in (1.4.9) can be written in the form

$$V_1^- = S_{11}V_1^+ + S_{12}V_2^+$$

$$V_2^- = S_{21}V_1^+ + S_{22}V_2^+$$

and

$$I_1^- = S_{11}I_1^+ + S_{12}I_2^+$$

$$I_2^- = S_{21}I_1^+ + S_{22}I_2^+$$

- 1.5** Verify the S - and T -parameter conversions given in (1.4.11) and (1.4.12).
- 1.6** Show that the Thévenin voltage $E_{1,TH}$ in Fig. 1.6.3 is given by $E_{1,TH} = E_1 e^{-i\beta l}$.
- 1.7** (a) Find the $ABCD$ matrix of the series impedance Z and shunt admittance Y of Example 1.6.1.
- (b) Use Fig. 1.8.1 to convert the $ABCD$ parameters obtained in part (a) to S parameters. Compare the answers with the results in Example 1.6.1.
- 1.8** Find the scattering matrix and the chain scattering matrix of a transmission line of length l and characteristic impedance Z_o .
- 1.9** Find the scattering matrix and the chain scattering matrix of an open-circuited shunt stub of length l and characteristic impedance Z_o .

1.10 Determine the S parameters of the two-port network shown in Fig. P1.10.

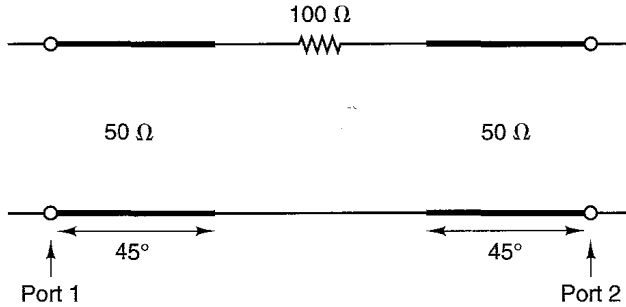


Figure P1.10

1.11 Find the S parameters of the 1-to- n turns ratio transformer shown in Fig. P1.11 at ports 1-2 and 1'-2'.

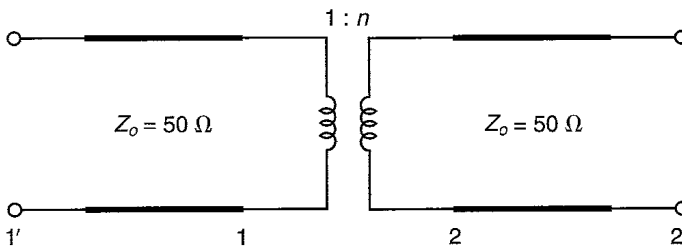


Figure P1.11

1.12 Show that the overall S_{21} parameter of two cascade two-port networks with scattering matrices $[S_A]$ and $[S_B]$, respectively, is given by

$$S_{21} = \frac{S_{21,A} S_{21,B}}{1 - S_{22,A} S_{11,B}}$$

- 1.13 (a) Calculate the reflection coefficient from the 100-Ω load and the VSWR in the $\lambda/4$ line in Fig. P1.13.
- (b) Calculate $V(0)$, P_{AVS} , and the power delivered to the 100-Ω load.
- 1.14 (a) Find the value of the source impedance that results in maximum power delivered to the load in Fig. P1.14. Evaluate the maximum power delivered to the load.
- (b) Using the value of Z_s from part (a), find the Thévenin's equivalent circuit at the load end and evaluate the power delivered to the load.
- 1.15 In Example 1.6.3, calculate $V_2(0)$ and $I_2(0)$ and evaluate the power delivered to the load using $\frac{1}{2}|I_2(0)|^2(50)$ and $\frac{1}{2}|V_2(0)|^2/50$.
- 1.16 In the network shown in Fig. P1.16, $Z_{T1} = 150 + j150 \Omega$, $Z_1 = Z_2 = Z_o = 50 \Omega$, and $l_1 = l_2 = \lambda/8$.

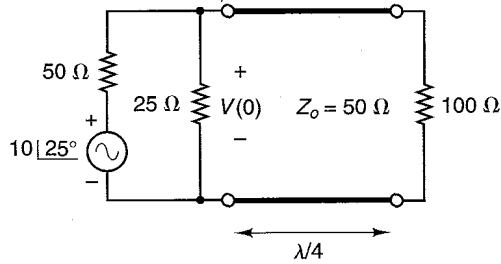


Figure P1.13

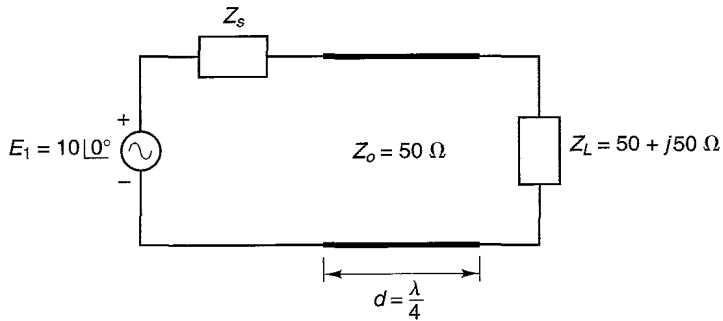


Figure P1.14

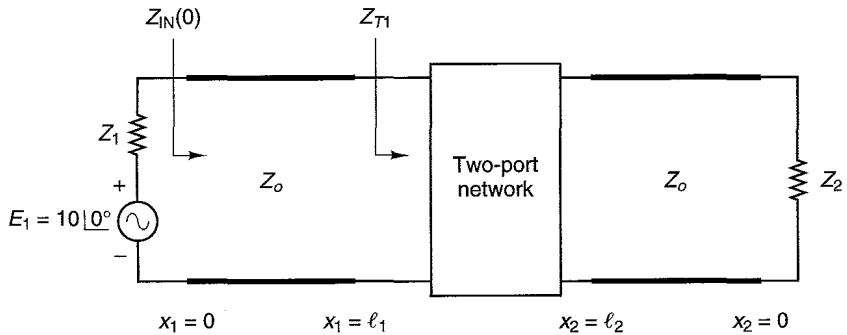


Figure P1.16

- Find $Z_{IN}(0)$.
- Find $a_1(0)$, $b_1(0)$, $a_1(\lambda/8)$, $b_1(\lambda/8)$, and $a_2(0)$.
- Evaluate $V_1(0)$, $V_1(\lambda/8)$, $I_1(0)$, and $I_1(\lambda/8)$.
- Evaluate the average input power at $x_1 = 0$ and the average input power at $x_1 = \lambda/8$.
- Show that $P_1(0) = P_1(\lambda/8)$.
- Evaluate $S_{11}(0)$ and $S_{11}(\lambda/8)$.

- (g) Evaluate the input and output VSWR.
 - (h) Find the electrical length and the length in centimeters of the $\lambda/8$ transmission line at $f = 1$ GHz.
 - (i) If the scattering parameters of the two-port network at $x_1 = l_1$ and $x_2 = l_2$ are $S_{12} = 0$, $S_{21} = 3 \angle 60^\circ$, and $S_{22} = 0.7 \angle 30^\circ$, calculate the power delivered to Z_2 .
- 1.17** In the network shown in Fig. P1.16, $Z_{T1} = 150 + j150 \Omega$, $Z_o = 75 \Omega$, $Z_1 = 100 \Omega$, $Z_2 = 75 \Omega$, $l_1 = \lambda/8$, and $l_2 = \lambda/4$.
- (a) Find $Z_{IN}(0)$.
 - (b) Determine the VSWR in the $\lambda/8$ and $\lambda/4$ lines.
 - (c) Evaluate $a_1(0)$, $b_1(0)$, $a_1(\lambda/8)$, $b_1(\lambda/8)$, and $a_2(0)$.
 - (d) Evaluate $P_1(0)$ and $P_1(\lambda/8)$.
 - (e) Evaluate P_{AVS} and $\frac{1}{2} |a_1(0)|^2$. Are they equal? Explain.
- 1.18** (a) Calculate a_p , b_p , V_p^+ , V_p^- , I_p^+ , and I_p^- for the circuit in Fig. P1.18.
 (b) Evaluate V and I using the values of a_p and b_p from part (a).
 (c) Evaluate V and I using the values of V_p^+ and V_p^- from part (a).

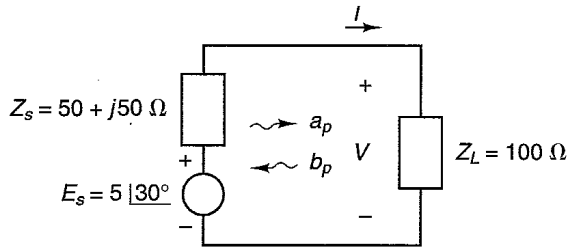


Figure P1.18

- 1.19** (a) Calculate the incident and reflected voltages V_p^+ and V_p^- in the circuit shown in Fig. 1.7.6.
 (b) Evaluate a_p and b_p using the values of V_p^+ and V_p^- [i.e., using (1.7.13) and (1.7.14)].
- 1.20** (a) Calculate the incident and reflected voltages V_p^+ and V_p^- in the circuit shown in Fig. 1.7.7b.
 (b) Evaluate a_p and b_p using the values of V_p^+ and V_p^- [i.e., using (1.7.13) and (1.7.14)].
- 1.21** Consider the circuit shown in Fig. P1.21.

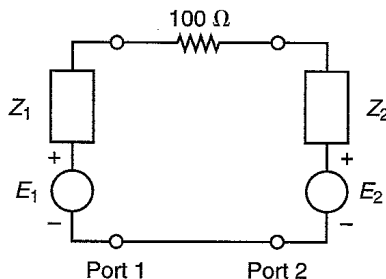


Figure P1.21

- (a) Evaluate S_{p11} , S_{p22} , S_{p21} , and S_{p12} with $Z_1 = Z_2 = 200 \Omega$.
 (b) Evaluate S_{p11} , S_{p22} , S_{p21} , and S_{p12} with $Z_1 = Z_2 = 50 \Omega$.
 (c) Evaluate S_{11} , S_{22} , S_{21} , and S_{12} in a $50\text{-}\Omega$ system.
- 1.22** For the two-port network in Fig. 1.7.8,
 (a) Evaluate the S_p parameters of the 1.59-nH inductor if $Z_1 = Z_2 = 50 \Omega$.
 (b) Evaluate the S parameters of the 1.59-nH inductor in a $50\text{-}\Omega$ system.
- 1.23** Show that in the indefinite scattering matrix given in (1.6.34) the sum of the coefficient of any row is equal to 1 and the sum of the coefficient of any column is equal to 1.
Hint: Since (1.6.34) is valid for any values of a_1 , a_2 , and a_3 , consider the case where $a_2 = a_3 = 0$, as shown in Fig. P1.23a. Then $b_1 = S_{11}a_1$, $b_2 = S_{21}a_1$, and $b_3 = S_{31}a_1$, and at P we can write

$$I_1^+ = I_1^- + I_2^- + I_3^-$$

Therefore, it follows that

$$S_{11} + S_{21} + S_{31} = 1$$

The circuit shown in Fig. P1.23b can be used to show that the sum of the coefficients in any row is equal to 1.

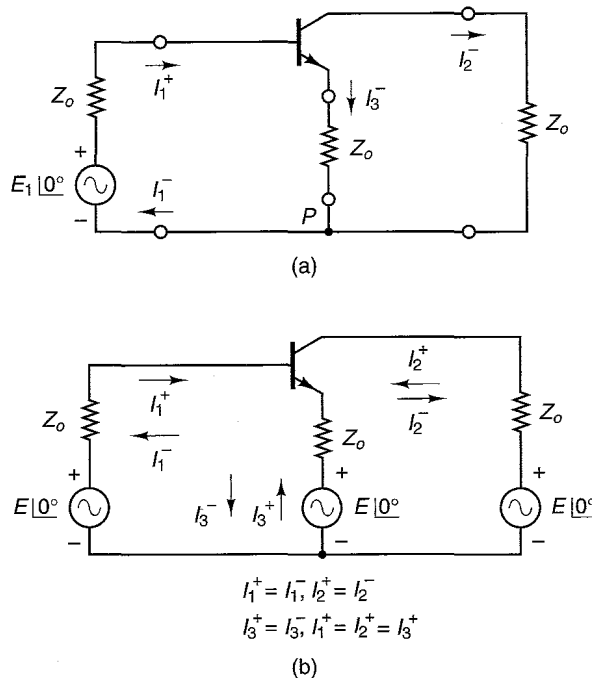


Figure P1.23

- 1.24** In Fig. 1.8.1, verify the conversions between
 (a) z and y parameters
 (b) z and $ABCD$ parameters.

1.25 (a) Show that

$$[S] = -([y] + [Y_o])^{-1}([y] - [Y_o])$$

and

$$[y] = [Y_o] ([\mathbf{1}] - [S]) ([\mathbf{1}] + [S])^{-1}$$

where

$$[Y_o] = \begin{bmatrix} Y_o & 0 \\ 0 & Y_o \end{bmatrix}$$

(b) Verify the conversion between S and y parameters in Fig. 1.8.1.

1.26 In the network shown in Fig. P1.26, the S parameters of the BJT and the value of L are known. Explain how the overall S parameters of the two-port can be calculated.

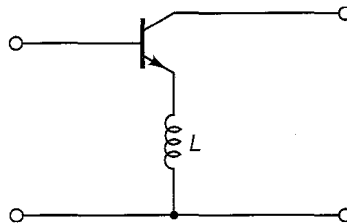


Figure P1.26

1.27 The common-emitter S parameters of a GaAs FET at $f = 10$ GHz are

$$S_{11} = 0.73 \angle -128^\circ$$

$$S_{21} = 1.73 \angle 73^\circ$$

$$S_{12} = 0.045 \angle 114^\circ$$

$$S_{22} = 0.75 \angle -52^\circ$$

Determine the common-base and common-collector S parameters.

1.28 (a) Derive the equations for f_T and f_β , for a BJT, given in (1.11.1) and (1.11.3).

(b) Derive the equation for f_T , for a GaAs FET, given in (1.11.4).

REFERENCES

- [1.1] "S Parameter Design," Hewlett-Packard Application Note 154, April 1972.
- [1.2] T. H. Hsu and C. P. Snapp, "Low-Noise Microwave Bipolar Transistor with Sub-Half-Micrometer Emitter Width," *IEEE Transaction on Electron Devices*, Vol. ED-25, June 1978, pp. 723–730.
- [1.3] D. V. Morgan and M. J. Howes, editors, *Microwave Solid State Devices and Applications*, Peter Peregrinus Ltd., New York, 1980.
- [1.4] R. S. Pengelly, *Microwave Field-Effect Transistors—Theory, Design, and Applications*, 2nd edition, Research Studies Press, Letchworth, England, 1986.

2

MATCHING NETWORKS AND SIGNAL FLOW GRAPHS

2.1 INTRODUCTION

The analysis of transmission-line problems and of matching circuits at microwave frequencies can be cumbersome in analytical form. The Smith chart provides a very useful graphical aid to the analysis of these problems. The Smith chart is basically a plot of all passive impedances in a reflection coefficient chart of unit radius. The reading accuracy from the Smith chart is sufficient for most practical microwave transistor amplifier design problems.

Matching circuits that provide optimum performance in a microwave amplifier can be easily and quickly designed using the normalized impedance and admittance Smith chart. The Smith chart is also used to present the frequency dependence of scattering parameters and other amplifier characteristics.

The characteristics of microstrip transmission lines are presented in this chapter. The mode of propagation in a microstrip line is assumed to be quasi-transverse electromagnetic. Although radiation losses in a microstrip line can be severe, the use of a thin material, having a high dielectric constant, between the top strip conductor and the ground plane of a microstrip line reduces the radiation losses to a minimum.

Microstrip lines find extensive use as passive circuit elements and as a medium in which the complete microwave amplifier can be built. The interconnection features of the microstrip line are unsurpassed. Transistors in chip or packaged form can be easily attached to the strip conductors of the microstrip line. Some practical circuit construction techniques using microstrips are presented.

In this chapter signal flow graphs are discussed. The description of two-port networks in terms of S parameters permits the use of signal flow graphs in the analysis of microwave amplifiers. Power-gain expressions, as well as other relations, are derived in Section 2.6 using signal flow graphs. In Section 2.7 the power-gain expressions are derived using direct manipulations of the traveling wave relations.

2.2 THE SMITH CHART

The Smith chart is the representation in the reflection coefficient plane, called the Γ plane, of the relation

$$\Gamma = \frac{Z - Z_o}{Z + Z_o} \quad (2.2.1)$$

for all values of Z , such that $\text{Re}[Z] \geq 0$. Z_o is the characteristic impedance of the transmission line or a reference impedance value. Defining the normalized impedance z as

$$z = \frac{Z}{Z_o} = \frac{R + jX}{Z_o} = r + jx$$

we can write (2.2.1) in the form

$$\Gamma = \frac{z - 1}{z + 1} \quad (2.2.2)$$

Figure 2.2.1a illustrates the properties of the transformation (2.2.2) for some values of z . For example, if $Z = 50 \Omega$ and $Z_o = 50 \Omega$, then $z = 1$ and $\Gamma = 0$. That is, the point $z = 1$ in the normalized z plane maps into the origin of the Γ plane. From (2.2.2) it also follows that the point $z = 0$ maps into the point $\Gamma = -1$ (i.e., $U = -1$ and $V = 0$).

Next we consider the mapping of normalized impedances having constant real and imaginary parts. For example, for $z = 1 + jx$ the corresponding values of Γ are

$$\Gamma = \frac{jx}{2 + jx} \quad \text{or} \quad \left\{ \begin{array}{ll} \Gamma = 0 & \text{for } x = 0 \\ \Gamma = 0.447 \angle \pm 63.43^\circ & \text{for } x = \pm 1 \\ \Gamma = 0.707 \angle \pm 45^\circ & \text{for } x = \pm 2 \\ & \text{etc.} \end{array} \right.$$

The mapping of the various points along $z = 1 + jx$ is shown in Fig. 2.2.1a. In fact, we will show that the mapping is a circle of radius $1/2$ centered at $U = 1/2$ and $V = 0$. Since this circle represents the mapping of all points with $r = 1$, the circle is known as the constant resistance circle for $r = 1$.

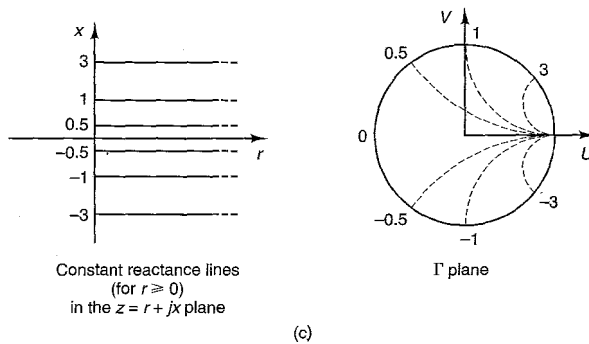
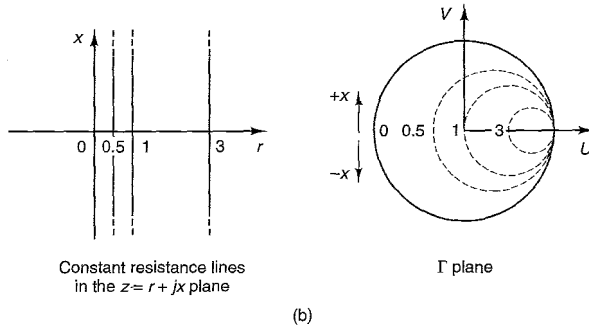
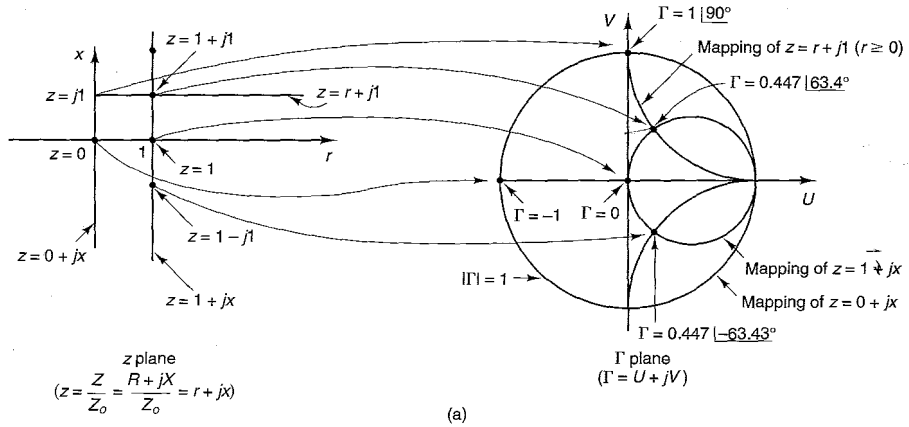


Figure 2.2.1 Development of the Smith chart.

From (2.2.2) it follows that the imaginary axis (i.e., $z = 0 + jx$) maps into the unit circle given by $|\Gamma| = 1$. Therefore, all passive impedances—that is, impedances having $r \geq 0$ —map inside the unit circle (i.e. $|\Gamma| \leq 1$) in the Γ plane.

Figure 2.2.1a also shows the mapping of $z = r + j1$ ($r \geq 0$) (i.e., a straight line having a constant imaginary value of one). For $z = r + j1$ ($r \geq 0$) it follows that the corresponding values of Γ lie along a portion of a circle inside $|\Gamma| \leq 1$

having radius 1, centered at $U = 1$ and $V = 1$. This circle is known as the constant reactance circle for $x = 1$. The portion of the circle outside the Smith chart corresponds to the mapping of $z = r + j1$ for $r < 0$ (i.e., for negative resistances).

The transformation (2.2.2) can be analyzed in general as follows. Let

$$\Gamma = U + jV = \frac{(r - 1) + jx}{(r + 1) + jx}$$

Then rationalize and separate the real and imaginary parts to obtain

$$U = \frac{r^2 - 1 + x^2}{(r + 1)^2 + x^2} \quad (2.2.3)$$

and

$$V = \frac{2x}{(r + 1)^2 + x^2} \quad (2.2.4)$$

Eliminating x from (2.2.3) and (2.2.4) results in

$$\left(U - \frac{r}{r + 1}\right)^2 + V^2 = \left(\frac{1}{r + 1}\right)^2$$

which is the equation of a family of circles centered at $U = r/(r + 1)$ and $V = 0$, with radii $1/(r + 1)$. The constant resistance circles for $r = 0, 0.5, 1$, and 3 are shown in Fig. 2.2.1b. Observe that in Fig. 2.2.1b the constant resistance circles in the Γ plane are labeled according to the constant resistance values (i.e., the value of r in the z plane).

Eliminating r from (2.2.3) and (2.2.4) results in

$$(U - 1)^2 + \left(V - \frac{1}{x}\right)^2 = \left(\frac{1}{x}\right)^2$$

which is the equation of a family of circles centered at $U = 1$ and $V = 1/x$, with radii $1/x$. The portion of constant-reactance circles for $x = -3, -1, -0.5, 0, 1, 0.5$, and 3 (with $r \geq 0$) is shown in Fig. 2.2.1c.

There is a one-to-one correspondence between points in the z plane and points in the Γ plane. The plot of the constant-resistance and constant-reactance circles for all values of z such that $\text{Re}[z] \geq 0$ in a graph is known as the *Smith chart*. The Smith chart is shown in Fig. 2.2.2. Observe that the upper half of the chart represents normalized impedances having a positive reactance (i.e., x is positive) and the lower half represents negative reactances (i.e., x is negative).

The Smith chart can also be used as an admittance chart. The appropriate transformation in this case is

$$\Gamma' = \frac{y - 1}{y + 1}$$

NAME	TITLE	DWG. NO.
SMITH CHART FORM 82-BSPR (9-66)	KAY ELECTRIC COMPANY, PINE BROOK, N.J. ©1966 PRINTED IN U.S.A.	DATE

IMPEDANCE OR ADMITTANCE COORDINATES

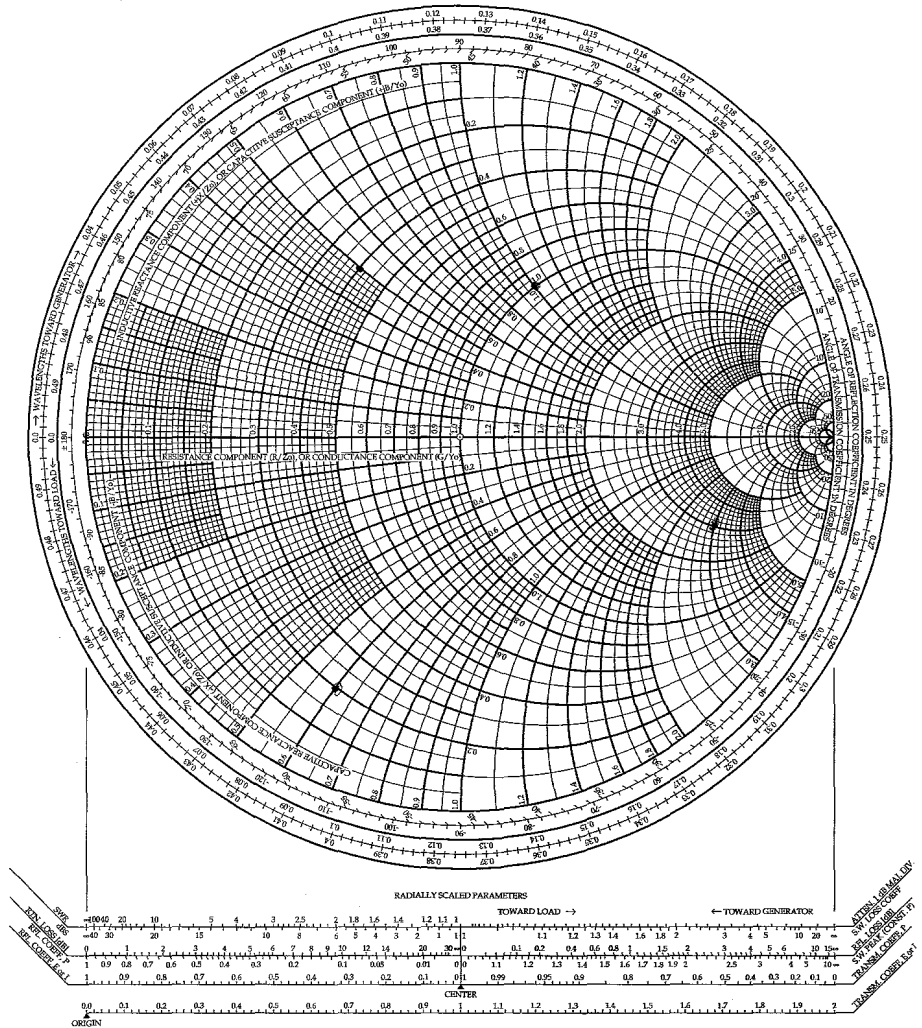


Figure 2.2.2 The Smith chart. (Reproduced with permission of Kay Electric Co., Pine Brook, N.J.)

where the normalized admittance is $y = Y/Y_o$. Y_o is the characteristic admittance of the transmission line or a reference admittance value. Since $z = 1/y$, it follows that Γ and Γ' are related by $\Gamma' = -\Gamma$ or $\Gamma' = \Gamma e^{j\pi}$.

In the admittance chart, since

$$y = \frac{Y}{Y_o} = \frac{G + jB}{Y_o} = g + jb$$

the previous constant-resistance (r) circles become constant-conductance (g) circles and the constant-reactance (x) circles become constant-susceptance (b) circles. Observe that the upper half of the chart represents normalized admittances having a positive susceptance (i.e., b is positive) and the lower half represents negative susceptances (i.e., b is negative).

When needed for clarity, we will call a Smith chart used as an impedance chart a “Z Smith chart,” and a Smith chart used as an admittance chart a “Y Smith chart.”

Example 2.2.1

Locate in the Smith chart the following normalized impedances and admittances:

$$z_1 = 1 + j1, \quad z_2 = 0.4 + j0.5, \quad z_3 = 3 - j3, \quad z_4 = 0.2 - j0.6, \quad z_5 = 0$$

$$y_1 = 1 + j1, \quad y_2 = 0.4 + j0.5, \quad y_3 = 2 - j1.4, \quad y_4 = 0.5 - j0.2, \quad y_5 = \infty$$

Solution. The values of z 's and y 's are shown in Fig. 2.2.3. The Smith chart in Fig. 2.2.3a is obviously used as a Z Smith chart, and that in Fig. 2.2.3b as a Y Smith chart.

The conversion of a normalized impedance to a normalized admittance can be done easily in the Smith chart. Since from (2.2.2)

$$z = \frac{1 + \Gamma}{1 - \Gamma}$$

and

$$y = \frac{1}{z} = \frac{1 - \Gamma}{1 + \Gamma}$$

we observe that rotating Γ by $e^{j\pi}$ we obtain a new value of z (denoted by z') given by

$$z' = \frac{1 + \Gamma e^{j\pi}}{1 - \Gamma e^{j\pi}} = \frac{1 - \Gamma}{1 + \Gamma}$$

which is identical to the value of the admittance y . In other words, the numerical value of the impedance z' is identical to the value of the admittance $y = 1/z$.

Example 2.2.2

Find y for $z = 1 + j1$ using the Smith chart.

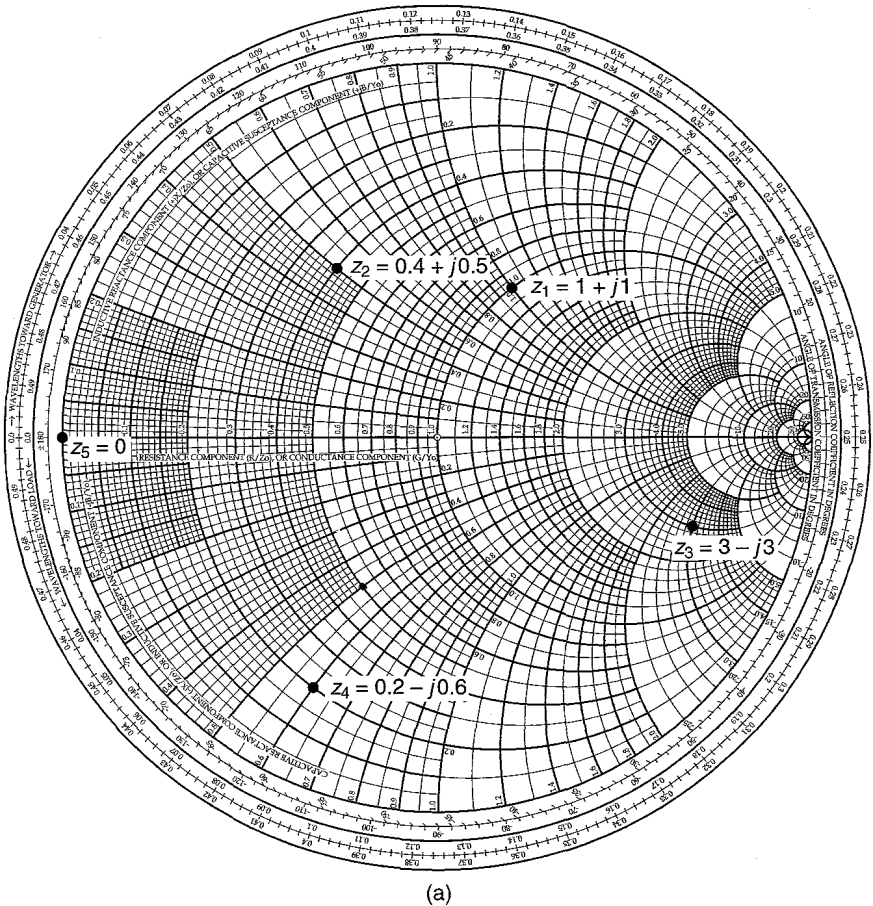


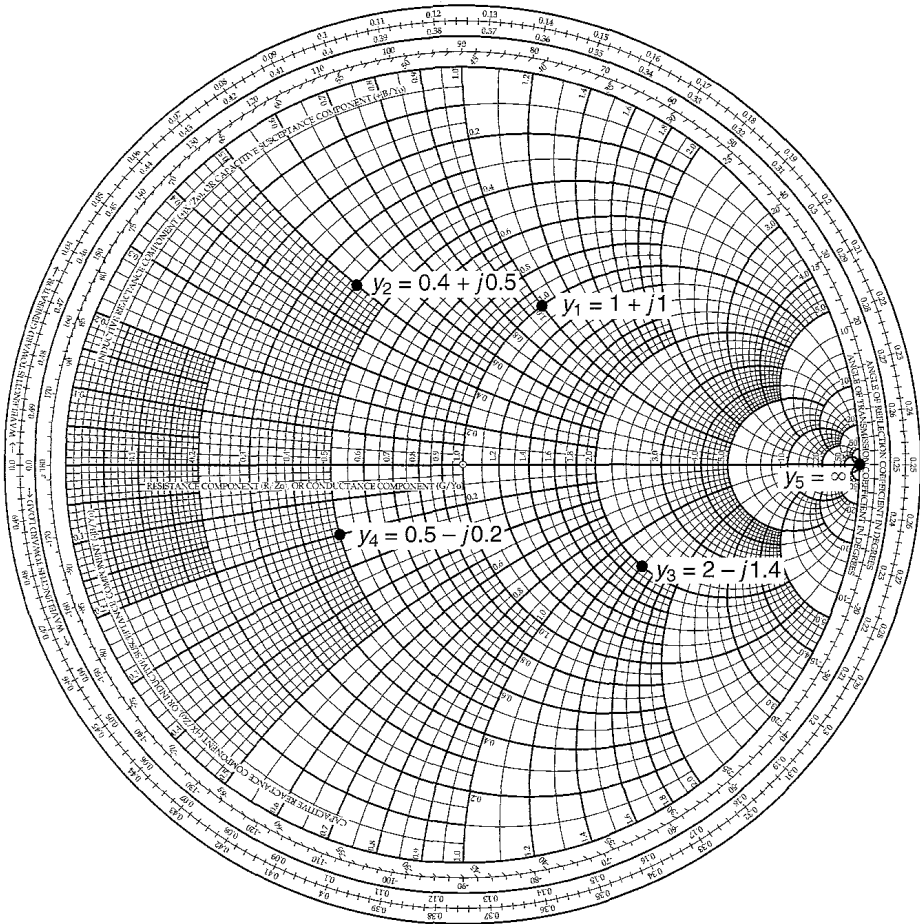
Figure 2.2.3 (a) Values of z in the Z Smith chart; (b) values of y in the Y Smith chart.

Solution. Locate the point $z = 1 + j1$ in Fig. 2.2.4. Associated with z there is a value of Γ . Rotating Γ by 180° (i.e., $e^{j\pi}$) results in the point z' , whose numerical value is that of y . The value of y is read as $0.5 - j0.5$, which of course agrees with

$$y = \frac{1}{z} = \frac{1}{1 + j1} = 0.5 - j0.5$$

Impedances having a negative real part will have a reflection coefficient whose magnitude is greater than 1. These impedances, therefore, map outside the Smith chart. Figure 2.2.5 shows a chart (known as the *compressed Smith chart*) that includes the Smith chart (i.e., $|\Gamma| \leq 1$) plus a portion of the negative impedance region.

An alternative way of handling negative resistances (i.e., $|\Gamma| > 1$) is to plot in the Smith chart $1/\Gamma^*$ and take the values of the resistance circles as being negative and the reactance circles as labeled.



(b)

Figure 2.2.3 Continued

Example 2.2.3

Find the impedance whose reflection coefficient is $2.236 \angle 26.56^\circ$.

Solution. If we plot in the Smith chart shown in Fig. 2.2.6 the quantity

$$\frac{1}{\Gamma^*} = 0.447 \angle 26.56^\circ$$

the resulting z is $-2 + j1$. Of course, from (2.2.2),

$$\Gamma = \frac{-2 + j1 - 1}{-2 + j1 + 1} = 2.236 \angle 26.56^\circ$$

The use of the Smith chart in a transmission-line calculation follows from (1.3.35), (1.3.38), and (1.3.39). With $z = Z_L/Z_o$, we can conveniently write these equations in the form

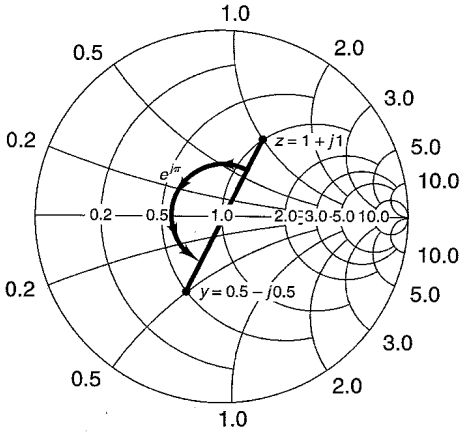


Figure 2.2.4 Conversion of z to y in the Smith chart.

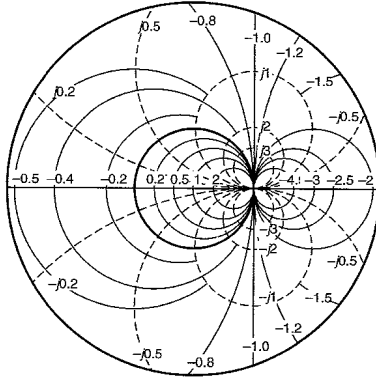


Figure 2.2.5 The compressed Smith chart. (From Ref. [1.1]; courtesy of Hewlett-Packard.)

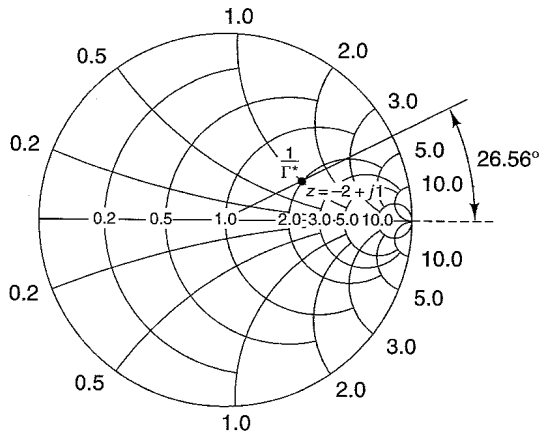


Figure 2.2.6 Negative resistances in the Smith chart.

$$\Gamma_0 = \frac{z - 1}{z + 1} \quad (2.2.5)$$

$$\Gamma_{\text{IN}}(d) = \Gamma_0 e^{-j2\beta d} \quad (2.2.6)$$

$$z_{\text{IN}}(d) = \frac{1 + \Gamma_{\text{IN}}(d)}{1 - \Gamma_{\text{IN}}(d)} \quad (2.2.7)$$

A typical transmission-line input impedance calculation involves the following steps:

1. Locate Γ_0 in the Z Smith chart for a given $z = Z_L/Z_o$ [i.e., (2.2.5)].
2. Rotate Γ_0 by $-2\beta d$ to obtain $\Gamma_{\text{IN}}(d)$ [i.e., (2.2.6)]. Observe that the rotation is along a vector of constant magnitude—namely, $|\Gamma_0| = |\Gamma_{\text{IN}}(d)|$.
3. Read the value of the normalized $z_{\text{IN}}(d)$ associated with $\Gamma_{\text{IN}}(d)$ [i.e., (2.2.7)].

Example 2.2.4

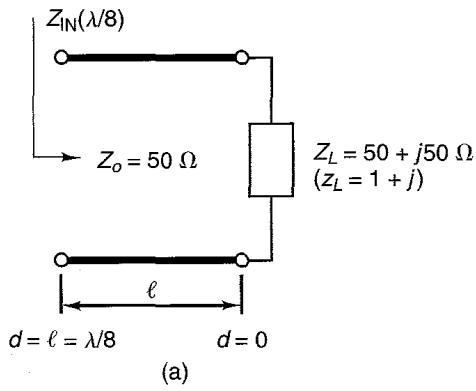
Find the input impedance, the load reflection coefficient, and the VSWR in a transmission line having an electrical length of 45° , characteristic impedance of 50Ω , and terminated in a load $Z_L = 50 + j50 \Omega$.

Solution. The transmission line is shown in Fig. 2.2.7a, where $z_L = Z_L/Z_o = 1 + j1$ and $\beta d = 2\pi d/\lambda = \pi/4$ or $d = \lambda/8 = 0.125\lambda$. In Fig. 2.2.7b, the point $z_L = 1 + j1$ is located and the vector representing Γ_0 drawn. To find Z_{IN} , we rotate along a constant Γ radius a distance of -90° (i.e., $-2\beta d$)—that is, from 63.4° to -26.6° . The input impedance is read directly from the Smith chart as $z_{\text{IN}} = 2 - j1$ or $Z_{\text{IN}}(\lambda/8) = 100 - j50 \Omega$.

The previous calculations can also be made using the wavelength scales on the Smith chart. The input impedance is at a distance $d = 0.125\lambda$ from the load. From Fig. 2.2.7b, at z_L we read from the “wavelengths toward generator” scale a value of 0.162λ . This is an arbitrary value assigned to the load location. Next we add 0.125λ to obtain $0.162\lambda + 0.125\lambda = 0.287\lambda$. That is, we rotate toward the generator a distance $d = 0.125\lambda$ along a constant $|\Gamma|$ circle to reach the input of the line, which is found to be located at 0.287λ . Hence z_{IN} is read from the Smith chart to be $z = 2 - j1$ or $100 - j50 \Omega$.

The magnitude and phase of Γ_0 are read as indicated in Fig. 2.2.7b. Observe the linear scale for the magnitude of the reflection coefficient. The distance from the origin to z_L can be measured with a ruler or compass and superimposed on the linear scale. The reading of Γ_0 gives $\Gamma_0 = 0.447 \angle 63.4^\circ$.

Finally, the VSWR can be calculated from (1.3.44), or the distance from the origin to z_L can be measured and superimposed on the VSWR scale. The value obtained is 2.62. It can also be shown that the value of the maximum resistance in the line is numerically equal to the VSWR. This value is indicated in Fig. 2.2.7b as $\text{VSWR} = r_{\text{max}} = 2.62$.



IMPEDANCE OR ADMITTANCE COORDINATES

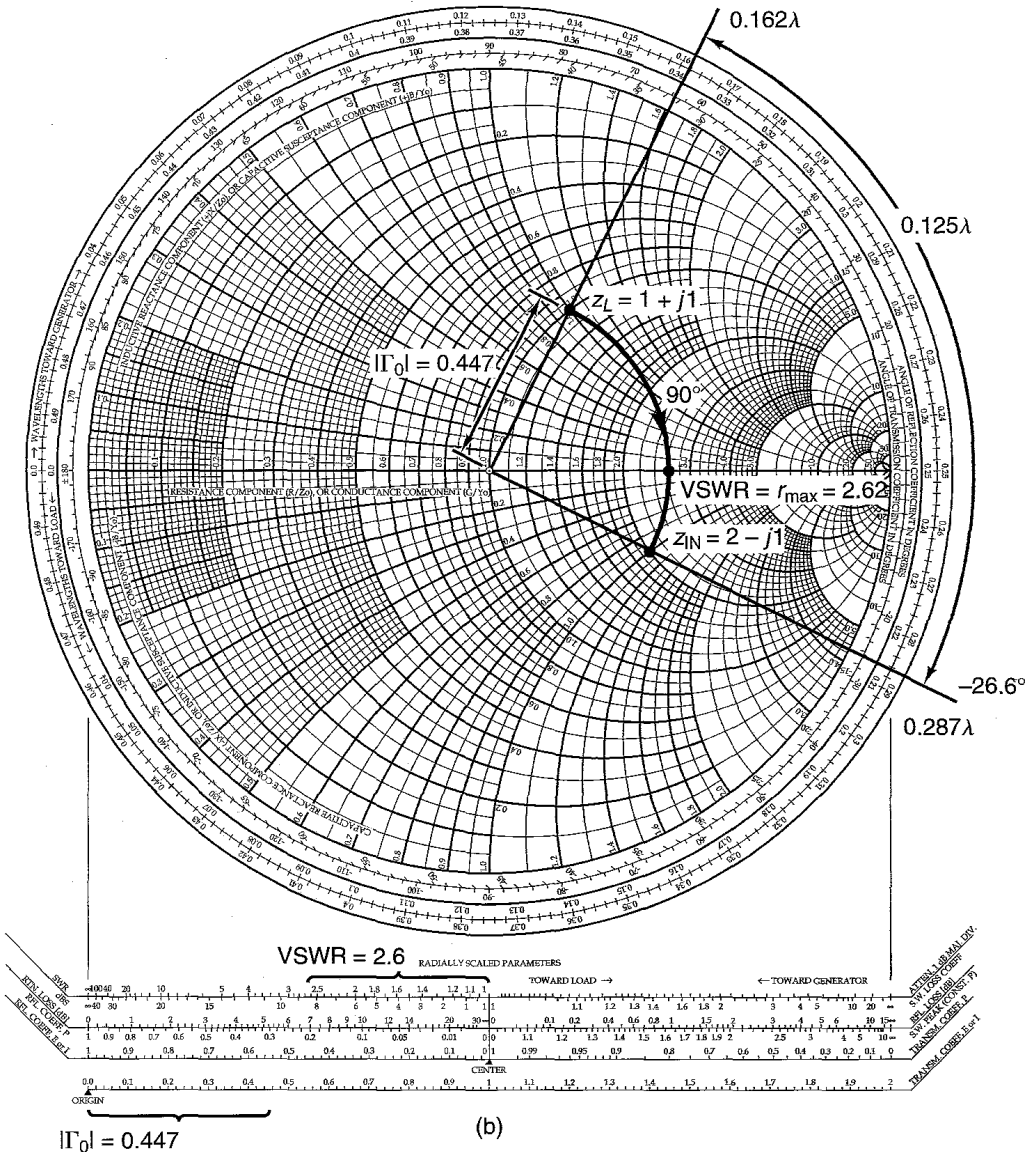


Figure 2.2.7 Typical transmission-line calculation using the Smith chart.

Example 2.2.5

(a) Determine the length l of the $50\text{-}\Omega$ short-circuited transmission line shown in Fig. 2.2.8a so that the input impedance is $Z_{\text{IN}}(l) = j100\ \Omega$.

(b) Determine the length l of the $50\text{-}\Omega$ open-circuited transmission line shown in Fig. 2.2.8b so that the input impedance is $Z_{\text{IN}}(l) = j100\ \Omega$.

Solution. (a) In the short-circuited transmission line, $z_L = 0$. From Fig. 2.2.8a, the length l required to transform the load impedance $z_L = 0$ to the input impedance $z_{\text{IN}}(l) = j100/50 = j2\ \Omega$ is $l = 0.176\ \lambda$. Observe that in a short-circuited line the motion is along the edge of the chart (since $|\Gamma| = 1$ in a short-circuited line).

The length could have been calculated using (1.3.45). That is,

$$Z_{\text{IN}}(l) = j100 = j50 \tan \beta l$$

which gives $\tan \beta l = 2$ or $\beta l = 63.43^\circ = 0.352\pi$. Then

$$l = \frac{0.352\pi\lambda}{2\pi} = 0.176\lambda$$

(b) In the open-circuited transmission line, $z_L = \infty$. Therefore, from Fig. 2.2.8b the length l is 0.426λ [i.e., $(0.5\lambda - 0.25\lambda) + 0.176\lambda = 0.426\lambda$].

In many cases it is convenient to make transmission-line calculations using the Y Smith chart. The following two examples illustrate some transmission-line calculations using the Y Smith chart.

Example 2.2.6

(a) Determine the input admittance of a short-circuited transmission line having a length of $\lambda/8$ and $Y_o = 1/Z_o = 20\ \text{mS}$.

(b) Determine the input admittance of an open-circuited transmission line having a length of $\lambda/8$ and $Y_o = 1/Z_o = 20\ \text{mS}$.

Solution. (a) For the short-circuited line, the load admittance is $y_L = \infty$. Plotting y_L in the Y Smith chart shown in Fig. 2.2.9a and rotating along the constant gamma circle $|\Gamma| = 1$ a distance $l = \lambda/8$, we obtain $y_{\text{IN}}(l) = -j$ or

$$Y_{\text{IN}}(l) = y_{\text{IN}}(l)Y_o = -j(20 \times 10^{-3}) = -j20\ \text{mS}$$

The input impedance is $Z_{\text{IN}}(l) = 1/Y_{\text{IN}}(l) = j50\ \Omega$.

(b) In the open-circuited line, the load admittance is $y_L = 0$. Therefore, as shown in Fig. 2.2.9b, at $l = \lambda/8$ we obtain $y_{\text{IN}}(l) = j$ or

$$Y_{\text{IN}}(l) = y_{\text{IN}}(l)Y_o = j(20 \times 10^{-3}) = j20\ \text{mS}$$

The input impedance is $Z_{\text{IN}}(l) = 1/Y_{\text{IN}}(l) = -j50\ \Omega$.

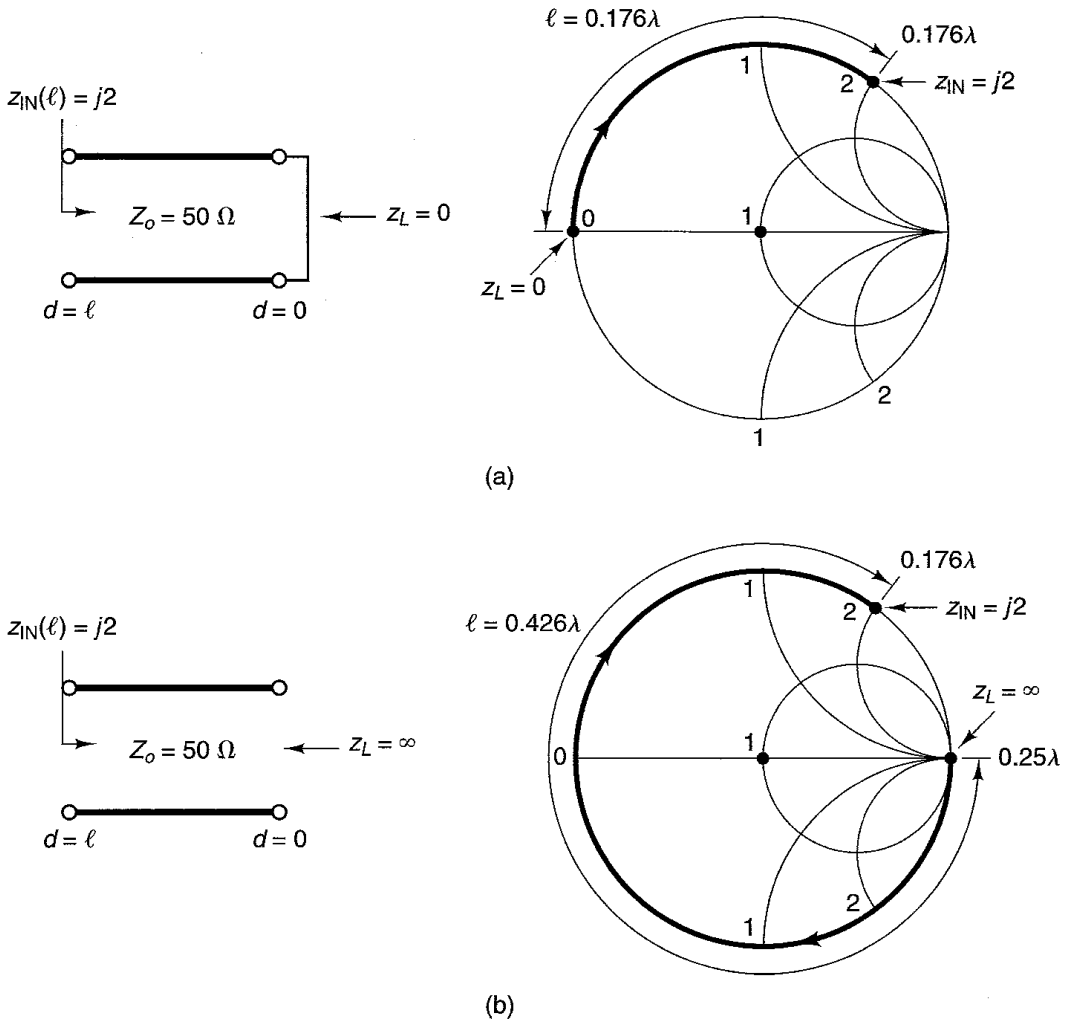


Figure 2.2.8 Circuit diagrams for Example 2.2.5.

Example 2.2.7

Solve Example 2.2.4 using a Y Smith chart.

Solution. Referring to Fig. 2.2.7a, the admittance associated with the load $z_L = Z_L/Z_o = 1 + j1$ can be obtained by rotating Γ_0 by 180° in Fig. 2.2.7b to obtain $y_L = 0.5 - j0.5$. The load y_L is shown in Fig. 2.2.10. At y_L , the “wavelengths toward generator” scale reads 0.412λ . Adding 0.125λ to 0.412λ results in the input being located at 0.537λ . Since the wavelength scale repeats every $\lambda/2$, it follows that 0.537λ is equivalent to 0.037λ . The motion from y_L to $y_{IN}(\lambda/8)$ along a constant $|\Gamma|$ circle is shown in Fig. 2.2.10. The value of $y_{IN}(\ell)$ is read from the Y Smith chart to be $0.4 + j0.2$, or $Y_{IN}(\ell) = (8 + j4)$ mS.

Comparing with Example 2.2.4, we observe that $y_{IN}(\ell) = 0.4 + j0.2$ is the admittance associated with $z_{IN}(\ell) = 1/y_{IN}(\ell) = 2 - j1$, and therefore $Z_{IN}(\ell) = 100 - j50 \Omega$, as expected.

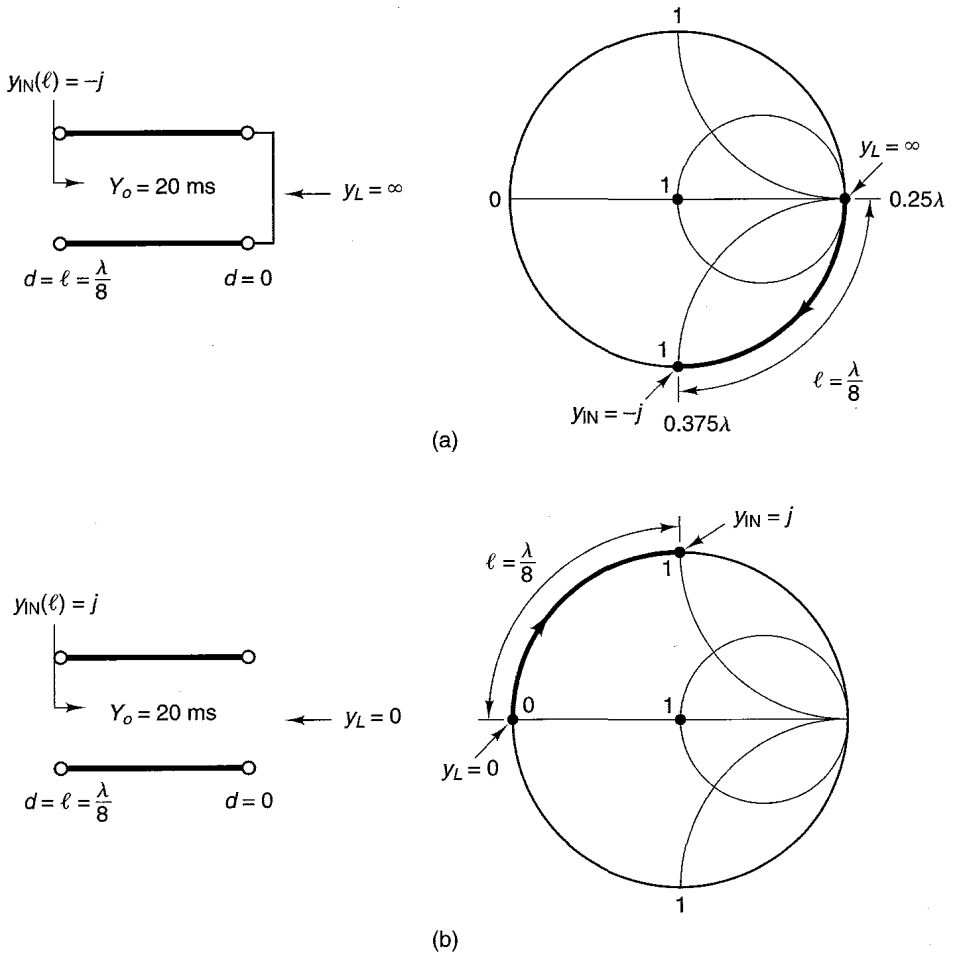


Figure 2.2.9 Circuit diagrams for Example 2.2.6.

2.3 THE NORMALIZED IMPEDANCE AND ADMITTANCE SMITH CHART

The impedance-to-admittance conversion can also be obtained by superimposing two Smith charts and rotating one of the charts by 180° . The rotated chart represents admittances and the other chart represents impedances. The superposition of the original and the rotated chart is known as the *normalized impedance and admittance coordinates Smith chart*. We will refer to this Smith chart as the *ZY Smith chart*. The ZY Smith chart is shown in Fig. 2.3.1, where the impedance values are shown in red and the admittance values in green. (See Fig. 2.3.1 in color on the inside cover of this book.)

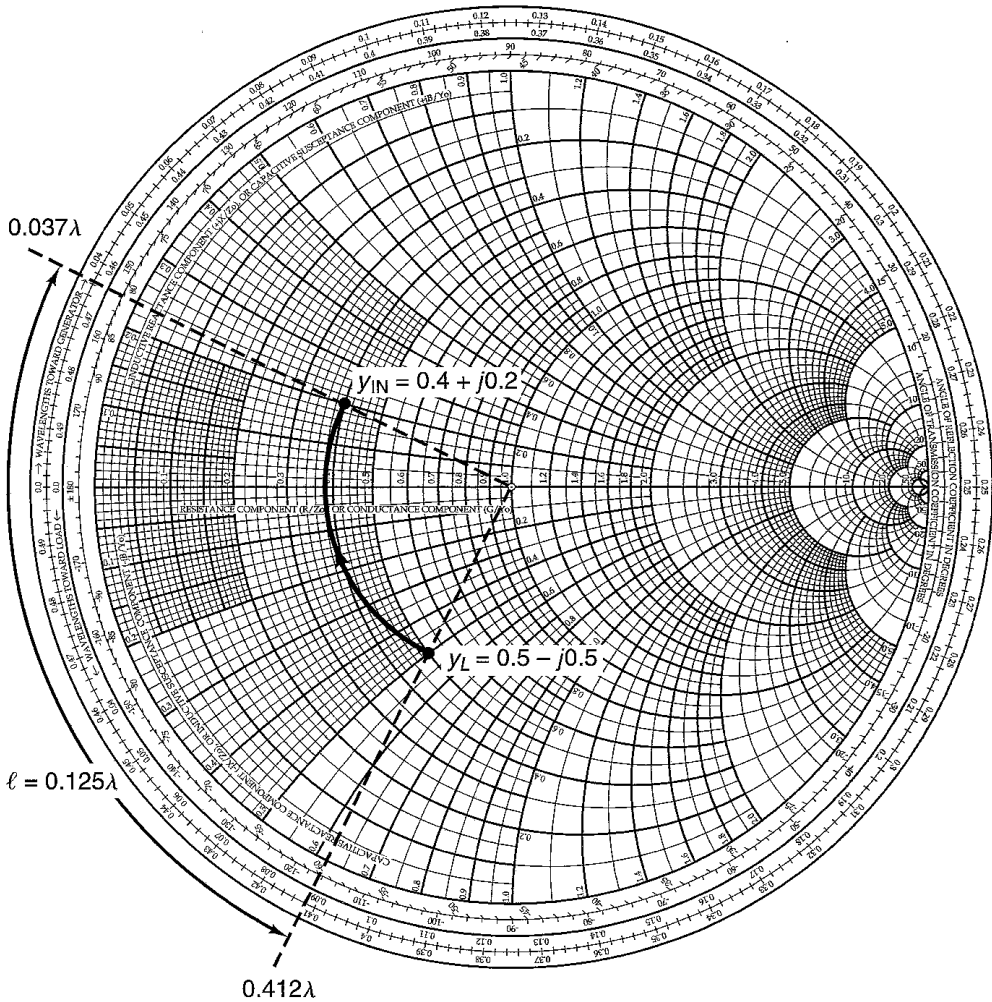


Figure 2.2.10 Solution in the Y Smith chart to the problem in Example 2.2.4.

On the left edge of the ZY Smith chart, one finds the symbols $+X_s$ and $-X_s$ to remind us that when using impedances values (red curves), the reactances are positive in the upper half of the chart and negative in the lower half. On the right edge of the ZY Smith chart, one finds $+B_p$ and $-B_p$ to remind us that when using the admittance values (i.e., green curves), the susceptances are negative in the upper half of the chart and positive in the lower half.

In the ZY Smith chart, for a given value of z the associated value of y is read directly from the admittance coordinates (shown in green), and vice versa.

Example 2.3.1

Find y for $z = 1 + j1$ using the ZY Smith chart.

NAME	TITLE	DWG. NO.
SMITH CHART FORM ZY-01-N	ANALOG INSTRUMENTS COMPANY, NEW PROVIDENCE, N.J. 07974	DATE

NORMALIZED IMPEDANCE AND ADMITTANCE COORDINATES

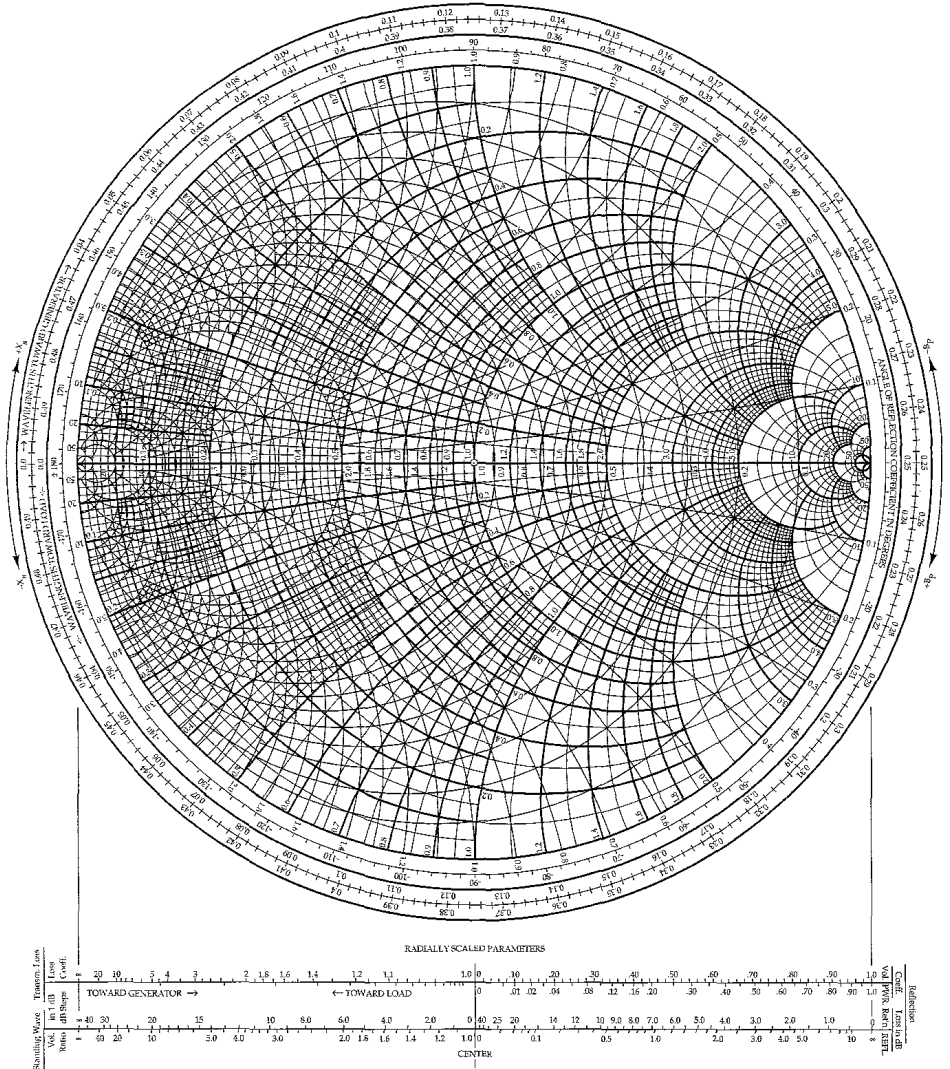


Figure 2.3.1 The normalized impedance and admittance coordinates Smith chart. (Reproduced with permission of Analog Instruments Co., New Providence, N.J.)

Solution. We can locate in the ZY Smith chart in Fig. 2.3.1 the point $z = 1 + j1$ (red curves) and read directly from the green curves the value $y = 0.5 - j0.5$.

The various Smith charts can be used to represent the frequency response of circuits, or from the frequency response of a circuit in the Smith chart an equivalent circuit model can be developed. The simplest frequency responses that can be represented in the Smith chart are those of a series RL circuit, a series RC circuit, a parallel RL circuit, and a parallel RC circuit.

In a series RL circuit, the normalized impedance is

$$z = \frac{Z}{Z_o} = \frac{R + j\omega L}{Z_o} = r + jx$$

As the frequency increases from f_a to f_b , the plot of the normalized impedance z follows a constant r circle with the reactance increasing linearly as a function of frequency, such as the typical plot for the series RL circuit shown in Fig. 2.3.2a, where $r = 0.2 \Omega$ and the reactance increases from $j0.24$ at f_a to $j0.5$ at f_b . In a series RL circuit, the reactance must change linearly with frequency.

The effect of adding a parallel capacitor to the series RL circuit is also shown in Fig. 2.3.2a. It is observed that the admittance of the capacitor (i.e., $y = jb = j\omega C/Y_o$) adds to the admittance of the series RL circuit. For the series RL circuit with a capacitor C in parallel in Fig. 2.3.2a, it is seen that at f_b the susceptance of the capacitor (i.e., $j0.9$) adds to the susceptance of the series RL circuit (i.e., $-j1.7$) to produce a series susceptance of $-j0.8$. Hence, the susceptance of the capacitor is $j0.9$ and at f_b the admittance of the circuit is $y = 0.7 - j0.8$. At f_a , the susceptance of the capacitor is such that the admittance of the circuit is $y = 2 - j1.4$.

In Fig. 2.3.2a, typical impedance plots for a series RC circuit and a series RC circuit with an inductor in parallel are also shown. In Fig. 2.3.2b, the admittance plots of parallel RL and parallel RC circuits are shown, as well as the effects of adding a series C to the parallel RL circuit and a series L to the parallel RC circuit.

Example 2.3.2

The frequency response of the normalized impedance (with $Z_o = 50 \Omega$) of a one-port network is shown in Fig. 2.3.3a as the frequency varies from 500 MHz to 1 GHz. Determine an equivalent circuit for the one-port network and the element values.

Solution. Since the frequency response follows a constant resistance circle of $r = 0.4$ and the reactance increases linearly with frequency, it follows that a series RL circuit simulates the behavior shown in Fig. 2.3.3a.

The value of R , with $Z_o = 50 \Omega$, is $R = rZ_o = 0.4(50) = 20 \Omega$. The value of L follows from

$$\frac{j\omega_b L}{Z_o} - \frac{j\omega_a L}{Z_o} = j0.4 - j0.2$$

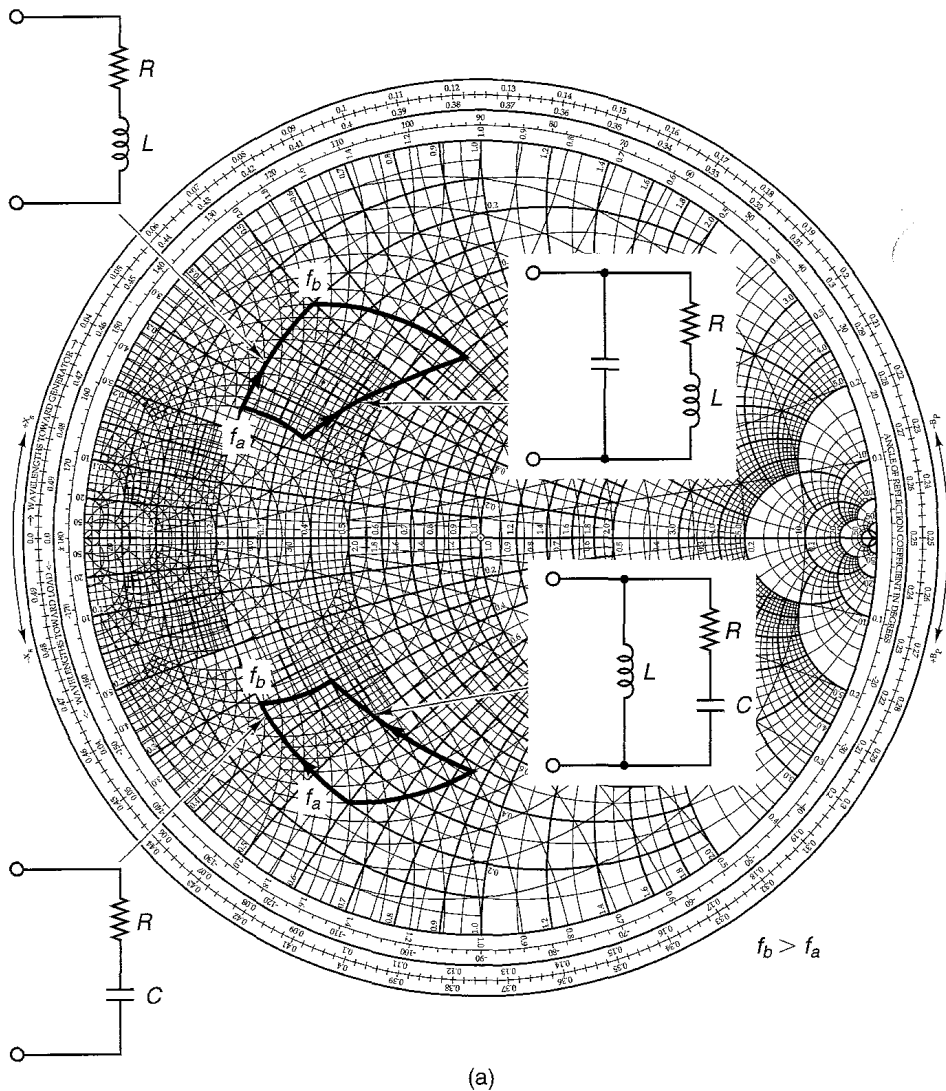


Figure 2.3.2 Characteristics of some networks in the ZY Smith chart.

or

$$L = 50 \frac{(0.4 - 0.2)}{(\omega_b - \omega_a)} = 50 \frac{0.2}{2\pi(1 \times 10^9 - 500 \times 10^6)} = 3.18 \text{ nH}$$

A typical plot of S_{11} for a transistor in the common-emitter configuration is shown in Fig. 1.10.2. It is observed that S_{11} for this transistor in chip form follows a constant-resistance circle, with a capacitive reactance at the lower frequencies and an inductive reactance at the higher frequencies. The equivalent

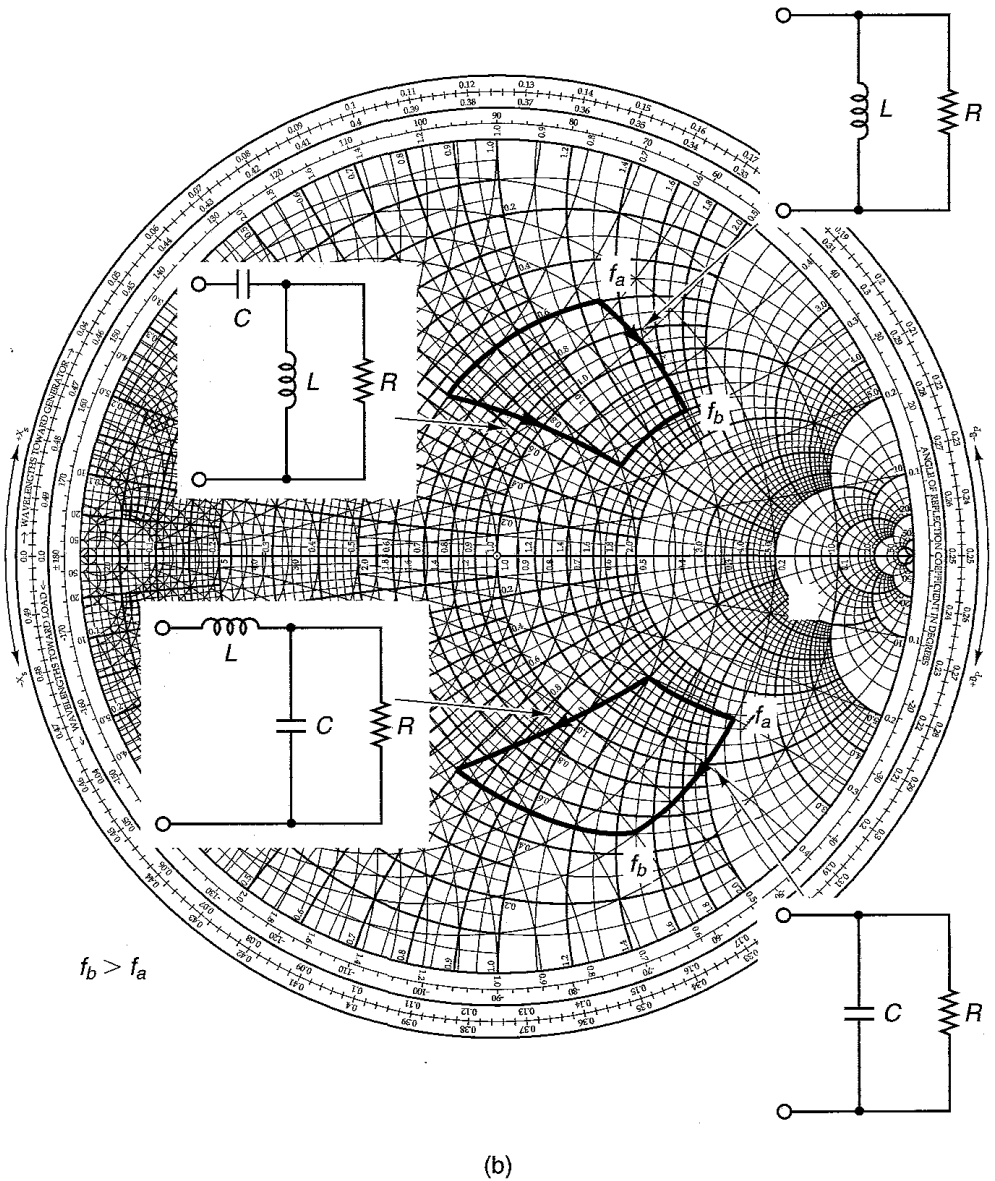


Figure 2.3.2 Continued

circuit for this transistor in chip form which exhibits the behavior of S_{11} is shown in Fig. 2.3.4a. The resistance R represents the base-to-emitter resistance plus any contact resistance. The capacitance C is due to the junction capacitance from base to emitter. The inductance L is due to the reflection properties of a transistor where the emitter resistance, when $h_{fe}(\omega)$ is complex, produces an inductive reactance across the base-to-emitter terminals.

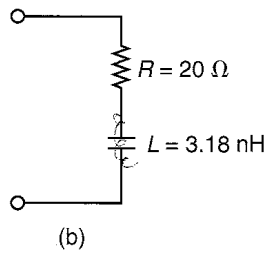
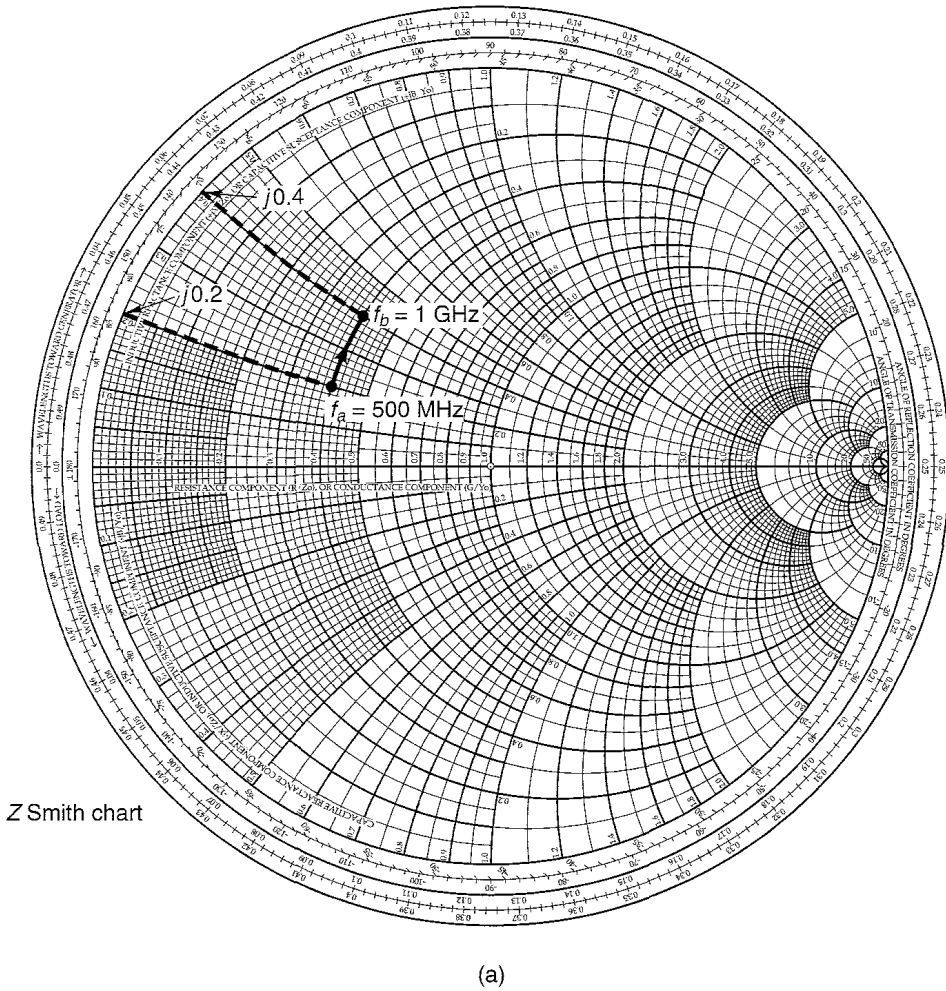


Figure 2.3.3 (a) Frequency response of a one-port network; (b) equivalent circuit of the one-port network.

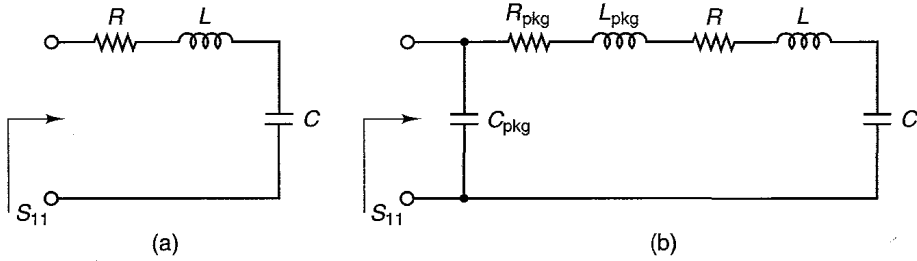


Figure 2.3.4 (a) Input equivalent circuit for a transistor in chip form; (b) input equivalent circuit for a packaged transistor.

Example 2.3.3

The frequency response of S_{11} for a transistor chip is shown in Fig. 1.10.2, and its input equivalent network is shown in Fig. 2.3.4a. Determine the values of R , L , and C .

Solution. From Fig. 1.10.2, at $f_a = 1$ GHz the input impedance associated with S_{11} is $Z_{IN} = 50(0.2 - j0.2) = 10 - j10 \Omega$, and at $f_b = 10$ GHz the input impedance is $Z_{IN} = 50(0.2 + j0.15) = 10 + j7.5 \Omega$. Hence, at $\omega_a = 2\pi f_a$ we obtain

$$10 - j10 = R + j\left(\omega_a L - \frac{1}{\omega_a C}\right) \quad (2.3.1)$$

and at $\omega_b = 2\pi f_b$ we obtain

$$10 + j7.5 = R + j\left(\omega_b L - \frac{1}{\omega_b C}\right) \quad (2.3.2)$$

From (2.3.1) and (2.3.2), it follows that $R = 10 \Omega$ and

$$-10 = 2\pi 10^9 L - \frac{1}{2\pi 10^9 C} \quad (2.3.3)$$

$$7.5 = 2\pi 10^{10} L - \frac{1}{2\pi 10^{10} C} \quad (2.3.4)$$

The simultaneous solution of (2.3.3) and (2.3.4) is $L = 0.1024$ nH and $C = 14.95$ pF.

The equivalent circuit for the transistor in packaged form is a little more difficult to obtain. One equivalent circuit that will closely simulate the response of S_{11} is shown in Fig. 2.3.4b. The resistor R_{pkg} represents the resistance of the package, the package inductance is L_{pkg} , and the package capacitance is C_{pkg} .

2.4 IMPEDANCE MATCHING NETWORKS

The need for matching networks arises because amplifiers, in order to deliver maximum power to a load or to perform in a certain desired way, must be properly terminated at both the input and the output ports. Figure 2.4.1 illustrates a

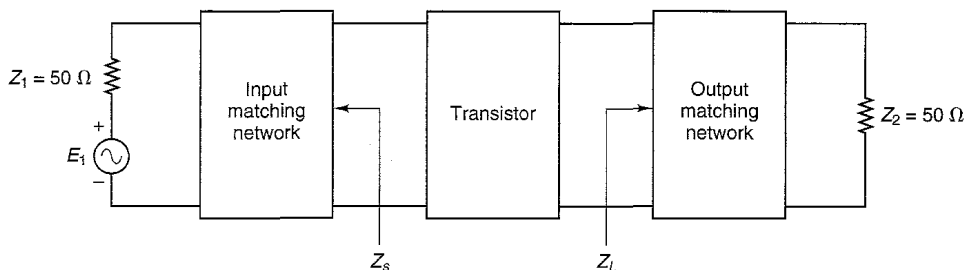


Figure 2.4.1 Block diagram of a microwave amplifier.

typical situation in which a transistor, in order to deliver maximum power to the 50- Ω load, must have the terminations Z_s and Z_L . The input matching network is designed to transform the generator impedance (shown as 50 Ω) to the source impedance Z_s , and the output matching network transforms the 50- Ω termination to the load impedance Z_L .

Although many different types of matching networks can be designed, the eight ELL sections (also denoted as L sections) shown in Fig. 2.4.2 are not only simple to design but quite practical. The matching networks are lossless in order not to dissipate any of the signal power.

The ZY Smith chart can be used conveniently in the design of matching networks. The effect of adding a series reactance element to an impedance or a parallel susceptance element to an admittance, in the ZY Smith chart, is illustrated in the following example.

Example 2.4.1

(a) Illustrate the effect of adding a series inductor L ($z_L = j0.8$) to an impedance z ($z = 0.3 - j0.3$) in the ZY Smith chart.

Solution. Figure 2.4.3 shows that the effect of adding a series inductance with $z_L = j0.8$ is to move along a constant-resistance circle from a reactance value of -0.3 to a reactance of 0.5 . In other words, the motion is in a clockwise direction along a constant-resistance circle.

(b) Illustrate the effect of adding a series capacitor C ($z_C = -j0.8$) to an impedance z ($z = 0.3 - j0.3$) in the ZY Smith chart.

Solution. Figure 2.4.4 shows that the effect of adding a series capacitor with $z_C = -j0.8$ is to move along a constant-resistance circle from a reactance value of -0.3 to a reactance of -1.1 . In other words, the motion is in a counterclockwise direction along a constant-resistance circle.

(c) Illustrate the effect of adding a shunt inductor L ($y_L = -j2.4$) to an admittance y ($y = 1.6 + j1.6$) in the ZY Smith chart.

Solution. Figure 2.4.5 shows that the effect of adding a shunt inductor with $y_L = -j2.4$ is to move along a constant-conductance circle from a susceptance of 1.6 to a

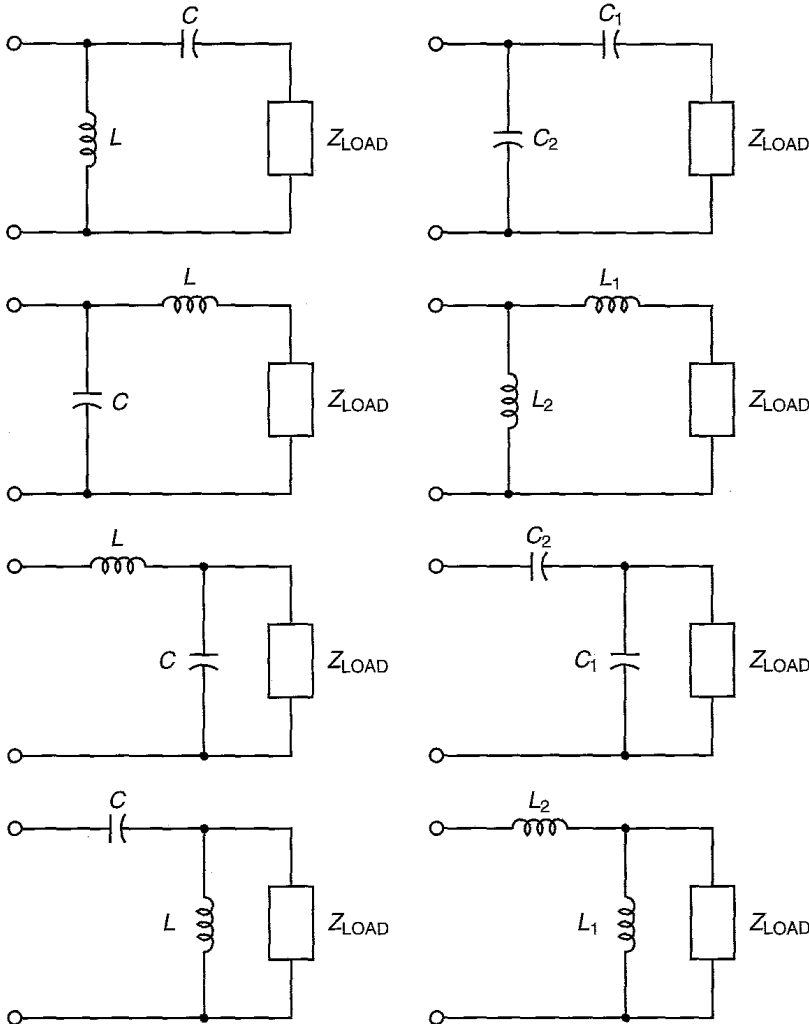


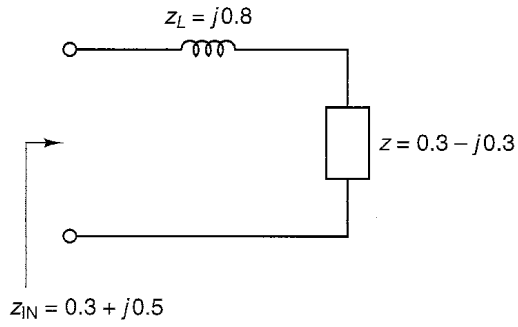
Figure 2.4.2 Matching networks.

susceptance of -0.8 . In other words, the motion is in a counterclockwise direction along a constant-conductance circle.

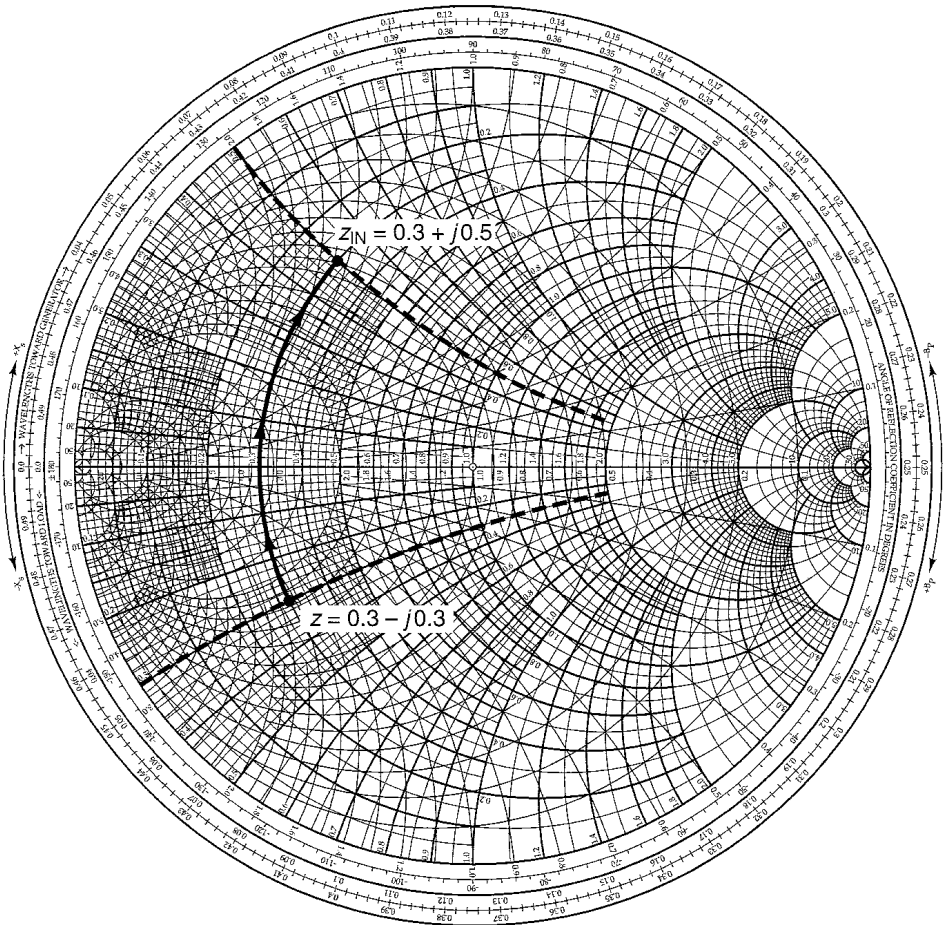
(d) Illustrate the effect of adding a shunt capacitor C ($y_C = j3.4$) to an admittance y ($y = 1.6 + j1.6$) in the ZY Smith chart.

Solution. Figure 2.4.6 shows that the effect of adding a shunt capacitor with $y_C = j3.4$ is to move along a constant-conductance circle from a susceptance of 1.6 to a susceptance of 5 . In other words, the motion is in a clockwise direction along a constant-conductance circle.

In conclusion, adding a series reactance produces a motion along a constant-resistance circle in the ZY Smith chart, and adding shunt susceptance

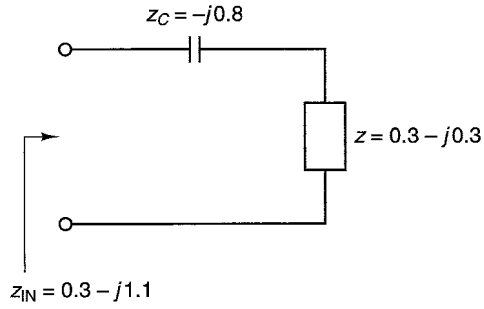


(a)

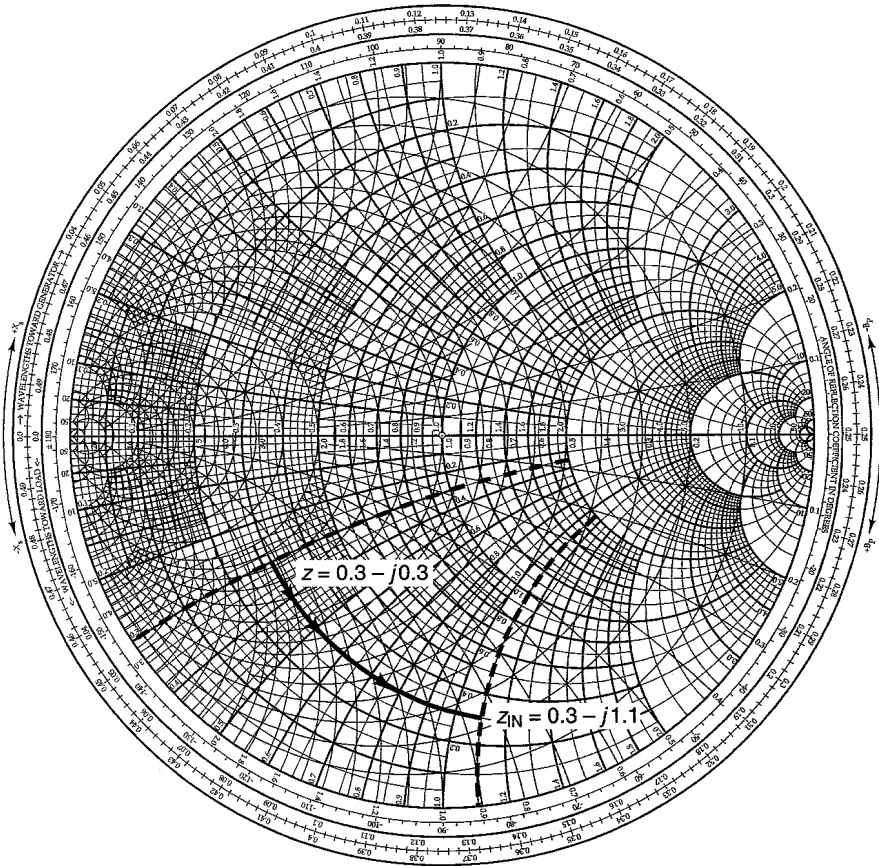


(b)

Figure 2.4.3 Effect of adding a series inductor to an impedance in the ZY Smith chart.

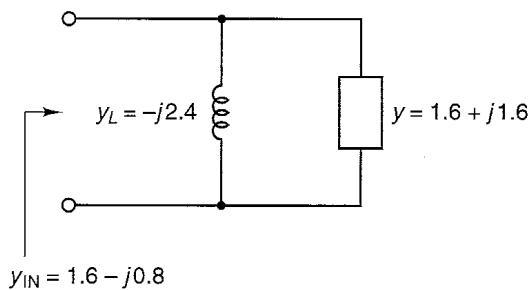


(a)

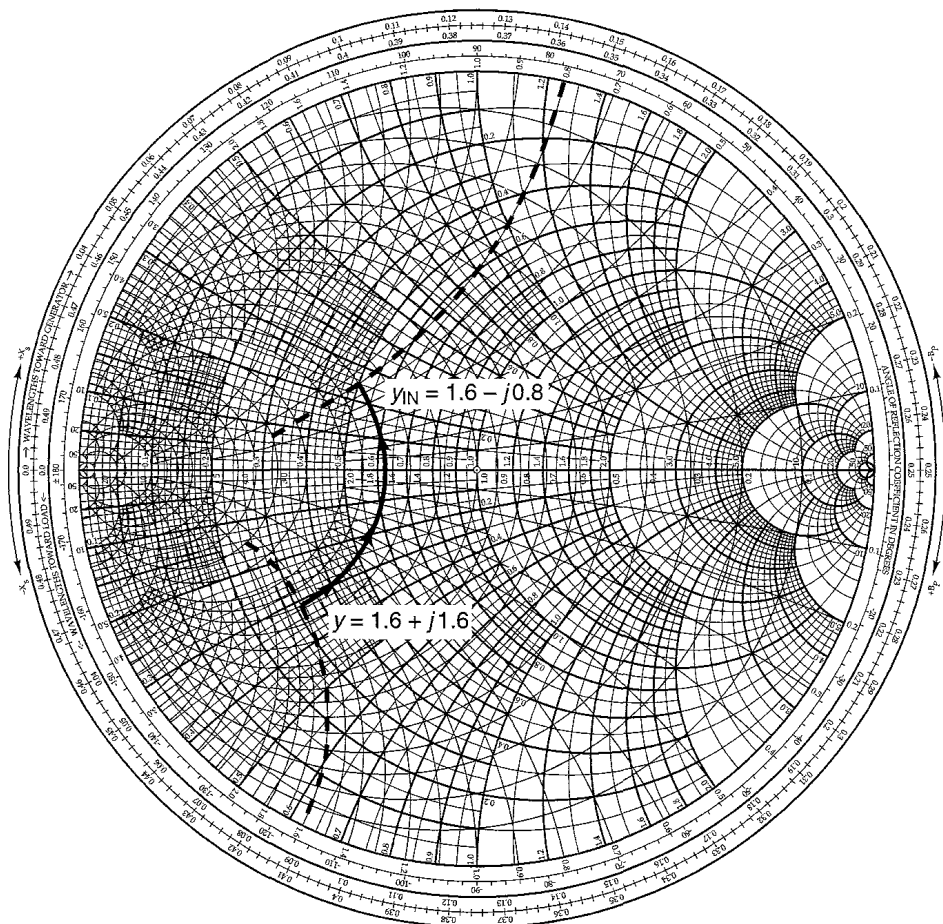


(b)

Figure 2.4.4 Effect of adding a series capacitor to an impedance in the ZY Smith chart.

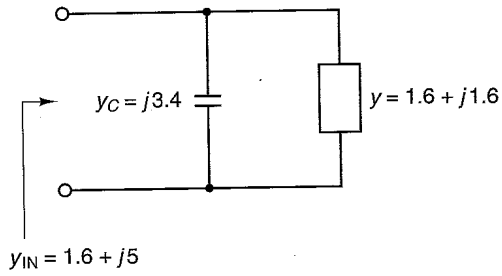


(a)

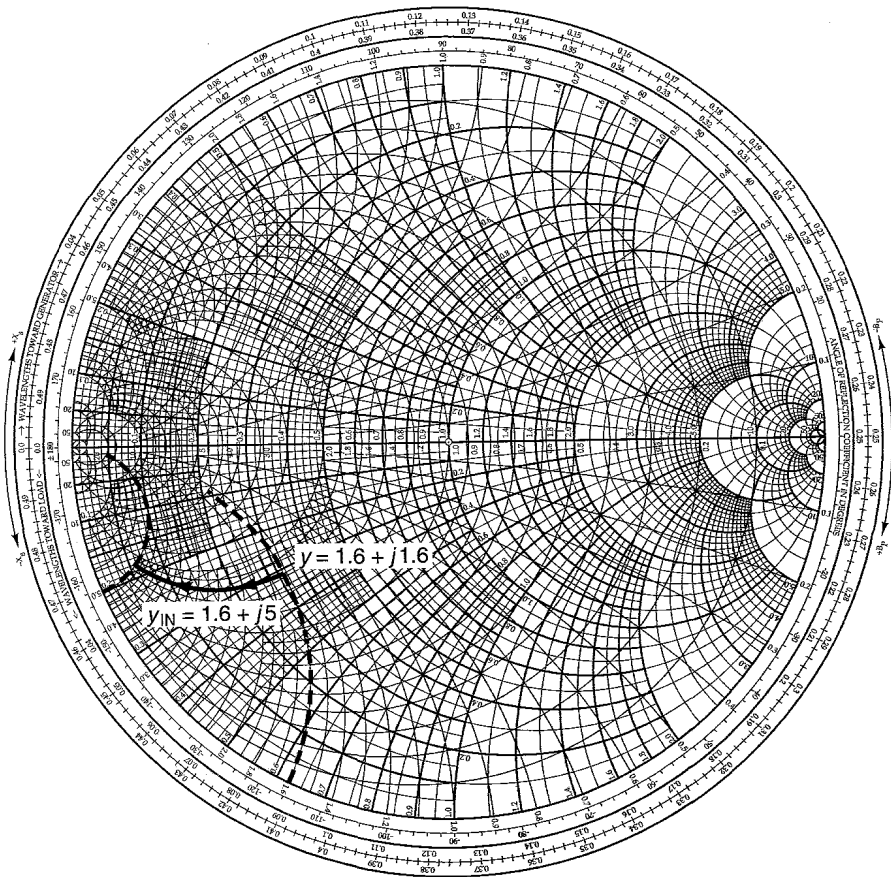


(b)

Figure 2.4.5 Effect of adding a shunt inductor to an admittance in the ZY Smith chart.



(a)



(b)

Figure 2.4.6 Effect of adding a shunt capacitor to an admittance in the ZY Smith chart.

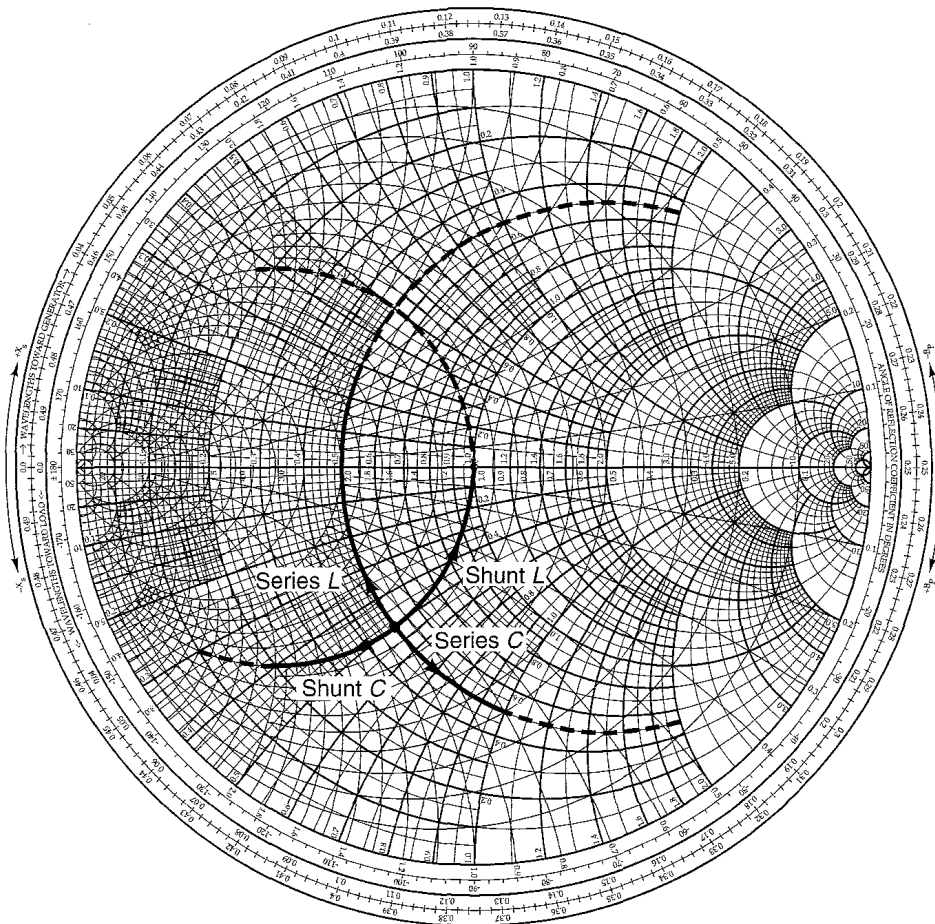


Figure 2.4.7 Effect of adding series and shunt elements in the ZY Smith chart.

produces a motion along a constant-conductance circle in the ZY Smith chart. The four types of motions are illustrated in Fig. 2.4.7.

Designing a matching network in the ZY Smith chart consists of moving along a constant-resistance or constant-conductance circle from one value of impedance or admittance to another. Each motion along a constant-resistance or constant-conductance circle gives the value of an appropriate element. The following examples illustrate the use of the ZY Smith chart in the design of matching networks.

Example 2.4.2

A load $Z_{\text{LOAD}} = 10 + j10 \Omega$ is to be matched to a $50\text{-}\Omega$ line. Design two matching networks and specify the values of L and C at a frequency of 500 MHz .

Solution. Selecting the series L -shunt C network shown in Fig. 2.4.8a, the matching network is designed as shown in Fig. 2.4.8b. (See Figure 2.4.8b on the inside cover.)

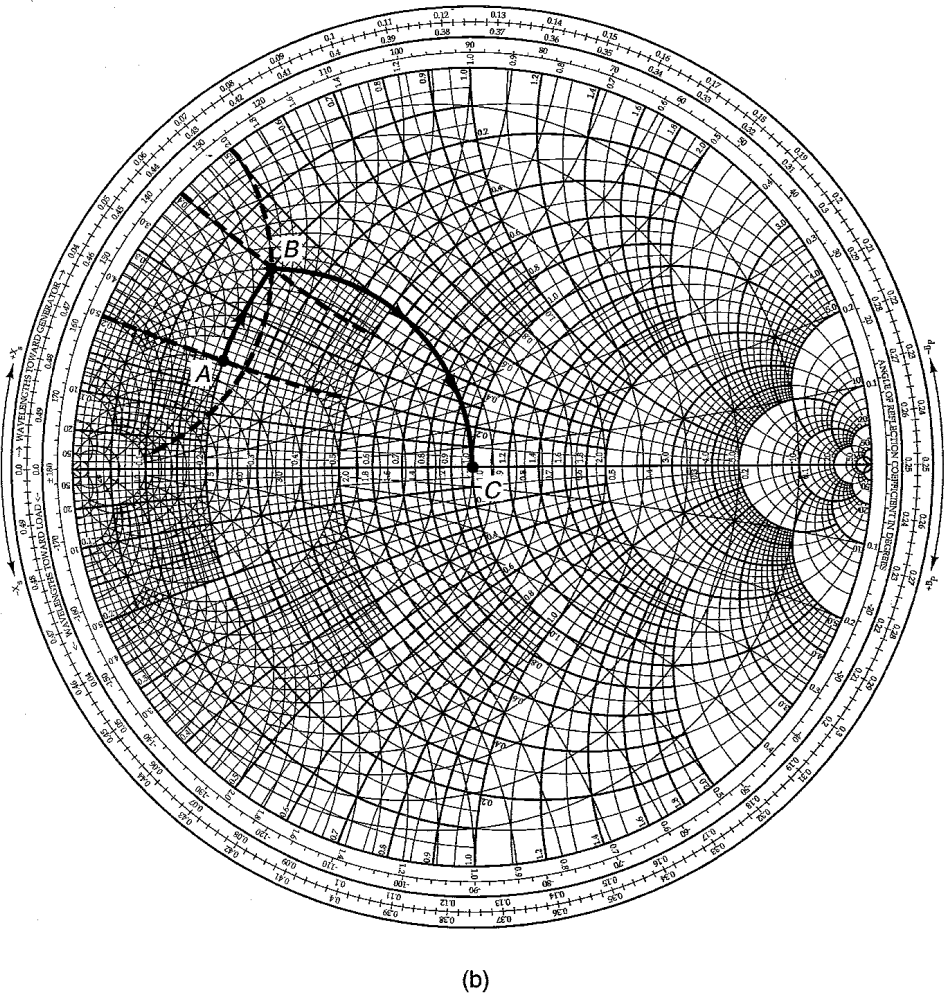
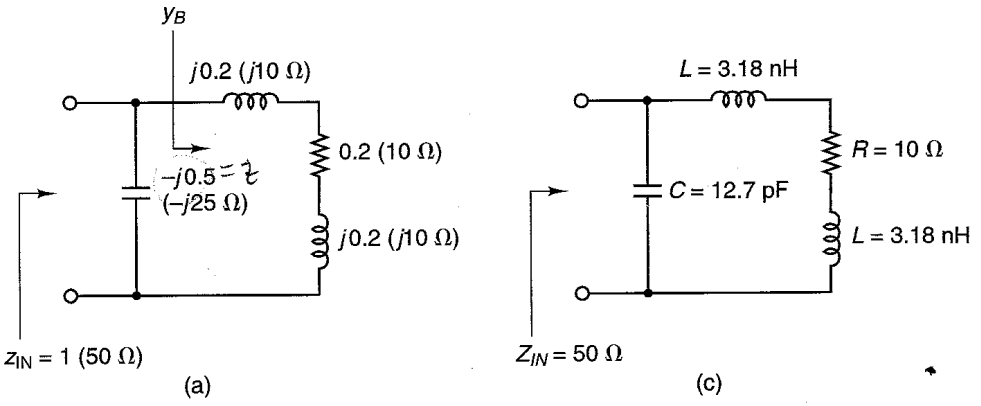


Figure 2.4.8 Design of a series L -shunt C matching network.

The motion from point A [i.e., $z_{\text{LOAD}} = (10 + j10)/50 = 0.2 + j0.2$] to point B is along a constant-resistance circle, and we obtain for the inductor impedance $z_L = j0.4 - j0.2 = j0.2$. Observe that point B is along the unit constant-conductance circle. The admittance at point B is $y_B = 1 - j2$. The motion from point B to point C (i.e., the origin) is along a constant-conductance circle, and we obtain the capacitor admittance $y_C = 0 - (-j2) = j2$ (or $z_C = 1/j2 = -j0.5$). Therefore, at point C , $y_{\text{IN}} = z_{\text{IN}} = 1$ (or $Z_{\text{IN}} = 50 \Omega$) and the network is matched to a $50\text{-}\Omega$ line. At 500 MHz, the value of L is

$$L = \frac{10}{2\pi(500 \times 10^6)} = 3.18 \text{ nH}$$

and the value of C is

$$C = \frac{1}{25(2\pi)500 \times 10^6} = 12.74 \text{ pF}$$

The matching network at 500 MHz is shown in Fig. 2.4.8c.

The second matching network is shown in Fig. 2.4.9a and the ZY Smith chart design in Fig. 2.4.9b. (See Figure 2.4.9b on the inside cover.) The motion from A to B in Fig. 2.4.9b is along a constant-resistance circle; therefore, the impedance of the series capacitor is $z_C = -j0.4 - j0.2 = -j0.6$. The motion from B to C is along a constant-conductance circle; therefore, the admittance of the shunt inductor is $y_L = 0 - j2 = -j2$ (or $z_L = 1/-j2 = j0.5$). The design at 500 MHz is shown in Fig. 2.4.9c.

Example 2.4.3

Design the matching network shown in Fig. 2.4.10a to transform a $50\text{-}\Omega$ load at the input to an admittance $Y_{\text{OUT}} = (8 - j12) \times 10^{-3} \text{ S}$ at the output.

Solution. Figure 2.4.10b illustrates a motion in the ZY Smith chart from the origin (i.e., $z_{\text{LOAD}} = 50/50 = 1$) to $y_{\text{OUT}} = 50(8 - j12) \times 10^{-3} = 0.4 - j0.6$. (See Figure 2.4.10b on the inside cover.) The motion from A to B produces a series capacitor having an impedance of $z_C = -j1.21$. The motion from B to C produces a shunt inductor having an admittance of $y_L = -j0.6 - j0.49 = -j1.09$ (or $z_L = 1/-j1.09 = j0.917$). The matching network is shown in Fig. 2.4.10c.

Example 2.4.4

Design a matching network to transform the load $Z_{\text{LOAD}} = 100 + j100 \Omega$ to an input impedance of $Z_{\text{IN}} = 50 + j20 \Omega$.

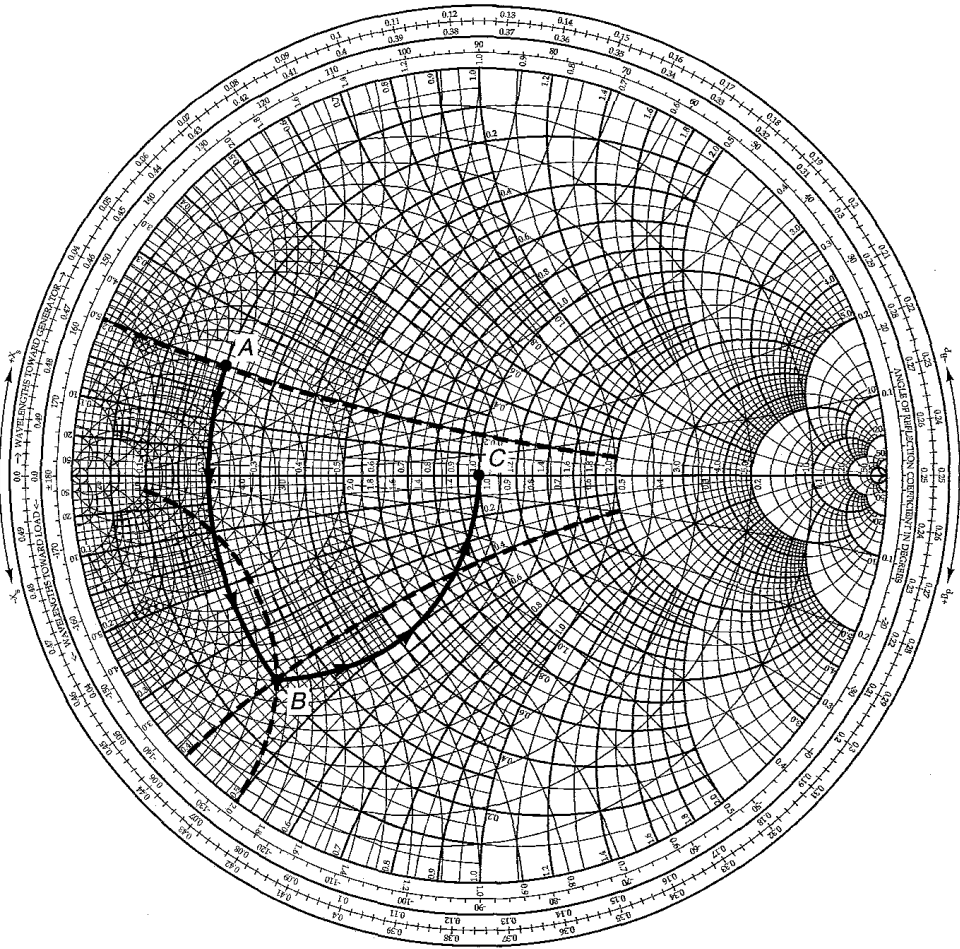
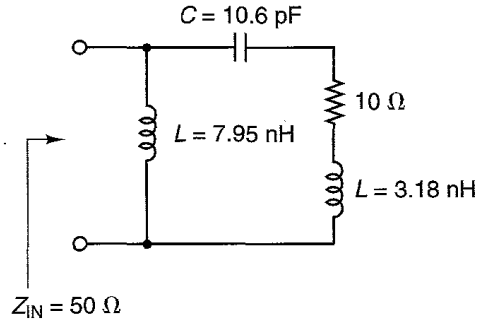
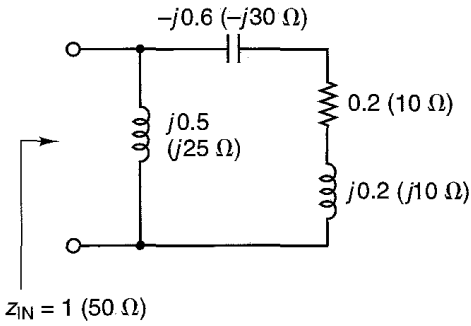
Solution. Using a normalized value of $Z_o = 100 \Omega$, we have $z_{\text{LOAD}} = Z_{\text{LOAD}}/Z_o = 1 + j$ and $z_{\text{IN}} = Z_{\text{IN}}/Z_o = 0.5 + j0.2$. Figure 2.4.11a shows one possible solution for the matching network. The motion from A to B is produced by a shunt capacitor whose normalized admittance is $y_C = j0.86 - (-j0.5) = j1.36$ (or $z_C = 1/y_C = -j0.735$). Then, the impedance of the capacitor is

$$Z_C = 100z_C = 100(-j0.735) = -j73.5 \Omega$$

The motion from B to C requires an inductor having a normalized impedance value of $z_L = j0.2 - (-j0.87) = j1.07$. Then

$$Z_L = 100z_L = 100(j1.07) = j107 \Omega$$

The matching network is shown in Fig. 2.4.11b.



(b)

Figure 2.4.9 Design of a series C-shunt L matching network.

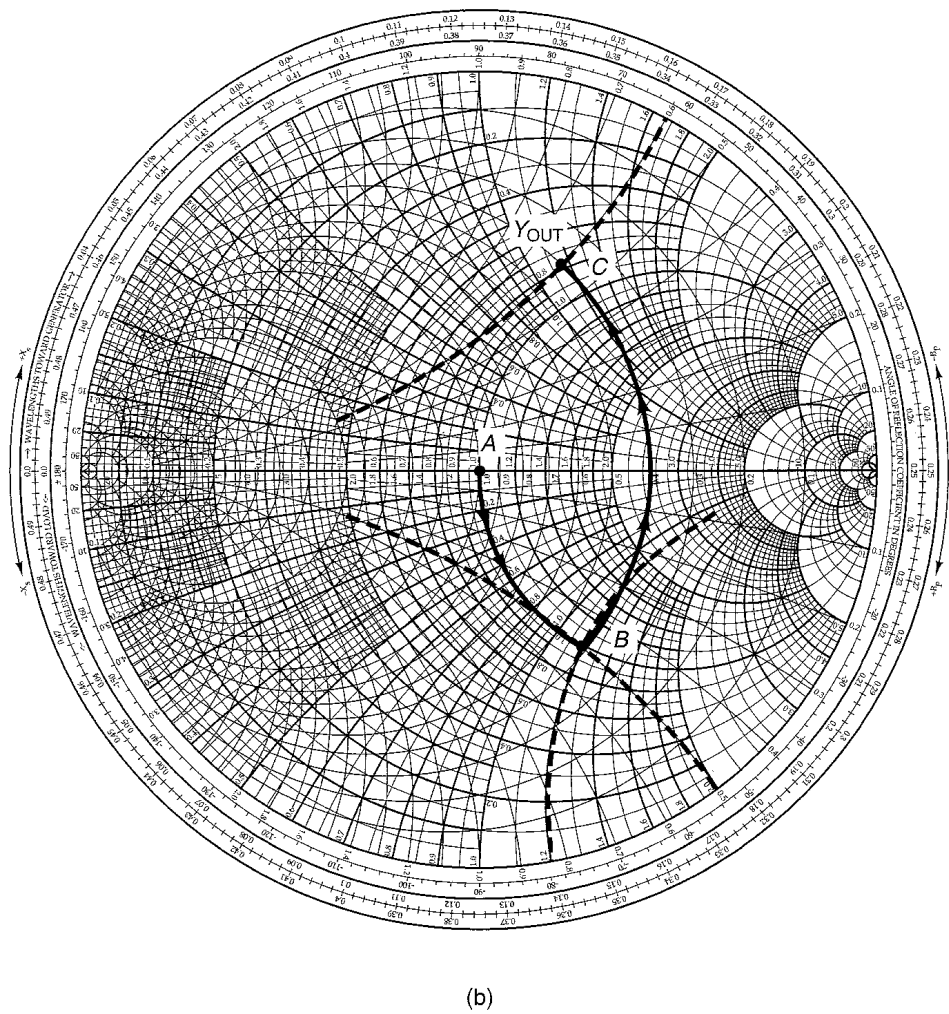
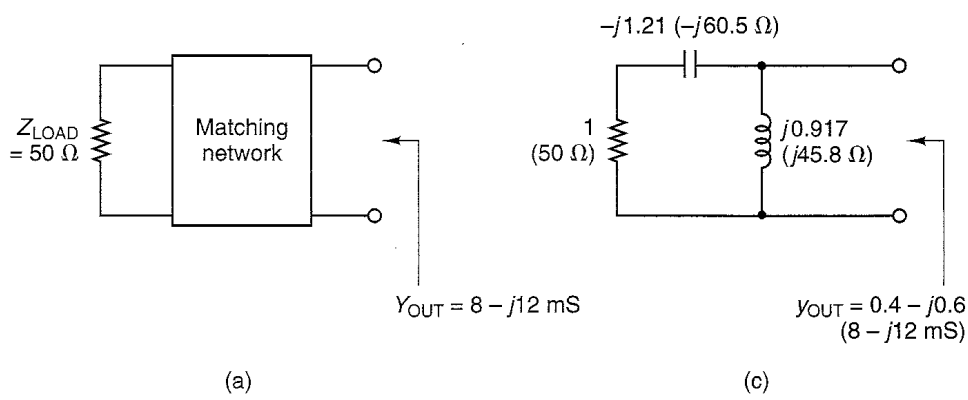
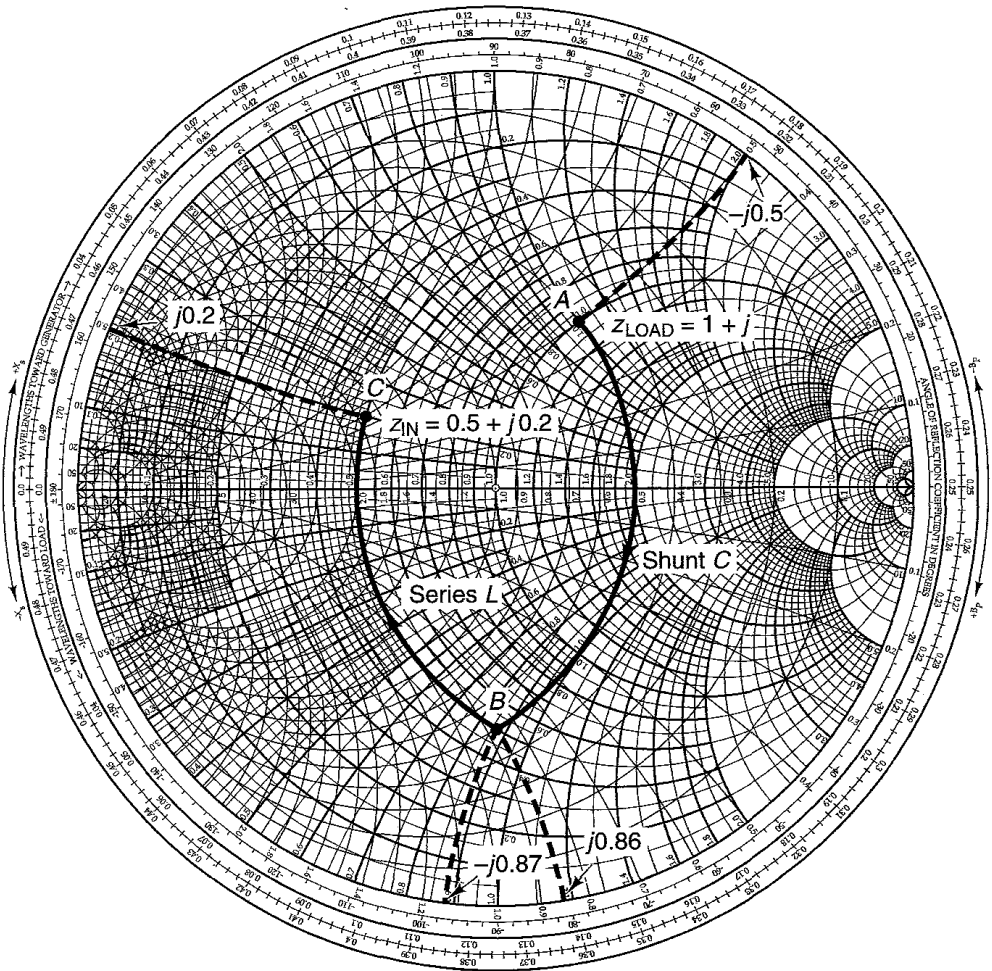
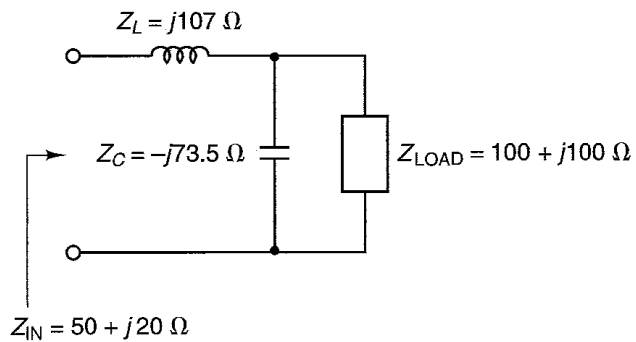


Figure 2.4.10 Matching a 50-Ω load to a given Y_{OUT} using a series C-shunt L matching network.



(a)



(b)

Figure 2.4.11 Matching a complex load to a given complex impedance Z_{IN} using a shunt C -series L network.

Sometimes a specific matching network cannot be used to accomplish a given match. For example, any load impedance falling in the marked region in Fig. 2.4.12a cannot be matched to $50\ \Omega$ with the network in Fig. 2.4.12b because adding a series L produces motion, in a clockwise direction, away from any constant-conductance circle that passes through the origin.

Another observation regarding the Ell matching networks is that only those with an inductor and a capacitor can be used to provide a match between a resistive load and an input resistance.

In a resonant circuit, the ratio of its resonant frequency f_o to its bandwidth (BW) is known as the loaded Q of the circuit. That is,

$$Q_L = \frac{\omega_o}{\text{BW}}$$

If the bandwidth is expressed in hertz, we write

$$Q_L = \frac{f_o}{\text{BW}} \quad (2.4.1)$$

The Ell matching networks in Fig. 2.4.2 are used to provide a match at a certain frequency. The frequency response of an Ell network can be classified as either a (two-pole) low-pass filter or a high-pass filter. At each node of the Ell matching networks, there is an equivalent series input impedance, denoted by $R_s + jX_s$. Hence, a circuit node Q , denoted by Q_n , can be defined at each node as

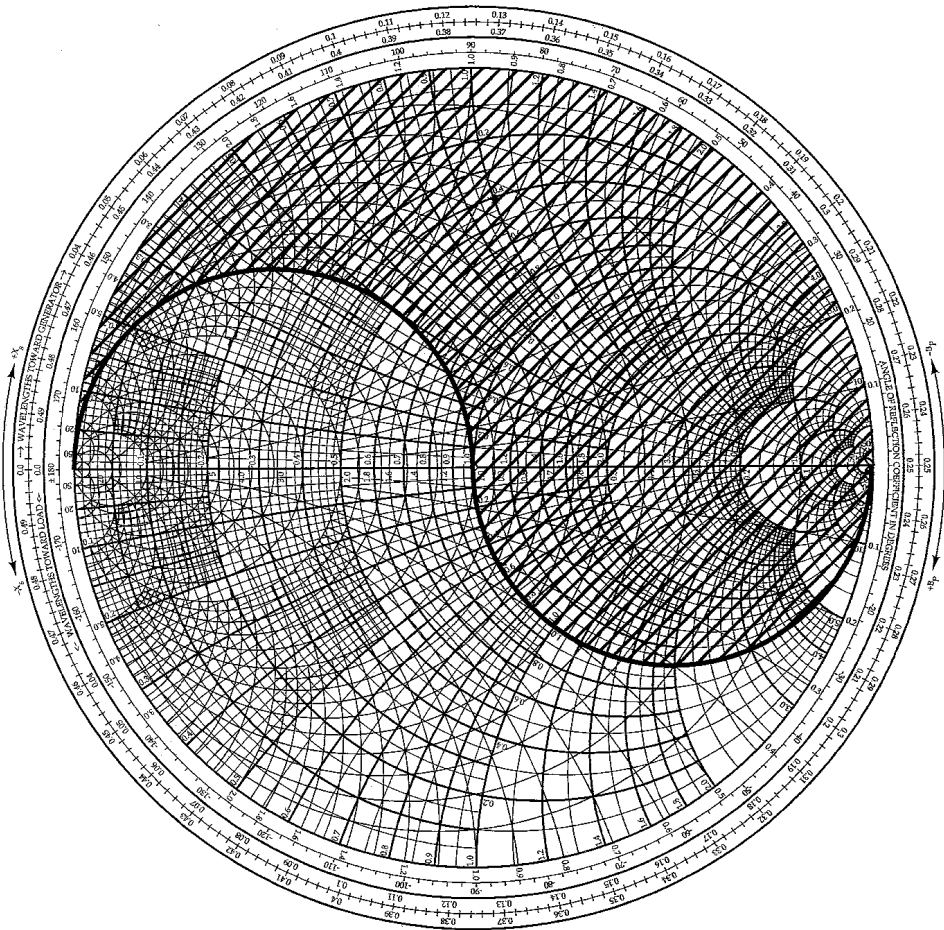
$$Q_n = \frac{|X_s|}{R_s} \quad (2.4.2)$$

If the equivalent parallel input admittance at the node is $G_p + jB_p$, the circuit node Q can be expressed in the form

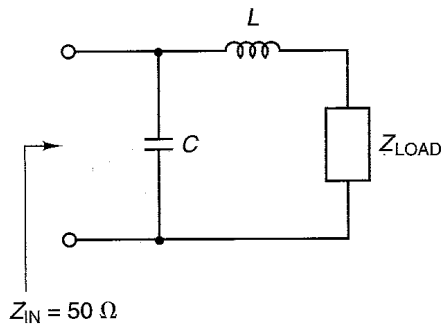
$$Q_n = \frac{|B_p|}{G_p} \quad (2.4.3)$$

For example, the normalized series input impedance of the circuit in Fig. 2.4.8a at point B (see Fig. 2.4.8b) is $0.2 + j0.4$; therefore, the circuit node Q , from (2.4.2), is $Q_n = 0.4/0.2 = 2$. Also, using the Smith chart, the equivalent parallel admittance is readily found to be $1 - j2$, producing a circuit node Q , according to (2.4.3), of $Q_n = 2/1 = 2$, which agrees with the result from (2.4.2).

The circuit in Fig. 2.4.8a is redrawn in Fig. 2.4.13a. The circuit is excited with a source voltage having a $50\text{-}\Omega$ source impedance (i.e., for a proper match at the input), and the output voltage is taken across the real part of the load impedance (i.e., the $10\text{-}\Omega$ resistor). For convenience, the two 3.18-nH inductors are combined, and the circuit can be viewed as performing a match between a $10\text{-}\Omega$ load and a $50\text{-}\Omega$ input resistance. The frequency response of the circuit



(a)



(b)

Figure 2.4.12 Forbidden region in the ZY Smith chart to match a given Z_{LOAD} to 50Ω using a series L -shunt C matching network.

is illustrated in Fig. 2.4.13b. Figure 2.4.13b shows that a peak occurs at the frequency f_o where the match occurs, and the filter attenuates the frequencies above and below f_o .

For a narrowband range of frequencies around f_o , the filter can be viewed as a bandpass filter with a loaded Q , which can be calculated using (2.4.1). The equivalent bandpass filter is shown in Fig. 2.4.13c, as well as the frequency response. This circuit was obtained by changing $Z_B = 10 + j20 \Omega$ to an equivalent admittance (i.e., 50Ω in parallel with $j25 \Omega$). The tuned circuit in Fig. 2.4.13c is loaded by the resistance $R_T = 50 \parallel 50 = 25 \Omega$. Hence, the loaded Q of the bandpass filter is given by

$$Q_L = \frac{\omega_o}{\text{BW}} = \omega_o R_T C = \frac{|B_C|}{G_T} = \frac{R_T}{|X_C|} = \frac{25}{25} = 1 \quad (2.4.4)$$

In Fig. 2.4.13c, since the gain at $f_o = 500$ MHz is -6 dB, it follows that the value of $|v_B|$ is $|v_s|/2$. Then, from Fig. 2.4.13a, we have

$$|v_o| = |v_B| \frac{10}{|10 + j20|} = \frac{|v_s|}{2} (0.447) = |v_s| (0.224)$$

or

$$20 \log \frac{|v_o|}{|v_s|} = -13 \text{ dB}$$

in agreement with the gain at $f_o = 500$ MHz in Fig. 2.4.13b.

The equivalent bandpass filter helps to explain the *bell-shape* response of the circuit in the neighborhood of f_o . Away from the neighborhood of f_o , the frequency responses of the circuit in Figs. 2.4.13a and 2.4.13c are quite different.

A question arises about the relation between the circuit node Q and the loaded Q associated with the response in the neighborhood of f_o . Referring to Fig. 2.4.13a, it is also observed that the circuit node Q looking toward the $50\text{-}\Omega$ source is 2 (since the normalized admittance of the $50\text{-}\Omega$ source and the $-j25 \Omega$ capacitor is $1 + j2$). Comparing Q_n in (2.4.3) with Q_L in (2.4.4), it follows that in the neighborhood of f_o the loaded Q of the Ell matching networks is given by

$$Q_L = \frac{Q_n}{2} \quad (2.4.5)$$

Using (2.4.5), the loaded Q of the circuit in Fig. 2.4.13a is

$$Q_L = \frac{Q_n}{2} = \frac{2}{2} = 1$$

Hence, the approximate bandwidth of the circuit in Fig. 2.4.13a is

$$\text{BW} \approx \frac{f_o}{Q_L} = \frac{500 \times 10^6}{1} = 500 \text{ MHz}$$

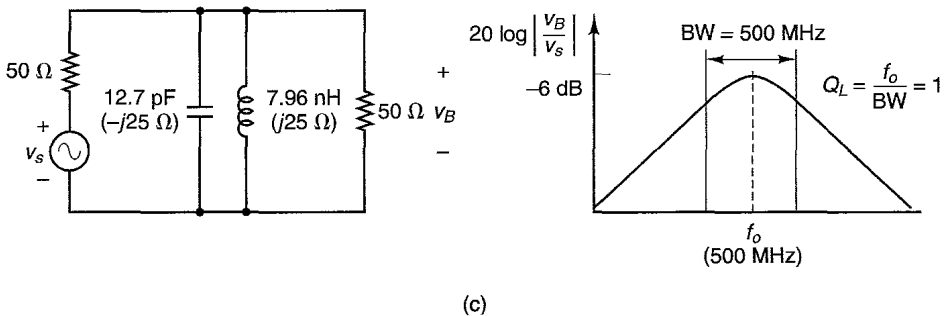
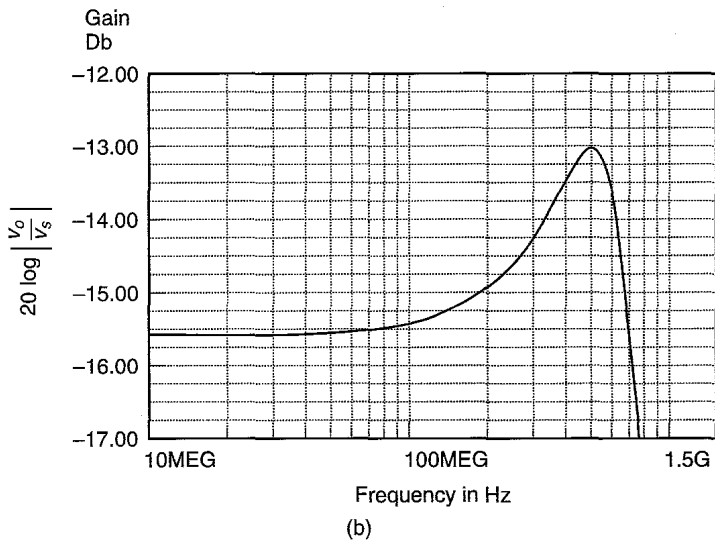
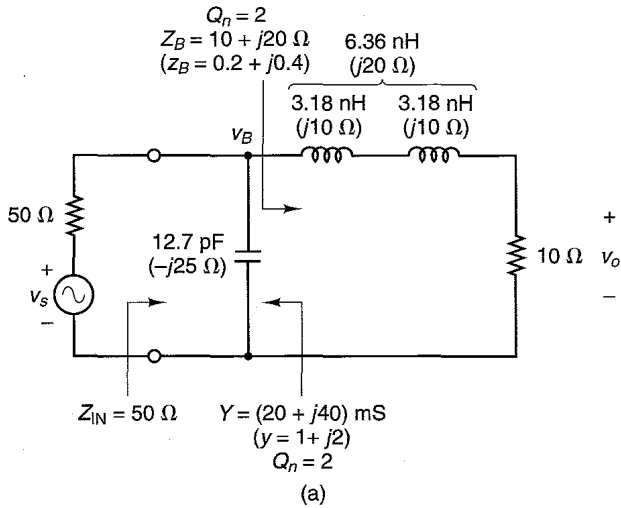


Figure 2.4.13 (a) The matching network from Fig. 2.4.8a; (b) its frequency response (the program *Microcap III* was used); (c) equivalent bandpass filter configuration in the neighborhood of f_o , and its frequency response.

The frequency response in Fig. 2.4.13b shows that the 3-dB point for $f > f_o$ occurs at $f = 720$ MHz. For $f < f_o$, there is no 3-dB point. This is due to the low value of Q_n in Fig. 2.4.13a and, consequently, to the frequency response characteristics of the circuit for $f < f_o$. However, if we assume that the bell-shape response is symmetrical around f_o , it follows that the bandwidth is approximately

$$\text{BW} \approx 2(720 \times 10^6 - 500 \times 10^6) = 440 \text{ MHz}$$

in reasonable agreement with the predicted bandwidth.

The following example illustrates the bandpass characteristics of an Ell network when a high value of Q_n is used.

Example 2.4.5

The low-pass Ell network shown in Fig. 2.4.14a was designed to transform a 200- Ω load to an input resistance of 20 Ω (see Fig. 2.4.14b) at 500 MHz. Determine the loaded Q of the circuit.

Solution. From Fig. 2.4.14b, the impedance at point B is $z_B = 0.1 - j0.3$. Hence, the circuit node Q is $Q_n = 0.3/0.1 = 3$. Also, observe that the normalized impedance looking toward the source is $z_B = 0.1 + j0.3$, giving $Q_n = 3$.

From (2.4.4), it follows that Q_L is

$$Q_L = \frac{Q_n}{2} = \frac{3}{2} = 1.5$$

and the expected bandwidth is

$$\text{BW} \approx \frac{f_o}{Q_L} = \frac{500 \times 10^6}{1.5} = 333.33 \text{ MHz}$$

The frequency response of the circuit in Fig. 2.4.14c shows that $f_o = 500$ MHz and $\text{BW} = 650 \times 10^6 - 275 \times 10^6 = 375$ MHz. Hence,

$$Q_L = \frac{500}{375} = 1.33$$

These values agree with the expected bandwidth and Q_L .

In conclusion, in order to obtain a high value of Q_L , the circuit node Q must be high. For the low-pass matching circuit, the attenuation characteristics for frequencies above f_o are obviously better than for frequencies below f_o . For bandpass applications, the attenuation of the harmonics above f_o is important, and the Ell filters will provide an attenuation of -12 dB/octave.

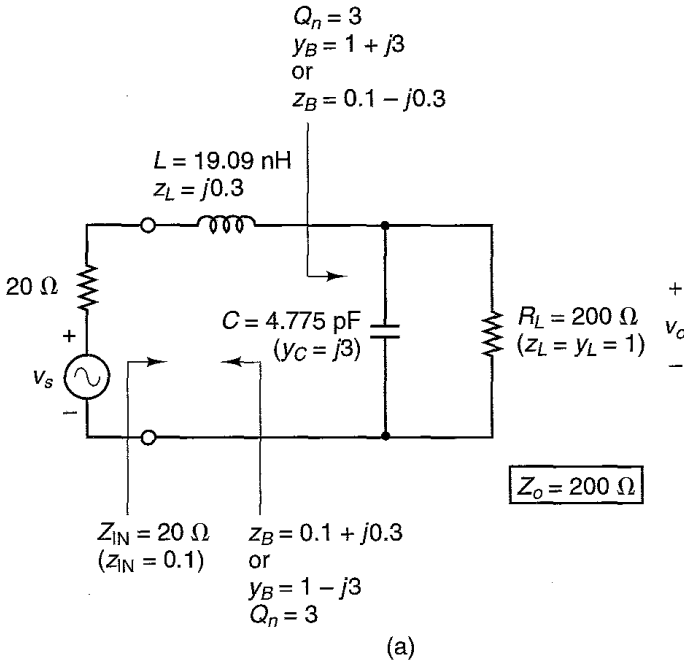
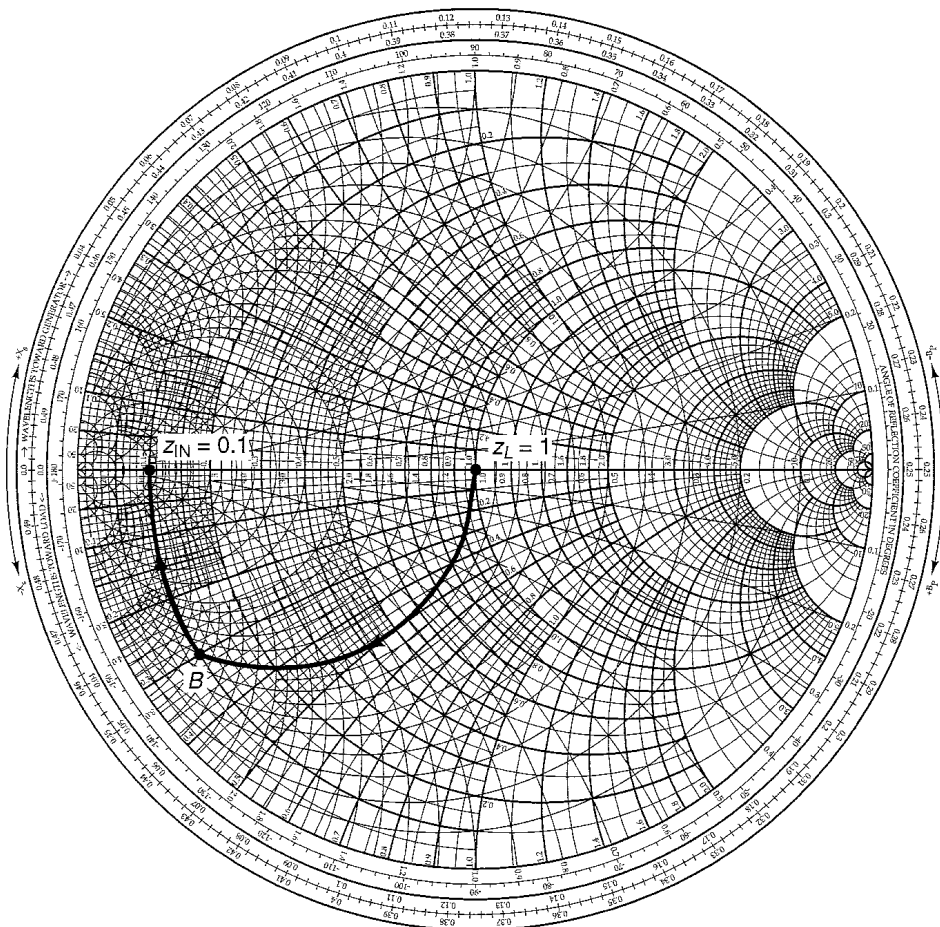


Figure 2.4.14 (a) The low-pass matching circuit for Example 2.4.5; (b) the design in the ZY Smith chart; (c) the frequency response (the program *Microcap-III* was used).

In many cases, the matching network provides a match to a complex impedance (or admittance). The frequency response of these circuits can be obtained using an excitation whose impedance (or admittance) is the complex conjugate of the impedance (or admittance) presented by the matching network. In some cases, it is convenient to represent the source excitation by its Norton's equivalent circuit. For example, in Fig. 2.4.10c the matching network was designed to present an output admittance of $Y_{OUT} = (8 - j12)$ mS. The frequency response of this circuit can be performed using a current source in parallel with a source admittance of $(8 + j12)$ mS.

When a high value of Q_L is a design consideration, the Ell matching networks in Fig. 2.4.2 might not be suitable since the Q_L cannot be controlled when matching with two elements. In fact, with the Ell matching networks we have to accept the resulting Q_n in the design. For example, in the design shown in Fig. 2.4.13a the value of Q_n is determined by the equivalent impedance at point B—namely, $z = 0.2 + j0.4$; therefore, in this circuit Q_n is fixed at the value of 2.

Higher values of Q_L than those obtained with the Ell circuits can be obtained using matching circuits with three elements. The addition of a third element to an Ell matching network results in either the lossless Tee network (also denoted as *T* network) or the lossless Pi network (also denoted as *Π* network) shown in Fig. 2.4.15.



(b)

Figure 2.4.14 Continued

The addition of a third element introduces flexibility in the selection of the loaded Q , since the equivalent series impedance (or the equivalent parallel admittance) at the nodes in the circuit will determine various values of Q_n . Obviously, a high value of Q_n in the circuit will result in a high value of Q_L . However, it is not simple to exactly relate Q_n to Q_L in these circuits. The Q of a Tee or Pi network is normally taken as the highest value of Q_n in the circuit.

Several equivalent series input impedances can have the same Q_n . For example, the normalized impedances $z = 0.5 \pm j0.5$ have a Q_n of 1, as well as the impedances $z = 1 \pm j1$. Constant Q_n contours can be drawn on the Smith chart. This is illustrated in Fig. 2.4.16, where constant Q_n contours of 1, 5, and 10 are shown.

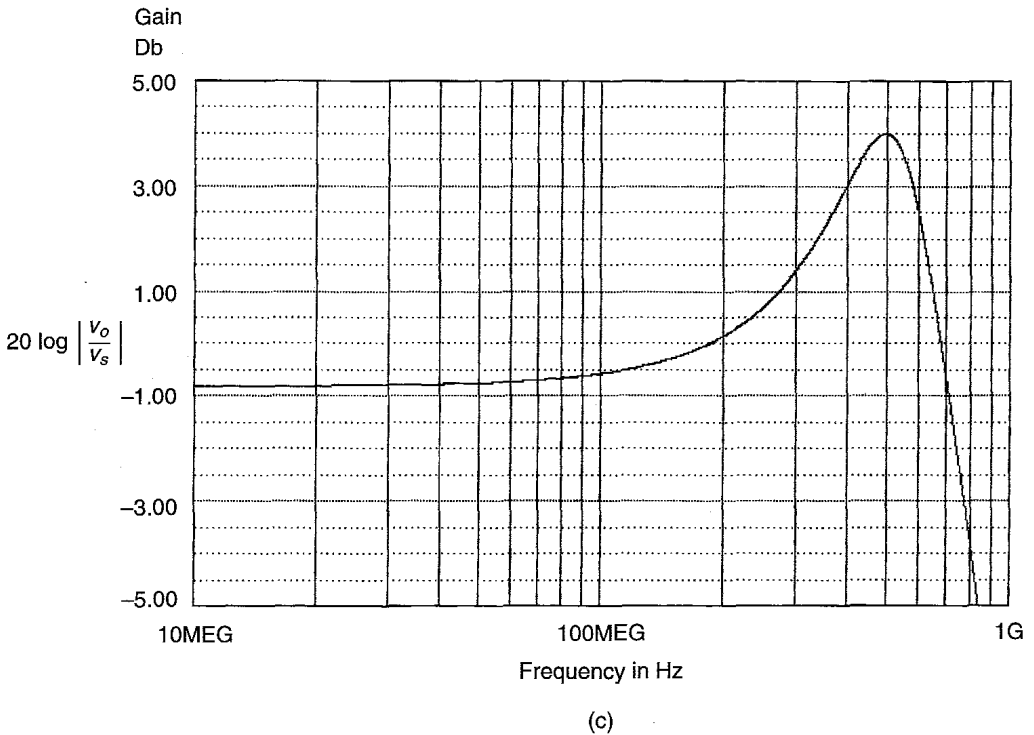


Figure 2.4.14 Continued

The upper and lower parts of the constant- Q contours can be shown to satisfy a circle equation as follows. Since

$$z = r + jx = \frac{1 + \Gamma}{1 - \Gamma} = \frac{1 - U^2 - V^2}{(1 - U)^2 + V^2} + j \frac{2U}{(1 - U)^2 + V^2}$$

then

$$Q_n = \frac{|x|}{r} = \frac{2U}{1 - U^2 - V^2}$$

which can be written as

$$U^2 + \left(V \pm \frac{1}{Q_n} \right)^2 = 1 + \frac{1}{Q_n^2} \quad (2.4.6)$$

The plus sign applies when x is positive, and the minus sign when x is negative.

Equation (2.4.6) is recognized as the equation of a circle. For $x > 0$, the center in the Γ plane is at $(0, -1/Q_n)$, and for $x < 0$ at $(0, 1/Q_n)$; the radius of the circle is

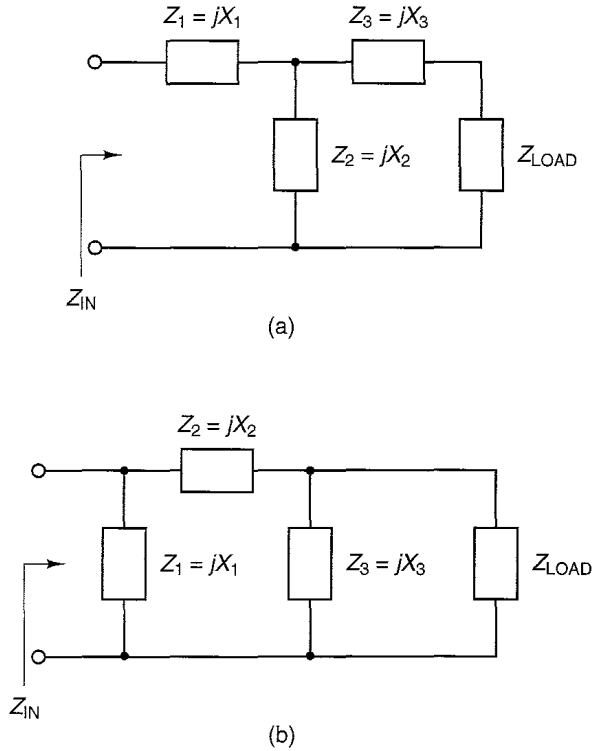


Figure 2.4.15 (a) Lossless Tee network; (b) lossless Pi network.

$$\sqrt{1 + \frac{1}{Q_n^2}}$$

For example, for the $Q_n = 5$ contour in Fig. 2.4.16, the upper and lower parts of the contour are simply one half of a circle centered at $(0, \mp 0.2)$, respectively, with radius of

$$\sqrt{1 + \frac{1}{25}} = 1.02$$

The following example illustrates the design of Tee and Pi networks for a given Q_n factor.

Example 2.4.6

Design two Tee networks to transform the load impedance $Z_{LOAD} = 50 \Omega$ to the input impedance $Z_{IN} = 10 - j15 \Omega$ with a Q_n of 5.

Solution. The design of a Tee matching network with a Q_n of 5 is illustrated in Fig. 2.4.17a, where a normalizing impedance of 50Ω was used. The motion from A to B produces a series inductor with impedance $z_{L_1} = j2$; the motion from B to C produces a

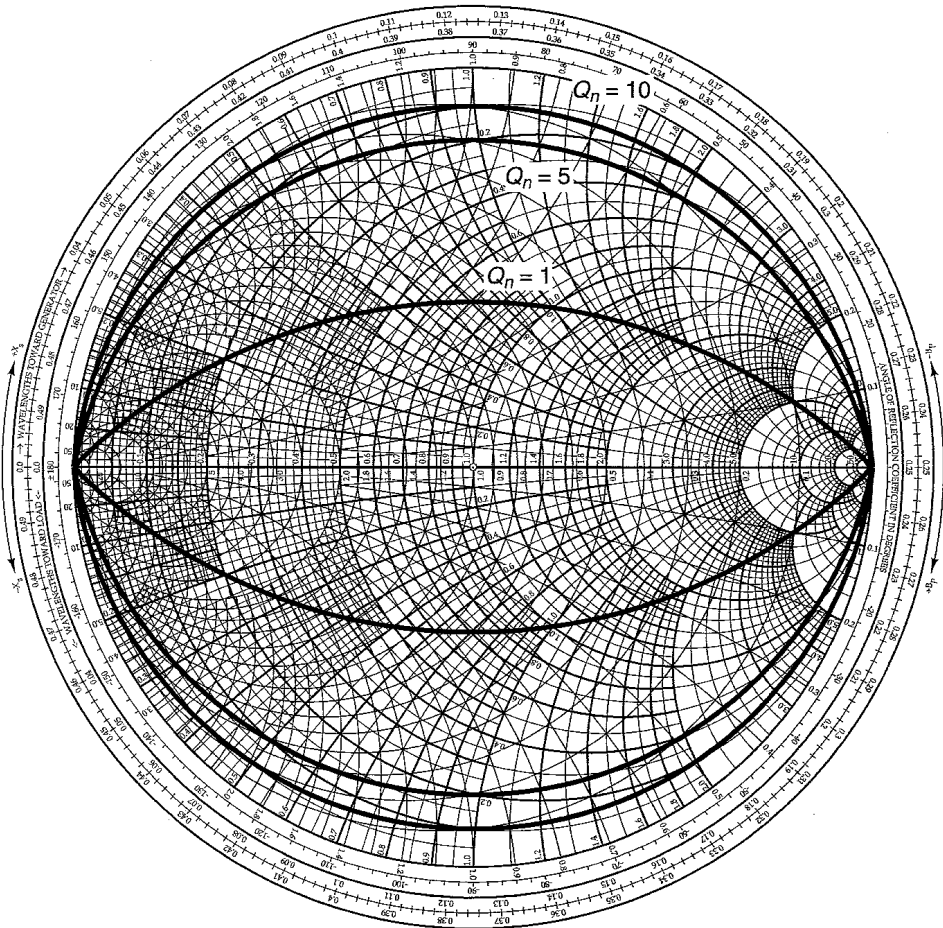


Figure 2.4.16 Constant Q_n contours for $Q_n = 1, 5,$ and 10 .

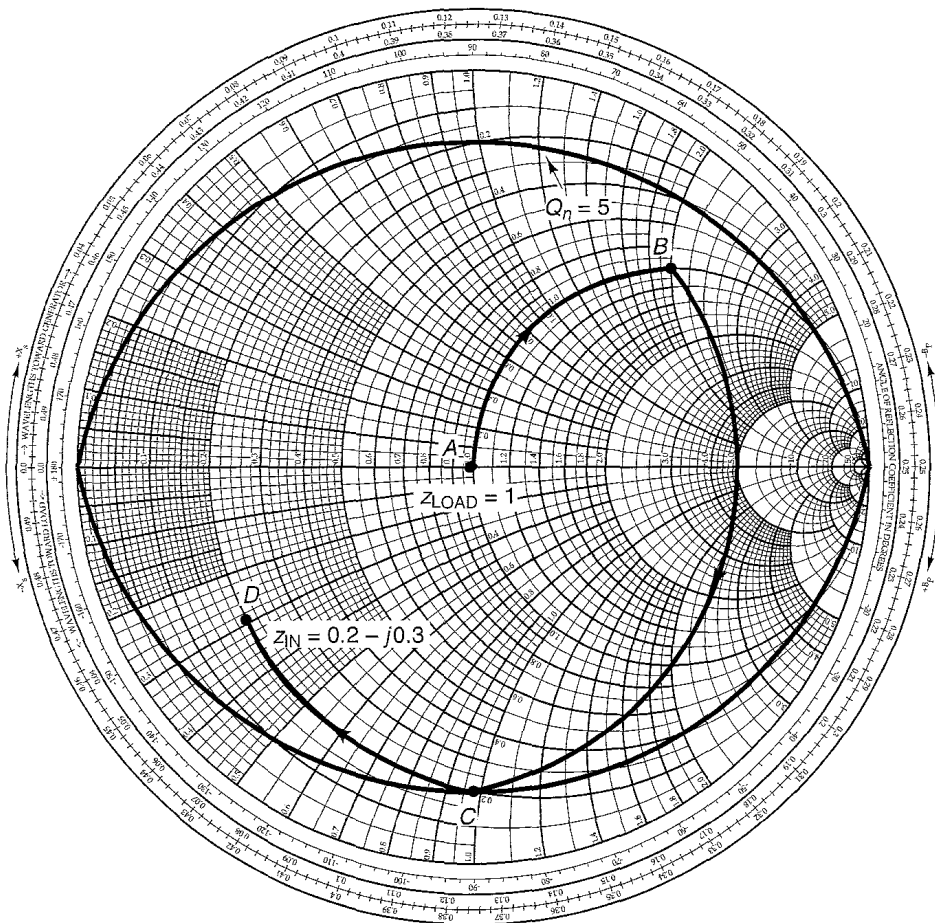
shunt capacitor with admittance $y_C = j0.96 - (-j0.4) = j1.36$ (or $z_C = 1/j1.36 = -j0.735$); and the motion from C to D produces a series inductor with impedance $z_{L_2} = -j0.3 - (-j1) = j0.7$. The impedance value at point C , which touches the $Q_n = 5$ contour, determines the Q of the network. The resulting Tee network is shown in Fig. 2.4.17b, and its frequency response at 500 MHz is shown in Fig. 2.4.17c. From Fig. 2.4.17c, the loaded Q is calculated to be

$$Q_L = \frac{f_o}{\text{BW}} = \frac{500 \times 10^6}{568 \times 10^6 - 382 \times 10^6} = 2.7$$

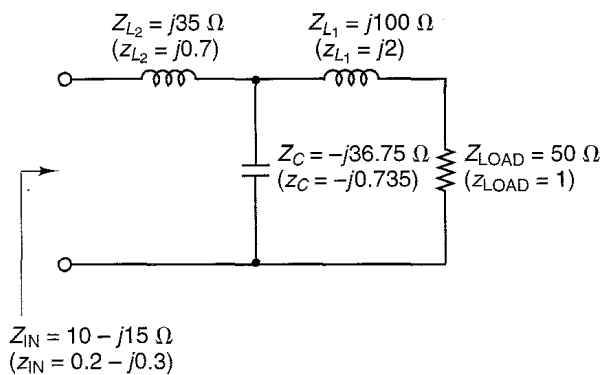
It is simple to verify that the other Tee network design, shown in Fig. 2.4.17d, transforms $Z_{\text{LOAD}} = 50 \Omega$ to $Z_{\text{IN}} = 10 - j15 \Omega$.

Example 2.4.7

Design two Pi networks to transform the load impedance $Z_{\text{LOAD}} = 50 \Omega$ to the input impedance $Z_{\text{IN}} = 150 \Omega$ with a Q_n of 5.

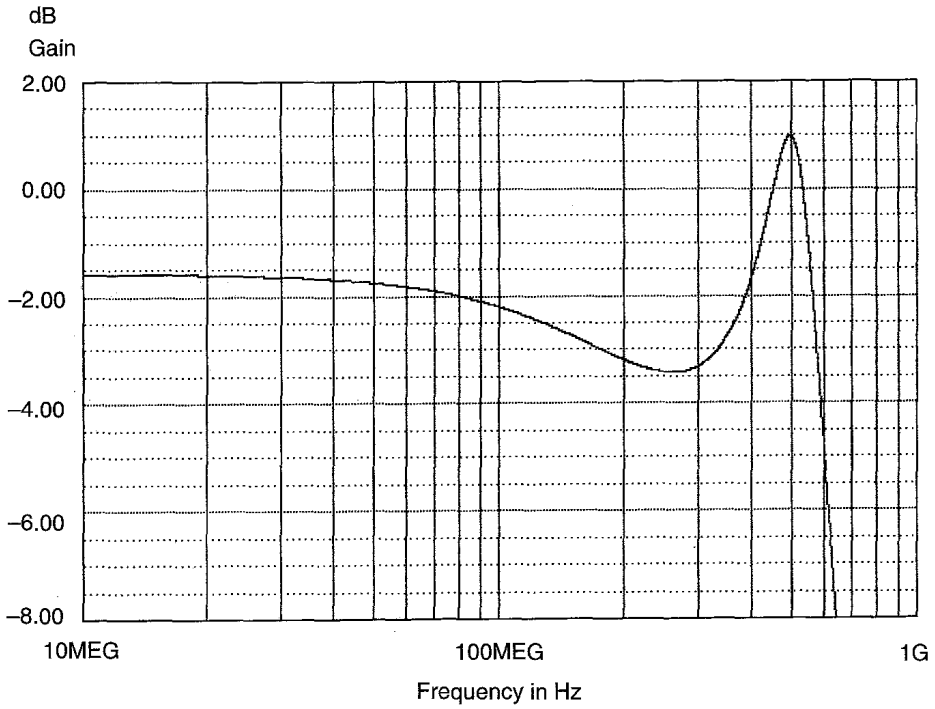


(a)

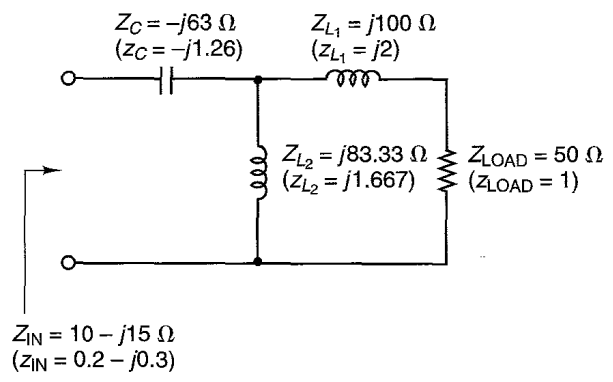


(b)

Figure 2.4.17 (a) Smith chart design of a Tee network for Example 2.4.6; (b) the Tee matching network; (c) the frequency response (the program *Microcap-III* was used); (d) another Tee network design.



(c)



$Z_{IN} = 10 - j15 \Omega$
 $(z_{IN} = 0.2 - j0.3)$

(d)

Figure 2.4.17 Continued

Solution. The design of a Pi network with a Q_n of 5 is illustrated in Fig. 2.4.18a. The motion from A to B requires a shunt inductor with admittance $y_{L_1} = -j2.9$ (or $z_{L_1} = j0.345$); the motion from B to C is produced by a series inductor with impedance $z_{L_2} = j0.55 - j0.31 = j0.24$. Point C is on the $Q_n = 5$ contour; therefore, the circuit Q is 5. Finally, the motion from C to D produces a shunt capacitor whose admittance is $y_C = 0 - (-j1.75) = j1.75$ (or $z_C = -j0.571$). The resulting Pi network is shown in Fig. 2.4.18b.

It is simple to verify that the other Pi network design, shown in Fig. 2.4.18c, transforms $Z_{\text{LOAD}} = 50 \Omega$ to $Z_{\text{IN}} = 150 \Omega$.

The design of lossless matching networks is accomplished by moving along constant-resistance and constant-conductance circles in the Smith chart. A question commonly asked is, “What happens if one moves along a constant-reactance or constant-susceptance circle in the Smith chart?”. The answer is simple: A motion along a constant-reactance circle introduces a series resistance, and a motion along a constant-susceptance circle introduces a shunt resistance. The resistor is positive if the motion is along the constant resistance circle in the direction that r increases, or along the constant susceptance circle in the direction that g increases. It is important to emphasize that resistors are lossy elements and, in general, are avoided in the design of matching networks.

Example 2.4.8

A matching network is designed as shown in the ZY Smith chart in Fig. 2.4.19a to transform a $50\text{-}\Omega$ load to the input impedance $Z_{\text{IN}} = 50(1.6 - j1.2) \Omega$. Draw the matching circuit and determine the component values.

Solution. The motion from A to B results in a series inductor of value $z_L = j0.6$ (or $Z_L = 50(j0.6) = j30 \Omega$). The motion from B to C , along the constant-reactance circle $x_L = 0.6$, results in a series resistor. The impedance at B is $z_B = 1 + j0.6$, and the impedance at C is $z_C = 2.3 + j0.6$. Therefore, the value of the series resistor is $r = r_C - r_B = 2.3 - 1 = 1.3$, or $R = 50r = 50(1.3) = 65 \Omega$. Finally, the motion from C to D results in a capacitor of value $y_C = j0.3 - (-j0.1) = j0.4$ [or $z_C = -j2.5$, $Z_C = 50(-j2.5) = -j125 \Omega$]. The matching circuit is shown in Fig. 2.4.19b.

In a microwave amplifier (see Fig. 2.4.1), the input and output matching networks provide the appropriate ac impedances to the transistor. The transistor must also be biased at an appropriate quiescent point. A complete microwave amplifier contains both dc bias components and the ac matching networks. RFCs, bypass capacitors, and coupling capacitors need to be introduced so the dc bias components do not affect the ac performance of the amplifier. An example of a discrete microwave amplifier is shown in Fig. 2.4.20a. The capacitors denoted by C_B are bypass capacitors (they behave like short circuits at the frequency of operation). The RFCs behave like open circuits at the frequency of operation. The resistors R_1 , R_2 , R_C , and R_E set the quiescent point of the transistor. The input matching circuit consists of C_1 and L_1 , and the output matching circuit consists of C_2 and L_2 . In addition, the capacitors C_1 and C_2 act like coupling capacitors. That is, they isolate the dc bias circuit from the

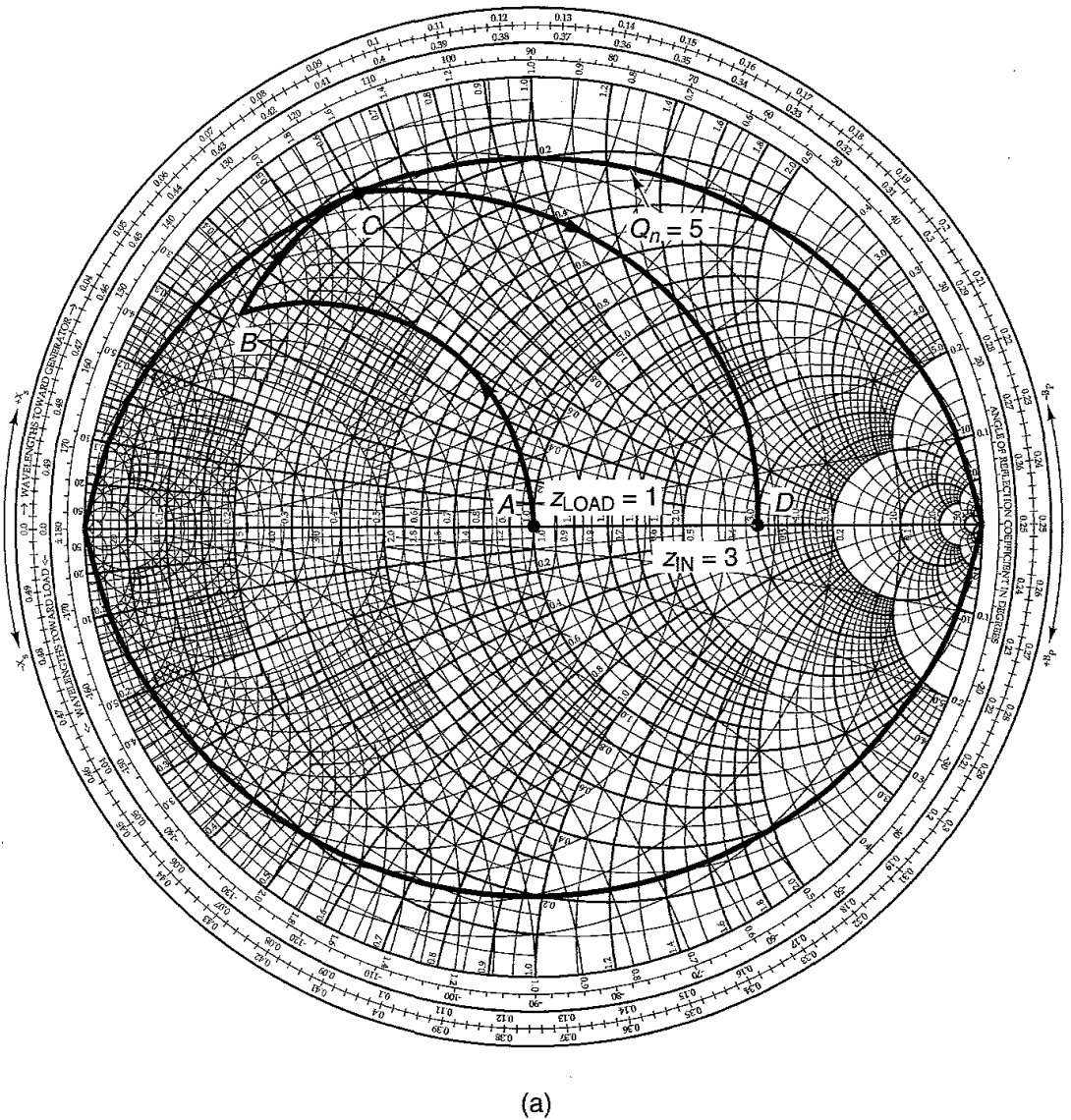
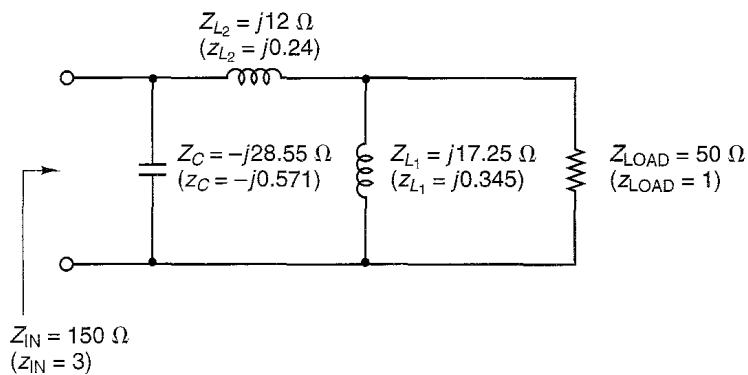
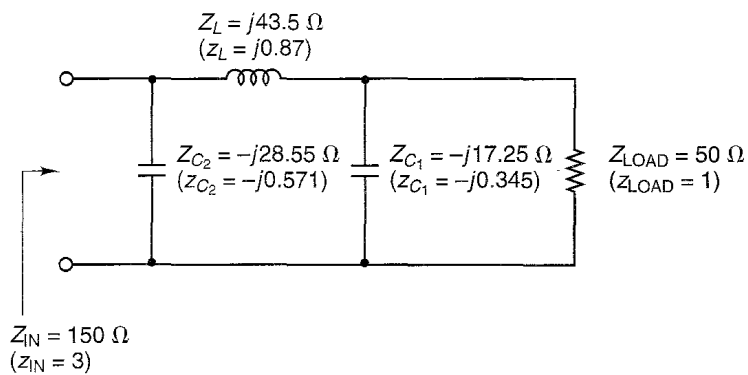


Figure 2.4.18 (a) Smith chart design of a Pi network for Example 2.4.7; (b) the Pi matching network; (c) another Pi network design.

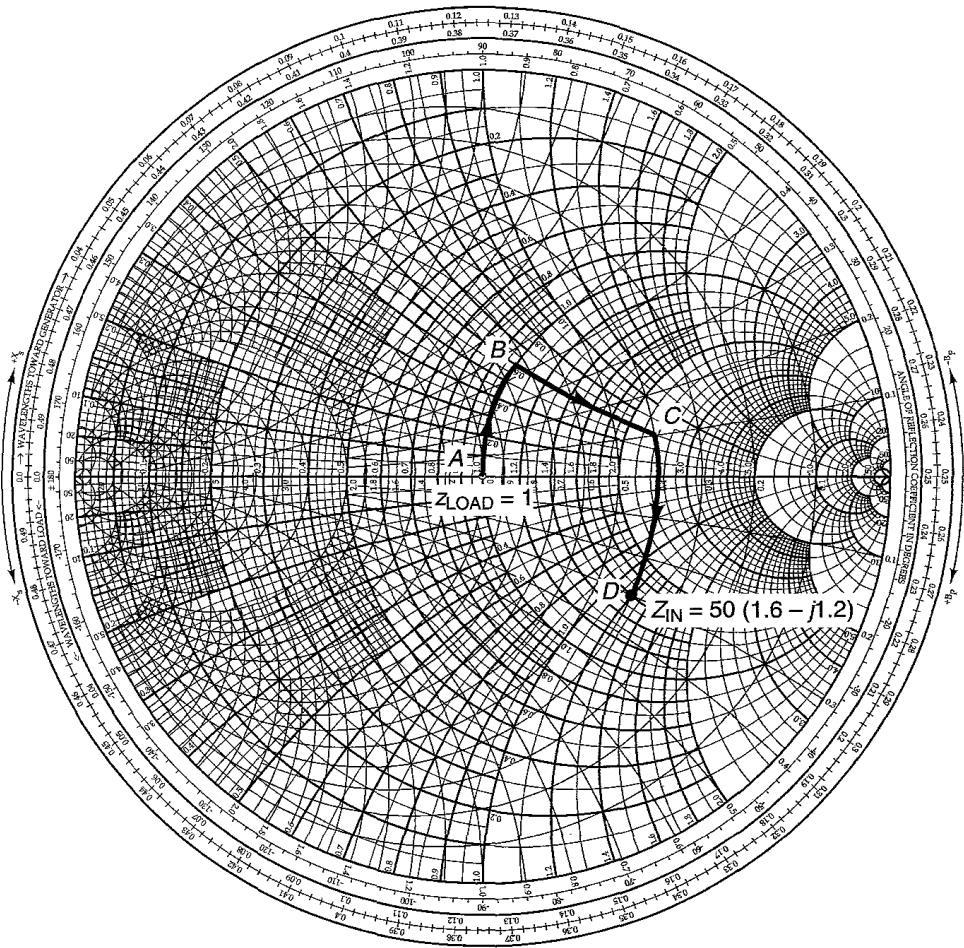


(b)

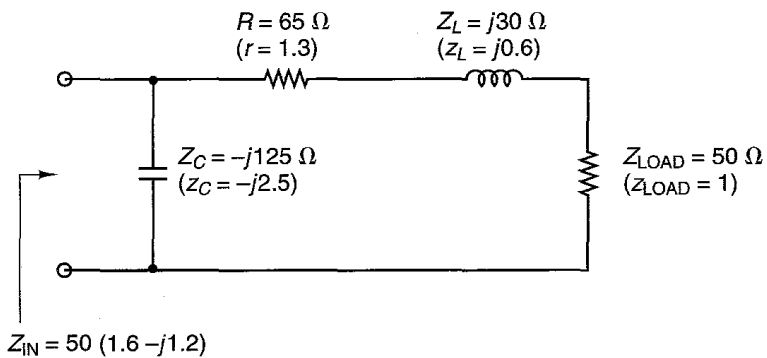


(c)

Figure 2.4.18 Continued



(a)



(b)

Figure 2.4.19 (a) Matching of $Z_{LOAD} = 1$ to $z_{IN} = 1.6 - j1.2$; (b) the matching circuit.

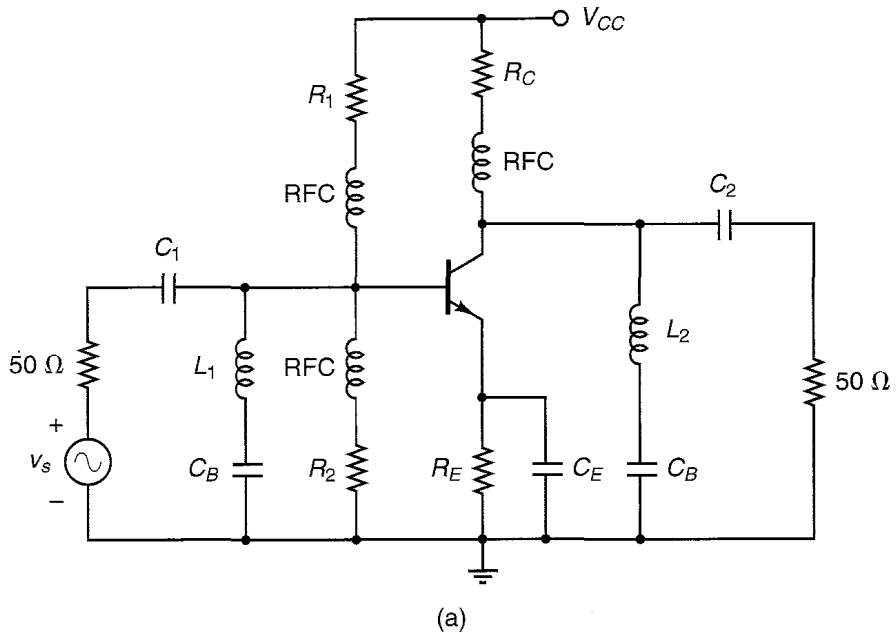


Figure 2.4.20 (a) A discrete microwave amplifier; (b) the dc model; (c) the ac model.

input source. The dc model of the amplifier is shown in Fig. 2.4.20b, and the ac model in Fig. 2.4.20c.

2.5 MICROSTRIP MATCHING NETWORKS

Microstrip lines

Microstrip lines are used extensively in building microwave transistor amplifiers because they are easily fabricated using printed-circuit techniques. Network interconnections and the placement of lumped and transistor devices

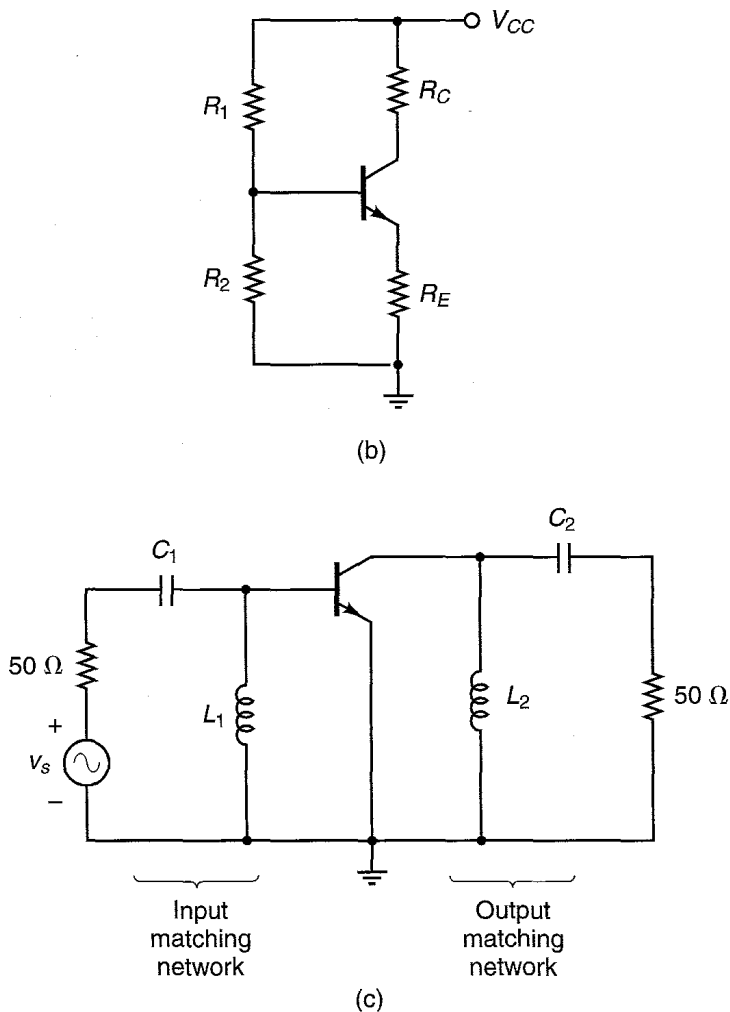


Figure 2.4.20 Continued

are easily made on its metal surface. The superior performance characteristics of the microstrip line make it one of the most important mediums of transmission in microwave transistor amplifiers and in microwave integrated-circuit technology.

A microstrip line is, by definition, a transmission line consisting of a strip conductor and a ground plane separated by a dielectric medium. Figure 2.5.1

illustrates the microstrip geometry. The dielectric material serves as a substrate and is sandwiched between the strip conductor and the ground plane. The relative dielectric constant of the substrate, ϵ_r , and ϵ are related by $\epsilon = \epsilon_r \epsilon_o$, where $\epsilon_o = 8.854 \times 10^{-12}$ F/m. Some typical dielectric substrates are RT/Duroid® (a trademark of Rogers Corporation, Chandler, Arizona), which is available with several values of ϵ_r (e.g., $\epsilon = 2.23\epsilon_o$, $\epsilon = 6\epsilon_o$, $\epsilon = 10.5\epsilon_o$, etc.); quartz ($\epsilon = 3.7\epsilon_o$), alumina ($\epsilon = 9\epsilon_o$); and Epsilam-10® ($\epsilon = 10\epsilon_o$).

The electromagnetic field lines in the microstrip are not contained entirely in the substrate. Therefore, the propagating mode in the microstrip is not a pure transverse electromagnetic mode (TEM mode) but a quasi-TEM. Assuming a quasi-TEM mode of propagation in the microstrip line, the phase velocity is given by

$$v_p = \frac{c}{\sqrt{\epsilon_{ff}}} \tag{2.5.1}$$

where c is the speed of light (i.e., 3×10^8 m/s) and ϵ_{ff} is the effective relative dielectric constant of the microstrip. The effective relative dielectric constant of the microstrip is related to the relative dielectric constant of the dielectric substrate and also takes into account the effect of the external electromagnetic fields (i.e., fringing effects must be considered).

Since $Z_o = \sqrt{L/C}$ and $v_p = 1/\sqrt{LC}$, the characteristic impedance of the microstrip line can be expressed in the form

$$Z_o = \frac{1}{v_p C} \tag{2.5.2}$$

where C is the capacitance per unit length of the microstrip. The wavelength in the microstrip line is given by

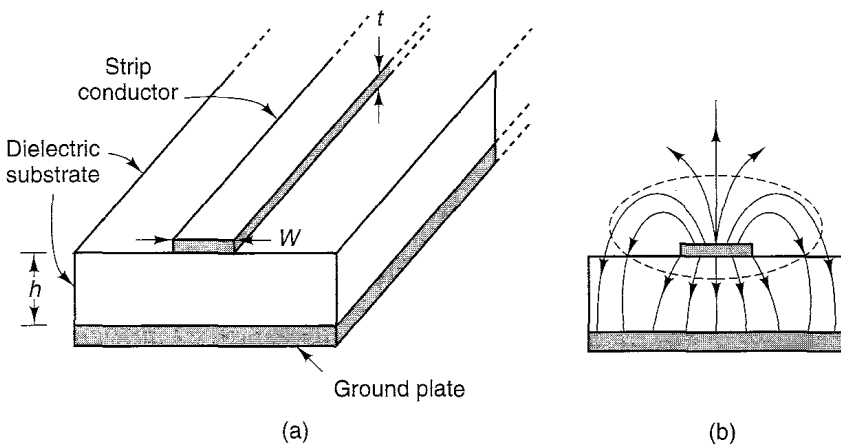


Figure 2.5.1 Microstrip geometry and field configuration. In (b), the solid lines represent electric field lines and the dashed line represents a magnetic field line.

$$\lambda = \frac{v_p}{f} = \frac{c}{f\sqrt{\epsilon_{ff}}} = \frac{\lambda_0}{\sqrt{\epsilon_{ff}}} \quad (2.5.3)$$

where λ_0 is the free-space wavelength.

As seen from (2.5.1), (2.5.2), and (2.5.3), the evaluation of v_p , Z_o , and λ in a microstrip line requires the evaluation of ϵ_{ff} and C . There are different methods for determining ϵ_{ff} and C and, of course, closed-form expressions are of great importance in microstrip-line design. The evaluation of ϵ_{ff} and C based on a quasi-TEM mode is accurate for design purposes at lower microwave frequencies. However, at higher microwave frequencies the longitudinal components of the electromagnetic fields are significant and the quasi-TEM assumption is no longer valid.

A useful set of relations for the characteristic impedance, assuming zero or negligible thickness of the strip conductor (i.e., $t/h < 0.005$), is as follows [2.1]:

For $W/h \leq 1$:

$$Z_o = \frac{60}{\sqrt{\epsilon_{ff}}} \ln \left(8 \frac{h}{W} + 0.25 \frac{W}{h} \right) \quad (2.5.4)$$

where

$$\epsilon_{ff} = \frac{\epsilon_r + 1}{2} + \frac{\epsilon_r - 1}{2} \left[\left(1 + 12 \frac{h}{W} \right)^{-1/2} + 0.04 \left(1 - \frac{W}{h} \right)^2 \right] \quad (2.5.5)$$

For $W/h \geq 1$:

$$Z_o = \frac{120\pi/\sqrt{\epsilon_{ff}}}{W/h + 1.393 + 0.667 \ln(W/h + 1.444)} \quad (2.5.6)$$

where

$$\epsilon_{ff} = \frac{\epsilon_r + 1}{2} + \frac{\epsilon_r - 1}{2} \left(1 + 12 \frac{h}{W} \right)^{-1/2} \quad (2.5.7)$$

Plots of the characteristic impedance, as well as the normalized wavelength, as a function of W/h are shown in Figs. 2.5.2 and 2.5.3.

Based on the results in (2.5.3), (2.5.5), and (2.5.7) and/or in experimental data, the wavelength in the microstrip line, assuming zero or negligible thickness (i.e., $t/h \leq 0.005$) for the strip conductor, is given by the following relations [2.3]:

For $W/h \geq 0.6$:

$$\lambda = \frac{\lambda_0}{\sqrt{\epsilon_r}} \left[\frac{\epsilon_r}{1 + 0.63(\epsilon_r - 1)(W/h)^{0.1255}} \right]^{1/2} \quad (2.5.8)$$

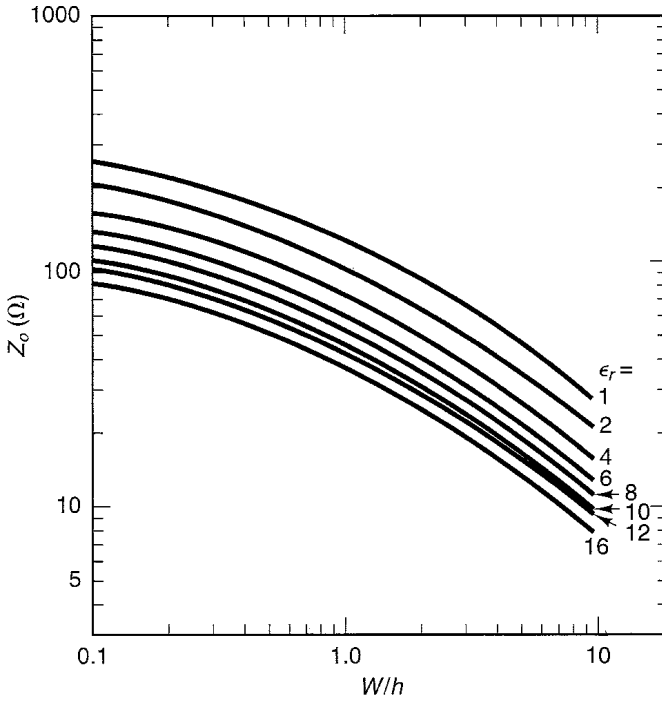


Figure 2.5.2 Characteristic impedance of the microstrip line versus W/h . (From H. Sobol [2.2]; copyright 1971, IEEE; reproduced with permission of IEEE.)

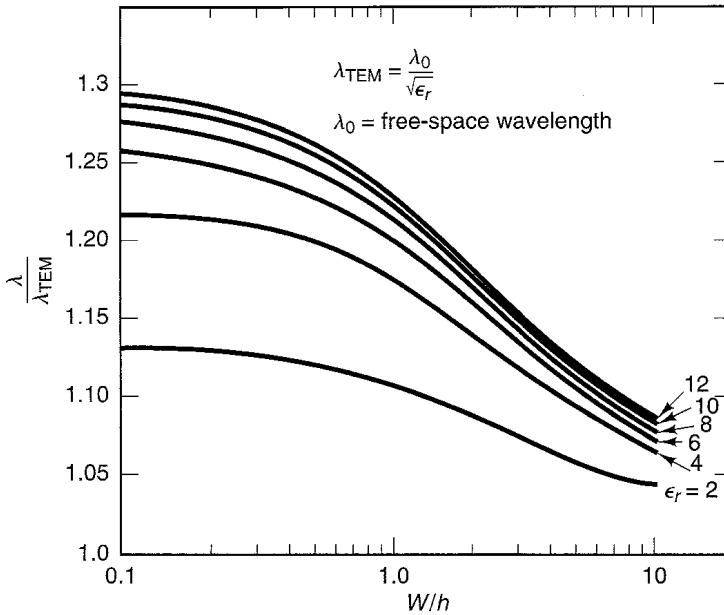


Figure 2.5.3 Normalized wavelength of the microstrip line versus W/h . (From H. Sobol [2.2]; copyright 1971, IEEE; reproduced with permission of IEEE.)

For $Wh < 0.6$:

$$\lambda = \frac{\lambda_0}{\sqrt{\epsilon_r}} \left[\frac{\epsilon_r}{1 + 0.6(\epsilon_r - 1)(W/h)^{0.0297}} \right]^{1/2} \quad (2.5.9)$$

For design purposes, a set of equations relating Z_o and ϵ_r to the ratio W/h of the microstrip line is desirable. Assuming zero or negligible thickness of the strip conductor (i.e., $t/h \leq 0.005$), the expressions are as follows [2.2]:

For $Wh \leq 2$:

$$\frac{W}{h} = \frac{8e^A}{e^{2A} - 2} \quad (2.5.10)$$

For $Wh \geq 2$:

$$\frac{W}{h} = \frac{2}{\pi} \left\{ B - 1 - \ln(2B - 1) + \frac{\epsilon_r - 1}{2\epsilon_r} \left[\ln(B - 1) + 0.39 - \frac{0.61}{\epsilon_r} \right] \right\} \quad (2.5.11)$$

where

$$A = \frac{Z_o}{60} \sqrt{\frac{\epsilon_r + 1}{2}} + \frac{\epsilon_r - 1}{\epsilon_r + 1} \left(0.23 + \frac{0.11}{\epsilon_r} \right)$$

and

$$B = \frac{377\pi}{2Z_o\sqrt{\epsilon_r}}$$

The zero or negligible thickness formulas given in (2.5.4) to (2.5.11) can be modified to include the thickness of the strip conductor. The first-order effect of a strip conductor of finite thickness t is to increase the capacitance. Therefore, an approximate correction is made by replacing the strip width W by the effective width W_{eff} . The following relations for W_{eff}/h are useful when $t < h$ and $t < W/2$:

For $W/h \geq 1/2\pi$:

$$\frac{W_{\text{eff}}}{h} = \frac{W}{h} + \frac{t}{\pi h} \left(1 + \ln \frac{2h}{t} \right)$$

For $W/h \leq 1/2\pi$:

$$\frac{W_{\text{eff}}}{h} = \frac{W}{h} + \frac{t}{\pi h} \left(1 + \ln \frac{4\pi W}{t} \right)$$

The restrictions $t < h$ and $t < W/2$ are usually satisfied since for dielectric substrates a typical thickness is $t = 0.002$ in.

Various substrate materials are available for the construction of microstrip lines, with practical values of ϵ_r ranging from 2 to 10. The substrate material comes plated on both sides with copper, and an additional layer of gold

plating on top of the cooper is usually added after the circuit pattern is etched in order to prevent oxidation. Typical plating thickness of copper is from 1/2 mils to 2 mils (1 inch = 1000 mils).

The value of ϵ_r and the dielectric thickness (h) determine the width of the microstrip line for a given Z_o . These parameters also determine the speed of propagation in the line, and consequently its length. Typical dielectric thickness are 25, 30, 40, 50, and 100 mils.

Example 2.5.1

A microstrip material with $\epsilon_r = 10$ and $h = 1.016$ mm is used to build a transmission line. Determine the width for the microstrip transmission line to have a characteristic impedance of 50Ω . Also determine the wavelength and the effective relative dielectric constant of the microstrip line.

Solution. Figures 2.5.2 and 2.5.3 can be used to obtain the approximate values of W , λ , and ϵ_{ff} . From Fig. 2.5.2, with $Z_o = 50 \Omega$ and $\epsilon_r = 10$, the value of W/h is approximate 1. Hence,

$$W = h = 1.016 \text{ mm} = 0.1016 \text{ cm}$$

Sometimes W and h are expressed in mils. Since 1 inch = 1000 mils and 1 inch = 2.54 cm, it follows that the width and height in mils are

$$W = h = 0.1016 \left(\frac{1000}{2.54} \right) = 40 \text{ mils}$$

From Fig. 2.5.3, with $W/h = 1$ and $\epsilon_r = 10$, it follows that the value of $\lambda/\lambda_{\text{TEM}}$ is approximately 1.23, or

$$\lambda = 1.23\lambda_{\text{TEM}} = 1.23 \frac{\lambda_0}{\sqrt{\epsilon_r}} = \frac{1.23}{\sqrt{10}} \lambda_0 = 0.389\lambda_0$$

Hence [see (2.5.3)],

$$\epsilon_{ff} = \left(\frac{1}{0.389} \right)^2 = 6.61$$

More accurate values for W , λ , and ϵ_{ff} can be obtained using (2.5.8) to (2.5.11). From (2.5.10),

$$A = \frac{50}{60} \sqrt{\frac{10+1}{2}} + \frac{10-1}{10+1} \left(0.23 + \frac{0.11}{10} \right) = 2.1515$$

and

$$\frac{W}{h} = \frac{8e^{2.1515}}{e^{2(2.1515)} - 2} = 0.9563$$

Then

$$W = 0.9563(40) = 38.2 \text{ mils}$$

From (2.5.8),

$$\lambda = \frac{\lambda_0}{\sqrt{10}} \left[\frac{10}{1 + 0.63(10 - 1)(0.9563)^{0.1255}} \right]^{1/2} = 0.387\lambda_0$$

and

$$\epsilon_{ff} = \left(\frac{1}{0.387} \right)^2 = 6.68$$

The width and ϵ_{ff} of several 50-Ω microstrip lines for various values of ϵ_r and h were calculated and are tabulated in Fig. 2.5.4. For example, for a microstrip line having an alumina substrate with $h = 25$ mils and $\epsilon_r = 9.6$, it follows from Fig. 2.5.4 that $W = 24.7$ mils for $Z_o = 50 \Omega$ and $\epsilon_{ff} = 6.46$.

The formulas presented thus far are valid at frequencies where the quasi-TEM assumption can be made. When the quasi-TEM assumption is not valid, ϵ_{ff} and Z_o are functions of frequency and, therefore, the microstrip line becomes dispersive. The phase velocity of the microstrip line decreases with increasing frequency. Therefore, $\epsilon_{ff}(f)$ increases with frequency. Also, the characteristic impedance of the microstrip line increases with frequency, and it follows that the effective width $W_{eff}(f)$ decreases.

The frequency below which dispersion may be neglected is given by

$$f_o(\text{GHz}) = 0.3 \sqrt{\frac{Z_o}{h\sqrt{\epsilon_r - 1}}}$$

where h must be expressed in centimeters.

An analytical expression that shows the effect of dispersion in $\epsilon_{ff}(f)$ is [2.1]

$$\epsilon_{ff}(f) = \epsilon_r - \frac{\epsilon_r - \epsilon_{ff}}{1 + G(f/f_p)^2} \quad (f \text{ in GHz})$$

	$\epsilon_r = 2.23$	4.54	6	9.6	10	30
$h = 25$ mils	$W = 76.4$ mils	46.7	37.5	24.7	23.8	6.01
	$\epsilon_{ff} = 1.91$	3.42	4.33	6.46	6.68	17.7
30	$W = 91.7$	56.1	45.0	29.7	28.5	7.21
	$\epsilon_{ff} = 1.91$	3.42	4.33	6.46	6.68	17.7
40	$W = 122.2$	74.7	60.0	39.6	38.0	9.6
	$\epsilon_{ff} = 1.91$	3.43	4.34	6.47	6.69	17.8
50	$W = 152.8$	93.4	75.0	49.4	47.6	12.0
	$\epsilon_{ff} = 1.91$	3.43	4.34	6.48	6.71	17.8
100	$W = 305.6$	186.8	150.1	98.9	95.1	24.1
	$\epsilon_{ff} = 1.91$	3.45	4.37	6.55	6.78	18.1

Figure 2.5.4 Width and ϵ_{ff} of microstrip lines for $Z_o = 50 \Omega$ for various ϵ_r and h values.

where

$$f_p = \frac{Z_o}{8\pi h} \quad (h \text{ in cm})$$

and

$$G = 0.6 + 0.009Z_o$$

Observe that when $f_p \gg f$, then $\epsilon_{ff}(f) \approx \epsilon_{ff}$. In other words, high-impedance lines on thin substrates are less dispersive.

The expression for the dispersion in Z_o is [2.1]

$$Z_o(f) = \frac{377h}{W_{\text{eff}}(f)\sqrt{\epsilon_{ff}}}$$

where

$$W_{\text{eff}}(f) = W + \frac{W_{\text{eff}}(0) - W}{1 + (f/f_p)^2}$$

and

$$W_{\text{eff}}(0) = \frac{377h}{Z_o(0)\sqrt{\epsilon_{ff}(0)}}$$

Another characteristic of the microstrip line is its attenuation. The attenuation constant is a function of the microstrip geometry, the electrical properties of the dielectric substrate and the conductors, and the frequency.

There are two types of losses in a microstrip line: a dielectric substrate loss and the ohmic skin loss in the conductors. The losses can be expressed as a loss per unit length along the microstrip line in terms of the attenuation factor α . Since the power carried by a wave traveling in the positive direction in a quasi-TEM mode is given by

$$P^+(z) = \frac{1}{2} \frac{|V^+|^2}{Z_o} e^{-2\alpha z} = P_0 e^{-2\alpha z} \quad (2.5.12)$$

where $P_0 = |V^+|^2/2Z_o$ is the power at $z = 0$. Then, from (2.5.12), we can write

$$\alpha = \frac{-dP(z)/dz}{2P(z)} = \alpha_d + \alpha_c$$

where α_d is the dielectric loss factor and α_c the conduction loss factor.

A useful set of expressions for calculating α_d is [2.1]

For a dielectric with low losses:

$$\alpha_d = 27.3 \frac{\epsilon_r}{\sqrt{\epsilon_{ff}}} \frac{\epsilon_{ff} - 1}{\epsilon_r - 1} \frac{\tan \delta}{\lambda_0} \quad \frac{\text{dB}}{\text{cm}} \quad (2.5.13)$$

where the loss tangent δ is given by

$$\tan \delta = \frac{\sigma}{\omega \epsilon}$$

For a dielectric with high losses:

$$\alpha_d = 4.34 \frac{\epsilon_{ff} - 1}{\sqrt{\epsilon_{ff}(\epsilon_r - 1)}} \left(\frac{\mu_0}{\epsilon_0} \right)^{1/2} \sigma \quad \frac{\text{dB}}{\text{cm}} \quad (2.5.14)$$

In (2.5.13) and (2.5.14), σ is the conductivity of the dielectric and $\mu_0 = 4\pi \times 10^{-7}$ H/m.

A set of expressions for calculating α_c is [2.1]

For $W/h \rightarrow \infty$:

$$\alpha_c = \frac{8.68}{Z_o W} R_s$$

where

$$R_s = \sqrt{\frac{\pi f \mu_0}{\sigma}}$$

For $W/h \leq 1/2\pi$:

$$\alpha_c = \frac{8.68 R_s P}{2\pi Z_o h} \left[1 + \frac{h}{W_{\text{eff}}} + \frac{h}{\pi W_{\text{eff}}} \left(\ln \frac{4\pi W}{t} + \frac{t}{W} \right) \right]$$

For $1/2\pi < W/h \leq 2$:

$$\alpha_c = \frac{8.68 R_s}{2\pi Z_o h} P Q$$

For $W/h \geq 2$:

$$\alpha_c = \frac{8.68 R_s Q}{Z_o h} \left\{ \frac{W_{\text{eff}}}{h} + \frac{2}{\pi} \ln \left[2\pi e \left(\frac{W_{\text{eff}}}{2h} + 0.94 \right) \right] \right\}^{-2} \left[\frac{W_{\text{eff}}}{h} + \frac{W_{\text{eff}}/\pi h}{(W_{\text{eff}}/2h) + 0.94} \right]$$

where

$$P = 1 - \left(\frac{W_{\text{eff}}}{4h} \right)^2$$

and

$$Q = 1 + \frac{h}{W_{\text{eff}}} + \frac{h}{\pi W_{\text{eff}}} \left(\ln \frac{2h}{t} - \frac{t}{h} \right)$$

In dielectric substrates, the dielectric losses are normally smaller than conductor losses. However, dielectric losses in silicon substrates can be of the same order or larger than conductor losses.

The quality factor Q of a microstrip line is calculated from

$$Q = \frac{\beta}{2\alpha}$$

where

$$\beta = \frac{2\pi}{\lambda}$$

and α is the total loss. Therefore,

$$Q = \frac{\pi}{\lambda\alpha}$$

or in decibels we can write

$$\begin{aligned} Q &= \frac{8.686\pi}{\lambda\alpha} \quad \text{dB} \\ &= \frac{27.3}{\alpha} \quad \frac{\text{dB}}{\lambda} \end{aligned}$$

where we used the fact that 1 dB = 8.686 nepers.

A microstrip line also has radiation losses. The effect of radiation losses can be accounted for in terms of the radiation quality factor Q_r given by [2.1]

$$Q_r = \frac{Z_o}{480\pi(h/\lambda_0)F}$$

where

$$F = \frac{\epsilon_{ff}(f) + 1}{\epsilon_{ff}(f)} - \frac{(\epsilon_{ff}(f) - 1)^2}{2[\epsilon_{ff}(f)]^{2/3}} \ln \frac{\sqrt{\epsilon_{ff}(f)} + 1}{\sqrt{\epsilon_{ff}(f)} - 1}$$

is known as the *radiation factor*.

The total Q , called Q_T , of a microstrip resonator can be expressed as

$$\frac{1}{Q_T} = \frac{1}{Q_c} + \frac{1}{Q_d} + \frac{1}{Q_r}$$

where Q_d and Q_c are the quality factors of the dielectric (i.e., $Q_d = \pi/\lambda\alpha_d$) and conductor (i.e., $Q_c = \pi/\lambda\alpha_c$), respectively.

Microstrip lines can be etched to a typical accuracy of ± 1 mils for width greater than 5 mils. Circuit layouts using microstrips are easily done using a layout CAD program. For example, the Hewlett-Packard MDS program has a circuit layout capability that generates the circuit pattern from the circuit schematic. If a layout program is not available, a typical circuit layout first

involves making a scaled drawing of the circuit. A typical scale factor is 10. For example, a width of 24.7 mils in alumina microstrip with $h = 25$ mils produces a line with $Z_o = 50 \Omega$. A 1-to-1 scale drawing of a circuit using these lines would be almost impossible to obtain. Thus, it is common practice to draw the circuit in graph paper using a 10-to-1 scale. On a 10-to-1 scale, the previous 50- Ω line would have a width of 247 mils, which is certainly a drawable quantity.

Electronic components come in various sizes. Some standard component size are as follows:

	Width (mils)	Length (mils)	Height (mils)
Transistors	100	120	20
Diodes	100	120	20
Chip capacitors	50	80	20
Chip coils (RFCs)	80	100	50
Chip resistors	50	80	15

Lumped components and microstrip lines are drawn in graph paper, scaled by a factor of 10, to obtain the complete circuit layout. For example, a typical chip resistor in the scaled layout would have dimensions of $W = 500$ mils by $L = 800$ mils. Once the circuit drawing is done on a 10-to-1 scale, it is brought back to a 1-to-1 scale through photographic methods in which the reduction process is exact.

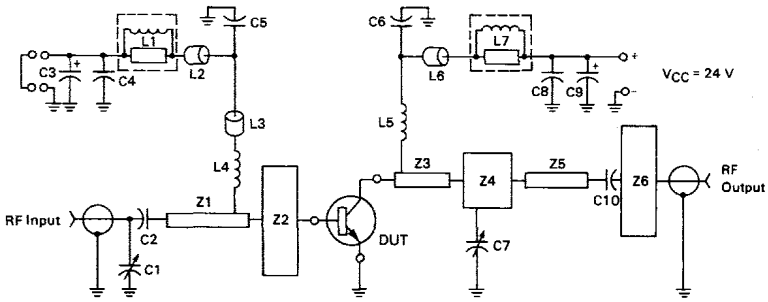
Manufacturers commonly provide test circuits for their transistors, as well as the photomaster of the test circuit (see Fig. 2.5.5).

Design of Matching Networks

The impedance transforming properties of transmission lines can be used in the design of matching networks. A microstrip line can be used as a series transmission line, as an open-circuited stub, or as a short-circuited stub. In fact, a series microstrip line together with a short- or open-circuited shunt stub can transform a 50- Ω resistor into any value of impedance.

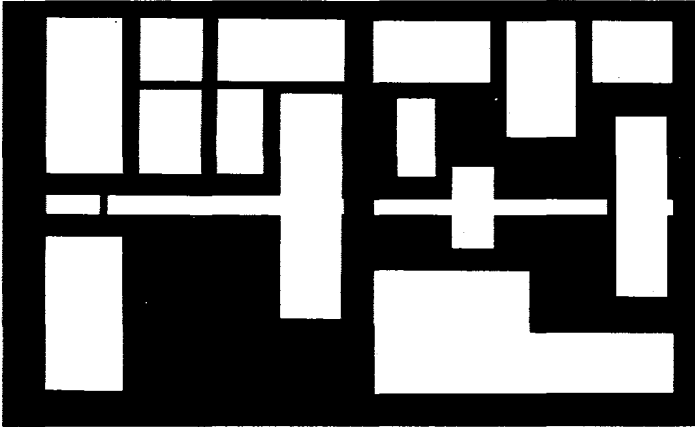
The matching circuit configuration in which a short-circuited stub is connected in parallel with the load Z_L followed by a series microstrip transmission line is shown in Fig. 2.5.6a. The characteristic impedance of the microstrip lines is shown as 50 Ω . Another way that is used to draw the schematic in Fig. 2.5.6a is shown in Fig. 2.5.6b. For comparison purposes, the same schematic drawn with 50- Ω two-wire transmission lines is shown in

— 850 - 900 MHz TEST CIRCUIT



- C1, C7 — Johanson 0.5 - 4.0 pF Giga-Trim
- C2, C5, C6 — 91 pF Mini Underwood Mica
- C3, C9 — 1.0 μ F Electrolytic
- C4, C8 — 250 pF Unelco
- C10 — 39 pF Mini Underwood
- L1, L7 — 10 Turns Around 10 Ω 1/2 W Resistor
- L2, L3, L6 — Ferrite Bead
- L4, L5 — 4 Turns 26 AWG 0.1" ID
- Z1, Z2, Z3, Z4, Z5, Z6 — Distributed Microstrip Elements (see photomask)
- Board Material — Glass Teflon $\epsilon_r = 2.55$ $t = 0.031"$

— PHOTOMASTER FOR TEST FIXTURE



NOTE: The Printed Circuit Board shown is 75% of the original.

— 850-900 MHz TEST CIRCUIT

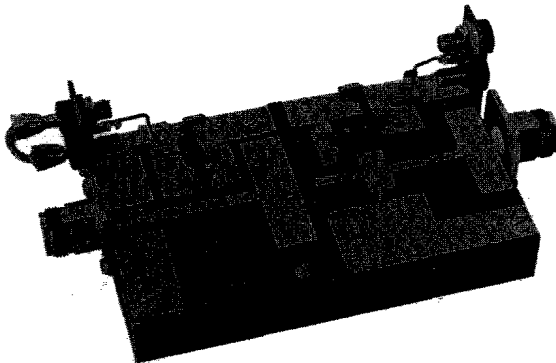


Figure 2.5.5 Test circuit, photomaster, and circuit construction for the MRF890 transistor. (From *Motorola RF Device Data*, Vol. 1, 6th edition; copyright of Motorola, used by permission.)

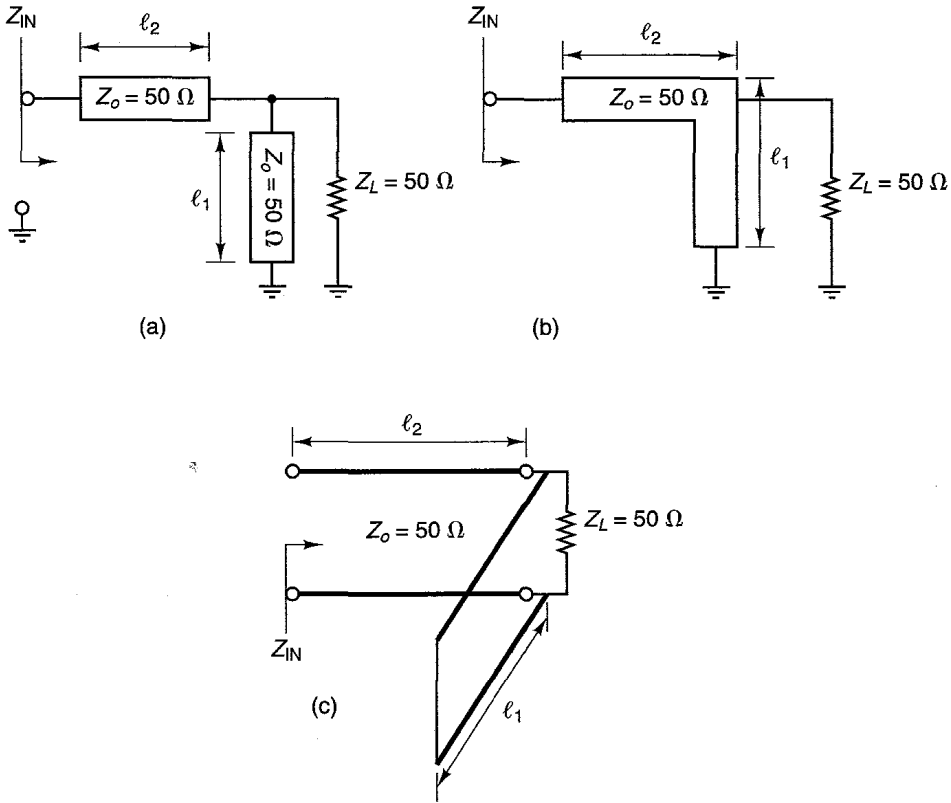


Figure 2.5.6 (a) A matching network using microstrip lines; (b) an alternative drawing; (c) schematic using two-wire transmission lines.

Fig. 2.5.6c. The shunt element in Fig. 2.5.6 could have been an open-circuited shunt stub instead of the short-circuited shunt stub shown in the figure. While the design procedure is discussed for a 50-Ω load, it can be applied to an arbitrary load impedance.

The Smith chart design procedure for the matching circuit in Fig. 2.5.6a is now discussed. Since the admittance of the shunt stub adds to the load admittance, it is convenient to use the Y Smith chart to design the circuit. Figure 2.5.7a shows the matching circuit where $z_L = Z_L/Z_o = 50/50 = 1$ (or $y_L = 1/Z_L = 1$). The normalized admittance of the shunt stub is written, for convenience, in the form $y_{sc} = jb_s$ ($b_s > 0$) for a capacitive susceptance, or $y_{sc} = -jb_s$ ($b_s > 0$) for an inductive susceptance. Using this notation, b_s is always positive and the length l_1 determines the value of $\pm jb_s$. The admittance y_x is given by

$$y_x = y_L + y_{sc} = 1 \pm jb_s$$

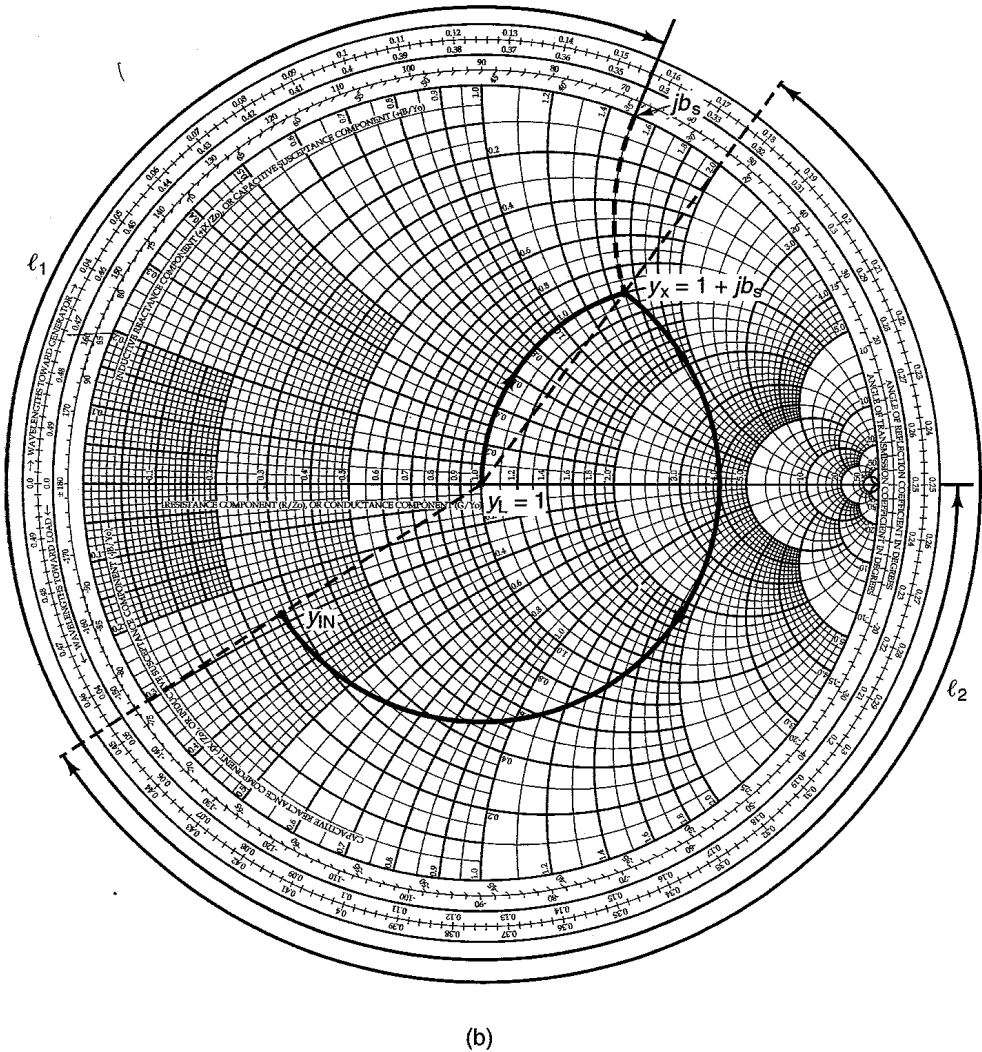
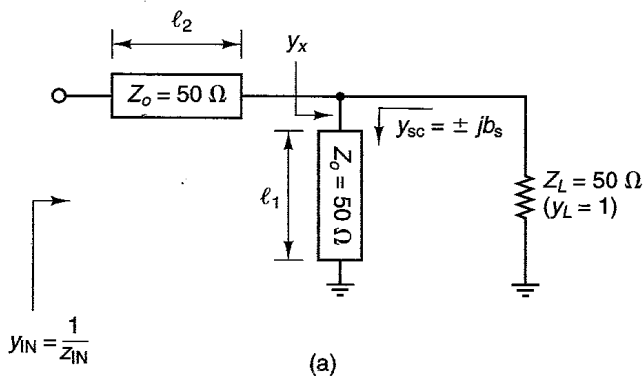
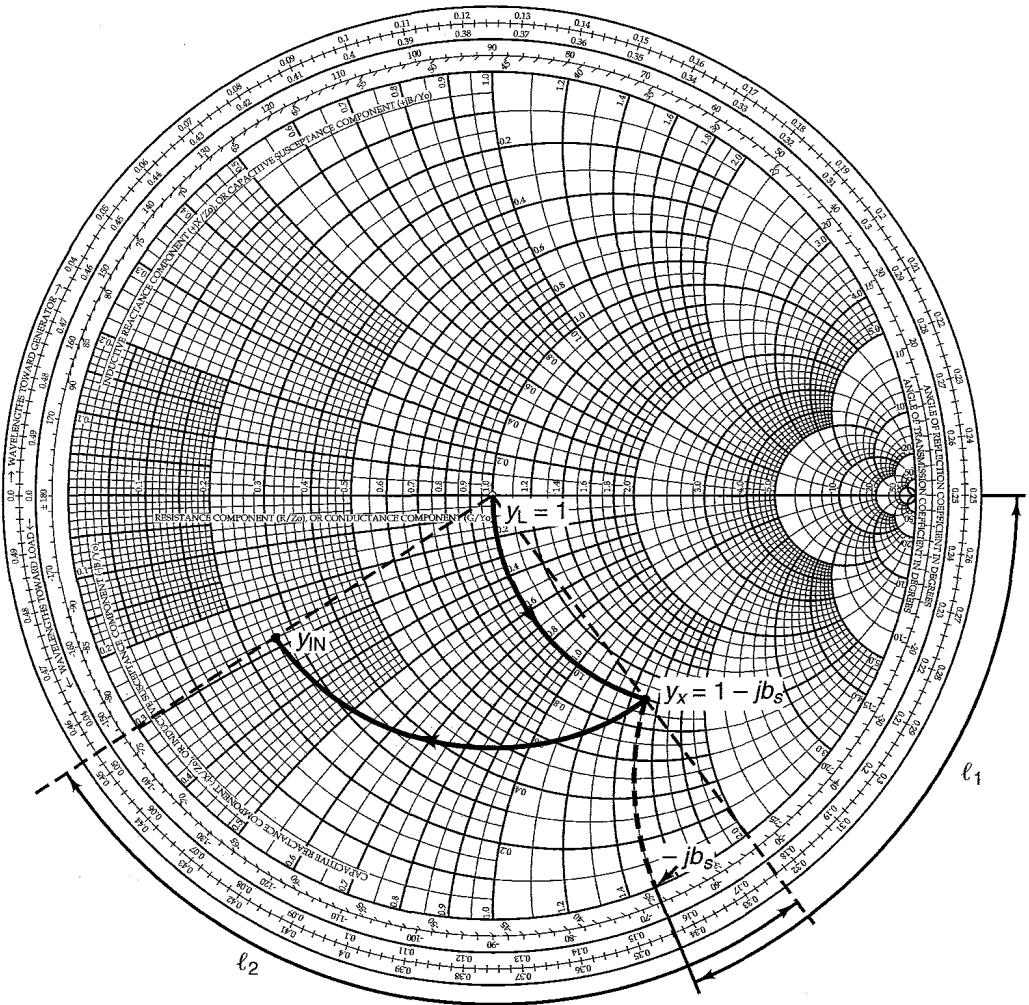


Figure 2.5.7 (a) A microstrip network to transform $y_L = 1$ to y_{IN} ; (b) the design in the Y Smith chart; with $y_{sc} = j b_s$ ($b_s > 0$); (c) the design in the Y Smith chart with $y_{sc} = -j b_s$ ($b_s > 0$).



(c)

Figure 2.5.7 Continued

As shown in the Y Smith chart in Fig. 2.5.7b, the addition of $y_{sc} = jb_s$ to y_L produces a motion along the unity constant-conductance circle from $y_L = 1$ to $y_x = 1 + jb_s$. The design of the series transmission line of length l_2 is such that y_x is transformed to the admittance y_{IN} (a typical y_{IN} is shown in Fig. 2.5.7b). Consequently, the value of b_s must be selected so that y_x and y_{IN} are on a con-

stant $|\Gamma|$ circle. The readings of l_1 and l_2 in the Y Smith chart are also shown in Fig. 2.5.7b. Observe that l_1 is the length of the short-circuited stub that produces the admittance $y_{sc} = jb_s$. The value of l_1 is easily read from the edge of the Y Smith chart.

The matching design with $y_{sc} = -jb_s$ is illustrated in Fig. 2.5.7c. In this case, the shunt stub of length l_1 produces $y_{sc} = -jb_s$ and the series microstrip line of length l_2 is designed to change y_x to y_{IN} .

If an open-circuited shunt stub is used instead of the short-circuited shunt stub shown in Fig. 2.5.6, the design procedure is quite similar. In fact, the only difference is that the length l_1 in Figs. 2.5.7a and 2.5.7b is read starting from an open-circuited termination (i.e., starting from $y = 0$).

In Fig. 2.5.7a, the shunt stub simply behaves like either a shunt capacitor (see Fig. 2.5.7b with $y_{sc} = jb_s$) or a shunt inductor (see Fig. 2.5.7c with $y_{sc} = -jb_s$), changing $y_L = 1$ to the admittance $y_x = 1 \pm jb_s$. In fact, the same design procedure applies if the shunt stub is replaced by a lumped capacitor or inductor with admittance jb_s or $-jb_s$, respectively.

A practical design using the matching network topology in Fig. 2.5.6 is found in Example 2.5.2, Design 1.

The microstrip matching circuit shown in Fig. 2.5.8a can be designed to match an arbitrary load impedance Z_L to a 50- Ω input impedance. This configuration resembles the one in Fig. 2.5.6. While in Fig. 2.5.6 the matching was from $Z_L = 50 \Omega$ to an arbitrary Z_{IN} , in Fig. 2.5.8a the matching is from an arbitrary Z_L to $Z_{IN} = 50 \Omega$. The design procedure in the Y Smith chart is shown in Fig. 2.5.8b, where the load admittance $y_L = 1/Z_L$ is transformed to $y_{IN} = 1/Z_{IN} = 1$. The length l_1 is selected so that y_L is transformed to the admittance $y_x = 1 + jb_s$ ($b_s > 0$). The motion from y_L to y_x is along a constant $|\Gamma|$ circle. Since $y_x = 1 + jb_s$, we design the short-circuited stub admittance to be $y_{sc} = -jb_s$ so that $y_{IN} = 1$. That is,

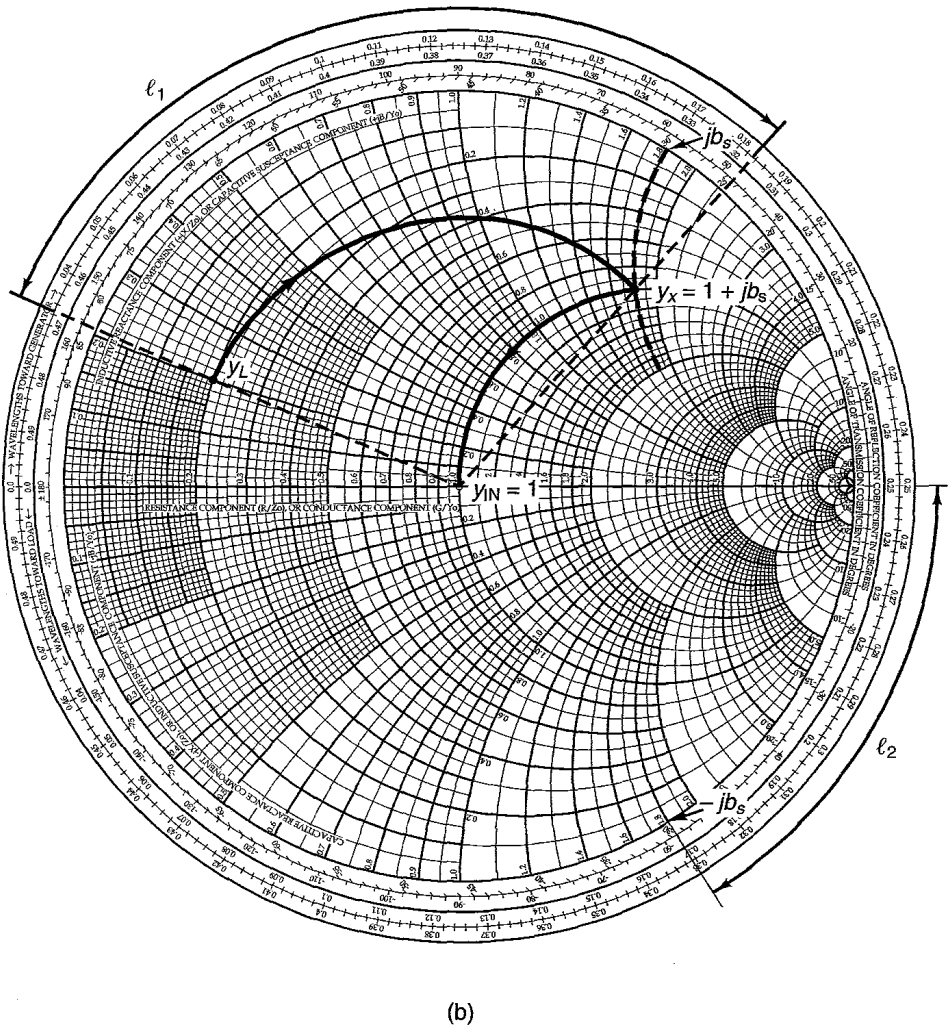
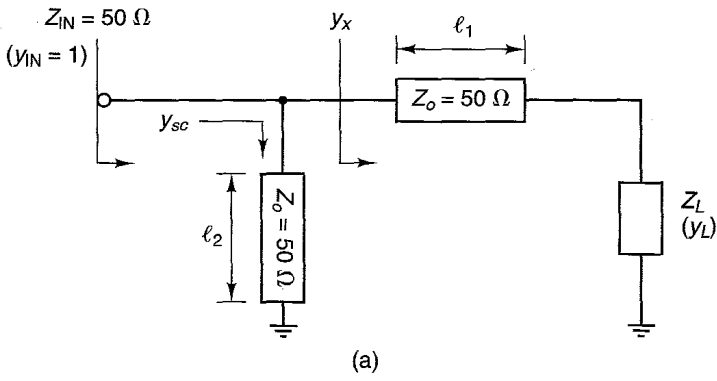
$$y_{IN} = y_x + y_{sc} = (1 + jb_s) - jb_s = 1$$

In other words, y_x must be located on the unit conductance circle at the location $y_x = 1 + jb_s$, and $y_{sc} = -jb_s$ cancels the imaginary part of y_x . The length l_2 (measured as shown in Fig. 2.5.8b) produces the short-circuited admittance $y_{sc} = -jb_s$.

The matching design with $y_{sc} = jb_s$ is illustrated in Fig. 2.5.8c. In this case, $y_x = 1 - jb_s$, so $y_{IN} = y_x + y_{sc} = (1 - jb_s) + jb_s = 1$.

Another practical microstrip matching circuit, shown in Fig. 2.5.9a, uses a series quarter-wave line with characteristic impedance Z_{o1} followed by a short-circuited shunt stub of length $\lambda/8$ or $3\lambda/8$ and characteristic impedance Z_{o2} to transform a 50- Ω load to any value of input impedance. An open-circuited shunt stub can be used instead of the short-circuited shunt stub.

The design procedure for the matching circuit in Fig. 2.5.9a is as follows. Letting $Y_{IN} = G_{IN} + jB_{IN}$, where $B_{IN} > 0$, the quarter-wave transformer is used



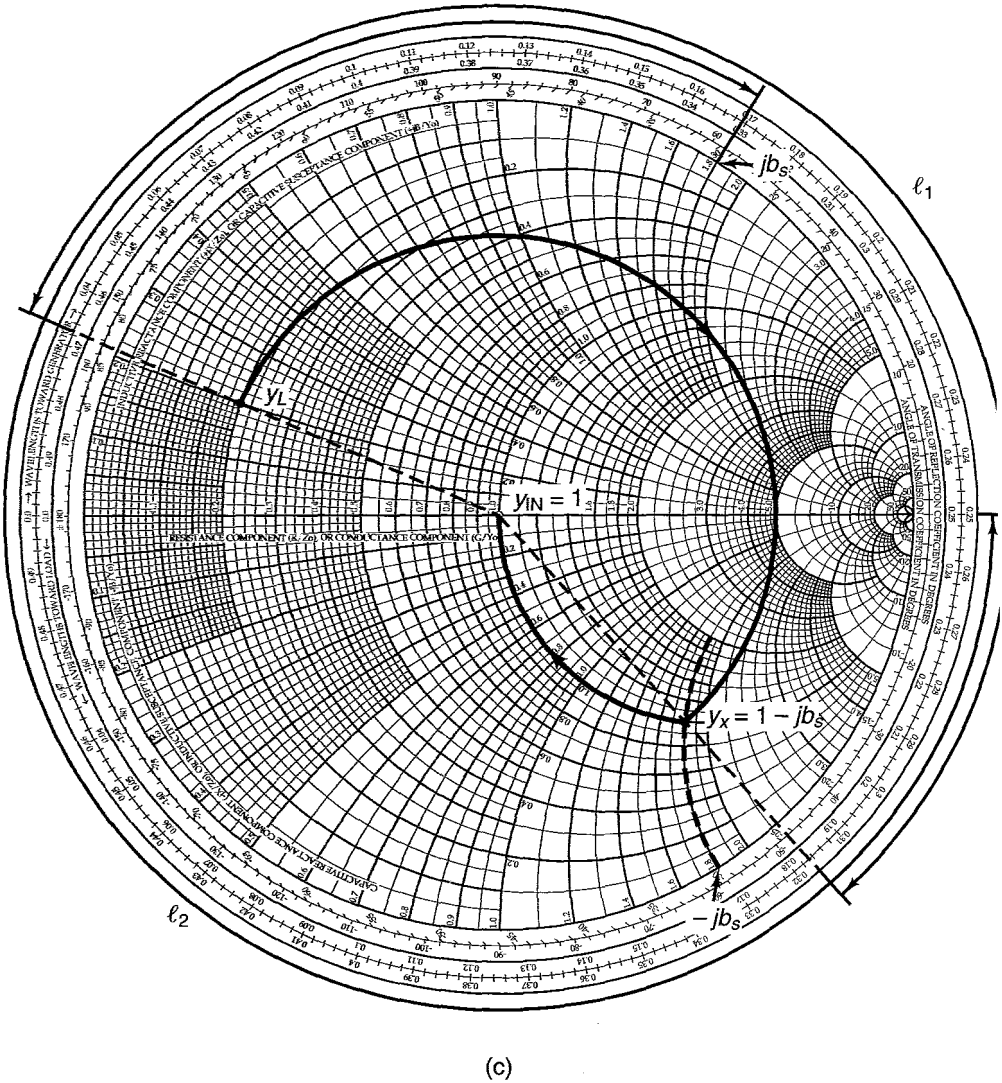


Figure 2.5.8 (a) A microstrip network to transform Z_{LOAD} to Z_{IN} ; (b) the design in the Y Smith chart with $y_{sc} = -jb_s$; (c) the design in the Y Smith chart with $y_{sc} = jb_s$.

to transform $Z_L = 50 \Omega$ to the input resistance $R_{IN} = 1/G_{IN}$. The short-circuited shunt stub is designed to produce the admittance jb_{IN} . Hence, the addition of G_{IN} and jb_{IN} produces the desired Y_{IN} .

The characteristic impedance of the quarter-wave line Z_{o1} is calculated using

$$Z_{o1} = \sqrt{Z_L R_{IN}} = \sqrt{50 R_{IN}} \tag{2.5.15}$$

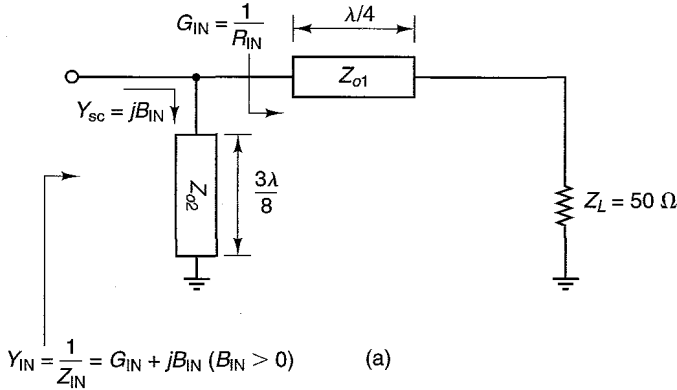


Figure 2.5.9 (a) A microstrip matching network; (b) admittance produced by a short-circuited stub of length $3\lambda/8$; (c) admittance produced by an open-circuited shunt stub of length $\lambda/8$.

Then, since a short-circuited shunt stub of length $3\lambda/8$ produces a shunt admittance of value $Y_{sc} = jY_{o2}$ (see Fig. 2.5.9b), we let jY_{o2} be equal to jB_{IN} . That is,

$$Y_{o2} = B_{IN}$$

or

$$Z_{o2} = \frac{1}{Y_{o2}} = \frac{1}{B_{IN}} \quad (2.5.16)$$

In conclusion, a characteristic impedance for the quarter-wave line Z_{o1} given by (2.5.15) produces the input conductance G_{IN} , and a characteristic impedance for the shunt stub Z_{o2} given by (2.5.16) produces the input susceptance B_{IN} . If an open-circuited shunt stub is used instead of the short-circuited shunt stub, then its length would have been $\lambda/8$ to produce $Y_{oc} = jY_{o2}$ (see Fig. 2.5.9c).

If the input admittance is given by $Y_{IN} = G_{IN} - jB_{IN}$, where $B_{IN} > 0$, as shown in Fig. 2.5.10a, Z_{o1} is calculated using (2.5.15), and a short-circuited shunt stub of length is $\lambda/8$ will produce $Y_{sc} = -jY_{o2}$ (see Fig. 2.5.10b). Therefore, letting $-jY_{o2}$ equal $-jB_{IN}$, we obtain

$$-jY_{o2} = -jB_{IN}$$

or

$$Z_{o2} = \frac{1}{Y_{o2}} = \frac{1}{B_{IN}}$$

If an open-circuited shunt stub is used instead of the short-circuited shunt stub, its length would have been $3\lambda/8$ to produce $Y_{oc} = -jY_{o2}$ (see Fig. 2.5.10c).

A practical design using the matching network topology in Fig. 2.5.9a is found in Example 2.5.2, Design 2.

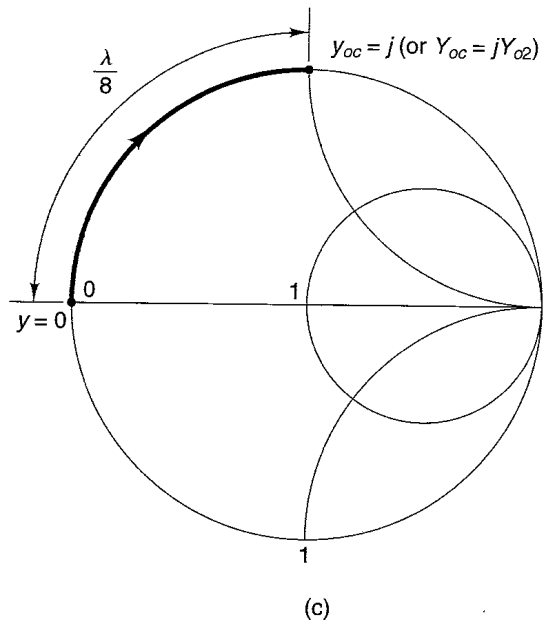
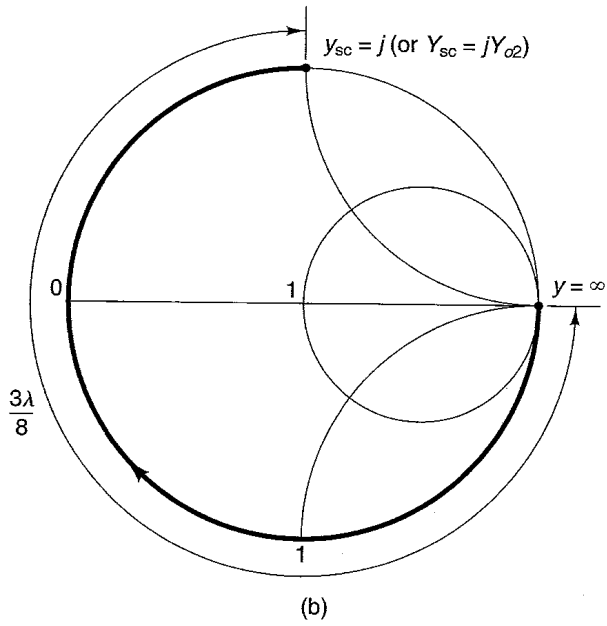


Figure 2.5.9 Continued

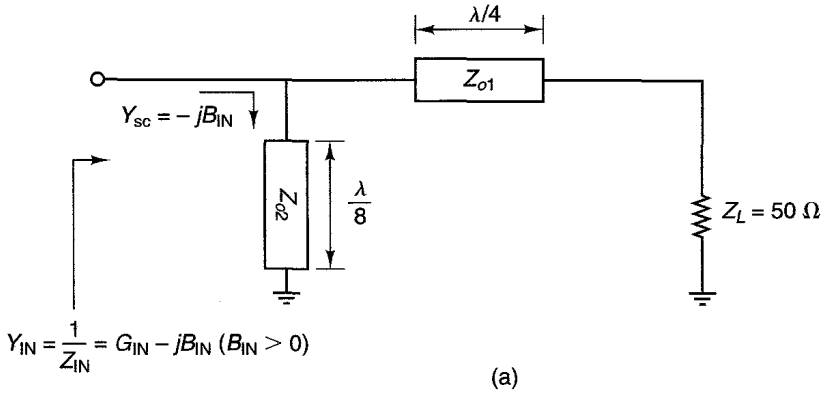


Figure 2.5.10 (a) A microstrip matching network; (b) admittance produced by a short-circuited stub of length $\lambda/8$; (c) admittance produced by an open-circuited shunt stub of length $3\lambda/8$.

The microstrip matching circuits shown in Fig. 2.5.9a and 2.5.10a can also be designed by using any practical value of Z_{o2} but setting the shunt stub length l_2 to produce the admittance of $Y_{sc} = \pm jB_{IN}$. The configuration is shown in Fig. 2.5.11.

The following examples illustrate the uses of microstrip lines in matching networks.

Example 2.5.2

Design two microstrip matching networks for the amplifier shown in Fig. 2.5.12 whose reflection coefficients for a good match, in a 50- Ω system, are $\Gamma_s = 0.614 \angle 160^\circ$ and $\Gamma_L = 0.682 \angle 97^\circ$.

Solution. *Design 1:* The amplifier block diagram is shown in Fig. 2.5.12. The normalized impedances and admittances associated with Γ_s and Γ_L can be read, to reasonable accuracy, from the ZY chart—namely,

$$y_s = \frac{1}{z_s} = \frac{1}{0.245 + j0.165} = 2.8 - j1.9$$

and

$$y_L = \frac{1}{z_L} = \frac{1}{0.325 + j0.83} = 0.4 - j1.05$$

In order to design the input matching network, we locate y_s in the Y Smith chart shown in Fig. 2.5.13a. The shortest length of microstrip line plus stub is obtained by using an open-circuited shunt stub of length 0.159λ to move from the origin (i.e., 50 Ω) to point A on the Smith chart, and then using a transmission line length of 0.099λ to move from A to y_s .

Next, we locate y_L in Fig. 2.5.13b and follow a similar procedure. In this case, the shortest length of microstrip line plus stub is obtained by using a short-circuited shunt

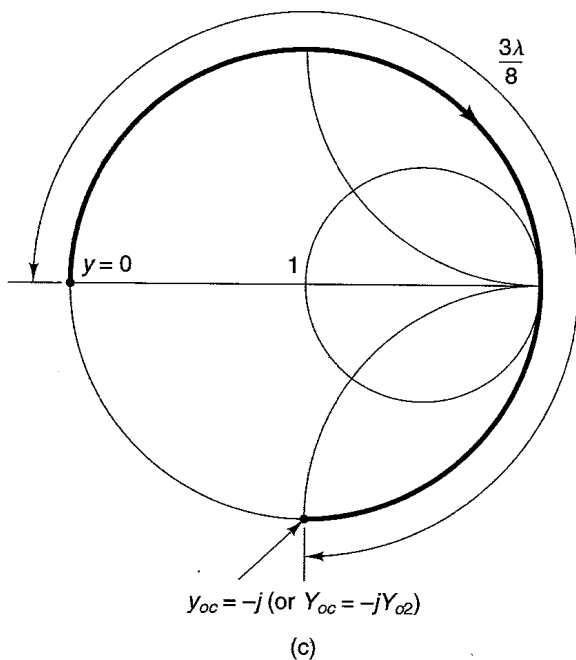
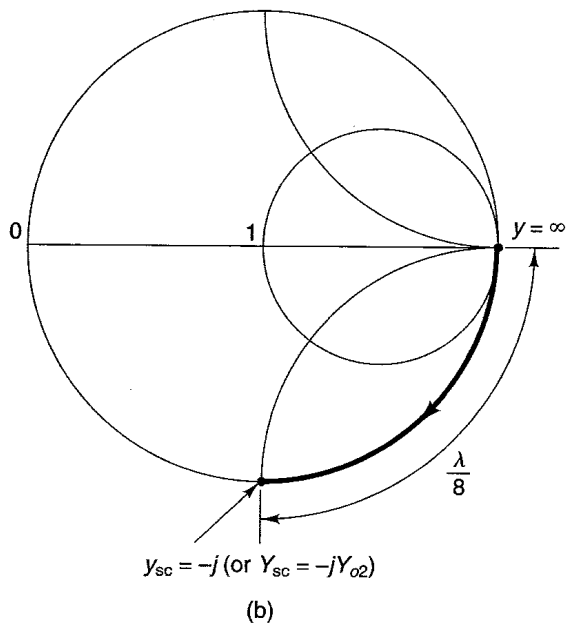


Figure 2.5.10 Continued

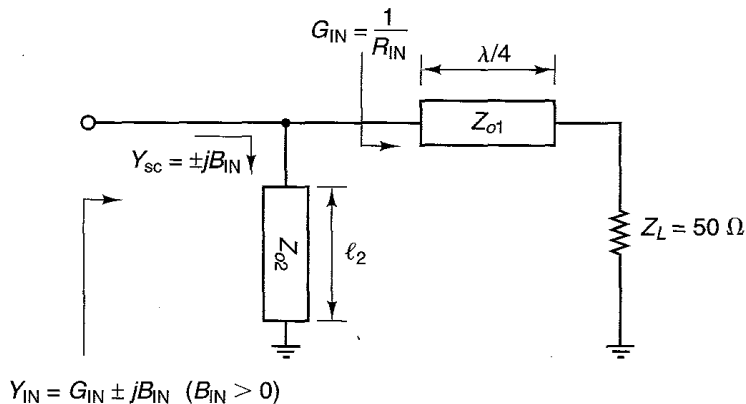


Figure 2.5.11 A microstrip matching circuit.

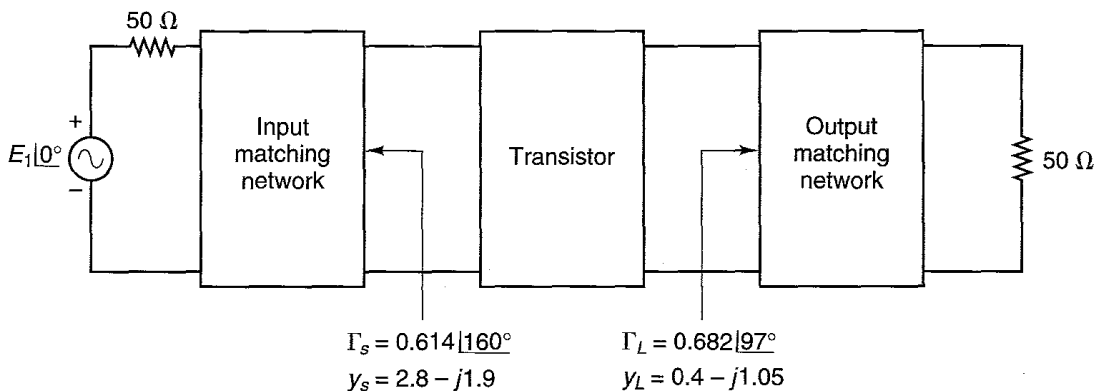


Figure 2.5.12 Amplifier block diagram.

stub of length 0.077λ to move from the origin to point B . Then a series transmission line of length 0.051λ is used to move from B to y_L .

The complete design, showing the transistor, the microstrip matching network, and the dc supply, is shown in Fig. 2.5.14. The characteristic impedance of all microstrip lines is 50Ω .

The capacitors C_A are coupling capacitors. Typical values for the chip capacitors C_A are 200 to 1000 pF, high- Q capacitor. The bypass capacitors C_B (i.e., chip capacitors, 50 to 500 pF) provide the ac short circuits for the 0.077λ and $\lambda/4$ short-circuited stubs. The $\lambda/4$ short-circuited stub, high-impedance line (denoted by $Z_o \gg$), provides the dc path for the base supply voltage. It also presents an open circuit to the ac signal at the base of the transistor. The narrowest practical line (i.e., large Z_o) should be used for the $\lambda/4$ short-circuited stub to avoid unwanted ac coupling. Typical dc bias circuits are shown in Figs. 3.9.2 and 3.9.4.

To minimize transition interaction between the shunt stubs and the series transmission lines, the shunt stubs are usually balanced along the series transmission lines. A schematic of the amplifier using balanced shunt stubs is shown in Fig. 2.5.15. The

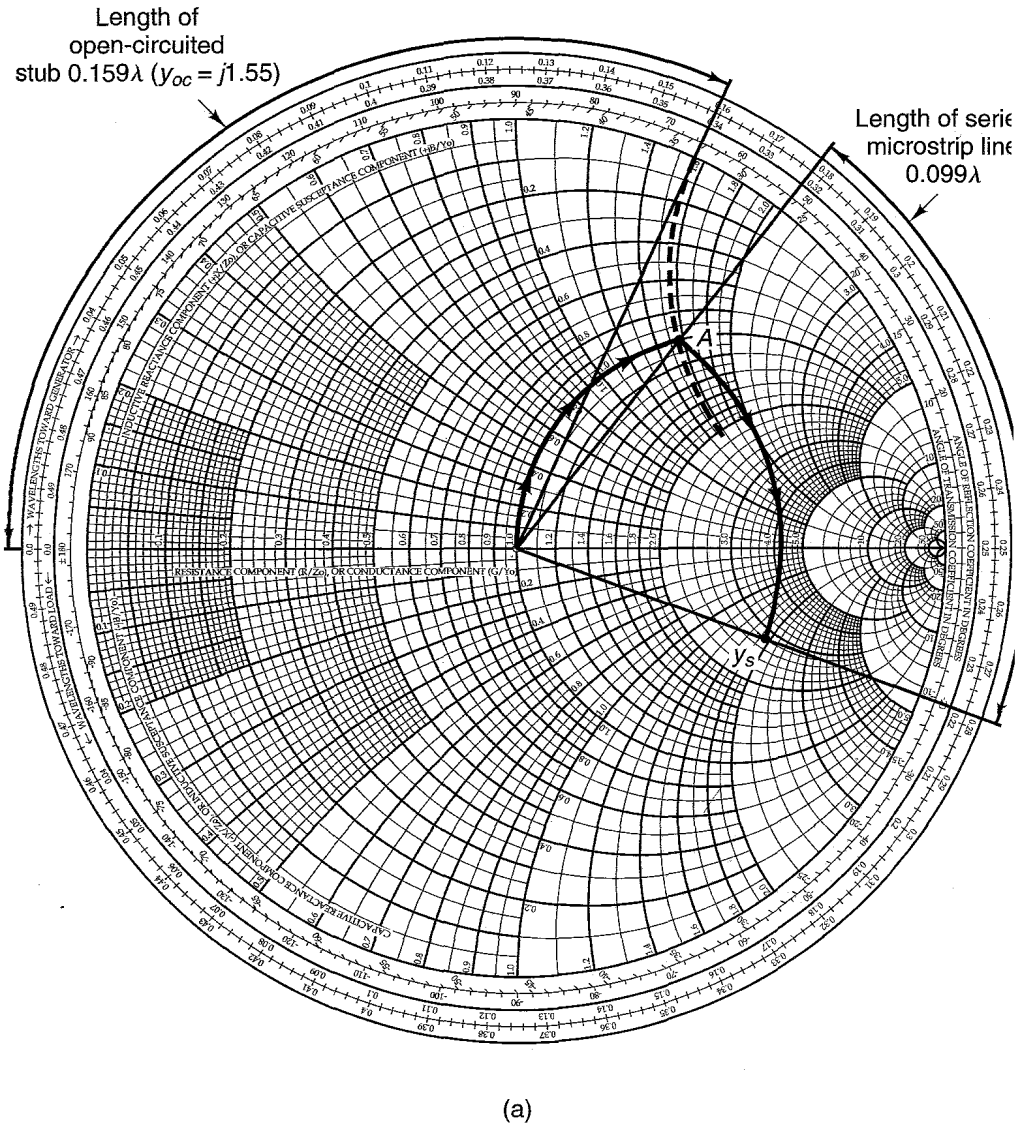
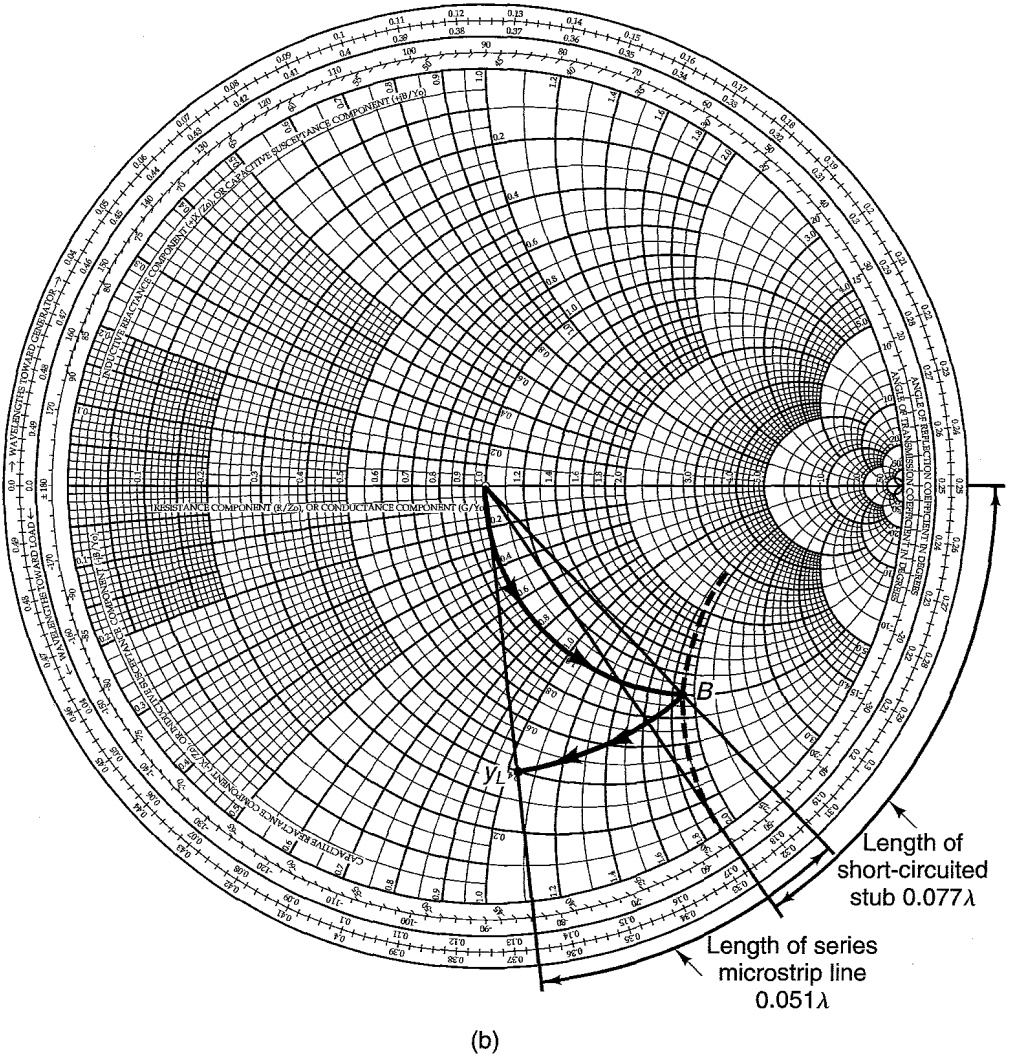


Figure 2.5.13 (a) Input matching network design; (b) output matching network design.

schematic also shows that 50-Ω lines were added on both sides of C_A to provide a soldering area.

In Fig. 2.5.15, two parallel shunt stubs must provide the same admittance as the single stub in Fig. 2.5.14. Therefore, the admittance of each side of the balanced stub must be equal to half of the total admittance. For example, each side of the input balanced shunt stubs must have an admittance of $y = j1.55/2 = j0.775$. Using the Smith



(b)

Figure 2.5.13 Continued

chart, we obtain that the length of each side must be 0.105λ . Observe that the length of the shunt stubs in Fig. 2.5.14 is not equal to the total length of the balance stubs in Fig. 2.5.15. Of course, a simple check will show that the admittance seen by the series transmission line is the same in both cases.

If we use RT/Duroid® with $\epsilon_r = 2.23$ and $h = 0.7874$ mm to build the amplifier, we find from (2.5.8) to (2.5.11) (or from Figs. 2.5.2 and 2.5.3) that a characteristic impedance of 50Ω is obtained with $W = 2.42$ mm and $\epsilon_{eff} = 1.91$. The microstrip wave-

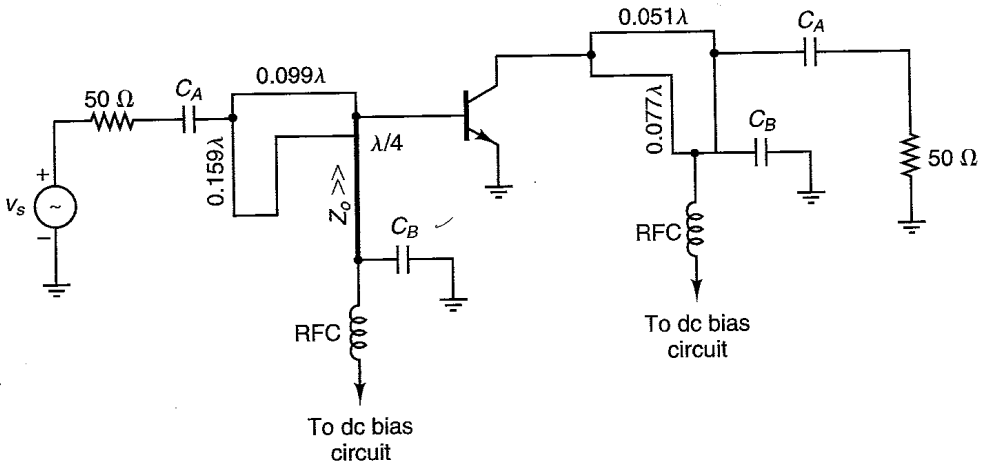


Figure 2.5.14 Complete amplifier schematic. The characteristic impedance of the microstrip lines is $50\ \Omega$.

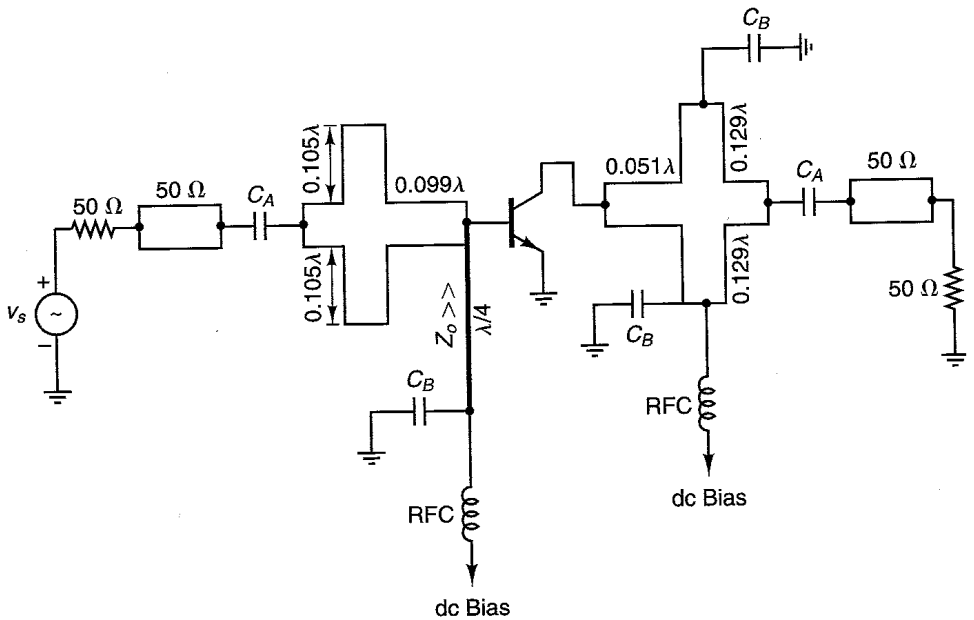


Figure 2.5.15 Complete amplifier schematic using balanced shunt stubs. The characteristic impedance of the microstrip lines is $50\ \Omega$.

length in the 50- Ω Duroid microstrip line is $\lambda = \lambda_0/\sqrt{1.91} = 0.7236\lambda_0$, where $\lambda_0 = 30$ cm at $f = 1$ GHz. For a characteristic impedance of 100 Ω in the $\lambda/4$ line, the width must be $W = 0.7$ mm. The line lengths in Fig. 2.5.15 are

$$0.105\lambda = 2.28 \text{ cm}$$

$$0.099\lambda = 2.15 \text{ cm}$$

$$0.051\lambda = 1.10 \text{ cm}$$

$$0.129\lambda = 2.80 \text{ cm}$$

$$\lambda/4 = 5.43 \text{ cm}$$

Design 2: This method uses microstrip lines with different characteristic impedances, as shown in Fig. 2.5.10a. The design requires the transformation of 50 Ω to $Y_s = (2.8 - j1.9)/50 = 0.056 - j0.038$ S. A quarter-wave transformer can be used to transform the source impedance of 50 Ω to the resistance $1/0.056 = 17.86$ Ω . The characteristic impedance of the quarter-wave transformer is

$$Z_{o1} = \sqrt{50(17.86)} = 29.9 \text{ } \Omega$$

An open-circuited shunt stub can be used to obtain the admittance $-j0.038$ S. Therefore, as shown in Fig. 2.5.10c, an open-circuited shunt stub of length $3\lambda/8$ looks like a shunt inductor having the admittance $-jY_{o2}$. Equating $-jY_{o2}$ to $-j0.038$ S, we find the characteristic impedance Z_{o2} to be

$$Z_{o2} = \frac{1}{Y_{o2}} = \frac{1}{0.038} = 26.32 \text{ } \Omega$$

If the design is done using a short-circuited shunt stub (see Fig. 2.5.10a), its length would be $\lambda/8$ and $Z_{o2} = 26.3$ Ω .

Similarly, for the output matching network [$Y_L = (0.4 - j1.05)/50 = 0.008 - j0.021$ S], a quarter-wave line of characteristic impedance

$$Z_{o1} = \sqrt{50(125)} = 79.1 \text{ } \Omega$$

transforms the 50- Ω load to a resistance of value $1/0.008 = 125$ Ω . An open-circuited shunt stub of length $3\lambda/8$ and characteristic impedance $Z_{o2} = 1/Y_{o2} = 1/0.021 = 47.6$ Ω produces the required admittance of $-j0.021$ S.

The complete amplifier is shown in Fig. 2.5.16a. Figure 2.5.16b shows the amplifier using balanced shunt stubs of length $3\lambda/8$ to minimize the microstrip transition interaction. Observe that in the balance stubs the lengths were kept at $3\lambda/8$, but the characteristic impedance was doubled. For example, in Fig. 2.5.16b each half of the input balance stub must provide the admittance $-j0.038/2$ (since each half must contribute half of the total admittance). Therefore, the value of Z_{o2} for the balanced stubs at the input is $Z_{o2} = 2/0.038 = 52.6$ Ω .

Example 2.5.3

Design a microstrip matching network to transform the load $Z_L = 75 - j60$ Ω to an input impedance of value $Z_{IN} = 15 + j30$ Ω .

Solution. In this design, let us select a Z_o different from 50 Ω —for example, $Z_o = 75$ Ω . With $Z_o = 75$ Ω , the design consists of transforming a normalized load $z_L = Z_L/Z_o = 1 - j0.8$ (or $y_L = 0.61 + j0.49$) to the normalized input impedance $z_{IN} =$

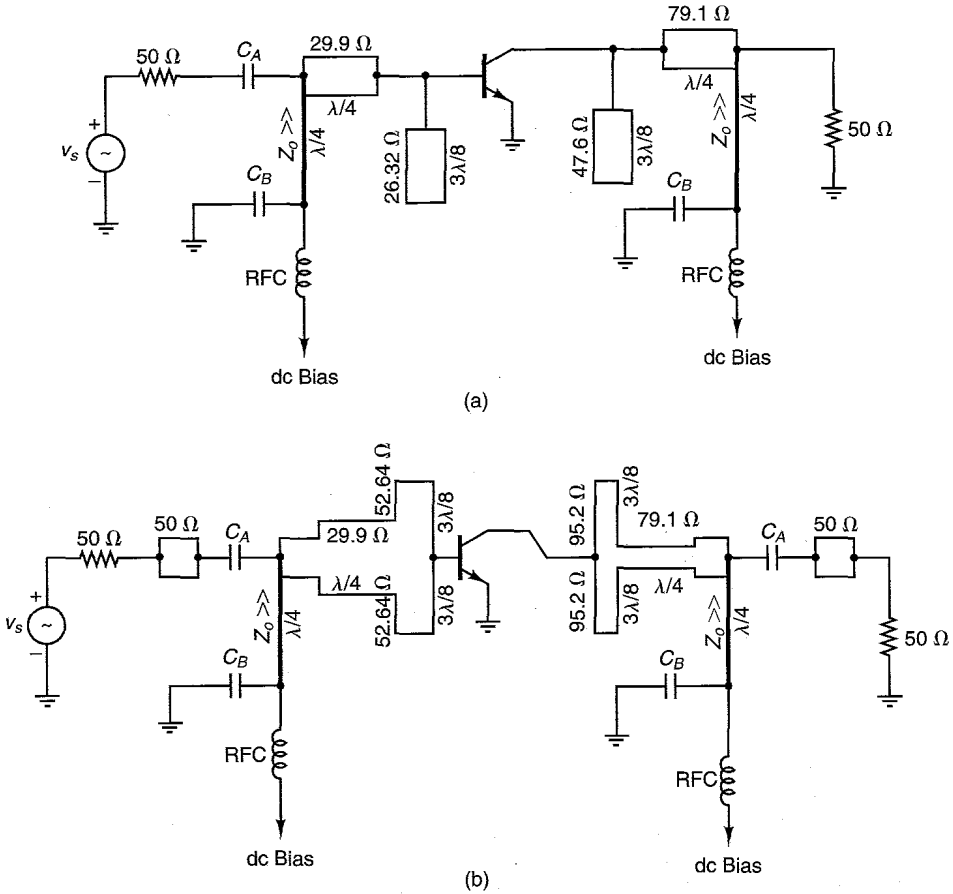


Figure 2.5.16 Matching network design using microstrip lines with different characteristic impedances.

$Z_{IN}/Z_o = 0.2 + j0.4 \Omega$ (or $y_{IN} = 1 - j2$). The matching topology selected is shown in Fig. 2.5.17a, and the design in the Y Smith chart is shown in Fig. 2.5.17b. From Fig. 2.5.17b, the shunt admittance required to move from y_L to point A is $j1.5 - j0.49 = j1.01$. The admittance at point A is $y_A = 0.61 + j1.5$. An open-circuited shunt stub of length $l_1 = 0.126\lambda$ provides the admittance of $j1.01$. Then a series transmission line of length $l_2 = 0.313\lambda - 0.164\lambda = 0.149\lambda$ moves the admittance value, along a constant $|\Gamma|$ circle, from that at point A to y_{IN} .

A microstrip matching network which can be easily designed using a Z Smith chart is shown in Fig. 2.5.18a. This matching network uses a $\lambda/4$ line with characteristic impedance Z_{o1} to transform the $50\text{-}\Omega$ load ($z_L = 1$) to a resistance R_x ($r_x = R_x/50$) that lies on the constant $|\Gamma|$ circle that passes through $z_{IN} = Z_{IN}/50$. The value of Z_{o1} is given by

$$Z_{o1} = \sqrt{50R_x}$$

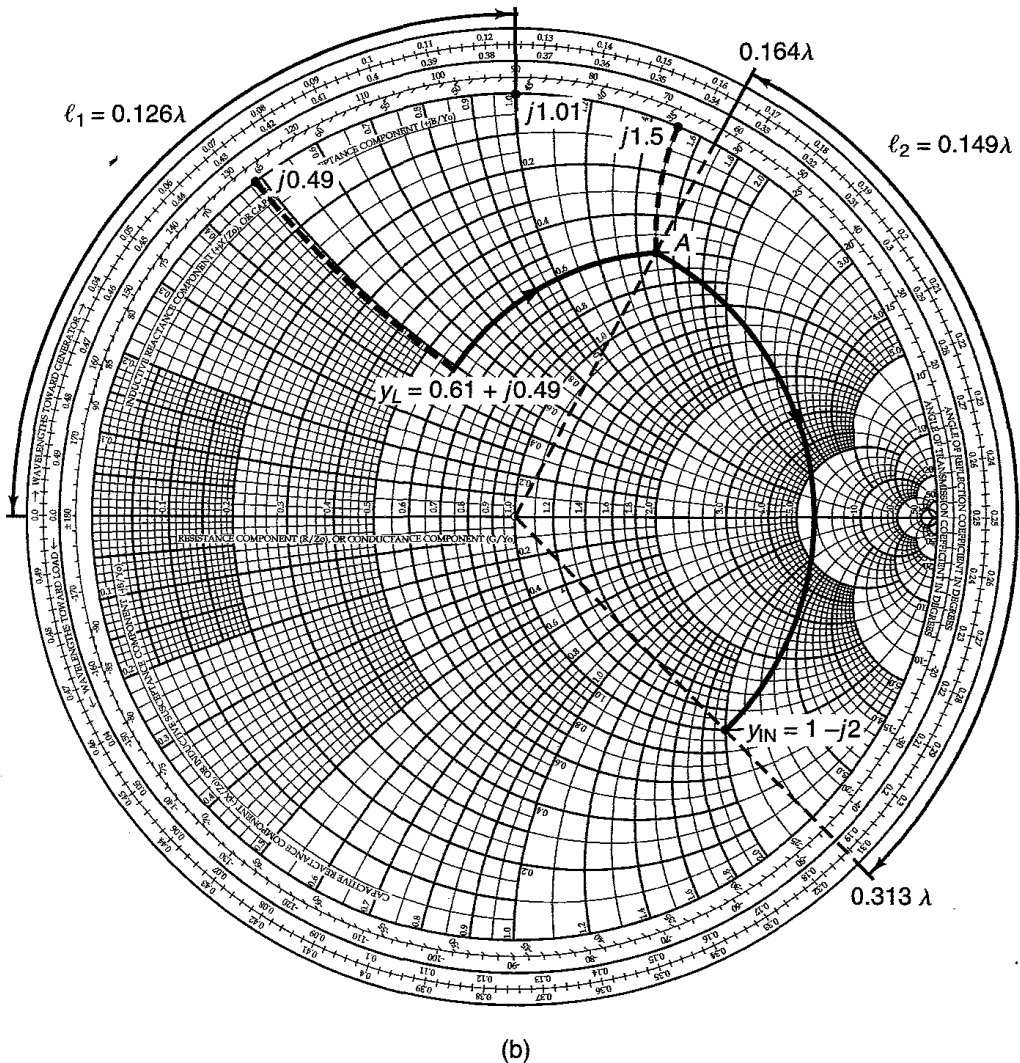
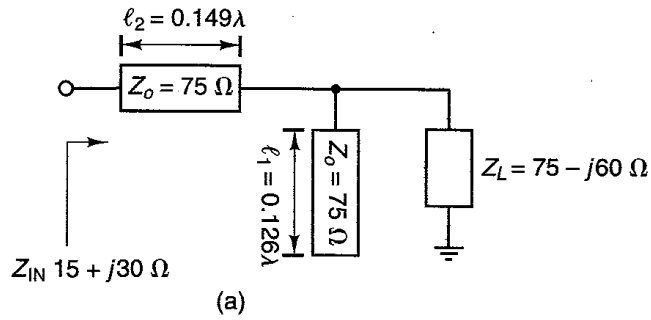


Figure 2.5.17 (a) Matching network for Example 2.5.3; (b) design in the Y Smith chart using $Z_o = 75 \Omega$.

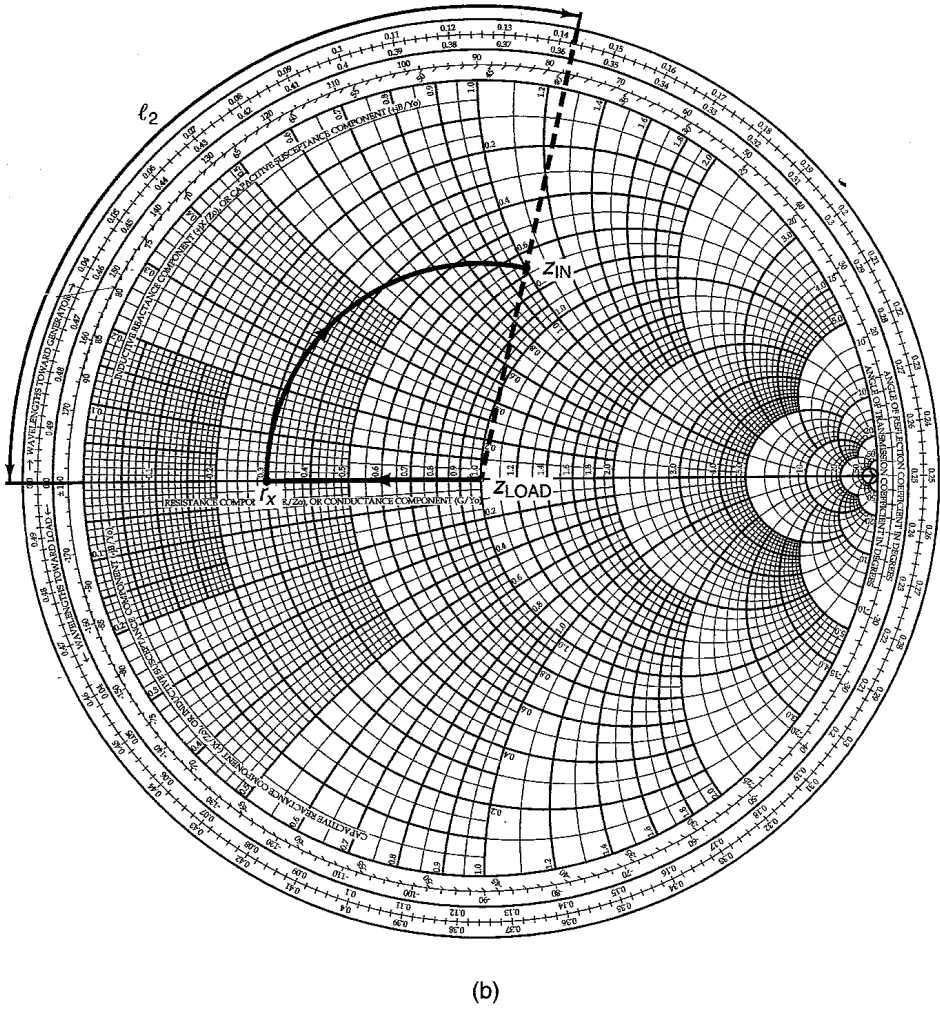
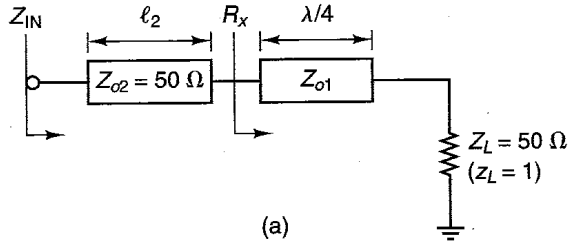
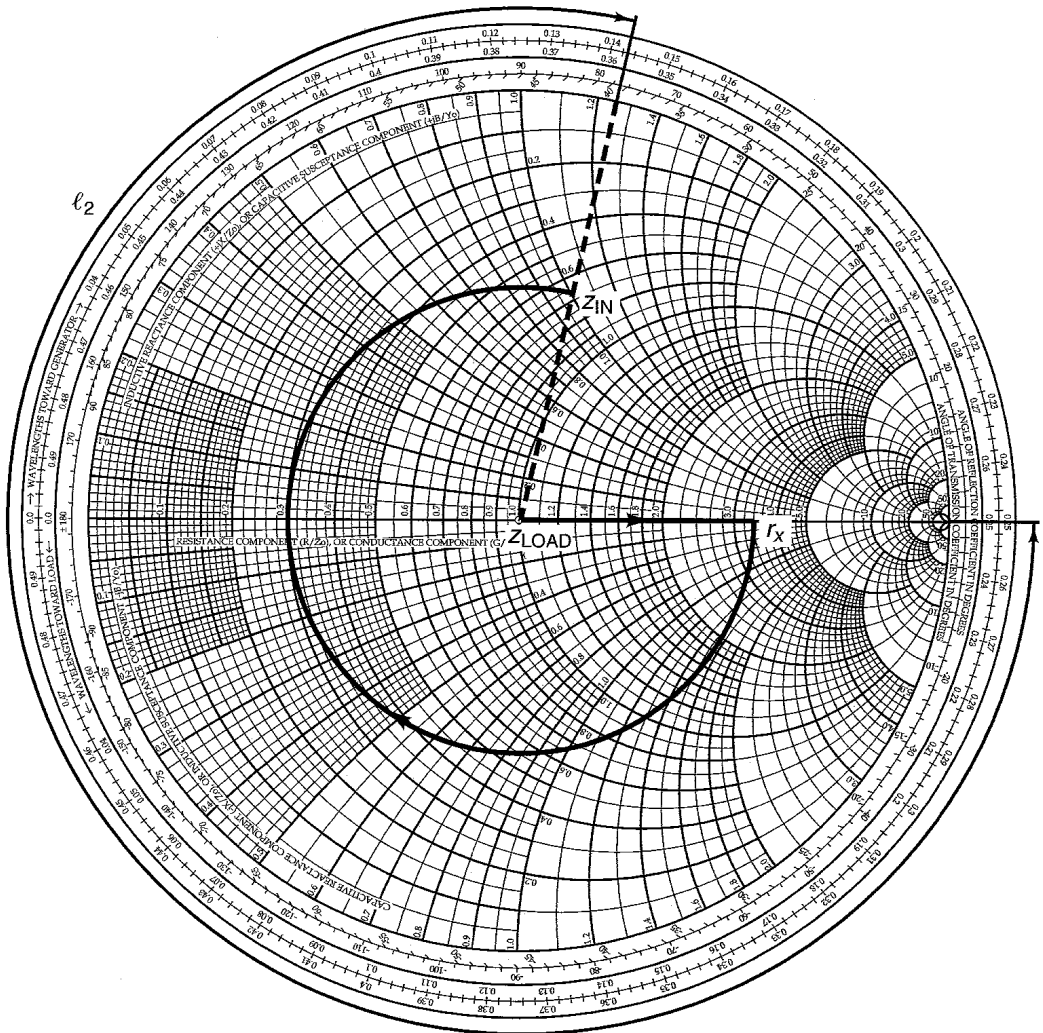


Figure 2.5.18 (a) A microstrip matching circuit; (b) design in the Z Smith chart that results in Z_{o1} smaller than 50Ω ; (c) design in the Z Smith chart that results in Z_{o1} greater than 50Ω .



(c)

Figure 2.5.18 Continued

Then, the $50\text{-}\Omega$ line of length l_2 changes the normalized resistance r_x to the input impedance Z_{IN} . The design procedure in the Z Smith chart for an arbitrary value of Z_{IN} is shown in Fig. 2.5.18b. An alternate solution is shown in Fig. 2.5.18c. The solution described in Fig. 2.5.18b produces a Z_{o1} smaller than $50\ \Omega$, while the solution in Fig. 2.5.18c produces a Z_{o1} greater than $50\ \Omega$.

Example 2.5.4

Design the microstrip matching network in Fig. 2.5.18a to transform a $50\text{-}\Omega$ load to the input impedance $Z_{IN} = 33 + j50\ \Omega$.

Solution. The location of $z_{IN} = Z_{IN}/50 = 0.66 + j1$ corresponds to the z_{IN} shown in Fig. 2.5.18b. From the constant $|\Gamma|$ circle through z_{IN} , we observe that $r_x = 0.3$, or $R_x = 50(0.3) = 15 \Omega$. The $\lambda/4$ line is designed to transform $Z_L = 50 \Omega$ to $R_x = 15 \Omega$. Hence,

$$Z_{o1} = \sqrt{50(15)} = 27.4 \Omega$$

Then, the $50\text{-}\Omega$ series transmission line of length $l_2 = 0.143\lambda$ produces an input impedance equal to $z_{IN} = 0.66 + j1$, or $Z_{IN} = 50(z_{IN}) = 33 + j50 \Omega$.

The design of matching networks containing lumped components and microstrip transmission lines can also be done using the various Smith charts. The following example illustrates one such design.

Example 2.5.5

(a) An oscillator is designed at 2.5 GHz using the output matching topology shown in Fig. 2.5.19a. The length of the microstrips is shown for $\epsilon_{ff} = 1$ (i.e., for $v = c = 3 \times 10^{10}$ cm/s). The matching network uses a varactor diode as a voltage-variable capacitor for the control of the oscillator frequency. Determine the value of the load reflection coefficient.

(b) Specify the width, height, and length of the microstrip lines if they are constructed using an alumina substrate ($\epsilon_r = 9.6$).

Solution. (a) The wavelength in free space is

$$\lambda_0 = \frac{c}{f} = \frac{3 \times 10^{10}}{2.5 \times 10^9} = 12 \text{ cm}$$

Hence, the shunt microstrip of length $l_1 = 43$ mm (or $l_1 = 0.358\lambda_0$) has an open-circuited admittance of $y_{oc} = -j1.25$. This shunt microstrip acts like a shunt inductor. Hence, the admittance value of 50Ω in parallel with the shunt microstrip produces the admittance $y_A = 1 - j1.25$, shown as point *A* in the *Y* Smith chart in Fig. 2.5.19b.

The series microstrip of length $l_2 = 10$ mm (or $l_2 = 0.083\lambda_0$) produces the matching from point *A* to point *B* (see Fig. 2.5.19b). This motion is along a constant $|\Gamma|$ circle. The admittance at *B* is $y_B = 0.41 - j0.53$. Then, the shunt capacitance of the varactor diode (3 pF or $y_C = j2.36$) produces the motion from point *B* to point *C*. At point *C* the admittance is $0.41 + j1.83$, which corresponds to $\Gamma_L = 0.83 \angle -124.5^\circ$.

In practice, the capacitance of the varactor diode is 3 pF when a specific dc voltage is applied to it. Let us assume that 3 pF occurs when the dc voltage is 4 V. A practical dc bias circuit for the varactor diode and for the transistor is shown in Fig. 2.5.19c.

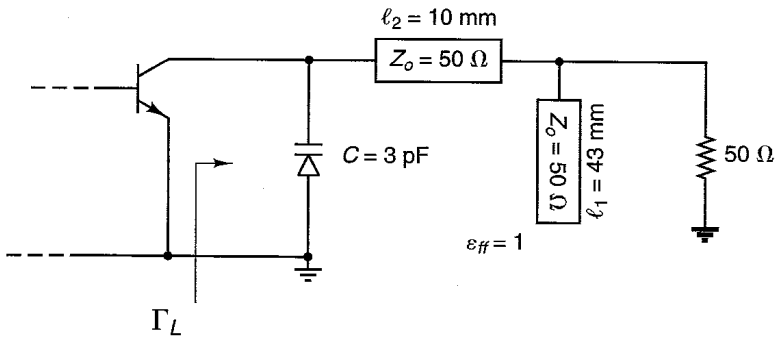
(b) If the microstrip lines are built using alumina with $\epsilon_r = 9.6$, then from Fig. 2.5.4 a characteristic impedance of 50Ω can be obtained with $W = 24.7$ mils and $h = 25$ mils.

It also follows that $\epsilon_{ff} = 6.46$ (or $\lambda = \lambda_0/\sqrt{\epsilon_{ff}} = 12/\sqrt{6.46} = 4.72$ cm) in the alumina. Hence, the length of the shunt stub, denoted by l'_1 , is

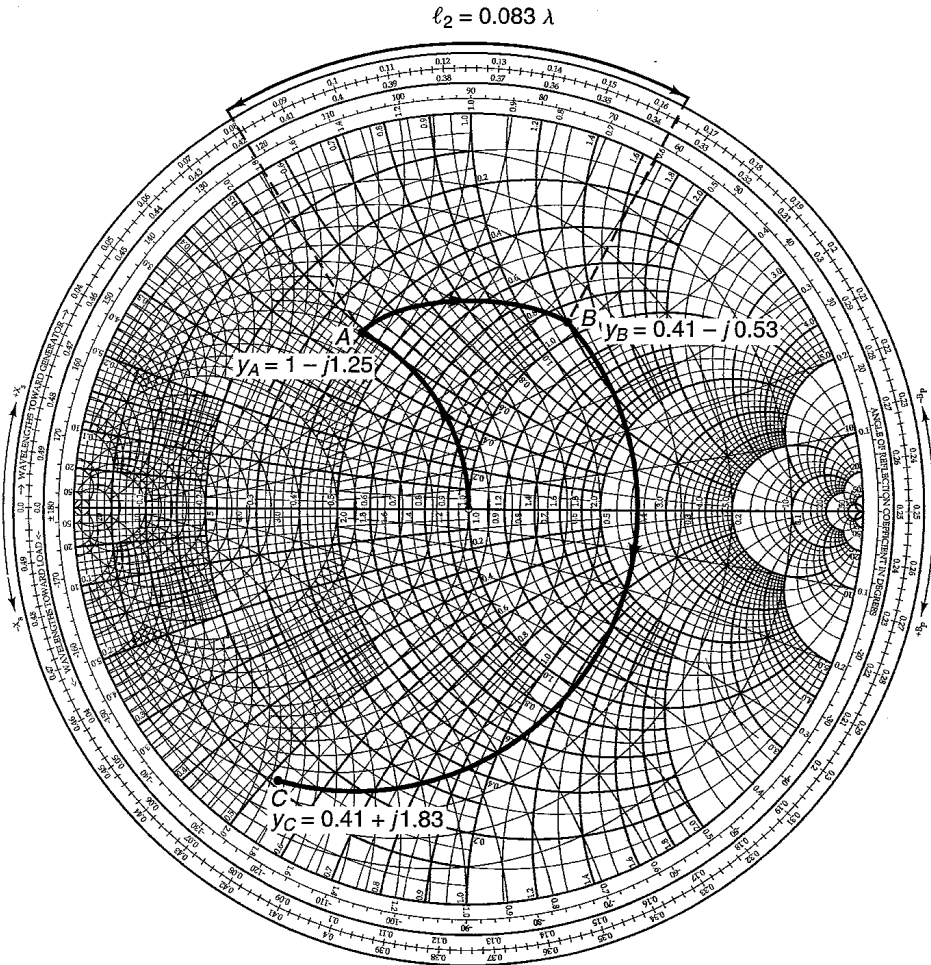
$$l'_1 = \frac{l_1}{\sqrt{\epsilon_{ff}}} = \frac{43}{\sqrt{6.46}} = 16.9 \text{ mm}$$

and that of the series microstrip line, denoted by, l'_2 is

$$l'_2 = \frac{l_2}{\sqrt{\epsilon_{ff}}} = \frac{10}{\sqrt{6.46}} = 3.93 \text{ mm}$$



(a)



(b)

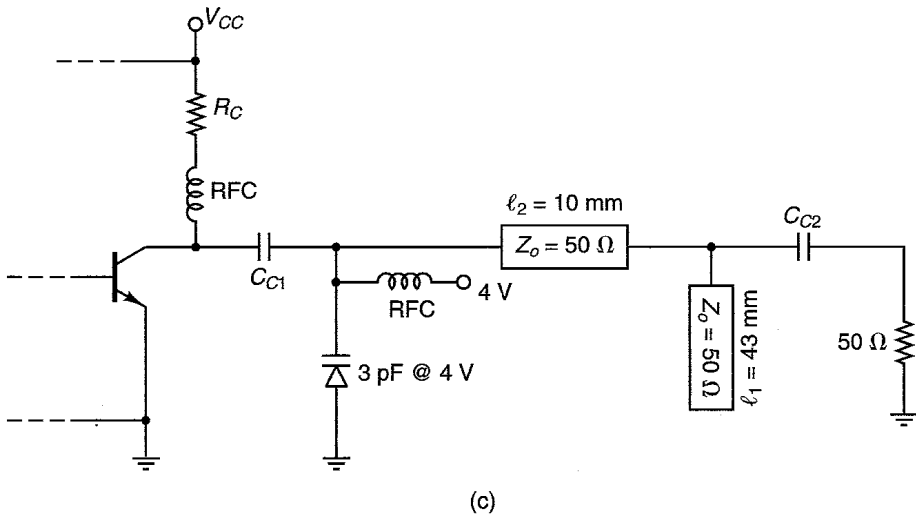


Figure 2.5.19 (a) Circuit schematic for Example 2.5.5; (b) calculation of Γ_L using the Y Smith chart; (c) an implementation of the dc bias circuit.

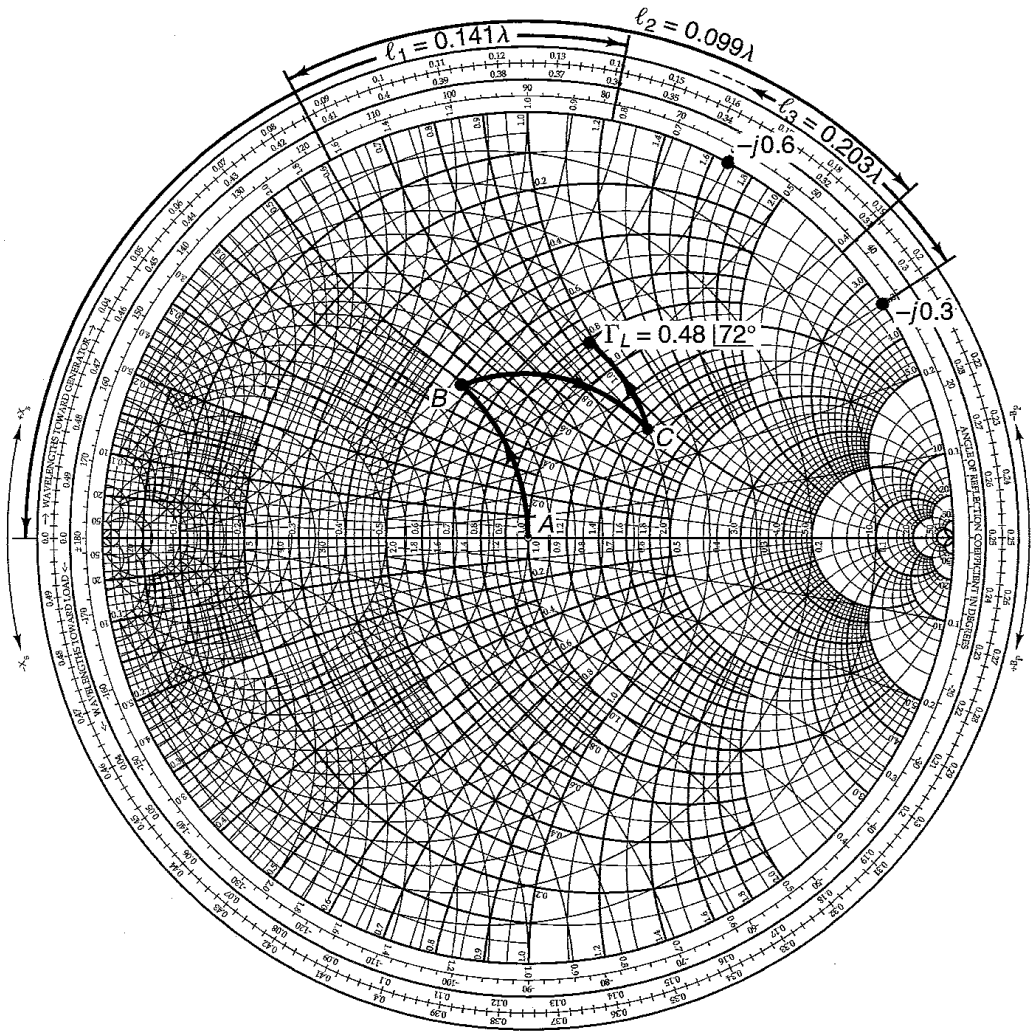
Example 2.5.6

Design a three-element microstrip matching network to transform a $50\text{-}\Omega$ termination to a load reflection coefficient given by $\Gamma_L = 0.48 \angle 72^\circ$.

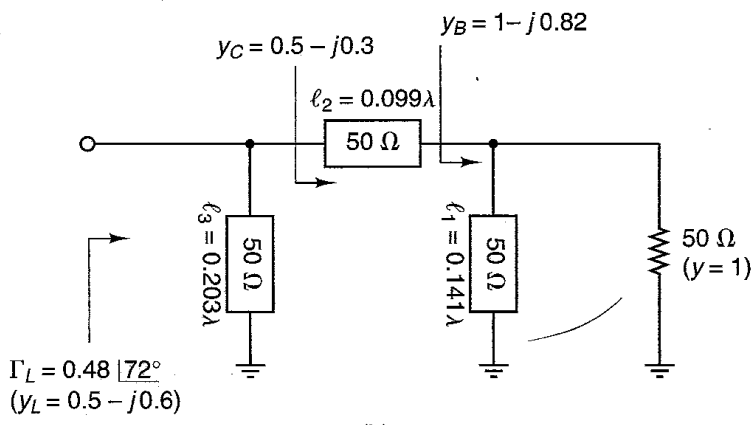
Solution. We will solve this problem using the ZY Smith chart. The solution using this chart should be of interest to the reader (it is recommended that the reader also work this problem using the Y Smith chart). Figure 2.5.20a shows Γ_L in the ZY Smith chart, as well as the path selected for the matching network, using $Z_o = 50 \Omega$. The first element transforms the normalized admittance from point A to point B in Fig. 2.5.20a. The normalized admittance at B is $y_B = 1 - j0.82$. As shown in Fig. 2.5.20b, this can be implemented with a short-circuited shunt stub of length $l_1 = 0.141\lambda$. The second element produces the admittance $y_C = 0.5 - j0.3$ at point C . This element is implemented using a series microstrip line of length $l_2 = 0.099\lambda$. Finally, the third element changes the susceptance along a constant conductance circle of 0.5 from $-j0.3$ to $-j0.6$. This element can be implemented using a short-circuited shunt stub of length $l_3 = 0.203\lambda$ (i.e., having an admittance of $-j0.3$). The matching network is shown in Fig. 2.5.20b.

2.6 SIGNAL FLOW GRAPHS AND APPLICATIONS

A signal flow graph is a convenient technique to represent and analyze the transmission and reflection of waves in a microwave amplifier. Once the signal flow graph is developed, relations between the variables can be obtained using Mason’s rule. The flow graph technique permits expressions, such as power gains and voltage gains of complex microwave amplifiers, to be derived easily. Certain rules are followed in constructing a signal flow graph:



(a)



(b)

Figure 2.5.20 (a) Design in the ZY Smith chart for Example 2.5.6; (b) the matching network.

1. Each variable is designated as a node.
2. The S parameters and reflection coefficients are represented by branches.
3. Branches enter dependent variable nodes and emanate from independent variable nodes. The independent variable nodes are the incident waves, and the reflected waves are dependent variables nodes.
4. A node is equal to the sum of the branches entering it.

The signal flow graph of the S parameters of a two-port network is shown in Fig. 2.6.1. Observe that b_1 and b_2 are the dependent nodes and a_1 and a_2 the independent nodes. The complete signal flow graph of the two-port network is shown in Fig. 2.6.2.

The signal flow graph in Fig. 2.6.2 shows the relationship between the traveling waves. The incident wave a_1 at port 1 gets partly transmitted (i.e., $S_{21}a_1$) to become part of b_2 , and partly reflected (i.e., $S_{11}a_1$) to become part of b_1 . Similarly, the incident wave a_2 at port 2 gets partly transmitted (i.e., $S_{12}a_2$) to become part of b_1 and partly reflected (i.e., $S_{22}a_2$) to become part of b_2 .

In order to obtain the signal flow graph of a microwave amplifier, we need to obtain the signal flow graph of a signal generator with some internal impedance and the signal flow graph of a load impedance.

Figure 2.6.3a shows a voltage-source generator with impedance Z_s . At the terminals we can write

$$V_g = E_s + I_g Z_s \quad (2.6.1)$$

Using (1.4.1) and (1.4.2), we can express (2.6.1) in terms of traveling waves—namely,

$$V_g^+ + V_g^- = E_s + \left(\frac{V_g^+}{Z_o} - \frac{V_g^-}{Z_o} \right) Z_s$$

Solving for V_g^- , we obtain

$$b_g = b_s + \Gamma_s a_g \quad (2.6.2)$$

where

$$b_g = \frac{V_g^-}{\sqrt{Z_o}}$$

$$a_g = \frac{V_g^+}{\sqrt{Z_o}}$$

$$b_s = \frac{E_s \sqrt{Z_o}}{Z_s + Z_o}$$

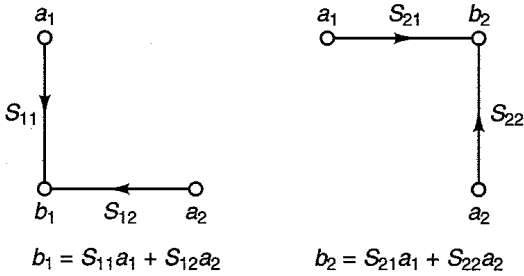


Figure 2.6.1 Signal flow graph for the scattering parameter equations.

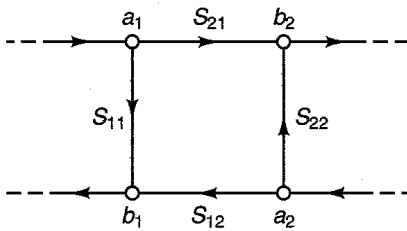


Figure 2.6.2 Signal flow graph of a two-port network.

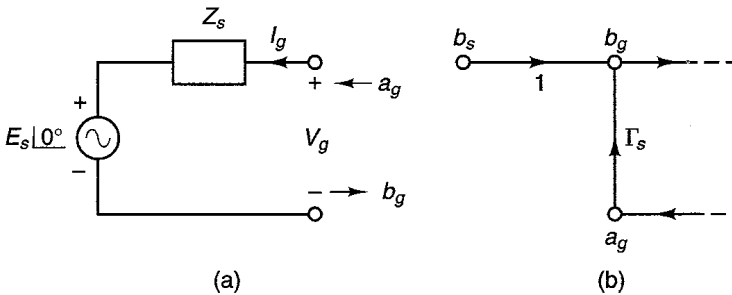


Figure 2.6.3 Signal flow graph of a voltage-source generator.

and

$$\Gamma_s = \frac{Z_s - Z_o}{Z_s + Z_o}$$

From (2.6.2), the signal flow graph in Fig. 2.6.3b follows.

For the load impedance shown in Fig. 2.6.4a, we can write

$$V_L = Z_L I_L$$

In terms of traveling waves, we obtain

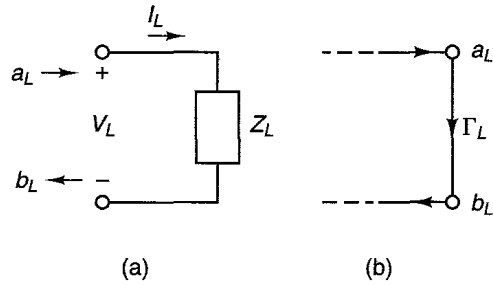


Figure 2.6.4 Signal flow graph of a load impedance.

$$V_L^+ + V_L^- = Z_L \left(\frac{V_L^+}{Z_o} - \frac{V_L^-}{Z_o} \right)$$

or

$$b_L = \Gamma_L a_L \tag{2.6.3}$$

where

$$b_L = \frac{V_L^-}{\sqrt{Z_o}}$$

$$a_L = \frac{V_L^+}{\sqrt{Z_o}}$$

and

$$\Gamma_L = \frac{Z_L - Z_o}{Z_L + Z_o}$$

The signal flow graph follows from (2.6.3) and is shown in Fig. 2.6.4b.

We can now combine the signal flow graph for the two-port network in Fig. 2.6.2 with the signal flow graphs of the signal generator (i.e., Fig. 2.6.3b) and the load (i.e., Fig. 2.6.4b). Observe that the nodes $b_g, a_g, b_L,$ and a_L are identical to $a_1, b_1, a_2,$ and $b_2,$ respectively. The resulting signal flow graph of a microwave amplifier is shown in Fig. 2.6.5.

To determine the ratio or transfer function T of a dependent to an independent variable, we apply Mason's rule—namely,

$$T = \frac{P_1[1 - \Sigma L(1)^{(1)} + \Sigma L(2)^{(1)} - \dots] + P_2[1 - \Sigma L(1)^{(2)} + \dots] + \dots}{1 - \Sigma L(1) + \Sigma L(2) - \Sigma L(3) + \dots}$$

where the different terms are defined as follows.

The terms $P_1, P_2,$ and so on are the different paths connecting the dependent and independent variables whose transfer function T is to be determined. A path is defined as a set of consecutive, codirectional branches along which no node is encountered more than once as we move in the graph from the independent to

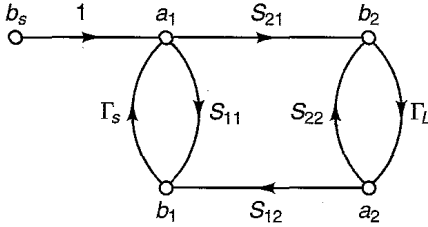


Figure 2.6.5 Signal flow graph of a microwave amplifier.

the dependent node. The value of the path is the product of all branch coefficients along the path. For example, in Fig. 2.6.5, b_s is the only independent variable. To determine the ratio b_1/b_s , we identify two paths, $P_1 = S_{11}$ and $P_2 = S_{21}\Gamma_L S_{12}$.

The term $\sum L(1)$ is the sum of all first-order loops. A first-order loop is defined as the product of the branches encountered in a round trip as we move from a node in the direction of the arrows back to that original node. In Fig. 2.6.5, $S_{11}\Gamma_s$, $S_{21}\Gamma_L S_{12}\Gamma_s$, and $S_{22}\Gamma_L$ are first-order loops.

The term $\sum L(2)$ is the sum of all second-order loops. A second-order loop is defined as the product of any two nontouching first-order loops. In Fig. 2.6.5, $S_{11}\Gamma_s$ and $S_{22}\Gamma_L$ do not touch; therefore, the product $S_{11}\Gamma_s S_{22}\Gamma_L$ is a second-order loop.

The term $\sum L(3)$ is the sum of all third-order loops. A third-order loop is defined as the product of three nontouching first-order loops. In Fig. 2.6.5, there are no third-order loops. Of course, the terms $\sum L(4)$, $\sum L(5)$, and so on represent fourth-, fifth-, and higher-order loops.

The terms $\sum L(1)^{(P)}$ is the sum of all first-order loops that do not touch the path P between the independent and dependent variables. In Fig. 2.6.5, for the path $P_1 = S_{11}$ we find that $\sum L(1)^{(1)} = \Gamma_L S_{22}$, and for the path $P_2 = S_{21}\Gamma_L S_{12}$ we find that $\sum L(1)^{(2)} = 0$.

The term $\sum L(2)^{(P)}$ is the sum of all second-order loops that do not touch the path P between the independent and dependent variables. In Fig. 2.6.5, we find that $\sum L(2)^{(P)} = 0$. Of course, $\sum L(3)^{(P)}$, $\sum L(4)^{(P)}$, and so on represent higher-order loops that do not touch the path P .

For the transfer function b_1/b_s in Fig. 2.6.5, we have found that $P_1 = S_{11}$, $P_2 = S_{21}\Gamma_L S_{12}$, $\sum L(1) = S_{11}\Gamma_s + S_{22}\Gamma_L + S_{21}\Gamma_L S_{12}\Gamma_s$, $\sum L(2) = S_{11}\Gamma_s S_{22}\Gamma_L$, and $\sum L(1)^{(1)} = \Gamma_L S_{22}$. Therefore, using Mason's rule, we obtain

$$\frac{b_1}{b_s} = \frac{S_{11}(1 - \Gamma_L S_{22}) + S_{21}\Gamma_L S_{12}}{1 - (S_{11}\Gamma_s + S_{22}\Gamma_L + S_{21}\Gamma_L S_{12}\Gamma_s) + S_{11}\Gamma_s S_{22}\Gamma_L}$$

Applications of Signal Flow Graphs

The first application of signal flow graph analysis is in the calculation of the input reflection coefficient, called Γ_{IN} , when a load is connected to the output of a two-port network. The signal flow graph is shown in Fig. 2.6.6.

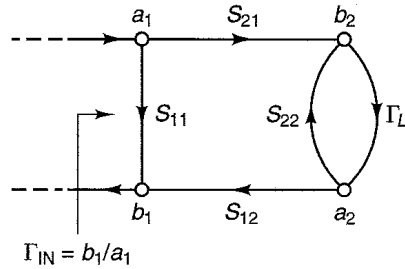


Figure 2.6.6 Signal flow graph for the input reflection coefficient Γ_{IN} .

The input reflection coefficient Γ_{IN} is defined as

$$\Gamma_{IN} = \frac{b_1}{a_1}$$

Observing that $P_1 = S_{11}$, $P_2 = S_{21}\Gamma_L S_{12}$, $\Sigma L(1) = S_{22}\Gamma_L$, and $\Sigma L(1)^{(1)} = S_{22}\Gamma_L$, we can use Mason's rule to obtain

$$\begin{aligned} \Gamma_{IN} &= \frac{S_{11}(1 - S_{22}\Gamma_L) + S_{21}\Gamma_L S_{12}}{1 - S_{22}\Gamma_L} \\ &= S_{11} + \frac{S_{12}S_{21}\Gamma_L}{1 - S_{22}\Gamma_L} \end{aligned} \tag{2.6.4}$$

If $\Gamma_L = 0$, it follows from (2.6.4) that $\Gamma_{IN} = S_{11}$. Also, when there is no transmission from the output to the input (i.e., when $S_{12} = 0$), it follows that $\Gamma_{IN} = S_{11}$. When $S_{12} = 0$, we call the device represented by the two-port a unilateral device.

Similarly, we can calculate the output reflection coefficient $\Gamma_{OUT} = b_2/a_2$ with $b_s = 0$ from the signal flow graph shown in Fig. 2.6.7. The expression for Γ_{OUT} is

$$\Gamma_{OUT} = S_{22} + \frac{S_{12}S_{21}\Gamma_s}{1 - S_{11}\Gamma_s} \tag{2.6.5}$$

Next, we use signal flow graphs to calculate power gain and voltage gain. The square of the magnitude of the incident and reflected waves represents

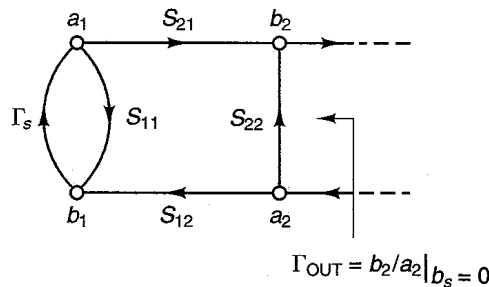


Figure 2.6.7 Signal flow graph for the output reflection coefficient Γ_{OUT} .

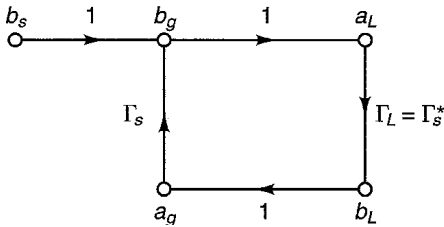


Figure 2.6.8 Signal flow graph of a voltage source connected to a conjugate matched load.

power. Therefore, the power delivered to the load in Fig. 2.6.5 is given by the difference between the incident and reflected power—namely,

$$P_L = \frac{1}{2} |b_2|^2 - \frac{1}{2} |a_2|^2 = \frac{1}{2} |b_2|^2 (1 - |\Gamma_L|^2) \quad (2.6.6)$$

The power available from a source is defined as the power delivered by the source to a conjugately matched load. Figure 2.6.8 shows the signal flow graph of a source connected to a conjugate match load (i.e., $\Gamma_L = \Gamma_s^*$). Therefore, the power available from the source, in Fig. 2.6.8, is given by

$$P_{AVS} = \frac{1}{2} |b_g|^2 - \frac{1}{2} |a_g|^2 \quad (2.6.7)$$

Observing that $b_g = b_s + b_g \Gamma_s \Gamma_s^*$ and $a_g = b_g \Gamma_s^*$, we obtain

$$b_g = \frac{b_s}{1 - |\Gamma_s|^2} \quad (2.6.8)$$

and

$$a_g = \frac{b_s \Gamma_s^*}{1 - |\Gamma_s|^2} \quad (2.6.9)$$

Substituting (2.6.8) and (2.6.9) into (2.6.7) gives

$$P_{AVS} = \frac{\frac{1}{2} |b_s|^2}{1 - |\Gamma_s|^2} \quad (2.6.10)$$

The previous results could have also been obtained as follows. Observe that the power delivered to the load Γ_L in Fig. 2.6.8 is given by

$$P_L = |a_L|^2 (1 - |\Gamma_L|^2) = \frac{\frac{1}{2} |b_s|^2 (1 - |\Gamma_L|^2)}{|1 - \Gamma_s \Gamma_L|^2}$$

Therefore, with $\Gamma_L = \Gamma_s^*$ the power delivered to the load is equal to the available power from the source, and (2.6.10) follows.

The transducer power gain, called G_T , is defined as the ratio of the power delivered to a load to the power available from the source. From (2.6.6) and (2.6.10), we obtain

$$G_T = \frac{P_L}{P_{AVS}} = \frac{|b_2|^2}{|b_s|^2} (1 - |\Gamma_L|^2) (1 - |\Gamma_s|^2) \quad (2.6.11)$$

The ratio b_2/b_s can be obtained using Mason's rule—namely,

$$\begin{aligned} \frac{b_2}{b_s} &= \frac{S_{21}}{1 - (S_{11}\Gamma_s + S_{22}\Gamma_L + S_{21}\Gamma_L S_{12}\Gamma_s) + S_{11}\Gamma_s S_{22}\Gamma_L} \\ &= \frac{S_{21}}{(1 - S_{11}\Gamma_s)(1 - S_{22}\Gamma_L) - S_{21}S_{12}\Gamma_L\Gamma_s} \end{aligned} \quad (2.6.12)$$

Substituting (2.6.12) into (2.6.11) results in

$$G_T = \frac{|S_{21}|^2 (1 - |\Gamma_s|^2) (1 - |\Gamma_L|^2)}{|(1 - S_{11}\Gamma_s)(1 - S_{22}\Gamma_L) - S_{21}S_{12}\Gamma_L\Gamma_s|^2} \quad (2.6.13)$$

The denominator of (2.6.13) can be further manipulated, and G_T can be expressed in the form

$$G_T = \frac{1 - |\Gamma_s|^2}{|1 - \Gamma_{IN}\Gamma_s|^2} |S_{21}|^2 \frac{1 - |\Gamma_L|^2}{|1 - S_{22}\Gamma_L|^2} \quad (2.6.14)$$

or

$$G_T = \frac{1 - |\Gamma_s|^2}{|1 - S_{11}\Gamma_s|^2} |S_{21}|^2 \frac{1 - |\Gamma_L|^2}{|1 - \Gamma_{OUT}\Gamma_L|^2} \quad (2.6.15)$$

where Γ_{IN} and Γ_{OUT} are given by (2.6.4) and (2.6.5), respectively.

The power gain G_p is defined as the ratio of the power delivered to the load P_L to the input power to the network P_{IN} . P_L is given by (2.6.6), and the input power is given by

$$P_{IN} = \frac{1}{2} |a_1|^2 - \frac{1}{2} |b_1|^2 = \frac{1}{2} |a_1|^2 (1 - |\Gamma_{IN}|^2)$$

Hence, we can express the power gain in the form

$$G_p = \frac{P_L}{P_{IN}} = \frac{|b_2|^2 (1 - |\Gamma_L|^2)}{|a_1|^2 (1 - |\Gamma_{IN}|^2)}$$

Dividing the numerator and denominator by $|b_s|^2$ gives

$$G_p = \frac{P_L}{P_{IN}} = \frac{\left|\frac{b_2}{b_s}\right|^2 (1 - |\Gamma_L|^2)}{\left|\frac{a_1}{b_s}\right|^2 (1 - |\Gamma_{IN}|^2)} \quad (2.6.16)$$

The ratio b_2/b_s is given by (2.6.12), and using Mason's rule, the ratio a_1/b_s is

$$\frac{a_1}{b_s} = \frac{1 - S_{22}\Gamma_L}{1 - (S_{11}\Gamma_s + S_{22}\Gamma_L + S_{21}\Gamma_L S_{12}\Gamma_s) + S_{11}\Gamma_s S_{22}\Gamma_L} \quad (2.6.17)$$

Substituting (2.6.12) and (2.6.17) into (2.6.16), we can express G_p in the form

$$G_p = \frac{1}{1 - |\Gamma_{IN}|^2} |S_{21}|^2 \frac{1 - |\Gamma_L|^2}{|1 - S_{22}\Gamma_L|^2} \quad (2.6.18)$$

The available power gain G_A is defined as the ratio of the power available from the network P_{AVN} to the power available from the source P_{AVS} . The power available from the network is the power delivered by the network to a conjugate matched load. That is,

$$\begin{aligned} P_{AVN} &= P_L|_{\Gamma_L=\Gamma_{OUT}^*} = \left[\frac{1}{2} |b_2|^2 - \frac{1}{2} |a_2|^2 \right] \Big|_{\Gamma_L=\Gamma_{OUT}^*} \\ &= \left[\frac{1}{2} |b_2|^2 (1 - |\Gamma_L|^2) \right] \Big|_{\Gamma_L=\Gamma_{OUT}^*} = \frac{1}{2} |b_2|^2 (1 - |\Gamma_{OUT}|^2) \end{aligned} \quad (2.6.19)$$

Therefore, from (2.6.19) and (2.6.10), G_A is given by

$$G_A = \frac{P_{AVN}}{P_{AVS}} = \frac{|b_2|^2}{|b_s|^2} (1 - |\Gamma_{OUT}|^2) (1 - |\Gamma_s|^2) \quad (2.6.20)$$

From (2.6.12), the ratio b_2/b_s with $\Gamma_L = \Gamma_{OUT}^*$ can be expressed as

$$\begin{aligned} \frac{b_2}{b_s} &= \frac{S_{21}}{(1 - S_{11}\Gamma_s)(1 - S_{22}\Gamma_L) - S_{21}S_{12}\Gamma_L\Gamma_s} \\ &= \frac{S_{21}}{(1 - S_{11}\Gamma_s)(1 - \Gamma_{OUT}\Gamma_L)} \Big|_{\Gamma_L=\Gamma_{OUT}^*} \\ &= \frac{S_{21}}{(1 - S_{11}\Gamma_s)(1 - |\Gamma_{OUT}|^2)} \end{aligned} \quad (2.6.21)$$

Substituting (2.6.21) into (2.6.20) results in the expression

$$G_A = \frac{1 - |\Gamma_s|^2}{|1 - S_{11}\Gamma_s|^2} |S_{21}|^2 \frac{1}{1 - |\Gamma_{OUT}|^2} \quad (2.6.22)$$

The voltage gain of the amplifier is defined as the ratio of the output voltage to the input voltage. That is,

$$A_v = \frac{a_2 + b_2}{a_1 + b_1}$$

Dividing by b_s gives

$$A_v = \frac{a_2/b_s + b_2/b_s}{a_1/b_s + b_1/b_s}$$

Therefore, we need to calculate the ratios a_2/b_s , b_2/b_s , a_1/b_s , and b_1/b_s using Mason's rule. The expression for A_v can be shown to be

$$A_v = \frac{S_{21}(1 + \Gamma_L)}{(1 - S_{22}\Gamma_L) + S_{11}(1 - S_{22}\Gamma_L) + S_{21}\Gamma_L S_{12}} \tag{2.6.23}$$

2.7 POWER-GAIN EXPRESSIONS: ALTERNATE DERIVATIONS

In the previous section, the power-gain expressions were derived using signal flow graph theory. In this section, the power-gain expressions are derived using a direct manipulation of the S -parameters relations.

For the microwave amplifier shown in Fig. 2.7.1, the source and load reflection coefficients in a Z_o system are

$$\Gamma_s = \frac{Z_s - Z_o}{Z_s + Z_o} \tag{2.7.1}$$

and

$$\Gamma_L = \frac{Z_L - Z_o}{Z_L + Z_o} \tag{2.7.2}$$

For the transistor, the input and output traveling waves measured in a Z_o system are related by

$$b_1 = S_{11}a_1 + S_{12}a_2 \tag{2.7.3}$$

and

$$b_2 = S_{21}a_1 + S_{22}a_2 \tag{2.7.4}$$

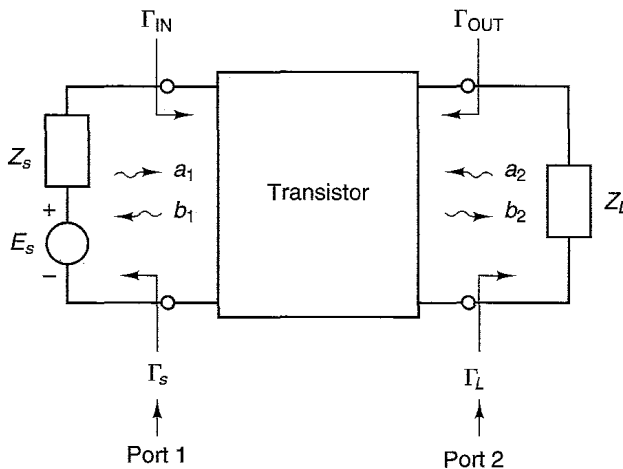


Figure 2.7.1 Block diagram of a microwave amplifier.

One should observe that the concepts of a reflection coefficient and traveling waves can be used even if there are no transmission lines at port 1 and port 2 in Fig. 2.7.1. The reflection coefficients Γ_s and Γ_L and the traveling waves a_1 , b_1 , a_2 , and b_2 are the reflection coefficients and traveling waves that would exist if transmission lines with characteristic impedances Z_o were inserted at ports 1 and 2. Alternatively, we could think of the reflection coefficients and the traveling waves as those in a transmission line of zero length and characteristic impedance Z_o connected at ports 1 and 2.

The input reflection coefficient Γ_{IN} is

$$\Gamma_{IN} = \frac{b_1}{a_1}$$

The ratio b_1/a_1 can be evaluated as follows. Since

$$a_2 = \Gamma_L b_2 \quad (2.7.5)$$

substituting (2.7.5) into (2.7.4) gives

$$b_2 = S_{21}a_1 + S_{22}\Gamma_L b_2$$

or

$$b_2 = \frac{S_{21}a_1}{1 - S_{22}\Gamma_L} \quad (2.7.6)$$

Then, substituting (2.7.5) and (2.7.6) into (2.7.3) gives

$$b_1 = S_{11}a_1 + S_{12}\Gamma_L b_2 = S_{11}a_1 + \frac{S_{12}S_{21}\Gamma_L}{1 - S_{22}\Gamma_L} a_1$$

or

$$\Gamma_{IN} = \frac{b_1}{a_1} = S_{11} + \frac{S_{12}S_{21}\Gamma_L}{1 - S_{22}\Gamma_L}$$

The output reflection coefficient is defined as

$$\Gamma_{OUT} = \left. \frac{b_2}{a_2} \right|_{E_s=0}$$

With $E_s = 0$, it follows that

$$a_1 = \Gamma_s b_1 \quad (2.7.7)$$

Substituting (2.7.7) into (2.7.3) gives

$$b_1 = S_{11}\Gamma_s b_1 + S_{12}a_2$$

or

$$b_1 = \frac{S_{12}a_2}{1 - S_{11}\Gamma_s} \quad (2.7.8)$$

Then, substituting (2.7.7) and (2.7.8) into (2.7.4) gives

$$b_2 = S_{21}\Gamma_s b_1 + S_{22}a_2 = \frac{S_{12}S_{21}\Gamma_s}{1 - S_{11}\Gamma_s} a_2 + S_{22}a_2$$

Therefore, Γ_{OUT} is given by

$$\Gamma_{OUT} = \frac{b_2}{a_2} \Big|_{E_s=0} = S_{22} + \frac{S_{12}S_{21}\Gamma_s}{1 - S_{11}\Gamma_s}$$

The power delivered to the input port of the transistor is

$$P_{IN} = \frac{1}{2} |a_1|^2 - \frac{1}{2} |b_1|^2 = \frac{1}{2} |a_1|^2 (1 - |\Gamma_{IN}|^2) \tag{2.7.9}$$

At the input port (see Fig. 2.7.2),

$$V_1 = E_s + I_1 Z_s \tag{2.7.10}$$

Therefore, in terms of traveling waves, (2.7.10) is written as

$$a_1 = b_s + \Gamma_s b_1 \tag{2.7.11}$$

where

$$a_1 = \frac{V_1^-}{\sqrt{Z_o}}$$

$$b_1 = \frac{V_1^+}{\sqrt{Z_o}}$$

$$b_s = \frac{E_s \sqrt{Z_o}}{Z_s + Z_o}$$

and

$$\Gamma_s = \frac{Z_s - Z_o}{Z_s + Z_o}$$

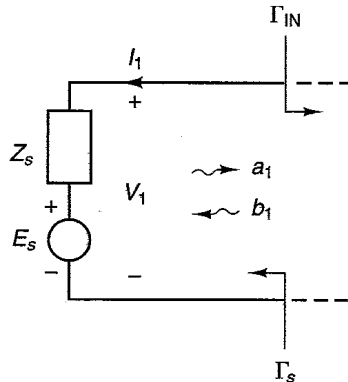


Figure 2.7.2 The input port.

Except for a nonmenclatural difference, (2.7.11) is identical to (2.6.2).

Since $b_1 = \Gamma_{\text{IN}} a_1$, (2.7.11) can be written as

$$a_1 = b_s + \Gamma_s \Gamma_{\text{IN}} a_1$$

or

$$a_1 = \frac{b_s}{1 - \Gamma_s \Gamma_{\text{IN}}} \quad (2.7.12)$$

Substituting (2.7.12) into (2.7.9) gives

$$P_{\text{IN}} = \frac{1}{2} |b_s|^2 \frac{1 - |\Gamma_{\text{IN}}|^2}{|1 - \Gamma_s \Gamma_{\text{IN}}|^2} \quad (2.7.13)$$

The power available from the source is equal to the input power when $\Gamma_{\text{IN}} = \Gamma_s^*$. With $\Gamma_{\text{IN}} = \Gamma_s^*$, (2.7.13) gives

$$P_{\text{AVS}} = P_{\text{IN}}|_{\Gamma_{\text{IN}}=\Gamma_s^*} = \frac{\frac{1}{2} |b_s|^2}{1 - |\Gamma_s|^2} \quad (2.7.14)$$

Observe that (2.7.14) agrees with (2.6.10).

Substituting (2.7.14) into (2.7.13), we can express P_{IN} in the form

$$P_{\text{IN}} = P_{\text{AVS}} \frac{(1 - |\Gamma_s|^2)(1 - |\Gamma_{\text{IN}}|^2)}{|1 - \Gamma_s \Gamma_{\text{IN}}|^2} \quad (2.7.15)$$

Equation (2.7.15) can be written as

$$P_{\text{IN}} = P_{\text{AVS}} M_s \quad (2.7.16)$$

where

$$M_s = \frac{(1 - |\Gamma_s|^2)(1 - |\Gamma_{\text{IN}}|^2)}{|1 - \Gamma_s \Gamma_{\text{IN}}|^2} \quad (2.7.17)$$

The factor M_s is known as the source mismatch factor (or the source mismatch loss). This factor is used to quantize what portion of P_{AVS} is delivered to the input of the transistor. Observe that if $\Gamma_{\text{IN}} = \Gamma_s^*$, (2.7.17) gives $M_s = 1$ and it follows that $P_{\text{IN}} = P_{\text{AVS}}$. This fact is expressed in the form

$$P_{\text{IN}} = P_{\text{AVS}}|_{\Gamma_{\text{IN}}=\Gamma_s^*}$$

A Thévenin's equivalent circuit at the output port of the transistor is shown in Fig. 2.7.3, where Z_{OUT} (i.e., the output impedance) is the Thévenin's impedance seen from the output terminals of the transistor. From Fig. 2.7.3, we have

$$V_L = E_{\text{TH}} - I_L Z_{\text{OUT}}$$

This expression is similar to (2.7.10) and can be expressed in terms of traveling waves as

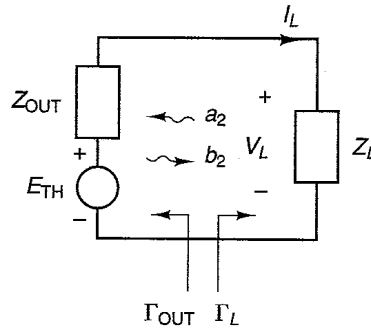


Figure 2.7.3 A Thévenin's equivalent circuit at the output port of the transistor.

$$b_2 = b_{TH} + \Gamma_{OUT}a_2 \tag{2.7.18}$$

where

$$b_2 = \frac{V_L^-}{\sqrt{Z_o}}$$

$$a_2 = \frac{V_L^+}{\sqrt{Z_o}}$$

$$b_{TH} = \frac{E_{TH} \sqrt{Z_o}}{Z_{OUT} + Z_o}$$

and

$$\Gamma_{OUT} = \frac{Z_{OUT} - Z_o}{Z_{OUT} + Z_o}$$

Since $a_2 = \Gamma_L b_2$, (2.7.18) gives

$$b_2 = b_{TH} + \Gamma_{OUT} \Gamma_L b_2$$

or

$$b_2 = \frac{b_{TH}}{1 - \Gamma_{OUT} \Gamma_L} \tag{2.7.19}$$

The power delivered to the load Z_L is

$$P_L = \frac{1}{2} |b_2|^2 - \frac{1}{2} |a_2|^2 = \frac{1}{2} |b_2|^2 (1 - |\Gamma_L|^2) \tag{2.7.20}$$

Substituting (2.7.19) into (2.7.20), we obtain

$$P_L = \frac{1}{2} |b_{TH}|^2 \frac{1 - |\Gamma_L|^2}{|1 - \Gamma_{OUT} \Gamma_L|^2} \tag{2.7.21}$$

The power available from the network P_{AVN} is equal to the power delivered to the load when $\Gamma_L = \Gamma_{OUT}^*$. With $\Gamma_L = \Gamma_{OUT}^*$, (2.7.21) gives

$$P_{AVN} = P_L|_{\Gamma_L = \Gamma_{OUT}^*} = \frac{\frac{1}{2} |b_{TH}|^2}{1 - |\Gamma_{OUT}|^2} \quad (2.7.22)$$

Substituting (2.7.22) into (2.7.21), we can express P_L in the form

$$P_L = P_{AVN} \frac{(1 - |\Gamma_L|^2)(1 - |\Gamma_{OUT}|^2)}{|1 - \Gamma_{OUT}\Gamma_L|^2} \quad (2.7.23)$$

Equation (2.7.23) can be written in the form

$$P_L = P_{AVN} M_L \quad (2.7.24)$$

where

$$M_L = \frac{(1 - |\Gamma_L|^2)(1 - |\Gamma_{OUT}|^2)}{|1 - \Gamma_{OUT}\Gamma_L|^2} \quad (2.7.25)$$

Observe the similarity between (2.7.24) and (2.7.16). The factor M_L is known as the load mismatch factor. This factor is used to quantize what portion of P_{AVN} is delivered to the load. For $\Gamma_L = \Gamma_{OUT}^*$, (2.7.25) gives $M_L = 1$ and it follows that $P_L = P_{AVN}$. This fact is expressed in the form

$$P_L = P_{AVN}|_{\Gamma_L = \Gamma_{OUT}^*}$$

The power gain is given by

$$G_p = \frac{P_L}{P_{IN}}$$

Therefore, using (2.7.9) and (2.7.20), we can write

$$G_p = \frac{P_L}{P_{IN}} = \frac{\frac{1}{2} |b_2|^2 (1 - |\Gamma_L|^2)}{\frac{1}{2} |a_1|^2 (1 - |\Gamma_{IN}|^2)} \quad (2.7.26)$$

Then, substituting (2.7.6) into (2.7.26), we obtain

$$G_p = \frac{1}{1 - |\Gamma_{IN}|^2} |S_{21}|^2 \frac{1 - |\Gamma_L|^2}{|1 - S_{22}\Gamma_L|^2} \quad (2.7.27)$$

The transducer power gain is given by

$$G_T = \frac{P_L}{P_{AVS}} = \frac{P_L}{P_{IN}} \frac{P_{IN}}{P_{AVS}} = G_p \frac{P_{IN}}{P_{AVS}} \quad (2.7.28)$$

From (2.7.16), the ratio P_{IN}/P_{AVS} is M_s ; therefore, (2.7.28) can be written as

$$G_T = G_p M_s \quad (2.7.29)$$

Substituting (2.7.17) and (2.7.27) into (2.7.29), we obtain

$$G_T = \frac{1 - |\Gamma_s|^2}{|1 - \Gamma_s \Gamma_{IN}|^2} |S_{21}|^2 \frac{1 - |\Gamma_L|^2}{|1 - S_{22} \Gamma_L|^2} \quad (2.7.30)$$

Manipulating the denominator, (2.7.30) can also be written in the form

$$G_T = \frac{1 - |\Gamma_s|^2}{|1 - S_{11} \Gamma_s|^2} |S_{21}|^2 \frac{1 - |\Gamma_L|^2}{|1 - \Gamma_{OUT} \Gamma_L|^2} \quad (2.7.31)$$

The available power gain can be expressed in the form

$$G_A = \frac{P_{AVN}}{P_{AVS}} = \frac{P_L}{P_{AVS}} \frac{P_{AVN}}{P_L} = \frac{G_T}{M_L}$$

Then, using (2.7.25) and (2.7.31), we can write G_A in the form

$$G_A = \frac{1 - |\Gamma_s|^2}{|1 - S_{11} \Gamma_s|^2} |S_{21}|^2 \frac{1}{1 - |\Gamma_{OUT}|^2} \quad (2.7.32)$$

It is of interest to investigate further the significance of the mismatch factors M_s and M_L . From (2.7.16), the factor M_s relates P_{AVS} to P_{IN} . Consider the network in Fig. 2.7.4a. For this network,

$$P_{AVS} = \frac{1}{8} \frac{|E_s|^2}{R_s}$$

and the input power is given by

$$P_{IN} = \frac{1}{2} \left| \frac{E_s}{Z_s + Z_{IN}} \right|^2 R_{IN} = \frac{1}{8} \frac{|E_s|^2}{R_s} \left(\frac{4R_s R_{IN}}{|Z_s + Z_{IN}|^2} \right) = P_{AVS} \left(\frac{4R_s R_{IN}}{|Z_s + Z_{IN}|^2} \right) \quad (2.7.33)$$

Comparing (2.7.33) with (2.7.16), it follows that the mismatch factor M_s is the term in parentheses in (2.7.33)—namely,

$$M_s = \frac{4R_s R_{IN}}{|Z_s + Z_{IN}|^2} \quad (2.7.34)$$

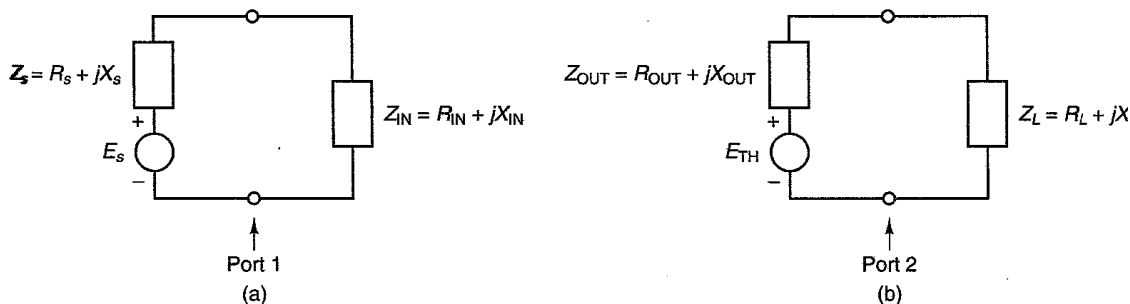


Figure 2.7.4 (a) The input port; (b) the output port.

Although it is not obvious at first sight, (2.7.34) and (2.7.17) are identical. To prove this, we use a normalizing impedance Z_o and write

$$Z_s = Z_o \frac{1 + \Gamma_s}{1 - \Gamma_s}$$

Then, the real part of Z_s is

$$R_s = \frac{1}{2} (Z_s + Z_s^*) = \frac{Z_o}{2} \left[\frac{1 + \Gamma_s}{1 - \Gamma_s} + \frac{1 + \Gamma_s^*}{1 - \Gamma_s^*} \right] = Z_o \frac{1 - |\Gamma_s|^2}{|1 - \Gamma_s|^2} \quad (2.7.35)$$

Similarly, we express the real part of Z_{IN} as

$$R_{IN} = Z_o \frac{1 - |\Gamma_{IN}|^2}{|1 - \Gamma_{IN}|^2} \quad (2.7.36)$$

Substituting (2.7.35) and (2.7.36) into (2.7.34), and simplifying a bit, it follows that

$$M_s = \frac{4R_s R_{IN}}{|Z_s + Z_{IN}|^2} = \frac{(1 - |\Gamma_{IN}|^2)(1 - |\Gamma_s|^2)}{|1 - \Gamma_s \Gamma_{IN}|^2}$$

At the output port in Fig. 2.7.4b, the factor M_L is given by

$$M_L = \frac{4R_{OUT} R_L}{|Z_{OUT} + Z_L|^2}$$

which is identical to (2.7.25).

Power-Gain Expressions in Terms of S_p Parameters

Consider the two-port network in Fig. 2.7.5, where the two-port network is characterized by its S_p parameters. In Section 1.7, the expression for G_T in terms of S_p parameters was derived [see (1.7.27)]. That is,

$$G_T = \frac{P_L}{P_{AVS}} = |S_{p21}|^2 \quad (2.7.37)$$

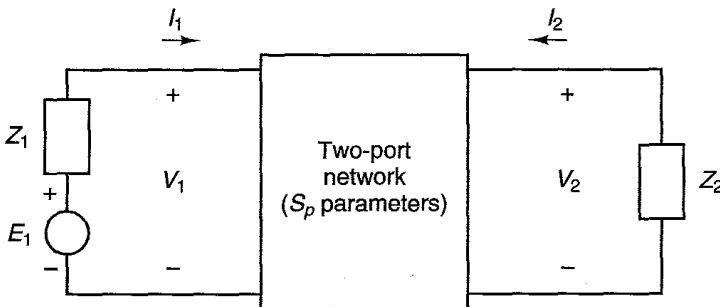


Figure 2.7.5 Two-port network characterized by its S_p parameters.

Using (2.7.28), the power gain G_p can be expressed as

$$G_p = G_T \frac{P_{AVS}}{P_{IN}} \quad (2.7.38)$$

In Fig. 2.7.5, the input power is given by

$$P_{IN} = P_{AVS}(1 - |S_{p11}|^2) \quad (2.7.39)$$

Substituting (2.7.37) and (2.7.39) into (2.7.38) gives

$$G_p = \frac{|S_{p21}|^2}{1 - |S_{p11}|^2} \quad (2.7.40)$$

Using (2.7.24), the power available from the network can be expressed as

$$G_A = \frac{G_T}{M_L} = \frac{G_T}{P_L} P_{AVN} \quad (2.7.41)$$

The power delivered to the load Z_L in Fig. 2.7.5 is given by

$$P_L = P_{AVN}(1 - |S_{p22}|^2) \quad (2.7.42)$$

Substituting (2.7.37) and (2.7.42) into (2.7.41) gives

$$G_A = \frac{|S_{p21}|^2}{1 - |S_{p22}|^2} \quad (2.7.43)$$

The power-gain expressions in terms of S_p parameters are given in (2.7.37), (2.7.40), and (2.7.43). Next, we will show that these relations are equivalent to the power-gain expressions in terms of S parameters given in (2.7.30), (2.7.27), and (2.7.32).

The derivation of the S_p parameters in terms of the S parameters is a difficult one. It consists of expressing the S parameters and S_p parameters in terms of z parameters and then eliminating the z parameters between the two relations to obtain the relation between the S_p parameters in terms of S parameters. The results are as follows:

$$S_{p11} = \frac{(1 - \Gamma_s)(1 - \Gamma_L S_{22})(S_{11} - \Gamma_s^*) + S_{12} S_{21} \Gamma_L}{(1 - \Gamma_s^*) D} \quad (2.7.44)$$

$$S_{p22} = \frac{(1 - \Gamma_L)(1 - \Gamma_s S_{11})(S_{22} - \Gamma_L^*) + S_{12} S_{21} \Gamma_s}{(1 - \Gamma_L^*) D} \quad (2.7.45)$$

$$S_{p21} = \frac{(1 - \Gamma_s) |1 - \Gamma_L| S_{21} [(1 - |\Gamma_s|^2)(1 - |\Gamma_L|^2)]^{1/2}}{|1 - \Gamma_s| (1 - \Gamma_L^*) D} \quad (2.7.46)$$

and

$$S_{p12} = \frac{(1 - \Gamma_L) |1 - \Gamma_s| S_{12} [(1 - |\Gamma_s|^2)(1 - |\Gamma_L|^2)]^{1/2}}{|1 - \Gamma_L| (1 - \Gamma_s^*) D} \quad (2.7.47)$$

where

$$D = (1 - \Gamma_s S_{11}) (1 - S_{22} \Gamma_L) - S_{21} S_{12} \Gamma_L \Gamma_s$$

Substituting (2.7.46) into (2.7.37), we obtain the expression for G_T in terms of S parameters—namely,

$$G_T = |S_{p21}|^2 = \frac{1 - |\Gamma_s|^2}{|1 - S_{11} \Gamma_s|^2} |S_{21}|^2 \frac{1 - |\Gamma_L|^2}{|1 - \Gamma_{OUT} \Gamma_L|^2}$$

which is recognized as (2.7.30). Similarly, substituting (2.7.44) and (2.7.46) into (2.7.40), we obtain the expression for G_p in (2.7.27); and substituting (2.7.45) and (2.7.46) into (2.7.43) gives the expression for G_A in (2.7.32).

2.8 VSWR CALCULATIONS

The VSWR in a transmission line is given by (1.3.44). Since the power delivered to the load in a transmission line, excited by a source with impedance Z_o , is given by

$$P_L = P_{AVS}(1 - |\Gamma_0|^2)$$

it follows that the magnitude of the load reflection coefficient, $|\Gamma_0|$ (which is related to the VSWR), provides a measure of what portion of P_{AVS} is delivered to the load.

For example, for a VSWR = 1 it follows that $|\Gamma_0| = 0$ and $P_L = P_{AVS}$ (i.e., all the incident power is delivered to the load). For a VSWR = 1.5, it follows that $|\Gamma_0| = 0.2$ and the ratio of the incident to the reflected power from the load is $|\Gamma_0|^2 = 0.04$, or 4%. Hence, 4% of the incident power is reflected by the load (96% of the incident power is delivered to the load). For a VSWR = 2, then $|\Gamma_0| = 1/3$ and $|\Gamma_0|^2 = 0.11$, or 11%. In this case, 11% of the incident power is reflected by the load.

The values of the input and output VSWR are important to the microwave amplifier designer. For example, many microwave amplifiers require the input VSWR to be less than 1.5. In other designs, higher VSWR values must be tolerated in order to obtain other performances, such as a particular noise performance.

Figure 2.8.1 shows the input portion of a microwave amplifier. The reflection coefficient at the input of the lossless matching network, normalized to Z_o , is denoted by Γ_a . The input VSWR, denoted by $(\text{VSWR})_{in}$, is related to Γ_a by

$$(\text{VSWR})_{in} = \frac{1 + |\Gamma_a|}{1 - |\Gamma_a|} \quad (2.8.1)$$

where

$$\Gamma_a = \frac{Z_a - Z_o}{Z_a + Z_o}$$

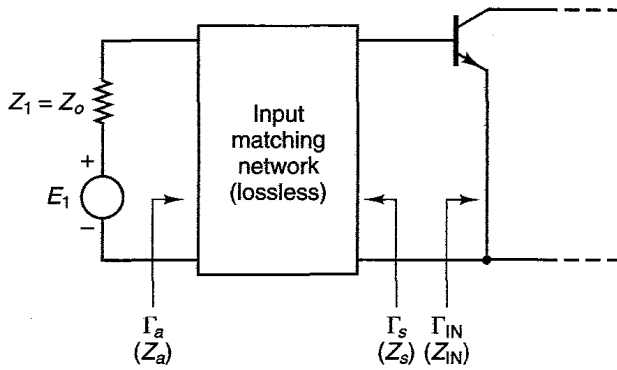


Figure 2.8.1 Input portion of a microwave amplifier.

Since the input power is given by

$$P_{IN} = P_{AVS}(1 - |\Gamma_a|^2)$$

and from (2.7.16) we have

$$P_{IN} = P_{AVS}M_s$$

it follows that

$$M_s = 1 - |\Gamma_a|^2$$

or

$$|\Gamma_a| = \sqrt{1 - M_s} \tag{2.8.2}$$

Equations (2.8.1) and (2.8.2) show that $(VSWR)_{in}$ can be calculated from a knowledge of the mismatch factor M_s .

Substituting (2.7.17) into (2.8.2) and simplifying results in the following expression for $|\Gamma_a|$:

$$|\Gamma_a| = \sqrt{1 - \frac{(1 - |\Gamma_s|^2)(1 - |\Gamma_{IN}|^2)}{|1 - \Gamma_s\Gamma_{IN}|^2}} = \left| \frac{\Gamma_{IN} - \Gamma_s^*}{1 - \Gamma_{IN}\Gamma_s} \right| \tag{2.8.3}$$

This relation shows that $|\Gamma_a|$ can be calculated from a knowledge of Γ_{IN} and Γ_s .

The concept of a reflection coefficient and of a VSWR can be used in a microwave amplifier even if there are no transmission lines. For example, in Fig. 2.8.1 this can occur when the input matching network is implemented using lumped components. The reflection coefficients and $(VSWR)_{in}$ in Fig. 2.8.1 can be thought of as those of a transmission line of zero length with characteristic impedance Z_o .

Similar relations can be defined for the output VSWR. The output portion of a microwave amplifier is shown in Fig. 2.8.2. For Fig. 2.8.2, we have

$$(VSWR)_{out} = \frac{1 + |\Gamma_b|}{1 - |\Gamma_b|} \tag{2.8.4}$$

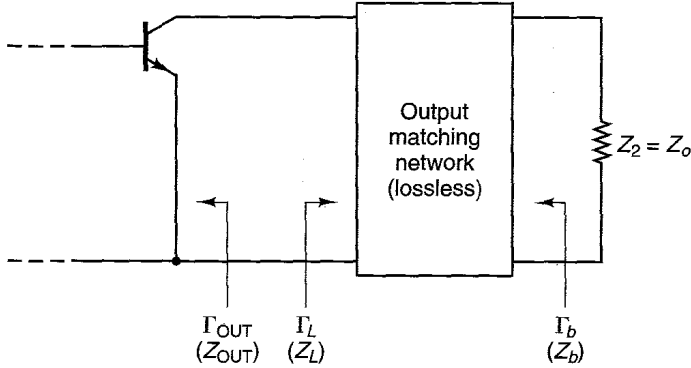


Figure 2.8.2 Output portion of a microwave amplifier.

$$\Gamma_b = \frac{Z_b - Z_o}{Z_b + Z_o}$$

$$|\Gamma_b| = \sqrt{1 - M_L} \quad (2.8.5)$$

and

$$|\Gamma_b| = \sqrt{1 - \frac{(1 - |\Gamma_L|^2)(1 - |\Gamma_{OUT}|^2)}{|1 - \Gamma_{OUT}\Gamma_L|^2}} = \left| \frac{\Gamma_{OUT} - \Gamma_L^*}{1 - \Gamma_{OUT}\Gamma_L} \right| \quad (2.8.6)$$

Example 2.8.1

(a) The input portion of the microwave amplifier in Fig. 2.5.14 is drawn in Fig. 2.8.3a. Assume that the S parameters of the transistor are such that the resulting Γ_{IN} is $0.614 \angle -160^\circ$. Calculate $(VSWR)_{in}$.

(b) Calculate $(VSWR)_{in}$ in Fig. 2.8.3a if Γ_{IN} is $0.4 \angle -145^\circ$.

Solution. (a) From (2.8.3), with $\Gamma_s = \Gamma_{IN}^* = 0.614 \angle 160^\circ$, it follows that $|\Gamma_a| = 0$. Therefore, using (2.8.1), we obtain $(VSWR)_{in} = 1$.

The previous calculation illustrates the fact that when $\Gamma_s = \Gamma_{IN}^*$, a conjugate matched condition exists at the input of the transistor and at the source. In other words, $Z_a = 50 \Omega$ (since $|\Gamma_a| = 0$) and the source sees a matched input impedance. This can also be verified by evaluating Z_a for the circuit in Fig. 2.8.3a. In Fig. 2.8.3b, we have plotted the normalized input admittance $y_{IN} = 1/z_{IN} = 2.8 + j1.9$ and calculated y_a to be 1, thus verifying that $Z_a = 50 \Omega$.

(b) In this case, Γ_{IN} is given as $0.4 \angle -145^\circ$. Therefore, $\Gamma_s \neq \Gamma_{IN}^*$, so the input of the transistor is not conjugate matched for maximum power transfer. Using (2.8.3), we obtain

$$|\Gamma_a| = \left| \frac{0.4 \angle -145^\circ - 0.614 \angle -160^\circ}{1 - 0.4 \angle -145^\circ (0.614 \angle 160^\circ)} \right| = 0.327$$

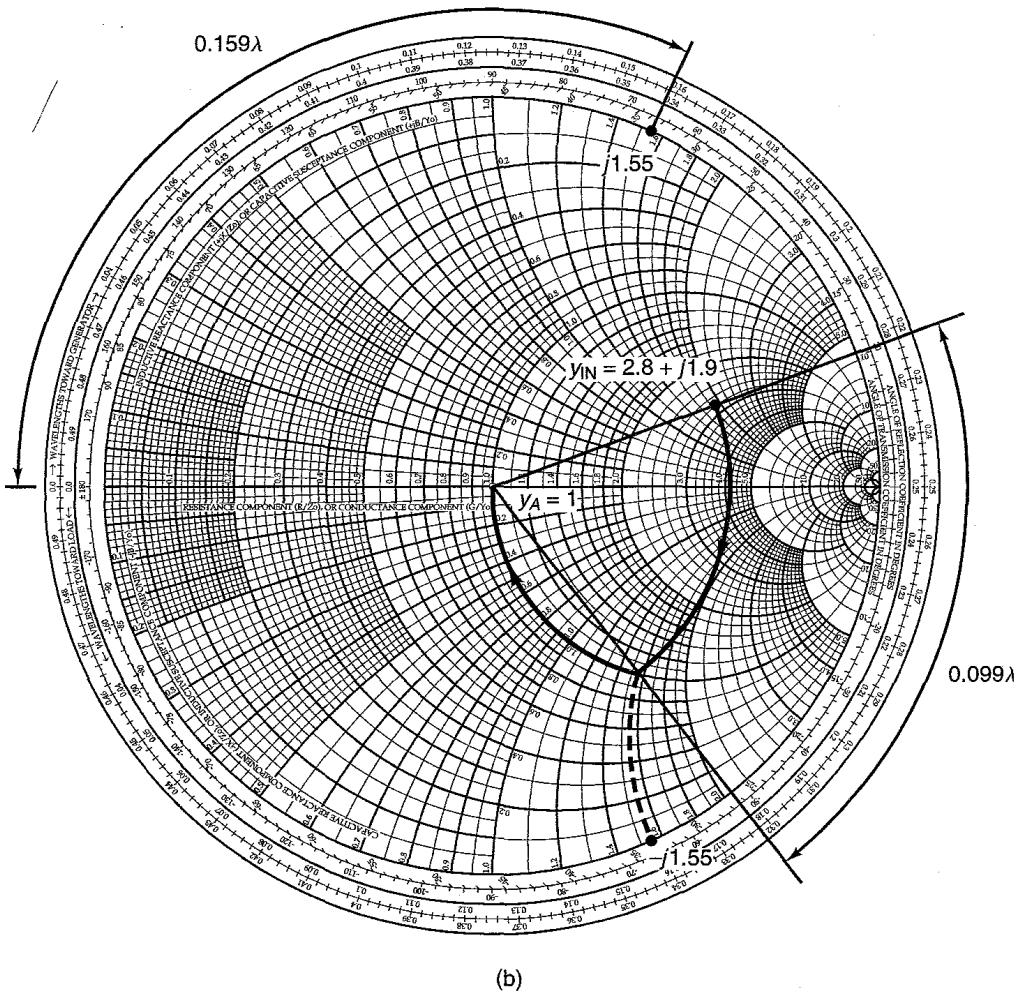
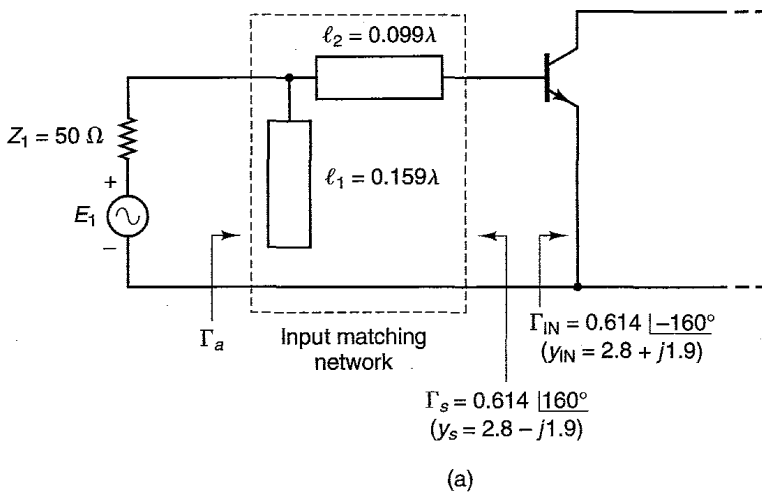


Figure 2.8.3 (a) Circuit for Example 2.8.1; (b) calculation of Z_a using the Smith chart.

Therefore, the value of $(VSWR)_{in}$ is

$$(VSWR)_{in} = \frac{1 + 0.327}{1 - 0.327} = 1.97$$

Let us proceed a little further with the analysis of the VSWR. Consider Fig. 2.8.4a, where the matching networks are assumed to be lossless. The indicated coefficients $\Gamma_a, \Gamma_b, \Gamma_{p,IN}$, and $\Gamma_{p,OUT}$ are power reflection coefficients. Since the impedances Z_1 and Z_2 are real (i.e., $Z_1 = Z_2 = Z_o$), it follows that Γ_a and Γ_b are identical to the traveling-wave reflection coefficients. The equivalent circuits at the input and output ports of the transistor are shown in Fig. 2.8.4b.

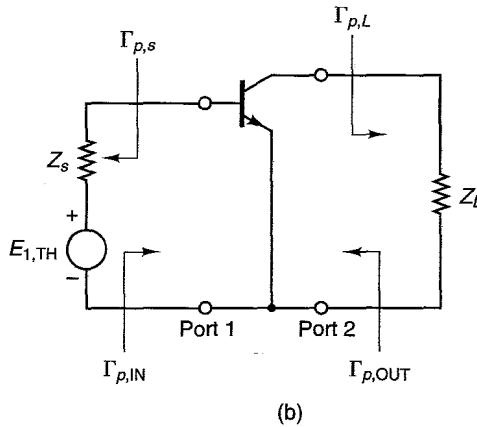
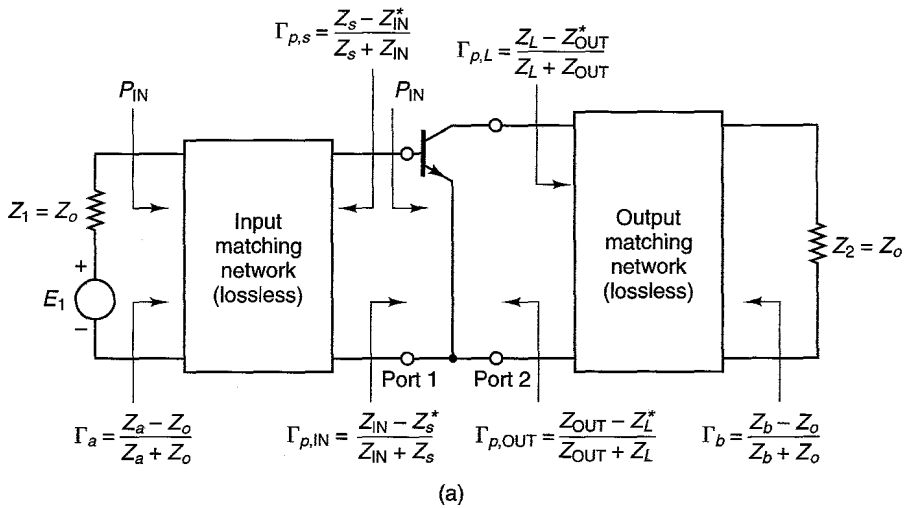


Figure 2.8.4 (a) Power reflection coefficients in a microwave amplifier; (b) an equivalent circuit.

The input power at the generator input in Fig. 2.8.4a can be written as

$$P_{\text{IN}} = P_{\text{AVS}}(1 - |\Gamma_a|^2) = P_{\text{AVS}}M_s \quad (2.8.7)$$

Since the matching circuits are assumed to be lossless, at the input of the transistor we can write

$$P_{\text{IN}} = P_{\text{AVS}}(1 - |\Gamma_{p,\text{IN}}|^2) = P_{\text{AVS}}M'_s \quad (2.8.8)$$

where $\Gamma_{p,\text{IN}}$ is the power reflection coefficient at the input of the transistor—namely,

$$\Gamma_{p,\text{IN}} = \frac{Z_{\text{IN}} - Z_s^*}{Z_{\text{IN}} + Z_s} \quad (2.8.9)$$

and

$$M'_s = 1 - |\Gamma_{p,\text{IN}}|^2$$

In writing (2.8.8), we used the fact that P_{AVS} is the same at the input and output ports of the lossless matching circuit. The parameter $\Gamma_{p,\text{IN}}$ is identical to the value of S_{p11} associated with the two-port network in Fig. 2.8.4b.

Equating (2.8.7) to (2.8.8) gives

$$M_s = M'_s \quad (2.8.10)$$

or

$$|\Gamma_a| = |\Gamma_{p,\text{IN}}|$$

It also follows that $|\Gamma_{p,\text{IN}}| = |\Gamma_{p,s}|$. From the previous results, $(\text{VSWR})_{\text{in}}$ can also be expressed in terms of $\Gamma_{p,\text{IN}}$ as

$$(\text{VSWR})_{\text{in}} = \frac{1 + |\Gamma_{p,\text{IN}}|}{1 - |\Gamma_{p,\text{IN}}|} \quad (2.8.11)$$

Equation (2.8.10) shows that the mismatch factor is an invariant quantity in a lossless matching network. That is, the mismatch factor M_s at the input of the input matching network is equal to the mismatch factor M'_s at the output of the input matching network. Using (2.7.34), we can express (2.8.10) in terms of impedances as

$$\frac{4Z_o R_a}{|Z_o + Z_a|^2} = \frac{4R_s R_{\text{IN}}}{|Z_s + Z_{\text{IN}}|^2}$$

where $R_a = \text{Re}[Z_a]$, $R_s = \text{Re}[Z_s]$, and $R_{\text{IN}} = \text{Re}[Z_{\text{IN}}]$.

Similarly, at the output of the amplifier in Fig. 2.8.4a, we can write

$$M_L = M'_L$$

$$M_L = 1 - |\Gamma_b|^2 = \frac{4Z_o R_b}{|Z_o + Z_b|^2}$$

$$M'_L = 1 - |\Gamma_{p,OUT}|^2 = \frac{4R_L R_{OUT}}{|Z_L + Z_{OUT}|^2}$$

$$|\Gamma_b| = |\Gamma_{p,OUT}| = |\Gamma_{p,L}|$$

$$\Gamma_{p,OUT} = \frac{Z_{OUT} - Z_L^*}{Z_{OUT} + Z_L}$$

and

$$(\text{VSWR})_{out} = \frac{1 + |\Gamma_{p,OUT}|}{1 - |\Gamma_{p,OUT}|} \quad (2.8.12)$$

where $R_b = \text{Re}[Z_b]$, $R_L = \text{Re}[Z_L]$, and $R_{OUT} = \text{Re}[Z_{OUT}]$. The parameter $\Gamma_{p,OUT}$ is identical to the value of S_{p22} associated with the two-port network in Fig. 2.8.4b.

Example 2.8.2

(a) Calculate the $(\text{VSWR})_{in}$ in Example 2.8.1, part (a), using (2.8.11).

(b) Calculate the $(\text{VSWR})_{in}$ in Example 2.8.1, part (b), using (2.8.11). Also, evaluate M'_s .

Solution. (a) With $\Gamma_s = \Gamma_{IN}^*$, it follows that $Z_s = Z_{IN}^* = 12.308 + j8.297 \Omega$. Therefore, from (2.8.9) it follows that $\Gamma_{p,IN} = 0$ and from (2.8.11), $(\text{VSWR})_{in} = 1$.

(b) With $\Gamma_{IN} = 0.4 \angle -145^\circ$ (or $Z_{IN} = 23.136 - j12.638 \Omega$), it follows from (2.8.9) that

$$\Gamma_{p,IN} = \frac{Z_{IN} - Z_s^*}{Z_{IN} + Z_s} = \frac{23.136 - j12.638 - (12.308 - j8.297)}{23.136 - j12.638 + (12.308 + j8.297)} = 0.327 \angle -14.86^\circ$$

and

$$(\text{VSWR})_{in} = \frac{1 + 0.327}{1 - 0.327} = 1.97$$

As expected, $|\Gamma_d| = |\Gamma_{p,IN}| = |\Gamma_{p,s}| = 0.327$.

The mismatch factor M'_s is

$$M'_s = M'_s = 1 - |\Gamma_{p,IN}|^2 = 1 - (0.327)^2 = 0.893$$

PROBLEMS

- 2.1 (a)** Locate in the Z Smith chart the impedance $Z = 100 + j100 \Omega$ using a reference impedance of 50Ω .
- (b)** Find the value of the normalized admittance y using the Z Smith chart, and evaluate the value of Y (i.e., $Y = yY_o = y/Z_o$).
- (c)** Find y using the ZY Smith chart.
- (d)** Repeat parts (a) to (c) for the following impedances: $Z = 50 - j100 \Omega$, $Z = 25 - j25 \Omega$, $Z = j50 \Omega$, and $Z = j0 \Omega$.
- 2.2 (a)** Show that impedances having a negative real part (i.e., $z = -r + jx$) have a reflection coefficient whose magnitude is greater than 1.

- (b) Prove that negative resistances can be handled in the Smith chart by plotting $1/\Gamma^*$ and interpreting the resistance circles as being negative and the reactance circles as marked.
- (c) Locate in the Smith chart the impedances $Z_1 = -20 + j16 \Omega$ and $Z_2 = -200 + j25 \Omega$ and find the associated reflection coefficient. Normalize the impedances to 50Ω .
- (d) Work the problem in part (c) in the compressed Smith chart.
- (e) What is the value of $|\Gamma|$ on the boundary of the compressed Smith chart in Fig. 2.2.5?

2.3 Show that the impedance along a transmission line repeats itself at every $\lambda/2$ distance. That is,

$$Z(d) = Z\left(d + \frac{n\lambda}{2}\right), \quad n = 1, 2, 3, \dots$$

2.4 Show that the impedance along a transmission line can be expressed in the form

$$Z(d) = R(d) + jX(d) = |Z(d)|e^{j\theta_d}$$

where

$$R(d) = Z_o \frac{1 - |\Gamma|^2}{1 - 2|\Gamma| \cos \phi + |\Gamma|^2}$$

$$X(d) = Z_o \frac{2|\Gamma| \sin \phi}{1 - 2|\Gamma| \cos \phi + |\Gamma|^2}$$

$$|Z(d)| = Z_o \sqrt{\frac{1 + 2|\Gamma| \cos \phi + |\Gamma|^2}{1 - 2|\Gamma| \cos \phi + |\Gamma|^2}}$$

$$\theta_d = \tan^{-1} \frac{X(d)}{R(d)} = \tan^{-1} \left(\frac{2|\Gamma| \sin \phi}{1 - |\Gamma|^2} \right)$$

$$\Gamma = |\Gamma_0|e^{j\phi}, \quad \Gamma_0 = |\Gamma_0|e^{j\phi_0}, \quad \phi = \phi_0 - 2\beta d$$

- 2.5 Find the input impedance, the load reflection coefficient, and the VSWR in a transmission line having an electrical length of 90° , $Z_o = 50 \Omega$, and terminated in the load $Z_L = 50 + j100 \Omega$. Work the problem in both the Z and Y Smith charts.
- 2.6 (a) Prove that the maximum normalized resistance in a transmission line is numerically equal to the VSWR.
- (b) Prove that the minimum normalized resistance in a transmission line is numerically equal to $1/\text{VSWR}$.
- 2.7 (a) Determine the length l of the $50\text{-}\Omega$ short-circuited transmission line shown in Fig. 2.2.8a so that the input impedance is $Z_{\text{IN}}(l) = -j25 \Omega$.
- (b) Determine the length l of the $50\text{-}\Omega$ open-circuited transmission line shown in Fig. 2.2.8b so that the normalized input admittance is $y_{\text{IN}}(l) = j2$.
- 2.8 The normalized admittance (with $Z_o = 50 \Omega$) of a one-port network is shown in Fig. P2.8 as the frequency varies from 500 MHz to 1 GHz. Determine an equivalent circuit for the one-port network and the element values.
- 2.9 (a) In the series RC circuit shown in Fig. 2.3.2, the value of C is 50 pF. Determine the values of f_a and f_b .

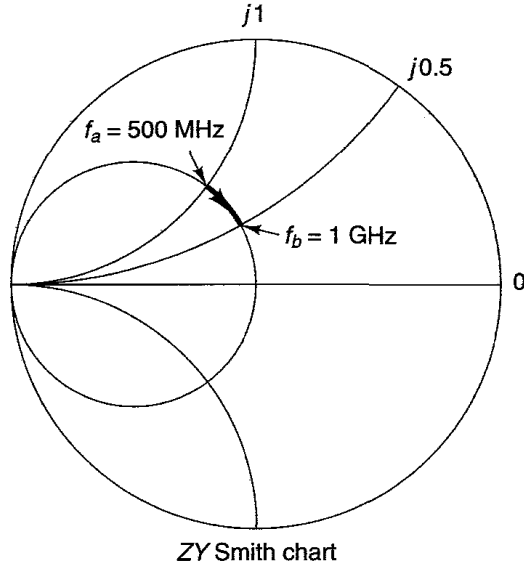


Figure P2.8

(b) In Example 2.3.2, assume that at $f_b = 1$ GHz the normalized impedance is $j0.6$. At $f_a = 500$ MHz, the normalized impedance remains at $j0.2$. Determine an equivalent circuit for the one-port network and the element values. Observe that in this problem the reactance does not increase linearly with frequency.

- 2.10 Design four different Ell matching networks to match the load $Z_{LOAD} = 10 + j40 \Omega$ to a $50\text{-}\Omega$ transmission line.
- 2.11 Design the matching network in Fig. P2.11 that provides $Y_L = (4 - j4) \times 10^{-3}$ S to the transistor. Find the element values at 700 MHz.

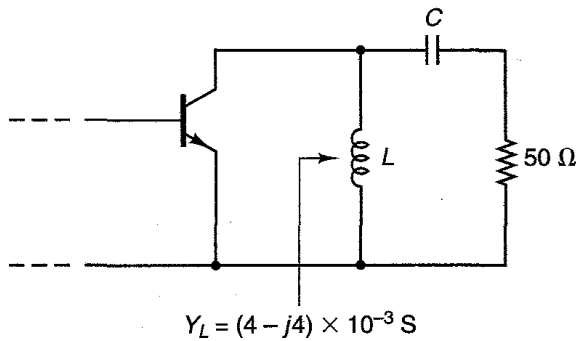


Figure P2.11

2.12 Two types of Ell matching networks are shown in Fig. P2.12. Select one that can match the load $Y_{LOAD} = (8 - j12) \times 10^{-3}$ S to a $50\text{-}\Omega$ transmission line. Find the element values at $f = 1$ GHz.

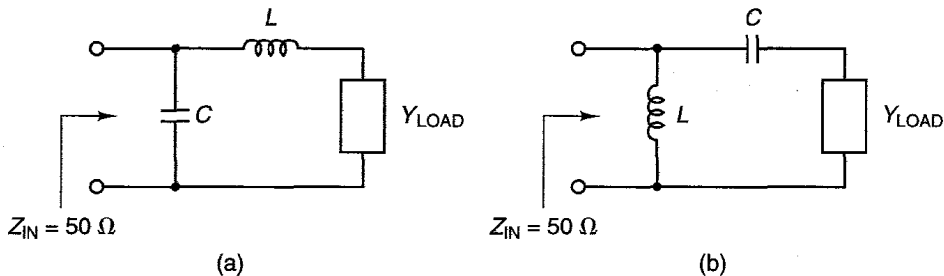


Figure P2.12

2.13 Show the impedance-admittance path in the ZY Smith chart for the circuit shown in Fig. P2.13 at $\omega = 10^9$ rad/s, and evaluate Z_{IN} .

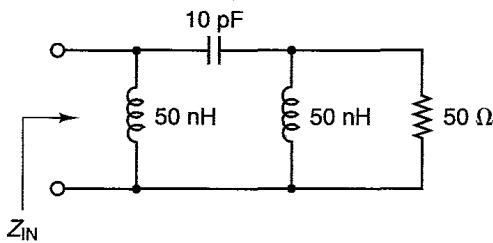


Figure P2.13

2.14 Design a two-element matching network to transform the load $Z_{LOAD} = 100 - j100 \Omega$ to an input impedance of $Z_{IN} = 25 + j25 \Omega$.

2.15 (a) Design a Tee matching network to transform $Z_{LOAD} = 50 \Omega$ to the input impedance $Z_{IN} = 20 + j20 \Omega$ with a Q of 5.

(b) Design a Pi matching network to transform $Z_{LOAD} = 50 \Omega$ to the input impedance $Z_{IN} = 25 \Omega$ with a Q of 2.5.

2.16 (a) Use Figs. 2.5.2 and 2.5.3 to calculate W , λ , and ϵ_{ff} for a characteristic impedance of 50Ω using RT/Duroid® with $\epsilon_r = 2.23$ and $h = 0.7874$ mm.

(b) Use (2.5.8) through (2.5.11) to show that for RT/Duroid® with $\epsilon_r = 2.23$ and $h = 0.7874$ mm, a $50\text{-}\Omega$ characteristic impedance is obtained with $W/h = 3.073$. Also, $\epsilon_{ff} = 1.91$ and $\lambda = 0.7236\lambda_0$.

2.17 The 10-nH inductor shown in Fig. P2.17 is to be implemented at 1 GHz using an open-circuited microstrip line with $Z_o = 50 \Omega$. The microstrip material has $\epsilon_r = 6$ and $h = 25$ mils. Determine the width and length of the microstrip line.

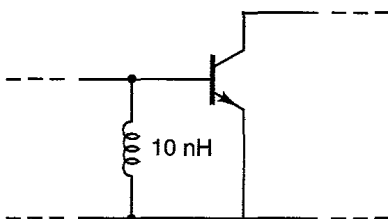


Figure P2.17

- 2.18** In the amplifier shown in Fig. 2.5.16b, calculate the width and the length of the lines at $f = 1$ GHz
- 2.19** (a) Design the matching circuit shown in Fig. P2.19 to transform the $50\text{-}\Omega$ load to the input impedance $Z_{\text{IN}} = 100 - j100\ \Omega$.
- (b) What is the length l_1 if the short-circuited shunt stub is replaced by an open-circuited shunt stub?
- (c) Repeat parts (a) and (b) for $Z_{\text{IN}} = 100 + j100\ \Omega$.

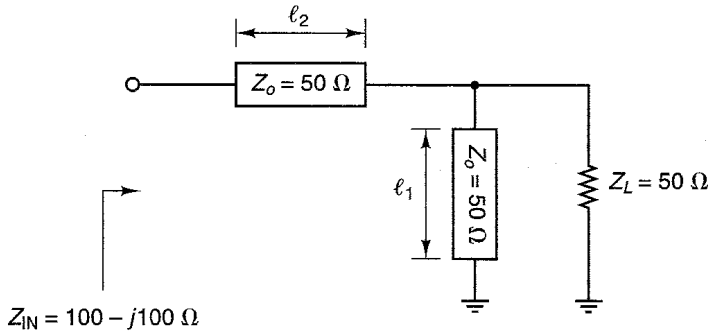


Figure P2.19

- 2.20** (a) Design a single-stub matching system (see Fig. P2.20) to match the load $Z_L = 15 + j25\ \Omega$ to a $50\text{-}\Omega$ transmission line. The characteristic impedance of the short-circuited stub is $50\ \Omega$.
- (b) Design the single-stub matching system in Fig. P2.20 assuming that the characteristic impedance of the stub is $100\ \Omega$.

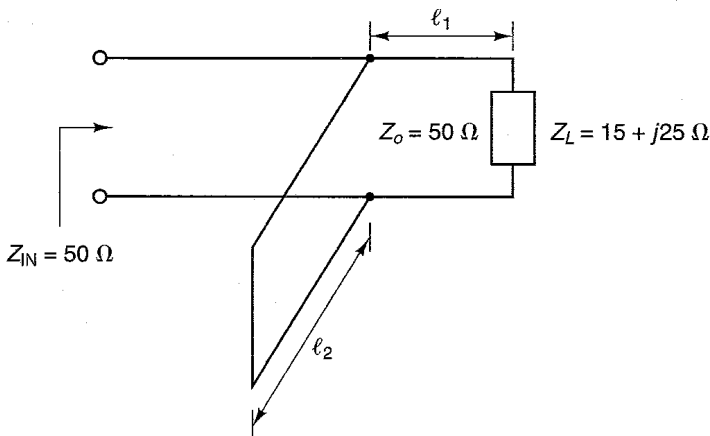


Figure P2.20

- 2.21** Design the matching circuits shown in Fig. P2.21 to transform the $50\text{-}\Omega$ load impedance to the input admittance given in the figures.

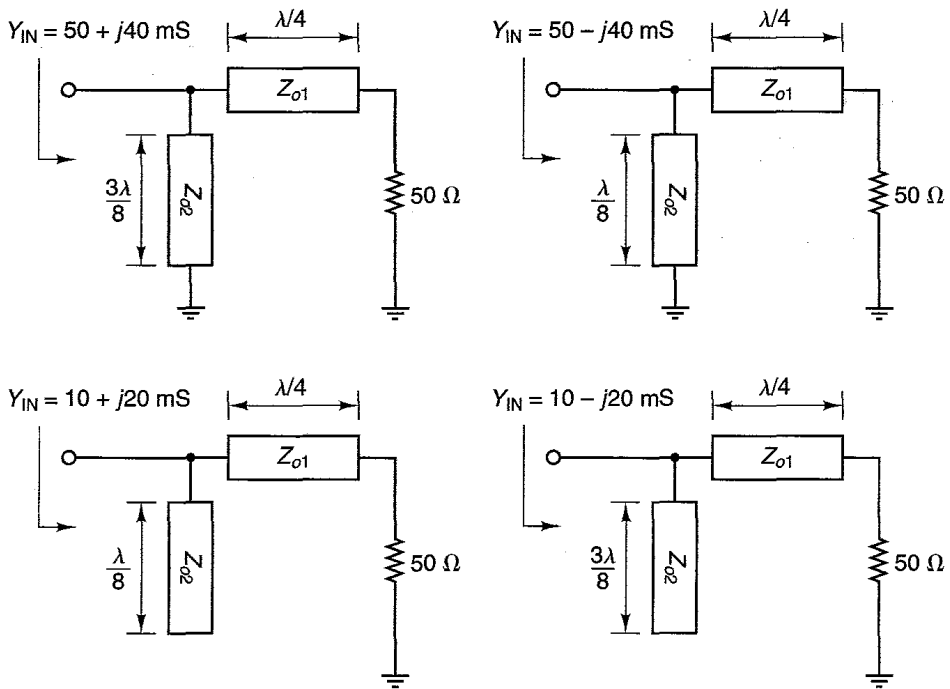


Figure P2.21

- 2.22 (a)** Design the matching networks shown in Fig. P2.22 to produce the source reflection coefficient $\Gamma_s = 0.5 \angle 90^\circ$. In Fig. P2.22b, the appropriate length for the short-circuited stub must be selected (i.e., $\lambda/8$ or $3\lambda/8$).
- (b)** Design the balance form of the shunt stubs.

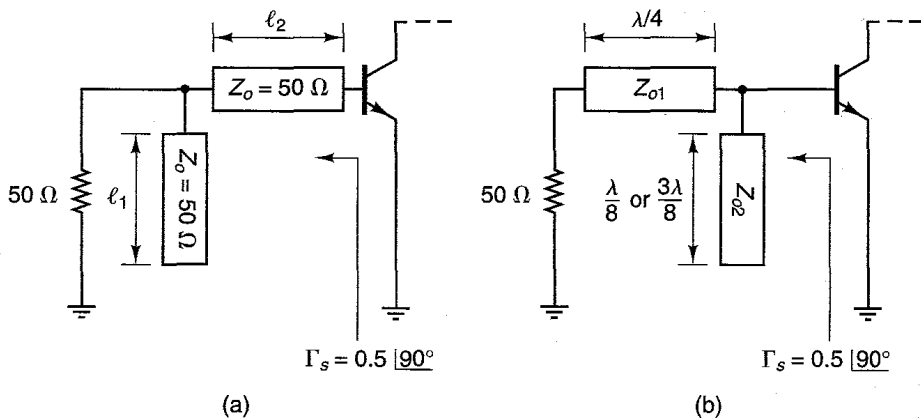


Figure P2.22

- 2.23** In the design shown in Fig. 2.5.16, the balance stubs of length $3\lambda/8$ were designed with characteristic impedances of 52.64Ω and 95.2Ω , respectively. Design the length of the balance stubs if the characteristic impedances are left at 26.32Ω and 47.6Ω , respectively.
- 2.24 (a)** Design the matching network in Fig. P2.24 to produce a load reflection coefficient of $\Gamma_L = 0.4 \angle -120^\circ$ to the transistor. The appropriate length for the balance stubs must be selected (i.e., $\lambda/8$ or $3\lambda/8$).
- (b)** Design the length of the balance stubs if the impedance Z_{o2} is changed to $Z_{o2}/2$.

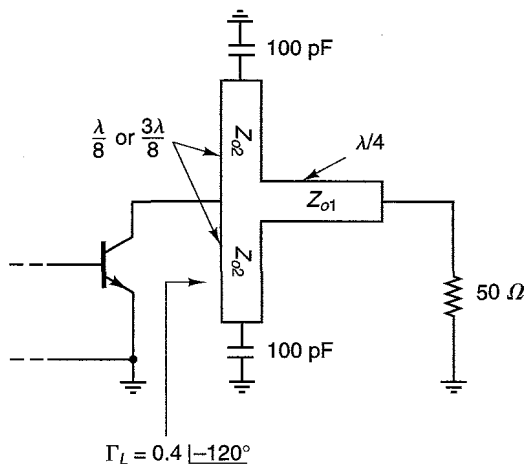


Figure P2.24

- 2.25** Design two microstrip matching networks for an amplifier whose reflection coefficients at $f = 800 \text{ MHz}$, in a $50\text{-}\Omega$ system, are $\Gamma_s = 0.8 \angle 160^\circ$ and $\Gamma_L = 0.7 \angle 20^\circ$. Show the diagram for the complete amplifier using balanced shunt stubs.
- 2.26 (a)** Determine the value of Γ_s in Fig. P2.26a.
- (b)** Determine the value of Γ_s in Fig. P2.26b. Observe that the 100-pF capacitor is a short circuit to the ac signal.
- 2.27 (a)** Determine the value of Γ_L in Fig. P2.27. The lengths shown are for $\epsilon_{ff} = 1$ and $f = 6 \text{ GHz}$.
- (b)** Show the balance form of the shunt stubs.
- 2.28** The input matching network shown in Fig. P2.28 was designed to obtain a certain gain. If the input reflection coefficient is $\Gamma_{IN} = 0.5 \angle 100^\circ$, determine the value of the impedance Z_A seen by the source.
- 2.29** Design a microstrip matching network to transform the load impedance $Z_L = 50 - j50 \Omega$ to the input impedance $Z_{IN} = 25 + j25 \Omega$ in Fig. P2.29.
- 2.30** Determine the value of Γ_L in Fig. P2.30.
- 2.31** Design a two-element matching network, as shown in the Smith chart in Fig. P2.31, that produces $\Gamma_s = 0.57 \angle 116^\circ$.

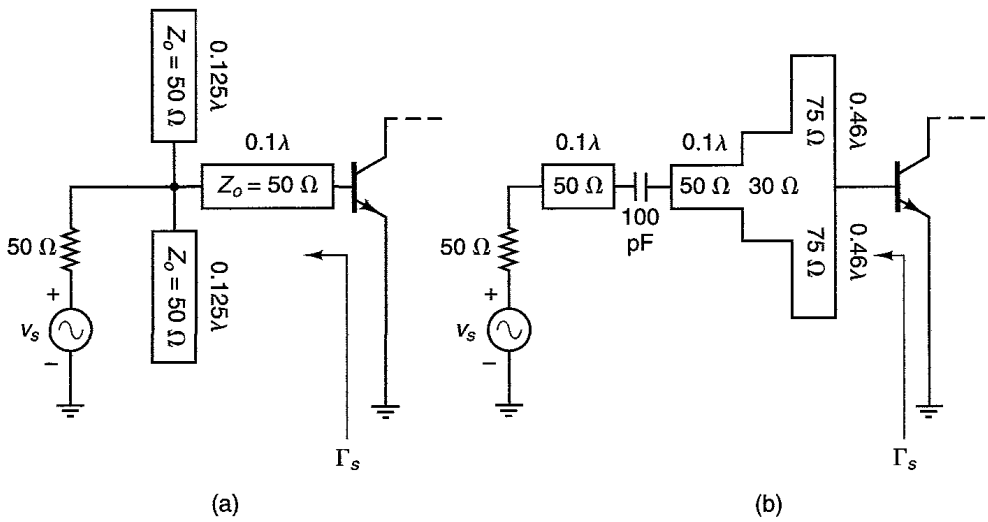


Figure P2.26

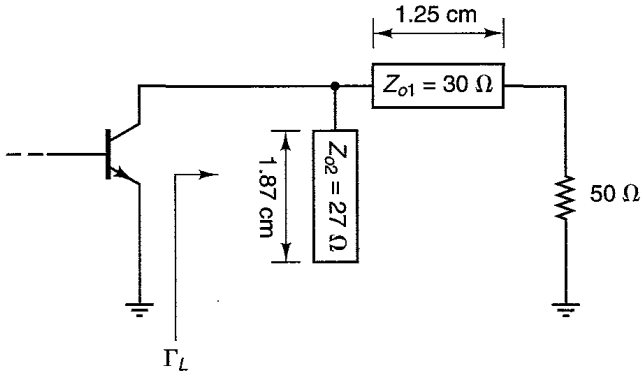


Figure P2.27

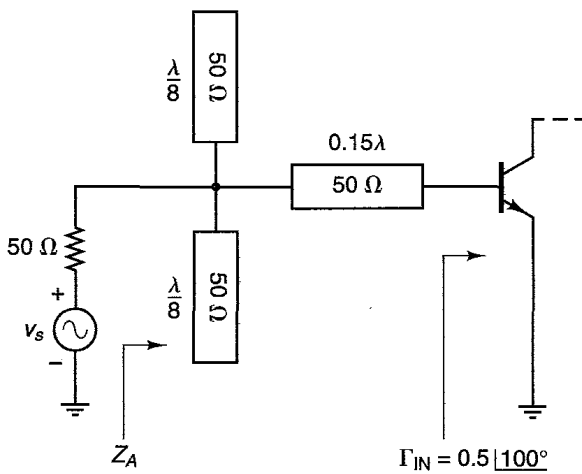


Figure P2.28

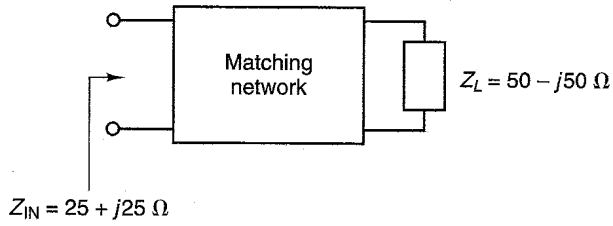


Figure P2.29

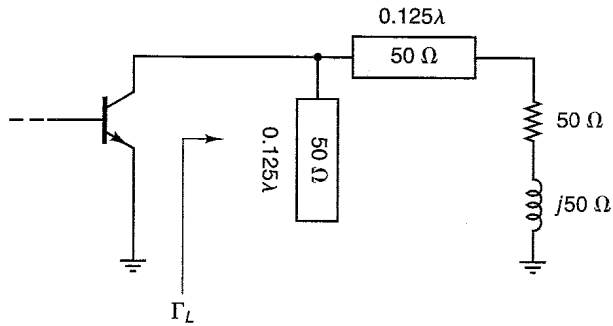


Figure P2.30

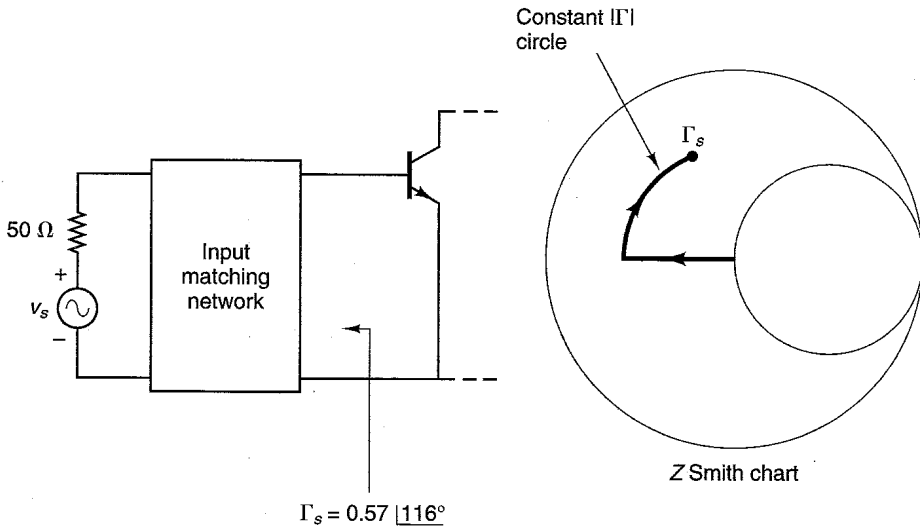


Figure P2.31

2.32 Design the matching networks in Fig. P2.32 to match the load $Z_L = 100 + j100 \Omega$ to a 50- Ω transmission line.

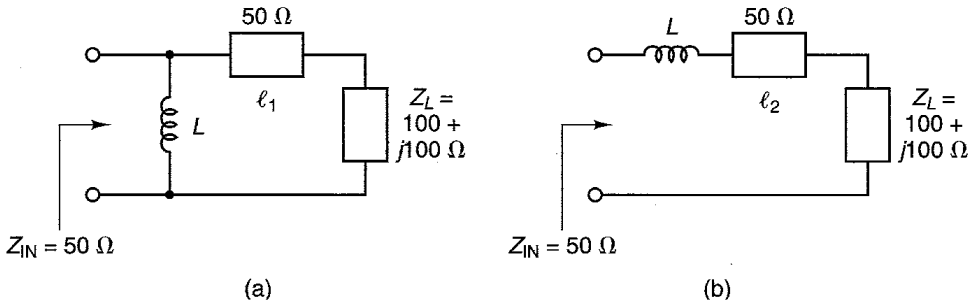


Figure P2.32

2.33 Design the matching networks in Fig. P2.33 to match a 50- Ω load to the impedance Z_{IN} .

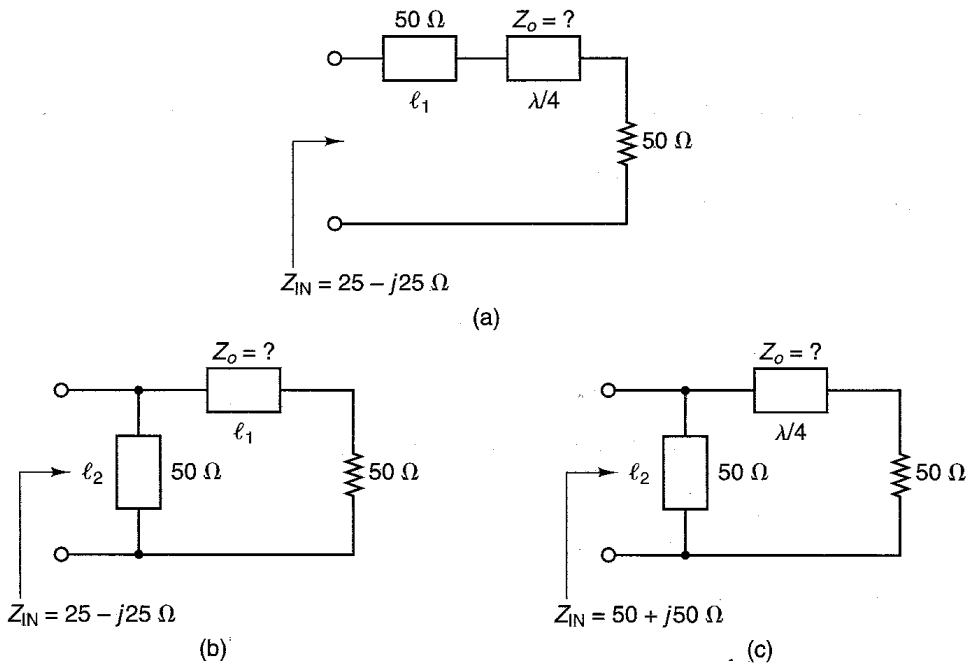


Figure P2.33

2.34 Verify the expressions for G_T in (2.6.14) and (2.6.15).

2.34 Verify the expression for A_v in (2.6.23).

- 2.36** (a) The output portion of a microwave amplifier is shown in Fig. P2.36. Calculate $(VSWR)_{out}$ if $\Gamma_{OUT} = 0.682 \angle -97^\circ$.
 (b) Verify the Z_b is 50Ω when $\Gamma_L = \Gamma_{OUT}^*$.
 (c) Calculate $(VSWR)_{out}$ if $\Gamma_{OUT} = 0.5 \angle -60^\circ$.

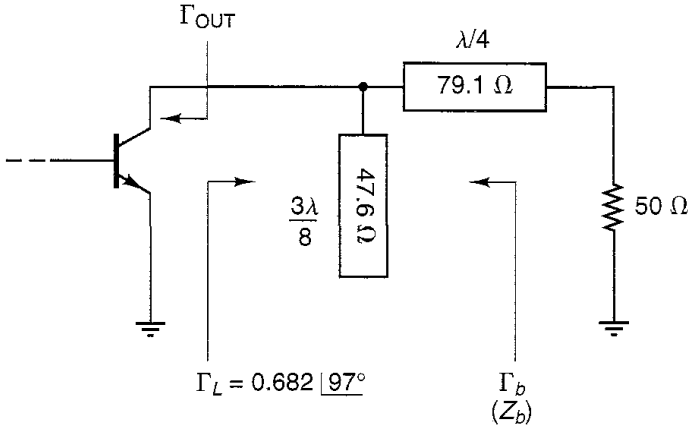


Figure P2.36

- 2.37** (a) The input portion of a microwave amplifier is shown in Fig. P2.37. Calculate $(VSWR)_{in}$ if $\Gamma_{IN} = 0.545 \angle -77.7^\circ$.
 (b) Verify that Z_a is 50Ω when $\Gamma_s = \Gamma_{IN}^*$.
 (c) Calculate $(VSWR)_{in}$ if $\Gamma_{IN} = 0.4 \angle 45^\circ$.

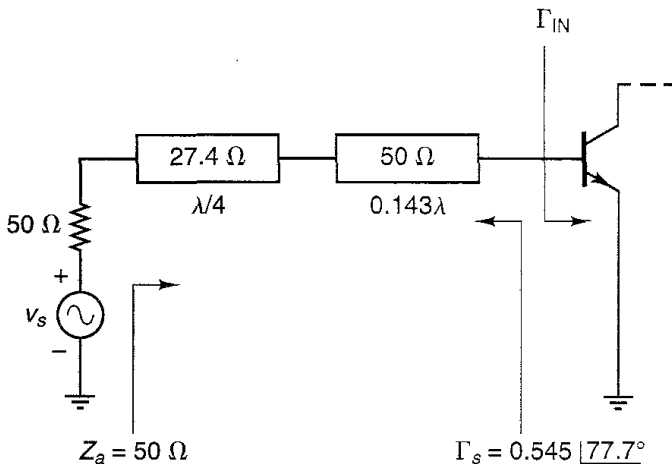


Figure P2.37

REFERENCES

- [2.1] I. J. Bahl and D. K. Trivedi, "A Designer's Guide to Microstrip Line," *Microwaves*, May 1977.
- [2.2] H. Sobol, "Applications of Integrated Circuit Technology to Microwave Frequencies," *Proceedings of the IEEE*, August 1971.
- [2.3] H. Sobol, "Extending IC Technology to Microwave Equipment," *Electronics*, March 1967.

3

MICROWAVE TRANSISTOR AMPLIFIER DESIGN

3.1 INTRODUCTION

This chapter develops some basic principles used in the analysis and design of microwave transistor amplifiers. Based on the S parameters of the transistor and certain performance requirements, a systematic procedure is developed for the design of a microwave transistor amplifier.

The most important design considerations in a microwave transistor amplifier are stability, power gain, bandwidth, noise, and dc requirements. This chapter deals mainly with the problems of stability and power gain in narrow-band amplifiers. VSWR considerations are also discussed. Low-noise amplifiers, broadband amplifiers, and power amplifiers are discussed in Chapter 4.

A design usually starts with a set of specifications and the selection of the proper transistor. Then a systematic mathematical solution, aided by graphical methods, is developed to determine the transistor loading (i.e., the source and load reflection coefficients) for a particular stability and gain criteria. An unconditionally stable transistor will not oscillate with any passive termination. On the other hand, a design using a potentially unstable transistor requires some analysis and careful considerations so that the passive terminations produce a stable amplifier.

Design procedures for both unilateral and bilateral transistors, based on stability and gain requirements, are described. Both passive and active dc bias networks for BJTs and GaAs FETs are analyzed. It is important to select the correct dc operating point and the proper dc network topology in order to obtain the desired ac performance.

3.2 POWER GAIN EQUATIONS

Several power gain equations appear in the literature and are used in the design of microwave amplifiers. Figure 3.2.1 illustrates a microwave amplifier signal flow graph and the different powers used in gain equations. The transducer power gain G_T , the power gain G_p (also called the *operating power gain*), and the available power gain G_A are defined as follows:

$$G_T = \frac{P_L}{P_{AVS}} = \frac{\text{power delivered to the load}}{\text{power available from the source}}$$

$$G_p = \frac{P_L}{P_{IN}} = \frac{\text{power delivered to the load}}{\text{power input to the network}}$$

and

$$G_A = \frac{P_{AVN}}{P_{AVS}} = \frac{\text{power available from the network}}{\text{power available from the source}}$$

The expressions for G_T , G_p , and G_A were already derived in (2.6.14), (2.6.15), (2.6.18), and (2.6.22)—namely,

$$G_T = \frac{1 - |\Gamma_s|^2}{|1 - \Gamma_{IN}\Gamma_s|^2} |S_{21}|^2 \frac{1 - |\Gamma_L|^2}{|1 - S_{22}\Gamma_L|^2} \quad (3.2.1)$$

$$G_T = \frac{1 - |\Gamma_s|^2}{|1 - S_{11}\Gamma_s|^2} |S_{21}|^2 \frac{1 - |\Gamma_L|^2}{|1 - \Gamma_{OUT}\Gamma_L|^2} \quad (3.2.2)$$

$$G_p = \frac{1}{1 - |\Gamma_{IN}|^2} |S_{21}|^2 \frac{1 - |\Gamma_L|^2}{|1 - S_{22}\Gamma_L|^2} \quad (3.2.3)$$

$$G_A = \frac{1 - |\Gamma_s|^2}{|1 - S_{11}\Gamma_s|^2} |S_{21}|^2 \frac{1}{1 - |\Gamma_{OUT}|^2} \quad (3.2.4)$$

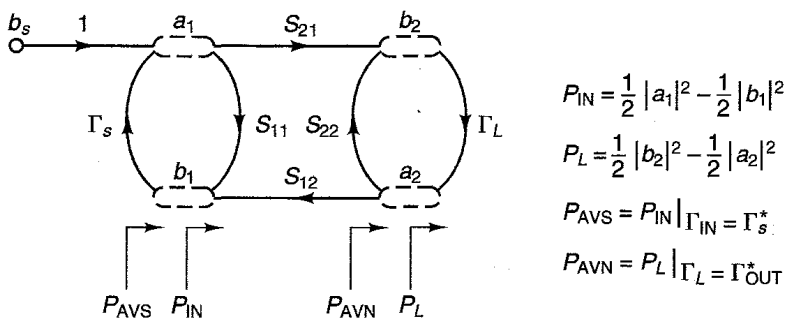


Figure 3.2.1 Different power definitions.

$$\Gamma_{IN} = S_{11} + \frac{S_{12}S_{21}\Gamma_L}{1 - S_{22}\Gamma_L} \tag{3.2.5}$$

$$\Gamma_{OUT} = S_{22} + \frac{S_{12}S_{21}\Gamma_s}{1 - S_{11}\Gamma_s} \tag{3.2.6}$$

G_T is a function of Γ_s, Γ_L , and the S parameters of the transistor (i.e., $G_T = f(\Gamma_s, \Gamma_L, [S])$, $G_p = f(\Gamma_L, [S])$, and $G_A = f(\Gamma_s, [S])$).

In terms of the amplifier shown in Fig. 3.2.2, the input matching network transforms the generator impedance Z_1 (usually 50Ω) to the impedance Z_s , or in other words to the source reflection coefficient Γ_s . The output matching network transforms the impedance Z_2 (usually 50Ω) to the load impedance Z_L or to the load reflection coefficient Γ_L . Observe that we use the nomenclature Z_s and Γ_s for the source impedance and source reflection coefficient at the input port of the transistor, and Z_L and Γ_L for the load impedance and load reflection coefficient at the output port of the transistor.

The values of Γ_s, Γ_L , and the S parameters of the transistor determine the gains of the amplifier according to (3.2.1) through (3.2.4).

The passive matching networks produce values of Γ_s and Γ_L such that $|\Gamma_s| < 1$ and $|\Gamma_L| < 1$. In other words, the resistive part associated with Z_s and Z_L is positive. However, from (3.2.5) and (3.2.6) it is possible that for certain values of the S parameters (where $|\Gamma_s| < 1$ and $|\Gamma_L| < 1$) that $|\Gamma_{IN}| > 1$ and/or $|\Gamma_{OUT}| > 1$. When $|\Gamma_{IN}| > 1$ or $|\Gamma_{OUT}| > 1$, the input or output ports of the transistor present a negative resistance and oscillations can occur. Obviously, this is a situation that we must avoid in amplifier design.

Example 3.2.1

(a) The input and output matching networks in Fig. 3.2.2 are designed to produce $\Gamma_s = 0.5 \angle 120^\circ$ and $\Gamma_L = 0.4 \angle 90^\circ$. Determine G_T, G_A , and G_p if the S parameters of the transistor are

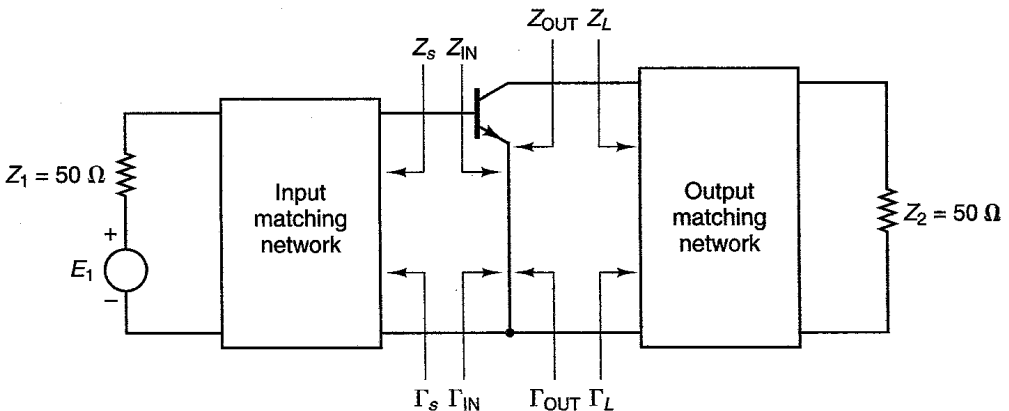


Figure 3.2.2 A microwave amplifier diagram.

$$S_{11} = 0.6 \angle -160^\circ$$

$$S_{12} = 0.045 \angle 16^\circ$$

$$S_{21} = 2.5 \angle 30^\circ$$

$$S_{22} = 0.5 \angle -90^\circ$$

(b) Calculate P_{AVS} , P_{IN} , P_{AVN} , and P_L in Fig. 3.2.2 if $E_1 = 10 \angle 0^\circ$, $Z_1 = 50 \Omega$, and $Z_2 = 50 \Omega$.

(c) Calculate $(VSWR)_{in}$ and $(VSWR)_{out}$.

Solution. (a) From (3.2.5) and (3.2.6) we obtain

$$\Gamma_{IN} = 0.6 \angle -160^\circ + \frac{0.045 \angle 16^\circ (2.5 \angle 30^\circ) 0.4 \angle 90^\circ}{1 - 0.5 \angle -90^\circ (0.4 \angle 90^\circ)} = 0.627 \angle -164.6^\circ$$

and

$$\Gamma_{OUT} = 0.5 \angle -90^\circ + \frac{0.045 \angle 16^\circ (2.5 \angle 30^\circ) 0.5 \angle 120^\circ}{1 - 0.6 \angle -160^\circ (0.5 \angle 120^\circ)} = 0.471 \angle -97.63^\circ$$

Then, from (3.2.1), (3.2.3), and (3.2.4) it readily follows that

$$G_T = \frac{1 - (0.5)^2}{|1 - 0.627 \angle -164.6^\circ (0.5 \angle 120^\circ)|^2} (2.5)^2 \frac{1 - (0.4)^2}{|1 - 0.5 \angle -90^\circ (0.4 \angle 90^\circ)|^2} = 9.43 \quad (\text{or } 9.75 \text{ dB})$$

$$G_p = \frac{1}{1 - (0.627)^2} (2.5)^2 \frac{1 - (0.4)^2}{|1 - 0.5 \angle -90^\circ (0.4 \angle 90^\circ)|^2} = 13.51 \quad (\text{or } 11.31 \text{ dB})$$

and

$$G_A = \frac{1 - (0.5)^2}{|1 - 0.6 \angle -160^\circ (0.5 \angle 120^\circ)|^2} (2.5)^2 \frac{1}{1 - (0.471)^2} = 9.55 \quad (\text{or } 9.8 \text{ dB})$$

Since the values of $G_p = P_L/P_{IN}$ and $G_T = P_L/P_{AVS}$ differ by 1.56 dB (i.e., 11.31 dB – 9.75 dB = 1.56 dB), it follows that the input power is less than the power available from the source. In fact, recall (2.7.16) and (2.7.29)—namely,

$$P_{IN} = P_{AVS} M_s \quad (3.2.7)$$

and

$$G_T = G_p M_s \quad (3.2.8)$$

where from (2.7.17) the source mismatch factor is

$$M_s = \frac{[1 - (0.5)^2][1 - (0.627)^2]}{|1 - 0.5 \angle 120^\circ (0.627 \angle -164.6^\circ)|^2} = 0.6983 \quad (\text{or } -1.56 \text{ dB})$$

Observe how G_T and G_p are related by (3.2.8). That is, 9.43 = 13.51(0.6983) or 9.75 dB = 11.31 dB – 1.56 dB.

Also, since $G_A = P_{AVN}/P_{AVS}$ and $G_T = P_L/P_{AVS}$ are fairly close (i.e., 9.8 dB and 9.75 dB, respectively), the power delivered to the load is close to the power available from the network. In fact,

$$P_L = P_{AVN}M_L \quad (3.2.9)$$

and

$$G_T = G_A M_L \quad (3.2.10)$$

where from (2.7.25) the load mismatch factor is

$$M_L = \frac{[1 - (0.4)^2][1 - (0.471)^2]}{|1 - 0.471 \angle -97.63^\circ (0.4 \angle 90^\circ)|^2} = 0.9874 \quad (\text{or } -0.055 \text{ dB})$$

Observe how G_T and G_A are related by (3.2.10). That is, $9.43 = 9.55(0.9874)$ or $9.75 \text{ dB} = 9.8 \text{ dB} - 0.055 \text{ dB}$.

(b) The power available from the source is

$$P_{AVS} = \frac{E_1^2}{8 \operatorname{Re}[Z_1]} = \frac{10^2}{8(50)} = 0.25 \text{ W}$$

Then, using (3.2.7) the input power is

$$P_{IN} = P_{AVS}M_s = 0.25(0.6983) = 0.1745 \text{ W}$$

The power delivered to the load can be calculated using the definition of G_T . That is,

$$P_L = G_T P_{AVS} = 9.43(0.25) = 2.358 \text{ W}$$

It can also be calculated using the definition of G_p . That is,

$$P_L = G_p P_{IN} = 13.51(0.1745) = 2.358 \text{ W}$$

The power available from the network can be calculated using (3.2.9). That is,

$$P_{AVN} = \frac{P_L}{M_L} = \frac{2.358}{0.9874} = 2.39 \text{ W}$$

It can also be calculated using the definition of G_A . That is,

$$P_{AVN} = G_A P_{AVS} = 9.55(0.25) = 2.39 \text{ W}$$

(c) Since the mismatch factor M_s has been calculated in part (a), it is simple to use (2.8.1) and (2.8.2) to calculate $(VSWR)_{in}$. That is,

$$(VSWR)_{in} = \frac{1 + |\Gamma_a|}{1 - |\Gamma_a|} = \frac{1 + \sqrt{1 - M_s}}{1 - \sqrt{1 - M_s}} = \frac{1 + \sqrt{1 - 0.6983}}{1 - \sqrt{1 - 0.6983}} = 3.44$$

Similarly, using (2.8.4) and (2.8.5) we obtain

$$(VSWR)_{out} = \frac{1 + |\Gamma_b|}{1 - |\Gamma_b|} = \frac{1 + \sqrt{1 - M_L}}{1 - \sqrt{1 - M_L}} = \frac{1 + \sqrt{1 - 0.9874}}{1 - \sqrt{1 - 0.9874}} = 1.25$$

3.3 STABILITY CONSIDERATIONS

The stability of an amplifier, or its resistance to oscillate, is a very important consideration in a design and can be determined from the S parameters, the matching networks, and the terminations. In a two-port network, oscillations are possible when either the input or output port presents a negative resistance. This occurs when $|\Gamma_{IN}| > 1$ or $|\Gamma_{OUT}| > 1$, which for a unilateral device occurs when $|S_{11}| > 1$ or $|S_{22}| > 1$. For example, a unilateral transistor is a transistor where $S_{12} = 0$ (or its effect so small that it can be set equal to zero). If $S_{12} = 0$, it follows from (3.2.5) and (3.2.6) that $|\Gamma_{IN}| = |S_{11}|$ and $|\Gamma_{OUT}| = |S_{22}|$. Hence, if $|S_{11}| > 1$ the transistor presents a negative resistance at the input, and if $|S_{22}| > 1$ the transistor presents a negative resistance at the output.

The two-port network shown in Fig. 3.3.1 is said to unconditionally stable at a given frequency if the real parts of Z_{IN} and Z_{OUT} are greater than zero for all passive load and source impedances. If the two-port is not unconditionally stable, it is potentially unstable. That is, some passive load and source terminations can produce input and output impedances having a negative real part.

In terms of reflection coefficients, the conditions for unconditional stability at a given frequency are

$$|\Gamma_s| < 1 \quad (3.3.1)$$

$$|\Gamma_L| < 1 \quad (3.3.2)$$

$$|\Gamma_{IN}| = \left| S_{11} + \frac{S_{12}S_{21}\Gamma_L}{1 - S_{22}\Gamma_L} \right| < 1 \quad (3.3.3)$$

and

$$|\Gamma_{OUT}| = \left| S_{22} + \frac{S_{12}S_{21}\Gamma_s}{1 - S_{11}\Gamma_s} \right| < 1 \quad (3.3.4)$$

where, of course, all coefficients are normalized to the same characteristic impedance Z_o .

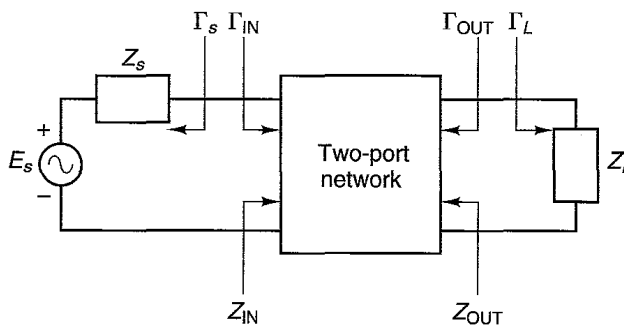


Figure 3.3.1 Stability of two-port networks.

Equations (3.3.1) and (3.3.2) state that the source and load are passive, while (3.3.3) and (3.3.4) state that the input and output impedances must also be passive (i.e., no negative resistance is associated with their real parts).

The solutions of (3.3.1) to (3.3.4) give the required conditions for the two-port network to be unconditionally stable. However, before we discuss the intricacies of the necessary and sufficient conditions for unconditional stability, a graphical analysis of (3.3.1) to (3.3.4) is presented. The graphical analysis is especially useful in the analysis of potentially unstable transistors.

When the two-port in Fig. 3.3.1 is potentially unstable, there may be values of Γ_s and Γ_L (i.e., source and load impedances) for which the real parts of Z_{IN} and Z_{OUT} are positive. These values of Γ_s and Γ_L (i.e., regions in the Smith chart) can be determined using the following graphical procedure.

First, the regions where values of Γ_L and Γ_s produce $|\Gamma_{IN}| = 1$ and $|\Gamma_{OUT}| = 1$ are determined, respectively. Setting the magnitude of (3.3.3) and (3.3.4) equal to 1 and solving for the values of Γ_L and Γ_s shows that the solutions for Γ_L and Γ_s lie on circles (called *stability circles*) whose equations are given by

$$\left| \Gamma_L - \frac{(S_{22} - \Delta S_{11}^*)^*}{|S_{22}|^2 - |\Delta|^2} \right| = \left| \frac{S_{12}S_{21}}{|S_{22}|^2 - |\Delta|^2} \right| \quad (3.3.5)$$

and

$$\left| \Gamma_s - \frac{(S_{11} - \Delta S_{22}^*)^*}{|S_{11}|^2 - |\Delta|^2} \right| = \left| \frac{S_{12}S_{21}}{|S_{11}|^2 - |\Delta|^2} \right| \quad (3.3.6)$$

where

$$\Delta = S_{11}S_{22} - S_{12}S_{21}$$

The derivations of (3.3.5) and (3.3.6) are given in Appendix A, Section A.2. For completeness, the reader can find in Appendix A, Section A.1, a review of circle equations and bilinear transformations.

The radii and centers of the circles where $|\Gamma_{IN}| = 1$ and $|\Gamma_{OUT}| = 1$ in the Γ_L plane and Γ_s plane, respectively, are obtained from (3.3.5) and (3.3.6), namely

Γ_L values for $|\Gamma_{IN}| = 1$ (Output Stability Circle):

$$r_L = \left| \frac{S_{12}S_{21}}{|S_{22}|^2 - |\Delta|^2} \right| \quad (\text{radius}) \quad (3.3.7)$$

$$C_L = \frac{(S_{22} - \Delta S_{11}^*)^*}{|S_{22}|^2 - |\Delta|^2} \quad (\text{center}) \quad (3.3.8)$$

Γ_s values for $|\Gamma_{OUT}| = 1$ (Input Stability Circle):

$$r_s = \left| \frac{S_{12}S_{21}}{|S_{11}|^2 - |\Delta|^2} \right| \quad (\text{radius}) \quad (3.3.9)$$

$$C_s = \frac{(S_{11} - \Delta S_{22}^*)^*}{|S_{11}|^2 - |\Delta|^2} \quad (\text{center}) \quad (3.3.10)$$

With the S parameters of a two-port device at one frequency, the expressions (3.3.7) to (3.3.10) can be calculated and plotted on a Smith chart, and the set of values of Γ_L and Γ_s that produce $|\Gamma_{IN}| = 1$ and $|\Gamma_{OUT}| = 1$ can be easily observed. Figure 3.3.2 illustrates the graphical construction of the stability circles where $|\Gamma_{IN}| = 1$ and $|\Gamma_{OUT}| = 1$. On one side of the stability circle boundary, in the Γ_L plane, we will have $|\Gamma_{IN}| < 1$ and on the other side $|\Gamma_{IN}| > 1$. Similarly, in the Γ_s plane on one side of the stability circle boundary, we will have $|\Gamma_{OUT}| < 1$ and on the other side $|\Gamma_{OUT}| > 1$.

Next we need to determine which area in the Smith chart represents the stable region—in other words, the region where values of Γ_L (where $|\Gamma_L| < 1$) produce $|\Gamma_{IN}| < 1$ and where values of Γ_s (where $|\Gamma_s| < 1$) produce $|\Gamma_{OUT}| < 1$. To this end, we observe that if $Z_L = Z_o$, then $\Gamma_L = 0$ and from (3.2.5) $|\Gamma_{IN}| = |S_{11}|$. If the magnitude of S_{11} is less than 1, then $|\Gamma_{IN}| < 1$ when $\Gamma_L = 0$. That is, the center of the Smith chart in Fig. 3.3.2a represents a stable operating point, because for $\Gamma_L = 0$ it follows that $|\Gamma_{IN}| < 1$. On the other hand, if $|S_{11}| > 1$ when $Z_L = Z_o$, then $|\Gamma_{IN}| > 1$ when $\Gamma_L = 0$ and the center of the Smith chart represents an unstable operating point. Figure 3.3.3 illustrates the two cases discussed. The shaded area represents the values of Γ_L that produce a stable operation. Similarly, Fig. 3.3.4 illustrates stable and unstable regions for Γ_s .

For unconditional stability any passive load or source in the network must produce a stable condition. From a graphical point of view, for $|S_{11}| < 1$ and $|S_{22}| < 1$, we want the stability circles shown in Figs. 3.3.3a and 3.3.4a to fall completely outside (or to completely enclose) the Smith chart. The case in which the stability circles fall completely outside the Smith chart is illustrated in Fig. 3.3.5. Therefore, the conditions for unconditional stability for all passive sources and loads can be expressed in the form

$$\|C_L| - r_L| > 1 \quad \text{for } |S_{11}| < 1 \quad (3.3.11)$$

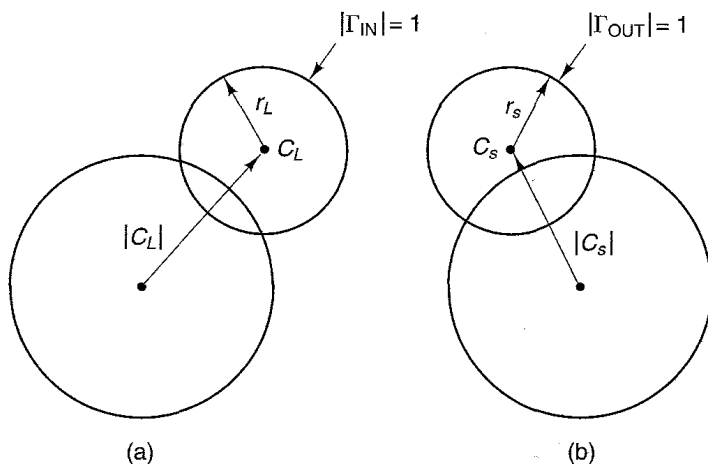


Figure 3.3.2 Stability circle construction in the Smith chart: (a) Γ_L plane; (b) Γ_s plane.

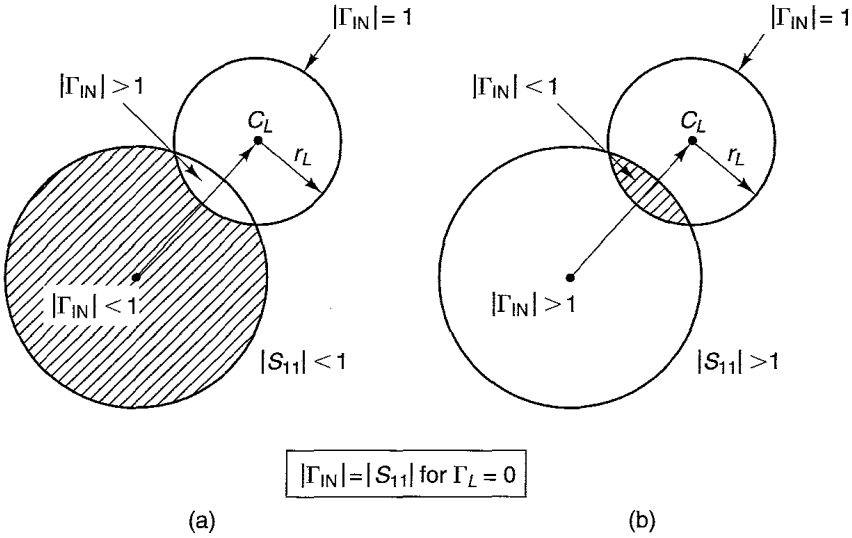


Figure 3.3.3 Smith chart illustrating stable and unstable regions in the Γ_L plane.

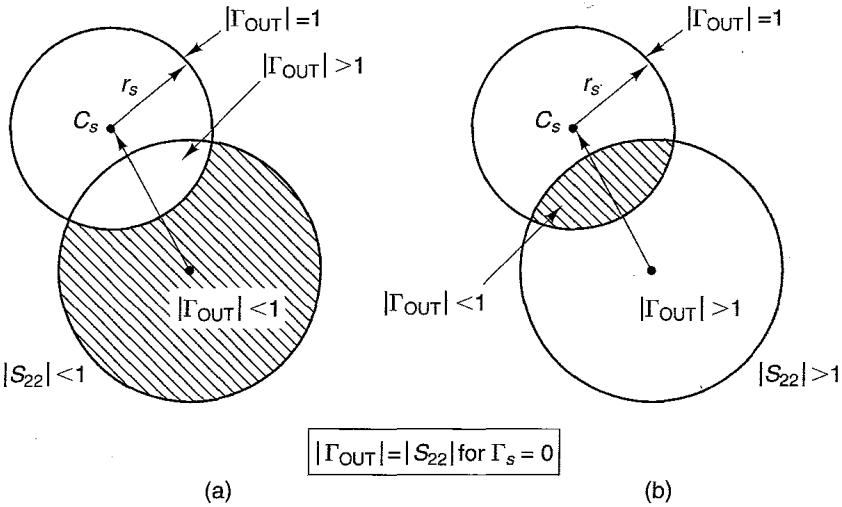


Figure 3.3.4 Smith chart illustrating stable and unstable regions in the Γ_s plane.

and

$$\|C_s - r_s\| > 1 \quad \text{for } |S_{22}| < 1 \tag{3.3.12}$$

If either $|S_{11}| > 1$ or $|S_{22}| > 1$, the network cannot be unconditionally stable because the termination $\Gamma_L = 0$ or $\Gamma_s = 0$ [see (3.3.3) and (3.3.4)] will produce $|\Gamma_{IN}| > 1$ or $|\Gamma_{OUT}| > 1$.

We now return to the necessary and sufficient conditions for a two-port to be unconditionally stable. A straightforward but somewhat lengthy manipu-

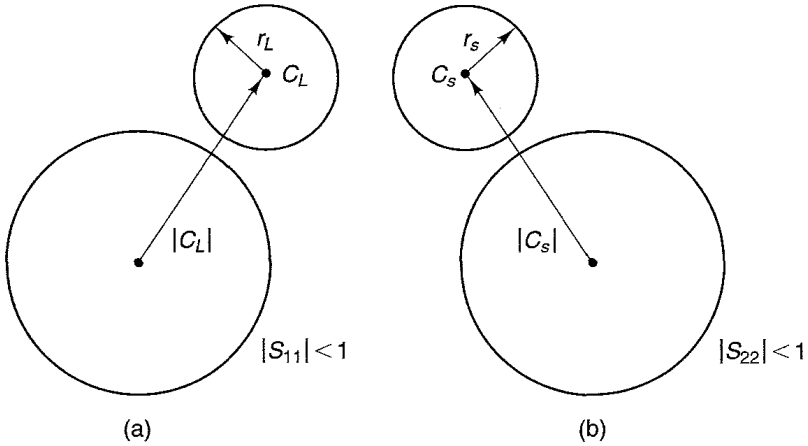


Figure 3.3.5 Conditions for unconditional stability: (a) Γ_L plane; (b) Γ_s plane.

lation of (3.3.1) to (3.3.4) results in the following necessary and sufficient conditions for unconditional stability (see Appendix B):

$$K > 1 \tag{3.3.13}$$

and

$$1 - |S_{11}|^2 > |S_{12}S_{21}| \tag{3.3.14}$$

$$1 - |S_{22}|^2 > |S_{12}S_{21}| \tag{3.3.15}$$

where

$$K = \frac{1 - |S_{11}|^2 - |S_{22}|^2 + |\Delta|^2}{2|S_{12}S_{21}|} \tag{3.3.16}$$

and

$$\Delta = S_{11}S_{22} - S_{12}S_{21} \tag{3.3.17}$$

There are other ways of expressing the necessary and sufficient conditions for unconditional stability [3.1]. Adding (3.3.14) and (3.3.15) gives

$$2 - |S_{11}|^2 - |S_{22}|^2 > 2|S_{12}S_{21}| \tag{3.3.18}$$

Since

$$|\Delta| = |S_{11}S_{22} - S_{12}S_{21}| \leq |S_{11}S_{22}| + |S_{12}S_{21}|$$

we use (3.3.18) to obtain

$$|\Delta| < |S_{11}S_{22}| + 1 - \frac{1}{2}|S_{11}|^2 - \frac{1}{2}|S_{22}|^2$$

$$|\Delta| < 1 - \frac{1}{2}(|S_{11}| - |S_{22}|)^2$$

or simply

$$|\Delta| < 1$$

Hence, a convenient way of expressing the necessary and sufficient conditions for unconditional stability is

$$K > 1 \quad (3.3.19)$$

and

$$|\Delta| < 1 \quad (3.3.20)$$

In this textbook we use (3.3.19) and (3.3.20) to test for unconditional stability.

Another way that the necessary and sufficient conditions for unconditional stability are found in the literature is (see Appendix C)

$$K > 1$$

and

$$B_1 = 1 + |S_{11}|^2 - |S_{22}|^2 - |\Delta|^2 > 0 \quad (3.3.21)$$

From a theoretical point of view, a two-port network can have any value of K and $|\Delta|$. From a practical point of view, most microwave transistors produced by manufacturers are either unconditionally stable or potentially unstable with $K < 1$ and $|\Delta| < 1$. In fact, in potentially unstable transistors most practical values of K are such that $0 < K < 1$. These potentially unstable transistors have source and load stability circles that intersect the boundary of the Smith chart (e.g., see Figs. 3.3.3a and 3.3.4a).

Negative values of K in the range $-1 < K < 0$ result in most of the Smith chart being unstable. Some transistor configurations (e.g., some CB configurations) used in oscillator designs are potentially unstable with negative values of K .

Example 3.3.1

The S parameters of a BJT at $V_{CE} = 15$ V and $I_C = 15$ mA at $f = 500$ MHz, 1 GHz, 2 GHz, and 4 GHz are as follows:

f (GHz)	S_{11}	S_{12}	S_{21}	S_{22}
0.5	0.761 $\angle -151^\circ$	0.025 $\angle 31^\circ$	11.84 $\angle 102^\circ$	0.429 $\angle -35^\circ$
1	0.770 $\angle -166^\circ$	0.029 $\angle 35^\circ$	6.11 $\angle 89^\circ$	0.365 $\angle -34^\circ$
2	0.760 $\angle -174^\circ$	0.040 $\angle 44^\circ$	3.06 $\angle 74^\circ$	0.364 $\angle -43^\circ$
4	0.756 $\angle -179^\circ$	0.064 $\angle 48^\circ$	1.53 $\angle 53^\circ$	0.423 $\angle -66^\circ$

Determine the stability. If the transistor is potentially unstable at a given frequency, draw the input and output stability circles.

Solution. At $f = 500$ MHz it follows from (3.3.16) and (3.3.17) that $K = 0.482$ and $\Delta = 0.221 \angle -123^\circ$. Therefore, for this transistor at 500 MHz we have $K < 1$ and $|\Delta| < 1$. Since $K < 1$, the transistor is potentially unstable. Using (3.3.10), the center of the input stability circle is

$$C_s = \frac{(0.761 \angle -151^\circ - 0.221 \angle -123^\circ (0.429 \angle 35^\circ))^*}{(0.761)^2 - (0.221)^2} = 1.36 \angle 157.6^\circ$$

and from (3.3.9) the radius is

$$r_s = \left| \frac{0.025 \angle 31^\circ (11.84 \angle 102^\circ)}{(0.761)^2 - (0.221)^2} \right| = 0.558$$

Similarly, from (3.3.8) and (3.3.7) the center and radius of the output stability circles are $C_L = 2.8 \angle 57.86^\circ$ and $r_L = 2.18$.

At $f = 1$ GHz, we find that $K = 0.857$ and $\Delta = 0.173 \angle -162.9^\circ$. Therefore, since $K < 1$, the transistor is potentially unstable at 1 GHz. The center and radius of the input stability circle at 1 GHz are $C_s = 1.28 \angle 169^\circ$ and $r_s = 0.315$; and for the output stability circle $C_L = 2.62 \angle 51.3^\circ$ and $r_L = 1.71$.

At $f = 2$ GHz, we find that $K = 1.31$ and $\Delta = 0.174 \angle 160^\circ$. Since $K > 1$ and $|\Delta| < 1$, it follows from (3.3.19) and (3.3.20) that the transistor is unconditionally stable at 2 GHz.

At $f = 4$ GHz, we find that $K = 1.535$ and $\Delta = 0.226 \angle 121^\circ$. Therefore, since $K > 1$ and $|\Delta| < 1$, the transistor is unconditionally stable at 4 GHz.

The stability circles are plotted in Fig. 3.3.6 at $f = 500$ MHz and $f = 1$ GHz.

Manufacturers do not fabricate transistors with $K > 1$ and $|\Delta| > 1$. However, the addition of certain feedback networks or certain terminations to a transistor can create a potentially unstable two-port network with $K > 1$ and $|\Delta| > 1$. For example, a two-port network whose S parameters are $S_{11} = 0.75 \angle -60^\circ$, $S_{21} = 6 \angle 90^\circ$, $S_{22} = 0.5 \angle 60^\circ$, and $S_{12} = 0.3 \angle 70^\circ$ has $K = 1.344$ and $|\Delta| = 2.156$. This two-port network has $K > 1$; however, it is potentially unstable because $|\Delta| > 1$. In fact, the input and output stability circles, from (3.3.7) to (3.3.10), are located at $C_s = 0.1 \angle 107.4^\circ$, $r_s = 0.44$, $C_L = 0.26 \angle -36.3^\circ$, and $r_L = 0.41$, which can be drawn inside the Smith chart to show the unstable regions. The evaluation of B_1 in (3.3.21) gives $B_1 = -3.34$. Hence, when $|\Delta| > 1$ it follows that $B_1 < 0$. This shows that when the condition (3.3.20) for stability is not satisfied, neither is the condition (3.3.21).

A two-port network is said to be unilateral when $S_{12} = 0$. In a unilateral two-port network, $\Gamma_{IN} = S_{11}$ and $\Gamma_{OUT} = S_{22}$. Hence, we have unconditional stability if $|S_{11}| < 1$ and $|S_{22}| < 1$ for all passive source and load terminations. In fact, from (3.3.16) and (3.3.17), with $S_{12} = 0$ we have $K = \infty$ and $\Delta = S_{11}S_{22}$, and it follows from (3.3.19) that

$$1 - |S_{11}|^2 - |S_{22}|^2 + |S_{11}S_{22}|^2 > 0$$

or

$$(1 - |S_{11}|^2)(1 - |S_{22}|^2) > 0$$

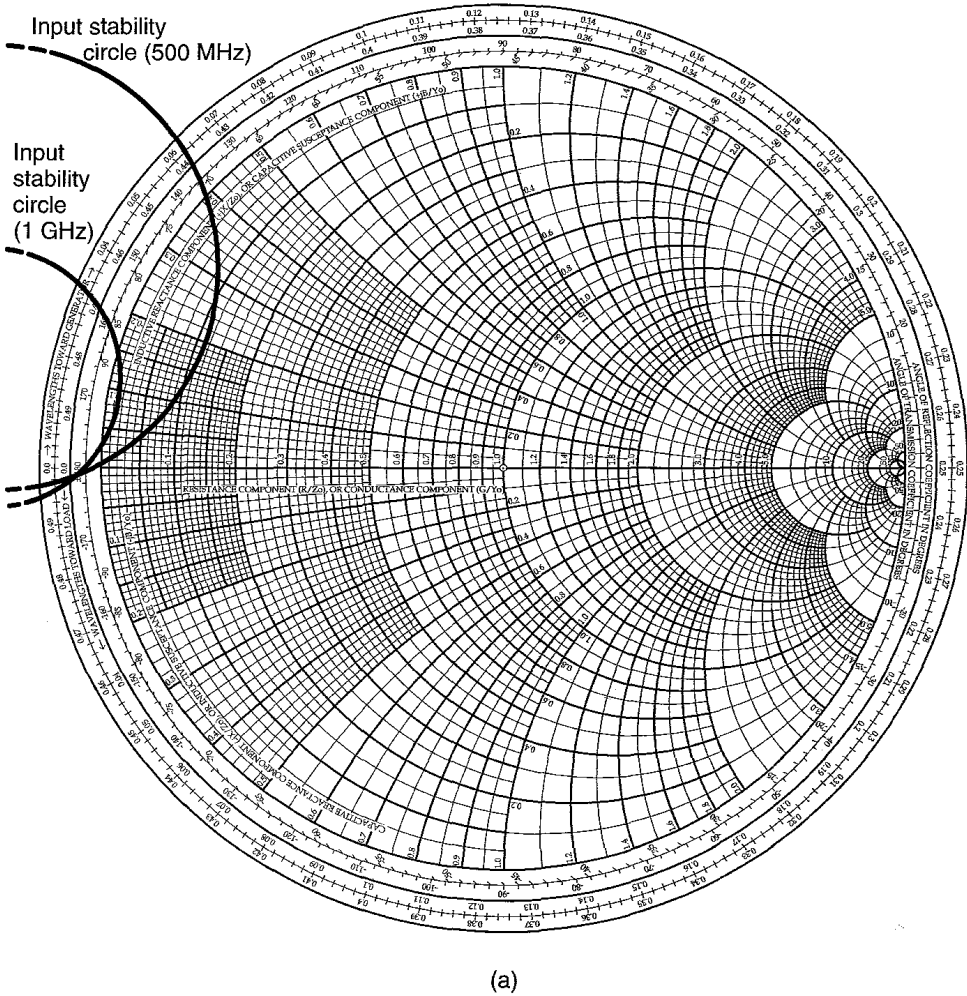


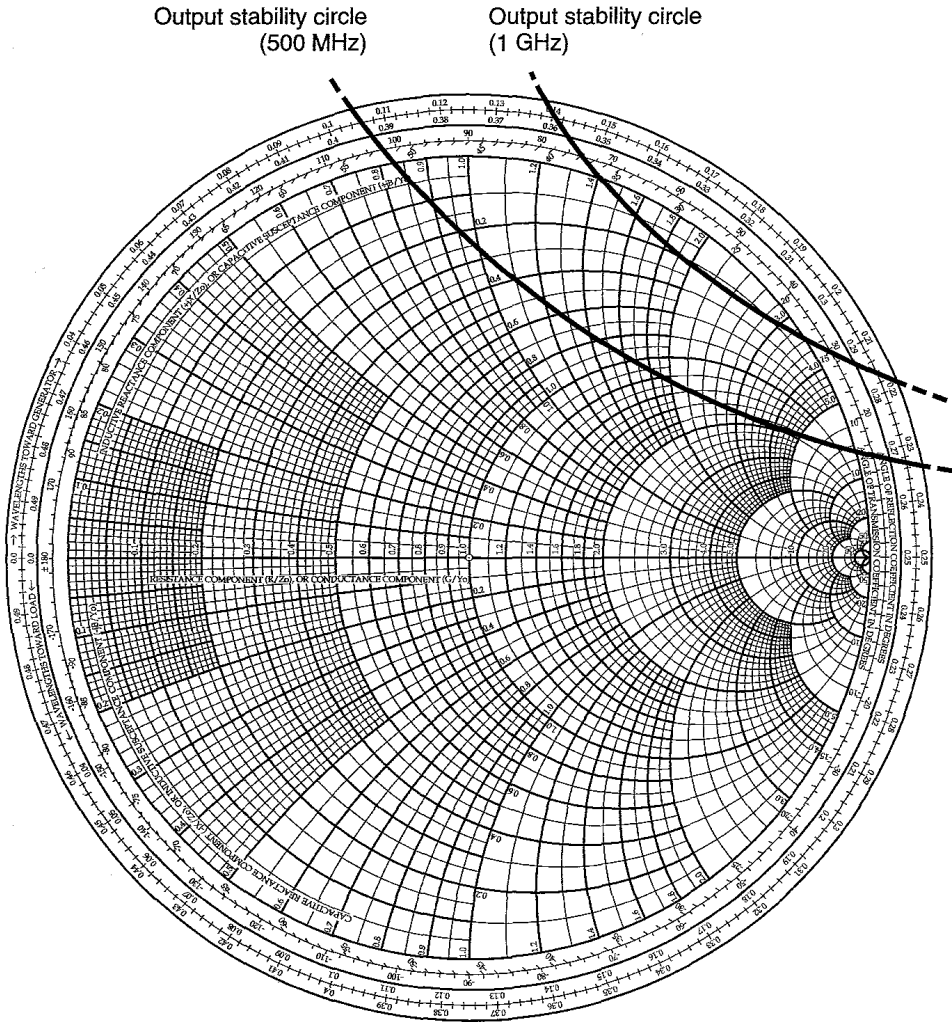
Figure 3.3.6 (a) Input stability circles for Example 3.3.1; (b) output stability circles.

The preceding inequality requires that $|S_{11}| < 1$ and $|S_{22}| < 1$ for unconditional stability of a unilateral two-port.

It is interesting to see what happens to the stability circles in the limit as $S_{12} \rightarrow 0$. The reader is referred to Problem 3.10 for this analysis.

In the potentially unstable situation illustrated in Figs. 3.3.3 and 3.3.4, the real part of the input and output impedances can be negative for some source and load reflection coefficients. In this case, selecting Γ_s and Γ_L in the stable region produces a stable operation.

Even when the selection of Γ_L and Γ_s produces $|\Gamma_{IN}| > 1$ or $|\Gamma_{OUT}| > 1$, the circuit can be made stable if the total input and output loop resistance in Fig. 3.3.1 is positive. In other words, the circuit is stable if



(b)

Figure 3.3.6 Continued

$$\text{Re}(Z_s + Z_{IN}) > 0$$

and

$$\text{Re}(Z_L + Z_{OUT}) > 0$$

A potentially unstable transistor can be made unconditionally stable by either resistively loading the transistor or by adding negative feedback. These techniques are not recommended in narrowband amplifiers because of the resulting degradation in power gain, noise figure, and VSWRs. Narrowband

amplifier design with potentially unstable transistors is best done by the proper selection of Γ_s and Γ_L to ensure stability. On the other hand, the techniques are popular in the design of some broadband amplifiers in which the transistor is potentially unstable.

The following example illustrates how resistive loading can stabilize a potentially unstable transistor.

Example 3.3.2

The S parameters of a transistor at $f = 800$ MHz are

$$S_{11} = 0.65 \angle -95^\circ$$

$$S_{12} = 0.035 \angle 40^\circ$$

$$S_{21} = 5 \angle 115^\circ$$

$$S_{22} = 0.8 \angle -35^\circ$$

Determine the stability and show how resistive loading can stabilize the transistor.

Solution. From (3.3.16) and (3.3.17) we find that $K = 0.547$ and $\Delta = 0.504 \angle 249.6^\circ$. Since $K < 1$, the transistor is potentially unstable at $f = 800$ MHz.

The input and output stability circles are calculated using (3.3.7) to (3.3.10):

$$\begin{aligned} C_s &= 1.79 \angle 122^\circ & C_L &= 1.3 \angle 48^\circ \\ r_s &= 1.04 & r_L &= 0.45 \end{aligned}$$

Figure 3.3.7 shows the plot of the stability circles, together with the stable region.

For the input stability circle the Smith chart in Fig. 3.3.7 represents the Γ_s plane and for the output stability circle the Γ_L plane. It can be seen that a series resistor with the input of approximately 9Ω assures stability at the input (see Fig. 3.3.8). The series addition of a $9\text{-}\Omega$ resistor produces an impedance Z_s equal to $Z'_s + 9 \Omega$. For any passive termination Z'_s , the real part of Z_s will be greater than 9Ω . Therefore, its associated reflection coefficient Γ_s will always be in the stable region in Fig. 3.3.7.

Also, a shunt resistor with the input of approximately $0.7/50 = 14$ mS (or 71.5Ω) produces stability at the input. Looking at the output stability circle, it follows that either a series resistor of approximately 29Ω or a shunt resistor of approximately 500Ω at the output produces stability at the output. The four choices of resistive loading are shown in Fig. 3.3.9. Usually, stabilizing one port of a transistor results in an unconditionally stable device.

All four choices of resistive loading affect the gain performance of the amplifier. In addition, from a practical point of view, resistive loading at the input (as shown in Figs. 3.3.9a and 3.3.9b) is not used because it produces a significant deterioration in the noise performance of the amplifier (see Chapter 4).

In some potentially unstable designs of broadband amplifiers, the shunt resistor loading at the output, as shown in Fig. 3.3.9d, produces a trade-off between gain and stability that is quite acceptable, resulting in a stable two-port with reasonable gain over a wide bandwidth (see Example 4.4.3).

For the stabilized shunt resistor configuration in Fig. 3.3.9d (i.e., with a $500\text{-}\Omega$ shunt resistor), the resulting S parameters are

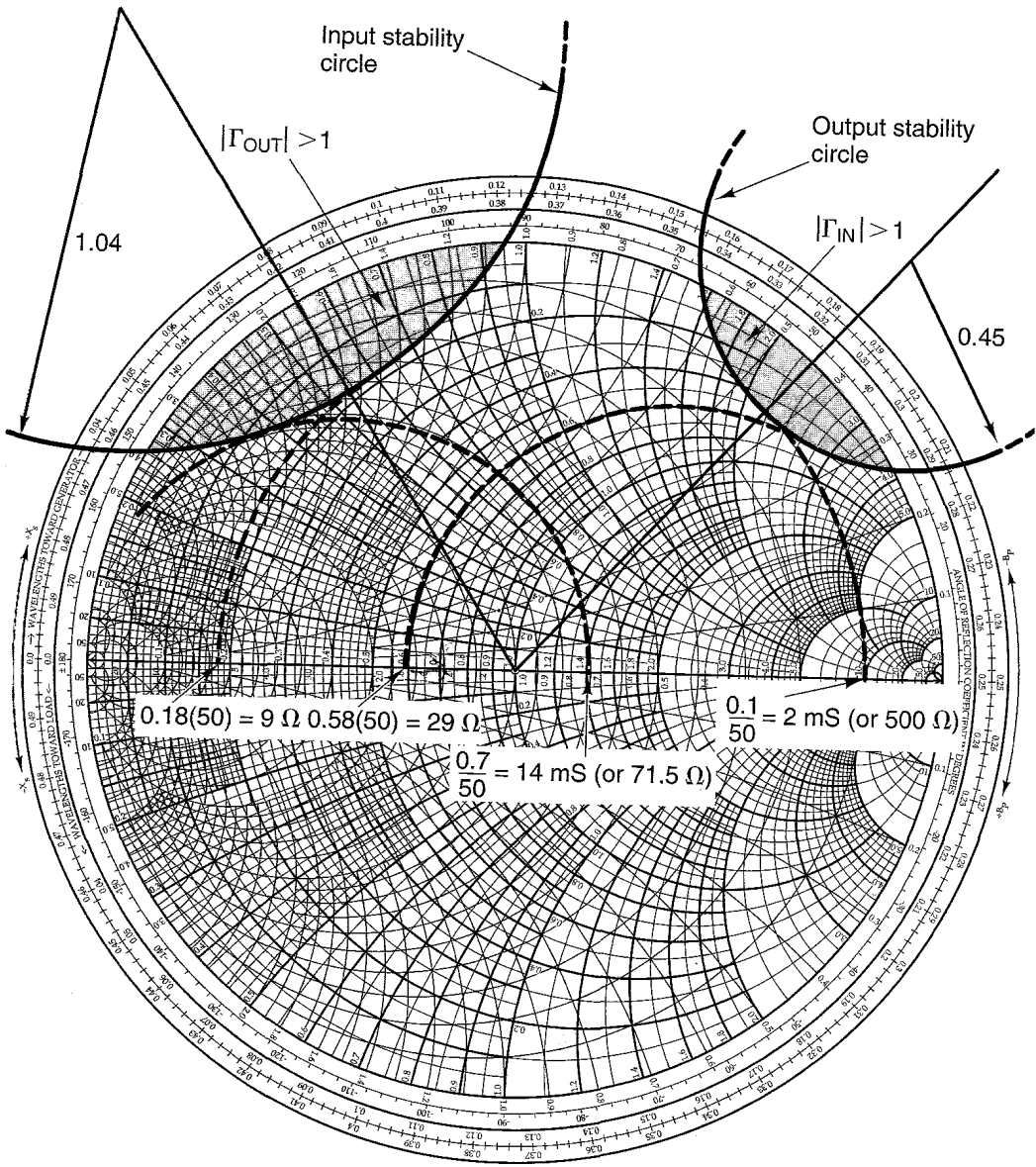


Figure 3.3.7 Input and output stability circles.

$$S_{11} = 0.65 \angle -94^\circ$$

$$S_{12} = 0.032 \angle 41.2^\circ$$

$$S_{21} = 4.62 \angle 116.2^\circ$$

$$S_{22} = 0.66 \angle -36^\circ$$

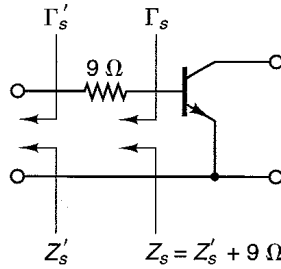


Figure 3.3.8 Series resistive loading of the transistor at the input port.

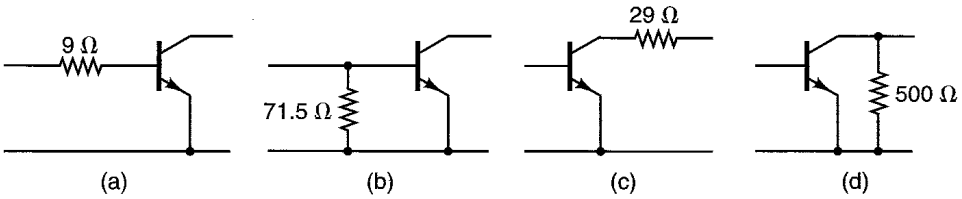


Figure 3.3.9 Four types of resistive loading to improve stability.

and from (3.3.16) and (3.3.17) $K = 1.04$ and $\Delta = 0.409 \angle 250.13^\circ$, which show that the stabilized network in Fig. 3.3.9d is unconditionally stable at $f = 800$ MHz.

Negative feedback can be used to stabilize a transistor by neutralizing S_{12} —that is, by making $S_{12} = 0$. However, this is not commonly done. In a broadband amplifier design using a potentially unstable transistor, a common procedure is to use resistive loading to stabilize the transistor and negative feedback to provide the proper ac performance—that is, to provide constant gain and low input and output VSWR.

3.4 CONSTANT-GAIN CIRCLES: UNILATERAL CASE

A two-port network is unilateral when $S_{12} = 0$. In a unilateral transistor, $\Gamma_{IN} = S_{11}$, $\Gamma_{OUT} = S_{22}$, and the unilateral transducer power gain from (3.2.1) and (3.2.2), called G_{TU} , is given by

$$G_{TU} = \frac{1 - |\Gamma_s|^2}{|1 - S_{11}\Gamma_s|^2} |S_{21}|^2 \frac{1 - |\Gamma_L|^2}{|1 - S_{22}\Gamma_L|^2} \tag{3.4.1}$$

The first term in (3.4.1) depends on the S_{11} parameter of the transistor and the source reflection coefficient. The second term, $|S_{21}|^2$, depends on the transistor scattering parameter S_{21} ; and the third term depends on the S_{22} parameter of the transistor and the load reflection coefficient. We can think of (3.4.1) as being composed of three distinct and independent gain terms. Therefore, we can write (3.4.1) in the form

$$G_{TU} = G_s G_o G_L \tag{3.4.2}$$

where

$$G_s = \frac{1 - |\Gamma_s|^2}{|1 - S_{11}\Gamma_s|^2} \quad (3.4.3)$$

$$G_o = |S_{21}|^2 \quad (3.4.4)$$

$$G_L = \frac{1 - |\Gamma_L|^2}{|1 - S_{22}\Gamma_L|^2} \quad (3.4.5)$$

and the microwave amplifier can be represented by three different gain (or loss) blocks, as shown in Fig. 3.4.1. The input matching network determines Γ_s and therefore the value of G_s according to (3.4.3); the transistor gain is $G_o = |S_{21}|^2$; and the output matching network determines Γ_L and therefore the value of G_L according to (3.4.5).

The terms G_s and G_L represent the gain or loss produced by the matching or mismatching of the input or output circuits, respectively. The term G_s affects the degree of matching or mismatching between Γ_s and S_{11} . Although the G_s block is made up of passive components, it can either have a gain contribution greater than unity or a loss. The reason we usually refer to G_s as a gain block is that there is an intrinsic mismatch loss between Z_o , the matching network, and S_{11} (i.e., between Γ_s and S_{11}). Therefore, decreasing the mismatch loss can be thought of as providing a gain. Similarly, the term G_L affects the output matching and can be thought of as the output gain block. The term G_o is related to the device and is equal to $|S_{21}|^2$. In terms of decibels, we can write from (3.4.2) to (3.4.5)

$$G_{TU}(\text{dB}) = G_s(\text{dB}) + G_o(\text{dB}) + G_L(\text{dB})$$

If we optimize Γ_s and Γ_L to provide maximum gain in G_s and G_L , we refer to the gain as the maximum unilateral transducer power gain, called $G_{TU,\max}$. For a unilateral unconditional stable transistor (i.e., for $|S_{11}| < 1$ and $|S_{22}| < 1$), the maximum values of G_s and G_L are obtained when (see Problem 3.15).

$$\Gamma_s = S_{11}^*$$

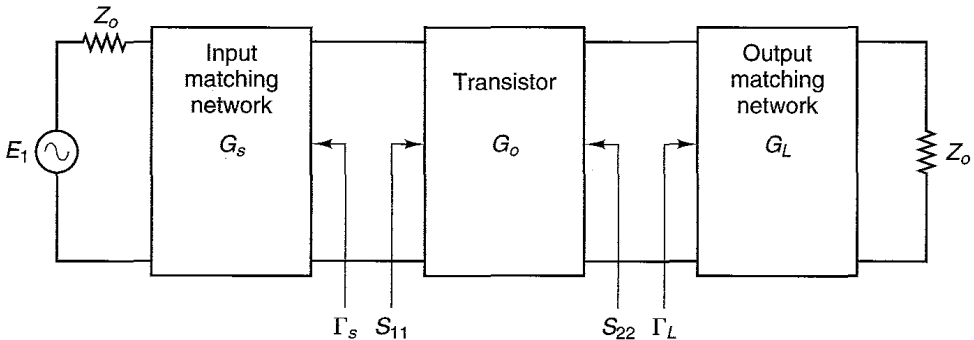


Figure 3.4.1 Unilateral transducer power gain block diagram.

and

$$\Gamma_L = S_{22}^*$$

Therefore, from (3.4.3) and (3.4.5) we obtain

$$G_{s,\max} = \frac{1}{1 - |S_{11}|^2}$$

$$G_{L,\max} = \frac{1}{1 - |S_{22}|^2}$$

and (3.4.2) gives

$$G_{TU,\max} = G_{s,\max} G_o G_{L,\max}$$

$$= \frac{1}{1 - |S_{11}|^2} |S_{21}|^2 \frac{1}{1 - |S_{22}|^2} \quad (3.4.6)$$

The appropriate block diagram for (3.4.6) is shown in Fig. 3.4.2.

Observing that in the unilateral case $\Gamma_{IN} = S_{11}$ and $\Gamma_{OUT} = S_{22}$, the maximum value of G_{TU} , which occurs when $\Gamma_s = S_{11}^* = \Gamma_{IN}^*$ and $\Gamma_L = S_{22}^* = \Gamma_{OUT}^*$, is equal to the maximum value of G_p and G_A [see (3.2.3) and (3.2.4)]. That is, $G_{TU,\max} = G_{pU,\max} = G_{AU,\max}$.

The unilateral transducer power gain is given by (3.4.1) or (3.4.2), and the maximum unilateral transducer power gain, obtained when $\Gamma_s = S_{11}^*$ and $\Gamma_L = S_{22}^*$, is given by (3.4.6). The expressions for G_s and G_L in (3.4.3) and (3.4.5) are similar in form and can be written in the general form

$$G_i = \frac{1 - |\Gamma_i|^2}{|1 - S_{ii}\Gamma_i|^2} \quad (3.4.7)$$

where $i = s$ with $ii = 11$ or $i = L$ with $ii = 22$. The design for a specific gain is based on (3.4.7).

Two cases must be considered in the analysis of (3.4.7): the unconditionally stable case, where $|S_{ii}| < 1$, and the potentially unstable case, where $|S_{ii}| > 1$.

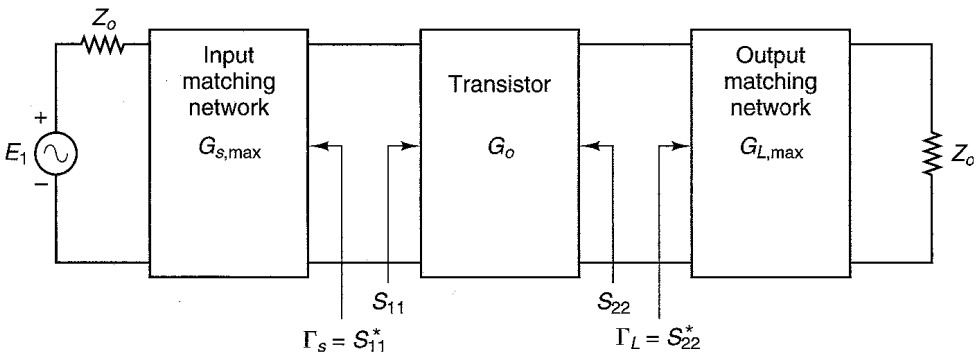


Figure 3.4.2 Maximum unilateral transducer power gain block diagram.

Unconditionally Stable Case, $|S_{ii}| < 1$

The maximum value of (3.4.7) is obtained when $\Gamma_i = S_{ii}^*$, and it is given by

$$G_{i,\max} = \frac{1}{1 - |S_{ii}|^2} \quad (3.4.8)$$

The terminations that produce $G_{i,\max}$ are called the *optimum terminations*.

From (3.4.7), G_i has a minimum value of zero when $|\Gamma_i| = 1$. Other values of Γ_i produce values of G_i between zero and $G_{i,\max}$. That is,

$$0 \leq G_i \leq G_{i,\max}$$

The values of Γ_i that produce a constant gain G_i will be shown to lie in a circle in the Smith chart. These circles are called *constant G_i circles* (i.e., for $i = s$ the circles are *constant G_s circles* and for $i = L$ the circles are *constant G_L circles*).

Define the normalized gain factor as

$$g_i = \frac{G_i}{G_{i,\max}} = G_i(1 - |S_{ii}|^2) = \frac{1 - |\Gamma_i|^2}{|1 - S_{ii}\Gamma_i|^2} (1 - |S_{ii}|^2) \quad (3.4.9)$$

such that

$$0 \leq g_i \leq 1$$

In Appendix D it is shown that the values of Γ_i that produce a constant value of g_i in (3.4.9) lie in a circle whose equation is

$$|\Gamma_i - C_{g_i}| = r_{g_i} \quad (3.4.10)$$

where the center of the circle is given by

$$C_{g_i} = \frac{g_i S_{ii}^*}{1 - |S_{ii}|^2(1 - g_i)} \quad (3.4.11)$$

and the radius is

$$r_{g_i} = \frac{\sqrt{1 - g_i}(1 - |S_{ii}|^2)}{1 - |S_{ii}|^2(1 - g_i)} \quad (3.4.12)$$

Each constant value of g_i generates a new constant G_i circle. Equations (3.4.11) and (3.4.12) can be used to generate the constant G_s circles and the constant G_L circles.

Figure 3.4.3 illustrates a constant G_i circle. The distance from the origin to the center of a constant G_i circle is given by $|C_{g_i}|$ in (3.4.11), and the angle of inclination, α_i , is equal to the phase of C_{g_i} (which is the phase of S_{ii}^*).

It is observed that when $g_i = 1$ (i.e., when $G_i = G_{i,\max}$), (3.4.12) gives $r_{g_i} = 0$ and (3.4.11) gives $C_{g_i} = S_{ii}^*$. Therefore, the constant G_i circle for maximum gain is represented by a point, located at S_{ii}^* .

In conclusion, the procedure for drawing the constant G_i circles in the Z Smith chart is as follows:

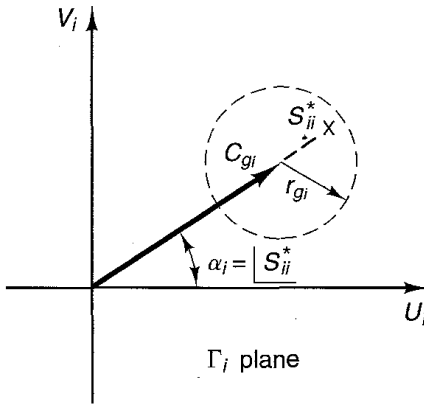


Figure 3.4.3 A constant G_i circle in the Smith chart.

1. Locate S_{ii}^* and draw a line from the origin to S_{ii}^* . At S_{ii}^* , the gain is $G_{i,max}$ and is given by (3.4.8).
2. Determine the values of G_i , where $0 \leq G_i \leq G_{i,max}$, for which the constant G_i circles are to be drawn, and calculate the corresponding values of $g_i = G_i/G_{i,max}$.
3. From (3.4.11), determine the values of C_{g_i} for each g_i .
4. From (3.4.12), determine the values of r_{g_i} for each g_i .

The 0-dB circle ($G_i = 1$) always passes through the origin of the Smith chart. This is not a coincidence. In fact, $G_i = 1$ occurs when $\Gamma_i = 0$, and from (3.4.9)

$$g_{i,0 \text{ dB}} = 1 - |S_{ii}|^2$$

Then, from (3.4.11) and (3.4.12),

$$r_{g_i,0 \text{ dB}} = |C_{g_i,0 \text{ dB}}| = \frac{|S_{ii}|}{1 + |S_{ii}|^2}$$

which shows that the radius and the distance from the origin to the center of the 0-dB constant G_i circle are identical.

A typical set of constant G_s circles is calculated in the following example and shown in Fig. 3.4.4.

Example 3.4.1

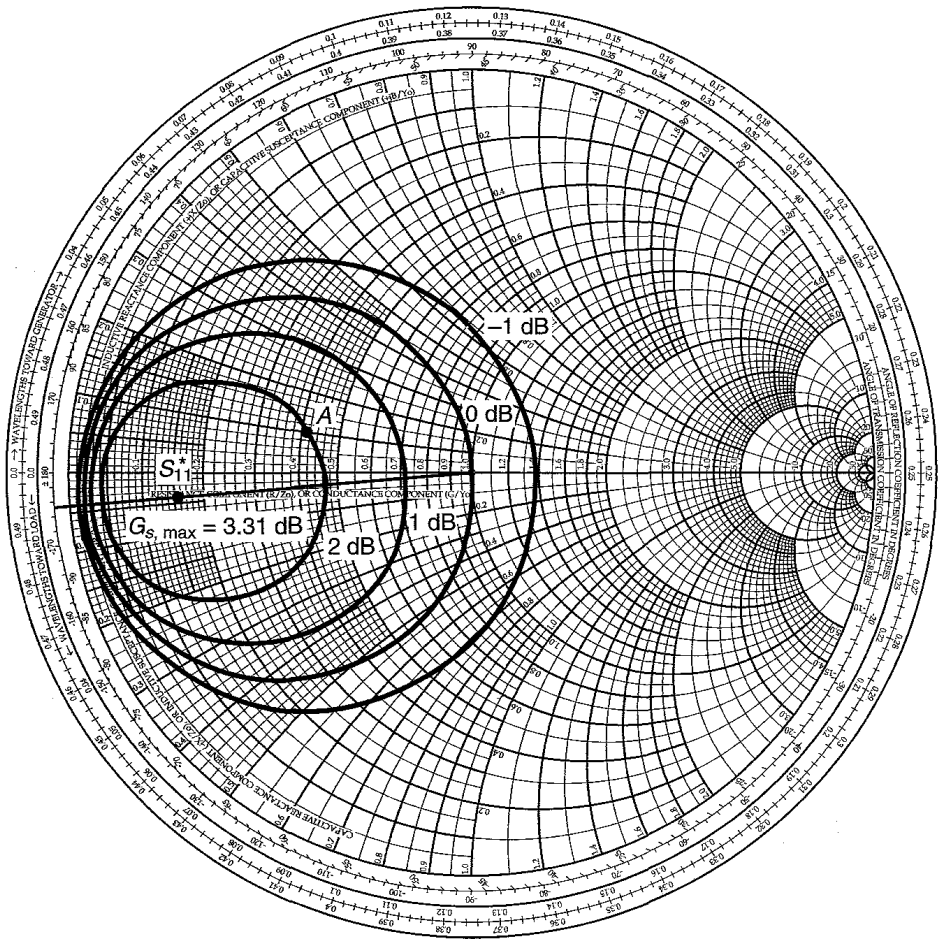
The S parameters of a BJT measured at $V_{CE} = 10 \text{ V}$, $I_C = 30 \text{ mA}$, and $f = 1 \text{ GHz}$, in a $50\text{-}\Omega$ system, are

$$S_{11} = 0.73 \angle 175^\circ$$

$$S_{12} = 0$$

$$S_{21} = 4.45 \angle 65^\circ$$

$$S_{22} = 0.21 \angle -80^\circ$$



(a)

G_s (dB):	2	1	0	-1
G_s	1.59	1.26	1	0.79
g_s	0.743	0.588	0.467	0.369
$ C_{g_s} $	0.629	0.55	0.476	0.406
r_{g_s}	0.274	0.384	0.476	0.559

(b)

Figure 3.4.4 (a) Constant-gain circles for $G_s = 2, 1, 0,$ and -1 dB; (b) calculations of constant-gain circles.

- Calculate the optimum terminations.
- Calculate $G_{s,\max}$, $G_{L,\max}$, and $G_{TU,\max}$ in decibels.
- Draw several G_s constant-gain circles.
- Design the input matching network for $G_s = 2$ dB.

Solution. (a) The optimum terminations are

$$\Gamma_s = S_{11}^* = 0.73 \angle -175^\circ$$

and

$$\Gamma_L = S_{22}^* = 0.21 \angle 80^\circ$$

Using the Smith chart, the impedances associated with Γ_s and Γ_L are $Z_s = 50(0.152 - j0.047) = 7.6 - j2.35 \Omega$ and $Z_L = 50(0.97 + j0.43) = 48.5 + j21.5 \Omega$.

(b) From (3.4.8) we find that

$$G_{s,\max} = \frac{1}{1 - |S_{11}|^2} = 2.141 \quad \text{or} \quad 3.31 \text{ dB}$$

$$G_{L,\max} = \frac{1}{1 - |S_{22}|^2} = 1.046 \quad \text{or} \quad 0.195 \text{ dB}$$

Since

$$G_o = |S_{21}|^2 = 19.8 \quad \text{or} \quad 12.97 \text{ dB}$$

then

$$G_{TU,\max}(\text{dB}) = 3.31 + 12.97 + 0.195 = 16.47 \text{ dB}$$

(c) Since $G_{s,\max} = 3.31$ dB, constant-gain circles at 2, 1, 0, and -1 dB are drawn in Fig. 3.4.4a. The necessary calculations are given in Fig. 3.4.4b.

(d) In an amplifier design using this transistor, we observe that the output gain block provides little gain (i.e., $G_{L,\max} = 0.195$ dB); therefore, the output matching network is designed to present the optimum termination $\Gamma_L = 0.21 \angle 80^\circ$.

Any Γ_s along the $G_s = 2$ dB circle provides the constant gain. Selecting Γ_s at point A (i.e., $\Gamma_s = 0.413 \angle 166^\circ$ or $z_s = 0.42 + j0.1$) in Fig. 3.4.4a results in the input matching network shown in Fig. 3.4.5a. The details of the matching network design are shown in Fig. 3.4.5b. With $\Gamma_s = 0.413 \angle 166^\circ$ and $\Gamma_L = 0.21 \angle 80^\circ$, it follows that $G_s = 2$ dB and $G_L = G_{L,\max} = 0.195$ dB; hence, the transducer gain of the amplifier is G_{TU} (dB) = $2 + 12.97 + 0.195 = 15.16$ dB.

Potentially Unstable Case, $|S_{ii}| > 1$

In this case $|S_{ii}| > 1$ and it is possible for a passive termination to produce an infinite value of G_i . The infinite value of G_i in (3.4.7) is produced by the critical value of Γ_i , called $\Gamma_{i,c}$, given by

$$\Gamma_{i,c} = \frac{1}{S_{ii}} \quad (3.4.13)$$

Equation (3.4.13) basically states that the real part of the impedance associated with $\Gamma_{i,c}$ is equal to the magnitude of the negative resistance associated

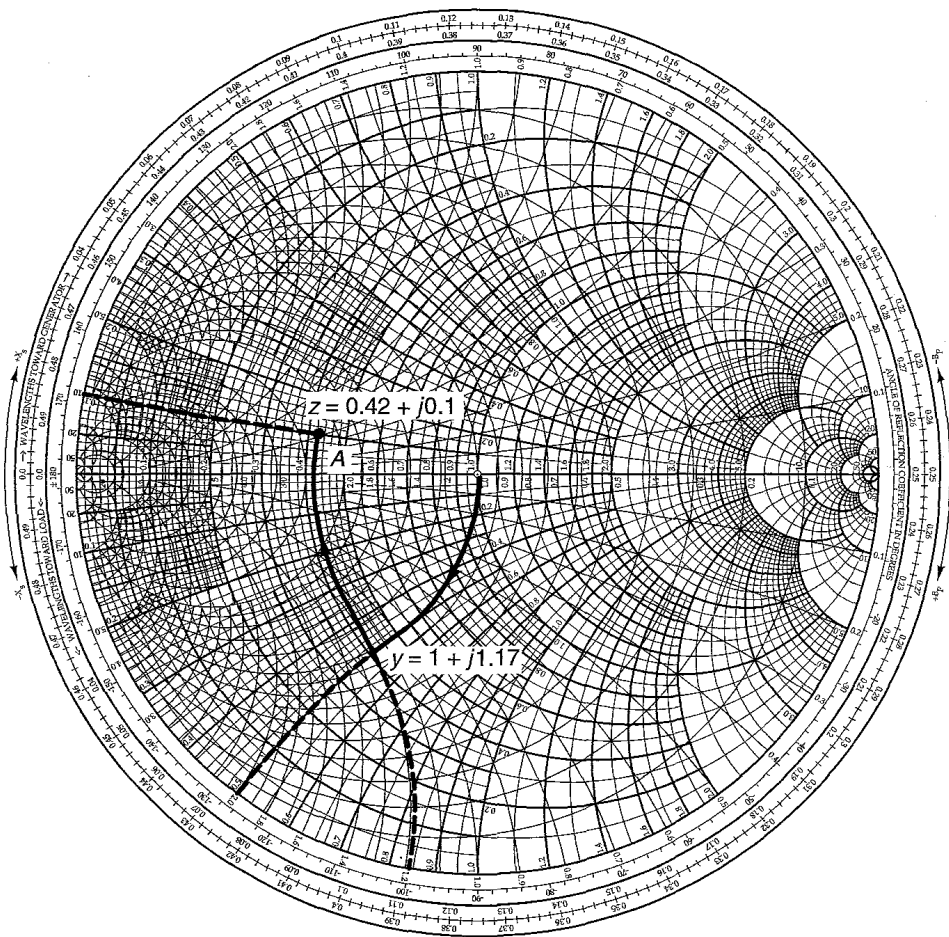
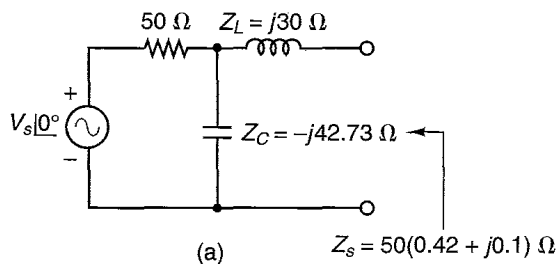


Figure 3.4.5 Input matching network for $G_s = 2$ dB.

with S_{ii} . Therefore, the total input or output loop resistance is zero, and oscillations will occur.

With g_i defined as in (3.4.9)—namely,

$$g_i = G_i(1 - |S_{ii}|^2) = \frac{1 - |\Gamma_i|^2}{|1 - S_{ii}\Gamma_i|^2} (1 - |S_{ii}|^2) \quad (3.4.14)$$

where now g_i can attain negative values because $|S_{ii}| > 1$ —the derivation of a constant G_i circle is identical to (3.4.10). Hence, with g_i given by (3.4.14), the center of a constant G_i circle is given by (3.4.11), and the radius is given by (3.4.12). The gain G_i is infinite at $\Gamma_i = \Gamma_{i,c} = 1/S_{ii}$. Since the argument of C_{g_i} (i.e., $|S_{ii}^*$) is identical to the argument of $1/S_{ii}$, it follows that the centers of the circles are located along a line drawn from the origin to the point $1/S_{ii}$.

As discussed in Section 2.2, the negative resistance associated with S_{ii} , where $|S_{ii}| > 1$, can be calculated using the Smith chart by locating the point $1/S_{ii}^*$ and interpreting the resistance circles as being negative and the reactance circles as labeled.

To prevent oscillations in the input or output port Γ_i must be selected such that the real part of the termination impedance is larger than the magnitude of the negative resistance associated with the point $1/S_{ii}^*$. When a negative resistance occurs at the input, the stable region is that region where values of Γ_s produce a source impedance such that

$$\text{Re}(Z_s) > |\text{Re}(Z_{IN})|$$

Similarly, when a negative resistance occurs at the output, Γ_L is selected such that

$$\text{Re}(Z_L) > |\text{Re}(Z_{OUT})|$$

A typical construction is illustrated in Fig. 3.4.6, where the critical value of Γ_s (i.e., $\Gamma_{s,c} = 1/S_{11}$) and two constant G_s circles are shown.

Example 3.4.2

The S parameters of a GaAs FET measured at $V_{DS} = 5\text{ V}$, $I_{DS} = 10\text{ mA}$, and $f = 1\text{ GHz}$ in a $50\text{-}\Omega$ system are

$$S_{11} = 2.27 \angle -120^\circ$$

$$S_{12} = 0$$

$$S_{21} = 4 \angle 50^\circ$$

$$S_{22} = 0.6 \angle -80^\circ$$

- Calculate the input impedance and the optimum output termination.
- Determine the unstable region in the Smith chart and construct constant-gain circles for $G_s = 5\text{ dB}$ and $G_s = 3\text{ dB}$.
- Design the input matching network for $G_s = 3\text{ dB}$ with the greatest degree of stability.
- Determine G_{TU} in decibels.

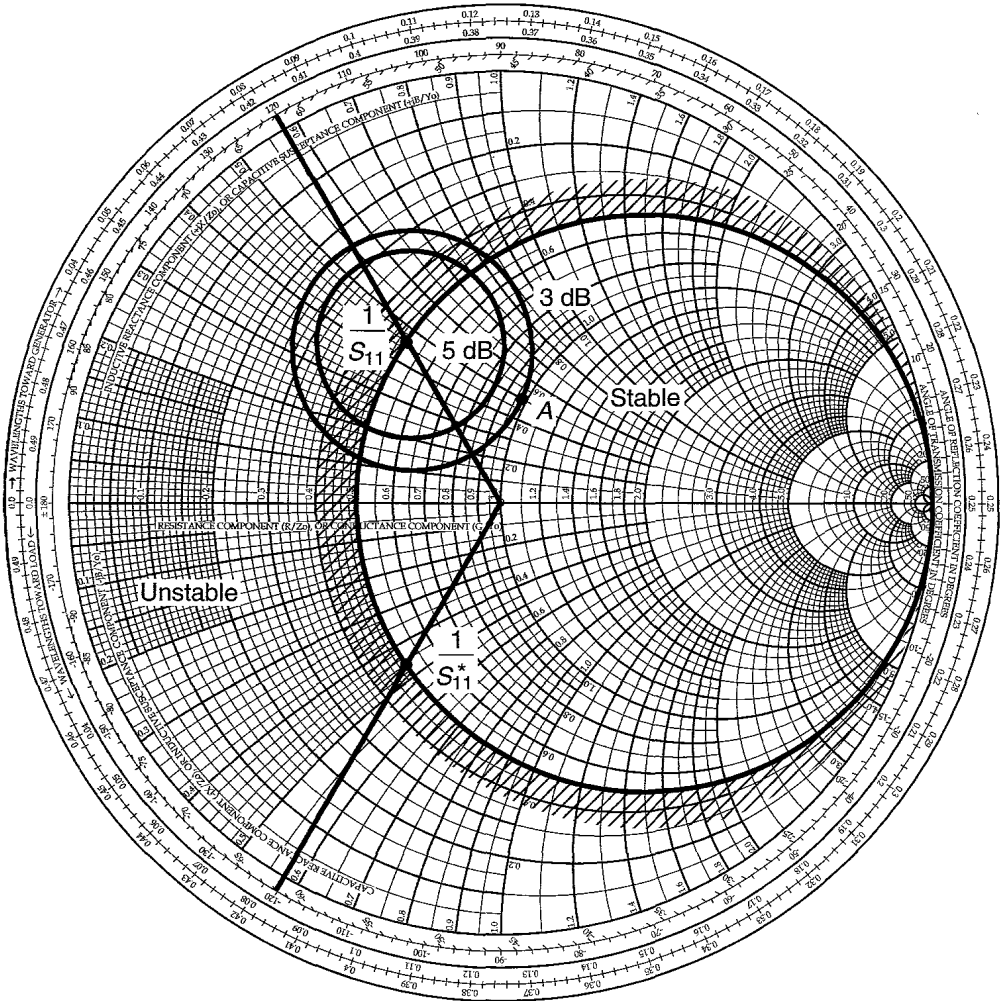


Figure 3.4.6 Stable and unstable regions and constant G_s circles for Example 3.4.2.

Solution. (a) The input impedance is obtained from the Smith chart at the point $1/S_{11}^* = 0.44 \angle -120^\circ$ (see Fig. 3.4.6)—namely,

$$Z_{IN} = 50(-0.5 - j0.46) = -25 - j23 \Omega$$

The optimum termination for G_L is

$$\Gamma_L = S_{22}^* = 0.6 \angle 80^\circ$$

The impedance associated with Γ_L is obtained from the Smith chart as $Z_L = 50(0.56 + j1.03) = 28 + j51.5 \Omega$.

(b) The unstable region is where $\text{Re}(Z_s) < |\text{Re}(Z_{IN})|$. The unstable region is marked in Fig. 3.4.6.

In order to construct the constant-gain circle for $G_s = 5$ dB, we first locate the point $1/S_{11}$ in Fig. 3.4.6. Then, from (3.4.14), (3.4.11), and (3.4.12), we find that

$$g_s = 3.16[1 - (2.27)^2] = -13.123$$

$$r_{g_s} = \frac{\sqrt{1 + 13.123} [1 - (2.27)^2]}{1 - (2.27)^2(1 + 13.123)} = 0.217$$

and

$$|C_{g_s}| = \frac{-13.123(2.27)}{1 - (2.27)^2(1 + 13.123)} = 0.415$$

The $G_s = 5$ dB circle is drawn in Fig. 3.4.6. Similarly, for the $G_s = 3$ dB circle, we find that $g_s = -8.286$, $|C_{g_s}| = 0.401$, and $r_{g_s} = 0.27$.

(c) In order to obtain the greatest degree of stability, we select Γ_s on the $G_s = 3$ dB circle such that it has the largest positive real part. That is, Γ_s is selected at point A in Fig. 3.4.6—namely,

$$\Gamma_s = 0.245 \angle 79^\circ$$

or

$$Z_s = 50(0.97 + j0.5) = 48.5 + j25 \Omega$$

Since the input loop resistance is $48.5 - 25 = 23.5 \Omega$, the input port is stable.

(d) Since $G_s = 3$ dB,

$$G_{L,\max} = \frac{1}{1 - |S_{22}|^2} = \frac{1}{1 - (0.6)^2} = 1.562 \quad \text{or} \quad 1.94 \text{ dB}$$

and

$$G_o = |S_{21}|^2 = (4)^2 = 16 \quad \text{or} \quad 12.04 \text{ dB}$$

and the unilateral transducer gain is

$$G_{TU}(\text{dB}) = 3 + 12.04 + 1.94 = 16.98 \text{ dB}$$

3.5 UNILATERAL FIGURE OF MERIT

When S_{12} can be set equal to zero, the design procedure is much simpler. In order to determine the error involved in assuming $S_{12} = 0$, we form the magnitude ratio of G_T and G_{TU} from (2.6.13) and (3.4.1)—namely,

$$\frac{G_T}{G_{TU}} = \frac{1}{|1 - X|^2} \quad (3.5.1)$$

where

$$X = \frac{S_{12}S_{21}\Gamma_s\Gamma_L}{(1 - S_{11}\Gamma_s)(1 - S_{22}\Gamma_L)}$$

From (3.5.1) the ratio of the transducer power gain to the unilateral transducer power gain is bounded by

$$\frac{1}{(1 + |X|)^2} < \frac{G_T}{G_{TU}} < \frac{1}{(1 - |X|)^2}$$

When $\Gamma_s = S_{11}^*$ and $\Gamma_L = S_{22}^*$, G_{TU} has a maximum value and, in this case, the maximum error introduced when using G_{TU} is bounded by

$$\frac{1}{(1 + U)^2} < \frac{G_T}{G_{TU}} < \frac{1}{(1 - U)^2} \quad (3.5.2)$$

where

$$U = \frac{|S_{12}| |S_{21}| |S_{11}| |S_{22}|}{(1 - |S_{11}|^2)(1 - |S_{22}|^2)} \quad (3.5.3)$$

is known as the *unilateral figure of merit*.

The value of U varies with frequency because of its dependence on the S parameters. A typical variation of U with frequency is shown in Fig. 3.5.1. In this case, the maximum value of U occurs at 100 MHz and 1 GHz and is given by $U = -15$ dB or $U = 0.03$. Therefore, from (3.5.2),

$$\frac{1}{(1 + 0.03)^2} < \frac{G_T}{G_{TU}} < \frac{1}{(1 - 0.03)^2}$$

or, in decibels,

$$-0.26 \text{ dB} < \frac{G_T}{G_{TU}} < 0.26 \text{ dB}$$

and the maximum error is ± 0.26 dB at 100 MHz and 1 GHz. In some designs this error is small enough to justify the unilateral assumption.

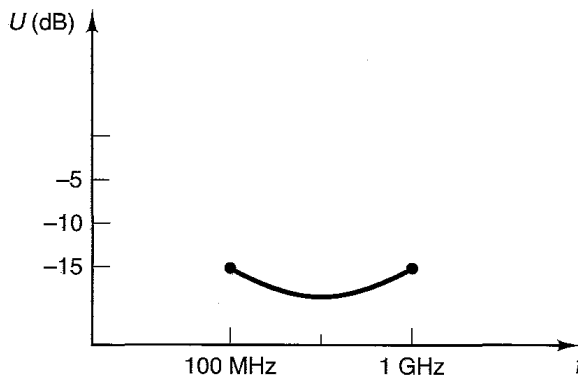


Figure 3.5.1 Frequency dependence of the unilateral figure of merit.

3.6 SIMULTANEOUS CONJUGATE MATCH: BILATERAL CASE

When $S_{12} \neq 0$ and the unilateral assumption cannot be made, the input and output reflection coefficients are given by (3.2.5) and (3.2.6), respectively. The conditions required to obtain maximum transducer power gain are

$$\Gamma_s = \Gamma_{IN}^* \quad (3.6.1)$$

and

$$\Gamma_L = \Gamma_{OUT}^* \quad (3.6.2)$$

These conditions are illustrated in Fig. 3.6.1 and are referred to as the simultaneous conjugate match conditions. When the input and output are matched, it follows that $(VSWR)_{in} = (VSWR)_{out} = 1$.

From (3.2.5), (3.2.6), (3.6.1), and (3.6.2), we can write

$$\Gamma_s^* = S_{11} + \frac{S_{12}S_{21}\Gamma_L}{1 - S_{22}\Gamma_L} \quad (3.6.3)$$

and

$$\Gamma_L^* = S_{22} + \frac{S_{12}S_{21}\Gamma_s}{1 - S_{11}\Gamma_s} \quad (3.6.4)$$

Solving (3.6.3) and (3.6.4) simultaneously gives the values Γ_s and Γ_L required for a simultaneous conjugate match. Calling these values Γ_{Ms} and Γ_{ML} , we obtain

$$\Gamma_{Ms} = \frac{B_1 \pm \sqrt{B_1^2 - 4|C_1|^2}}{2C_1} \quad (3.6.5)$$

$$\Gamma_{ML} = \frac{B_2 \pm \sqrt{B_2^2 - 4|C_2|^2}}{2C_2} \quad (3.6.6)$$

$$B_1 = 1 + |S_{11}|^2 - |S_{22}|^2 - |A|^2 \quad (3.6.7)$$

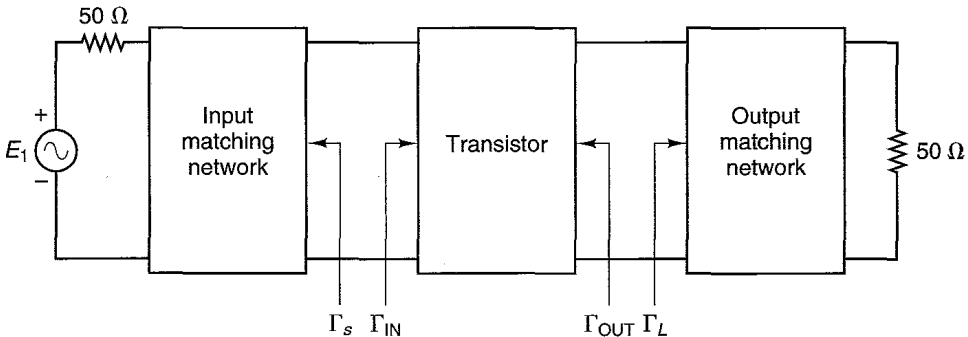


Figure 3.6.1 Simultaneous conjugate match exists when $\Gamma_s = \Gamma_{IN}^*$ and $\Gamma_L = \Gamma_{OUT}^*$.

$$B_2 = 1 + |S_{22}|^2 - |S_{11}|^2 - |\Delta|^2 \quad (3.6.8)$$

$$C_1 = S_{11} - \Delta S_{22}^*$$

$$C_2 = S_{22} - \Delta S_{11}^*$$

In what follows, we will show that for an unconditionally stable two-port network, the solutions with a minus sign in (3.6.5) and (3.6.6) are the useful ones [3.2, 3.3].

If $|B_1/2C_1| > 1$ and $B_1 > 0$ in (3.6.5), the solution with the minus sign produces $|\Gamma_{Ms}| < 1$ and the solution with the plus sign produces $|\Gamma_{Ms}| > 1$. If $|B_1/2C_1| > 1$ with $B_1 < 0$ in (3.6.5), the solution with the plus sign produces $|\Gamma_{Ms}| < 1$ and the solution with the minus sign produces $|\Gamma_{Ms}| > 1$. Similar considerations apply to (3.6.6). The proofs for the previous statements are given in Appendix E, Section E.1.

Since it can be shown that $|B_i/2C_i|^2 > 1$ ($i = 1$ or 2) is similar to $K^2 > 1$, it follows that the condition $|B_i/2C_i| > 1$ is similar to $|K| > 1$ (see Appendix E, Section E.2). Therefore, if $|K| > 1$ with K positive, one solution of (3.6.5) and (3.6.6) has a magnitude less than 1, and the other solution has a magnitude greater than 1. In fact, for $K > 1$ and $B_i > 0$, the solutions with the minus sign have magnitudes less than 1. The analysis for $|K| > 1$ with K negative is left as an exercise (see Problem 3.20); it follows that for $K < -1$ a simultaneous conjugate match does not exist.

Associated with Γ_{Ms} and Γ_{ML} are a source and a load impedance. The real parts of these impedances are positive if $|\Gamma_{Ms}| < 1$ and $|\Gamma_{ML}| < 1$. From the previous considerations, we conclude that in terms of K , the condition that a two-port network can be simultaneously matched with $|\Gamma_{Ms}| < 1$ and $|\Gamma_{ML}| < 1$ is

$$K > 1$$

The condition $K > 1$ is only a necessary condition for unconditional stability. Therefore, a simultaneous conjugate match having unconditional stability is possible if $K > 1$ and $|\Delta| < 1$. Since $|\Delta| < 1$ implies that $B_1 > 0$ and $B_2 > 0$, the minus signs must be used in (3.6.5) and (3.6.6) when calculating the simultaneous conjugate match for an unconditionally stable two-port network.

In what follows, any reference to a simultaneous conjugate match assumes that the two-port network is unconditionally stable. In a potentially unstable situation, the design procedure is best done in terms of G_p or G_A (see Section 3.7).

The maximum transducer power gain, under simultaneous conjugate match conditions, is obtained from (3.2.1) with $\Gamma_s = \Gamma_{IN}^* = \Gamma_{Ms}$ and $\Gamma_L = \Gamma_{OUT}^* = \Gamma_{ML}$. Thus, we obtain

$$G_{T,\max} = \frac{1}{1 - |\Gamma_{Ms}|^2} |S_{21}|^2 \frac{1 - |\Gamma_{ML}|^2}{|1 - S_{22}\Gamma_{ML}|^2} \quad (3.6.9)$$

Substituting (3.6.5) and (3.6.6) into (3.6.9), it can be shown (see Appendix F) that $G_{T,\max}$ can be expressed in the form

$$G_{T,\max} = \frac{|S_{21}|}{|S_{12}|} (K - \sqrt{K^2 - 1}) \quad (3.6.10)$$

Since under simultaneous conjugate match conditions $G_T = G_p = G_A$, it follows that $G_{T,max} = G_{p,max} = G_{A,max}$.

The maximum stable gain is defined as the value of $G_{T,max}$ when $K = 1$ —namely,

$$G_{MSG} = \frac{|S_{21}|}{|S_{12}|} \tag{3.6.11}$$

For a potentially unstable transistor, G_{MSG} is a figure of merit. Figure 3.6.2 illustrates a typical way in which $G_{T,max} = G_{p,max} = G_{A,max}$ and G_{MSG} are given by a manufacturer. At the frequencies where the transistor is unconditionally stable, $G_{A,max}$ is calculated and plotted in Fig. 3.6.2. In Fig. 3.6.2, $G_{A,max}$ is denoted by MAG (maximum available gain). At the frequencies where the transistor is potentially unstable, G_{MSG} is plotted in Fig. 3.6.2. From Fig. 3.6.2 it is seen that the transistor is potentially unstable below 1.5 GHz since MSG (i.e., G_{MSG}) is given; and above 2 GHz the transistor is unconditionally stable since $G_{A,max}$ is given.

A simultaneous conjugate match does not exist for $K < 1$. However, in a potentially unstable two-port network with $K > 1$ but $|A| > 1$ (which is similar to $B_1 < 0$ and $B_2 < 0$), solutions to (3.6.5) and (3.6.6) using the plus sign produce $|\Gamma_{Ms}| < 1$ and $|\Gamma_{ML}| < 1$. In such a case (i.e., for $K > 1$ and $|A| > 1$), the values of Γ_{Ms} and Γ_{ML} given by (3.6.5) and (3.6.6) using the plus sign result in a minimum value of G_T , and the input and output VSWR are unity. Substituting these values of Γ_{Ms} and Γ_{ML} into (3.6.9), the minimum value of G_T is given by

$$G_{T,min} = \frac{|S_{21}|}{|S_{12}|} (K + \sqrt{K^2 - 1}) \tag{3.6.12}$$

Recall that in a potentially unstable situation the maximum value of G_T approaches infinity as Γ_s and Γ_L approach the unstable region. Therefore, the expression (3.6.12) gives the minimum value that G_T can have when $K > 1$ and

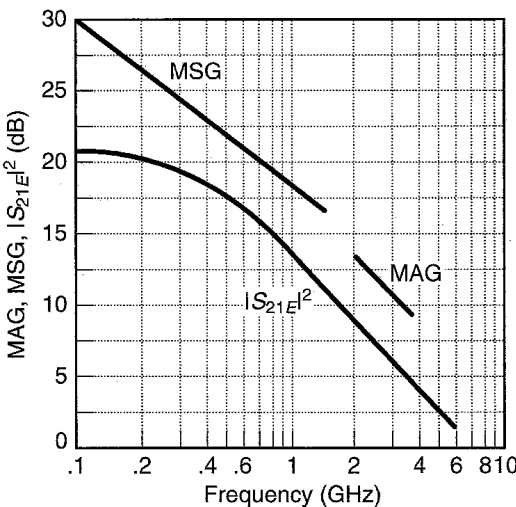


Figure 3.6.2 Typical MAG (i.e., $G_{A,max}$), MSG (i.e., G_{MSG}), and $|S_{21E}|^2$ versus frequency at $V_{CE} = 18$ V and $I_C = 30$ mA for the HXTR-5103. (From HP Microwave and RF Designer’s Catalog 1990–1991; courtesy of Hewlett Packard.)

$|\Delta| > 1$. Also, since the input and output ports are conjugate matched, it follows that $(\text{VSWR})_{\text{in}} = (\text{VSWR})_{\text{out}} = 1$.

Example 3.6.1

Design a microwave amplifier using a GaAs FET to operate $f = 6$ GHz with maximum transducer power gain. The transistor S parameters at the linear bias point, $V_{DS} = 4$ V and $I_{DS} = 0.5I_{DSS}$, are

$$S_{11} = 0.641 \angle -171.3^\circ$$

$$S_{12} = 0.057 \angle 16.3^\circ$$

$$S_{21} = 2.058 \angle 28.5^\circ$$

$$S_{22} = 0.572 \angle -95.7^\circ$$

Solution. From (3.3.16) and (3.3.17), we obtain $K = 1.504$ and $\Delta = 0.3014 \angle 109.88^\circ$. Since $K > 1$ and $|\Delta| < 1$, the GaAs FET is unconditionally stable.

It is of interest to check if the amplifier can be considered unilateral. From (3.5.3), $U = 0.1085$, and from (3.5.2),

$$-0.89 \text{ dB} < \frac{G_T}{G_{TU}} < 1 \text{ dB}$$

The preceding inequality shows that S_{12} cannot be neglected.

The reflection coefficients for a simultaneous conjugate match are calculated from (3.6.5) and (3.6.6) (using the minus sign) as follows:

$$B_1 = 0.9928$$

$$B_2 = 0.8255$$

$$C_1 = 0.4786 \angle -177.3^\circ$$

$$C_2 = 0.3911 \angle -103.9^\circ$$

$$\Gamma_{Ms} = 0.762 \angle 177.3^\circ$$

and

$$\Gamma_{ML} = 0.718 \angle 103.9^\circ$$

The maximum transducer power gain, from (3.6.10), is

$$G_{T,\text{max}} = \frac{2.058}{0.057} (1.504 - \sqrt{(1.504)^2 - 1}) = 13.74 \quad \text{or} \quad 11.38 \text{ dB}$$

The design of the matching networks using microstrip lines is illustrated in Fig. 3.6.3, where the admittances associated with Γ_{Ms} and Γ_{ML} are

$$Y_{Ms} = \frac{7.2 - j1.23}{50} = (144 - j24.6) \times 10^{-3} \text{ S}$$

and

$$Y_{ML} = \frac{0.414 - j1.19}{50} = (8.28 - j23.8) \times 10^{-3} \text{ S}$$

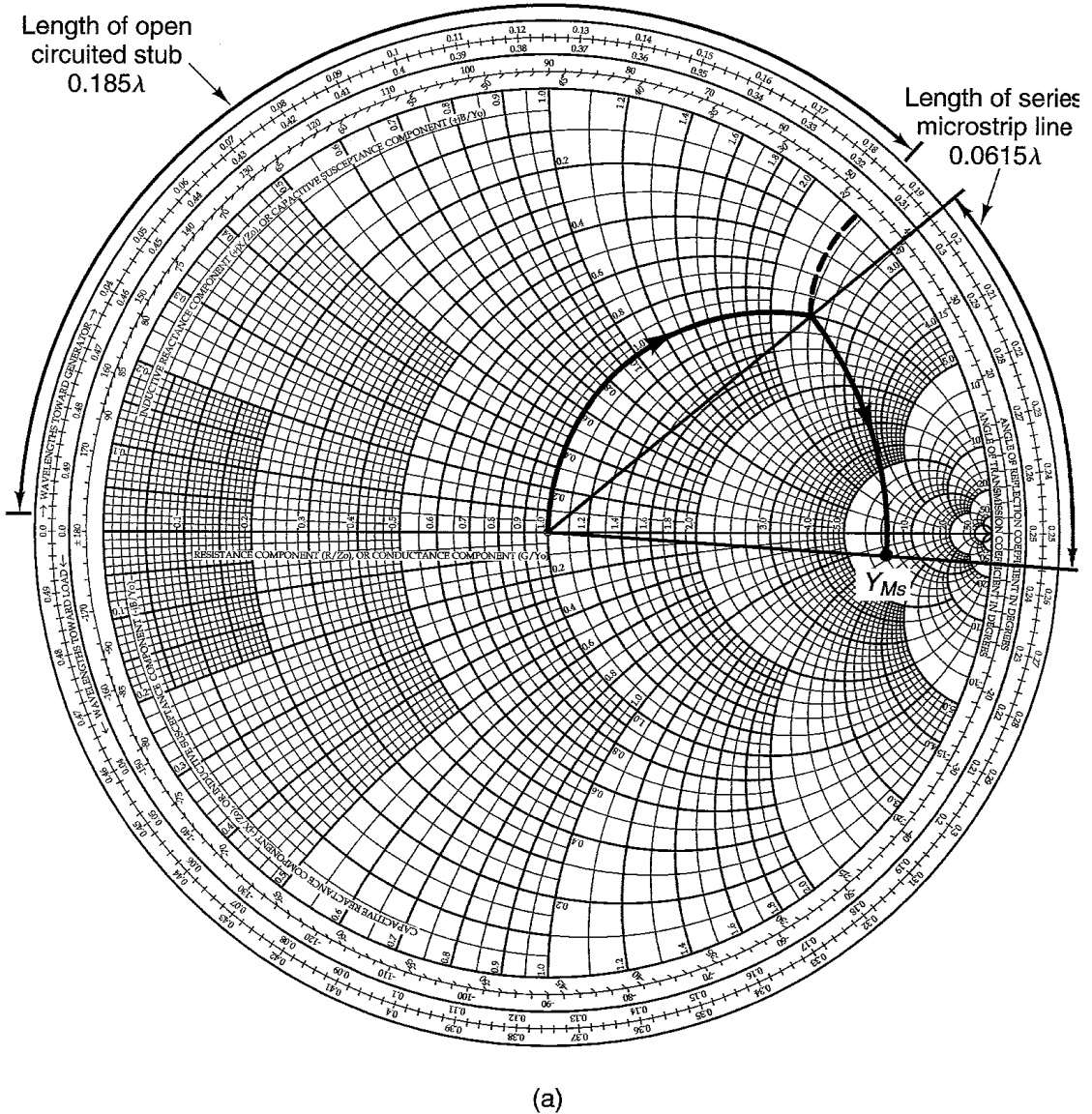
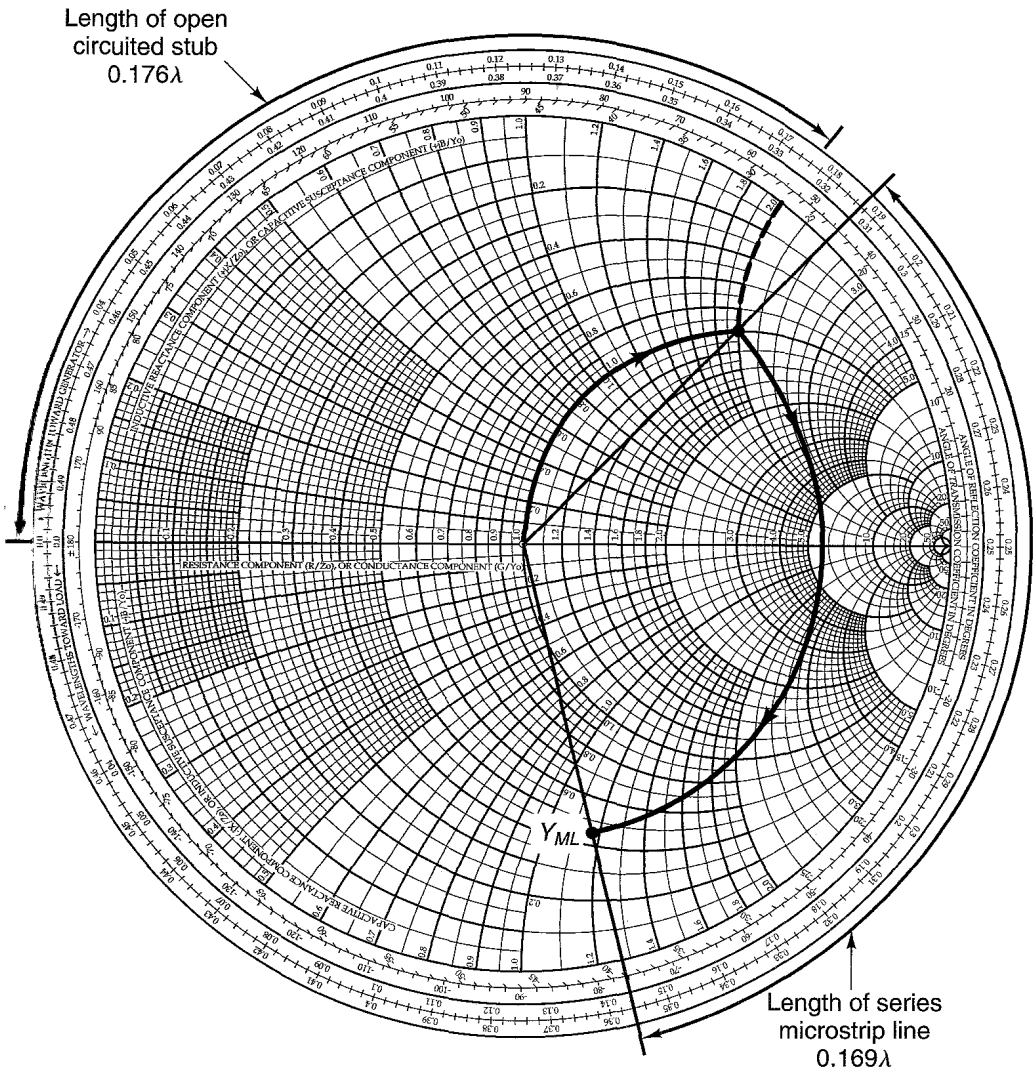


Figure 3.6.3 (a) Design of the input matching network; (b) design of the output matching network.

The input matching network can be designed with an open shunt stub of length 0.185λ and a series transmission line of length 0.0615λ . The output matching network is designed with an open shunt stub of length 0.176λ and a series transmission line of length 0.169λ .

The ac amplifier schematic is shown in Fig. 3.6.4. Using Duroid® ($\epsilon_r = 2.23$, $h = 0.7874$ mm) for the board material, we find that $W = 2.41$ mm for a characteristic impedance of 50Ω , $\epsilon_{ff} = 1.91$, and $\lambda = 0.7236\lambda_0$, where $\lambda_0 = 5$ cm at $f = 6$ GHz. The microstrip lengths at $f = 6$ GHz are



(b)

Figure 3.6.3 Continued

$$0.185\lambda = 6.70 \text{ mm}$$

$$0.0615\lambda = 2.23 \text{ mm}$$

$$0.169\lambda = 6.12 \text{ mm}$$

$$0.176\lambda = 6.37 \text{ mm}$$

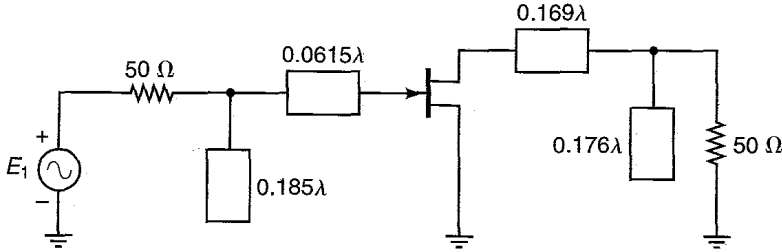


Figure 3.6.4 The ac schematic of a GaAs FET microwave amplifier. All microstrip lines have a characteristic impedance of $50\ \Omega$.

The design for $G_{T,\max}$ with Γ_{Ms} and Γ_{ML} , at 6 GHz assures that the input and output VSWR are 1.

This example is revisited in Chapter 4 (Section 4.3), where noise considerations are included. Finally, we should point out that the stability must be checked at all frequencies, so that the reflection coefficients Γ_{Ms} and Γ_{ML} provide stable operation.

We have seen that for an unconditional stable device, the terminations Γ_{Ms} and Γ_{ML} , given by (3.6.5) and (3.6.6), will produce a simultaneous conjugate match which results in the maximum value of the transducer power gain. If the design calls for a transducer power gain different from the maximum, a constant-gain circle procedure based on (3.2.1) or (3.2.2) can be attempted. As we will see, such a procedure is not practical.

A constant-gain circle procedure based on (3.2.1) could be attempted as follows. Write (3.2.1) in the form

$$G_T = G'_s G_o G_L \quad (3.6.13)$$

where

$$G'_s = \frac{1 - |\Gamma_s|^2}{|1 - \Gamma_{IN}\Gamma_s|^2} \quad (3.6.14)$$

$$G_o = |S_{21}|^2$$

and

$$G_L = \frac{1 - |\Gamma_L|^2}{|1 - S_{22}\Gamma_L|^2} \quad (3.6.15)$$

Then the design procedure is as follows:

1. From (3.6.15), the constant G_L circles can be drawn using (3.4.9) to (3.4.12). Select the desired Γ_L for a given G_L gain. Observe that $\Gamma_s = S_{22}^*$ produces $G_{L,\max}$ but not $G_{T,\max}$.

2. Calculate Γ_{IN} from (3.2.5). Observe that Γ_{IN} depends on Γ_L ; therefore, G'_s depends on G_L .
3. From (3.6.14), the constant G'_s circles can be drawn using (3.4.9) to (3.4.12) (observing that Γ_{IN} replaces S_{ii}). $\Gamma_s = \Gamma_{IN}^*$ produces $G'_{s,max}$, and constant G'_s circles can be drawn for $G'_s < G'_{s,max}$. Select the desired Γ_s for a given G'_s gain. Of course, the values of G'_s might not be satisfactory for the desired G_T . This will require the selection of another Γ_L and the procedure repeated.
4. Design the matching networks.

The procedure just outlined is not recommended for a practical design since Γ_{IN} is a function of Γ_L , making the G'_s function dependent of the G_L function. Furthermore, the centers of the gain circles at $\Gamma_L = S_{22}^*$ and $\Gamma_s = \Gamma_{IN}^*$ do not give $G_{T,max}$. In fact, the graphical approach becomes tedious because of the iterative process required for obtaining the desired gain.

As shown in the next section, the design of a microwave transistor amplified in the unconditional stable bilateral case, for a gain different from $G_{T,max}$, can be done using the operating power gain equation (the available power gain equation can also be used). When the transistor is unconditionally stable, a simultaneous conjugate match can be found, and the design procedure is based on $G_{T,max}$ or (as shown in the next section) on the operating power gain. In fact, when designing for $G_{T,max}$, which is equal to $G_{p,max}$ and to $G_{A,max}$, all design procedures result in $\Gamma_s = \Gamma_{Ms}$ and $\Gamma_L = \Gamma_{ML}$.

3.7 OPERATING AND AVAILABLE POWER-GAIN CIRCLES

Operating Power-Gain Circles

When S_{12} cannot be neglected, a design procedure based on the operating power gain G_p is commonly used. The operating power gain is independent of the source impedance; therefore, an operating power-gain circle procedure for both unconditionally stable and potentially unstable transistors is simple and recommended for practical designs.

Again we must consider two cases, the unconditionally stable case and the potentially unstable case.

Unconditionally stable bilateral case. To develop a design procedure with G_p , we write (3.2.3) in the form

$$\begin{aligned}
 G_p &= \frac{|S_{21}|^2(1 - |\Gamma_L|^2)}{\left(1 - \left| \frac{S_{11} - \Delta\Gamma_L}{1 - S_{22}\Gamma_L} \right|^2\right) |1 - S_{22}\Gamma_L|^2} \\
 &= |S_{21}|^2 g_p
 \end{aligned} \tag{3.7.1}$$

where

$$g_p = \frac{G_p}{|S_{21}|^2} = \frac{1 - |\Gamma_L|^2}{|1 - S_{22}\Gamma_L|^2 - |S_{11} - \Delta\Gamma_L|^2}$$

$$= \frac{1 - |\Gamma_L|^2}{1 - |S_{11}|^2 + |\Gamma_L|^2(|S_{22}|^2 - |\Delta|^2) - 2\operatorname{Re}(\Gamma_L C_2)} \quad (3.7.2)$$

and

$$C_2 = S_{22} - \Delta S_{11}^* \quad (3.7.3)$$

Here G_p and g_p are functions of the device S parameters and Γ_L .

In Appendix G the values of Γ_L in (3.7.2) that produce a constant value of g_p are shown to lie on a circle, known as an operating power-gain circle. The equation for an operating power-gain circle in the Γ_L plane, with g_p as a parameter, is

$$|\Gamma_L - C_p| = r_p$$

where the center of the circle C_p is located at

$$C_p = \frac{g_p C_2^*}{1 + g_p(|S_{22}|^2 - |\Delta|^2)} \quad (3.7.4)$$

and the radius of the circle is given by

$$r_p = \frac{[1 - 2K|S_{12}S_{21}|g_p + |S_{12}S_{21}|^2 g_p^2]^{1/2}}{|1 + g_p(|S_{22}|^2 - |\Delta|^2)|} \quad (3.7.5)$$

Equation (3.7.4) shows that the distance from the origin to the center of a power-gain circle is simply $|C_p|$, and the angle of inclination of the circle is C_2^* .

The maximum operating power gain occurs at the value of Γ_L when $r_p = 0$. Therefore, from (3.7.5) we can write

$$g_{p,\max}^2 |S_{12}S_{21}|^2 - 2K|S_{12}S_{21}|g_{p,\max} + 1 = 0 \quad (3.7.6)$$

where $g_{p,\max}$ is the maximum value of g_p . The solution to (3.7.6) for unconditional stability is

$$g_{p,\max} = \frac{1}{|S_{12}S_{21}|} (K - \sqrt{K^2 - 1}) \quad (3.7.7)$$

Therefore, substituting (3.7.7) into (3.7.1) gives

$$G_{p,\max} = \frac{|S_{21}|}{|S_{12}|} (K - \sqrt{K^2 - 1}) \quad (3.7.8)$$

As expected, (3.7.8) is identical to $G_{T,\max}$ in (3.6.10).

The value of Γ_L that produces $G_{p,\max}$ follows by substituting $g_p = g_{p,\max}$ in (3.7.4). This value of $\Gamma_L = C_{p,\max}$ must be equal to Γ_{ML} . That is, from (3.7.4)

$$\Gamma_{ML} = C_{p,\max} = \frac{g_{p,\max} C_2^*}{1 + g_{p,\max} (|S_{22}|^2 - |\Delta|^2)} \quad (3.7.9)$$

Substituting (3.7.7) into (3.7.9) and performing some manipulations, it follows that (3.7.9) is identical to (3.6.6), using the minus sign in (3.6.6). This derivation is presented in Appendix H.

The lowest value of g_p is zero, which corresponds to $G_p = 0$. From (3.7.1), $G_p = 0$ occurs when $|\Gamma_L| = 1$. In other words, the operating power gain is zero when all the output power is reflected from the load (i.e., when $|\Gamma_L| = 1$).

For a given G_p , Γ_L is selected from the constant operating power-gain circles. $G_{p,\max}$ results when Γ_L is selected at the distance where $g_{p,\max} = G_{p,\max}/|S_{21}|^2$. The maximum output power results when a conjugate match is selected at the input (i.e., $\Gamma_s = \Gamma_{IN}^*$). It also follows that when $\Gamma_s = \Gamma_{IN}^*$, the input power is equal to the maximum available input power. Therefore, under these circumstances the maximum transducer power gain ($G_{T,\max}$) and the operating power gain are equal, and the values of Γ_s and Γ_L that result in $G_{p,\max}$ are identical to Γ_{Ms} and Γ_{ML} , respectively.

The procedure for drawing a constant operating power-gain circle in the Z Smith chart is as follows:

1. For a given G_p , the center and radius of the constant operating power-gain circle are given by (3.7.4) and (3.7.5).
2. Select the desired Γ_L .
3. For the given Γ_L , maximum output power is obtained with a conjugate match at the input—namely, with $\Gamma_s = \Gamma_{IN}^*$, where Γ_{IN} is given by (3.2.5). This value of Γ_s produces the transducer power gain $G_T = G_p$.

Example 3.7.1

Design the amplifier in Example 3.6.1 to have an operating power gain of 9 dB instead of $G_{T,\max} = G_{p,\max} = 11.38$ dB.

Solution. Since

$$|S_{21}|^2 = (2.058)^2 = 4.235 \quad \text{or} \quad 6.27 \text{ dB}$$

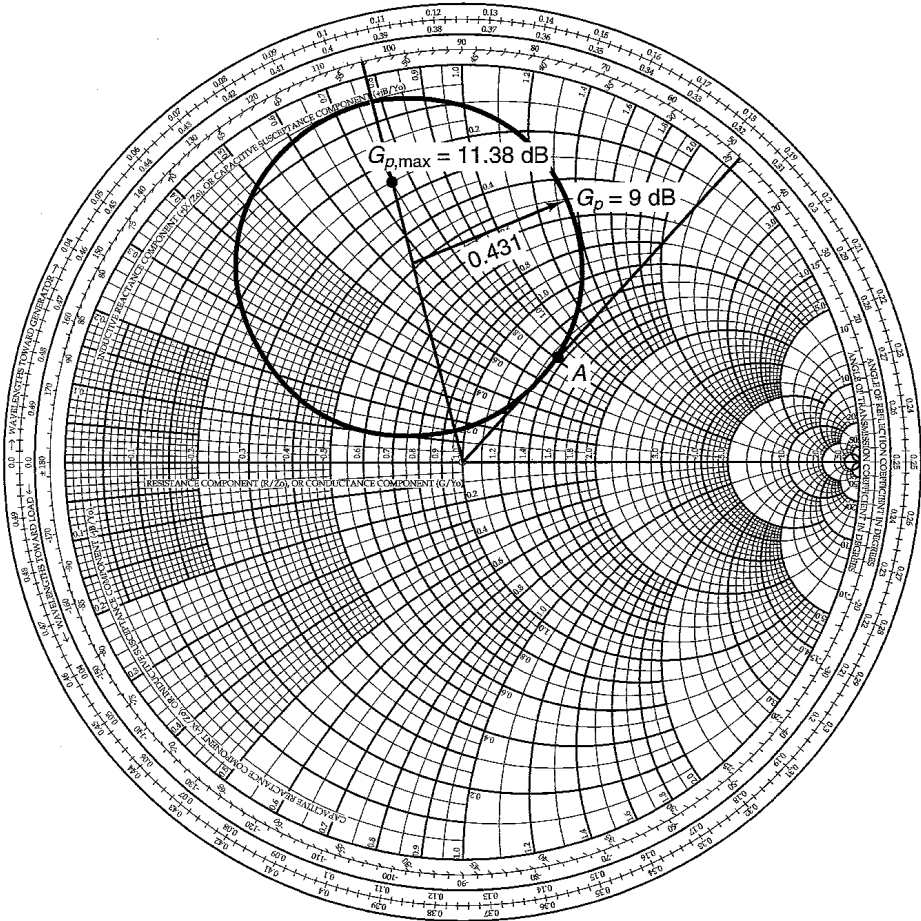
then

$$g_p = \frac{G_p}{|S_{21}|^2} = \frac{7.94}{4.235} = 1.875$$

From the results in Example 3.6.1, $K = 1.504$, $|\Delta| = 0.3014$, and $C_2 = 0.3911 \angle -103.9^\circ$. Therefore, the radius and center of the 9-dB operating power-gain circle, from (3.7.5) and (3.7.4), are $r_p = 0.431$ and $C_p = 0.508 \angle 103.9^\circ$.

The graphical construction is shown in Fig. 3.7.1a. The 9-dB operating power-gain circle shows all loads that produce $G_p = 9$ dB. The load reflection coefficient can be selected at point A —namely, $\Gamma_L = 0.36 \angle 47.5^\circ$. Then the required Γ_s for maximum output power is

$$\Gamma_s = \Gamma_{IN}^* = \left[S_{11} + \frac{S_{12} S_{21} \Gamma_L}{1 - S_{22} \Gamma_L} \right]^* = 0.629 \angle 175.51^\circ$$



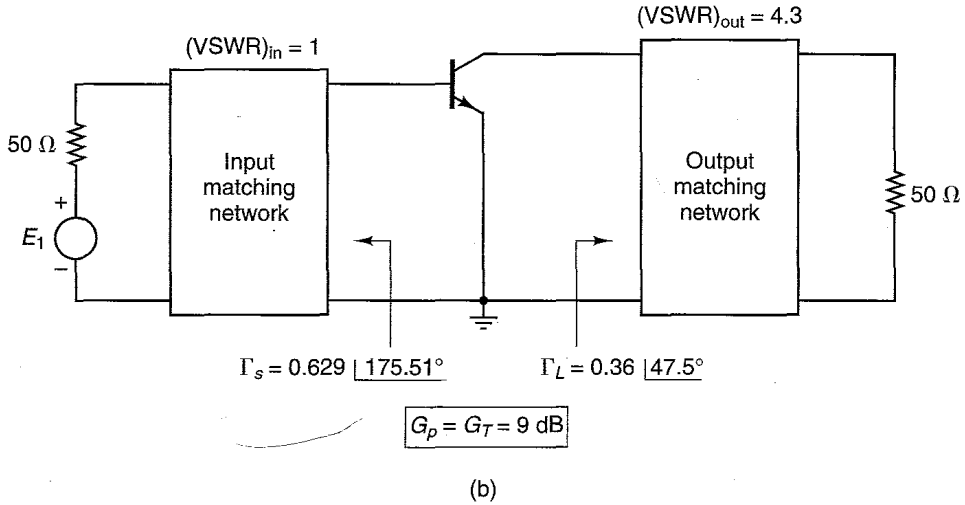
(a)

Figure 3.7.1 (a) Operating power-gain circle for $G_p = 9$ dB and location of $G_{p,max} = 11.38$ dB; (b) the block diagram of the amplifier.

Since $\Gamma_s = \Gamma_{IN}^*$, it follows that $G_T = G_p = 9$ dB. The block diagram of the amplifier is shown in Fig. 3.7.1b.

The input VSWR is 1 since $\Gamma_s = \Gamma_{IN}^*$. The output VSWR is calculated using (2.8.4) and (2.8.6). From (3.2.6) the output reflection coefficient is $\Gamma_{OUT} = 0.67 \angle -102.66^\circ$. Using (2.8.6), we obtain

$$|\Gamma_b| = \left| \frac{\Gamma_{OUT} - \Gamma_L^*}{1 - \Gamma_{OUT}\Gamma_L} \right| = \left| \frac{0.67 \angle -102.66^\circ - 0.36 \angle -47.5^\circ}{1 - 0.67 \angle -102.66^\circ (0.36 \angle 47.5^\circ)} \right| = 0.622$$


Figure 3.7.1 Continued

Therefore, the output VSWR is

$$(\text{VSWR})_{\text{out}} = \frac{1 + 0.622}{1 - 0.622} = 4.3$$

The location of $G_{p,\text{max}} = 11.38$ dB can be found as follows:

$$g_{p,\text{max}} = \frac{G_{p,\text{max}}}{|S_{21}|^2} = \frac{13.74}{(2.058)^2} = 3.24$$

$$r_{p,\text{max}} = 0$$

and the value of Γ_L that produces $G_{p,\text{max}}$ is

$$\Gamma_{ML} = C_{p,\text{max}} = \frac{g_{p,\text{max}} C_2^*}{1 + g_{p,\text{max}} (|S_{22}|^2 - |A|^2)} = 0.718 \angle 103.9^\circ$$

This value is identical to the value Γ_{ML} found in Example 3.6.1. The associated Γ_s for maximum output power, which is Γ_{Ms} , is obtained from

$$\Gamma_{Ms} = \left[S_{11} + \frac{S_{12} S_{21} \Gamma_{ML}}{1 - S_{22} \Gamma_{ML}} \right]^* = 0.762 \angle 177.3^\circ$$

As expected, this value is identical to the value of Γ_{Ms} in Example 3.6.1.

The previous example illustrates that for a given Γ_L on a constant G_p circle, there is an associated $\Gamma_s = \Gamma_{\text{IN}}^*$ that gives $(\text{VSWR})_{\text{in}} = 1$. Then for $\Gamma_s = \Gamma_{\text{IN}}^*$, there is a Γ_{OUT} . The mismatch at the output between Γ_L and Γ_{OUT} determines $(\text{VSWR})_{\text{out}}$ according to (2.8.4). We can try other values of Γ_L on the constant G_p circle and calculate for each Γ_L the associated $\Gamma_s = \Gamma_{\text{IN}}^*$. Then for each Γ_s the associated Γ_{OUT} is calculated and the resulting

$(VSWR)_{out}$. This analysis can be done for a series of points on the constant G_p circle to see if a better $(VSWR)_{out}$ can be obtained. In some cases, a certain mismatch at the input might be necessary in order to obtain the desired $(VSWR)_{out}$. Design considerations involving gain and VSWRs are discussed in Section 3.8.

Potentially unstable bilateral case. With a potentially unstable transistor, the design procedure for a given G_p is as follows:

1. For a given G_p , draw the constant operating power-gain circle using (3.7.4) and (3.7.5), and also draw the output stability circle as discussed in Section 3.3 [i.e., see (3.3.7) and (3.3.8)]. Select a value of Γ_L that is in the stable region and not too close to the stability circle.
2. Calculate Γ_{IN} using (3.2.5) and determine if a conjugate match at the input is feasible. That is, draw the input stability circle as discussed in Section 3.3 [i.e., see (3.3.9) and (3.3.10)] and determine if $\Gamma_s = \Gamma_{IN}^*$ lies in the input stable region.
3. If $\Gamma_s = \Gamma_{IN}^*$ is not in the stable region or is in the stable region but very close to the input stability circle, the value of Γ_s can be selected arbitrarily or a new value of G_p can be selected. Of course, we must be careful when selecting Γ_s arbitrarily since the value of Γ_s affects the output power and the VSWR.

The values of Γ_L and Γ_s should not be too close to their respective stability circles, because oscillations might occur due to component variations that can place Γ_s and Γ_L in the unstable regions.

Since G_p can be infinite in a potentially unstable case, it is practical to keep the value of G_p below the figure of merit value G_{MSG} [given in (3.6.11)]. The design for G_p lower than G_{MSG} can be performed with good stability and practical values of the input and output VSWR. On the other hand, a design for a G_p greater than G_{MSG} usually produces values of Γ_L and Γ_s close to the unstable regions and large values of the input and output VSWR. Design procedures involving potentially unstable transistors and VSWR considerations are discussed in Section 3.8.

In a potentially unstable situation with $K > 1$ and $|\Delta| > 1$, there is a $G_{p,min}$, just like $G_{T,min}$ in (3.6.12). In fact, in a potentially unstable situation with $K > 1$ and $|\Delta| > 1$, the other solution of (3.7.6), denoted by $g_{p,min}$, is

$$g_{p,min} = \frac{1}{|S_{12}S_{21}|} (K + \sqrt{K^2 - 1})$$

Hence,

$$G_{p,min} = \frac{|S_{21}|}{|S_{12}|} (K + \sqrt{K^2 - 1}) \quad (3.7.10)$$

Equation (3.7.10) gives the minimum value that G_p can have inside the stable region in a potentially unstable case with $K > 1$ and $|\Delta| > 1$. The maximum value that G_p can have is infinite.

The value of Γ_L that produces $G_{p,\min}$, denoted by $\Gamma_{L,\min}$, is

$$\Gamma_{L,\min} = \frac{g_{p,\min} C_2^*}{1 + g_{p,\min} (|S_{22}|^2 - |\Delta|^2)} \quad (3.7.11)$$

It also follows that $\Gamma_{L,\min}$ in (3.7.11) is identical to Γ_{ML} in (3.6.6) when the plus sign is used in (3.6.6).

Example 3.7.2

The S parameters of a GaAs FET at $I_D = 50\% I_{DSS}$, $I_{DSS} = 10$ mA, $V_{DS} = 5$ V, and $f = 8$ GHz are

$$S_{11} = 0.5 \angle -180^\circ$$

$$S_{12} = 0.08 \angle 30^\circ$$

$$S_{21} = 2.5 \angle 70^\circ$$

$$S_{22} = 0.8 \angle -100^\circ$$

The transistor is potentially unstable at 8 GHz with $G_{MSG} = 14.9$ dB. Design an amplifier with $G_p = 10$ dB.

Solution. First we will verify that the transistor is potentially unstable at 8 GHz. From (3.3.16) and (3.3.17), we obtain $K = 0.4$ and $\Delta = 0.223 \angle 62.12^\circ$. Since $K < 1$, the GaAs FET is potentially unstable. Also, from (3.6.11) the value of G_{MSG} is $G_{MSG} = 2.5/0.08 = 31.25$ or 14.9 dB.

In order to design for $G_p = 10$ dB (4.9 dB less than the G_{MSG}), the 10-dB operating power-gain circle and the output stability circle must be calculated. The radius and center of the 10-dB power gain circle, from (3.7.4) and (3.7.5), are $r_p = 0.473$ and $C_p = 0.572 \angle 97.2^\circ$. The radius and center of the output stability circle, from (3.3.7) and (3.3.8), are $r_L = 0.34$ and $C_L = 1.18 \angle 97.2^\circ$.

The Smith chart in Fig. 3.7.2 shows the construction of the 10-dB operating power-gain circle and the output stability circle. Since $|S_{11}| < 1$, the stable region is the region outside the output stability circle. Γ_L is selected on the 10-dB power-gain circle at location A —namely, $\Gamma_L = 0.1 \angle 97^\circ$ or $Z_L = 50 (0.96 + j0.19) \Omega$.

For a conjugate match at the input, Γ_s is given by $\Gamma_s = \Gamma_{IN}^* = 0.52 \angle 179.32^\circ$ and we must determine if the value of Γ_s is in the stable region. The radius and center of the input stability circle, from (3.3.9) and (3.3.10), are $r_s = 1.0$ and $C_s = 1.67 \angle 171^\circ$, where the stable region is the region outside the input stability circle. Therefore, Γ_s is a stable source reflection coefficient. Since $\Gamma_s = \Gamma_{IN}^*$, it follows that $G_T = G_p = 10$ dB and $(VSWR)_{in} = 1$.

From (3.2.6), the output reflection coefficient is $\Gamma_{OUT} = 0.934 \angle -97.18^\circ$. Using (2.8.6), we obtain $|\Gamma_b| = 0.918$ and the output VSWR is

$$(VSWR)_{out} = \frac{1 + |\Gamma_b|}{1 - |\Gamma_b|} = \frac{1 + 0.918}{1 - 0.918} = 23.5$$

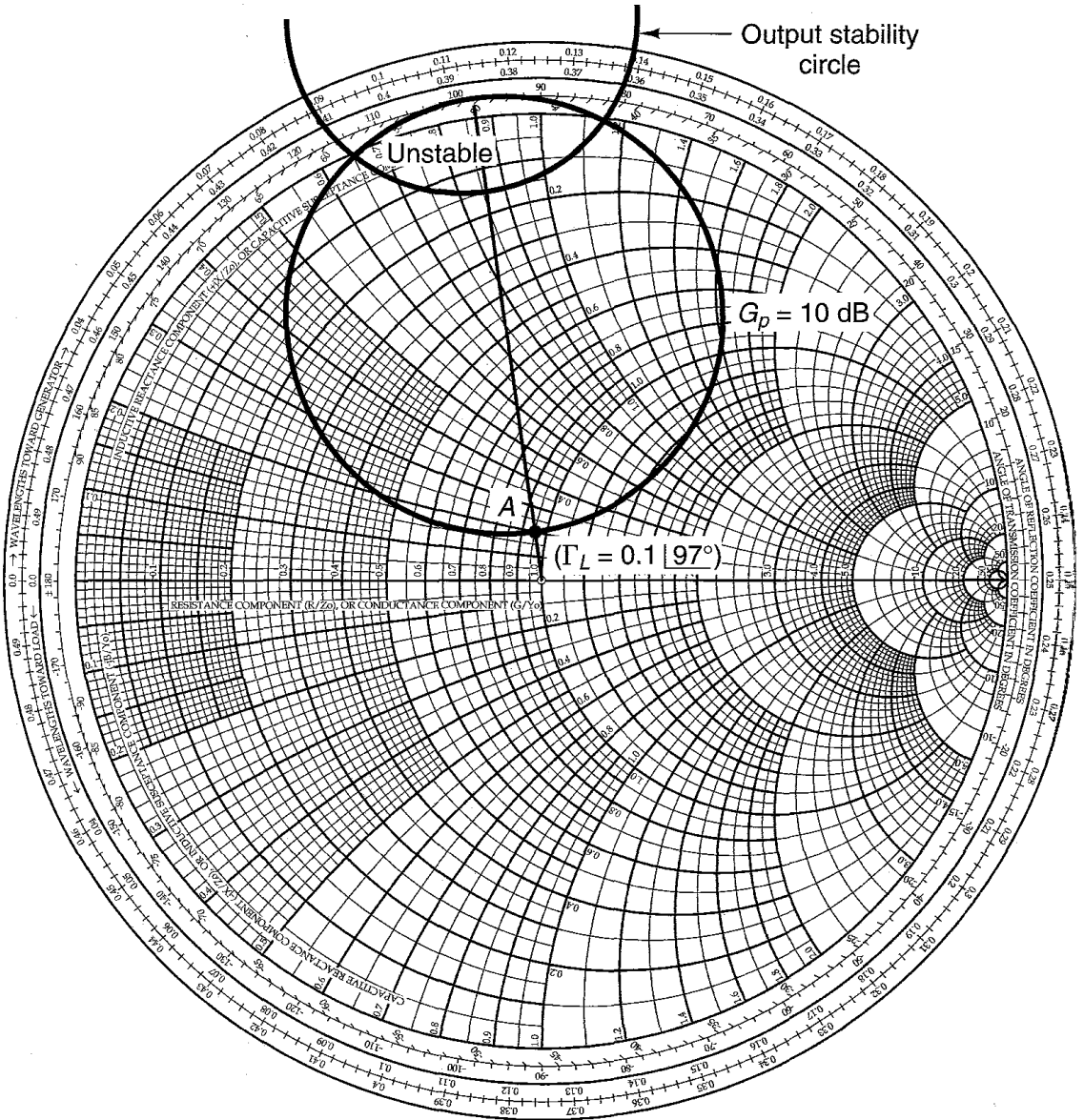


Figure 3.7.2 Power and stability circles construction for Example 3.7.2.

The previous calculations show that the output port of the amplifier is significantly mismatched in order to obtain $G_p = 10$ dB. The output VSWR can be lowered by accepting a higher-input VSWR or by changing the amplifier gain requirements. For example, with $\Gamma_s = 0.22 \angle 177^\circ$ and $\Gamma_L = 0.1 \angle 97^\circ$, it follows that $(\text{VSWR})_{\text{in}} = 2$ and $(\text{VSWR})_{\text{out}} = 9.9$. A formal procedure involving gain and VSWR considerations is discussed in Section 3.8.

Using the values of the S parameters in Example 3.7.2, the operating power-gain circles for $G_p = 0$ dB, 10 dB, 15 dB, 20 dB, and 30 dB were calculated and plotted in Fig. 3.7.3. Observe that the $G_p = 0$ (i.e., $-\infty$ dB) circle oc-

G_p (dB)	g_p	r_p	C_p
0	0.16	0.903	0.102 97.18°
15	5.06	0.277	0.882 97.18°
10	1.6	0.473	0.572 97.18°
20	16	0.282	1.060 97.18°
30	160	0.331	1.160 97.18°

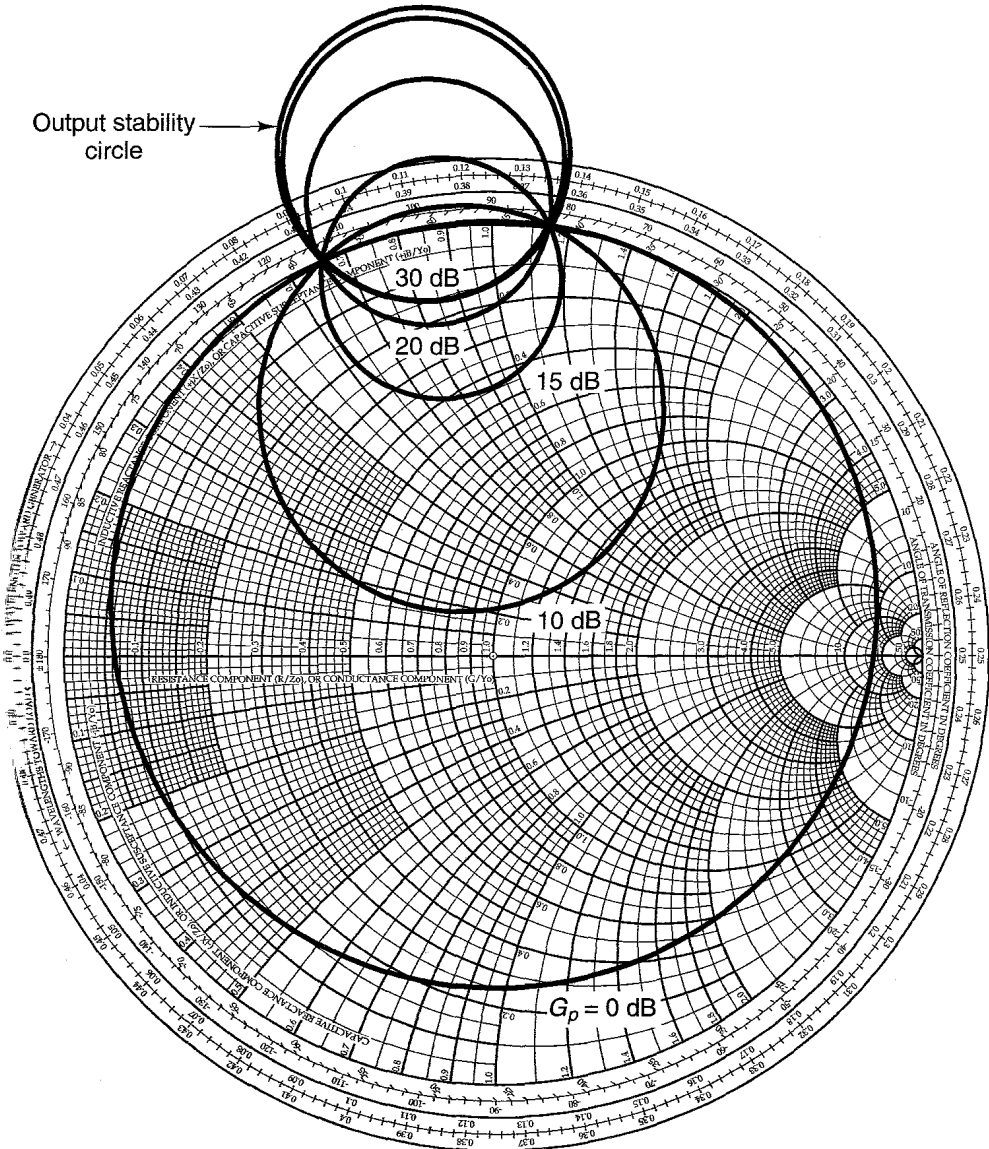


Figure 3.7.3 Typical behavior of the operating power-gain circles. The S parameters in Example 3.7.2 were used to calculate the constant gain circles.

curs when $|\Gamma_L| = 1$, and the operating power-gain circles approach the output stability circles as G_p becomes infinite.

Since G_p becomes infinite when Γ_L is on the output stability circle, it follows that the power-gain circle for $G_p = \infty$ is identical to the output stability circle. In fact, for $G_p \rightarrow \infty$ we have $g_p \rightarrow \infty$ and, taking the limit as g_p approaches infinity in (3.7.4), we obtain

$$C_p = \frac{C_2^*}{|S_{22}|^2 - |\Delta|^2}$$

and

$$r_p \approx \frac{[|S_{12}S_{21}|^2 g_p^2]^{1/2}}{|g_p(|S_{22}|^2 - |\Delta|^2)|} = \frac{|S_{12}S_{21}|}{\|S_{22}\|^2 - |\Delta|^2}$$

which are recognized as the equations for C_L and r_L in (3.3.8) and (3.3.7), respectively.

From the plots in Fig. 3.7.2, it is seen that the power-gain circles and the output stability circles intersect the Smith chart at the same points. This is not a coincidence, and it can be shown (see Problem 3.28) that for a potentially unstable device these circles intersect the Smith chart at the same points.

Example 3.7.3

(This example illustrates the power-gain circles for a two-port network with $K > 1$ and $|\Delta| > 1$.)

The S parameters of a two-port network at $f = 4$ GHz are

$$S_{11} = 0.7 \angle -50^\circ$$

$$S_{12} = 0.27 \angle 75^\circ$$

$$S_{21} = 5 \angle 120^\circ$$

$$S_{22} = 0.6 \angle 80^\circ$$

Plot several operating power-gain circles ranging from $G_p = G_{p,\min}$ to $G_p = \infty$.

Solution. For this two-port network, it follows that $K = 1.202$ and $\Delta = 1.76 \angle 18.54^\circ$ (i.e., $|\Delta| = 1.76$ is greater than 1). Since $K > 1$ and $|\Delta| > 1$ (or $B_2 < 0$), we obtain from (3.6.6), using the plus sign in (3.6.6),

$$B_1 = -1.964$$

$$B_2 = -2.224$$

$$C_1 = 0.395 \angle 97.92^\circ$$

$$C_2 = 0.654 \angle -121.95^\circ$$

$$\Gamma_{L,\min} = \Gamma_{ML} = \frac{-2.224 + \sqrt{(2.224)^2 - 4(0.654)^2}}{2(0.654 \angle -121.95^\circ)} = 0.325 \angle -58.05^\circ$$

Then, using (3.7.10),

$$G_{p,\min} = G_{T,\min} = \frac{5}{0.27} (1.202 + \sqrt{(1.202)^2 - 1}) = 34.61 \text{ (or 15.39 dB)}$$

The output stability circle ($C_L = 0.239 \angle -58.05^\circ$ and $r_L = 0.494$) and power-gain circles for $G_{p,\min} = 15.39$ dB and $G_p = 18$ dB, 20 dB, and 30 dB were calculated and are plotted in Fig. 3.7.4a. Observe that the operating power-gain circles approach the output stability circle as G_p becomes infinite.

It is simple to show that in the unstable region G_p in decibels becomes negative, approaching $-\infty$ dB at $|\Gamma| = 1$.

For maximum power transfer to the load, the source reflection coefficient is

$$\Gamma_s = \Gamma_{IN}^* = \left(0.7 \angle -50^\circ + \frac{0.27 \angle 75^\circ (5 \angle 120^\circ) 0.325 \angle -58.05^\circ}{1 - 0.6 \angle 80^\circ (0.325 \angle -58.05^\circ)} \right)^* = 0.21 \angle 82.08^\circ$$

This value of Γ_s is identical to the value of Γ_{Ms} in (3.6.5), using the plus sign in (3.6.5). That is,

$$\Gamma_s = \Gamma_{Ms} = 0.21 \angle 82.08^\circ$$

The input stability circle ($C_s = 0.152 \angle 82.08^\circ$ and $r_s = 0.518$) and Γ_{Ms} are shown in Fig. 3.7.4b.

Since a simultaneous conjugate match condition exists it follows that the input and output VSWR are equal to one.

Available Power-Gain Circles

Unconditionally stable bilateral case. The derivation of the constant available power-gain circles is similar to that of the operating power-gain circles. From (3.2.4), we write G_A in the form

$$G_A = \frac{|S_{21}|^2(1 - |\Gamma_s|^2)}{\left(1 - \left| \frac{S_{22} - \Delta\Gamma_s}{1 - S_{11}\Gamma_s} \right|^2 \right) |1 - S_{11}\Gamma_s|^2} = |S_{21}|^2 g_a \quad (3.7.12)$$

where

$$g_a = \frac{G_A}{|S_{21}|^2} = \frac{1 - |\Gamma_s|^2}{1 - |S_{22}|^2 + |\Gamma_s|^2(|S_{11}|^2 - |\Delta|^2) - 2 \operatorname{Re}(\Gamma_s C_1)} \quad (3.7.13)$$

and

$$C_1 = S_{11} - \Delta S_{22}^* \quad (3.7.14)$$

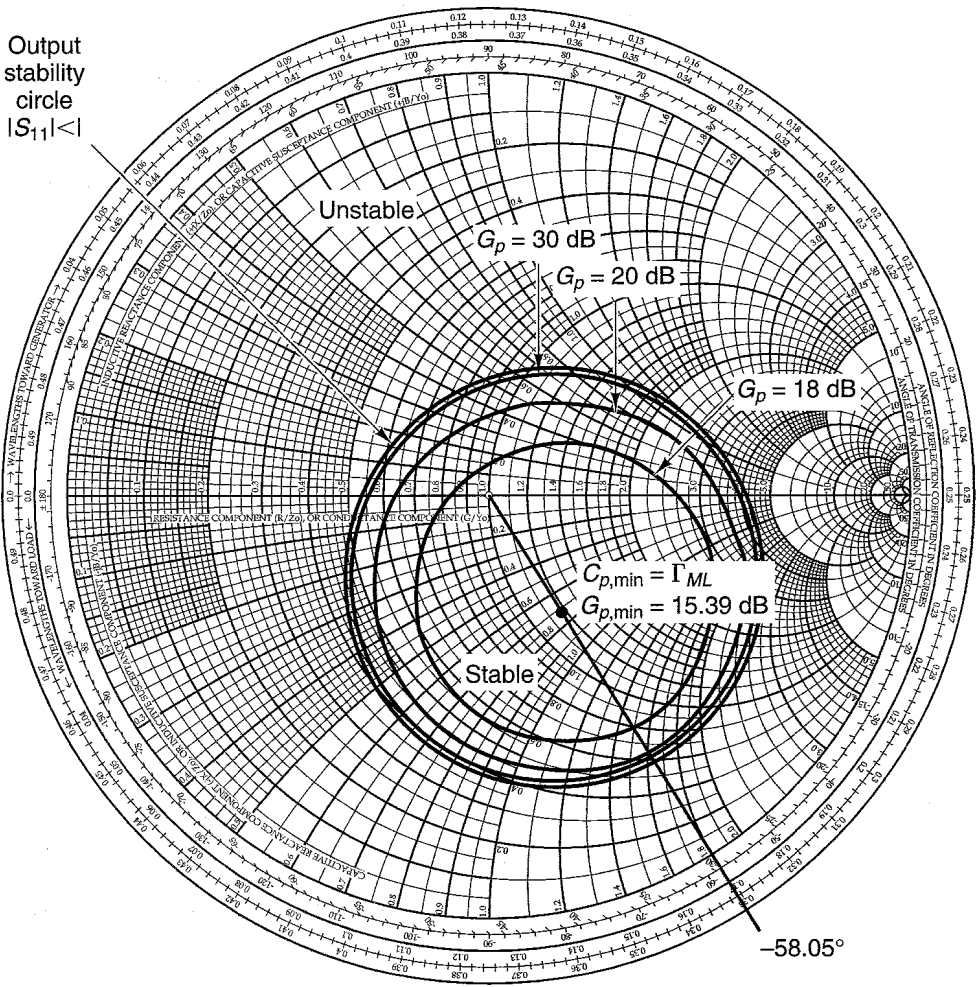
Since (3.7.12), (3.7.13), and (3.7.14) are identical in form to (3.7.1), (3.7.2), and (3.7.3), it follows that the center C_a and radius r_a of constant operating power-gain circles are given by

$$C_a = \frac{g_a C_1^*}{1 + g_a(|S_{11}|^2 - |\Delta|^2)} \quad (3.7.15)$$

and

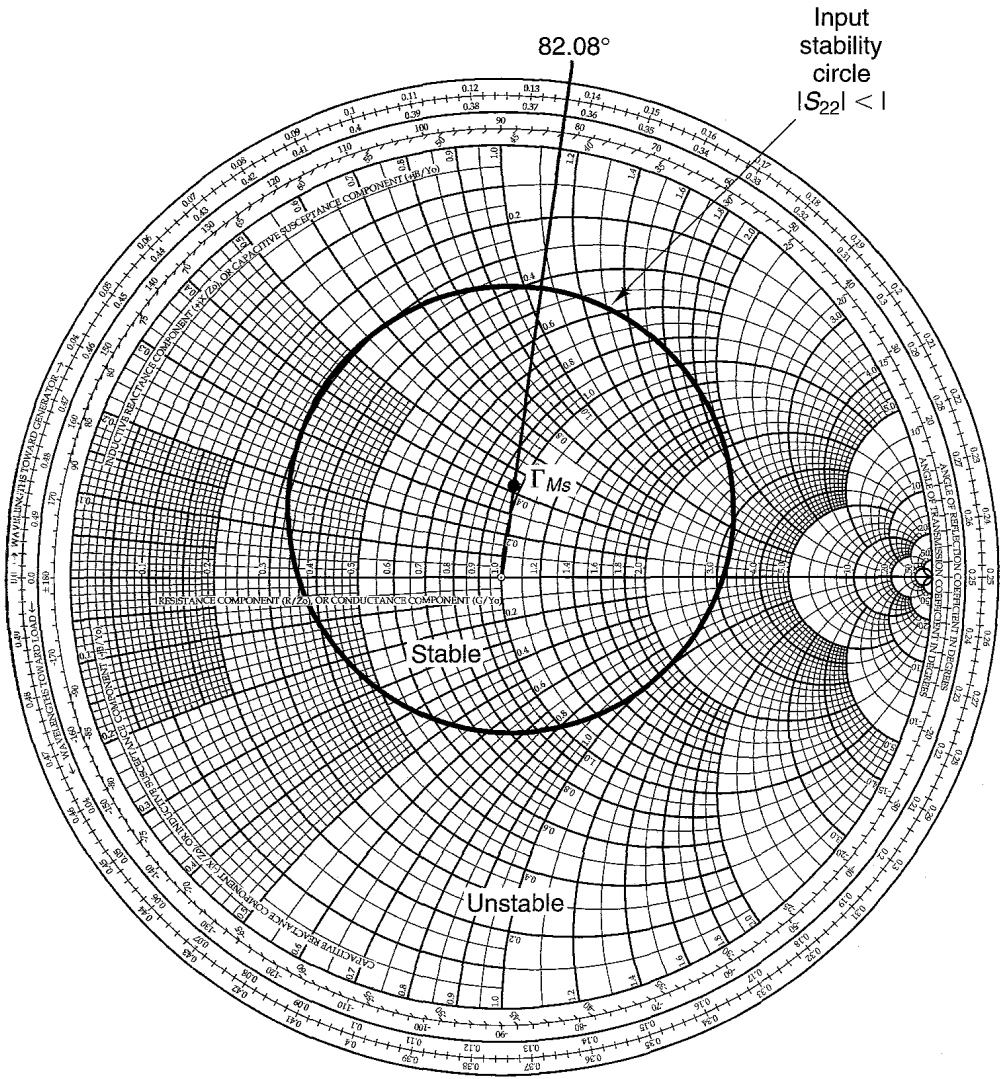
$$r_a = \frac{[1 - 2K|S_{12}S_{21}|g_a + |S_{12}S_{21}|^2 g_a^2]^{1/2}}{|1 + g_a(|S_{11}|^2 - |\Delta|^2)|} \quad (3.7.16)$$

G_p (dB)	g_p	r_p	C_p
18	2.524	0.356	0.280 -58.05°
20	4	0.417	0.263 -58.05°
30	40	0.487	0.242 -58.05°



(a)

Figure 3.7.4 (a) Output stability circle and operating power-gain circles for Example 3.7.3; (b) input stability circle and Γ_{Ms} .



(b)

Figure 3.7.4 Continued

For a given G_A , a constant available power-gain circle can be plotted using (3.7.15) and (3.7.16). All Γ_s on this circle produce the given G_A . For the given G_A , maximum output power is obtained with $\Gamma_L = \Gamma_{OUT}^*$, where Γ_{OUT} is given by (3.2.6). This value of Γ_L produces the transducer power gain $G_T = G_A$.

Since the constant available power-gain circles and the constant noise figure circles are functions of Γ_s , they can be plotted together on the Smith chart

and the trade-offs that result between gain and noise figure can be analyzed. These concepts are studied in Chapter 4.

Potentially unstable bilateral case. With a potentially unstable transistor, the design procedure for a given G_A is as follows:

1. For a given G_A , draw the constant available gain circle using (3.7.15) and (3.7.16), and also draw the input stability circle using (3.3.9) and (3.3.10). Select a value of Γ_s that is in the stable region and not too close to the stability circle.
2. Calculate Γ_{OUT} using (3.2.6) and determine if a conjugate match at the output is feasible. That is, draw the output stability circle and determine if $\Gamma_L = \Gamma_{OUT}^*$ lies in the stable region.
3. If $\Gamma_L = \Gamma_{OUT}^*$ is not in the stable region or is in the stable region but very close to the output stability circle, the value of Γ_L can be selected arbitrarily or a new value of G_A can be selected. Of course, we must be careful when selecting Γ_L arbitrarily since the value of Γ_L affects the output power and the VSWR.

The values of Γ_L and Γ_s should not be too close to their respective stability circles, because oscillations might occur due to component variations that can place Γ_L and Γ_s in their respective unstable regions.

3.8 CONSTANT VSWR CIRCLES

The design specifications of a microwave amplifier usually include the maximum allowable values of its input VSWR and of its output VSWR. Constant input VSWR circles can be drawn on the Γ_s plane, and constant output VSWR circles can be drawn on the Γ_L plane. These circles can be used in the development of certain designs.

Consider Fig. 3.8.1, which shows a microwave amplifier. The input VSWR is given by

$$(\text{VSWR})_{\text{in}} = \frac{1 + |\Gamma_a|}{1 - |\Gamma_a|} \quad (3.8.1)$$

where $|\Gamma_a|$ is given by (2.8.3)—namely,

$$|\Gamma_a| = \left| \frac{\Gamma_{\text{IN}} - \Gamma_s^*}{1 - \Gamma_{\text{IN}}\Gamma_s} \right| \quad (3.8.2)$$

Equation (3.8.2) shows that for a given Γ_{IN} , the reflection coefficients Γ_s and Γ_a are related by a bilinear transformation. Hence, constant values of $|\Gamma_a|$ are obtained by values of Γ_s that lie on a circle.

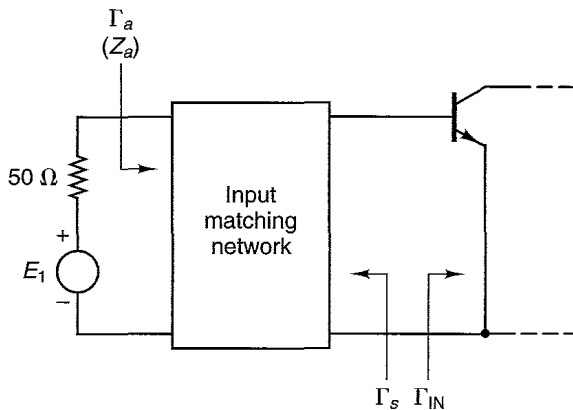


Figure 3.8.1 Input portion of a microwave amplifier.

The design for a given $(VSWR)_{in}$ can be performed as follows. From (3.8.1), the value of $(VSWR)_{in}$ fixes the value of $|\Gamma_a|$. Then (3.8.2) is used to plot the values of Γ_s that result in the constant value $|\Gamma_a|$. In Appendix I it is shown that from (3.8.2) a constant $|\Gamma_a|$ circle satisfies the equation

$$|\Gamma_s - C_{V_i}| = r_{V_i}$$

where the center C_{V_i} is given by

$$C_{V_i} = \frac{\Gamma_{IN}^*(1 - |\Gamma_a|^2)}{1 - |\Gamma_a \Gamma_{IN}|^2} \tag{3.8.3}$$

and the radius is

$$r_{V_i} = \frac{|\Gamma_a|(1 - |\Gamma_{IN}|^2)}{1 - |\Gamma_a \Gamma_{IN}|^2} \tag{3.8.4}$$

In an unconditional stable case, and in many potentially unstable cases, Γ_s can be selected equal to Γ_{IN}^* in order to get $(VSWR)_{in} = 1$. Equations (3.8.3) and (3.8.4) demonstrate this fact. That is, from (3.8.1) with $(VSWR)_{in} = 1$, it follows that $|\Gamma_a| = 0$, and from (3.8.3) and (3.8.4) we obtain

$$C_{V_i}|_{|\Gamma_a|=0} = \Gamma_{IN}^*$$

and

$$r_{V_i}|_{|\Gamma_a|=0} = 0$$

In other words, the value of $\Gamma_s = \Gamma_{IN}^*$ produces $|\Gamma_a| = 0$ and consequently $(VSWR)_{in} = 1$.

Similar relations are obtained for the output VSWR. The output VSWR is given by

$$(VSWR)_{out} = \frac{1 + |\Gamma_b|}{1 - |\Gamma_b|} \tag{3.8.5}$$

where $|\Gamma_b|$ is given by (2.8.6)—namely,

$$|\Gamma_b| = \left| \frac{\Gamma_{\text{OUT}} - \Gamma_L^*}{1 - \Gamma_{\text{OUT}}\Gamma_L} \right| \quad (3.8.6)$$

The constant $|\Gamma_b|$ circles satisfy the equation

$$|\Gamma_L - C_{V_o}| = r_{V_o}$$

where

$$C_{V_o} = \frac{\Gamma_{\text{OUT}}^*(1 - |\Gamma_b|^2)}{1 - |\Gamma_b\Gamma_{\text{OUT}}|^2} \quad (3.8.7)$$

and

$$r_{V_o} = \frac{|\Gamma_b|(1 - |\Gamma_{\text{OUT}}|^2)}{1 - |\Gamma_b\Gamma_{\text{OUT}}|^2} \quad (3.8.8)$$

Example 3.8.1

(a) The S parameters of a GaAs FET at 12 GHz, $V_{DS} = 3.5$ V, and $I_{DS} = 25$ mA are

$$S_{11} = 0.6 \angle 36^\circ$$

$$S_{12} = 0.14 \angle -85^\circ$$

$$S_{21} = 2.3 \angle -80^\circ$$

$$S_{22} = 0.15 \angle 45^\circ$$

Determine $G_{A,\text{max}}$ and draw the constant G_A circle that is 1 dB less than $G_{A,\text{max}}$.

(b) Select several values of Γ_s on the $G_A = G_{A,\text{max}} - 1$ dB circle. For each Γ_s value, determine the values of Γ_L that lie on the constant $(\text{VSWR})_{\text{out}} = 1.5$ circle, and draw the constant $(\text{VSWR})_{\text{out}} = 1.5$ circles.

(c) Select several values of Γ_L on the $(\text{VSWR})_{\text{out}} = 1.5$ circle. For each Γ_L value, calculate $(\text{VSWR})_{\text{in}}$.

Solution. (a) This transistor is unconditionally stable since $K = 1.17$ and $\Delta = 0.368 \angle 27.91^\circ$. This transistor can be simultaneously conjugate matched with $\Gamma_{M_s} = 0.714 \angle -40.45^\circ$ and $\Gamma_{M_L} = 0.387 \angle -129.36^\circ$, resulting in $(\text{VSWR})_{\text{in}} = (\text{VSWR})_{\text{out}} = 1$. From (3.6.10),

$$G_{A,\text{max}} = \frac{|S_{21}|}{|S_{12}|} (K - \sqrt{K^2 - 1}) = \frac{2.3}{0.14} (1.17 - \sqrt{1.17^2 - 1}) = 9.24 \text{ (or 9.66 dB)}$$

The analysis calls for a gain G_A different from $G_{A,\text{max}}$ and the selection of Γ_s and Γ_L for certain VSWR performance. The design methods used in this example have applications in the design of low-noise amplifiers (discussed in Chapter 4). In the design of low-noise amplifiers, we commonly make trade-offs between gain, noise performance, and VSWRs.

The constant G_A circle that is 1 dB less than $G_{A,\text{max}}$ is the circle for $G_A = 8.66$ dB. The center and radius of the $G_A = 8.66$ dB circle, from (3.7.15) and (3.7.16) with $g_a = 7.3451/(2.3)^2 = 1.3886$, are $C_a = 0.602 \angle -40.45^\circ$ and $r_a = 0.3$. The $G_A = 8.66$ dB constant gain circle is drawn in Fig. 3.8.2a.

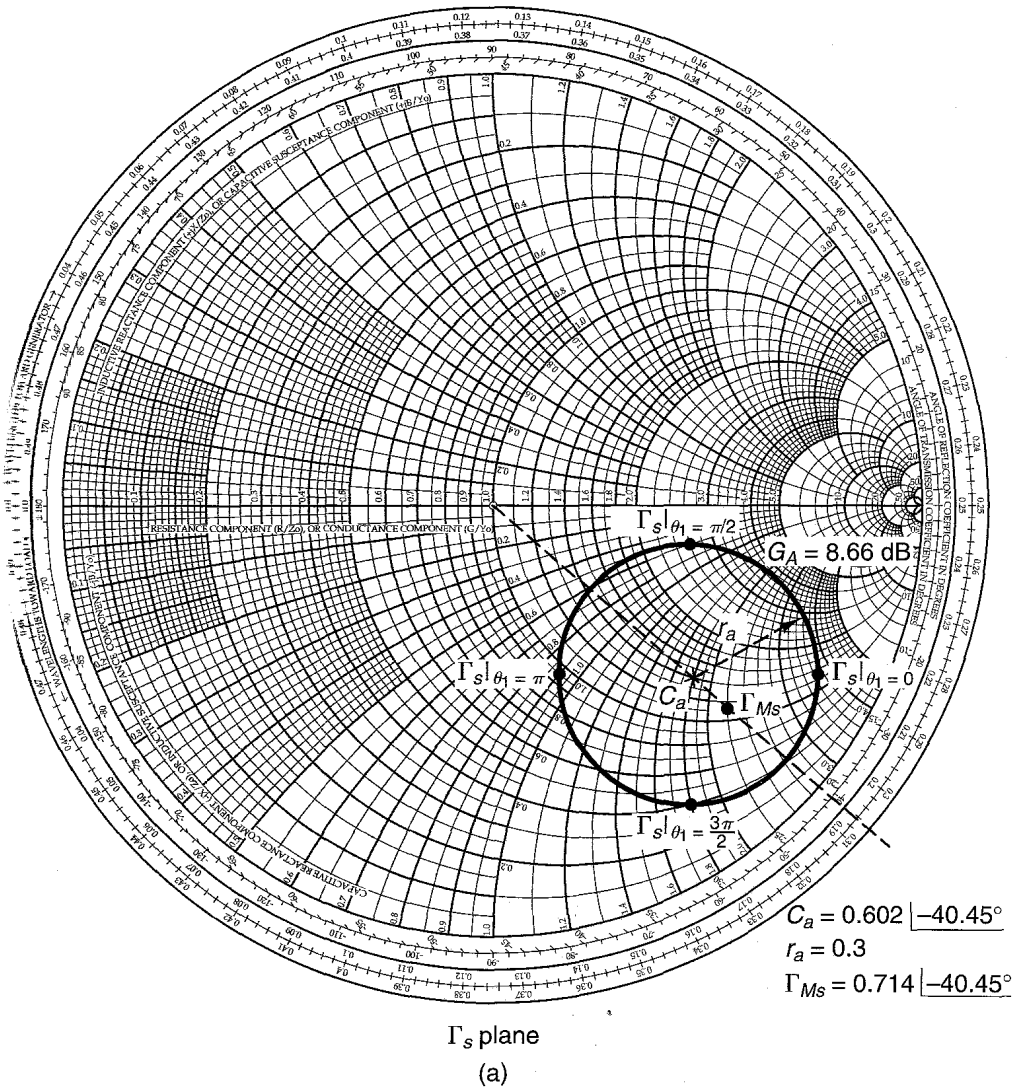


Figure 3.8.2 (a) The $G_A = 8.66$ dB constant gain circle and Γ_{Ms} ; (b) four values of Γ_s on the $G_A = 8.66$ dB circle and calculations of $(VSWR)_{in}$ for $(VSWR)_{out} = 1$; (c) the four $(VSWR)_{out} = 1.5$ circles; (d) four values of Γ_L on the $(VSWR)_{out} = 1.5$ circles, the corresponding values of Γ_{IN} and $|\Gamma_d|_in$, and the resulting values of $(VSWR)_{in}$.

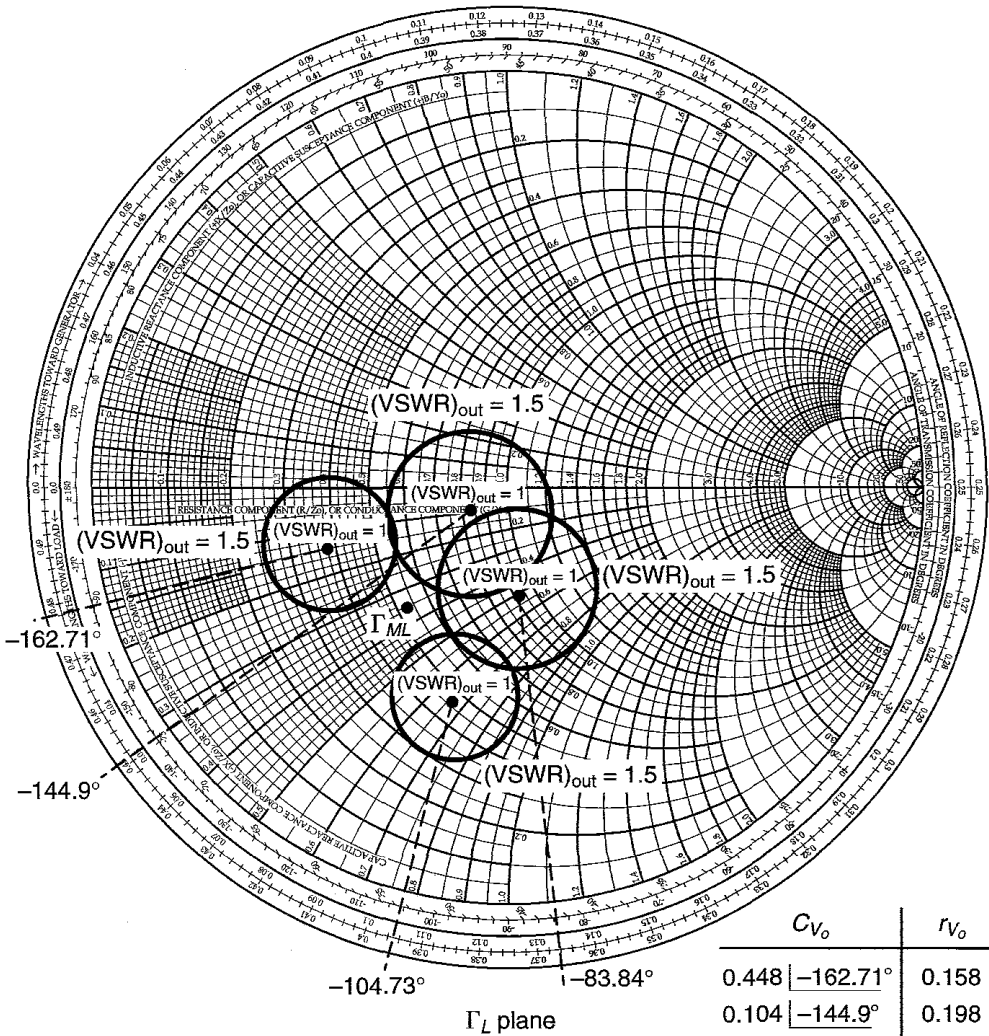
(b) The values of Γ_s on the $G_A = 8.66$ dB circle are given by

$$\Gamma_s = C_a + r_a e^{j\theta_1} = 0.602 \angle -40.45^\circ + 0.3e^{j\theta_1}$$

Four convenient values of Γ_s on this circle are shown in Fig. 3.8.2a. They correspond to $\theta_1 = 0, \pi/2, \pi,$ and $3\pi/2$. The values of Γ_s and the associated values of Γ_{OUT} are listed in

Γ_s	Γ_{OUT}	$\Gamma_L = \Gamma_{OUT}^*$	$(VSWR)_{out}$	Γ_{IN}	$ \Gamma_a $	$(VSWR)_{in}$
0.853 $\angle -27.25^\circ$ for $\theta_1 = 0$	0.463 $\angle 162.71^\circ$	0.463 $\angle -162.71^\circ$	1	0.743 $\angle 34.62^\circ$	0.395	2.31
0.467 $\angle -11.18^\circ$ for $\theta_1 = \pi/2$	0.108 $\angle 144.9^\circ$	0.108 $\angle -144.9^\circ$	1	0.634 $\angle 36.71^\circ$	0.394	2.30
0.421 $\angle -67.96^\circ$ for $\theta_1 = \pi$	0.259 $\angle 83.84^\circ$	0.259 $\angle -83.84^\circ$	1	0.630 $\angle 43.53^\circ$	0.394	2.30
0.829 $\angle -56.44^\circ$ for $\theta_1 = 3\pi/2$	0.533 $\angle 104.73^\circ$	0.533 $\angle -104.73^\circ$	1	0.727 $\angle 46.85^\circ$	0.395	2.31

(b)



C_{V_o}	r_{V_o}
0.448 $\angle -162.71^\circ$	0.158
0.104 $\angle -144.9^\circ$	0.198
0.249 $\angle -83.84^\circ$	0.187
0.518 $\angle -104.73^\circ$	0.144

(c)

Figure 3.8.2 Continued

Γ_s	Γ_{OUT}	Γ_L	Γ_{IN}	$ \Gamma_a $	$(VSWR)_{in}$
0.853 $\underline{-27.25^\circ}$ for $\theta_1 = 0$	0.463 $\underline{162.71^\circ}$	0.301 $\underline{-153.73^\circ}$ for $\theta_2 = 0$	0.695 $\underline{36.39^\circ}$	0.470	2.77
		0.428 $\underline{176.66^\circ}$ for $\theta_2 = \pi/2$	0.719 $\underline{31.29^\circ}$	0.371	2.18
		0.601 $\underline{-167.19^\circ}$ for $\theta_2 = \pi$	0.781 $\underline{33.11^\circ}$	0.320	1.94
		0.517 $\underline{-145.76^\circ}$ for $\theta_2 = 3\pi/2$	0.762 $\underline{37.91^\circ}$	0.460	2.70
0.467 $\underline{-11.18^\circ}$ for $\theta_1 = \pi/2$	0.108 $\underline{144.9^\circ}$	0.128 $\underline{-27.91^\circ}$ for $\theta_2 = 0$	0.573 $\underline{39.14^\circ}$	0.351	2.08
		0.162 $\underline{121.62^\circ}$ for $\theta_2 = \pi/2$	0.612 $\underline{31.30^\circ}$	0.320	1.94
		0.289 $\underline{-168.07^\circ}$ for $\theta_2 = \pi$	0.689 $\underline{34.54^\circ}$	0.447	2.62
		0.272 $\underline{-108.27^\circ}$ for $\theta_2 = 3\pi/2$	0.662 $\underline{41.79^\circ}$	0.470	2.77
0.421 $\underline{-67.96^\circ}$ for $\theta_1 = \pi$	0.259 $\underline{83.84^\circ}$	0.327 $\underline{-49.23^\circ}$ for $\theta_2 = 0$	0.573 $\underline{46.5^\circ}$	0.304	1.87
		0.066 $\underline{-66.19^\circ}$ for $\theta_2 = \pi/2$	0.599 $\underline{38.05^\circ}$	0.398	2.32
		0.295 $\underline{-122.88^\circ}$ for $\theta_2 = \pi$	0.682 $\underline{40.46^\circ}$	0.482	2.86
		0.435 $\underline{-86.48^\circ}$ for $\theta_2 = 3\pi/2$	0.665 $\underline{48^\circ}$	0.411	2.40
0.829 $\underline{-56.44^\circ}$ for $\theta_1 = 3\pi/2$	0.533 $\underline{104.73^\circ}$	0.501 $\underline{-88.59^\circ}$ for $\theta_2 = 0$	0.684 $\underline{49.28^\circ}$	0.390	2.28
		0.381 $\underline{-110.25^\circ}$ for $\theta_2 = \pi/2$	0.693 $\underline{43.43^\circ}$	0.477	2.82
		0.572 $\underline{-118.83^\circ}$ for $\theta_2 = \pi$	0.761 $\underline{44.22^\circ}$	0.449	2.63
		0.658 $\underline{-101.54^\circ}$ for $\theta_2 = 3\pi/2$	0.757 $\underline{49.53^\circ}$	0.311	1.90

(d)

Figure 3.8.2 Continued

Fig. 3.8.2b. For $\Gamma_L = \Gamma_{\text{OUT}}^*$, Fig. 3.8.2b shows the values of $(\text{VSWR})_{\text{out}}$, the corresponding values of Γ_{IN} , the values of $|\Gamma_d|$ [using (3.8.2)], and the resulting values of $(\text{VSWR})_{\text{in}}$ [using (3.8.1)]. From Fig. 3.8.2b, it is seen that with $\Gamma_L = \Gamma_{\text{OUT}}^*$, the input VSWR is approximately 2.3 for the four values of Γ_s .

For an output VSWR of 1.5, we have from (3.8.5) that $|\Gamma_b| = 0.2$. Then, using (3.8.7) and (3.8.8), the center and radius of the $(\text{VSWR})_{\text{out}} = 1.5$ circles are calculated and listed in Fig. 3.8.2c. The four $(\text{VSWR})_{\text{out}} = 1.5$ circles, as well as the four values where $\Gamma_L = \Gamma_{\text{OUT}}^*$ [i.e., $(\text{VSWR})_{\text{out}} = 1$], are drawn in Fig. 3.8.2c.

(c) The values of Γ_L on the $(\text{VSWR})_{\text{out}} = 1.5$ circles are given by

$$\Gamma_L = C_{V_o} + r_{V_o} e^{j\theta_2}$$

Four convenient values of Γ_L on the $(\text{VSWR})_{\text{out}} = 1.5$ circle correspond to $\theta_2 = 0, \pi/2, \pi,$ and $3\pi/2$. In Fig. 3.8.2d, four values of Γ_L are calculated on each $(\text{VSWR})_{\text{out}} = 1.5$ circle, as well as the corresponding values of Γ_{IN} and $|\Gamma_d|$ and the resulting values of $(\text{VSWR})_{\text{in}}$. From the tabulated values, it is seen that there are several values of Γ_s and Γ_L that result in $(\text{VSWR})_{\text{in}}$ values around 1.9 with $(\text{VSWR})_{\text{out}} = 1.5$. For example, with $\Gamma_s = 0.421 \angle -67.96^\circ$ and $\Gamma_L = 0.327 \angle -49.23^\circ$, we have $(\text{VSWR})_{\text{out}} = 1.5$ $(\text{VSWR})_{\text{in}} = 1.87$.

For further practice with this type of calculations, the reader is referred to Problem 3.30, where the analyses in this example are to be performed for the $G_A = G_{A,\text{max}} - 2$ dB circle (i.e., the $G_A = 7.66$ dB circle).

Since Γ_L and Γ_{IN} , as well as Γ_s and Γ_{OUT} , are related by bilinear transformations [see (3.2.5) and (3.2.6)], it follows that circles in the Γ_L plane map into circles in the Γ_{IN} plane, and circles in the Γ_s plane map into circles in the Γ_{OUT} plane. Specifically, these transformations are useful to map values of Γ_L on a constant G_p circle into a circle in the Γ_s plane, where $\Gamma_s = \Gamma_{\text{IN}}^*$ and values of Γ_s on a constant G_A circle into a circle in the Γ_L plane, where $\Gamma_L = \Gamma_{\text{OUT}}^*$.

In Appendix J it is shown that the values of Γ_L on a circle given by

$$|\Gamma_L - C_{oo}| = r_{oo}$$

map into a circle in the $\Gamma_s = \Gamma_{\text{IN}}^*$ plane given by

$$|\Gamma_s - C_i| = r_i$$

where the center of the circle is given by

$$C_i = \frac{(1 - S_{22}C_{oo})(S_{11} - \Delta C_{oo})^* - r_{oo}^2 \Delta^* S_{22}}{|1 - S_{22}C_{oo}|^2 - r_{oo}^2 |S_{22}|^2} \quad (3.8.9)$$

and the radius is

$$r_i = \frac{r_{oo} |S_{12} S_{21}|}{\left| |1 - S_{22}C_{oo}|^2 - r_{oo}^2 |S_{22}|^2 \right|} \quad (3.8.10)$$

Similarly, a circle in the Γ_s plane given by

$$|\Gamma_s - C_{ii}| = r_{ii}$$

maps into a circle in the $\Gamma_L = \Gamma_{\text{OUT}}^*$ plane given by

$$|\Gamma_L - C_o| = r_o$$

where

$$C_o = \frac{(1 - S_{11}C_{ii})(S_{22} - \Delta C_{ii})^* - r_{ii}^2 \Delta^* S_{11}}{|1 - S_{11}C_{ii}|^2 - r_{ii}^2 |S_{11}|^2} \quad (3.8.11)$$

and

$$r_o = \frac{r_{ii} |S_{12} S_{21}|}{|1 - S_{11}C_{ii}|^2 - r_{ii}^2 |S_{11}|^2} \quad (3.8.12)$$

Example 3.8.2

Design a microwave amplifier using a GaAs FET whose S parameters at 4 GHz, $V_{DS} = 2$ V, and $I_{DS} = 25$ mA are

$$\begin{aligned} S_{11} &= 0.55 \angle -120^\circ & S_{12} &= 0.14 \angle 30^\circ \\ S_{21} &= 3.5 \angle 60^\circ & S_{22} &= 0.2 \angle -50^\circ \end{aligned}$$

Analyze the trade-offs between operating power gain, stability, and VSWRs.

Solution. For this transistor, $K = 0.947$ and $\Delta = 0.521 \angle -102.01^\circ$. Since $K < 1$, the transistor is potentially unstable at 4 GHz. The centers and radii of the input and output stability circles are

$$\begin{aligned} C_s &= 16.47 \angle 130.7^\circ & C_L &= 1.22 \angle -59.25^\circ \\ r_s &= 15.52 & r_L &= 2.12 \end{aligned}$$

The maximum stable gain is

$$G_{\text{MSG}} = \frac{|S_{21}|}{|S_{12}|} = \frac{3.5}{0.14} = 25 \text{ (or 13.98 dB)}$$

Hence, we select a value of G_p lower than G_{MSG} . The value selected for this design is $G_p = 12$ dB, which is approximately 2 dB lower than G_{MSG} .

From (3.7.4) and (3.7.5), with $g_p = 15.849/(3.5)^2 = 1.294$, the center and radius of the $G_p = 12$ dB constant-gain circle are $C_p = 0.519 \angle 120.75^\circ$ and $r_p = 0.639$. Figure 3.8.3a shows the $G_p = 12$ dB constant-gain circle and the output stability circle. Next we select values of Γ_L on the 12-dB gain circle that are far away from the output stability circle. The values of Γ_L on the 12-dB gain circle are given by $\Gamma_L = C_p + r_p e^{j\theta_1}$. The design procedure is described for two values of Γ_L , shown as point a (where $\theta_1 = 0$) and point b (where $\theta_1 = 3\pi/2$). At point a the value of Γ_L is $0.582 \angle 50.05^\circ$, and at point b the value is $0.328 \angle -143.98^\circ$. Next we analyze the mapping of the $G_p = 12$ dB constant-gain circle onto the $\Gamma_s = \Gamma_{\text{IN}}^*$ plane. Using (3.8.9) and (3.8.10) with $C_{oo} = C_p = 0.519 \angle 120.75^\circ$ and $r_{oo} = r_p = 0.639$, we obtain $C_i = 0.8 \angle 130.7^\circ$ and $r_i = 0.338$. This circle is drawn in the $\Gamma_s = \Gamma_{\text{IN}}^*$ plane in Fig. 3.8.3b.

Several calculations are shown in Fig. 3.8.3c. Using (3.2.5), the second column shows the specific mapping of points a and b in the $\Gamma_s = \Gamma_{\text{IN}}^*$ plane. These points are denoted by a' and b' in Fig. 3.8.3b. The third column in Fig. 3.8.3c shows that $(\text{VSWR})_{\text{in}} = 1$ for $\Gamma_s = \Gamma_{\text{IN}}^*$. Using (3.2.6), the fourth column shows the corresponding values of Γ_{OUT} . From (3.8.6), the magnitude of $|\Gamma_b|$ is calculated in the fifth column. Finally, from (3.8.5),

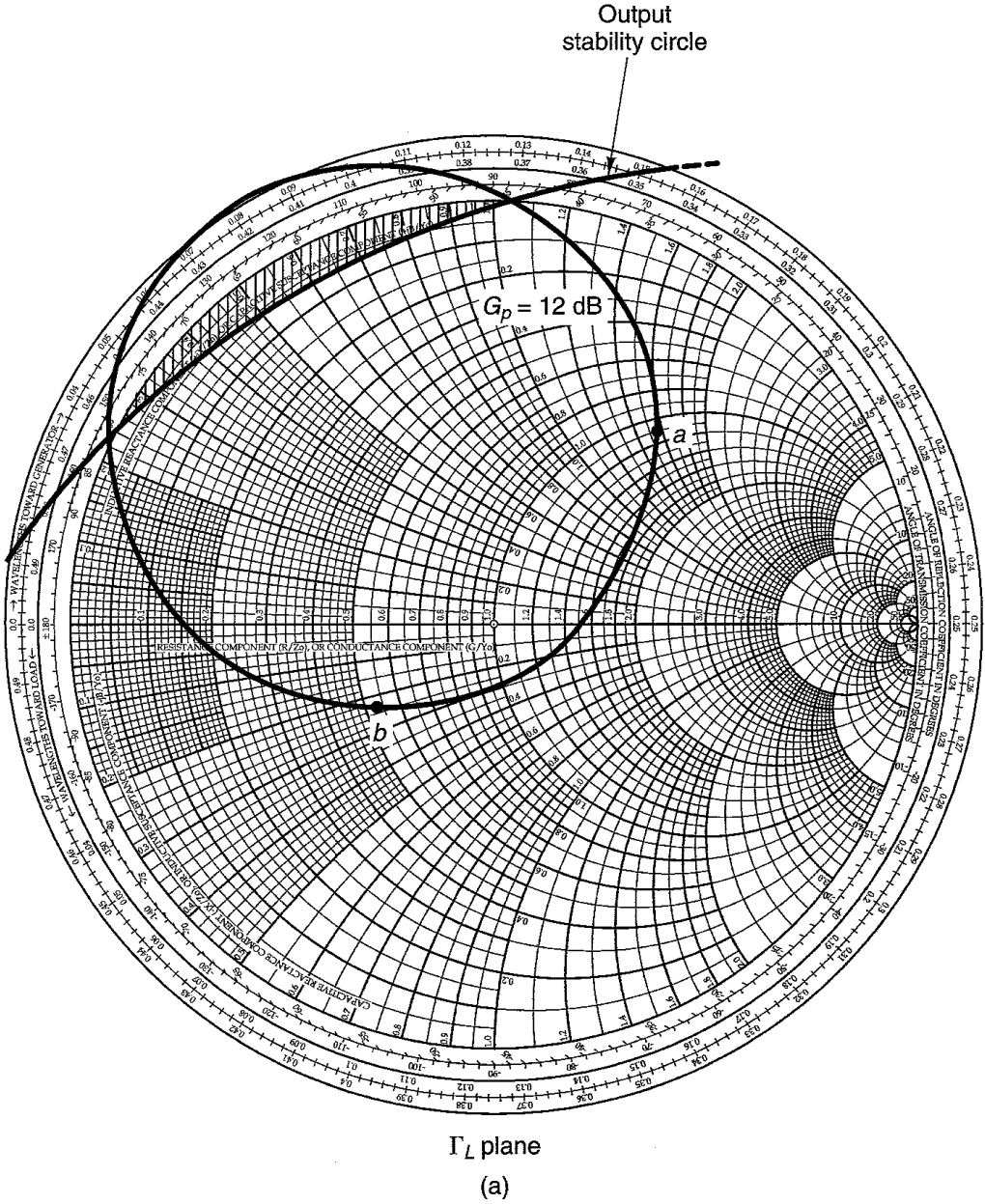


Figure 3.8.3 (a) The $G_p = 12 \text{ dB}$ constant-gain circle and the output stability circle; (b) mapping of the $G_p = 12 \text{ dB}$ constant-gain circle onto the $\Gamma_s = \Gamma_{IN}^*$ plane, the input stability circle, and the constant $(VSWR)_{in} = 1.5$ circles; (c) calculations for Γ_L values at point a and b with $\Gamma_s = \Gamma_{IN}^*$ [i.e., $(VSWR)_{in} = 1$]; (d) calculations for Γ_L values at points a and b with $(VSWR)_{in} = 1.5$.

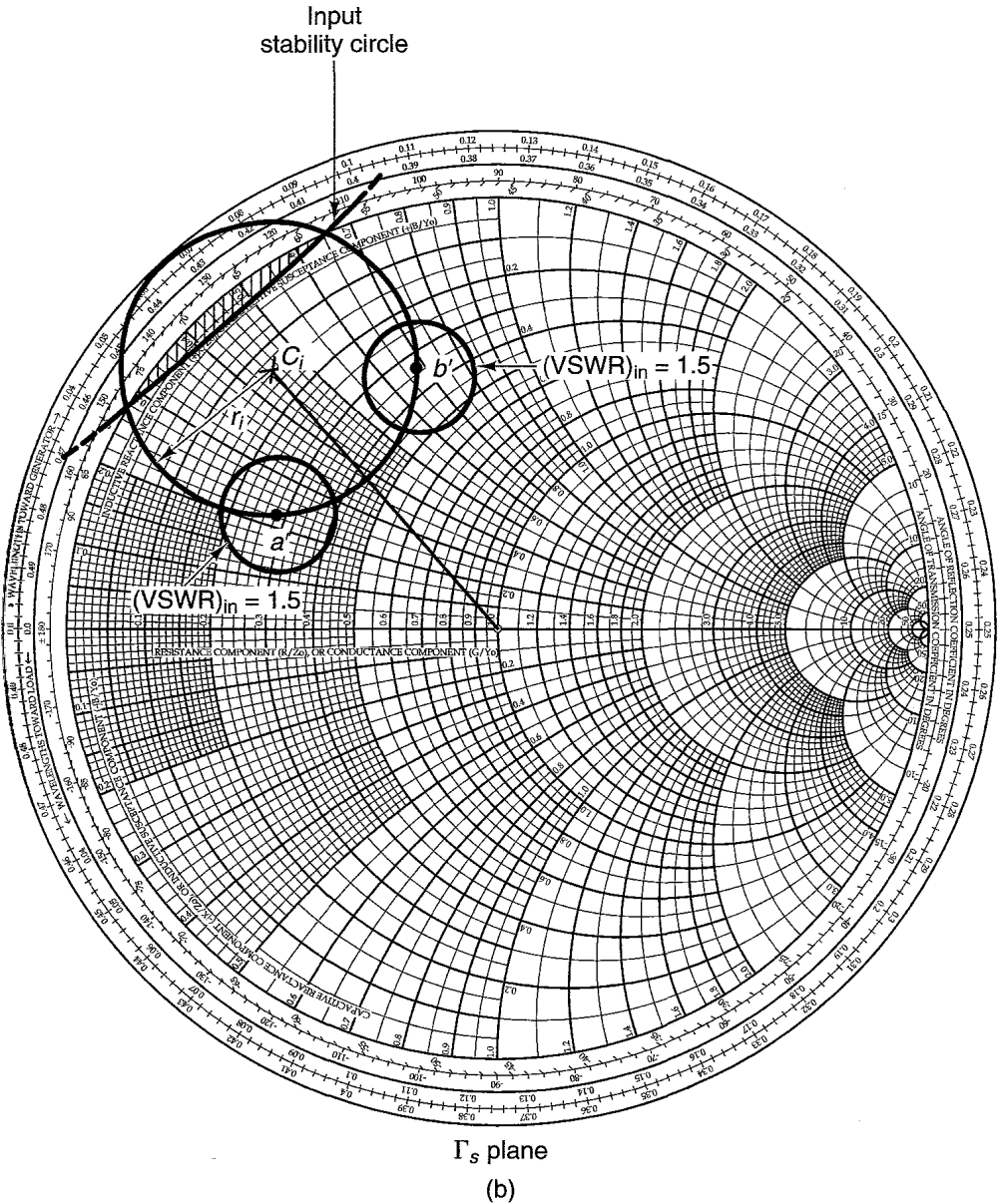


Figure 3.8.3 Continued

Γ_L	$\Gamma_s = \Gamma_{IN}^*$	$(VSWR)_{in}$	Γ_{OUT}	$ \Gamma_b $	$(VSWR)_{out}$
0.582 $\underline{50.05^\circ}$ for $\theta_1 = 0$	0.588 $\underline{152.74^\circ}$	1	0.528 $\underline{-85.97^\circ}$	0.448	2.62
0.328 $\underline{-143.98^\circ}$ for $\theta_1 = 270^\circ$	0.625 $\underline{107.15^\circ}$	1	0.399 $\underline{-143.55^\circ}$	0.447	2.62

(c)

Γ_L	Γ_{IN}	C_{V_i} and r_{V_i} for $(VSWR)_{in} = 1.5$	Γ_s	Γ_{OUT}	$ \Gamma_b $	$(VSWR)_{out}$
0.582 $\underline{50.05^\circ}$ for $\theta_1 = 0$	0.588 $\underline{-152.74^\circ}$	$C_{V_i} = 0.572 \underline{152.74^\circ}$ $r_{V_i} = 0.133$	0.458 $\underline{145.09^\circ}$ for $\theta_2 = 0$	0.410 $\underline{-90.33^\circ}$	0.454	2.66
			0.643 $\underline{142.16^\circ}$ for $\theta_2 = \pi/2$	0.483 $\underline{-74.36^\circ}$	0.324	1.96
			0.692 $\underline{157.78^\circ}$ for $\theta_2 = \pi$	0.569 $\underline{-97.81^\circ}$	0.572	3.67
			0.525 $\underline{165.77^\circ}$ for $\theta_2 = 3\pi/2$	0.621 $\underline{-80.87^\circ}$	0.451	2.64
0.328 $\underline{-143.98^\circ}$ for $\theta_1 = 270^\circ$	0.625 $\underline{-107.15^\circ}$	$C_{V_i} = 0.61 \underline{107.15^\circ}$ $r_{V_i} = 0.124$	0.586 $\underline{95.48^\circ}$ for $\theta_2 = 0$	0.293 $\underline{-156.53^\circ}$	0.324	1.96
			0.730 $\underline{104.28^\circ}$ for $\theta_2 = \pi/2$	0.485 $\underline{-156.23^\circ}$	0.460	2.70
			0.657 $\underline{117.53^\circ}$ for $\theta_2 = \pi$	0.315 $\underline{-125.74^\circ}$	0.453	2.66
			0.493 $\underline{111.40^\circ}$ for $\theta_2 = 3\pi/2$	0.496 $\underline{-130.80^\circ}$	0.571	3.66

(d)

Figure 3.8.3 Continued

the sixth column lists the values of $(VSWR)_{out}$. The values of Γ_s at a' and b' are far away from the input stability circle. Hence, if $(VSWR)_{out} = 2.62$ is satisfactory, the design for $G_p = 12$ dB can be implemented with the values of Γ_s and Γ_L listed in Fig. 3.8.3c.

A smaller value of $(VSWR)_{out}$ can be obtained by relaxing the input VSWR specifications. To illustrate this point, we design the amplifier with $(VSWR)_{in} = 1.5$. The design calculations are shown in Fig. 3.8.3d. The center and radius of the constant $(VSWR)_{in} = 1.5$ circle are made using (3.8.3) and (3.8.4) with $|\Gamma_a| = 0.2$. These values are listed in the third column in Fig. 3.8.3d, and the resulting $(VSWR)_{in} = 1.5$ circles are plotted in Fig. 3.8.3b.

The values of Γ_s on the $(VSWR)_{in} = 1.5$ circle are given by

$$\Gamma_s = C_{V_i} + r_{V_i} e^{j\theta_2}$$

Four convenient values on the $(VSWR)_{in} = 1.5$ circles are listed in the fourth column of Fig. 3.8.3d. They correspond to $\theta_2 = 0, \pi/2, \pi,$ and $3\pi/2$. Using (3.2.6), Γ_{OUT} is calculated in the fifth column. From (3.8.6), $|\Gamma_b|$ is calculated in the sixth column. Finally, using (3.8.5), $(VSWR)_{out}$ is calculated in the seventh column. From Fig. 3.8.3d, it is seen that the values associated with $(VSWR)_{out} = 1.96$ are far away from the input stability circle. Thus, a microwave amplifier with $G_p = 12$ dB can be designed with $\Gamma_L = 0.582 \underline{50.05^\circ}$ and $\Gamma_s = 0.643 \underline{142.16^\circ}$, or with $\Gamma_L = 0.328 \underline{-143.98^\circ}$ and $\Gamma_s = 0.586 \underline{95.48^\circ}$.

It is of interest to analyze the design for a value of G_p greater than G_{MSG} (e.g., $G_p = 15$ dB). From (3.7.4), with $g_p = 31.623/(3.5)^2 = 2.581$, the center and radius of the $G_p = 15$ dB constant-gain circle are $C_p = 1.8 \angle 120.75^\circ$ and $r_p = 1.12$. Using (3.8.9) and (3.8.10), the 15-dB gain circle is mapped into a circle in the $\Gamma_s = \Gamma_{IN}^*$ plane with center and radius given by $C_i = 1.53 \angle 130.7^\circ$ and $r_i = 0.652$.

The 15-dB gain circle is shown in Fig. 3.8.4a and its mapping in the $\Gamma_s = \Gamma_{IN}^*$ plane in Fig. 3.8.4b. Two values of Γ_L are selected on the 15-dB gain circle. These points are denoted by a and b in Fig. 3.8.4a. The mapping of the points a and b is shown in the $\Gamma_s = \Gamma_{IN}^*$

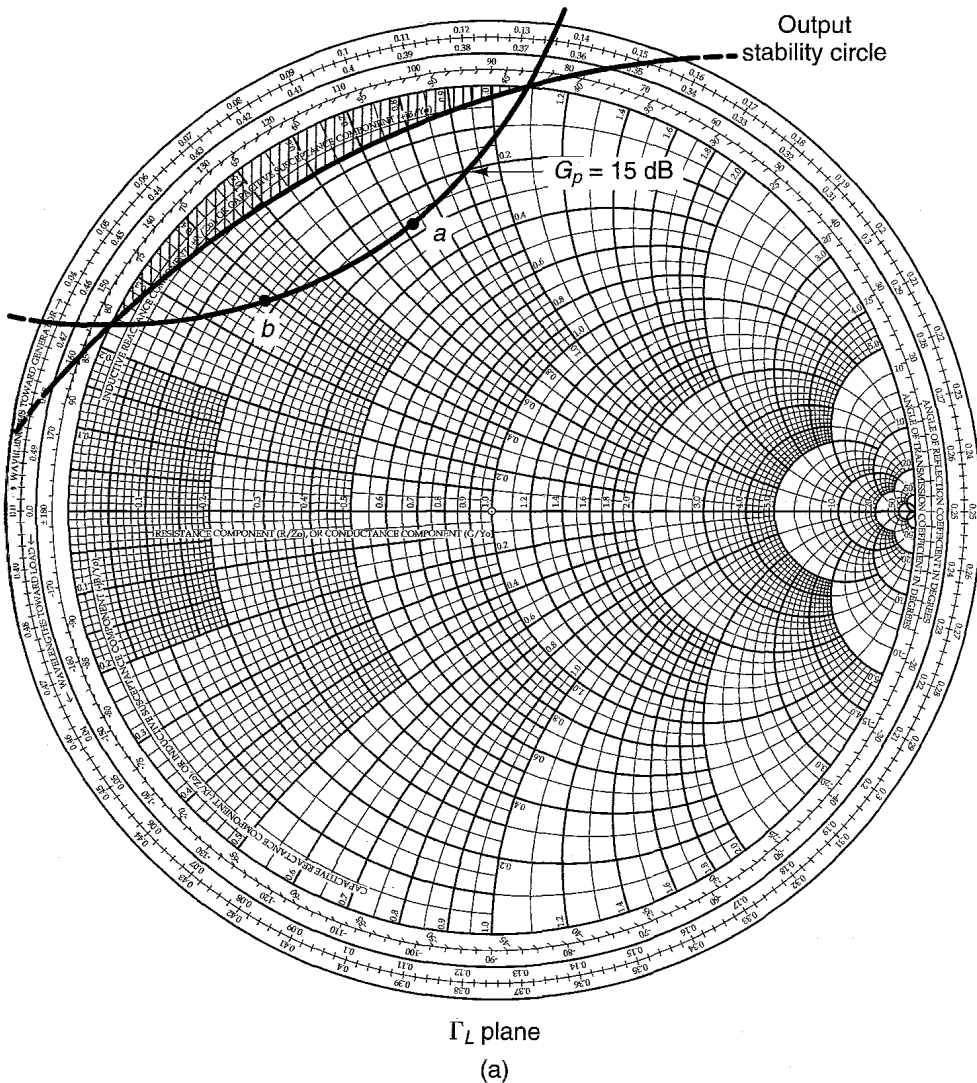
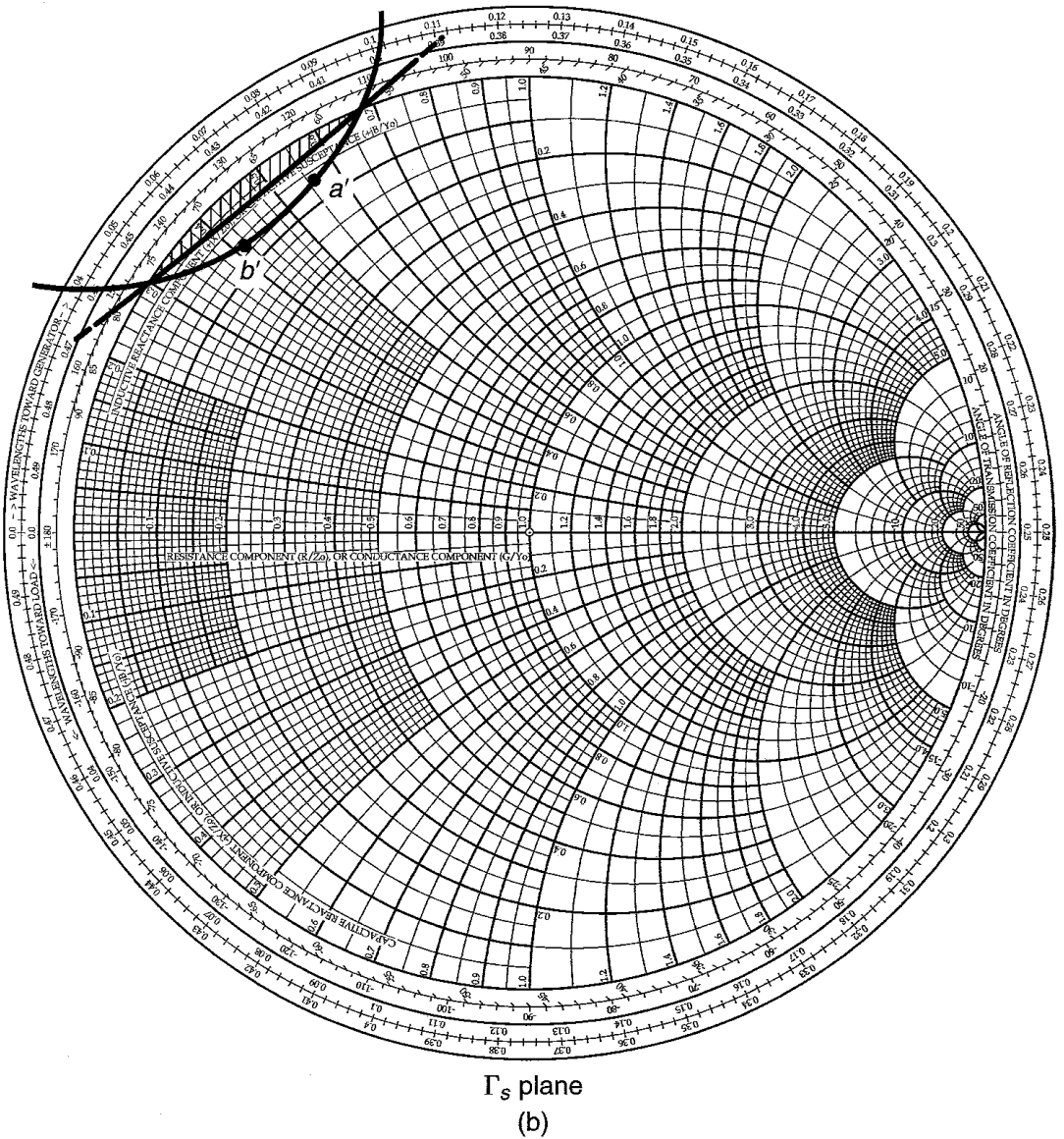


Figure 3.8.4 (a) The $G_p = 15$ dB constant-gain circle and the output stability circle; (b) mapping of the $G_p = 15$ dB constant-gain circle onto the $\Gamma_s = \Gamma_{IN}^*$ plane, and the input stability circle; (c) calculations for Γ_L values at points a and b with $\Gamma_s = \Gamma_{IN}^*$ [i.e., $(VSWR)_{in} = 1$].



Γ_L	$\Gamma_s = \Gamma_{IN}^*$	$(VSWR)_{in}$	Γ_{OUT}	$ \Gamma_b $	$(VSWR)_{out}$
0.717 $\angle 106.22^\circ$	0.884 $\angle 134.73^\circ$	1	0.878 $\angle -109.62^\circ$	0.449	2.63
0.730 $\angle 137.37^\circ$	0.906 $\angle 121.68^\circ$	1	0.884 $\angle -133.66^\circ$	0.453	2.65

(c)

Figure 3.8.4 Continued

plane as a' and b' in Fig. 3.8.4b. The values of Γ_L at points a and b are listed in Fig. 3.8.4c, as well as the design calculations. The third column shows that $(VSWR)_{in} = 1$ for $\Gamma_s = \Gamma_{in}^*$. The fourth column shows the corresponding values of Γ_{out} , the fifth column the values of $|\Gamma_b|$, and the sixth column the values of $(VSWR)_{out}$.

An examination of Fig. 3.8.4b shows that the points a' and b' are very close to the unstable region, and the resulting $(VSWR)_{out}$ is greater than 2.63. This is typical of a design when the value of G_p is selected close to the value of G_{MSG} or greater than G_{MSG} .

Further improvements can be done by performing calculations of the type illustrated in Figs. 3.8.3c and 3.8.3d. However, a CAD program can simplify the task considerably. In Appendix "Computer-Aided Designs," Example CAD.2, it is shown that with $\Gamma_L = 0.328 \angle -143.98^\circ$ and $\Gamma_s = 0.612 \angle 95.2^\circ$ it follows that $G_p = 12$ dB, $(VSWR)_{in} = 1.5$, and $(VSWR)_{out} = 1.93$. This is the smallest $(VSWR)_{out}$ that can be obtained with Γ_s on the $(VSWR)_{in} = 1.5$ circle shown in Fig. 3.8.3b. Furthermore, a CAD optimization to minimize the VSWRs shows that with $\Gamma_L = 0.319 \angle -176.51^\circ$ and $\Gamma_s = 0.642 \angle 102.61^\circ$, it follows that $G_p = 12.7$ dB, $(VSWR)_{in} = 1.52$, and $(VSWR)_{out} = 1.58$.

3.9 DC BIAS NETWORKS

It has been said that the least considered factor in microwave transistor amplifier design is the bias network [3.4]. While considerable effort is spent in designing for a given gain, noise figure, and bandwidth, little effort is spent in the dc bias network. The cost per decibel of microwave power gain or noise figure is high, and the designer cannot sacrifice the amplifier performance by having a poor dc bias design.

The purpose of a good dc bias design is to select the proper quiescent point and hold the quiescent point constant over variations in transistor parameters and temperature. A resistor bias network can be used with good results over moderate temperature changes. However, an active bias network is usually preferred for large temperature changes.

In the discussion that follows, we first consider the dc bias design for BJTs and then the bias design of GaAs FETs.

BJT Bias Networks

At low frequencies, a bypassed emitter resistor is an important contributor to the quiescent-point stability. At microwave frequencies, the bypass capacitor, which is in parallel with the emitter resistor, can produce oscillations by making the input port unstable at some frequencies. Furthermore, an emitter resistor will degrade the noise performance of the amplifier. Therefore, in most microwave transistor amplifiers, especially in the gigahertz region, the emitter lead of the transistor is grounded.

At microwave frequencies, the transistor parameters that are affected most by temperature are I_{CBO} , h_{FE} , and V_{BE} . The conventional reverse current I_{CBO} (i.e., I_{CBO} at low frequencies) doubles every 10°C rise in temperature. That is,

$$I_{CBO,T_2} = I_{CBO,T_1} 2^{(T_2 - T_1)/10}$$

where I_{CBO,T_2} and I_{CBO,T_1} are the values of I_{CBO} at temperatures T_2 and T_1 , respectively. The temperature T_1 is usually the temperature at which the manufacturer measures I_{CBO} . This temperature is usually 25°C .

A microwave transistor has a more complicated reverse current flow. The reverse current flow of a microwave transistor is composed of two components; one is the conventional I_{CBO} and the other is a surface current, I_s , that flows across the top of the silicon lattice. The reverse current in a microwave transistor, which is referred to simply as I_{CBO} , increases at a rate much slower than the conventional I_{CBO} . A typical plot of the reverse current versus temperature for a microwave transistor is shown in Fig. 3.9.1. The conventional I_{CBO} slope is also shown in the figure for comparison.

The base-to-emitter voltage V_{BE} has a negative temperature coefficient, approximately given by

$$\frac{\Delta V_{BE}}{\Delta T} \approx -2 \times 10^{-3} \frac{\text{V}}{^\circ\text{C}}$$

The dc value of the current gain h_{FE} is defined as the value of the collector-to-base current at a constant value of V_{CE} . That is,

$$h_{FE} = \left. \frac{I_C}{I_B} \right|_{V_{CE}=\text{constant}}$$

The dc value of h_{FE} is typically found to increase linearly with temperature at the rate of $0.5\%/^\circ\text{C}$.

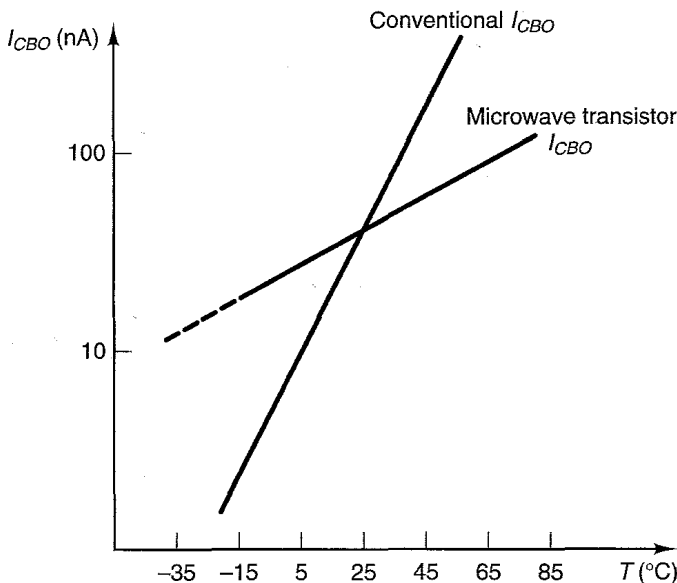


Figure 3.9.1 Typical reverse current versus temperature for a microwave transistor.

In order to find the change in collector current as a function of temperature in a dc bias network, we first find the expression for the collector current valid for any temperature. Then, observing that the temperature-sensitive parameters are I_{CBO} , h_{FE} , and V_{BE} , we can write

$$I_C = f(I_{CBO}, h_{FE}, V_{BE})$$

and

$$\Delta I_C = \left(\frac{\Delta I_C}{\Delta I_{CBO}} \right) \bigg|_{\substack{\Delta h_{FE}=0 \\ \Delta V_{BE}=0}} \Delta I_{CBO} + \left(\frac{\Delta I_C}{\Delta h_{FE}} \right) \bigg|_{\substack{\Delta I_{CBO}=0 \\ \Delta V_{BE}=0}} \Delta h_{FE} + \left(\frac{\Delta I_C}{\Delta V_{BE}} \right) \bigg|_{\substack{\Delta I_{CBO}=0 \\ \Delta h_{FE}=0}} \Delta V_{BE} \quad (3.9.1)$$

Defining the stability factors as

$$S_i = \frac{\Delta I_C}{\Delta I_{CBO}} \bigg|_{\substack{\Delta h_{FE}=0 \\ \Delta V_{BE}=0}}$$

$$S_{h_{FE}} = \frac{\Delta I_C}{\Delta h_{FE}} \bigg|_{\substack{\Delta I_{CBO}=0 \\ \Delta V_{BE}=0}}$$

and

$$S_{V_{BE}} = \frac{\Delta I_C}{\Delta V_{BE}} \bigg|_{\substack{\Delta I_{CBO}=0 \\ \Delta h_{FE}=0}}$$

we can write (3.9.1) in the form

$$\Delta I_C = S_i \Delta I_{CBO} + S_{h_{FE}} \Delta h_{FE} + S_{V_{BE}} \Delta V_{BE} \quad (3.9.2)$$

For a given dc bias network, the stability factors can be calculated and (3.9.2) can be used to predict the variations of I_C with temperature. In a design procedure, the maximum variation of I_C in a temperature range can be selected and (3.9.2) can be used to find the required stability factors. In turn, the stability factors together with the Q -point location will fix the value of the resistors in the bias network.

Two grounded-emitter dc bias networks that can be used at microwave frequencies are shown in Fig. 3.9.2. The network in Fig. 3.9.2b produces lower values of resistance and therefore is more compatible with thin- or thick-film resistor values.

Example 3.9.1

Design the dc bias network shown in Fig. 3.9.2b for $V_{CE} = 10$ V and $I_C = 10$ mA. Assume that $I_{CBO} = 0$, $V_{BE} = 0.7$ V, and $h_{FE} = 50$.

Solution. In this example we follow a procedure that results in good stability factors. Let the supply voltage V_{CC} be 20 V. The base current (I_B) is

$$I_B = \frac{I_C}{h_{FE}} = \frac{10 \times 10^{-3}}{50} = 200 \mu\text{A}$$

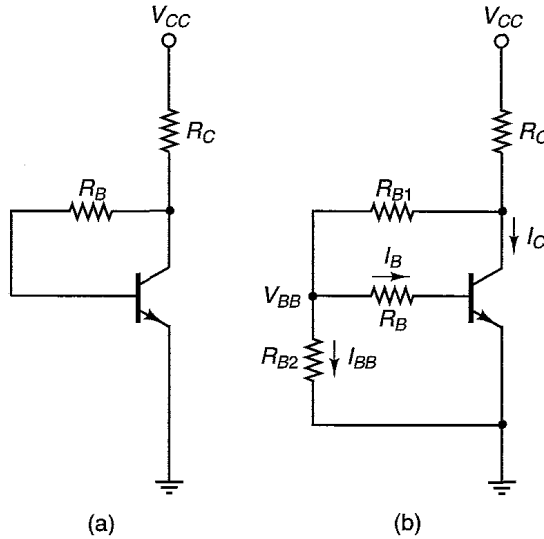


Figure 3.9.2 (a) Voltage feedback bias network; (b) voltage feedback bias network with constant-base current source.

Assuming V_{BB} to be 2 V, we find that

$$R_B = \frac{V_{BB} - V_{BE}}{I_B} = \frac{2 - 0.7}{200 \times 10^{-6}} = 6.5 \text{ k}\Omega$$

R_{B2} is calculated assuming that $I_{BB} = 1 \text{ mA}$ (i.e., $I_{BB} = 5I_B$)—namely,

$$R_{B2} = \frac{V_{BB}}{I_{BB}} = \frac{2}{1 \times 10^{-3}} = 2 \text{ k}\Omega$$

R_{B1} is obtained from

$$R_{B1} = \frac{V_{CE} - V_{BB}}{I_{BB} + I_B} = \frac{10 - 2}{(1 + 0.2) \times 10^{-3}} = 6.66 \text{ k}\Omega$$

and R_C is obtained from

$$R_C = \frac{V_{CC} - V_{CE}}{I_C + I_{BB} + I_B} = \frac{20 - 10}{(10 + 1 + 0.2) \times 10^{-3}} = 893 \Omega$$

The assumption $I_{BB} \gg I_B$ and $V_{BB} \approx 10\% V_{CC}$ produces good stability factors.

At the lower microwave frequencies, the dc biasing network shown in Fig. 3.9.3 with a bypassed emitter resistor can be used. The bypassed emitter resistor provides excellent stability. For this network, it is easy to show that

$$I_C = \frac{h_{FE}(V_{TH} - V_{BE})}{R_{TH} + (h_{FE} + 1)R_E} + \frac{(h_{FE} + 1)I_{CBO}(R_{TH} + R_E)}{R_{TH} + (h_{FE} + 1)R_E}$$

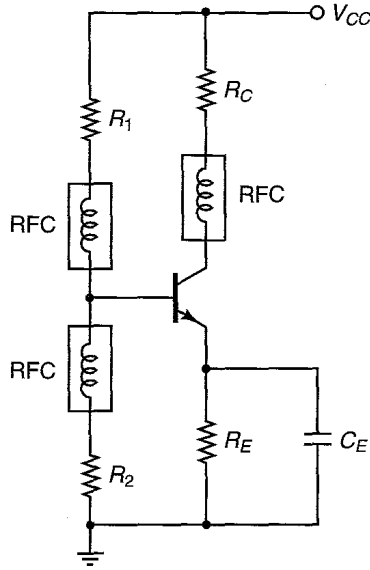


Figure 3.9.3 A dc bias network with a bypassed emitter resistor.

where

$$V_{TH} = \frac{V_{CC}R_2}{R_1 + R_2}$$

and

$$R_{TH} = \frac{R_1R_2}{R_1 + R_2}$$

The stability factors are

$$S_i = \frac{(h_{FE} + 1)(R_{TH} + R_E)}{R_{TH} + (h_{FE} + 1)R_E}$$

$$S_{h_{FE}} \approx \frac{I_{C1}}{h_{FE}} \frac{S_{I2}}{h_{FE,2}} \tag{3.9.3}$$

and

$$S_{V_{BE}} = \frac{-h_{FE}}{R_{TH} + (h_{FE} + 1)R_E}$$

In (3.9.3), $\Delta h_{FE} = h_{FE,2} - h_{FE}$ and S_{I2} is the value of S_i with $h_{FE} = h_{FE,2}$.

An active dc biasing network is shown in Fig. 3.9.4. A pnp BJT is used to stabilize the operating point of the microwave transistor. The bypass capacitors C_1 and C_2 are typically $0.01\text{-}\mu\text{F}$ disk capacitors. The radio frequency chokes (RFCs) are typically made of two or three turns of No. 36 enameled wire on 0.1-in. air core. The operation of the network is as follows. If I_{C2} tends to increase, the current I_3 increases and the emitter-to-base voltage of Q_1 ($V_{EB,1}$) decreases. The decrease of $V_{EB,1}$ decreases I_{E1} , which in turn decreases I_{C2} and I_{B2} . The decrease in I_{B2} and I_{C2} produces the desired bias stability.

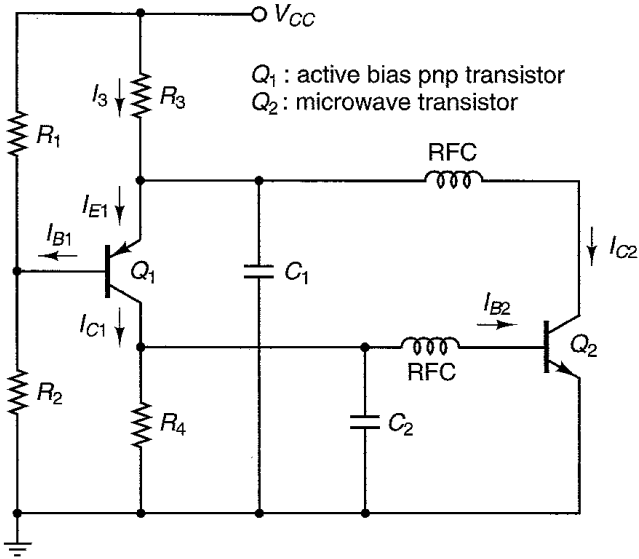


Figure 3.9.4 Active bias network for a BJT.

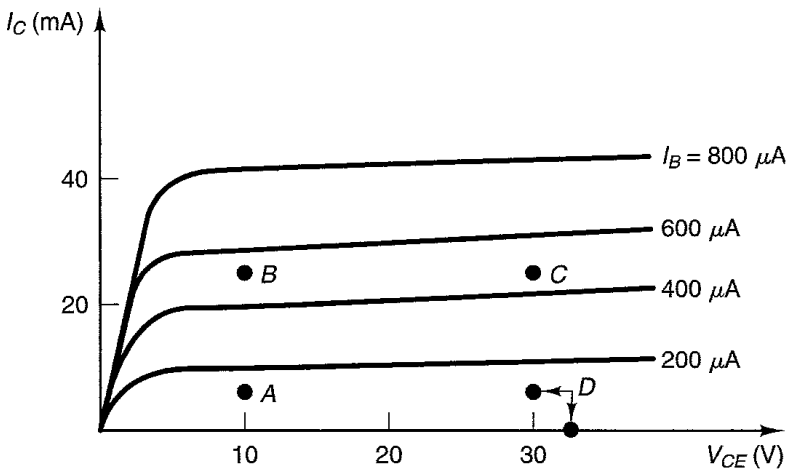


Figure 3.9.5 Selection of the dc operating point.

The selection of the dc quiescent point for a BJT depends on the particular application. For low-noise and low-power applications, the quiescent point *A* in Fig. 3.9.5 is recommended. At *A*, the BJT operates at low values of collector current. For low noise and higher power gain, the quiescent point at *B* is recommended. For high output power, in class A operation, the quiescent point at *C* is recommended. For higher output power and higher efficiency, the BJT is operated in class AB or B, using the quiescent point at *D*.

Example 3.9.2

(a) Design the bias circuit in Fig. 3.9.3 to have a quiescent point at $V_{CE} = 8 \text{ V}$ and $I_C = 2 \text{ mA}$. Use $\beta = 100$ and $V_{BE} = 0.7 \text{ V}$.

(b) Design the active bias network in Fig. 3.9.4 to set the quiescent point of transistor Q_2 at $V_{CE2} = 8\text{ V}$ and $I_{C2} = 2\text{ mA}$. Use $\beta = 100$ and $V_{BE} = 0.7\text{ V}$.

Solution. (a) Let $V_{CC} = 15\text{ V}$ in Fig. 3.9.3. Then, with $I_C \approx I_E$, the dc load-line equation is

$$V_{CC} = V_{CE} + I_C(R_C + R_E)$$

or

$$R_C + R_E = \frac{15 - 8}{2 \times 10^{-3}} = 3.5\text{ k}\Omega \quad (3.9.4)$$

The value of R_E is usually selected using the assumption that the voltage across R_E is 10% to 20% of V_{CC} . Selecting 10% of V_{CC} , we obtain

$$R_E = \frac{10\% V_{CC}}{I_C} = \frac{0.1(15)}{2 \times 10^{-3}} = 750\ \Omega$$

Then, from (3.9.4),

$$R_C = 3500 - 750 = 2.75\text{ k}\Omega$$

A Thévenin's equivalent circuit between the base and ground of the transistor gives

$$V_{TH} = \frac{V_{CC}R_2}{R_2 + R_1} \quad (3.9.5)$$

and

$$R_{TH} = \frac{R_1R_2}{R_1 + R_2} \quad (3.9.6)$$

From (3.9.5) and (3.9.6), we can solve for R_1 and R_2 in terms of V_{TH} and R_{TH} —namely,

$$R_1 = R_{TH} \frac{V_{CC}}{V_{TH}} \quad (3.9.7)$$

and

$$R_2 = \frac{R_{TH}}{1 - \frac{V_{TH}}{V_{CC}}} \quad (3.9.8)$$

For good beta stability, the value of R_{TH} is selected such that $\beta R_E = 10 R_{TH}$, or

$$R_{TH} = \frac{\beta R_E}{10} = \frac{100(750)}{10} = 7.5\text{ k}\Omega$$

The value of V_{TH} is calculated using the loop equation:

$$V_{TH} = I_B R_{TH} + 0.7 + I_E R_E = \frac{2 \times 10^{-3}}{100} (7.5 \times 10^3) + 0.7 + 2 \times 10^{-3}(750) = 2.35\text{ V}$$

From (3.9.7) and (3.9.8), it follows that

$$R_1 = (7.5 \times 10^3) \frac{15}{2.35} = 47.9\text{ k}\Omega$$

and

$$R_2 = \frac{7.5 \times 10^3}{1 - \frac{2.35}{15}} = 8.9 \text{ k}\Omega$$

(b) Let $V_{CC} = 15 \text{ V}$ in Fig. 3.9.4. The base voltage of transistor Q_2 , which is equal to the voltage across R_4 , is 0.7 V . The current I_3 is equal to the sum of I_{C1} and I_{C2} (where $I_{C2} = 2 \text{ mA}$). Designing for I_3 equal to 4 mA , it follows that

$$I_{C1} = I_3 - I_{C2} = 4 \times 10^{-3} - 2 \times 10^{-3} = 2 \text{ mA}$$

Then

$$R_4 = \frac{0.7}{I_{C1}} = \frac{0.7}{2 \times 10^{-3}} = 350 \Omega$$

Since the collector voltage of transistor Q_2 is 8 V , R_3 is calculated from

$$R_3 = \frac{V_{CC} - 8}{I_3} = \frac{15 - 8}{4 \times 10^{-3}} = 1.75 \text{ k}\Omega$$

In the active bias circuit of Fig. 3.9.4, good beta stability is obtained by letting the current in R_1 and R_2 be 20 times the base current of transistor Q_1 . That is,

$$I_{R_1} \approx I_{R_2} = 20I_{B1} = 20 \left(\frac{2 \times 10^{-3}}{100} \right) = 0.4 \text{ mA}$$

Since the base voltage of transistor Q_1 is a 7.3 V , we can write

$$R_1 = \frac{V_{CC} - 7.3}{I_{R_1}} = \frac{15 - 7.3}{0.4 \times 10^{-3}} = 19.25 \text{ k}\Omega$$

and

$$R_2 = \frac{7.3}{I_{R_2}} = \frac{7.3}{0.4 \times 10^{-3}} = 18.25 \text{ k}\Omega$$

In the active bias circuit, the resistors R_2 and R_3 are implemented using a potentiometer in order to set the quiescent point of transistor Q_2 at exactly 8 V and 2 mA . An optimization and beta stability analysis of the active bias circuit in this design is performed in Appendix "Computer-Aided Designs," Example CAD.1.

GaAs FET Bias Networks

The GaAs FETs can be biased in several ways. Five basic dc network configurations for GaAs FET amplifiers are shown in Fig. 3.9.6 [3.5]. The dc bias network in Fig. 3.9.6a requires a bipolar power source, while the networks in Figs. 3.9.6b to 3.9.6e require a unipolar supply. The column "How" in Fig. 3.9.6 indicates the polarity of the sources, as well as the sequence in which the voltages must be applied to prevent transient burnout of the GaAs FET device during turn-on. For example, in the dc bias network in Fig. 3.9.6a, if the drain is biased

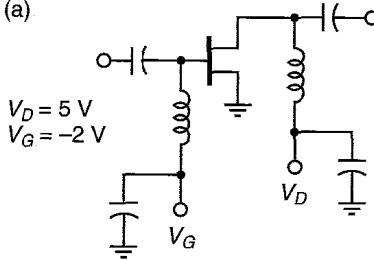
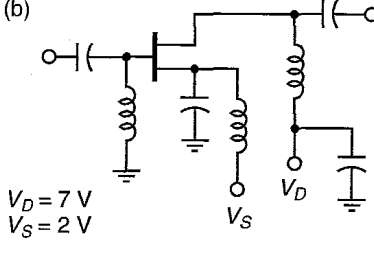
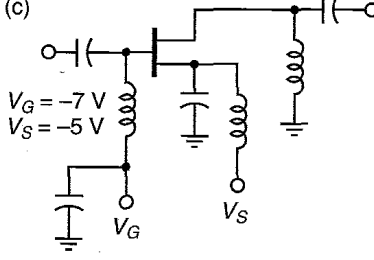
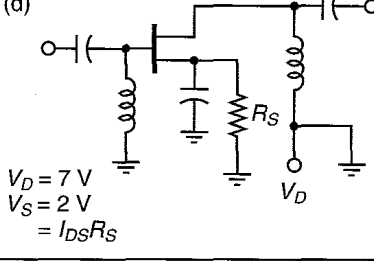
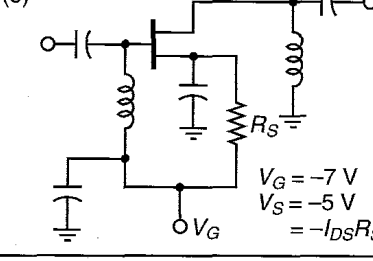
Figure	How	Amplifier characteristics	Power supply used
<p>(a)</p>  <p>$V_D = 5\text{ V}$ $V_G = -2\text{ V}$</p>	Apply V_G , then V_D	Low noise High gain High power High efficiency	Bipolar, Minimum source inductance
<p>(b)</p>  <p>$V_D = 7\text{ V}$ $V_S = 2\text{ V}$</p>	Apply V_S , then V_D	[same as (a)]	Positive supply
<p>(c)</p>  <p>$V_G = -7\text{ V}$ $V_S = -5\text{ V}$</p>	Apply V_S , then V_G	[same as (a)]	Negative supply
<p>(d)</p>  <p>$V_D = 7\text{ V}$ $V_S = 2\text{ V}$ $= I_{DS}R_S$</p>	Apply V_D	Low noise High gain High power Lower efficiency Gain easily adjusted by varying R_S	Unipolar, incorporating R_S automatic transient protection
<p>(e)</p>  <p>$V_G = -7\text{ V}$ $V_S = -5\text{ V}$ $= -I_{DS}R_S$</p>	Apply V_G	[same as (d)]	Negative unipolar, incorporating R_S

Figure 3.9.6 Five basic dc bias networks. (From G. D. Vendelin [3.5]; reproduced with permission of *Microwaves & RF*.)

positive before the gate, the transistor will operate momentarily beyond its safe operating region. Therefore, the proper turn-on sequence is: first apply a negative bias to the gate (i.e., $V_G < 0$) and then apply the drain voltage ($V_D > 0$). One method to accomplish the previous turn-on procedure is to turn both sources at the same time and to include a long RC time constant network in the V_D supply and a short RC time constant network in the negative supply V_G .

The bias networks in Figs. 3.9.6d and 3.9.6e use a source resistor. The source resistor provides automatic transient protection. However, the source resistor will degrade the noise-figure performance, and the source bypass capacitor can cause low-frequency oscillations.

The decoupling capacitors shown in Fig. 3.9.6 are sometimes shunted with zener diodes. The zener diodes provide additional protection against transients, reverse biasing, and overvoltage.

The dc bias network of a GaAs FET must provide a stable quiescent point. It is not difficult to show that the negative feedback resistor R_s decreases the effect of variations of I_D with respect to temperature and I_{DSS} .

The selection of the dc quiescent point in a GaAs FET depends on the particular application. Figure 3.9.7 shows typical GaAs FET characteristics with four quiescent points located at A, B, C, and D.

For low-noise, low-power application, the quiescent point A is recommended. At A, the FET operates at a low value of current (i.e., $I_{DS} \approx 0.15I_{DSS}$).

For low noise and higher power gain, the recommended quiescent point is at B. The bias voltage remains the same as for point A, but the drain current is increased to $I_{DS} \approx 0.9I_{DSS}$.

The GaAs FET output power level can be increased by selecting the quiescent point at C with $I_{DS} \approx 0.5I_{DSS}$. The quiescent point at C maintains class A operation. For higher efficiency, or to operate the GaAs FET in class

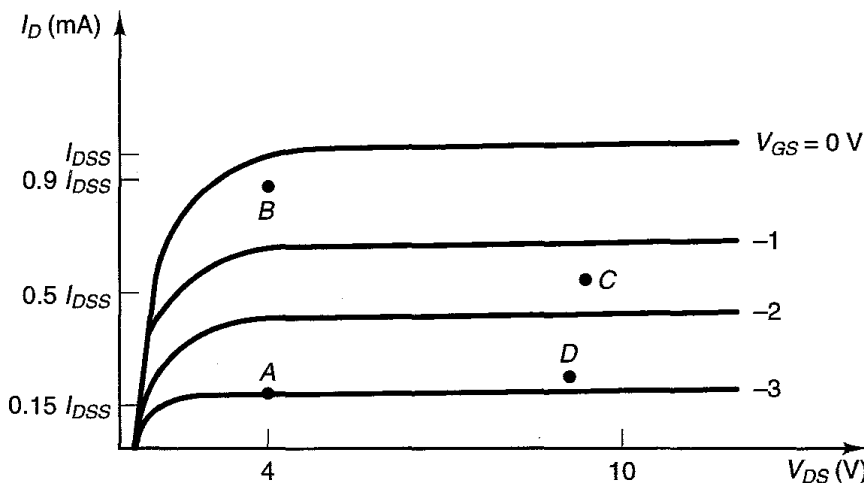


Figure 3.9.7 Typical GaAs FET characteristics and recommended quiescent points.

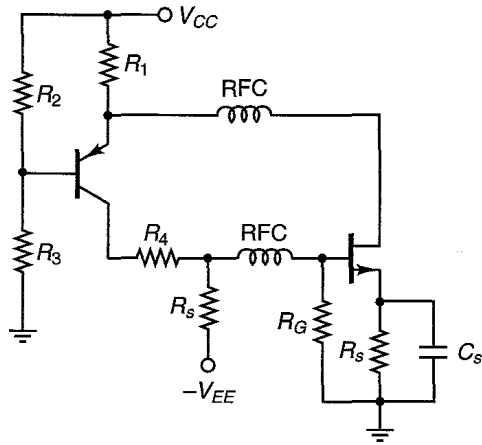


Figure 3.9.8 Active bias for a common-source GaAs FET.

AB or B, the drain-to-source current must be decreased and the quiescent point *D* is recommended.

An active bias network for a common-source GaAs FET is shown in Fig. 3.9.8.

PROBLEMS

- 3.1 (a)** Show that $G_T \leq G_A$ and $G_T \leq G_p$. When is the equality sign satisfied?
- (b)** Show that (3.2.3) can be obtained from (3.2.1) when $\Gamma_s = \Gamma_{IN}^*$, and (3.2.4) from (3.2.2) when $\Gamma_L = \Gamma_{OUT}^*$.
- 3.2 (a)** Show that the transducer power gain is given by $G_T = |S_{21}|^2$ when the source and load impedances to the transistor are equal to the reference impedance Z_o (usually 50 Ω).
- (b)** Determine the expression for G_p and G_A when the source and load impedances are real and equal to Z_o .
- 3.3 (a)** A microwave amplifier diagram is shown in Fig. 3.2.2. Determine G_T , G_A , and G_p if $\Gamma_s = 0.49 \angle -150^\circ$, $\Gamma_L = 0.56 \angle 90^\circ$, and the *S* parameters of the transistor are

$$\begin{aligned} S_{11} &= 0.54 \angle 165^\circ & S_{12} &= 0.09 \angle 20^\circ \\ S_{21} &= 2 \angle 30^\circ & S_{22} &= 0.5 \angle -80^\circ \end{aligned}$$

- (b)** Calculate P_{AVS} , P_{IN} , P_{AVN} , and P_L if $E_1 = 10 \angle 30^\circ$, $Z_1 = 50 \Omega$, and $Z_2 = 50 \Omega$.

- 3.4** The *S* parameters of a transistor are

$$\begin{aligned} S_{11} &= 0.7 \angle 30^\circ & S_{12} &= 0 \\ S_{21} &= 4 \angle 90^\circ & S_{22} &= 0.5 \end{aligned}$$

The transistor is used in the amplifier shown in Fig. P3.4, where the output matching network produces $\Gamma_L = 0.5 \angle 90^\circ$. Determine the values of G_T , G_p , and G_A .

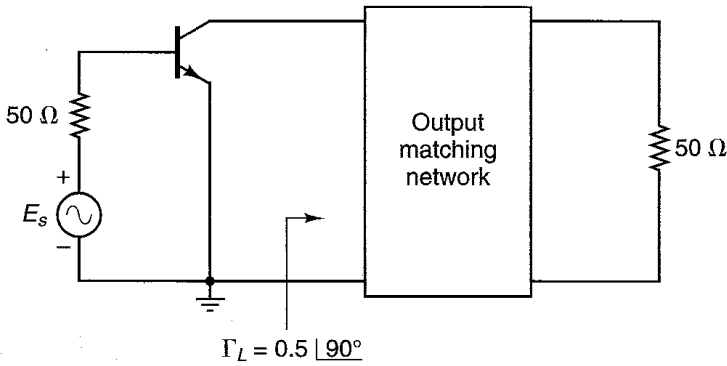


Figure P3.4

- 3.5 In each of the stability circle drawings shown in Fig. P3.5, indicate clearly the possible locations for a stable source reflection coefficient.
- 3.6 Two output stability circles are shown in Fig. P3.6. Determine the stable region for the load reflection coefficient.
- 3.7 The scattering parameters for three different transistors are given below. Determine the stability in each case and in a potentially unstable case, draw the input and output stability circles.
- (a) $S_{11} = 0.674 \angle -152^\circ$ (b) $S_{11} = 0.385 \angle -55^\circ$ (c) $S_{11} = 0.7 \angle -50^\circ$
 $S_{12} = 0.075 \angle 6.2^\circ$ $S_{12} = 0.045 \angle 90^\circ$ $S_{12} = 0.27 \angle 75^\circ$
 $S_{21} = 1.74 \angle 36.4^\circ$ $S_{21} = 2.7 \angle 78^\circ$ $S_{21} = 5 \angle 120^\circ$
 $S_{22} = 0.6 \angle -92.6^\circ$ $S_{22} = 0.89 \angle -26.5^\circ$ $S_{22} = 0.6 \angle 80^\circ$
- 3.8 The S parameters of a GaAs FET at a given Q point are

f (GHz)	S_{11}	S_{12}	S_{21}	S_{22}
4	$0.9 \angle -67^\circ$	$0.076 \angle 43^\circ$	$2.3 \angle 118^\circ$	$0.68 \angle -39^\circ$
6	$0.84 \angle -97^\circ$	$0.112 \angle 24^\circ$	$2.06 \angle 87^\circ$	$0.6 \angle -58^\circ$
8	$0.73 \angle -140^\circ$	$0.135 \angle -5^\circ$	$2.04 \angle 53^\circ$	$0.47 \angle -85^\circ$
10	$0.67 \angle -178^\circ$	$0.146 \angle -27^\circ$	$1.81 \angle 18^\circ$	$0.42 \angle -120^\circ$
14	$0.63 \angle 115^\circ$	$0.133 \angle -66^\circ$	$1.42 \angle -38^\circ$	$0.36 \angle -172^\circ$

Draw the input stability circles (at each frequency) in a Smith chart and the output stability circles in another Smith chart. Indicate the unstable regions.

- 3.9 This problem analyzes some interesting (theoretical) cases of the stability circles. The S parameters of several two-port networks are
- (a) $S_{11} = 1/\sqrt{2}$, $S_{12} = 1/\sqrt{2} \angle -180^\circ$, $S_{21} = 1/\sqrt{2}$, and $S_{22} = 1/\sqrt{2}$.
 (b) $S_{11} = 1/\sqrt{2}$, $S_{12} = 1.707$, $S_{21} = 1.707$, and $S_{22} = 1/\sqrt{2}$.
 (c) $S_{11} = 1/\sqrt{2}$, $S_{12} = 0.292$, $S_{21} = 0.292$, and $S_{22} = 1/\sqrt{2}$.
 (d) $S_{11} = 1$, $S_{12} = \sqrt{2}$, $S_{21} = \sqrt{2}$, and $S_{22} = 1$.
- Determine K and $|\Delta|$ and draw the input and output stability circles.

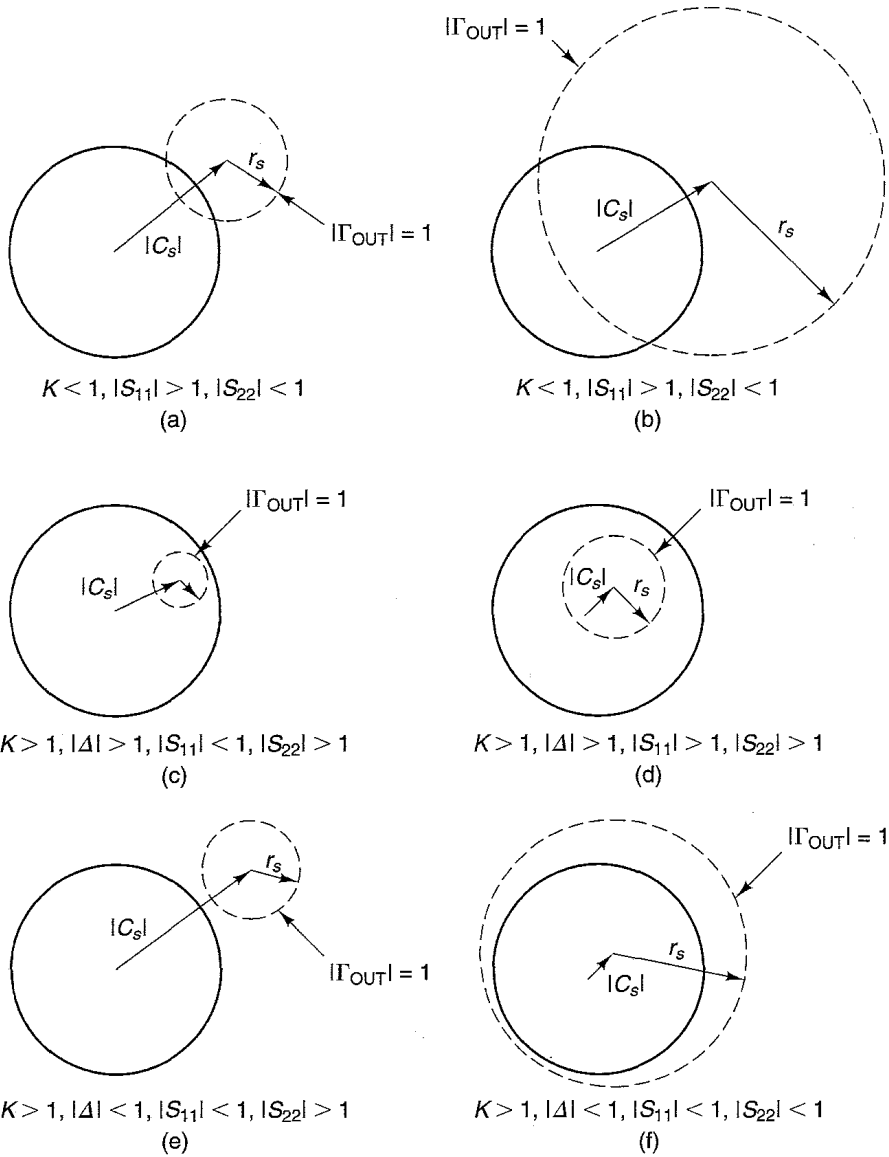


Figure P3.5

- 3.10 (a)** Show that in the limit as S_{12} approaches zero, the center and radius of the stability circles are $C_S \approx 1/S_{22}, r_s \approx 0, C_L \approx 1/S_{11}$, and $r_L \approx 0$.
- (b)** The S parameters of a two-port network are

$$\begin{aligned} S_{11} &= 2 \angle 90^\circ & S_{12} &= 0 \\ S_{21} &= 2 & S_{22} &= 0.1 \angle 45^\circ \end{aligned}$$

Draw the stability circles and show the unstable regions.

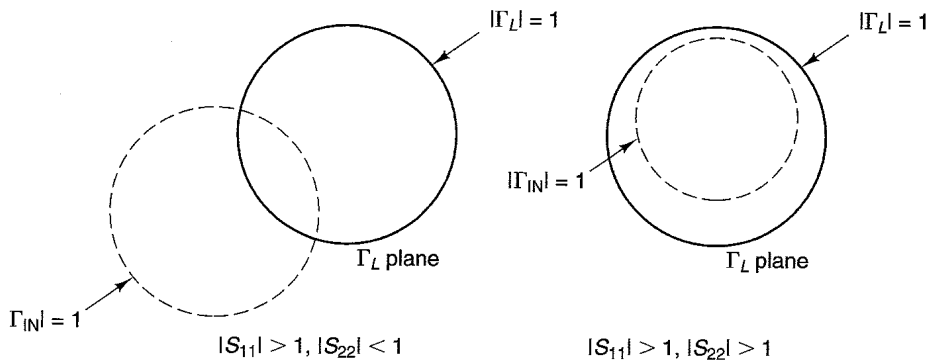


Figure P3.6

3.11 Show that the source stability circle does not enclose the center of the Smith chart when

$$|S_{22}| < 1 \text{ and } |\Delta| < S_{11}$$

or

$$|S_{22}| > 1 \text{ and } |\Delta| > S_{11}$$

Also show that the load stability circle does not enclose the center of Smith chart when

$$|S_{11}| < 1 \text{ and } |\Delta| < S_{22}$$

or

$$|S_{11}| > 1 \text{ and } |\Delta| > S_{22}$$

3.12 The conditions for unconditional stability were analyzed by considering the values in the Γ_s and Γ_L plane that result in $|\Gamma_{IN}| < 1$ and $|\Gamma_{OUT}| < 1$. An alternative approach is to consider the values in the Γ_{IN} and Γ_{OUT} plane, where $|\Gamma_{IN}| < 1$ and $|\Gamma_{OUT}| < 1$, that results in $|\Gamma_s| < 1$ and $|\Gamma_L| < 1$. Using this approach, show that the plot of the $|\Gamma_s| = 1$ circle in the Γ_{OUT} plane has radius and center given by

$$r_{OUT} = \frac{|S_{12}S_{21}|}{1 - |S_{11}|^2}$$

and

$$C_{OUT} = S_{22} + \frac{S_{12}S_{21}S_{11}^*}{1 - |S_{11}|^2} = \frac{S_{22} - \Delta S_{11}^*}{1 - |S_{11}|^2}$$

Also, the plot of the $|\Gamma_L| = 1$ circle in the Γ_{IN} plane has radius and center given by

$$r_{IN} = \frac{|S_{12}S_{21}|}{1 - |S_{22}|^2}$$

and

$$C_{IN} = S_{11} + \frac{S_{12}S_{21}S_{22}^*}{1 - |S_{22}|^2} = \frac{S_{11} - \Delta S_{22}^*}{1 - |S_{22}|^2}$$

3.13 (a) Show that

$$|A| \leq |S_{11}| |S_{22}| + |S_{12} S_{21}|$$

and

$$|S_{11}| |S_{22}| \leq |A| + |S_{12} S_{21}|$$

Substitute these inequalities in (3.3.13) and verify that

$$(1 - |A|)^2 > (|S_{11}|^2 - |S_{22}|^2)^2$$

Therefore, show that

$$B_1 B_2 > 0$$

and

$$B_1 + B_2 = 2(1 - |A|^2)$$

where B_1 is given by (3.3.21) and

$$B_2 = 1 + |S_{22}|^2 - |S_{11}|^2 - |A|^2$$

(b) Use the previous results to show that the conditions $K > 1$ and $B_1 > 0$ are similar to $K > 1$ and $B_2 > 0$ (see Appendix C).

(c) Show that the condition $|A| < 1$ is similar to $B_1 > 0$.

3.14 Show how resistive loading can stabilize a transistor whose S parameters at $f = 750$ MHz are

$$\begin{aligned} S_{11} &= 0.69 \angle -78^\circ & S_{12} &= 0.033 \angle 41.4^\circ \\ S_{21} &= 5.67 \angle 123^\circ & S_{22} &= 0.84 \angle -25^\circ \end{aligned}$$

Consider the four types of resistive loading shown in Fig. 3.3.9.

3.15 Prove that the maximum unilateral transducer power gain in (3.4.6) is obtained when $\Gamma_s = S_{11}^*$ and $\Gamma_L = S_{22}^*$.

3.16 (a) Design a microwave transistor amplifier for $G_{TU, \max}$ using a BJT whose S parameters in a $50\text{-}\Omega$ system at $V_{CE} = 10$ V, $I_C = 20$ mA, and $f = 1$ GHz are

$$\begin{aligned} S_{11} &= 0.706 \angle -160^\circ \\ S_{12} &= 0 \\ S_{21} &= 5.01 \angle 85^\circ \\ S_{22} &= 0.508 \angle -20^\circ \end{aligned}$$

(b) Draw the constant-gain circles for $G_s = 2, 1, 0$, and -1 dB.

3.17 The scattering parameters of a GaAs FET in a $50\text{-}\Omega$ system are

$$\begin{aligned} S_{11} &= 2.3 \angle -135^\circ \\ S_{12} &= 0 \\ S_{21} &= 4 \angle 60^\circ \\ S_{22} &= 0.8 \angle -60^\circ \end{aligned}$$

- (a) Determine the unstable region in the Smith chart and construct the constant-gain circle for $G_s = 4$ dB.
- (b) Design the input matching network for $G_s = 4$ dB with the greatest degree of stability.
- (c) Draw the complete ac amplifier schematic.

3.18 A microwave amplifier is to be designed for $G_{TU,max}$ using a transistor with

$$\begin{aligned} S_{11} &= 0.5 \angle 140^\circ & S_{12} &= 0 \\ S_{21} &= 5 \angle 45^\circ & S_{22} &= 0.6 \angle -95^\circ \end{aligned}$$

The S parameters were measured in a $50\text{-}\Omega$ system at $f = 900$ MHz, $V_{CE} = 15$ V, and $I_C = 15$ mA.

- (a) Determine $G_{TU,max}$.
- (b) Design two different microstrip matching networks.
- (c) Draw the constant gain circle for $G_L = 1$ dB.
- (d) If the S parameters at 1 GHz are

$$\begin{aligned} S_{11} &= 0.48 \angle 137^\circ & S_{12} &= 0 \\ S_{21} &= 4.6 \angle 48^\circ & S_{22} &= 0.57 \angle -99^\circ \end{aligned}$$

calculate the gain G_T at 1 GHz for the designs in part (b).

- 3.19** (a) Verify the equations for a simultaneous conjugate match in (3.6.5) and (3.6.6).
 - (b) Show that for small S_{12} , Γ_{Ms} and Γ_{ML} are close to S_{11}^* and S_{22}^* , respectively.
- 3.20** (a) Prove the identities

$$|C_1|^2 = |S_{11} - \Delta S_{22}^*|^2 = |S_{12} S_{21}|^2 + (1 - |S_{22}|^2)(|S_{11}|^2 - |\Delta|^2)$$

and

$$|C_2|^2 = |S_{22} - \Delta S_{11}^*|^2 = |S_{12} S_{21}|^2 + (1 - |S_{11}|^2)(|S_{22}|^2 - |\Delta|^2)$$

- (b) Analyze the solutions to (3.6.5) and (3.6.6) when $|K| > 1$ with K negative.

3.21 Design a microwave transistor amplifier for $G_{T,max}$ using a BJT whose S parameters in a $50\text{-}\Omega$ system at $V_{CE} = 10$ V, $I_C = 4$ mA, and $f = 750$ MHz are

$$\begin{aligned} S_{11} &= 0.277 \angle -59^\circ \\ S_{12} &= 0.078 \angle 93^\circ \\ S_{21} &= 1.92 \angle 64^\circ \\ S_{22} &= 0.848 \angle -31^\circ \end{aligned}$$

(This problem is based on a design given in Ref. [3.6]).

- 3.22** The output matching network shown in Fig. P3.22 was designed at 2 GHz for a simultaneous conjugate match.
 - (a) Determine Γ_{ML} .
 - (b) If the microstrip is alumina ($\epsilon_r = 10$) and $h = 30$ mils, determine the length of the 0.25λ line.
- 3.23** The matching network in Fig. P3.23 was designed for $\Gamma_{ML} = 0.718 \angle 103.9^\circ$. Determine Γ_x .

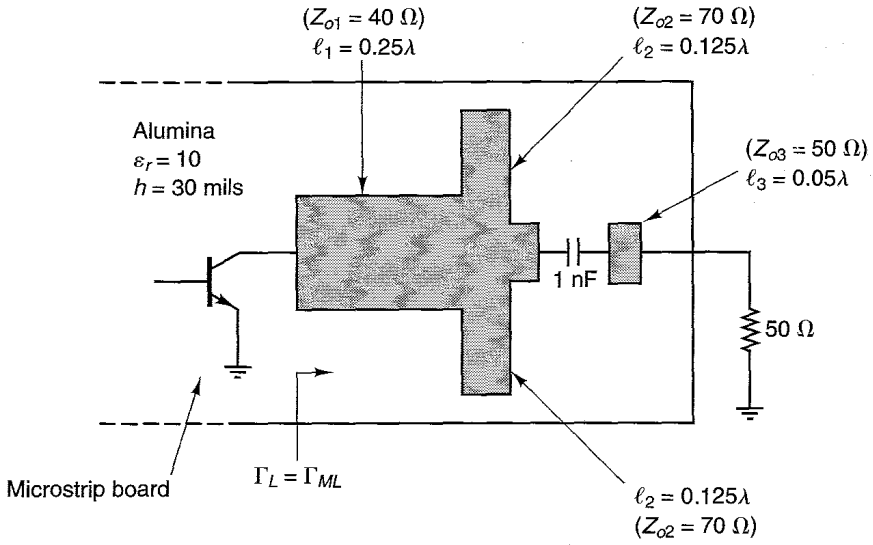


Figure P3.22

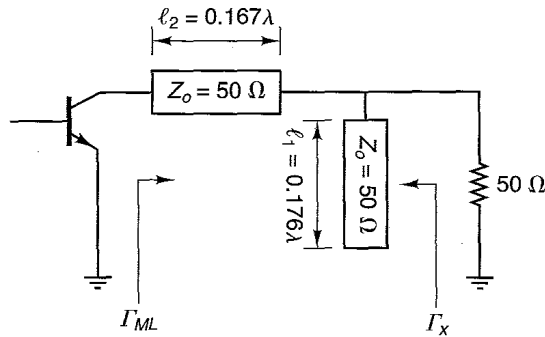


Figure P3.23

3.24 The S parameters from 3 GHz to 4 GHz of a BJT are

f (GHz)	S_{11}	S_{12}	S_{21}	S_{22}
3	0.575 $\angle -173^\circ$	0.043 $\angle 25^\circ$	2.21 $\angle 48^\circ$	0.773 $\angle -58^\circ$
3.5	0.56 $\angle 180^\circ$	0.046 $\angle 25^\circ$	1.95 $\angle 37^\circ$	0.795 $\angle -64^\circ$
4	0.548 $\angle 173^\circ$	0.049 $\angle 24^\circ$	1.67 $\angle 29^\circ$	0.816 $\angle -71^\circ$

- (a) Can you design for a simultaneous conjugate match at 3.5 GHz?
- (b) Design an amplifier for $G_{T,max}$ at 3.5 GHz.
- (b) Plot G_T in decibels versus frequency from 3 GHz to 4 GHz.

- 3.25** Design a microwave transistor amplifier at $f = 750$ MHz to have $G_p = 10$ dB using the BJT in Problem 3.21. For the value of Γ_L selected and with $\Gamma_s = \Gamma_{IN}^*$, determine $(VSWR)_{in}$ and $(VSWR)_{out}$.
- (b)** Determine the reflection coefficients for $G_{p,max}$ and show that they are identical to Γ_{Ms} and Γ_{ML} in Problem 3.21.
- 3.26** At 2 GHz, a GaAs FET has the following S parameters:

$$S_{11} = 0.7 \angle -65^\circ$$

$$S_{12} = 0.03 \angle 60^\circ$$

$$S_{21} = 3.2 \angle 110^\circ$$

$$S_{22} = 0.8 \angle -30^\circ$$

Determine the stability and design an amplifier with $G_p = 10$ dB. For the value of Γ_L selected and with $\Gamma_s = \Gamma_{IN}^*$, determine $(VSWR)_{in}$ and $(VSWR)_{out}$.

- 3.27** The S parameters of a transistor are

$$S_{11} = 0.78 \angle -102^\circ \quad S_{12} = 0.063 \angle 46^\circ$$

$$S_{21} = 2.43 \angle 84^\circ \quad S_{22} = 0.7 \angle -57^\circ$$

- (a)** Draw the $G_p = 10$ dB constant-gain circle.
- (b)** Select several values of Γ_L on the 10-dB gain circles. For each value of Γ_L selected, and with $\Gamma_s = \Gamma_{IN}^*$, determine $(VSWR)_{in}$ and $(VSWR)_{out}$.
- (c)** Draw the 15-dB, 20-dB, and 40-dB constant operating power-gain circle. Observe that as G_p becomes infinite, the power-gain circles approach the output stability circle.
- 3.28** Show that in a potentially unstable case when the operating power-gain circles and the output stability circle intersect the edge of the Smith chart, the points of intersection are identical (see Figs. 3.7.2 and 3.7.3).
- 3.29** The S parameters of a transistor are

$$S_{11} = 0.5 \angle 45^\circ \quad S_{12} = 0.4 \angle 145^\circ$$

$$S_{21} = 4 \angle 120^\circ \quad S_{22} = 0.4 \angle -40^\circ$$

- (a)** Draw the stability circles and show the stable regions.
- (b)** Calculate G_p if the transistor is used with $\Gamma_s = 0.2 \angle 145^\circ$ and $\Gamma_L = 0$.
- (c)** What is the value of the largest operating power gain that can be obtained?
- 3.30** Perform the analyses in Example 3.8.1 for the constant-gain circle $G_A = G_{A,max} - 2$ dB (i.e., $G_A = 7.66$ dB).
- 3.31** The parameters of a two-port network at 5 GHz are

$$S_{11} = 0.75 \angle -60^\circ \quad S_{12} = 0.3 \angle 70^\circ$$

$$S_{21} = 6 \angle 90^\circ \quad S_{22} = 0.5 \angle 60^\circ$$

- (a)** Verify that this two-port network is potentially unstable with $K > 1$ and $|\Delta| > 1$.
- (b)** Draw the output stability circle.
- (c)** Calculate Γ_{ML} .
- (d)** Calculate $G_{p,min}$ and $G_{T,min}$.

- (e) Draw the constant operating power-gain circles that are 2 dB, 5 dB, 10 dB, and 20 dB larger than $G_{p,min}$.
- (f) Draw the input stability circle and calculate Γ_{Ms} .
- (g) Determine $(VSWR)_{in}$ and $(VSWR)_{out}$ if the circuit is designed with $\Gamma_s = \Gamma_{Ms}$ and $\Gamma_L = \Gamma_{ML}$.

3.32 The S parameters of a GaAs FET at $f = 12$ GHz, $V_{DS} = 3.5$ V, and $I_D = 25$ mA are

$$\begin{aligned} S_{11} &= 0.6 \angle 36^\circ & S_{12} &= 0.14 \angle -85^\circ \\ S_{21} &= 2.3 \angle -80^\circ & S_{22} &= 0.15 \angle 45^\circ \end{aligned}$$

- (a) Determine $G_{p,max}$ and draw the constant G_p circle that is 1 dB less than $G_{p,max}$.
 - (b) Select several values of Γ_L on the $G_p = G_{p,max} - 1$ dB circle. For each Γ_L value, determine the values of Γ_s that lie on the constant $(VSWR)_{in} = 1.5$ circle, and draw the constant $(VSWR)_{in} = 1.5$ circle.
 - (c) Select several values of Γ_s on the $(VSWR)_{in} = 1.5$ circle. For each Γ_s value, calculate $(VSWR)_{out}$.
- 3.33 (a) Map the $G_p = 10$ dB circle in Fig. 3.7.2 to the $\Gamma_s = \Gamma_{IN}^*$ plane.
 (b) For $\Gamma_L = 0.1 \angle 97^\circ$, show the values of Γ_s that produce $(VSWR)_{in} = 2$.

3.34 Design a microwave amplifier using a BJT whose S parameters at 1 GHz are

$$\begin{aligned} S_{11} &= 0.6 \angle -170^\circ & S_{12} &= 0.03 \angle 50^\circ \\ S_{21} &= 8 \angle 80^\circ & S_{22} &= 0.45 \angle -30^\circ \end{aligned}$$

Analyze the trade-offs between operating power gain, stability, and VSWRs.

3.35 Design a microwave amplifier using a GaAs FET whose S parameters at 6 GHz, $V_{DS} = 3$ V, and $I_{DS} = 20$ mA are

$$\begin{aligned} S_{11} &= 0.6 \angle -170^\circ & S_{12} &= 0.125 \angle -12^\circ \\ S_{21} &= 3.1 \angle 25^\circ & S_{22} &= 0.4 \angle -90^\circ \end{aligned}$$

Analyze the trade-offs between available power gain, stability, and VSWRs.

3.36 The discrete amplifier in Fig. P3.36 was designed to operate at 500 MHz for $G_{T,max}$.

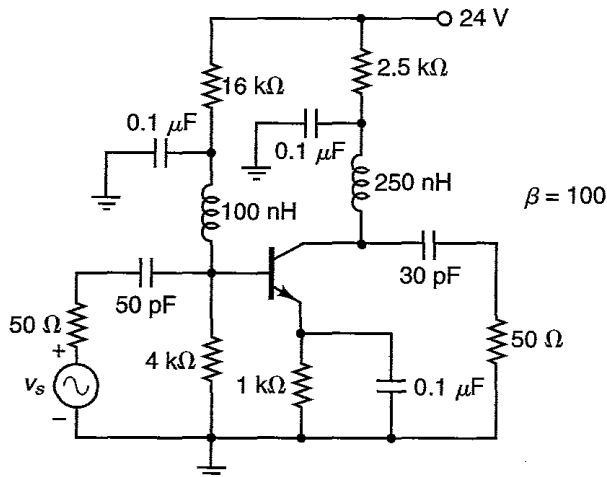


Figure P3.36

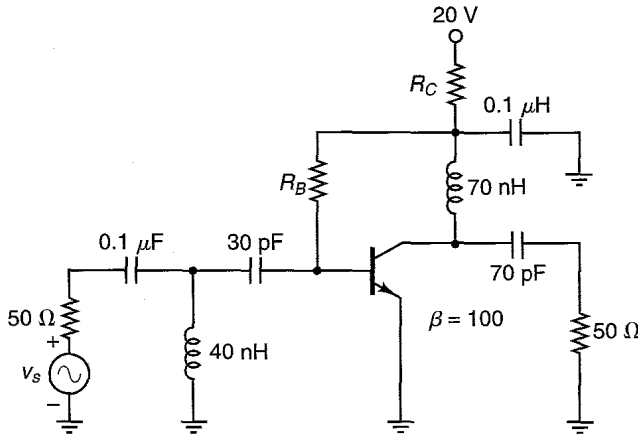


Figure P3.37

- (a) Draw the dc model.
- (b) Determine the approximate value of I_C and V_{CE} at the Q point.
- (c) Radio frequency coils could be connected in series with the $4\text{ k}\Omega$, $16\text{ k}\Omega$, and $2.5\text{ k}\Omega$ resistors. Are they necessary?
- (d) Draw the ac model.
- (e) Determine the value of Γ_s and Γ_L .
- 3.37** A 300-MHz low-noise amplifier is shown in Fig. P3.37. The dc bias circuit is recognized as the dc voltage feedback bias configuration in Fig. 3.9.2.
- (a) Draw the dc model.
- (b) Determine the values of R_L and R_B for a Q point at 10 V , 5 mA .
- (c) Determine the values of Γ_s and Γ_L .
- 3.38** Design the bias circuit in Fig. 3.9.3 to have a Q point at $V_{CE} = 10\text{ V}$ and $I_C = 10\text{ mA}$. Use $\beta = 100$ and $V_{BE} = 0.75\text{ V}$.
- 3.39** Design the active bias network in Fig. 3.9.4 to set the quiescent point of transistor Q_2 at $V_{CE2} = 10\text{ V}$ and $I_{C2} = 10\text{ mA}$. Use $\beta = 100$ and $V_{BE} = 0.75\text{ V}$.
- 3.40** (a) Derive the stability factors for the dc bias networks in Fig. 3.9.2a.
- (b) Design the circuit for a quiescent point at $V_{CE} = 10\text{ V}$ and $I_C = 10\text{ mA}$. Use $h_{FE} = 50$ and $V_{CC} = 20\text{ V}$.
- (c) What happens to the quiescent point if h_{FE} changes from 50 to 100.
- 3.41** Design the dc bias network shown in Fig. 3.9.3 for $V_{CE} = 6\text{ V}$, $I_C = 1\text{ mA}$, and $S_i = 5$. Assume that $h_{FE} = 100$ and $I_{CBO} = 1\text{ }\mu\text{A}$ at 25°C . Calculate the resulting stability factors and find what happens to the operating point if the temperature increases to 75°C .
- 3.42** Design the active bias network in Fig. 3.9.8 to set the quiescent point of GaAs FET at $V_{DS} = 3\text{ V}$ and $I_{DS} = 10\text{ mA}$. The pinchoff voltage is -3 V , and the drain saturation current is 30 mA .

REFERENCES

- [3.1] D. Woods, "Reappraisal of the Unconditional Stability Criteria for Active 2-Port Networks in Terms of S Parameters," *IEEE Transactions on Circuits and Systems*, February 1976.

- [3.2] K. Kurokawa, "Power Waves and the Scattering Matrix," *IEEE Transactions on Microwave Theory and Techniques*, March 1965.
- [3.3] G. E. Bodway, "Two Port Power Flow Analysis Using Generalized Scattering Parameters," *Microwave Journal*, May 1967.
- [3.4] "Microwave Transistor Bias Considerations," Hewlett-Packard Application Note 944-1, April 1975.
- [3.5] G. D. Vendelin, "Five Basic Bias Designs for GaAs FET Amplifiers," *Microwaves & RF*, February 1978.
- [3.6] W. H. Froehner, "Quick Amplifier Design with Scattering Parameters," *Electronics*, October 1967.

4

NOISE, BROADBAND, AND HIGH-POWER DESIGN METHODS

4.1 INTRODUCTION

In Chapter 3, design methods for given stability, VSWRs, and gain criteria were discussed. This chapter presents the basic principles involved in the design of low-noise, broadband, and high-power transistor amplifiers.

In some applications the design objective is for a minimum noise figure. Since a minimum noise figure and maximum power gain cannot be obtained simultaneously, constant noise figure circles, together with constant available power-gain circles, can be drawn on the Smith chart, and reflection coefficients can be selected that compromise between the noise figure and gain performance. The trade-offs that result from noise considerations, stability, VSWRs, and gain are discussed in this chapter.

The noise performance of the GaAs FET is superior to that of the BJT above 4 GHz. A minimum noise figure in both BJTs and GaAs FETs is obtained at low collector or drain current.

The design philosophy in a broadband amplifier is to obtain flat gain over the prescribed range of frequencies. This can be obtained by the use of compensated matching networks, negative feedback, or balance amplifiers.

The small-signal S parameters can be used in the design of microwave transistor amplifiers with linear power output (i.e., class A operation). However, the small-signal S parameters are not useful in the design of large-output power amplifiers. In this case, large-signal impedance or reflection coefficient data as a function of output power and gain are needed.

4.2 NOISE IN TWO-PORT NETWORKS

In a microwave amplifier, even when there is no input signal, a small output voltage can be measured. We refer to this small output power as the *amplifier noise power*. The total noise output power is composed of the amplified noise input power plus the noise output power produced by the amplifier. A review of basic noise concepts is given in Appendix K.

The model of a noisy two-port microwave amplifier is shown in Fig. 4.2.1. The noise input power can be modeled by a source resistor that produces thermal or Johnson noise. This noise is produced by the random fluctuations of the electrons due to thermal agitation. The rms value of the noise voltage ($v_{n,rms}$) produced by the noisy resistor R over a frequency range $f_H - f_L$ is given by

$$v_{n,rms} = \sqrt{4kTBR} \tag{4.2.1}$$

where k is Boltzmann’s constant (i.e., $k = 1.374 \times 10^{-23} \text{ J/}^\circ\text{K}$), T is the resistor noise temperature, and B is the noise bandwidth (i.e., $B = f_H - f_L$).

Equation (4.2.1) shows that the thermal noise power depends on the bandwidth and not on a given center frequency. Such a distribution of noise is called *white noise*.

The available noise power from R is

$$P_N = \frac{v_{n,rms}^2}{4R} = kTB \tag{4.2.2}$$

Example 4.2.1

- (a) Calculate the available noise power from a resistor at the standard temperature of $T = T_o = 290^\circ\text{K}$ in a 1-Hz bandwidth.
- (b) Calculate the noise voltage and the available noise power produced by a 2-M Ω resistor at a standard temperature ($T = 290^\circ\text{K}$) in a 5-kHz bandwidth.

Solution. (a) Using (4.2.2),

$$P_N = (1.374 \times 10^{-23})(290)(1) = 3.985 \times 10^{-21} \text{ W}$$

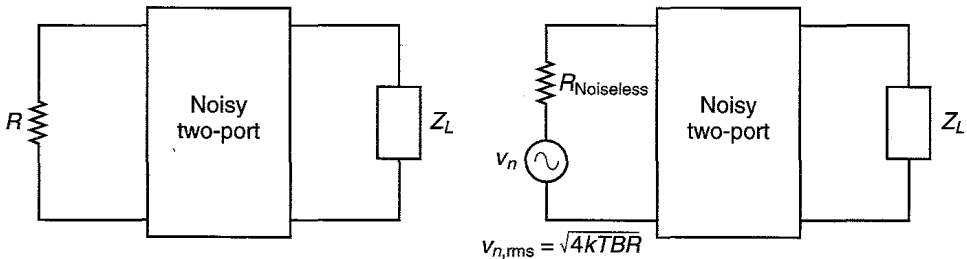


Figure 4.2.1 Model of a noisy microwave amplifier.

or in decibels above 1 mW (i.e., in dBm),

$$P_N(\text{dBm}) = 10 \log \frac{P_N}{10^{-3}} = 10 \log 3.985 \times 10^{-18} = -174 \text{ dBm}$$

Since this noise power is found in a 1-Hz bandwidth, it is common to express it as -174 dBm/Hz .

(b) Using (4.2.1) and (4.2.2), the noise voltage and maximum available noise power are

$$V_{n,\text{rms}} = \sqrt{4(1.374 \times 10^{-23})(290)(5 \times 10^3)(2 \times 10^6)} = 12.6 \mu\text{V}$$

and

$$P_N = \frac{(12.6 \times 10^{-6})^2}{4(2 \times 10^6)} = 19.9 \times 10^{-18} \text{ W}$$

The noise figure (F) describes quantitatively the performance of a noisy microwave amplifier. The noise figure of a microwave amplifier is defined as the ratio of the total available noise power at the output of the amplifier to the available noise power at the output due to thermal noise from the input termination R , where R is at the standard temperature $T = T_o = 290^\circ\text{K}$. The noise figure can be expressed in the form

$$F = \frac{P_{N_o}}{P_{N_i} G_A} \quad (4.2.3)$$

where P_{N_o} is the total available noise power at the output of the amplifier, $P_{N_i} = kT_o B$ is the available noise power due to R at $T = T_o = 290^\circ\text{K}$ in a bandwidth B , and G_A is the available power gain.

Since G_A can be expressed in the form

$$G_A = \frac{P_{S_o}}{P_{S_i}}$$

where P_{S_o} is the available signal power at the output and P_{S_i} is the available signal power at the input, then (4.2.3) can be written as

$$F = \frac{P_{S_i}/P_{N_i}}{P_{S_o}/P_{N_o}}$$

In other words, F can also be defined as the ratio of the available signal-to-noise power ratio at the input to the available signal-to-noise power ratio at the output. A minimum noise figure is obtained by properly selecting the source reflection coefficient of the amplifier.

A model for the calculation of the noise figure of a two-stage amplifier is shown in Fig. 4.2.2. P_{N_i} is the available input noise power, G_{A1} and G_{A2} are the available power gains of each stage, and P_{n1} and P_{n2} represent the noise power appearing at the output of amplifiers 1 and 2, respectively, due to the internal amplifier noise.

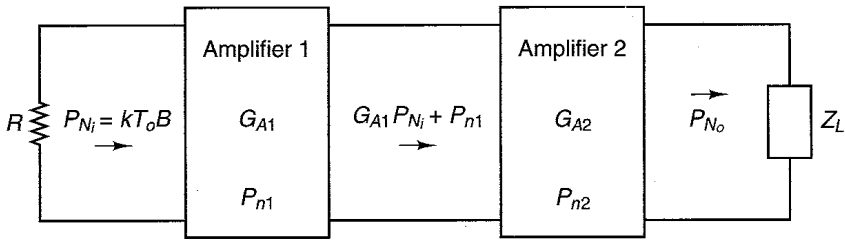


Figure 4.2.2 Noise figure model of a two-stage amplifier.

The total available noise power at the output (P_{N_o}) is given by

$$P_{N_o} = G_{A2}(G_{A1}P_{N_i} + P_{n1}) + P_{n2}$$

$$F = \frac{P_{N_o}}{P_{N_i}G_{A1}G_{A2}} = 1 + \frac{P_{n1}}{P_{N_i}G_{A1}} + \frac{P_{n2}}{P_{N_i}G_{A1}G_{A2}}$$

or

$$F = F_1 + \frac{F_2 - 1}{G_{A1}} \tag{4.2.4}$$

where

$$F_1 = 1 + \frac{P_{n1}}{P_{N_i}G_{A1}}$$

and

$$F_2 = 1 + \frac{P_{n2}}{P_{N_i}G_{A2}}$$

F_1 and F_2 are recognized as the individual noise figures of the first and second stages, respectively.

Equation (4.2.4) shows that the noise figure of the second stage is reduced by G_{A1} . Therefore, the noise contribution from the second stage is small if G_{A1} is large and can be significant if the gain G_{A1} is low. It is not always important to minimize the first-stage noise if the gain reduction is too large. In fact, we can select a higher gain, even if F_1 is higher than the minimum noise figure of the first stage, such that a low value of F is obtained. In a design, a trade-off between gain and noise figure is usually made.

A specific calculation can be made for two cascaded amplifiers to determine which one should be used first in order to achieve the lowest noise figure. Consider two amplifiers with noise figures F_1 and F_2 and gains G_{A1} and G_{A2} . If amplifier 1 is connected before amplifier 2, the total noise figure, denoted by F_{12} , is

$$F_{12} = F_1 + \frac{F_2 - 1}{G_{A1}}$$

On the other hand, if amplifier 2 is connected at the input, the total noise figure, denoted by F_{21} , is

$$F_{21} = F_2 + \frac{F_1 - 1}{G_{A2}}$$

The configuration with amplifier 1 connected at the input produces a lower total noise figure when $F_{12} < F_{21}$ or

$$F_1 + \frac{F_2 - 1}{G_{A1}} < F_2 + \frac{F_1 - 1}{G_{A2}} \quad (4.2.5)$$

Equation (4.2.5) can be manipulated to read

$$(F_1 - 1) + \frac{F_2 - 1}{G_{A1}} < (F_2 - 1) + \frac{F_1 - 1}{G_{A2}}$$

or

$$\frac{F_1 - 1}{1 - \frac{1}{G_{A1}}} < \frac{F_2 - 1}{1 - \frac{1}{G_{A2}}} \quad (4.2.6)$$

The inequality (4.2.6) can be written as

$$M_1 < M_2 \quad (4.2.7)$$

where

$$M = \frac{F - 1}{1 - \frac{1}{G_A}} \quad (4.2.8)$$

The quantity M is known as the noise measure.

Equation (4.2.7) shows that placing amplifier 1 before amplifier 2 produces a lower total noise figure when the noise measure of amplifier 1 (i.e., M_1) is smaller than the noise measure of amplifier 2 (i.e., M_2).

We conclude that when two amplifiers are cascaded, the lower total noise figure is achieved when the amplifier with the lowest value of M is connected at the input.

For the case of a chain of n amplifiers, the total noise figure is given by (see Problem 4.1)

$$F = F_1 + \frac{F_2 - 1}{G_{A1}} + \frac{F_3 - 1}{G_{A1}G_{A2}} + \frac{F_4 - 1}{G_{A1}G_{A2}G_{A3}} + \dots \quad (4.2.9)$$

If the amplifiers are identical with $F_1 = F_2 = \dots = F_n$ and $G_{A1} = G_{A2} = \dots = G_{An}$, (4.2.9) reduces to

$$F = 1 + \frac{F_1 - 1}{1 - \frac{1}{G_{A1}}} = 1 + M_1$$

4.3 CONSTANT NOISE FIGURE CIRCLES

The noise figure of a two-port amplifier is given by [4.1] (see Appendix L):

$$F = F_{\min} + \frac{r_n}{g_s} |y_s - y_{\text{opt}}|^2 \quad (4.3.1)$$

where r_n is the equivalent normalized noise resistance of the two-port (i.e., $r_n = R_n/Z_o$), $y_s = g_s + jb_s$ represents the normalized source admittance, and $y_{\text{opt}} = g_{\text{opt}} + jb_{\text{opt}}$ represents the normalized source admittance which results in the minimum (or optimum) noise figure, called F_{\min} .

We can express y_s and y_{opt} in terms of the reflection coefficients Γ_s and Γ_{opt} —namely,

$$y_s = \frac{1 - \Gamma_s}{1 + \Gamma_s} \quad (4.3.2)$$

and

$$y_{\text{opt}} = \frac{1 - \Gamma_{\text{opt}}}{1 + \Gamma_{\text{opt}}} \quad (4.3.3)$$

Substituting (4.3.2) and (4.3.3) into (4.3.1) results in the relation

$$F = F_{\min} + \frac{4r_n |\Gamma_s - \Gamma_{\text{opt}}|^2}{(1 - |\Gamma_s|^2) |1 + \Gamma_{\text{opt}}|^2} \quad (4.3.4)$$

Equation (4.3.4) depends on F_{\min} , r_n , and Γ_{opt} . These quantities are known as the *noise parameters* and are given by the manufacturer of the transistor or can be determined experimentally. The source reflection coefficient can be varied until a minimum noise figure is read in a noise figure meter. The value of F_{\min} , which occurs when $\Gamma_s = \Gamma_{\text{opt}}$, can be read from the meter, and the source reflection coefficient that produces F_{\min} can be determined accurately using a network analyzer. The noise resistance r_n can be measured by reading the noise figure when $\Gamma_s = 0$, called $F_{\Gamma_s=0}$. Then, using (4.3.4), we obtain

$$r_n = (F_{\Gamma_s=0} - F_{\min}) \frac{|1 + \Gamma_{\text{opt}}|^2}{4|\Gamma_{\text{opt}}|^2}$$

F_{\min} is a function of the device operating current and frequency, and there is one value of Γ_{opt} associated with each F_{\min} . A typical plot of F_{\min} versus current for a BJT is illustrated in Fig. 4.3.1.

Equation (4.3.4) can be used to design Γ_s for a given noise figure $F = F_i$. Rearranging (4.3.4) as follows

$$\frac{|\Gamma_s - \Gamma_{\text{opt}}|^2}{1 - |\Gamma_s|^2} = \frac{F_i - F_{\min}}{4r_n} |1 + \Gamma_{\text{opt}}|^2 \quad (4.3.5)$$

we observe that for a given noise figure F_i the right-hand side of (4.3.5) is a constant. Hence, defining the noise figure parameter N_i as

$$N_i = \frac{F_i - F_{\min}}{4r_n} |1 + \Gamma_{\text{opt}}|^2 \quad (4.3.6)$$

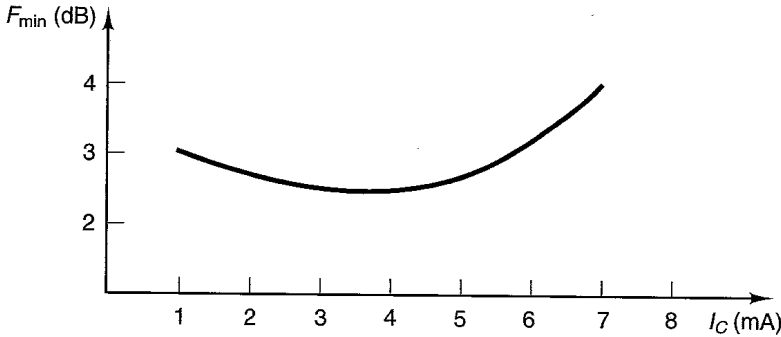


Figure 4.3.1 Typical F_{\min} versus collector current measured at $V_{CE} = 10$ V and $f = 4$ GHz.

it follows that (4.3.5) can be written as

$$\frac{|\Gamma_s - \Gamma_{\text{opt}}|^2}{1 - |\Gamma_s|^2} = N_i$$

$$(\Gamma_s - \Gamma_{\text{opt}})(\Gamma_s^* - \Gamma_{\text{opt}}^*) = N_i - N_i |\Gamma_s|^2$$

$$|\Gamma_s|^2(1 + N_i) - 2 \operatorname{Re}(\Gamma_s \Gamma_{\text{opt}}^*) + |\Gamma_{\text{opt}}|^2 = N_i$$

or

$$|\Gamma_s|^2 - \frac{2}{1 + N_i} \operatorname{Re}(\Gamma_s \Gamma_{\text{opt}}^*) + \frac{|\Gamma_{\text{opt}}|^2}{1 + N_i} = \frac{N_i}{1 + N_i}$$

This equation is recognized as the equation of a circle in the Γ_s plane (see Appendix A). In fact, it can be expressed in the form

$$\left| \Gamma_s - \frac{\Gamma_{\text{opt}}}{1 + N_i} \right|^2 = \frac{N_i^2 + N_i(1 - |\Gamma_{\text{opt}}|^2)}{(1 + N_i)^2}$$

For a given N_i , the center of the circle is located at

$$C_{F_i} = \frac{\Gamma_{\text{opt}}}{1 + N_i} \quad (4.3.7)$$

and the radius is

$$r_{F_i} = \frac{1}{1 + N_i} \sqrt{N_i^2 + N_i(1 - |\Gamma_{\text{opt}}|^2)} \quad (4.3.8)$$

Using (4.3.6), the parameter N_i is calculated for various F_i . Then, using (4.3.7) and (4.3.8), a family of constant noise circles can be drawn in the Γ_s plane.

Equations (4.3.6), (4.3.7), and (4.3.8) show that when $F_i = F_{\min}$, then $N_i = 0$, $C_{F_{\min}} = \Gamma_{\text{opt}}$, and $r_{F_{\min}} = 0$. That is, the center of the F_{\min} circle is located

at Γ_{opt} with zero radius. From (4.3.7), the centers of the other noise figure circles are located along the Γ_{opt} vector.

A typical set of constant noise figure circles is shown in Fig. 4.3.2. This set of curves show that $F_{min} = 3$ dB is obtained when $\Gamma_s = \Gamma_{opt} = 0.58 \angle 138^\circ$ and at point A, $\Gamma_s = 0.38 \angle 119^\circ$ produces $F_i = 4$ dB.

In a design there is always a difference between the designed noise figure and the measured noise figure of the final amplifier. This occurs because of the loss associated with the matching elements and the transistor noise figure variations from unit to unit. Typically, the noise figure difference can be from a fraction of a decibel to 1 dB in a narrowband design.

A low-noise design usually involves trade-offs between gain, noise figure, and VSWRs. A simple example that illustrates the trade-offs involved between gain and noise figure is shown in Fig. 4.3.3. The transistor in this example is unilateral, and a set of G_s constant-gain circles has been drawn in the Smith chart

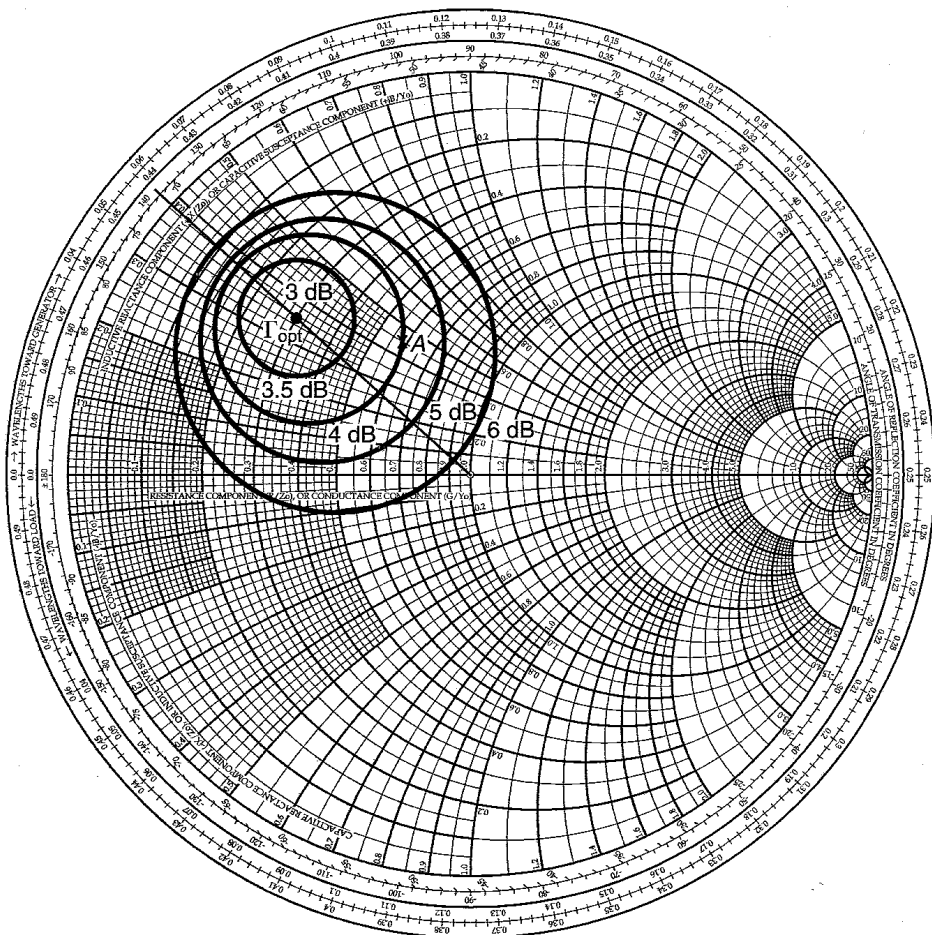


Figure 4.3.2 Typical constant noise figure circles in the Γ_s plane.

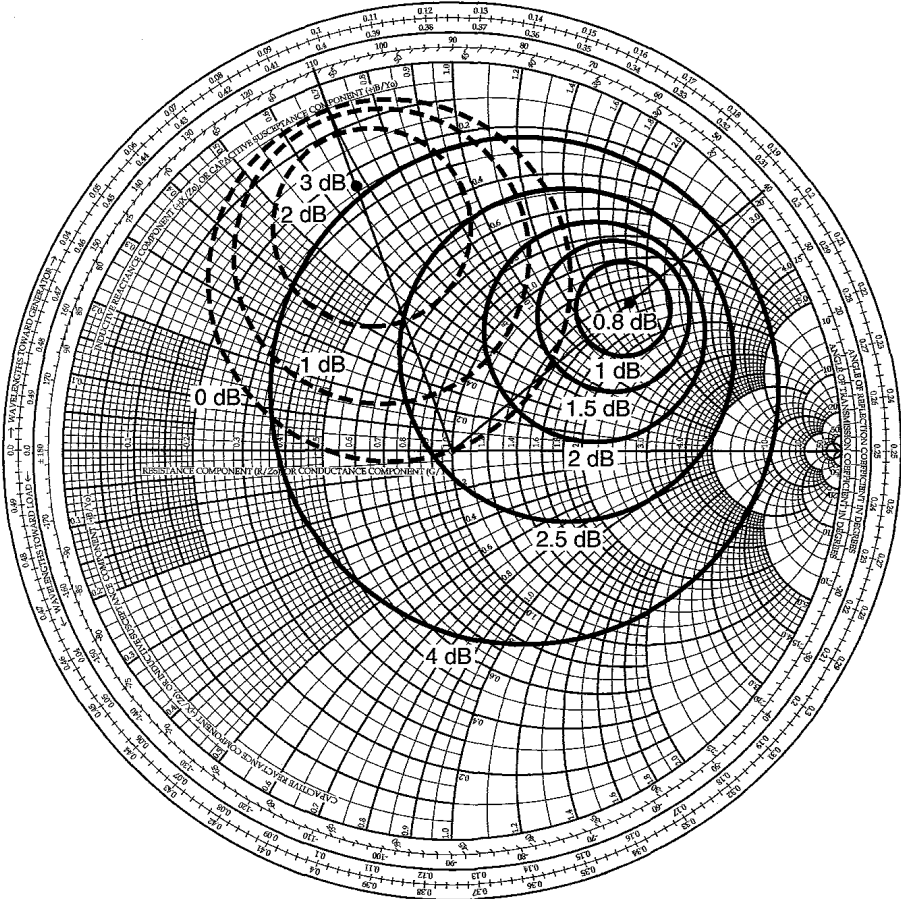


Figure 4.3.3 Noise figure circles (solid curves) and G_s constant-gain circles (dashed curves). The transistor is a GaAs FET with $V_{DS} = 4\text{ V}$, $I_{DS} = 12\text{ mA}$, and $f = 6\text{ GHz}$.

(i.e., in the Γ_s plane) containing the noise figure circles. Maximum gain and minimum noise figure cannot, in general, be obtained simultaneously. In Fig. 4.3.3, the maximum G_s gain of 3 dB, obtained with $\Gamma_s = 0.7\angle 110^\circ$, results in a noise figure of $F_i \approx 4\text{ dB}$; and the minimum noise figure $F_{\min} = 0.8\text{ dB}$, obtained with $\Gamma_s = 0.6\angle 40^\circ$, results in a gain $G_s \approx -1\text{ dB}$.

In a bilateral case the available gain circles and the noise figure circles are drawn in the Γ_s plane, and the trade-offs that can be made are easily analyzed. The following example illustrates such a case.

Example 4.3.1

The scattering and noise parameters of a BJT measured at a bias point for low-noise operation ($V_{CE} = 10\text{ V}$, $I_C = 4\text{ mA}$) at $f = 4\text{ GHz}$ are

$$S_{11} = 0.552\angle 169^\circ$$

$$S_{12} = 0.049\angle 23^\circ$$

$$S_{21} = 1.681 \angle 26^\circ$$

$$S_{22} = 0.839 \angle -67^\circ$$

and

$$F_{\min} = 2.5 \text{ dB}$$

$$\Gamma_{\text{opt}} = 0.475 \angle 166^\circ$$

$$R_n = 3.5 \ \Omega$$

Design a microwave transistor amplifier to have a minimum noise figure. (This example is based on a design from Hewlett-Packard Application Note 967 [4.2].)

Solution. For this transistor, it follows that $K = 1.012$ and $|A| = 0.419 \angle 111.04^\circ$. Therefore, the transistor is unconditionally stable at 4 GHz. Using (3.6.10), (3.6.5), and (3.6.6), it also follows that $G_{T,\max} = G_{A,\max} = 14.7 \text{ dB}$, $\Gamma_{M_s} = 0.941 \angle -154^\circ$, and $\Gamma_{ML} = 0.979 \angle 70^\circ$.

A minimum noise figure of 2.5 dB is obtained with $\Gamma_s = \Gamma_{\text{opt}} = 0.475 \angle 166^\circ$. The constant noise figure circles in Fig. 4.3.4 for $F_i = 2.5$ to 3 dB were calculated using (4.3.6), (4.3.7), and (4.3.8). For example, the $F_i = 2.8$ -dB circle was obtained as follows:

$$N_i = \frac{1.905 - 1.778}{4(3.5/50)} |1 + 0.475 \angle 166^\circ|^2 = 0.1378$$

$$C_{F_i} = \frac{0.475 \angle 166^\circ}{1 + 0.1378} = 0.417 \angle 166^\circ$$

and

$$r_{F_i} = \frac{1}{1 + 0.1378} \sqrt{(0.1378)^2 + 0.1378[1 - (0.475)^2]} = 0.312$$

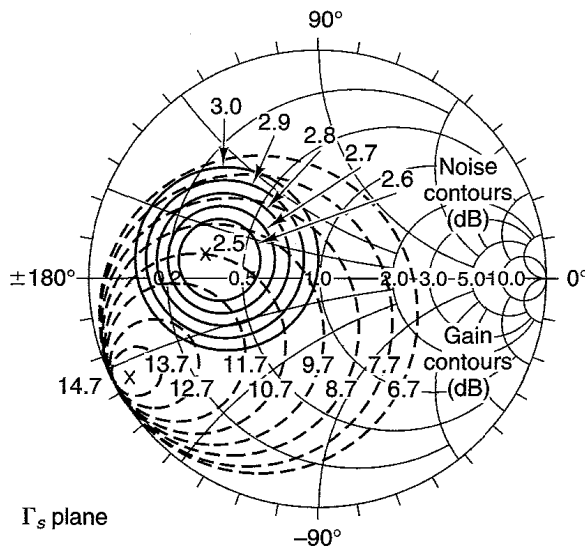


Figure 4.3.4 Constant noise figure circles and available power gain circles. (From Ref. [4.2]; courtesy of Hewlett-Packard.)

The gain contours in Fig. 4.3.4, which are the available gain circles in the Γ_s plane, were drawn using (3.7.15) and (3.7.16). Observe that since the transistor is unconditionally stable, all the available gain circles are completely inside the Smith chart.

Figure 4.3.4 shows that for this transistor F_{\min} is not very sensitive to small variations in Γ_s around Γ_{opt} . In fact, the 2.6-dB constant noise circle (i.e., a 0.1-dB increase in noise figure) results when Γ_s changes in magnitude by 0.2, from its value at Γ_{opt} .

With $\Gamma_s = \Gamma_{\text{opt}}$, the resulting available gain is $G_A = 11$ dB. Therefore, a sacrifice in gain was needed to obtain optimum noise performance. The load reflection coefficient is selected to provide maximum power transfer to the load (i.e., $\Gamma_L = \Gamma_{\text{OUT}}^*$). With $\Gamma_s = \Gamma_{\text{opt}}$, the value of Γ_L is

$$\Gamma_L = \left(S_{22} + \frac{S_{12}S_{21}\Gamma_{\text{opt}}}{1 - S_{11}\Gamma_{\text{opt}}} \right)^* = 0.844 \angle 70.4^\circ$$

Since $\Gamma_L = \Gamma_{\text{OUT}}^*$, the VSWR at the output is 1, and the resulting gains are $G_T = G_A = 11$ dB and $G_p = 12.7$ dB. Also, $\Gamma_{\text{IN}} = 0.744 \angle 157^\circ$ and, using (3.8.1) and (3.8.2), the input VSWR is 4.26.

The amplifier was designed, built, and tested by Hewlett-Packard [4.2]. The ac amplifier schematic is shown in Fig. 4.3.5. The input matching network was designed with a short-circuited stub and a quarter-wave transformer with $Z_o = 31.1 \Omega$. The output matching network was designed with a 0.61-cm microstrip line to provide soldering area, followed by a $\lambda/8$ short-circuited stub to tune out most of the susceptance component of $Y_1 = 1/Z_1$. Then, another series microstrip line followed by an open stub that provides some tuning capabilities was used. A final series microstrip line was used to obtain the match to 50Ω .

Of course, the output matching network could have been designed differently. The form selected (see Fig. 4.3.5) provides flexibility for tuning by adjusting the lengths of the series lines (i.e., the $l = 1.35$ -cm and $l = 0.19$ -cm lines), by changing the width (i.e., the characteristic impedance) of the open-circuited stub and by modifying the lengths of the short-circuited stub.

The complete amplifier schematic and the microstrip board layout are shown in Fig. 4.3.6. The board material is Duroid® ($\epsilon_r = 2.23$, $h = 0.031$ in).

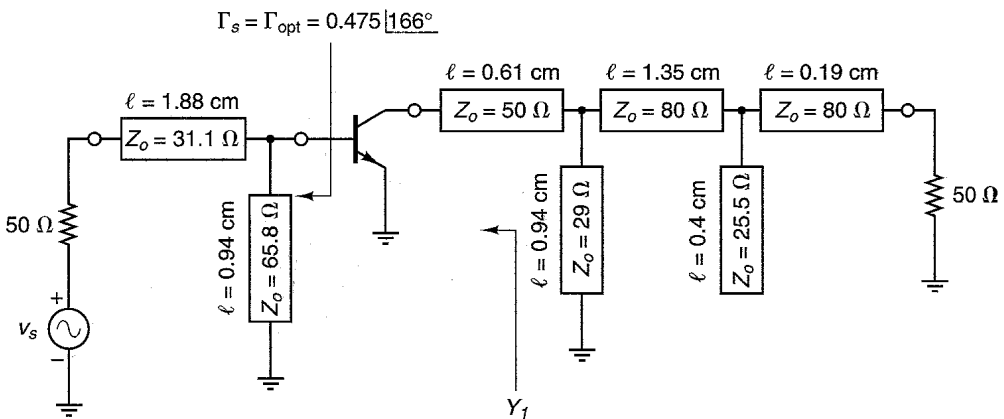
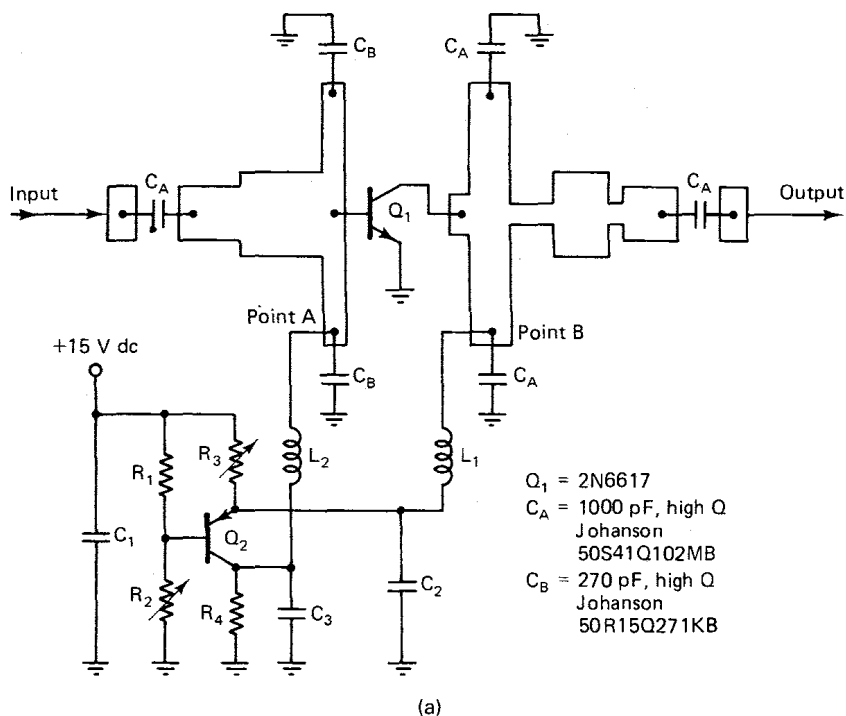
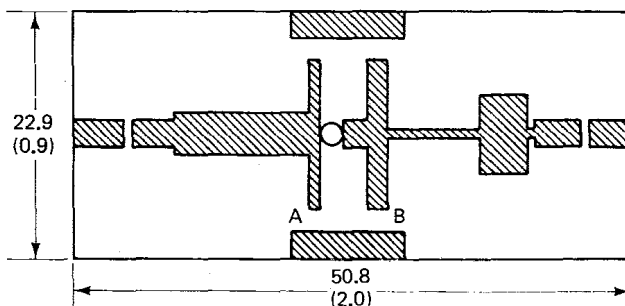


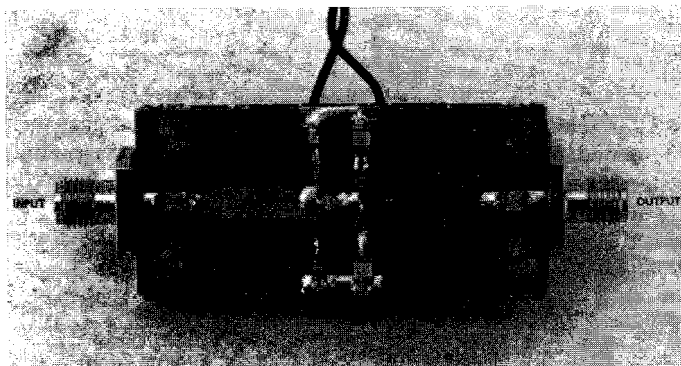
Figure 4.3.5 Amplifier schematic. The microstrip lengths are given for $\epsilon_{\text{eff}} = 1$ at $f = 4$ GHz. (From Ref. [4.2]; courtesy of Hewlett-Packard.)



(a)

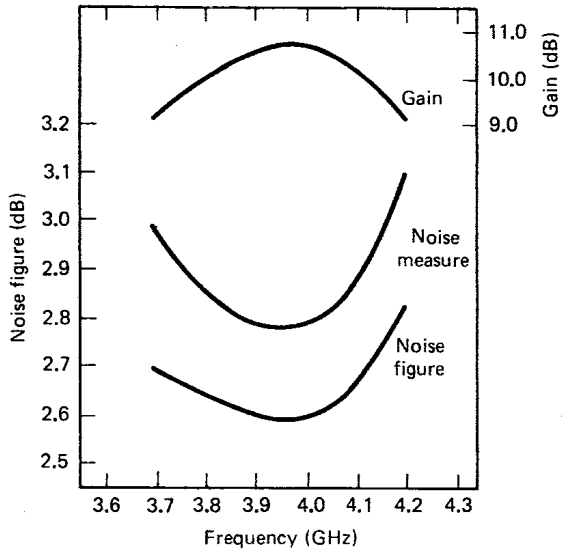


Dimensions in millimeters (inches)

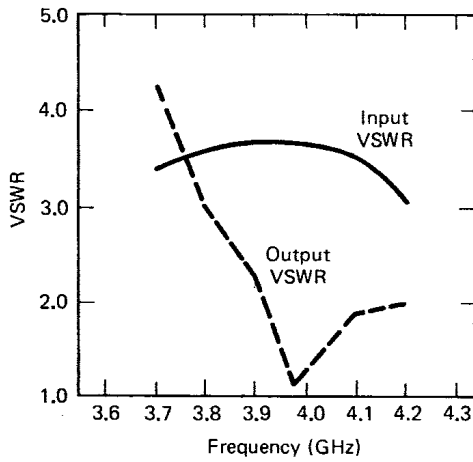


(b)

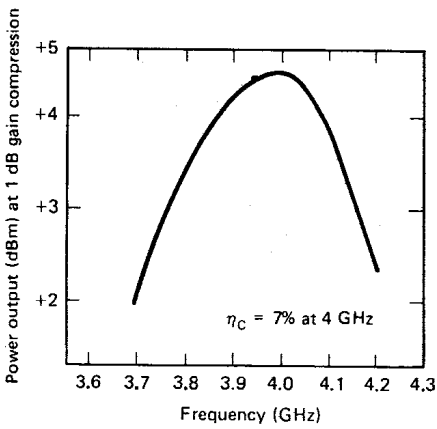
Figure 4.3.6 (a) Complete amplifier schematic; (b) microstrip board layout. (From Ref. [4.2]; courtesy of Hewlett-Packard.)



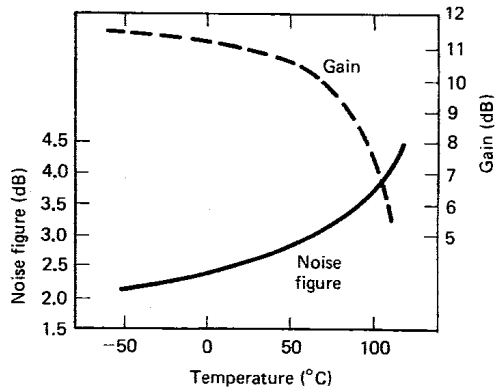
(a)



(b)



(c)



(d)

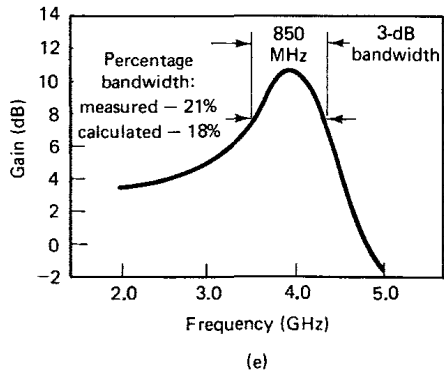


Figure 4.3.7 Measured amplifier characteristics: (a) noise and gain performance; (b) input-output VSWR performance; (c) power output performance; (d) temperature performance at 4 GHz; (e) wide-band gain performance. (From Ref. [4.2]; courtesy of Hewlett-Packard.)

The measured characteristics of the amplifier are shown in Fig. 4.3.7. Figure 4.3.7 shows that the amplifier performance is very good in the frequency range 3.7 to 4.2 GHz. The 3-dB bandwidth (see Fig. 4.3.7e) is 850 MHz, which corresponds to a 21% bandwidth.

The following two examples discuss the design of low-noise amplifiers and some of the trade-offs involved between noise figure, available gain, and VSWRs.

Example 4.3.2

The S parameters and the noise parameters of the AT-41470 (a low-noise silicon BJT) at 4 GHz, $V_{CE} = 8$ V, and $I_C = 10$ mA are

$$\begin{aligned}
 S_{11} &= 0.6 \angle 146^\circ & F_{\min} &= 3 \text{ dB} \\
 S_{12} &= 0.085 \angle 62^\circ & \Gamma_{\text{opt}} &= 0.45 \angle -150^\circ \\
 S_{21} &= 1.97 \angle 32^\circ & r_n &= 0.2 \\
 S_{22} &= 0.52 \angle -63^\circ
 \end{aligned}$$

Design a low-noise amplifier with $(\text{VSWR})_{\text{in}} < 1.8$.

Solution. This transistor is unconditionally stable at 4 GHz since $K = 1.172$ and $|A| = 0.151$. From (3.6.5) and (3.6.6), the simultaneous conjugate match terminations are $\Gamma_{M_s} = 0.824 \angle -147.81^\circ$ and $\Gamma_{M_L} = 0.791 \angle 60.45^\circ$; and $G_{A,\text{max}} = 11.15$ dB.

In Fig. 4.3.8a, the values of Γ_{opt} and Γ_{M_s} are plotted, as well as three other values of Γ_s , located on a straight line drawn from Γ_{opt} to Γ_{M_s} . In Fig. 4.3.8b, we have tabulated the resulting values of the noise, $(\text{VSWR})_{\text{in}}$, and G_A at the values of Γ_s indicated in Fig. 4.3.8a.

An examination of Fig. 4.3.8b shows that the design target of low noise with $(\text{VSWR})_{\text{in}} < 1.8$ can be obtained with $\Gamma_s = 0.64 \angle -148.2^\circ$. In fact, with this value of Γ_s , the noise figure is only 0.25 dB higher than F_{\min} , the gain $G_A = 10.64$ dB is only 0.51 dB lower than $G_{A,\text{max}}$, and the value of $(\text{VSWR})_{\text{in}} = 1.78$ represents an improvement of 33.83% over the $(\text{VSWR})_{\text{in}}$ value of 2.69 at Γ_{opt} . The block diagram of the low-noise amplifier is shown in Fig. 4.3.8c.

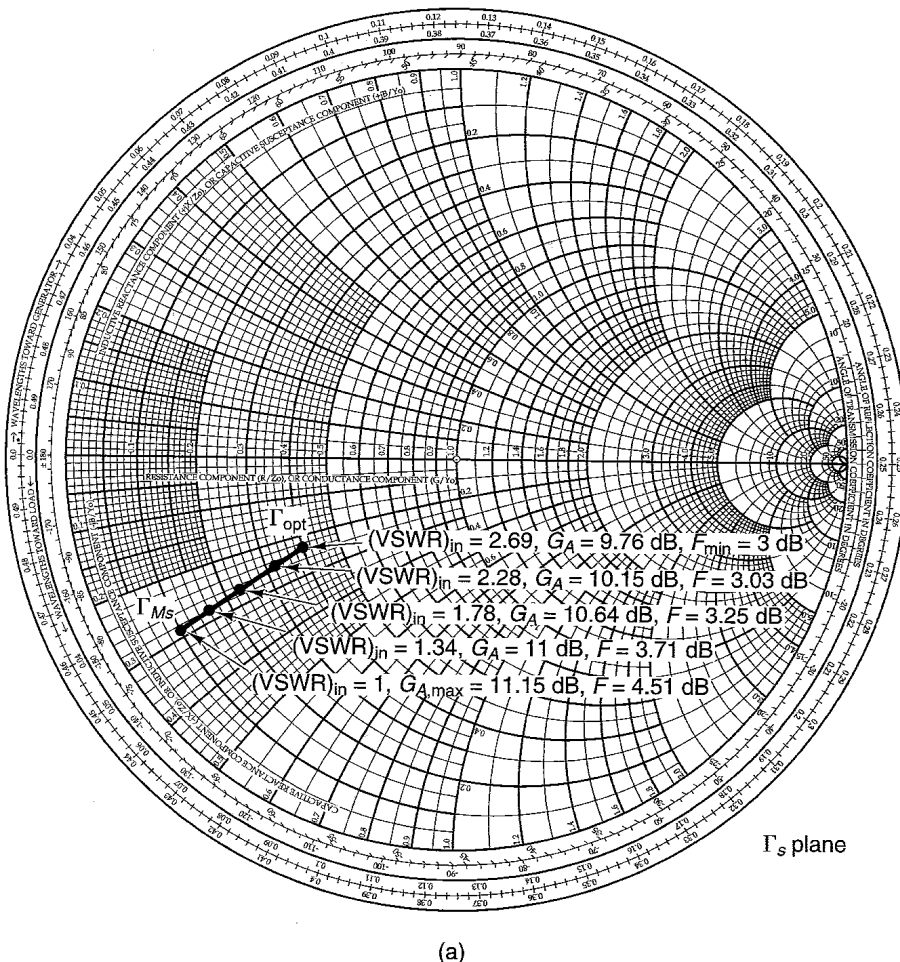


Figure 4.3.8 (a) Trade-offs between noise figure, available gain, and $(VSWR)_{in}$; (b) calculations of F , G_A , and $(VSWR)_{in}$ at the values of Γ_s indicated in (a); (c) the block diagram of the low-noise amplifier.

Example 4.3.3

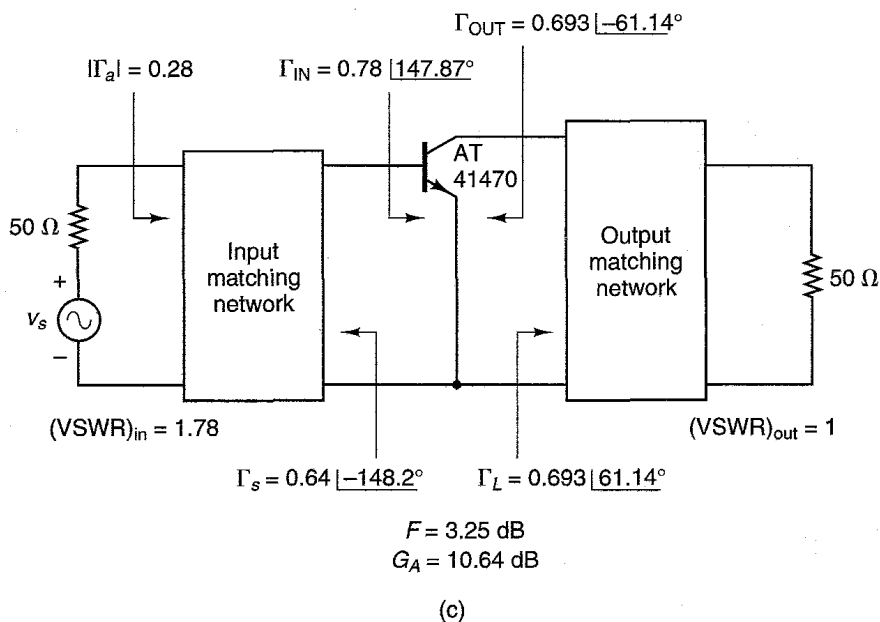
The scattering and noise parameters of a GaAs FET measured at three different optimum bias settings at $f = 6$ GHz are

Minimum Noise Figure ($V_{DS} = 3.5$ V, $I_{DS} = 15\%$ I_{DSS}):

$$\begin{aligned} S_{11} &= 0.674 \angle -152^\circ & F_{\min} &= 2.2 \text{ dB} \\ S_{12} &= 0.075 \angle 6.2^\circ & \Gamma_{\text{opt}} &= 0.575 \angle 138^\circ \\ S_{21} &= 1.74 \angle 36.4^\circ & R_n &= 6.64 \Omega \\ S_{22} &= 0.6 \angle -92.6^\circ \end{aligned}$$

	Γ_s	$\Gamma_L = \Gamma_{OUT}^*$	Γ_{IN}	$ \Gamma_a $	$(VSWR)_{in}$	G_A (dB)	F (dB)
0.45	$ -150^\circ$	0.623 $ 62.09^\circ$	0.753 $ 147.97^\circ$	0.458	2.69	9.76	3
0.53	$ -149^\circ$	0.649 $ 61.68^\circ$	0.762 $ 147.87^\circ$	0.39	2.28	10.15	3.03
0.64	$ -148.2^\circ$	0.693 $ 61.14^\circ$	0.78 $ 147.87^\circ$	0.28	1.78	10.64	3.25
0.74	$ -148^\circ$	0.741 $ 60.78^\circ$	0.8 $ 147.86^\circ$	0.147	1.34	11	3.71
0.824	$ -147.81^\circ$	0.791 $ 60.45^\circ$	0.824 $ 147.81^\circ$	0	1	11.15	4.51

(b)



(c)

Figure 4.3.8 Continued

Linear Power Output ($V_{DS} = 4$ V, $I_{DS} = 50\%$ I_{DSS}):

$$\begin{aligned}
 S_{11} &= 0.641 \angle -171.3^\circ & F_{\min} &= 2.9 \text{ dB} \\
 S_{12} &= 0.057 \angle 16.3^\circ & \Gamma_{\text{opt}} &= 0.542 \angle 141^\circ \\
 S_{21} &= 2.058 \angle 28.5^\circ & R_n &= 9.42 \ \Omega \\
 S_{22} &= 0.572 \angle -95.7^\circ
 \end{aligned}$$

Maximum Gain ($V_{DS} = 4$ V, $I_{DS} = 100\%$ I_{DSS}):

$$\begin{aligned}
 S_{11} &= 0.614 \angle -167.4^\circ \\
 S_{12} &= 0.046 \angle 65^\circ \\
 S_{21} &= 2.187 \angle 32.4^\circ \\
 S_{22} &= 0.716 \angle -83^\circ
 \end{aligned}$$

Design a microwave transistor amplifier to have good ac performance. (This example is based on a design from Hewlett-Packard Application Note 970 [4.3].)

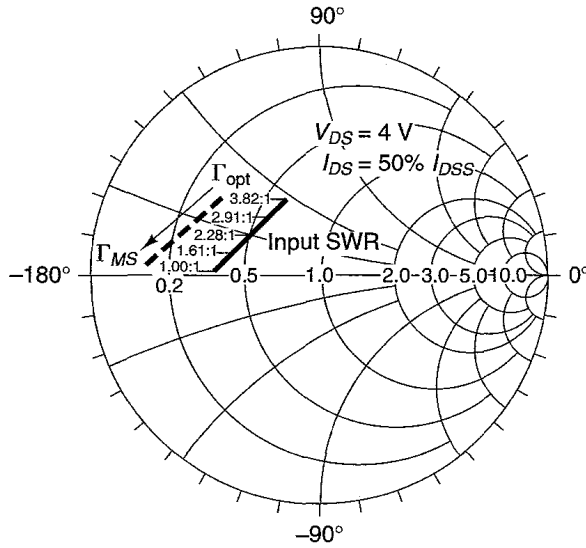
Solution. The three bias settings are referred to as minimum noise figure, linear power output, and maximum gain. From the data given, it is seen that for this transistor the lowest minimum noise figure is obtained at a bias setting of $V_{DS} = 3.5$ V and $I_{DS} = 15\% I_{DSS}$ with $\Gamma_s = \Gamma_{opt} = 0.575 \angle 138^\circ$. A larger output power is obtained by setting $V_{DS} = 4$ V and $I_{DS} = 50\% I_{DSS}$ (i.e., the optimum bias point for class A operation). At this Q point, a minimum noise figure of 2.9 dB is obtained with $\Gamma_s = \Gamma_{opt} = 0.542 \angle 141^\circ$. The largest output power is obtained by biasing the transistor at $I_{DS} = 100\% I_{DSS}$. No noise parameter data are given for this bias point since the noise degradation is significant at $I_{DS} = 100\% I_{DSS}$. Hence, it is a very poor Q point selection for a low-noise design.

There are four ac performances that must be considered: noise figure, available power gain, power output, and input and output VSWR. The linear power-output bias point ($V_{DS} = 4$ V, $I_{DS} = 50\% I_{DSS}$) provides a good compromise between the minimum noise figure bias point and the maximum gain bias point. At the linear power-output bias point, the values of Γ_s , Γ_L , F , G_A , and $P_{1\text{ dB}}$ are calculated for three different design goals (see Fig. 4.3.9)—namely, for a minimum noise figure design, for a simultaneous conjugate match design, and for a maximum output power design. $P_{1\text{ dB}}$ is the output power at the 1-dB compression point (see Section 4.7 for the definition of the 1-dB compression point). The output power performance, measured at the 1-dB compression point, was experimentally measured and is given in the figure. The data for the output power were taken with an input power drive of 8.3 dBm.

The input VSWR with $\Gamma_s = \Gamma_{Ms}$ is 1, and $(\text{VSWR})_{in} = 3.82$ with $\Gamma_s = \Gamma_{opt}$. Figure 4.3.10 shows the noise figure, G_A , and input and output VSWR as the reflection coefficient is varied from Γ_{opt} to Γ_{Ms} , along a straight line, in the Smith chart. Figure 4.3.10 shows that a good compromise between noise figure, G_A , and VSWR is to use $\Gamma_s = 0.614 \angle 160^\circ$ and $\Gamma_L = 0.627 \angle 106^\circ$. The noise figure is increased by 0.24 dB from the minimum noise, but G_A is increased by 1.22 dB and the input VSWR is improved by 40% [i.e., $(\text{VSWR})_{in} = 2.28$]. The ac schematic of the amplifier for the selected values of Γ_s and Γ_L is shown in Fig. 4.3.11a and the microstrip board layout is shown in Fig. 4.3.11b. The board material is Duroid ($\epsilon_r = 2.23$, $h = 0.031$ in.). The measured characteristics of the amplifier are shown in Fig. 4.3.12.

Minimum Noise Figure	Simultaneous Conjugate Match	Maximum Output Power
$\Gamma_s = \Gamma_{opt} = 0.542 \angle 141^\circ$	$\Gamma_{Ms} = 0.762 \angle 177.3^\circ$	$\Gamma_{PS} = 0.729 \angle 166^\circ$
$\Gamma_L = 0.575 \angle 104.5^\circ$	$\Gamma_{ML} = 0.718 \angle 103.9^\circ$	$\Gamma_{PL} = 0.489 \angle 101^\circ$
$F_{min} = 2.9$ dB	$F = 4.44$ dB	$F = 3.69$ dB
$G_A = 9.33$ dB	$G_{A,max} = 11.38$ dB	$G_p = 8.2$ dB
$P_{1\text{ dB}} = 9.3$ dBm	$P_{1\text{ dB}} = 13.4$ dBm	$P_{1\text{ dB}} = 15.5$ dBm

Figure 4.3.9 Values of Γ_s , Γ_L , F , G_A , and $P_{1\text{ dB}}$ for minimum noise figure design, simultaneous conjugate match design, and maximum output power design at the linear output bias point ($V_{DS} = 4$ V and $I_D = 50\% I_{DSS}$).



Γ_s	Mag./Ang.	Γ_L Mag./Ang.	F (dB)	G_A (dB)	Input VSWR	Output VSWR
Γ_{opt}	0.542 141°	0.575 104°	2.90	9.33	3.82:1	1.00:1
	0.572 152°	0.601 105°	2.97	10.04	2.91:1	1.00:1
	0.614 160°	0.627 106°	3.14	10.55	2.28:1	1.00:1
	0.678 169°	0.667 105°	3.57	11.10	1.61:1	1.00:1
Γ_{Ms}	0.762 177°	0.718 104°	4.44	11.38	1.00:1	1.00:1

Figure 4.3.10 Trade-offs between noise figure, power gain, and VSWR. (From Ref. [4.3]; courtesy of Hewlett-Packard.)

In the last two examples, the transistors were unconditionally stable. In a potentially unstable situation, we must check that the noise reflection coefficient Γ_s is in the stable region of the source stability circle. Once Γ_s is selected, Γ_L is selected for maximum gain (i.e., $\Gamma_L = \Gamma_{OUT}^*$), and again we must check that the value of Γ_L is in the stable region of the load stability circle.

Example 4.3.4

The parameters of a GaAs FET at $V_{DS} = 3$ V, $I_{DS} = 20$ mA, and $f = 6$ GHz are

$$\begin{aligned}
 S_{11} &= 0.7 \angle -105^\circ & F_{min} &= 0.8 \text{ dB} \\
 S_{12} &= 0.11 \angle 20^\circ & \Gamma_{opt} &= 0.7 \angle 55^\circ \\
 S_{21} &= 3 \angle 75^\circ & r_n &= 0.95 \\
 S_{22} &= 0.46 \angle -70^\circ
 \end{aligned}$$

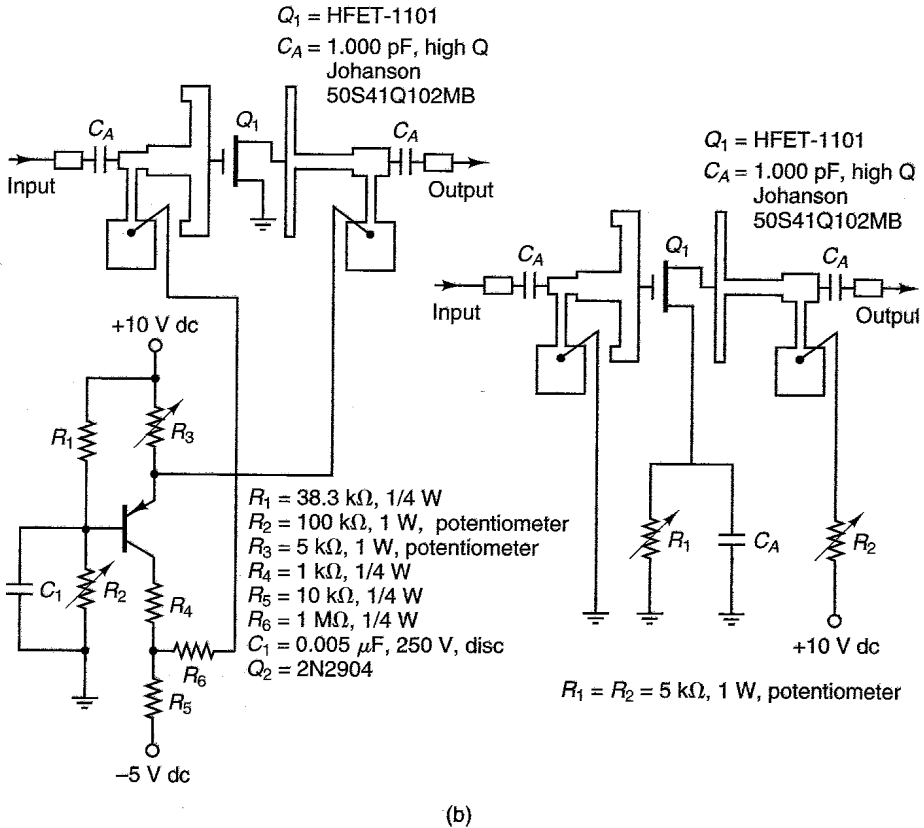
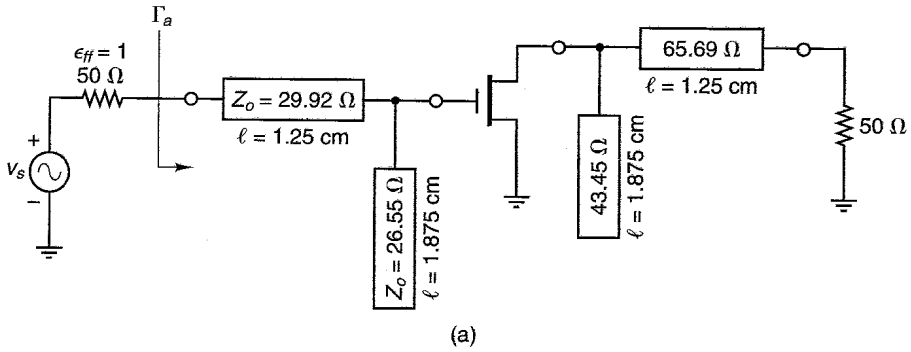
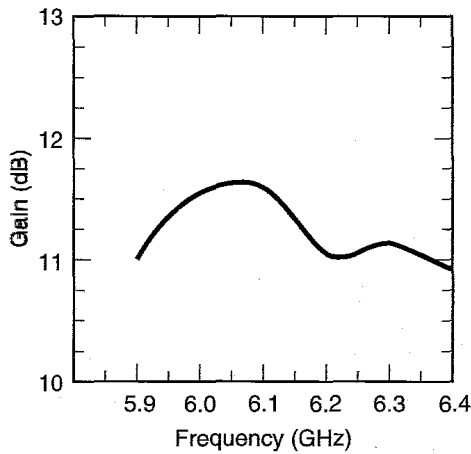
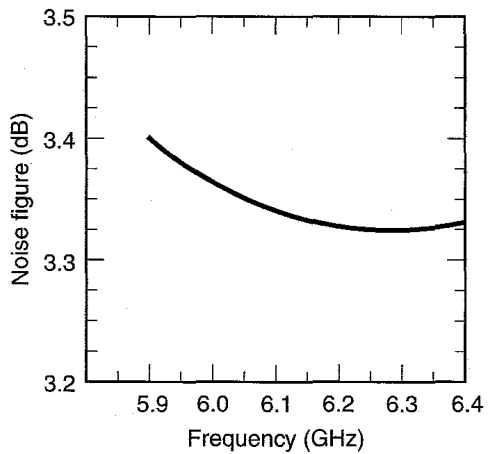


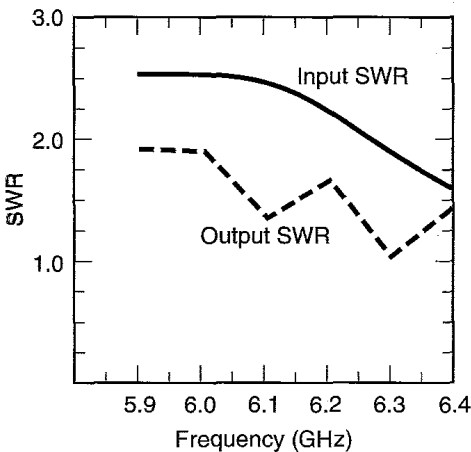
Figure 4.3.11 (a) The ac schematic of the amplifier with $\epsilon_{ff} = 1$; (b) microstrip layout with two different dc bias networks. (From Ref. [4.3]; courtesy of Hewlett-Packard.)



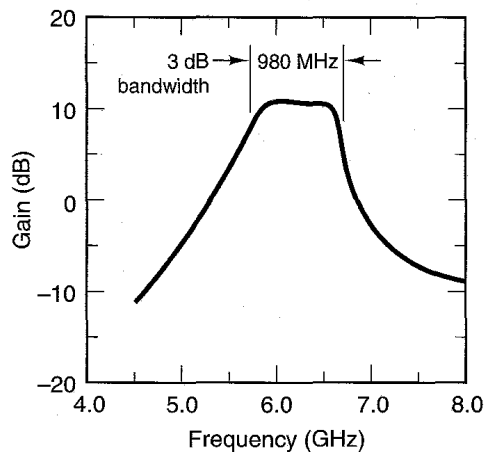
(a)



(b)



(c)



(d)

Figure 4.3.12 Measured characteristics of the amplifier: (a) gain performance; (b) noise performance; (c) input–output VSWR performance; (d) wideband gain performance. (From Ref. [4.3]; courtesy of Hewlett-Packard.)

Design a low-noise amplifier.

Solution. For this transistor, we find that $K = 0.774$ and $\Delta = 0.46 \angle -129.3^\circ$. Therefore, the transistor is potentially unstable. The maximum stable gain is

$$G_{MSG} = \frac{|S_{21}|}{|S_{12}|} = \frac{3}{0.11} = 27.27 \text{ (or 14.36 dB)}$$

Figure 4.3.13a shows the source stability circle; the constant-gain circles for $G_A = 10$ dB, 11 dB, and 12 dB; and the constant noise circles for $F_i = 1$ dB and 1.5 dB. The trade-offs between available gain and the noise figure can be analyzed using the

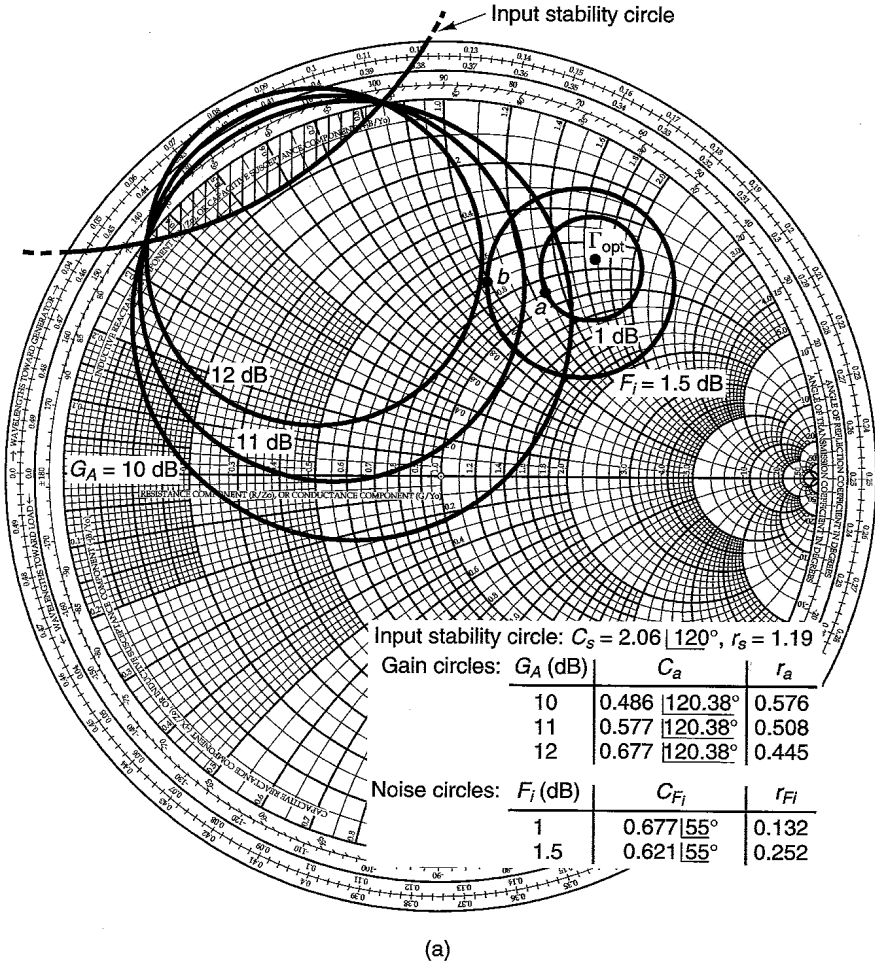


Figure 4.3.13 (a) Input stability circle, gain circles, and noise figure circles for Example 4.3.4; (b) the constant $(VSWR)_{out} = 1.5$ circle; (c) block diagram of a low-noise amplifier with $F = 1$ dB; (d) block diagram of a low-noise amplifier with $F = 1.5$ dB.

information in Fig. 4.3.13a. Next, the design of the low-noise amplifier at different values of Γ_s in Fig. 4.3.13a is considered.

First, with $\Gamma_s = \Gamma_{opt}$, the noise figure is a minimum at 0.8 dB, and the available gain is $G_A = 8.9$ dB. It also follows that $\Gamma_L = \Gamma_{OUT}^* = 0.18 \angle 88.79^\circ$, $(VSWR)_{out} = 1$, $\Gamma_{IN} = 0.725 \angle -109.78^\circ$, $|\Gamma_a| = 0.8$, and $(VSWR)_{in} = 9$. Certainly, we can increase the noise figure a little in order to get a higher gain and a better $(VSWR)_{in}$. To this end, we observe from Fig. 4.3.13a that a design with a noise figure of 1 dB is possible with G_A around 10.5 dB. For this design, we selected Γ_s on the 1-dB noise circle at point *a* in Fig. 4.3.13a. At point *a*, $\Gamma_s = 0.563 \angle 61^\circ$, $F_i = 1$ dB, and $G_A = 10.5$ dB. It also follows that

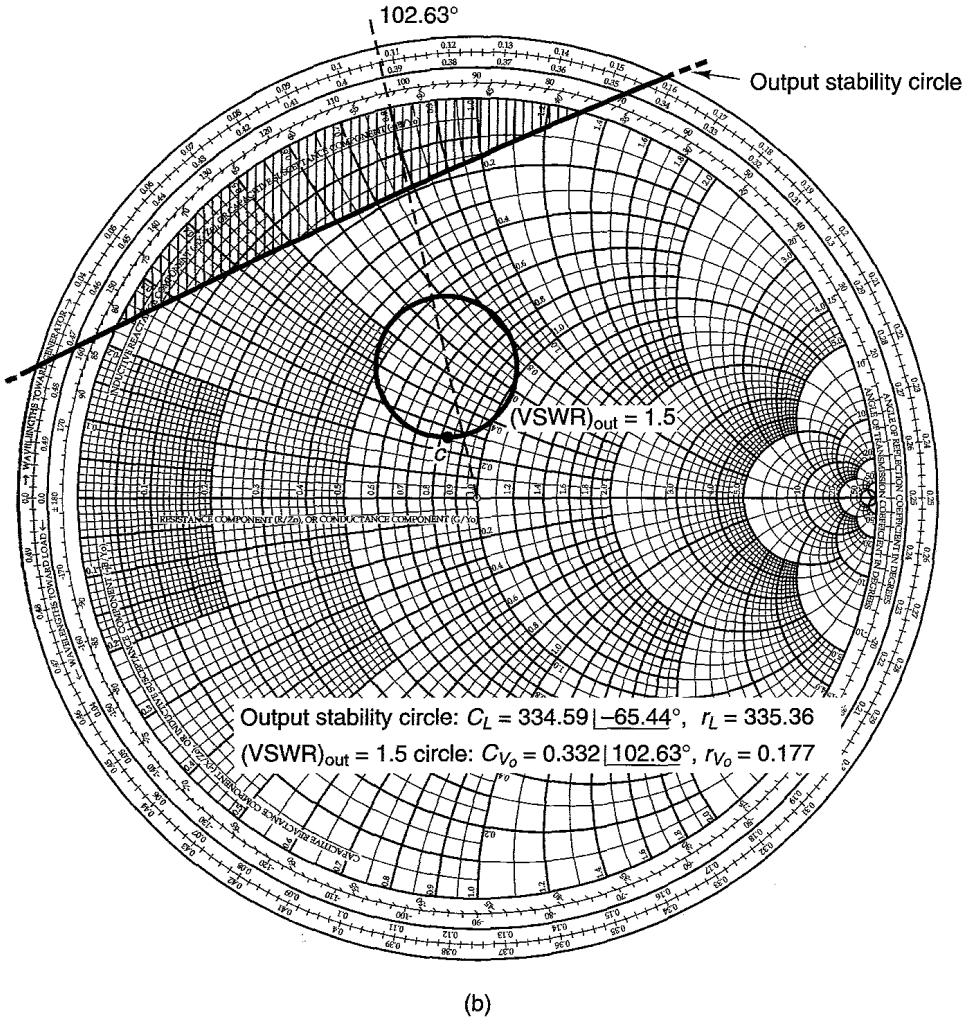


Figure 4.3.13 Continued

$\Gamma_L = \Gamma_{OUT}^* = 0.262 \angle 93.11^\circ$, $(VSWR)_{out} = 1$, $\Gamma_{IN} = 0.748 \angle -111.69^\circ$, $|\Gamma_a| = 0.73$, and $(VSWR)_{in} = 6.41$. Hence, a good improvement in G_A and $(VSWR)_{in}$ is obtained by allowing a noise figure of 1 dB.

The value of $(VSWR)_{in}$ can be improved further by designing for a higher value of G_A , a higher value of noise figure, and a higher value of $(VSWR)_{out}$. For example, with $\Gamma_s = 0.53 \angle 77^\circ$, shown as point *b* in Fig. 4.3.13a, it follows that $G_A = 11.8$ dB, $F_i = 1.5$ dB, and $\Gamma_{OUT} = 0.344 \angle -102.63^\circ$. Designing for $(VSWR)_{out} = 1.5$, the constant $(VSWR)_{out} = 1.5$ circle is drawn in Fig. 4.3.13b. Selecting $\Gamma_L = 0.164 \angle 115.81^\circ$, shown as point *c* in Fig. 4.3.13b, it follows that $\Gamma_{IN} = 0.744 \angle -107.88^\circ$, $|\Gamma_a| = 0.575$, and $(VSWR)_{in} = 3.71$.

Further reduction of the VSWRs can be obtained at the expense of increasing the noise figure. The use of CAD methods to design a low-noise amplifier is illustrated in the Appendix “Computer-Aided Designs,” Example CAD.4.

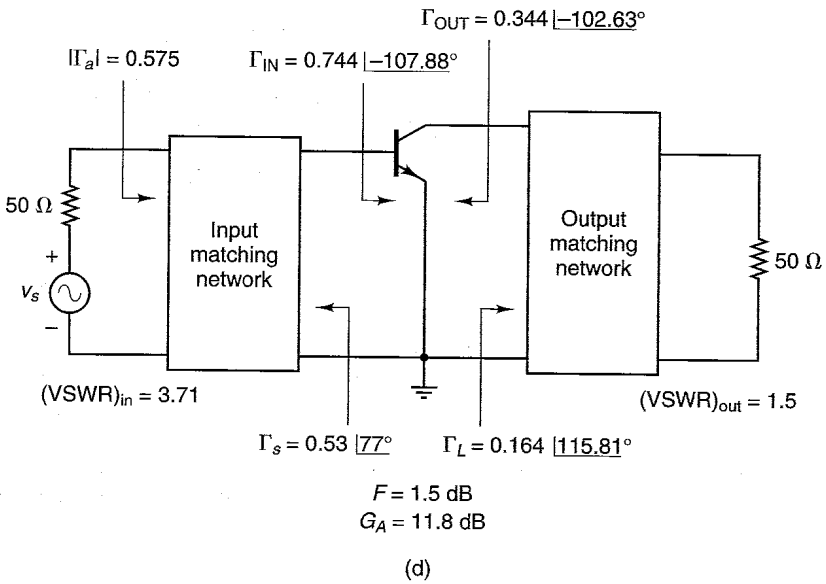
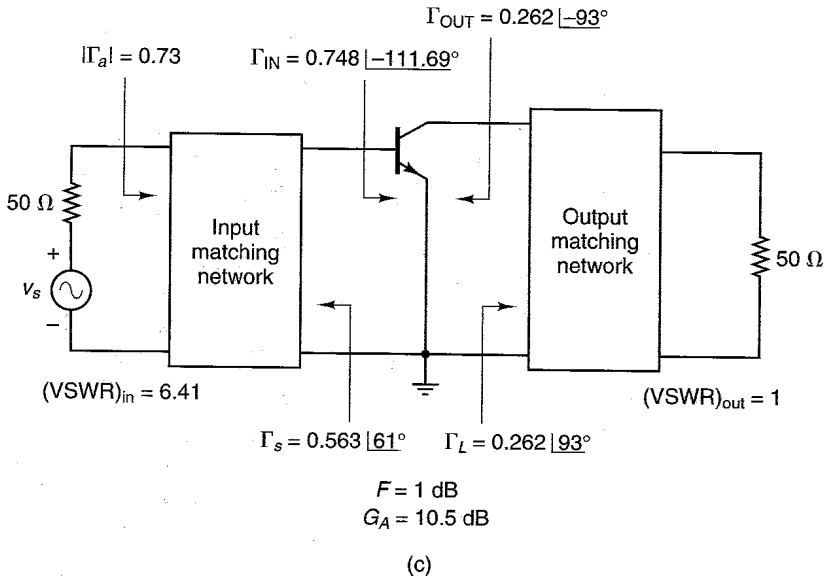


Figure 4.3.13 Continued

The circuit diagrams for the two low-noise amplifiers designed with $F_i = 1 \text{ dB}$ and $F_i = 1.5 \text{ dB}$ are shown in Figs. 4.3.13c and 4.3.13d.

The following example illustrates the design of low-noise amplifiers starting with the constant G_p circles.

Example 4.3.5

The parameters of a GaAs FET at $V_{DS} = 2.5$ V, $I_{DS} = 20$ mA, and $f = 8$ GHz are

$$\begin{aligned} S_{11} &= 0.55 \angle 144^\circ & F_{\min} &= 1.2 \text{ dB} \\ S_{12} &= 0.135 \angle -30^\circ & \Gamma_{\text{opt}} &= 0.41 \angle -150^\circ \\ S_{21} &= 3.1 \angle -4^\circ & r_n &= 0.22 \\ S_{22} &= 0.33 \angle -110^\circ \end{aligned}$$

Design a low-noise amplifier with $(\text{VSWR})_{\text{in}} \leq 1.5$.

Solution. The transistor is potentially unstable since $K = 0.883$ and $\Delta = 0.389 \angle 120.35^\circ$. The center and radius of the input stability circle are $C_s = 3.68 \angle -130.7^\circ$ and $r_s = 2.77$, and for the output stability circle they are $C_L = 9.03 \angle -36^\circ$ and $r_L = 9.9$. The maximum stable gain is

$$G_{\text{MSG}} = \frac{|S_{21}|}{|S_{12}|} = \frac{3.1}{0.135} = 22.96 \text{ (or 13.61 dB)}$$

In Fig 4.3.14a the load stability circle and the constant-gain circles for $G_p = 10$ dB, 11 dB, and 12 dB are drawn. We will try to satisfy the design requirements with Γ_L selected on the $G_p = 12$ dB circle. The transformation of the $G_p = 12$ dB circle to the $\Gamma_s = \Gamma_{\text{IN}}^*$ plane is shown in Fig. 4.3.14b. That is, using (3.8.9) and (3.8.10), we obtain $C_i = 0.923 \angle -130.71^\circ$ and $r_i = 0.351$. Also, in Fig. 4.3.14b the constant noise circles for $F_i = 1.3$ dB, 1.5 dB, and 2 dB are drawn.

Next we determine the values of Γ_L on the $G_p = 12$ dB circle that produce values of $\Gamma_s = \Gamma_{\text{IN}}^*$ close to Γ_{opt} . An examination of Fig. 4.3.14b shows that if the resulting values of Γ_s are far from Γ_{opt} , the resulting noise figure will not be acceptable and, furthermore, these values of Γ_s will probably be close to the unstable region.

Consider the following values of Γ_L : $\Gamma_L = 0.397 \angle 90.3^\circ$ and $\Gamma_L = 0.133 \angle 152.23^\circ$, shown as point a and b in Fig. 4.3.14a, respectively. These points transform to the corresponding points a' and b' in Fig. 4.3.14b. The calculations for the VSWRs and noise figure at these points are shown in Fig. 4.3.14c. Also, the VSWRs with $\Gamma_s = \Gamma_{\text{opt}} = 0.41 \angle -150^\circ$ and $\Gamma_L = 0.133 \angle 152.23^\circ$ are shown in Fig. 4.3.14c. The resulting noise figure is excessive at points a' and b' , and at $\Gamma_s = \Gamma_{\text{opt}}$ the input VSWR of 1.83 is too large.

The noise figure can be lowered by selecting a value of Γ_s close to Γ_{opt} that results in $(\text{VSWR})_{\text{in}} \leq 1.5$. To this end, we draw the constant $(\text{VSWR})_{\text{in}} = 1.5$ circle associated with point b' in Fig. 4.3.14b. That is, with $\Gamma_{\text{IN}} = 0.603 \angle 141.77^\circ$ and $|\Gamma_a| = 0.2$, it follows that the center and radius of the $(\text{VSWR})_{\text{in}} = 1.5$ circle are $C_{V_i} = 0.587 \angle -141.77^\circ$ and $r_{V_i} = 0.129$.

Figure 4.3.14b shows that selecting Γ_s at point c —namely, $\Gamma_s = 0.465 \angle -146^\circ$ —results in $(\text{VSWR})_{\text{in}} = 1.5$ with a noise figure of $F = 1.2$ dB. It also follows that $\Gamma_{\text{OUT}} = 0.484 \angle -140.64^\circ$ and $(\text{VSWR})_{\text{out}} = 2.2$. Hence, the design requirements are satisfied with Γ_s selected at point c . The block diagram of the amplifier is shown in Fig. 4.3.14d.

In the case of a two-stage (or n -stage) amplifier, (4.2.8) shows that the stage with the lowest M should be first. Also, (4.2.8) expresses the fact that the lowest total noise figure is not obtained with $\Gamma_s = \Gamma_{\text{opt}}$ in each stage but with a

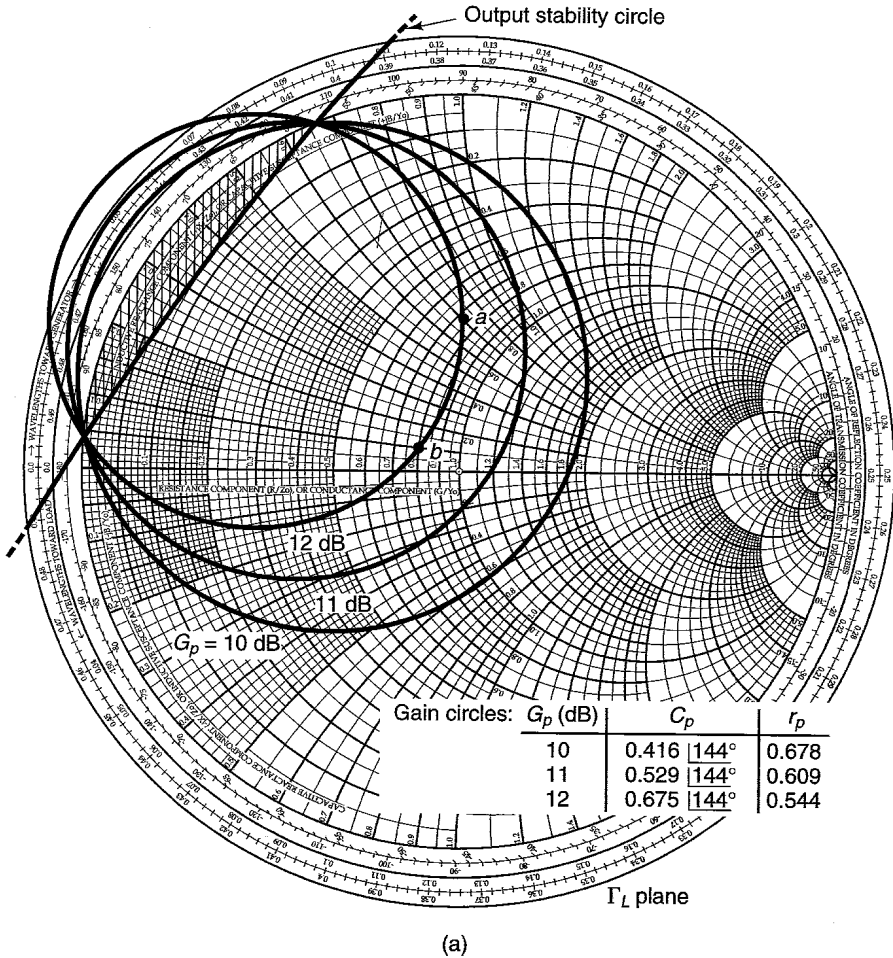
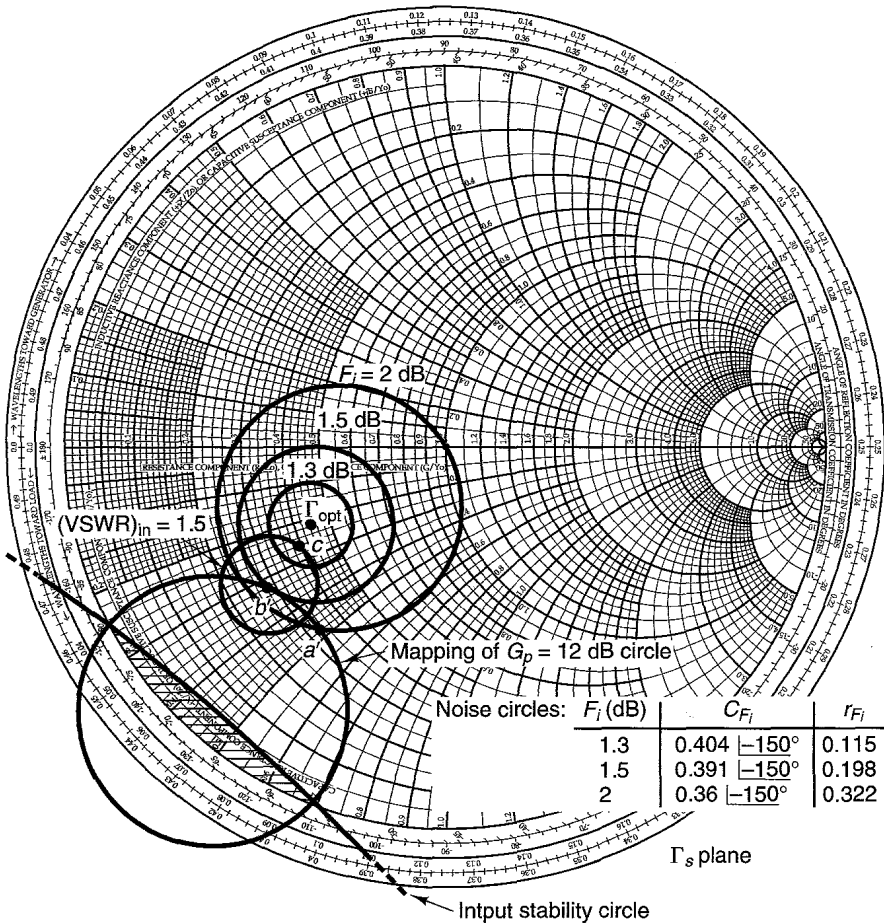


Figure 4.3.14 (a) Output stability circle and gain circles; (b) input stability circle, noise circles, mapping of the $G_p = 12$ dB circle and $(VSWR)_{in} = 1.5$ circle; (c) calculations of VSWRs and noise figure at points *a* and *b*; (d) block diagram of the amplifier.

value of Γ_s , that minimizes each stage noise measure. In most designs, the values of G_A are sufficiently large so that the value of $\Gamma_s = \Gamma_{opt}$ that minimizes a given stage noise figure also minimizes its noise measure.

In a design where G_A is low and the transistor is unconditionally stable, an analytical method that works well for the selection of Γ_s is to plot Γ_{opt} and Γ_{Ms} for the amplifier in the Smith chart, then draw a straight line from Γ_{opt} to Γ_{Ms} , and divide the line in several equal increments (e.g., three or four). Then calculate for each Γ_s on the line the values of M , G_A , and $(VSWR)_{in}$



(b)

Figure 4.3.14 Continued

and select the value of Γ_s that produces the best compromise between M , G_A , and $(VSWR)_{in}$.

For those who have access to a CAD program, a preliminary design can simply be done by selecting $\Gamma_s = \Gamma_{opt}$ in each stage and letting the program optimize the component values for the desired noise figure, gain, and VSWR performances.

For those interested, the relation for the value of Γ_s that minimizes M , as well as the constant noise measure circles, can be found in the papers by Fukui [4.4] and Poole and Paul [4.5]. The derivation of these results is involved.

Γ_L	$\Gamma_s = \Gamma_{IN}^*$	$(VSWR)_{in}$	F (dB)	Γ_{OUT}	$ \Gamma_b $	$(VSWR)_{out}$
0.397 $\angle 90.3^\circ$	0.580 $\angle -124.95^\circ$	1	1.8	0.632 $\angle -130.67^\circ$	0.507	3.06
0.133 $\angle 152.23^\circ$	0.603 $\angle -141.77^\circ$	1	1.6	0.598 $\angle -144.76^\circ$	0.506	3.05

Γ_L	$\Gamma_s = \Gamma_{opt}$	$ \Gamma_a $	$(VSWR)_{in}$	F (dB)	Γ_{OUT}	$ \Gamma_b $	$(VSWR)_{out}$
0.133 $\angle 152.23^\circ$	0.41 $\angle -150^\circ$	0.293	1.83	1.2	0.44 $\angle -139.13^\circ$	0.331	1.99

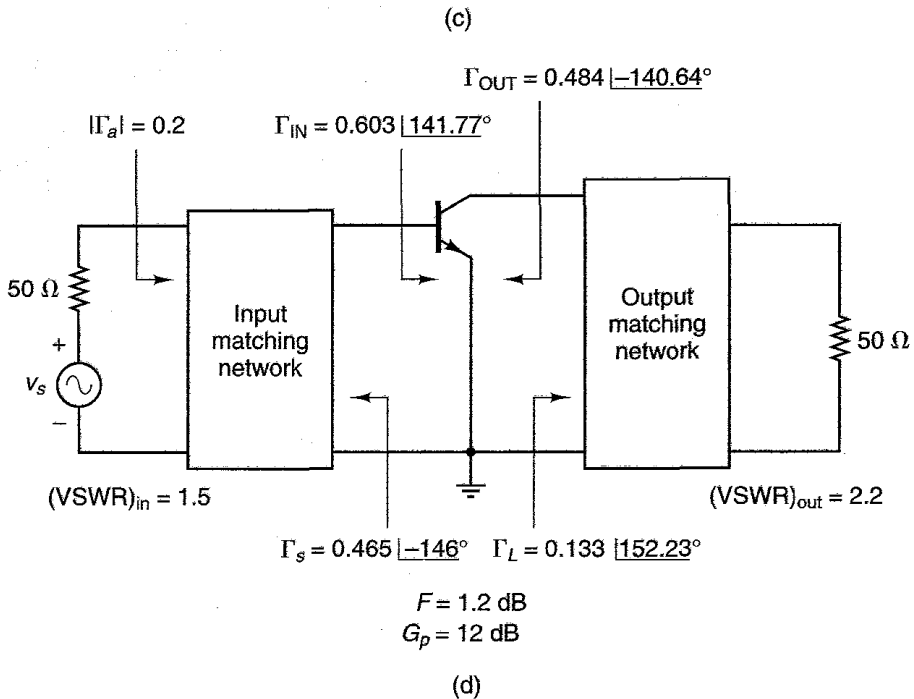


Figure 4.3.14 Continued

Example 4.3.6

(a) A suggested 4-GHz amplifier configuration in the *Avantek Microwave Semiconductors Data Book 1989* is shown in Fig. 4.3.15. This type of configuration is commonly called a low-noise block (LNB). It consists of a three-stage low-noise amplifier (LNA) section followed by a down-converter mixer and by an amplifier. Calculate the total noise figure and the available gain.

(b) Repeat the calculations in part (a) for the 12-GHz LNB shown in Fig. 4.3.16.

Solution. (a) The available gain of the LNA section is

$$G_A \text{ (dB)}|_{\text{LNA section}} = G_{A1} \text{ (dB)} + G_{A2} \text{ (dB)} + G_{A3} \text{ (dB)} = 15 + 15 + 14 = 44 \text{ dB}$$

and the available gain of the LNB is

$$G_A \text{ (dB)} = G_A \text{ (dB)}|_{\text{LNA section}} + G_{A4} \text{ (dB)} + G_{A5} \text{ (dB)} = 44 + 9 + 14 = 67 \text{ dB}$$

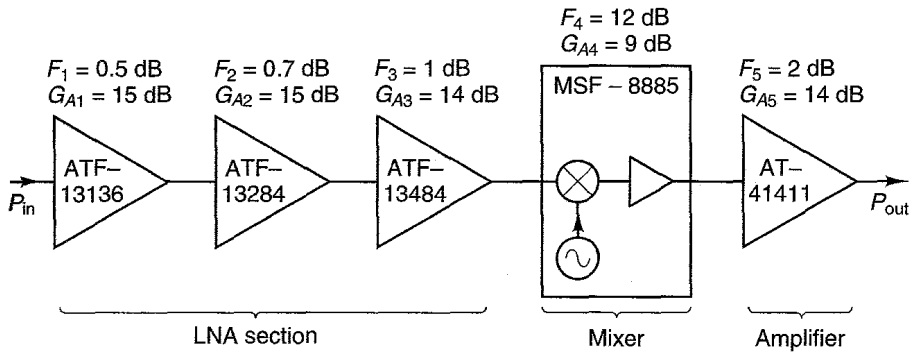


Figure 4.3.15 A 4-GHz LNB consisting of two low-noise GaAs FET amplifiers using the ATF-13136 and ATF-13284 transistors, a general purpose GaAs FET amplifier using the ATF-13484 transistor, an active mixer MMIC using the MSF-8885, and a BJT amplifier using the AT-41411 transistor.

The noise figure of the LNA section is

$$F|_{\text{LNA section}} = F_1 + \frac{F_2 - 1}{G_{A1}} + \frac{F_3 - 1}{G_{A1}G_{A2}} = 1.122 + \frac{1.175 - 1}{31.62} + \frac{1.259 - 1}{31.62(31.62)} = 1.127 \text{ (or 0.52 dB)}$$

and the total noise figure of the LNB is

$$F = F|_{\text{LNA section}} + \frac{F_4 - 1}{G_{A1}G_{A2}G_{A3}} + \frac{F_5 - 1}{G_{A1}G_{A2}G_{A3}G_{A4}} \approx 1.127 \text{ (or 0.52 dB)}$$

For this LNB the total noise figure is basically determined by the noise figure of the first stage of the LNA section (i.e., 0.5 dB). The contribution to the total noise from the second through the fourth stages is only 0.02 dB.

(b) In Fig. 4.3.16, the available gain of the LNA section is

$$G_A \text{ (dB)}|_{\text{LNA section}} = G_{A1} \text{ (dB)} + G_{A2} \text{ (dB)} + G_{A3} \text{ (dB)} = 9.5 + 9 + 9 = 27.5 \text{ dB}$$

and the available gain of the LNB is

$$G_A \text{ (dB)} = G_A \text{ (dB)}|_{\text{LNA section}} + G_{A4} \text{ (dB)} + G_{A5} \text{ (dB)} + G_{A6} \text{ (dB)} + G_{A7} \text{ (dB)} = 27.5 - 7 + 14 + 14 + 14 = 62.5 \text{ dB}$$

Observe that the mixer used in Fig. 4.3.16 introduces a gain loss (i.e., $G_{A4} = -7$ dB).

The noise figure of the LNA section is

$$F|_{\text{LNA section}} = F_1 + \frac{F_2 - 1}{G_{A1}} + \frac{F_3 - 1}{G_{A1}G_{A2}} = 1.318 + \frac{1.38 - 1}{8.913} + \frac{1.514 - 1}{8.913(7.943)} = 1.368 \text{ (or 1.36 dB)}$$

and the total noise figure of the LNB is

$$F = F|_{\text{LNA section}} + \frac{F_4 - 1}{G_{A1}G_{A2}G_{A3}} + \dots + \frac{F_7 - 1}{G_{A1}G_{A2} \dots G_{A6}} \approx 1.39 \text{ (or 1.43 dB)}$$

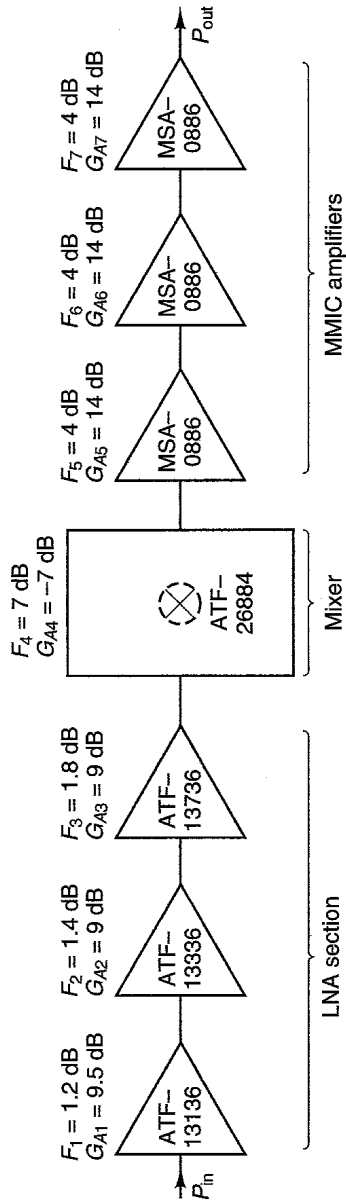


Figure 4.3.16 A 12-GHz LNB consisting of two low-noise GaAs FET amplifiers using the ATF-13136 and ATF-13336 transistors, a general purpose GaAs FET amplifier using the ATF-13736 transistor, a mixer using a GaAs FET (ATF-26884) for the oscillator, and three MMIC amplifiers (MSA-0886).

4.4 BROADBAND AMPLIFIER DESIGN

The design of broadband amplifiers introduces new difficulties which require careful considerations. Basically, the design of a constant-gain amplifier over a broad frequency range is a matter of properly designing the matching networks, or the feedback network, in order to compensate for the variations of $|S_{21}|$ with frequency. The design specifications might require the use of rather sophisticated synthesis procedures in the design of the matching networks.

Some of the difficulties encountered in the design of a broadband amplifier are:

1. The variations of $|S_{21}|$ and $|S_{12}|$ with frequency. Typically, $|S_{21}|$ decreases with frequency at the rate of 6 dB/octave and $|S_{12}|$ increases with frequency at the same rate. Typical variations of $|S_{21}|$, $|S_{12}|$, and $|S_{12}S_{21}|$ with frequency are illustrated in Fig. 1.10.3. The variations of $|S_{12}S_{21}|$ with frequency are important since the stability of the circuit depends on this quantity. It is in the flat region that we have to check the amplifier stability.
2. The scattering parameters S_{11} and S_{22} are also frequency dependent and their variations are significant over a broad range of frequencies.
3. There is a degradation of the noise figure and VSWR in some frequency range of the broadband amplifier.

Two techniques that are commonly used to design broadband amplifiers are (1) the use of compensated matching networks and (2) the use of negative feedback.

The technique of compensated matching networks involves mismatching the input and output matching networks to compensate for the changes with frequency of $|S_{21}|$. The matching networks are designed to give the best input and output VSWR. However, because of the broad bandwidth the VSWR will be optimum around certain frequencies, and a balanced amplifier design may be required.

The design of compensated matching networks can be done in analytical form with the help of the Smith chart. However, the use of a computer is usually required because of the complex analytical procedures. Of course, the use of a proper analytical procedure produces a starting design which can be optimized using computer-aided design (CAD) methods.

The matching networks can also be designed using network synthesis techniques. Passive network synthesis for the design of networks using lumped elements is well developed, and the techniques to implement the filter with microwave components are also well known [4.6, 4.7, 4.8, 4.9]. The microwave filters typically operate between two different impedances and must provide a prescribed insertion loss and bandwidth.

Synthesis methods usually produces a lumped-element network with the desired frequency characteristics. Then, certain transformations and manipulations (such as the Richard's transformation and Kuroda's identities) [4.8] are used to transform the lumped-element design to a microstrip implementation (or other desired implementation).

An interesting method for broadband amplifier design suitable to CAD has been developed by Mellor [4.10]. The broadband design involves the use of an interstage matching network. The amplifier schematic is shown in Fig. 4.4.1.

Transistors Q_1 and Q_2 have a gain that decreases with increasing frequency. The specifications for a good input and output match will require that the input and output matching networks have a constant gain over the frequency range of the amplifier (i.e., a flat frequency response). The interstage matching network must provide a gain having a positive slope with increasing frequency to compensate for the transistor roll-off and, therefore, to give an overall flat frequency response. The synthesis approach involves modeling the transistors with lumped elements and using an insertion-loss method to obtain the matching networks. The design of a broadband amplifier for a specific gain and noise figure requires, in general, the use of CAD techniques.

There are several CAD programs for synthesis of matching networks with prescribed responses. One such program is available from EAGLEWARE CORP. [4.11]. Another program is found in the software and user's manual by Sussman-Fort [4.12].

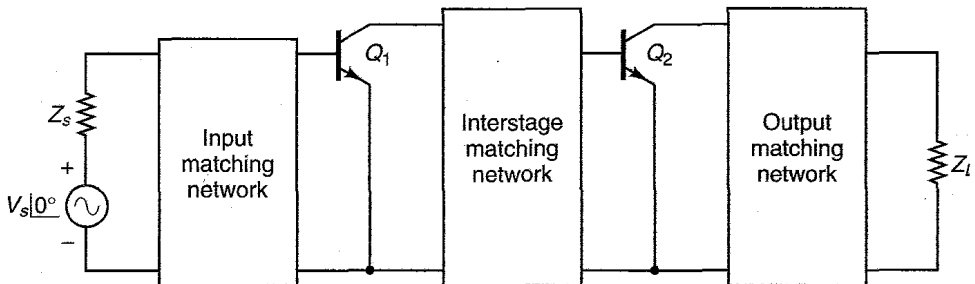


Figure 4.4.1 Broadband amplifier schematic.

Example 4.4.1

The S parameters of a BJT are given in Fig. 4.4.2. Design a broadband amplifier with a transducer power gain of 10 dB in the frequency range 300 to 700 MHz. (This example is based on a design from Hewlett-Packard Application Note 94-1 [4.13].)

Solution. The values in Fig. 4.4.2 show that

$$\begin{aligned} |S_{21}|^2 &= 13 \text{ dB at } 300 \text{ MHz} \\ &= 10 \text{ dB at } 450 \text{ MHz} \\ &= 6 \text{ dB at } 700 \text{ MHz} \end{aligned}$$

Therefore, in order to compensate for the variations of $|S_{21}|$, the matching networks must decrease the gain by 3 dB at 300 MHz and 0 dB at 450 MHz, and increase the gain by 4 dB at 700 MHz.

f (MHz)	S_{11}	S_{21}	S_{22}
300	0.3 $\angle -45^\circ$	4.47 $\angle 40^\circ$	0.86 $\angle -5^\circ$
450	0.27 $\angle -70^\circ$	3.16 $\angle 35^\circ$	0.855 $\angle -14^\circ$
700	0.2 $\angle -95^\circ$	2.0 $\angle 30^\circ$	0.85 $\angle -22^\circ$

Figure 4.4.2 Scattering parameters of a BJT.

For this transistor

$$G_{s,\max} = \frac{1}{1 - |S_{11}|^2} = \begin{cases} 0.409 \text{ dB at 300 MHz} \\ 0.329 \text{ dB at 450 MHz} \\ 0.177 \text{ dB at 700 MHz} \end{cases}$$

and little is to be gained by matching the source. Therefore, only the output matching network needs to be designed. Observe that $|S_{22}| \approx 0.85$ over the frequency range. Therefore,

$$G_{L,\max} = \frac{1}{1 - |S_{22}|^2} = 5.6 \text{ dB}$$

and the gain of 4 dB from G_L at 700 MHz is possible.

The output matching network is designed by plotting the constant-gain circles for $G_L = -3$ dB at 300 MHz, $G_L = 0$ dB at 450 MHz, and $G_L = 4$ dB at 700 MHz (see Fig. 4.4.3). The matching networks must transform the 50- Ω load to some point on the -3 -dB circle at 300 MHz, to some point on the 0-dB circle at 450 MHz, and to some point on the 4-dB gain circle at 700 MHz. Of course, there are many matching networks that can perform the required transformation. The matching network selected is an EII network consisting of a shunt and series inductor combination (see Fig. 4.4.4).

The shunt inductor susceptance decreases with frequency and transforms the 50- Ω load along the constant-conductance circle, as shown in Fig. 4.4.3. The series inductor reactance increases with frequency and transforms the parallel combination of 50 Ω and shunt inductance along a constant-resistance circle, as shown in Fig. 4.4.3. Optimizing the values of L_1 and L_2 is a trial-and-error procedure. The graphical construction is illustrated in Fig. 4.4.3, and the final ac schematic of the amplifier is shown in Fig. 4.4.4.

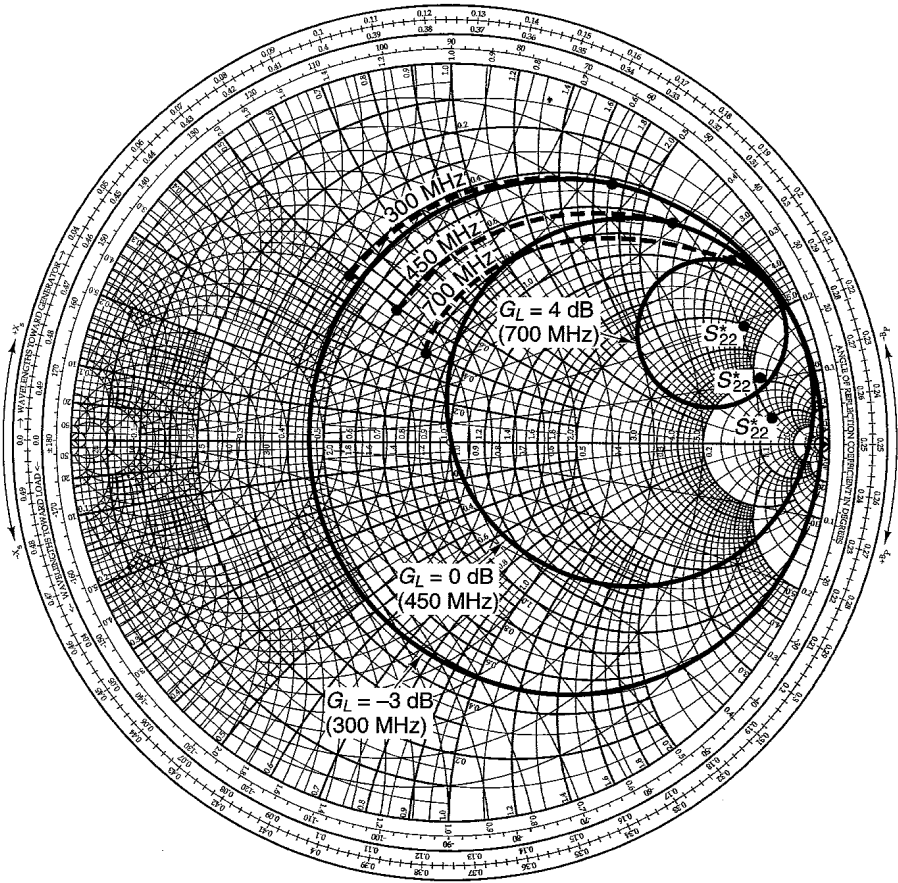
Figure 4.4.3 shows the trial that produced the desired matching at 300 MHz, 450 MHz, and 700 MHz. The values of L_1 and L_2 were calculated at 300 MHz as follows:

$$y_{L_1} = -j1.2 = \frac{-jZ_o}{\omega L_1} = \frac{-j50}{2\pi(300 \times 10^6)L_1} \Rightarrow L_1 = 22.1 \text{ nH}$$

and

$$z_{L_2} = j(1.7 - 0.5) = \frac{j\omega L_2}{Z_o} = \frac{j2\pi(300 \times 10^6)L_2}{50} \Rightarrow L_2 = 31.8 \text{ nH}$$

Then, it is simple to verify that at 450 MHz the output matching network in Fig. 4.4.4 with $L_1 = 22.1$ nH and $L_2 = 31.8$ nH produces a load reflection coefficient on the $G_L = 0$ dB gain circle, as shown in Fig. 4.4.3. Similarly, at 700 MHz the load reflection coefficient is on the $G_L = 4$ dB gain circle, as shown in Fig. 4.4.3.



G_L constant-gain circles calculations

F (MHz)	Center	Radius
300	0.31	0.68
450	0.49	0.49
700	0.76	0.2

Figure 4.4.3 Broadband design in the Smith chart.

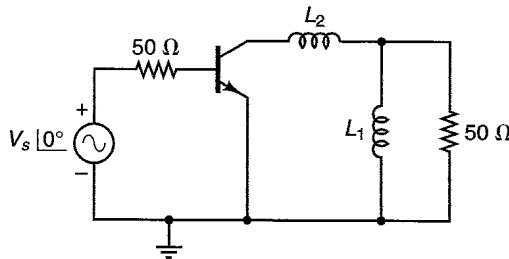


Figure 4.4.4 The ac schematic of the broadband amplifier.

At the input, the direct connection of the 50-Ω source resistor to the base of the transistor results in $G_s = 0$ dB and an input VSWR smaller than 1.86 [i.e., $(1 + 0.3)/(1 - 0.3) = 1.86$]. The VSWR can be improved by matching the 50-Ω source to S_{11} over the frequency band. The corresponding improvement in gain is small since $G_{s,max} = 0.409$ dB at $f = 300$ MHz.

Balanced Amplifiers

The design of compensated matching networks to obtain gain flatness results in impedance mismatching that can significantly degrade the input and output VSWR. The use of balanced amplifiers is a practical method for implementing a broadband amplifier that has flat gain and good input and output VSWR. The most popular arrangement of a balanced amplifier, shown in Fig. 4.4.5, uses two 3-dB hybrid couplers.

The input coupler is also known as a 3-dB power divider and the output coupler as a 3-dB power combiner. Two microstrip realizations of a 3-dB hybrid coupler are the 3-dB *Lange coupler* (shown in Fig. 4.4.6) and the 3-dB *branch-line coupler* (shown in Fig. 4.4.7). The theory and design of couplers is discussed in the texts by Rizzi [4.14], Elliott [4.8], and Ha [4.6].

In the Lange coupler, bonding wires are used to interconnect the microstrip lines. The design of a 3-dB Lange coupler involves specifications of the microstrip substrate, the spacing d , and the microstrip width w . The length $l = \lambda/4$ at the center frequency of operation produces output signals at terminals 2 and 3 that are 90° out of phase. Practical design relations for the Lange coupler have been obtained by Presser [4.15].

The design equations for the $\lambda/4$ branch-line coupler in Fig. 4.4.7. are

$$C = 10 \log \frac{1}{1 - \left(\frac{Z_{o1}}{Z_o}\right)^2} \tag{4.4.1}$$

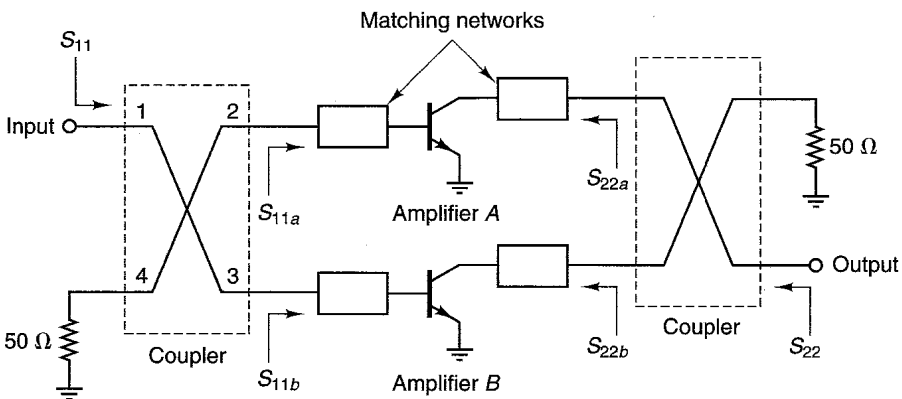


Figure 4.4.5 Balanced amplifier configuration.

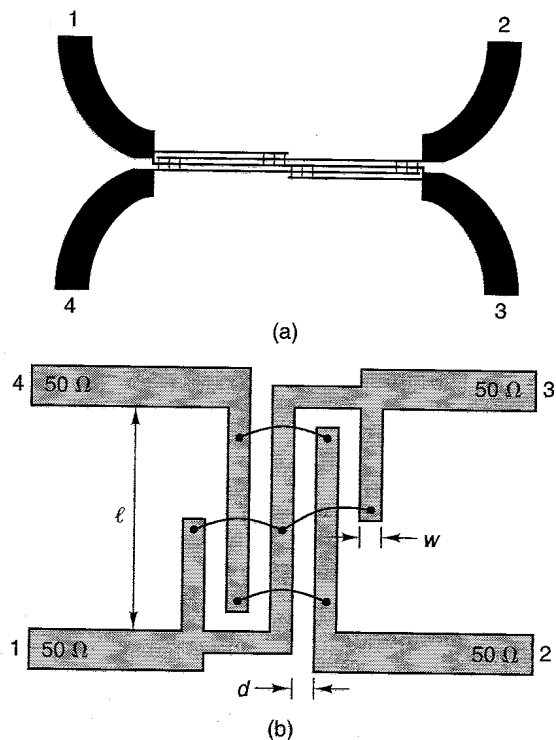


Figure 4.4.6 (a) A 3-dB Lange coupler. (From J. Lange [4.16]; copyright 1969, IEEE; reproduced with permission of IEEE.) (b) Another microstrip implementation of the 3-dB Lange coupler showing the bonding wires.

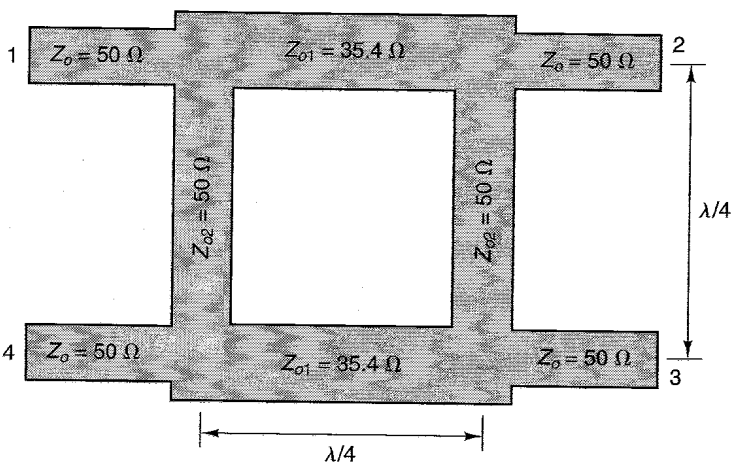


Figure 4.4.7 A 3-dB microstrip branch-line coupler.

and

$$\frac{Z_{o2}}{Z_o} = \frac{\frac{Z_{o1}}{Z_o}}{\sqrt{1 - \left(\frac{Z_{o1}}{Z_o}\right)^2}} \tag{4.4.2}$$

where C is the coupling coefficient. For $C = 3$ dB and with $Z_o = 50 \Omega$, it follows from (4.4.1) and (4.4.2) that $Z_{o1} = Z_o/\sqrt{2} = 35.4 \Omega$ and $Z_{o2} = Z_o = 50 \Omega$.

In Fig. 4.4.7, with $l = \lambda/4$ and 50- Ω terminations at ports 2, 3, and 4, the input power at port 1 divides equally between ports 2 and 3, with zero power at port 4 (i.e., port 4 is isolated). Specifically, the operation of the couplers is as follows. With an input source of 50- Ω impedance applied to port 1, and with ports 2, 3, and 4 terminated in 50 Ω , the incident wave a_1 at port 1 appears as $a_1 e^{-j\pi/2}/\sqrt{2}$ at port 2 and as $a_1 e^{-j\pi}/\sqrt{2}$ at port 3. Port 1 sees a matched input impedance (i.e., 50 Ω), and the phase shift between ports 2 and 3 is $\pi/2$. From the symmetry of the couplers, it also follows that after exciting port 2, the signal power divides and couples to port 1 and 4; exciting port 3, the signal power divides and couples to ports 4 and 1; and exciting port 4, the signal power divides and couples to ports 3 and 2. The driven port sees a matched impedance when the other ports are terminated in their matched impedances (i.e., in 50 Ω). The S parameter matrix of the coupler is

$$[S] = \begin{bmatrix} 0 & \frac{e^{-j\pi/2}}{\sqrt{2}} & \frac{e^{-j\pi}}{\sqrt{2}} & 0 \\ \frac{e^{-j\pi/2}}{\sqrt{2}} & 0 & 0 & \frac{e^{-j\pi}}{\sqrt{2}} \\ \frac{e^{-j\pi}}{\sqrt{2}} & 0 & 0 & \frac{e^{-j\pi/2}}{\sqrt{2}} \\ 0 & \frac{e^{-j\pi}}{\sqrt{2}} & \frac{e^{-j\pi/2}}{\sqrt{2}} & 0 \end{bmatrix}$$

When a 3-dB coupler is used in a balanced amplifier, port 4 is terminated in $Z_o = 50 \Omega$. Then the coupler becomes a three-port divider/combiner whose S parameters are

$$[S] = \begin{bmatrix} 0 & \frac{e^{-j\pi/2}}{\sqrt{2}} & \frac{e^{-j\pi}}{\sqrt{2}} \\ \frac{e^{-j\pi/2}}{\sqrt{2}} & 0 & 0 \\ \frac{e^{-j\pi}}{\sqrt{2}} & 0 & 0 \end{bmatrix}$$

The S parameters of the coupler show that when used as as divider with incident wave a_1 at port 1 and with $a_2 = a_3 = 0$, the output waves at ports 2 and

3 are $b_2 = a_1 e^{-j\pi/2}/\sqrt{2}$ and $b_3 = a_1 e^{-j\pi}/\sqrt{2}$, respectively. These output waves have equal amplitude and phase difference of $\pi/2$. Hence, the power delivered to 50- Ω terminations at ports 2 and 3 is $|b_2|^2 = |b_3|^2 = |a_1|^2/2$. That is, the output power is half of the input power (i.e., a 3-dB coupler).

When used as a combiner with incident waves at ports 2 and 3 of equal amplitudes and phase difference of $\pi/2$ (i.e., with $a_3 = a_2 e^{j\pi/2}$), the output at port 1 is

$$b_1 = \frac{e^{-j\pi/2}}{\sqrt{2}} (a_2 + a_3 e^{-j\pi/2}) = \frac{e^{-j\pi/2}}{\sqrt{2}} (2a_2)$$

Hence, the power delivered to a 50- Ω termination at port 1 is $|b_1|^2 = 2|a_2|^2$, which is twice the input power at port 2 (or port 3).

When port 1 is excited, port 4 is terminated in $Z_o = 50 \Omega$, and ports 2 and 3 are connected to amplifiers with input reflection coefficients S_{11a} and S_{11b} , the reflected voltages $a_1 e^{-j\pi/2}/\sqrt{2} S_{11a}$ and $a_1 e^{-j\pi}/\sqrt{2} S_{11b}$ are generated at ports 2 and 3, respectively, which travel back to port 1. Hence, the total reflected signal at port 1 is

$$b_1 = \frac{a_1}{2} e^{-j\pi} S_{11a} + \frac{a_1}{2} S_{11b} = \frac{a_1}{2} e^{-j\pi} (S_{11a} - S_{11b})$$

and the S_{11} parameter at port 1 is

$$S_{11} = \frac{e^{-j\pi}}{2} (S_{11a} - S_{11b})$$

In the balanced amplifier shown in Fig. 4.4.5, the input 3-dB coupler divides the input power equally to amplifiers *A* and *B*, and the output 3-dB coupler combines the output signals from the amplifiers. It follows that the S parameters of the balanced amplifier, where the input and output ports are indicated in Fig. 4.4.5, are

$$S_{11} = \frac{e^{-j\pi}}{2} (S_{11a} - S_{11b})$$

$$S_{21} = \frac{e^{-j\pi/2}}{2} (S_{21a} + S_{21b})$$

$$S_{12} = \frac{e^{-j\pi/2}}{2} (S_{12a} + S_{12b})$$

and

$$S_{22} = \frac{e^{-j\pi}}{2} (S_{22a} - S_{22b})$$

Hence,

$$\begin{aligned}
 |S_{11}| &= 0.5|S_{11a} - S_{11b}| \\
 |S_{21}| &= 0.5|S_{21a} + S_{21b}| \\
 |S_{12}| &= 0.5|S_{12a} + S_{12b}| \\
 |S_{22}| &= 0.5|S_{22a} - S_{22b}|
 \end{aligned}
 \tag{4.4.3}$$

If the two amplifiers are identical, then $S_{11} = 0$ and $S_{22} = 0$ and the gain S_{21} (and also S_{12}) is equal to the gain of one side of the coupler. The bandwidth of the balanced amplifier is limited by the bandwidth of the coupler (about two octaves).

The advantages of the balanced amplifier configuration are many:

1. The individual amplifiers can be designed for flat gain, noise figure, and so on (even if the individual amplifier VSWR is high), with the balanced amplifier input and output VSWR dependent on the coupler (i.e., ideally the VSWR is 1 if the amplifiers are identical).
2. There is a high degree of stability.
3. The output power is twice that obtained from the single amplifier.
4. If one of the amplifiers fails, the balanced amplifier unit will still operate with reduced gain (i.e., the power gain decreases by about 6 dB).
5. Balanced amplifier units are easy to cascade with other units, since each unit is isolated by the coupler.

The disadvantages of the balanced amplifier configuration are that the unit uses two amplifiers, consumes more dc power, and is larger. Also, in practice there is a finite insertion loss associated with the amplifiers.

Example 4.4.1

The balanced amplifier shown in Fig. 4.4.5 is terminated at the output port in 50Ω , and the source resistance at the input port is 50Ω . The S parameters of amplifiers A and B are

Amplifier A	Amplifier B
$S_{11a} = 0.3 \angle -120^\circ$	$S_{11b} = 0.32 \angle -123^\circ$
$S_{12a} = 0.1 \angle -25^\circ$	$S_{12b} = 0.09 \angle -27^\circ$
$S_{21a} = 3.5 \angle 120^\circ$	$S_{21b} = 3.7 \angle 117^\circ$
$S_{22a} = 0.4 \angle 25^\circ$	$S_{22b} = 0.42 \angle 28^\circ$

(a) Determine the input reflection coefficient S_{11} , the input VSWR, the output reflection coefficient S_{22} , and the output VSWR.

(b) Calculate the power gain.

(c) Determine the power gain if amplifier B fails completely.

Solution. (a) The input reflection coefficient is

$$S_{11} = \frac{e^{-j\pi}}{2} (S_{11a} - S_{11b}) = \frac{e^{-j\pi}}{2} (0.3 \angle -120^\circ - 0.32 \angle -123^\circ) = 0.013 \angle -160.6^\circ$$

and $(VSWR)_{in}$ is

$$(VSWR)_{in} = \frac{1 + |S_{11}|}{1 - |S_{11}|} = \frac{1 + 0.013}{1 - 0.013} = 1.03$$

Similarly, the output reflection coefficient and $(VSWR)_{out}$ are

$$S_{22} = \frac{e^{-j\pi}}{2} (S_{22a} - S_{22b}) = \frac{e^{-j\pi}}{2} (0.4 \angle 25^\circ - 0.42 \angle 28^\circ) = 0.015 \angle 73.5^\circ$$

and

$$(VSWR)_{out} = \frac{1 + |S_{22}|}{1 - |S_{22}|} = \frac{1 + 0.015}{1 - 0.015} = 1.03$$

(b) The transducer power gain is

$$G_T = |S_{21}|^2 = (0.5)^2 |3.5 \angle 120^\circ + 3.7 \angle 117^\circ|^2 = 12.95 \text{ (or 11.12 dB)}$$

(c) If amplifier B fails to operate, the transducer power gain is

$$G_T = (0.5)^2 |S_{21a}|^2 = (0.5)^2 (3.5)^2 = 3.06 \text{ (or 4.9 dB)}$$

Hence, the gain is decreased by approximately 6 dB.

Another type of power divider/combiner that can be used in a balanced amplifier is the 3-dB Wilkinson coupler. The 3-dB Wilkinson coupler is shown in Fig. 4.4.8. It is a three-port network that divides equally the input power at port 1 between ports 2 and 3, when the ports are terminated in $Z_o = 50 \Omega$. The signals at ports 2 and 3 are of equal amplitude and phase.

The operation of the Wilkinson coupler is as follows. When ports 2 and 3 are terminated in 50Ω , the input port 1 should see an input impedance of 50Ω

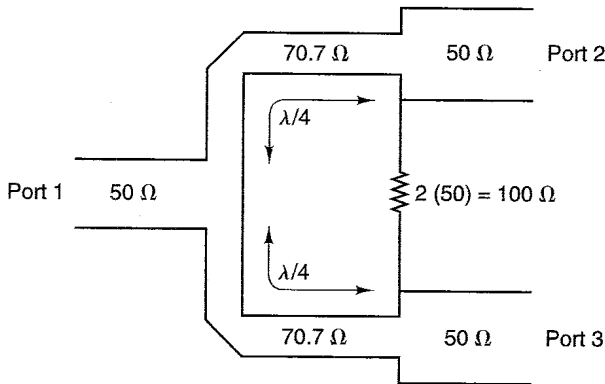


Figure 4.4.8 Microstrip implementation of a Wilkinson coupler.

(i.e., the input port 1 is matched). Therefore, each $\lambda/4$ line transforms the $50\ \Omega$ termination to an input impedance of $100\ \Omega$. Then port 1 sees $100\ \Omega$ in parallel with $100\ \Omega$, which produces the desired $50\text{-}\Omega$ input impedance. The transformation of $50\ \Omega$ to $100\ \Omega$ by the $\lambda/4$ line is accomplished by selecting its characteristic impedance as $Z_o = \sqrt{100(50)} = 70.7\ \Omega$. No power is dissipated in the $100\text{-}\Omega$ resistor connected between ports 2 and 3 when equal loads are connected to ports 2 and 3.

When a mismatch occurs at an output port (e.g., at port 2), a reflected signal is generated which splits between the transmission line and the $100\text{-}\Omega$ resistor. These two signals appear at port 3 with a 180° phase shift, and cancellation occurs. The value of the resistor (i.e., $2Z_o = 100\ \Omega$) was selected so that the two parts of the reflected signal have equal amplitude and, therefore, perfect cancellation results. Similar considerations apply if a mismatch occurs at port 3. The scattering matrix of the Wilkinson coupler is

$$[S] = \begin{bmatrix} 0 & \frac{e^{-j\pi/2}}{\sqrt{2}} & \frac{e^{-j\pi/2}}{\sqrt{2}} \\ \frac{e^{-j\pi/2}}{\sqrt{2}} & 0 & 0 \\ \frac{e^{-j\pi/2}}{\sqrt{2}} & 0 & 0 \end{bmatrix}$$

The Wilkinson coupler can be used as a two-way combiner by applying the input signals at ports 2 and 3 and taking the output at port 1. If input signals are applied to ports 2 and 3 and port 1 is terminated in $50\ \Omega$, then the signal at port 1 is equal to $e^{-j\pi/2}(a_2 + a_3)/\sqrt{2}$. If $a_2 = a_3$, then the power delivered to a $50\text{-}\Omega$ termination at port 1 is $|b_1|^2 = 2|a_2|^2$. That is, the power at port 1 is twice the input power at port 2 (or at port 3).

A balanced amplifier using 3-dB Wilkinson couplers is shown in Fig. 4.4.9. Since the signals are in phase at the output of the input coupler, it is necessary to shift the phase of the signal before amplifier A_1 and the signal after amplifier A_2 by 90° in order for (4.4.3) to apply.

The bandwidth of the branch-line coupler and the Wilkinson coupler is limited by the frequency response of the $\lambda/4$ lines. In general, the bandwidth is about 50% of the center frequency. Another practical limitation of the branch-line coupler and the Wilkinson coupler is that they occupy more space than the Lange coupler. Large bandwidths extending to a decade can be obtained using a multisection Wilkinson coupler [4.17].

Feedback Amplifiers

Negative feedback can be used in broadband amplifiers to provide a flat gain response and to reduce the input and output VSWR. It also controls the amplifier performance due to variations in the S parameters from transistor to

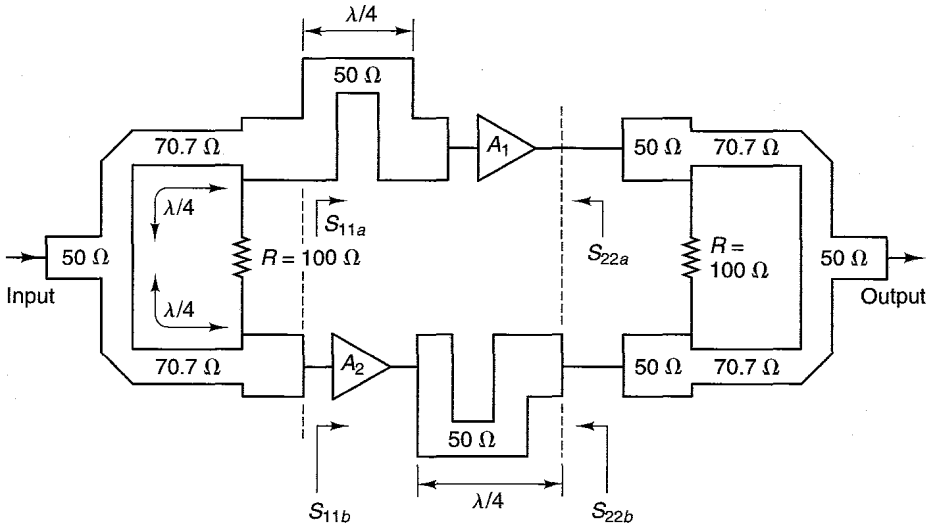


Figure 4.4.9 A balanced amplifier using 3-dB Wilkinson couplers.

transistor. As the bandwidth requirements of the amplifier approach a decade of frequency, gain compensation based on matching networks only is very difficult, and negative feedback techniques are used. In fact, a microwave transistor amplifier using negative feedback can be designed to have very wide bandwidths (greater than two decades) with small gain variations (tenths of a decibel). On the minus side, negative feedback will degrade the noise figure and reduce the maximum power gain available from a transistor.

The most common methods of applying negative feedback are by the series and shunt resistor feedback configurations shown in Fig. 4.4.10. The coupling capacitors and the dc bias network have been omitted.

The following simple analysis illustrates the use of negative feedback. The GaAs FET and BJT can be represented by the equivalent circuit shown in Fig. 4.4.11 when the parasitic elements can be neglected (i.e., at low frequencies). The resulting negative-feedback equivalent networks, including both series and shunt feedback, are shown in Fig. 4.4.12.

The admittance matrix for the network shown in Fig. 4.4.12a can be written in the form

$$\begin{bmatrix} i_1 \\ i_2 \end{bmatrix} = \begin{bmatrix} \frac{1}{R_2} & -\frac{1}{R_2} \\ \frac{g_m}{1 + g_m R_1} - \frac{1}{R_2} & \frac{1}{R_2} \end{bmatrix} \begin{bmatrix} v_1 \\ v_2 \end{bmatrix}$$

and a similar matrix can be written for Fig. 4.4.12b (assuming that $r_{b'e} + \beta R_1 \gg R_2$). Using Fig. 1.8.1 to convert from y parameters to S parameters gives

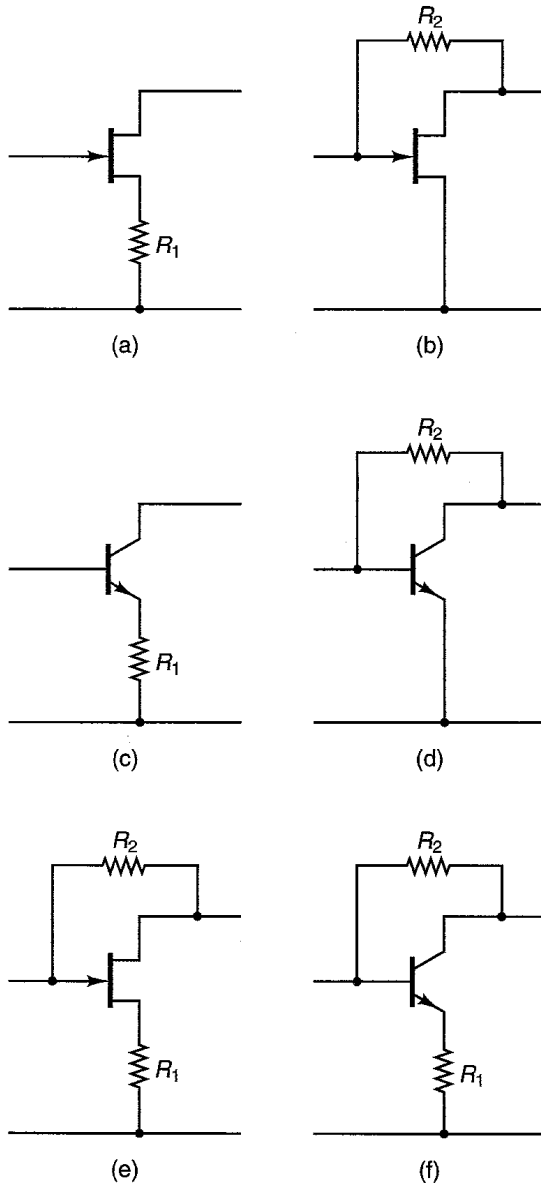


Figure 4.4.10 (a) GaAs FET with series feedback resistor; (b) GaAs FET with shunt feedback resistor; (c) BJT with series feedback resistor; (d) BJT with shunt feedback resistor; (e) GaAs FET with series-shunt feedback resistors; (f) BJT with series-shunt feedback resistors.

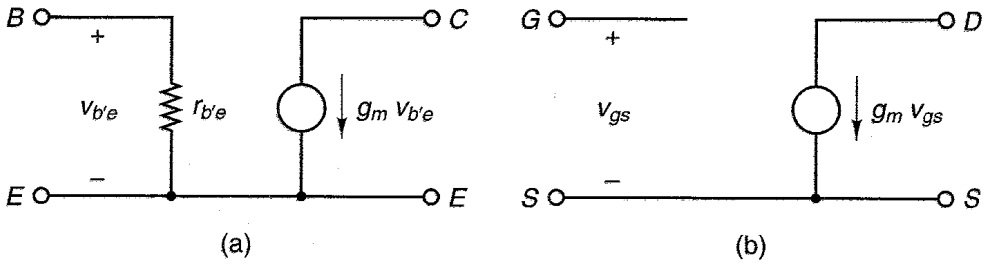


Figure 4.4.11 (a) BJT equivalent network; (b) GaAs FET equivalent network.

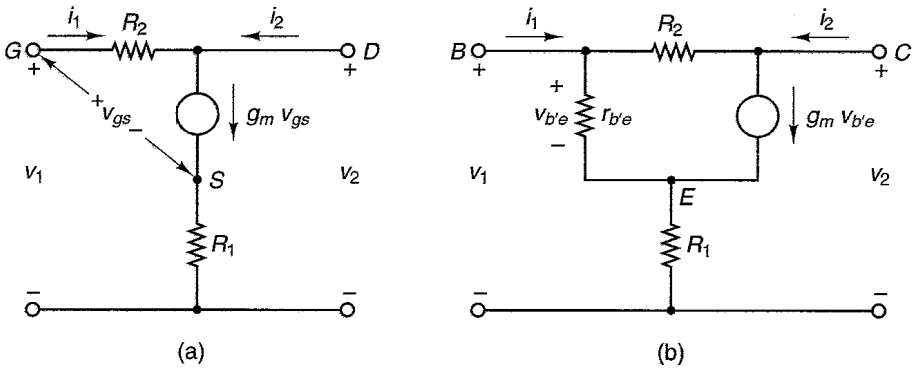


Figure 4.4.12 (a) GaAs FET negative-feedback model; (b) BJT negative-feedback model.

$$S_{11} = S_{22} = \frac{1}{D} \left[1 - \frac{g_m Z_o^2}{R_2(1 + g_m R_1)} \right] \tag{4.4.4}$$

$$S_{21} = \frac{1}{D} \left(\frac{-2g_m Z_o}{1 + g_m R_1} + \frac{2Z_o}{R_2} \right) \tag{4.4.5}$$

and

$$S_{12} = \frac{2Z_o}{DR_2} \tag{4.4.6}$$

where

$$D = 1 + \frac{2Z_o}{R_2} + \frac{g_m Z_o^2}{R_2(1 + g_m R_1)}$$

From (4.4.4), the conditions $S_{11} = S_{22} = 0$ (i.e., input and output VSWR = 1) are satisfied when

$$1 + g_m R_1 = \frac{g_m Z_o^2}{R_2}$$

or

$$R_1 = \frac{Z_o^2}{R_2} - \frac{1}{g_m} \quad (4.4.7)$$

Substituting (4.4.7) into (4.4.5) and (4.4.6) gives

$$S_{21} = \frac{Z_o - R_2}{Z_o} \quad (4.4.8)$$

and

$$S_{12} = \frac{Z_o}{R_2 + Z_o}$$

Equation (4.4.8) shows that S_{21} depends only on R_2 and not on the transistor parameters. Therefore, gain flattening can be achieved with negative feedback.

The shunt-feedback configurations in Figs. 4.4.10b and 4.4.10d can be analyzed by setting $R_1 = 0$ in the previous relations (for a BJT the condition $r_{b'e} \gg R_2$ must also be satisfied). Hence, from (4.4.7), with $R_1 = 0$ we obtain

$$g_m = \frac{R_2}{Z_o^2} \quad (4.4.9)$$

and from (4.4.8) we obtain

$$R_2 = Z_o(1 - S_{21}) \quad (4.4.10)$$

In a design, given the desired constant value of S_{21} , (4.4.10) is used to calculate R_2 , and (4.4.9) gives the required value of g_m for the transistor. If the transistor's g_m is different from the required value in (4.4.9), then S_{11} and S_{22} will not be exactly zero.

In the low-frequency models in Fig. 4.4.12, S_{21} is a negative number. Hence, (4.4.10) is commonly written as

$$R_2 = Z_o(1 + |S_{21}|)$$

For example, consider the design of the GaAs FET shunt feedback configuration in Fig. 4.4.10b for a transducer power gain of 10 dB in a 50- Ω system (i.e., $10 \log |S_{21}|^2 = 10$ dB or $S_{21} = -3.16$). Using (4.4.10), the required shunt feedback resistor is

$$R_2 = 50(1 + 3.16) = 208 \Omega$$

Then, from (4.4.9), the required value of g_m is

$$g_m = \frac{208}{50^2} = 83 \text{ mS}$$

The design of the BJT shunt feedback configuration in Fig. 4.4.10d is identical, provided that $r_{b'e} \gg R_2$. This condition places certain restrictions on the transistor's β and dc bias current.

Equation (4.4.10) is a well-known relation in feedback amplifiers. Consider the shunt feedback configuration shown in Fig. 4.4.13, where A_v is the voltage gain of the amplifier (A_v is a negative number) and the input current of the amplifier is negligible. Since

$$v_o = A_v v_1 \quad (4.4.11)$$

and

$$i_1 = \frac{v_1 - v_o}{R_2} \quad (4.4.12)$$

then substituting (4.4.11) into (4.4.12) gives

$$R_{in} = \frac{v_1}{i_1} = \frac{R_2}{1 - A_v} \quad (4.4.13)$$

If R_{in} is set equal to $Z_o = 50 \Omega$ and observing that $A_v = S_{21}$, it follows that (4.4.13) and (4.4.10) are identical.

In the general case that both series and shunt feedbacks are used (as shown in Fig. 4.4.12), R_2 is calculated using (4.4.8) and R_1 is calculated using (4.4.7). R_1 is positive if $(Z_o^2/R_2) \geq 1/g_m$. Hence, a minimum value of transconductance, denoted by $g_m(\min)$, is required. The minimum transconductance is given by

$$g_m(\min) = \frac{R_2}{Z_o^2}$$

Using (4.4.8), we can write

$$g_m(\min) = \frac{1 - S_{21}}{Z_o} \quad (4.4.14)$$

Any transistor having a g_m greater than $g_m(\min)$ can be used in the series-shunt feedback configuration.

When both R_1 and R_2 are used and g_m has a high value, (4.4.7) shows that the minimum input and output VSWR is obtained when $R_1 R_2 \approx Z_o^2$.

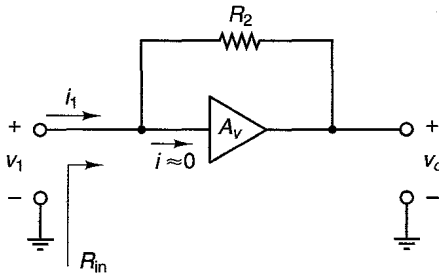


Figure 4.4.13 A shunt feedback configuration.

Example 4.4.2

Consider the series-shunt feedback configuration in Fig. 4.4.14. The S parameters of the BJT are fairly constant from 1 MHz to 10 MHz and are given by

f (in MHz)	S_{11}	S_{21}	S_{22}
1	$0.7 \angle 0^\circ$	$35 \angle 180^\circ$	$0.99 \angle 0^\circ$
10	$0.7 \angle 0^\circ$	$35 \angle 180^\circ$	$0.99 \angle 0^\circ$

Design the amplifier to have a constant transducer power gain of 10 dB in a 50- Ω system, with $(VSWR)_{in}$ and $(VSWR)_{out}$ equal to 1.

Solution. With no feedback applied the transducer power gain with 50- Ω terminations is $G_T = |S_{21}|^2 = 1225$ or 30.9 dB. Hence, the transistor is certainly capable of producing $G_T = 10$ dB with feedback. The value of $S_{11} = 0.7 \angle 0^\circ$ corresponds to an $r_{b'e}$ of 283 Ω , and $S_{22} = 0.99 \angle 0^\circ$ shows that r_{ce} is essentially an open circuit. The transconductance of the transistor is (see Example 1.11.1)

$$g_m = \frac{-S_{21}}{2Z_o} = \frac{35}{2(50)} = 350 \text{ mS}$$

Using (4.4.10) with $|S_{21}|^2 = 10$ dB or $S_{21} = -3.16$, we obtain

$$R_2 = 50(1 + 3.16) = 208 \Omega$$

Observe that the condition $r_{b'e} \gg R_2$ is not satisfied. Hence, the series feedback resistor R_1 in Fig. 4.4.14 is needed.

From (4.4.14), the minimum transconductance for a positive value of R_1 is

$$g_{m(\min)} = \frac{1 + 3.16}{50} = 83 \text{ mS}$$

Since the transistor's transconductance is greater than $g_{m(\min)}$, the value of R_1 , calculated using (4.4.7), is positive. That is,

$$R_1 = \frac{50^2}{208} - \frac{1}{0.350} = 9 \Omega$$

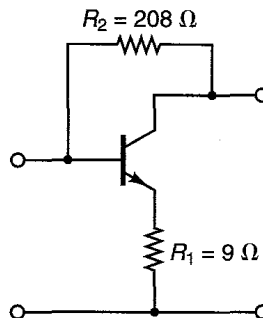


Figure 4.4.14 Feedback amplifier for Example 4.4.2.

For the feedback amplifier in Fig. 4.4.14 with $R_2 = 208 \Omega$ and $R_1 = 9 \Omega$, it follows that the S parameters from 1 MHz to 10 MHz are $S_{11} = -0.035$, $S_{21} = -3.16$, and $S_{22} = -0.007$. Hence, a constant gain of 10 dB with input and output VSWRs close to unity has been achieved.

The feedback analysis discussed in this section, although based on low-frequency models of the transistors, is useful in the design of microwave amplifiers. The low-frequency feedback analysis provides a preliminary design. Then, CAD methods can be used to calculate the S parameters of the transistor with the feedback network connected and to obtain the required Γ_s and Γ_L for optimum performance. Problem 4.20 considers the design of a 100 MHz to 1500 MHz BJT amplifier using series-shunt feedback. At microwave frequencies, the use of the series feedback resistor R_1 improves the amplifier stability; however, it also degrades the noise performance of the amplifier.

An important consideration in negative-feedback design is the phase of S_{21} . At low frequencies the phase of S_{21} is close to 180° , and as the frequency increases (above f_β) the phase of S_{21} varies rapidly. At some frequency the phase of S_{21} is such that a portion of the output voltage is in phase with the input voltage (i.e., positive feedback). This problem can be solved by decreasing the feedback when the phase shift of S_{21} approaches 90° . For example, in the case of shunt negative feedback (see Fig. 4.4.10), an inductor can be connected in series with R_2 such that after a certain frequency the negative feedback decreases in proportion to the S_{21} roll-off.

Example 4.4.3

Perform a preliminary analysis in the design of a BJT broadband amplifier having a transducer power gain of 10 dB from 10 to 1500 MHz. The S parameters of the transistor (in a 50- Ω system) at 10 V and 4 mA, the associated K factors, and $|S_{21}|^2$ in decibels (i.e., the transducer power gain in a 50- Ω system) are given in Fig. 4.4.15. (This example is based on a design from Ref. [4.18].)

Solution. The transistor is certainly capable of providing a transducer power gain of 10 dB. However, since $K < 1$, the transistor is potentially unstable and a stabil-

F (MHz)	S_{11}		S_{21}		S_{12}		S_{22}		$ S_{21} ^2$ (dB)	K
	Mag.	Ang.	Mag.	Ang.	Mag.	Ang.	Mag.	Ang.		
10	0.95	-2°	7.35	174.6°	0.003	84.3°	1.01	-1°	17.3	0.11
100	0.92	-11°	7.15	168.0°	0.007	79.0°	0.99	-4°	17.1	0.18
250	0.87	-28°	6.83	154.5°	0.015	69.2°	0.96	-10°	16.7	0.29
500	0.78	-54°	6.28	135.0°	0.026	54.0°	0.90	-18°	16.0	0.42
750	0.69	-78°	5.67	123.0°	0.033	41.4°	0.84	-25°	15.1	0.53
1000	0.63	-98°	5.04	113.0°	0.037	33.0°	0.79	-30°	14.1	0.67
1250	0.60	-114°	4.42	99.9°	0.038	29.3°	0.77	-33°	13.0	0.81
1500	0.60	-127°	3.88	87.0°	0.039	28.0°	0.76	-35°	11.8	0.91

Figure 4.4.15 S parameters of the transistor, K factors, and $|S_{21}|^2$ in decibels.

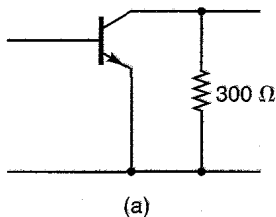
ity analysis must be performed. Also, observe that above 1250 MHz the phase of S_{21} is less than 90° , and a portion of the output voltage is in phase with the input.

The input and output stability circles are given in Fig. 4.4.16. Analysis of the output stability circles shows that a shunt resistor of $300\ \Omega$ at the output of the transistor provides stability. The resulting S parameters for the network shown in Fig. 4.4.17a are given in Fig. 4.4.17b. The stability of the network in Fig. 4.4.17a is much improved.

The gain $|S_{21}|^2$ is reduced because the $300\text{-}\Omega$ resistor dissipates some of the output power. Still, the network in Fig. 4.4.17a can easily provide the transducer power gain of

F (MHz)	C_s		r_s	Stable Region	C_L		r_L	Stable Region
	Mag.	Ang.			Mag.	Ang.		
10	1.27	-43°	0.90	Inside	1.05	13°	0.24	Outside
100	30.53	88°	30.34	Outside	1.13	21°	0.37	Outside
250	4.61	89°	4.24	Outside	1.26	32°	0.54	Outside
500	3.61	103°	3.08	Outside	1.40	39°	0.64	Outside
750	2.63	117°	1.96	Outside	1.39	42°	0.58	Outside
1000	2.26	129°	1.46	Outside	1.41	44°	0.53	Outside
1250	2.14	140°	1.24	Outside	1.40	44°	0.46	Outside
1500	1.99	150°	1.04	Outside	1.39	45°	0.42	Outside

Figure 4.4.16 Stability circles locations.



F (MHz)	S_{11}		S_{21}		S_{12}		S_{22}		$ S_{21} ^2$ (dB)	K	$ A $
	Mag.	Ang.	Mag.	Ang.	Mag.	Ang.	Mag.	Ang.			
10	0.95	-2°	6.30	174.7°	0.003	84.4°	0.72	-1°	15.98	1.4	0.69
100	0.92	-11°	6.13	168.3°	0.006	79.3°	0.71	-4°	15.75	1.1	0.66
250	0.87	-28°	5.88	155.2°	0.013	69.9°	0.69	-10°	15.38	0.94	0.61
500	0.79	-53°	5.44	136.1°	0.023	55.1°	0.65	-19°	14.71	1.0	0.54
750	0.70	-77°	4.94	124.5°	0.029	42.9°	0.61	-26°	13.88	1.2	0.45
1000	0.64	-97°	4.42	114.7°	0.032	34.7°	0.57	-32°	12.90	1.4	0.37
1250	0.61	-113°	3.89	101.7°	0.033	31.1°	0.56	-35°	11.79	1.6	0.34
1500	0.60	-126°	3.42	88.8°	0.034	29.8°	0.55	-38°	10.67	1.9	0.33

(b)

Figure 4.4.17 (a) Stabilized transistor network; (b) the resulting S parameters.

10 dB. The S_{11} and S_{22} parameters show that the input and output VSWR are poor. The phase of S_{21} above 1250 MHz remains less than 90° .

The value of $r_{b'e}$ can be calculated at the lower frequencies using the data in Fig. 4.4.17b. Assuming that $S_{11} \approx 0.95$, it follows that $r_{b'e} = 1950 \Omega$. Hence, the shunt-feedback configuration can be used since the condition $r_{b'e} \gg R_2$ will be satisfied.

The shunt negative-feedback resistor-inductor combination, shown in Fig. 4.4.18a, can now be designed to provide a flat gain of 10 dB (i.e., $|S_{21}|^2 = 10$ dB or $|S_{21}| = 3.16$) with 50- Ω input and output impedances. The value of R_2 is calculated using (4.4.10)—namely,

$$R_2 = 50(1 + 3.16) = 208 \Omega$$

The value of L_2 is designed to provide negative feedback above 1200 MHz (i.e., to decrease the gain, so that the phase of S_{21} in the feedback network remains above 90°). That is, the value of L_2 is selected from

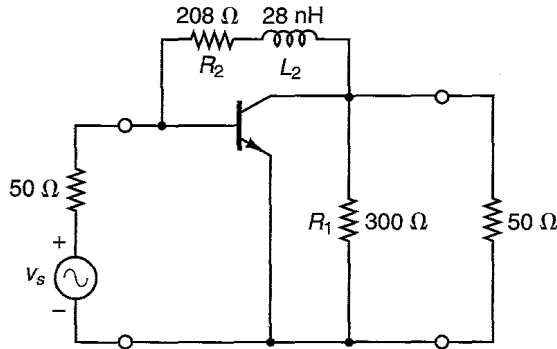
$$R_2 = \omega L_2|_{f=1200 \text{ MHz}} \quad \text{or} \quad L_2 = \frac{208}{2\pi(1200 \times 10^6)} = 28 \text{ nH}$$

The resulting S parameters of the feedback network in Fig. 4.4.18a are given in Fig. 4.4.18b. We can observe from Fig. 4.4.18b that negative feedback has reduced S_{11} and S_{22} considerably. The input VSWR is less than 2, except at 1500 MHz. Also, the gain $|S_{21}|^2$ in decibels in a 50- Ω system is close to the designed value of 10 dB over the frequency band.

To improve the performance of the circuit in Fig. 4.4.18a, the feedback network elements (i.e., R_2 and L_2) can be varied using trial and error. Obviously, the number of calculations required is considerable and CAD methods are necessary. In the Appendix “Computer-Aided Designs,” Example CAD.5, CAD methods are used to optimize the feedback network design in Fig. 4.4.18a. It is shown that using $R_2 = 275.8 \Omega$ and $L_2 = 13.9$ nH results in the S parameters given in Fig. 4.4.18c. These values of R_2 and L_2 improve the gain flatness of the amplifier. However, the VSWRs are high. For example, $(\text{VSWR})_{\text{in}}$ at $f = 1500$ MHz is 2.12.

Further performance improvements can be obtained by adding input and output matching networks, and using CAD methods to optimize the overall design for a flat transducer power gain of 10 dB with good input and output VSWR. To this end, an initial design using two-element matching networks at the input and output to provide a simultaneous conjugate match at 1500 MHz is performed (i.e., with $\Gamma_{Ms} = 0.236 \angle 130.3^\circ$ and $\Gamma_{ML} = 0.365 \angle -12.2^\circ$). The initial values used in the amplifier design are shown in Fig. 4.4.19a. The optimization of this amplifier is discussed in the Appendix “Computer-Aided Designs,” Example CAD.5. The optimized values are shown in parentheses in Fig. 4.4.19a, and the results of the optimization in Fig. 4.4.19b. From the values in Fig. 4.4.19b, it is seen that the transducer power gain of the broadband amplifier exhibits excellent gain flatness, since its gain varies from 9.90 dB to 10.07 dB (i.e., a gain ripple of 0.17 dB). The input VSWR is less than 1.49, and the output VSWR is less than 1.36. For comparison purposes, Fig. 4.4.19c shows how G_T varies as the design progresses—specifically, the G_T of the transistor, the G_T of the transistor with the feedback network, and the G_T of the complete broadband amplifier.

A matching network produces the desired match at one frequency and matching degradation occurs at the other frequencies. Fano [4.19] has derived a complete set of integrals that predict the gain-bandwidth restrictions for



(a)

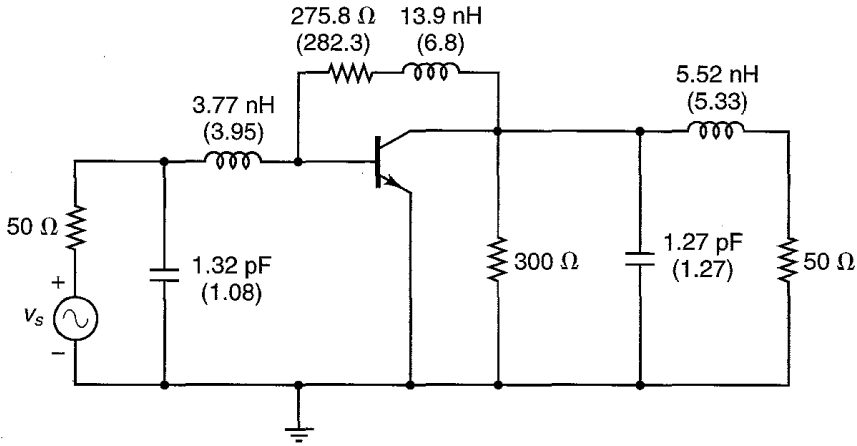
F (MHz)	S_{11}		S_{21}		S_{12}		S_{22}		$ S_{21} ^2$ (dB)	K	$ \Delta $
	Mag.	Ang.	Mag.	Ang.	Mag.	Ang.	Mag.	Ang.			
10	0.08	17°	2.68	176.7°	0.184	1.0°	0.04	140°	8.58	1.25	0.50
100	0.07	17°	2.67	175.5°	0.182	-2.9°	0.07	113°	8.53	1.26	0.48
250	0.08	11°	2.73	171.5°	0.180	-9.6°	0.14	93°	8.74	1.23	0.48
500	0.10	-5°	3.03	163.7°	0.172	-20.4°	0.26	77°	9.62	1.14	0.51
750	0.12	-46°	3.37	156.6°	0.154	-32.6°	0.35	62°	10.56	1.11	0.53
1000	0.18	-77°	3.65	146.3°	0.133	-43.6°	0.44	45°	11.25	1.10	0.54
1250	0.28	-93°	3.79	128.9°	0.112	-54.4°	0.56	26°	11.58	1.08	0.56
1500	0.39	-109°	3.70	109.5°	0.087	-64.1°	0.65	8°	11.35	1.12	0.55

(b)

F (MHz)	S_{11}		S_{21}		S_{12}		S_{22}		$ S_{21} ^2$ (dB)	K	$ \Delta $
	Mag.	Ang.	Mag.	Ang.	Mag.	Ang.	Mag.	Ang.			
10.00	0.19	5°	3.15	176.3°	0.161	1.0°	0.07	20°	9.97	1.22	0.52
100.00	0.18	-4°	3.12	173.0°	0.159	-1.9°	0.08	32°	9.87	1.23	0.51
250.00	0.17	-21°	3.11	165.5°	0.156	-7.0°	0.11	45°	9.85	1.25	0.50
500.00	0.18	-50°	3.18	153.9°	0.148	-14.4°	0.17	49°	10.05	1.26	0.49
750.00	0.21	-85°	3.23	146.0°	0.134	-21.9°	0.21	44°	10.18	1.33	0.47
1000.00	0.25	-108°	3.22	137.6°	0.120	-27.5°	0.26	36°	10.15	1.40	0.45
1250.00	0.30	-119°	3.19	124.4°	0.10	-32.3°	0.35	25°	10.05	1.44	0.45
1500.00	0.36	-126°	3.10	109.5°	0.09	-37.1°	0.44	14°	9.83	1.48	0.46

(c)

Figure 4.4.18 (a) The feedback network and the matching networks; (b) S parameters of the feedback network with $R_2 = 208 \Omega$ and $L_2 = 28 \text{ nH}$; (c) S parameters of the feedback network with $R_2 = 275.8 \Omega$ and $L_2 = 13.9 \text{ nH}$.



(a)

f (MHz)	G_T	$(VSWR)_{in}$	$(VSWR)_{out}$
10	10.07	1.49	1.17
100	9.96	1.46	1.19
250	9.90	1.42	1.26
500	10.00	1.35	1.36
750	10.06	1.34	1.34
1000	10.01	1.38	1.29
1250	9.99	1.36	1.21
1500	9.96	1.35	1.14

(b)

Figure 4.4.19 (a) Initial values used in the design of the broadband amplifier. The optimized values are shown in parentheses; (b) the results of the optimization; (c) G_T of the transistor, G_T of the transistor with the 300-Ω resistor, G_T of the transistor with the 300-Ω resistor and the feedback network, and G_T for the complete broadband amplifier.

lossless matching networks terminated in an arbitrary load impedance. The derivations of the results are covered in Fano’s paper, and only the appropriate results will be given. For the network shown in Fig. 4.4.20a, the best Γ that can be achieved over a frequency range is restricted by the integral

$$\int_0^\infty \ln \left| \frac{1}{\Gamma} \right| d\omega \leq \frac{\pi}{RC} \tag{4.4.15}$$

Equation (4.4.15) expressed the fact that the area under the curve $\ln|1/\Gamma|$ cannot be greater than π/RC . Therefore, if matching is required over a certain bandwidth, it can be obtained at the expense of less power transfer.

The best utilization of the area under the curve $\ln|1/\Gamma|$ is obtained when $|\Gamma|$ is constant over the frequency range ω_a to ω_b and equal to 1 outside that range. This situation is illustrated in Fig. 4.4.21, and it follows from (4.4.15) that

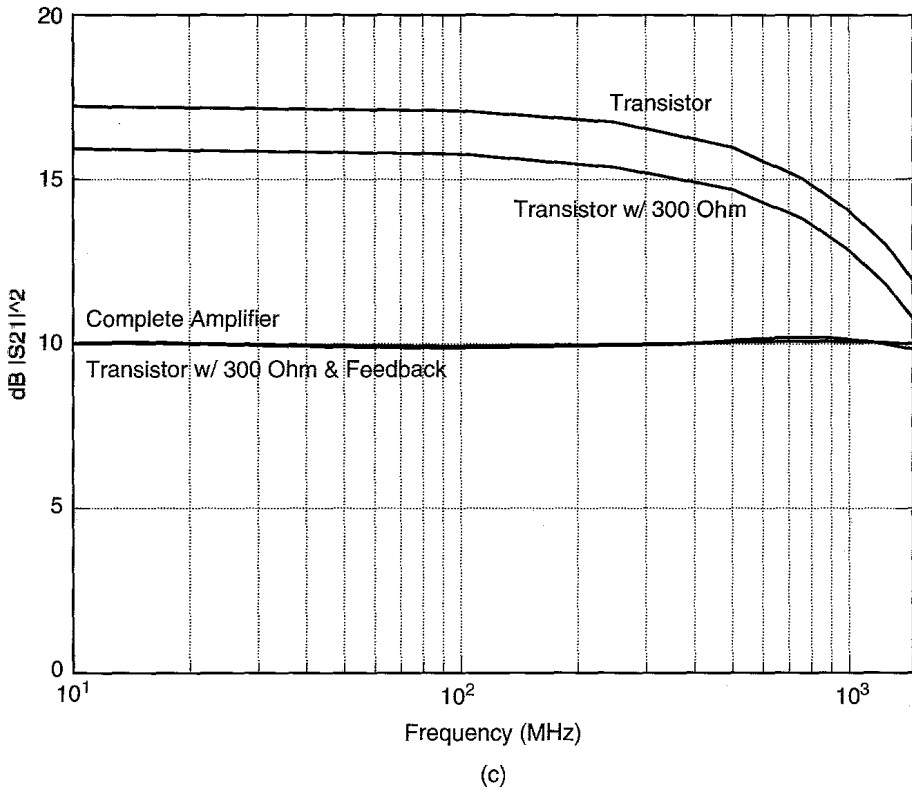


Figure 4.4.19 Continued

$$|\Gamma| = \Gamma_x = e^{-\pi/(\omega_b - \omega_a)RC}$$

or

$$\Gamma_x = e^{-\pi(Q_2/Q_1)} \tag{4.4.16}$$

where

$$Q_1 = \frac{R}{X_c}$$

and

$$Q_2 = \frac{\omega_o}{\omega_b - \omega_a}$$

Equation (4.4.16) gives the best ideally achievable Γ_x that can be obtained in the band ω_a to ω_b with no power transfer outside the band. Although a matching network satisfying the aforementioned requirements cannot be obtained in practice, the relation (4.4.16) can be used as a guideline for the best Γ_x .

The expression (4.4.16) can also be used for the networks shown in Figs. 4.4.20b to 4.4.20d when the appropriate definition of Q_1 and Q_2 are used. These are given in the figures.

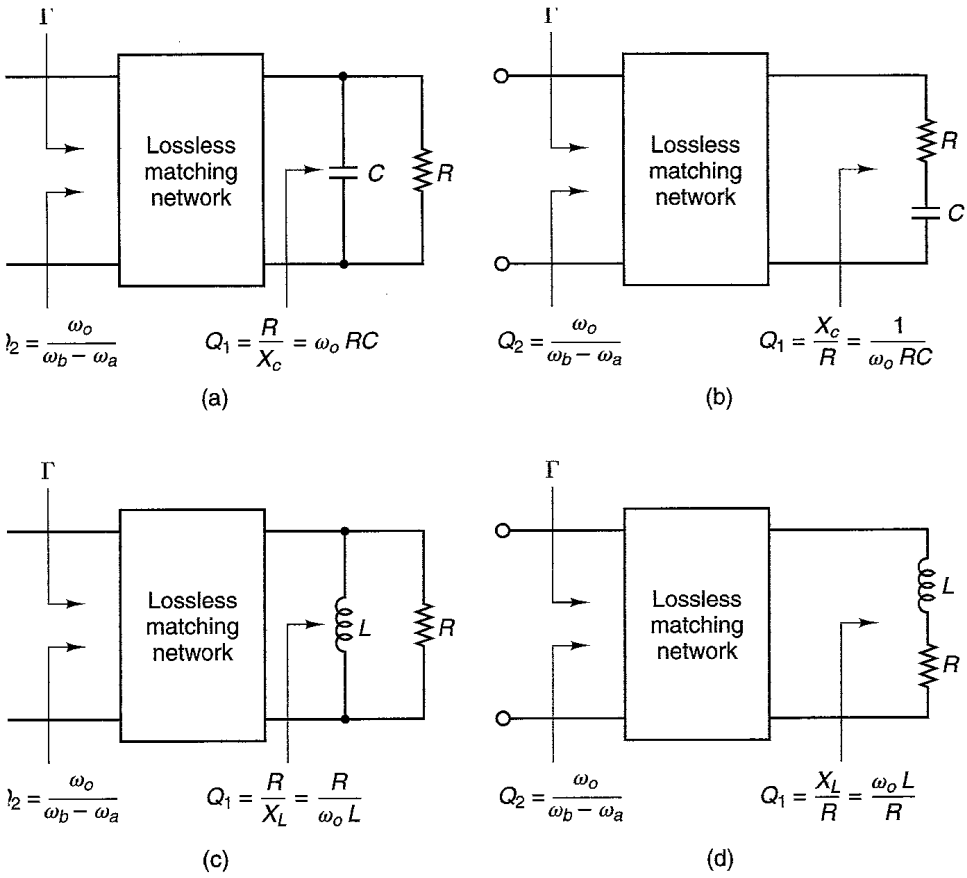


Figure 4.4.20 Network topologies used in the calculations of the gain-bandwidth limitations.

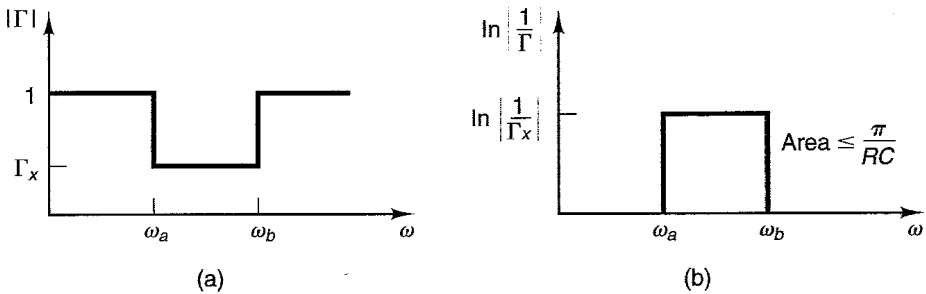


Figure 4.4.21 Optimum values of $|\Gamma|$

Example 4.4.4

Over the frequency range $f_a = 500$ MHz to $f_b = 900$ MHz, find the best Γ_x that can be achieved in the network shown in Fig. 4.4.22.

Solution. At $f_o = 700$ MHz, we obtain

$$Q_1 = \frac{1}{\omega_o RC} = \frac{1}{2\pi(700 \times 10^6)14(6.8 \times 10^{-12})} = 2.39$$

and

$$Q_2 = \frac{7}{4} = 1.75$$

Then, from (4.4.16), the value of Γ_x is

$$\Gamma_x = e^{-\pi(1.75/2.39)} = 0.1$$

The normalized load impedance of the network in Fig. 4.4.22 (i.e., $z = 0.28 - j468 \times 10^6/f$) is plotted in Fig. 4.4.23 over the frequency range f_a to f_b . Also, the region $\Gamma_x < 0.1$ for the ideally achievable match is shown shaded.

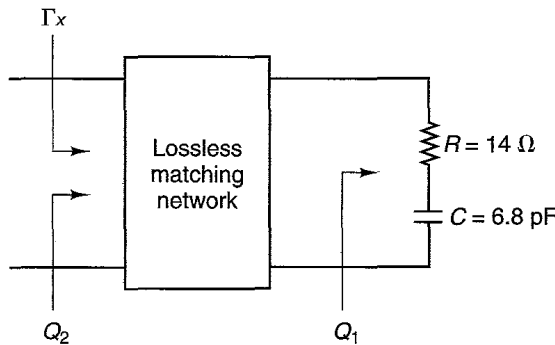


Figure 4.4.22 Calculation of Γ_x .

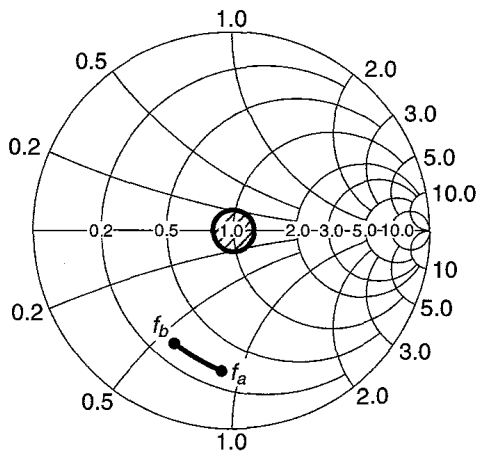


Figure 4.4.23 Best achievable match Γ_x .

4.5 AMPLIFIER TUNING

The input reflection coefficient in the bilateral case is a function of the load reflection coefficient. Therefore, Γ_{IN} varies with output tuning and Γ_{OUT} varies with input tuning.

After an amplifier is built, tuning or alignment is necessary in order for the amplifier to provide optimum performance. The tuning is usually done by performing minor changes and adjusting the components of the matching networks.

An amplifier is easy to tune when the ratios of the fractional changes in Γ_{IN} due to Γ_L , and Γ_{OUT} due to Γ_s , are small.

The input reflection tuning factor δ_{IN} is defined as

$$\delta_{\text{IN}} = \left| \frac{d\Gamma_{\text{IN}}/\Gamma_{\text{IN}}}{d\Gamma_L/\Gamma_L} \right|$$

which, in terms of the two-port network S parameters, can be written as

$$\delta_{\text{IN}} = \frac{|S_{21}| |S_{12}| |\Gamma_L|}{|1 - S_{22}\Gamma_L| |S_{11} - \Delta\Gamma_L|} \quad (4.5.1)$$

In practice, a value of $\delta_{\text{IN}} < 0.3$ produces good tunability. Equation (4.5.1) shows that δ_{IN} can be zero under some circumstances. That is, $\delta_{\text{IN}} = 0$ when $S_{12} = 0$, which occurs when the unilateral assumption can be made. In this case, the output tuning does not affect the input. Also, $\delta_{\text{IN}} = 0$ when $\Gamma_L = 0$, which is a very specific value of Γ_L that probably degrades the gain and noise performance of the amplifier. Of course, $\delta_{\text{IN}} = 0$ when $S_{21} = 0$ —that is, when there is no power gain. The derivation for the output tunability factor δ_{OUT} is left as an exercise.

Equation (4.5.1) can be solved for Γ_L in terms of δ_{IN} —namely,

$$|\Gamma_L| = \left| \alpha \pm \left| \alpha^2 - \frac{S_{11}}{S_{22}\Delta} \right|^{1/2} \right| \quad (4.5.2)$$

where

$$\alpha = \frac{\Delta + S_{11}S_{22} + S_{12}S_{21}\delta_{\text{IN}}^{-1}}{2S_{22}\Delta} \quad (4.5.3)$$

The value of $|\Gamma_L|$ obtained from (4.5.2) and (4.5.3) for a given δ_{IN} is, in general, different from the value that produces maximum power gain or optimum noise performance. Therefore, this value of Γ_L produces good tunability but mismatches the amplifier.

4.6 BANDWIDTH ANALYSIS

The conditions for a conjugate match at the input and output ports are satisfied at one frequency. One reason the output power varies with frequency is the frequency dependence of the matching networks. However, the most important

factor that limits the frequency response is the variations of the transistor S parameters with frequency.

The input port, under conjugate matched conditions, is shown in Fig. 4.6.1a. A conjugate match means that $\Gamma_s = \Gamma_{IN}^*$ or $Y_s = Y_{IN}^*$. With

$$Y_{IN} = G_{s,M} + jB_{s,M}$$

and

$$Y_s = G_{s,M} - jB_{s,M}$$

the network in Fig. 4.6.1a can be represented by the RLC network shown in Fig. 4.6.1b. The values $G_{s,M}$ and $B_{s,M}$ represent the conductance and susceptance obtained under conjugate matched conditions.

The input inherent bandwidth, $(BW)_{IN}^i$, is the bandwidth obtained under conjugate matched conditions where the matched terminations are determined by the S parameters of the two-port device. The input inherent bandwidth is given by

$$(BW)_{IN}^i = \frac{f_o}{Q_{IN}} \quad \text{Hz} \tag{4.6.1}$$

where f_o is the frequency at which the conjugate matched values were obtained and Q_{IN} is the “ Q ” of the equivalent input network. The value of Q_{IN} , for the network in Fig. 4.6.1b, can be expressed in different forms—namely,

$$Q_{IN} = \omega_o RC = \frac{R}{\omega_o L} \tag{4.6.2}$$

where $\omega_o = 2\pi f_o = 1/\sqrt{LC}$. Substituting (4.6.2) into (4.6.1), we obtain

$$(BW)_{IN}^i = \frac{2f_o G_{s,M}}{|B_{s,M}|} \tag{4.6.3}$$

where $R = 1/2G_{s,M}$ and $|B_{s,M}| = \omega_o C = 1/\omega_o L$. Similarly, the output inherent bandwidth is given by

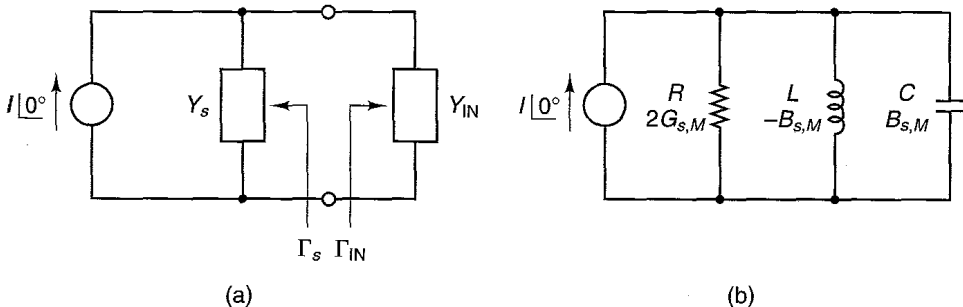


Figure 4.6.1 Equivalent networks of the input port under conjugate matched conditions.

$$(\text{BW})_{\text{OUT}}^i = \frac{2f_o G_{L,M}}{|B_{L,M}|} \quad (4.6.4)$$

where $Y_L = Y_{\text{OUT}}^*$.

Example 4.6.1

In the microwave transistor amplifier of Example 3.6.1, we found that for a simultaneous conjugate match at $f = 6$ GHz, $\Gamma_{M_s} = 0.762 \angle 177.3^\circ$, and $\Gamma_{M_L} = 0.718 \angle 103.9^\circ$. Calculate the amplifier bandwidth limitation due to the matching networks.

Solution. The admittances $Y_{\text{IN}} = Y_s^*$ and $Y_{\text{OUT}} = Y_L^*$ associated with Γ_{M_s} and Γ_{M_L} are

$$Y_{\text{IN}} = (144 + j24.6) \times 10^{-3} \text{ S}$$

and

$$Y_{\text{OUT}} = (8.28 + j23.8) \times 10^{-3} \text{ S}$$

The equivalent network at the input port is illustrated in Fig. 4.6.1. The equivalent network for the output port is similar. From Y_{IN} and Y_{OUT} , it follows that $G_{s,M} = 144 \times 10^{-3}$, $|B_{s,M}| = 24.6 \times 10^{-3}$, $G_{L,M} = 8.28 \times 10^{-3}$, and $|B_{L,M}| = 23.8 \times 10^{-3}$. Therefore, from (4.6.3) and (4.6.4),

$$(\text{BW})_{\text{IN}}^i = \frac{2(6 \times 10^9)144 \times 10^{-3}}{24.6 \times 10^{-3}} = 70.2 \text{ GHz}$$

and

$$(\text{BW})_{\text{OUT}}^i = \frac{2(6 \times 10^9)8.28 \times 10^{-3}}{23.8 \times 10^{-3}} = 4.17 \text{ GHz}$$

Since $(\text{BW})_{\text{IN}}^i \gg (\text{BW})_{\text{OUT}}^i$, the bandwidth limitations due to the matching networks are determined by $(\text{BW})_{\text{OUT}}^i$.

The broad bandwidth $(\text{BW})_{\text{OUT}}^i$ cannot be obtained in practice because of the transistor S -parameter variations with frequency. In fact, the overall bandwidth of the amplifier, as shown in Fig. 4.3.12d, is 980 MHz.

The inherent bandwidth of either the input or output port can be decreased by increasing the Q of the network. From (4.6.2), we can increase Q by increasing the capacitance or decreasing the inductance of the network. When Y_{IN} has a capacitive susceptance, the bandwidth is decreased by adding capacitance, and when Y_{IN} has an inductive susceptance, the bandwidth is decreased by adding inductance.

Consider the case where Y_{IN} has a capacitive susceptance. The admittance Y_{IN} is given by

$$Y_{\text{IN}} = G_{\text{IN},M} + jB_{\text{IN},M}$$

If we add to the input port the capacitor C'_{IN} , shown in Fig. 4.6.2, the admittance Y'_{IN} is given by

$$Y'_{\text{IN}} = Y_{\text{IN}} + j\omega_o C'_{\text{IN}}$$

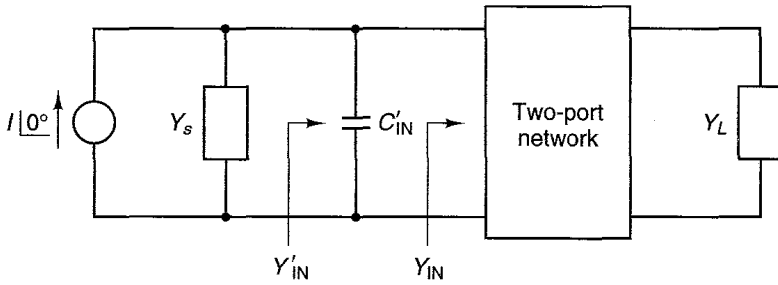


Figure 4.6.2 Increasing Q by adding the capacitance C'_{IN} .

and a conjugate match requires that $Y_s = (Y'_{IN})^*$. Therefore,

$$G_{s,M} = G_{IN,M}$$

and

$$B_{s,M} = -(B_{IN,M} + \omega_o C'_{IN})$$

The input port bandwidth is

$$(BW)_{IN} = \frac{2f_o G_{s,M}}{B_{IN,M} + \omega_o C'_{IN}}$$

which can be solved for C'_{IN} to obtain

$$C'_{IN} = \frac{B_{IN,M}}{\omega_o} \left[\frac{(BW)_{IN}^i}{(BW)_{IN}} - 1 \right] \tag{4.6.5}$$

where (4.6.3) was used.

Equation (4.6.5) gives the value of the additional capacitance required to obtain the bandwidth $(BW)_{IN}$. Similarly, for the output network the capacitance required to produce a bandwidth $(BW)_{OUT}$ is

$$C'_{OUT} = \frac{B_{OUT,M}}{\omega_o} \left[\frac{(BW)_{OUT}^i}{(BW)_{OUT}} - 1 \right]$$

When Y_{IN} has an inductive susceptance, the bandwidth is decreased by adding the inductor L'_{IN} shown in Fig. 4.6.3. It follows that the value of inductance required to obtain the bandwidth $(BW)_{IN}$ is

$$L'_{IN} = \frac{1}{\omega_o |B_{IN,M}| \left[\frac{(BW)_{IN}^i}{(BW)_{IN}} - 1 \right]}$$

In the output port, the value of inductance required to obtain $(BW)_{OUT}$ is

$$L'_{OUT} = \frac{1}{\omega_o |B_{OUT,M}| \left[\frac{(BW)_{OUT}^i}{(BW)_{OUT}} - 1 \right]}$$

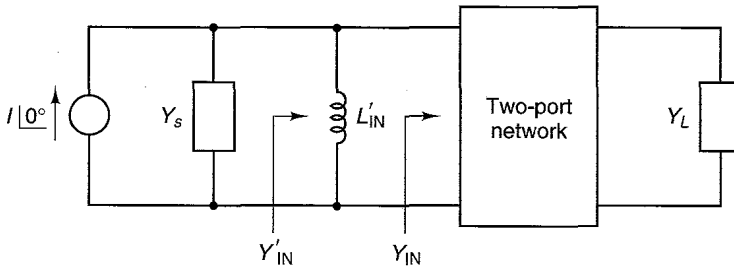


Figure 4.6.3 Increasing Q by adding the inductance L'_{IN} .

The previous methods of adding capacitance or inductance to narrow-band the amplifier response does not affect the original simultaneous conjugate matched calculations.

The overall bandwidth of n identical single tuned networks is related to the bandwidth of one stage, $(BW)_1$, by the relation

$$(BW)_n = (BW)_1 \sqrt{2^{1/n} - 1} \quad (4.6.6)$$

The factor

$$\sqrt{2^{1/n} - 1}$$

is called the *bandwidth reduction factor*. In the case of two single tuned networks (i.e., $n = 2$), (4.6.6) gives

$$(BW)_2 = (BW)_1(0.644)$$

4.7 HIGH-POWER AMPLIFIER DESIGN

Thus far we have presented design techniques, based on the small-signal S parameters of transistors, for maximum or arbitrary power gain, low noise, and broadband amplifiers. The small-signal S parameters are not useful for power amplifier design because power amplifiers usually operate in nonlinear regions. The small-signal S parameters can be used in large-signal amplifiers operating in class A (i.e., linear output power). However, for class AB, B, or C, the small-signal S parameters are not suitable for design purposes.

A set of large-signal S parameters is needed to characterize the transistor for power applications. Unfortunately, the measurement of large-signal S parameters is difficult and is not properly defined. Therefore, an alternative set of large-signal parameters is needed to characterize the transistor. This can be done by providing information of source and load reflection coefficients as a function of output power and gain.

We begin by discussing the large-signal parameters provided for transistors operating in class A at microwave frequencies. Then, the large-signal parameters provided for transistors operating in classes B and C are discussed.

Class-A Operation

Recall that small-signal class-A operation is linear, while large-signal class-A operation introduces some nonlinearities in the output signal. Hence, in large-signal class-A operation the output signal contains harmonics of the fundamental signal. Of course, if the Q of the output matching network is high, the harmonics can be suppressed and the output signal will be an amplified replica of the input signal.

At frequencies around 4 GHz and above, the size and fabrication of the transistors usually limit the maximum output power to about 1 W (or 30 dBm). In the UHF range (300 MHz to 3 GHz), linear output powers of several watts are possible.

One form of large-signal parameters provided by manufacturers is the measurement of the source and load reflection coefficients (or source and load impedances), together with the output power, when the transistor is operated at its 1-dB gain compression point. The listing of the 1-dB compression point data is used to specify the power-handling capabilities of the transistor.

The 1-dB gain compression point (called $G_{1\text{ dB}}$) is defined as the power gain where the nonlinearities of the transistor reduce the power gain by 1 dB over the small-signal linear power gain. That is

$$G_{1\text{ dB}}(\text{dB}) = G_o(\text{dB}) - 1 \quad (4.7.1)$$

where $G_o(\text{dB})$ is the small-signal linear power gain in decibels. Since the power gain is defined as

$$G_p = \frac{P_{\text{OUT}}}{P_{\text{IN}}}$$

or

$$P_{\text{OUT}}(\text{dBm}) = G_p(\text{dB}) + P_{\text{IN}}(\text{dBm})$$

we can write the output power at the 1-dB gain compression point, called $P_{1\text{ dB}}$, as

$$P_{1\text{ dB}}(\text{dBm}) = G_{1\text{ dB}}(\text{dB}) + P_{\text{IN}}(\text{dBm}) \quad (4.7.2)$$

or

$$G_{1\text{ dB}} = \frac{P_{1\text{ dB}}}{P_{\text{IN}}}$$

Substituting (4.7.1) into (4.7.2) gives

$$P_{1\text{ dB}}(\text{dBm}) - P_{\text{IN}}(\text{dBm}) = G_o(\text{dB}) - 1 \quad (4.7.3)$$

Equation (4.7.3) shows that the 1-dB gain compression point is that point at which the output power minus the input power in dBm is equal to the small-signal power gain minus 1 dB.

A typical plot of P_{OUT} versus P_{IN} which illustrates the 1-dB gain compression point is shown in Fig. 4.7.1. Observe the linear output power characteristics

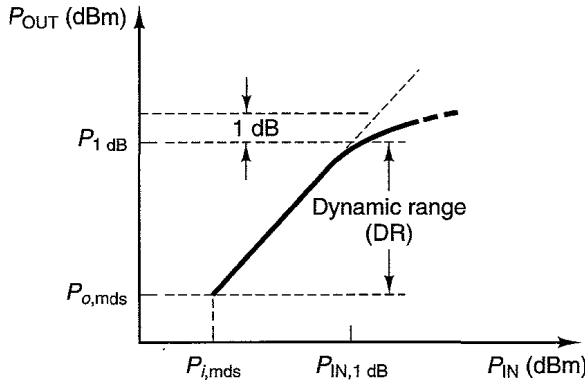


Figure 4.7.1 The 1-dB gain compression point and the dynamic range of microwave amplifiers.

for power levels between the minimum detectable signal output power ($P_{o,mds}$) and $P_{1\text{ dB}}$. The dynamic range (DR), shown in Fig. 4.7.1, is that range where the amplifier has a linear power gain. The dynamic range is limited at low power levels by the noise level. An input signal ($P_{i,mds}$) is detectable only if its output power level ($P_{o,mds}$) is above the noise power level.

The thermal noise power level of a two-port, with noise figure F , is given by

$$P_{N_o} = kTBG_A F$$

Observing that $kT = -174\text{ dBm}$ (or $kTB = -174\text{ dBm/Hz}$ at $T = 290^\circ\text{K}$) and assuming that the minimum detectable input signal is X decibels above thermal noise, we can write

$$P_{i,mds} = -174\text{ dBm} + 10\log B + F(\text{dB}) + X(\text{dB}) \quad (4.7.4)$$

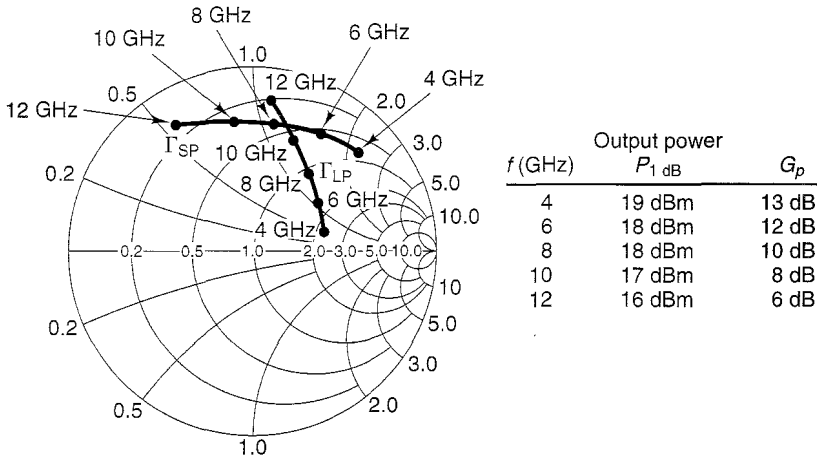
and

$$P_{o,mds} = -174\text{ dBm} + 10\log B + F(\text{dB}) + X(\text{dB}) + G_A(\text{dB}) \quad (4.7.5)$$

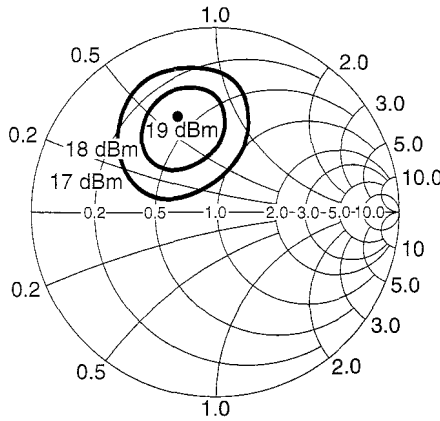
A typical value of $X(\text{dB})$ is 3 dB.

As previously discussed, a power transistor can be described in terms of the large-signal source and load reflection coefficients required to produce a given output power and gain. Of course, these parameters are functions of frequency and bias conditions. For example, in a GaAs FET the 1-dB gain compression point is usually measured at a drain-to-source voltage and gate-to-source voltage that optimizes the output power. From Fig. 3.9.7, this is usually at $I_{DS} = 50\% I_{DSS}$.

A typical set of power reflection coefficients is shown in Fig. 4.7.2a. The values of Γ_{SP} and Γ_{LP} denoted by points are the source and load power reflection coefficients for the output power $P_{1\text{ dB}}$. The values of Γ_{SP} and Γ_{LP} are given for $f = 4\text{ GHz}$ to $f = 12\text{ GHz}$. These values are certainly different from the si-



(a)



(b)

Figure 4.7.2 (a) Typical large-signal reflection coefficients. (b) Typical output power contours as a function of Γ_{LP} for a GaAs FET at $f = 10$ GHz, $V_{DS} = 10$ V, and $I_D = 50\% I_{DSS}$. For this transistor, the optimum output power is 19 dBm at 1-dB gain compression and $G_{1\text{ dB}} = 6$ dB.

multaneous conjugate matched reflection coefficients Γ_{Ms} and Γ_{ML} , which are obtained using the small-signal S parameters.

Another set of large-signal data that can be provided for a transistor is shown in Fig. 4.7.2b. Figure 4.7.2b illustrates typical output power contours as a function of the load reflection coefficient. For this transistor the maximum value of $P_{1\text{ dB}}$ is 19 dBm with $G_{1\text{ dB}} = 6$ dB. The output loadings (i.e., the values of Γ_{LP}) that result in $P_{1\text{ dB}}$ of 18 dBm and 17 dBm are also shown. Observe that

due to the nonlinear operation under large-signal conditions, the power contours are not circles. The measurements of the power contours are made with the input of the transistor conjugately matched at all times. Information on Γ_{SP} is normally given.

Figure 4.7.3 illustrates some of the large-signal information provided for the Motorola MRW52001 transistor. The values of Z_{IN} and Z_{OUT} are the large-signal input and output impedances of the transistor for an output power of 1.5 W, at a bias point of $V_{CE} = 20$ V and $I_C = 220$ mA. For this transistor, at $V_{CE} = 20$ V and $I_C = 220$ mA, the output power at the 1-dB compression point is 2 W. Therefore, the large-signal operation at 1.5 W is fairly linear. For proper matching, the source impedance Z_s should be equal to Z_{IN}^* and the load impedance Z_L should be equal to Z_{OUT}^* . Of course, this is equivalent to saying that $\Gamma_s = \Gamma_{IN}^*$ and $\Gamma_L = \Gamma_{OUT}^*$, where Γ_{IN} and Γ_{OUT} are the reflection coefficients associated with Z_{IN} and Z_{OUT} , respectively. The S parameters provided are, of course, the small-signal S parameters. Using these S parameters, it follows that at $f = 1$ GHz: $\Gamma_{OUT} = \Gamma_{ML}^* = 0.515 \angle -80.5^\circ$ and $\Gamma_{IN} = \Gamma_{Ms}^* = 0.918 \angle 165^\circ$. Observe the difference between the listed values of Γ_{IN} and Γ_{OUT} for 1.5 W of output power and the values for a simultaneous conjugate match. The largest difference is in the value of Γ_{OUT} .

Figure 4.7.4 shows some other forms in which large-signal impedance data are given. Figure 4.7.4a shows the large-signal data for the Motorola RF1030 transistor. This transistor provides 3 W of output power at $V_{CE} = 25$ V and $I_C = 0.4$ A. For this transistor the manufacturer provides large-signal input and output impedance data in rectangular form. Figure 4.7.4b shows the large-signal data for the Motorola MRW52104 transistor. Observe that the impedance data are normalized to 5 Ω .

A typical measuring system for large-signal parameters is illustrated in Fig. 4.7.5. The transistor under test is placed in a measuring setup where the dc bias and ac input signal level can be varied. The output tuning stubs are adjusted until the power meter C measures a given power level and the input tuning stubs are adjusted for zero reflected power (read at power meter B). The power meter A reads the incident power, and the power gain (at given output power level) can be obtained. Since there is no reflected power, the input port is conjugately matched, and the output impedance is that impedance required to produce the output power read at power meter C .

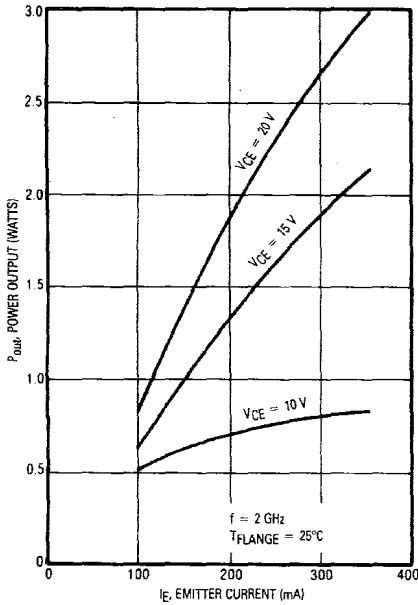
The transistor can then be disconnected from the test setup and the impedance at the reference planes A and B is measured with a network analyzer. These measurements produce the large-signal data for a given output power and gain.

Class-B and Class-C Operation

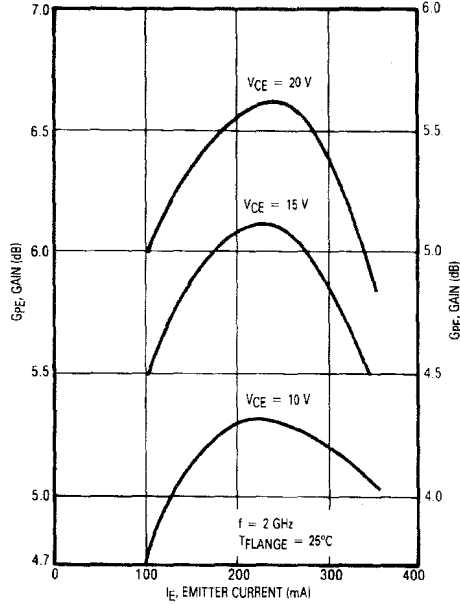
While most amplifiers operating at microwave frequencies above 1 GHz are class A, amplifiers operating in class B and class C are found at microwave frequencies below 1 GHz and in the RF range. The RF range (which is below the microwave range) extends from 300 kHz to 300 MHz. It includes the MF

MRW52001

TYPICAL CHARACTERISTICS



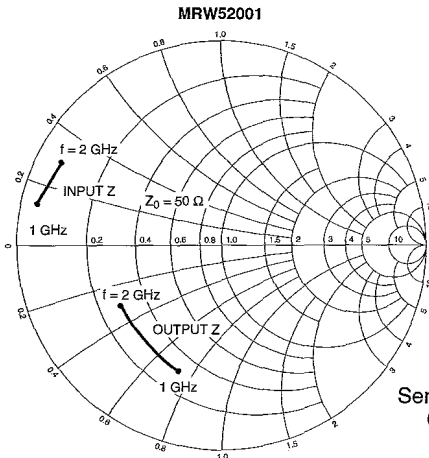
1 dB Compression Point versus Emitter Current



Gain versus Emitter Current

MRW52001

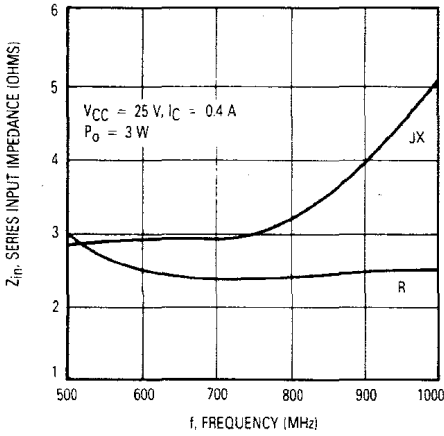
VCE (Volts)	I _C (mA)	f (GHz)	S ₁₁		S ₂₁		S ₁₂		S ₂₂	
			Mag	∠φ	Mag	∠φ	Mag	∠φ	Mag	∠φ
20	220	0.5	0.85	176	3.44	78	0.04	48	0.23	-142
		1	0.87	163	1.77	63	0.06	62	0.28	-147
		1.3	0.89	157	1.32	55	0.08	68	0.33	-155
		1.5	0.87	154	1.15	48	0.09	71	0.38	-156
		1.7	0.85	149	1.02	41	0.1	70	0.41	-157
		2	0.87	140	0.92	35	0.12	70	0.45	-161
		2.5	0.94	130	0.73	30	0.15	72	0.54	-170
		3	0.87	116	0.6	18	0.19	68	0.59	-177



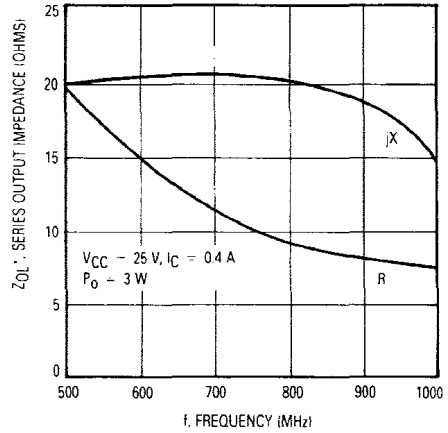
Series Equivalent Input/Output Impedance
Conditions: $V_{CE} = 20\text{ V}$, $I_E = 220\text{ mA}$,
 $T_{FLANGE} = 25^\circ\text{C}$

Figure 4.7.3 Data for the Motorola MRW52001 transistor. (From *Motorola RF Device Data*, Vol. 1, 6th edition; Copyright of Motorola, used by permission.)

TYPICAL CHARACTERISTICS

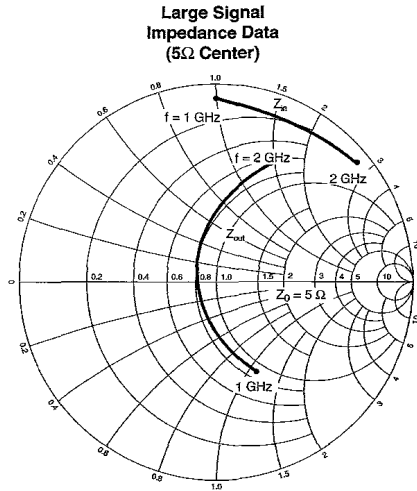


Input Impedance versus Frequency



Output Impedance versus Frequency

(a)



Series Equivalent Input/Output Impedance

(b)

Figure 4.7.4 (a) Data for the Motorola RF1030 transistor ($V_{CC} = V_{CE}$); (b) data for the Motorola MRW52104 transistor. (From *Motorola RF Device Data*, Vol. 1, 6th edition; Copyright of Motorola, used by permission.)

range (300 kHz to 3 MHz), the HF range (3 MHz to 30 MHz), and the VHF range (30 MHz to 300 MHz).

A short review of class-B and class-C operation is now presented. In class-B operation, the transistor conducts during half of the input signal cycle. This is accomplished by biasing the transistor at cutoff. Figure 4.7.6 describes the class-

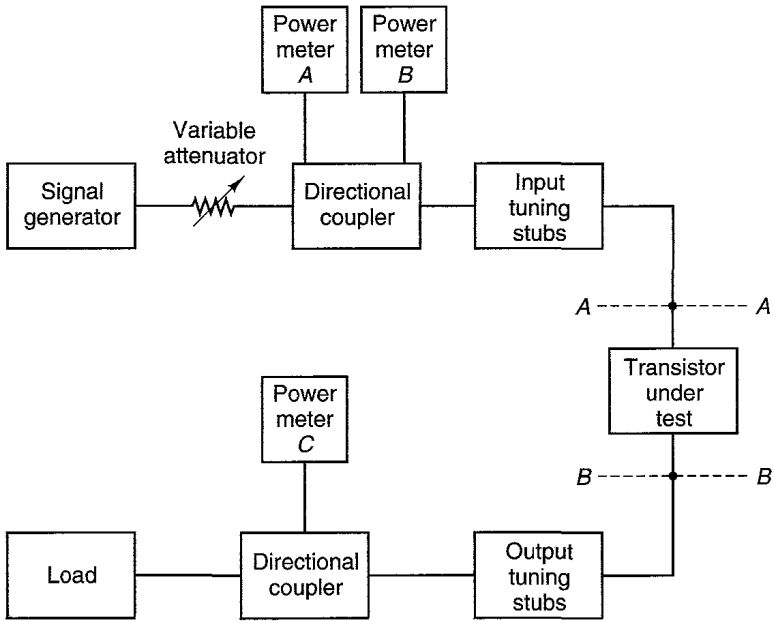


Figure 4.7.5 Measuring system for large-signal parameters.

B amplifier operation. The maximum efficiency of class-B amplifiers is 78.5%. The efficiency is defined as the ratio (in percent) of the ac power delivered to the load to the dc power required by the amplifier.

The linearity of class-A operation with the efficiency of class-B operation can be attained using two class-B transistors connected in a *complementary amplifier* configuration. A basic class-B complementary amplifier is shown in Fig. 4.7.7a.

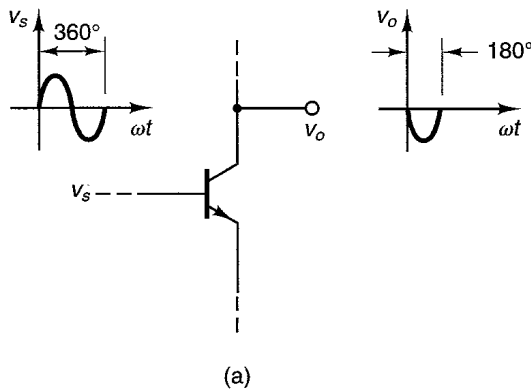


Figure 4.7.6 Input and output waveforms in class-B operation.

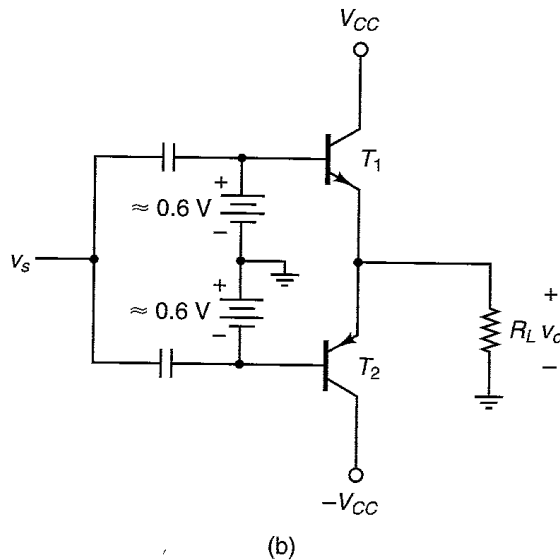
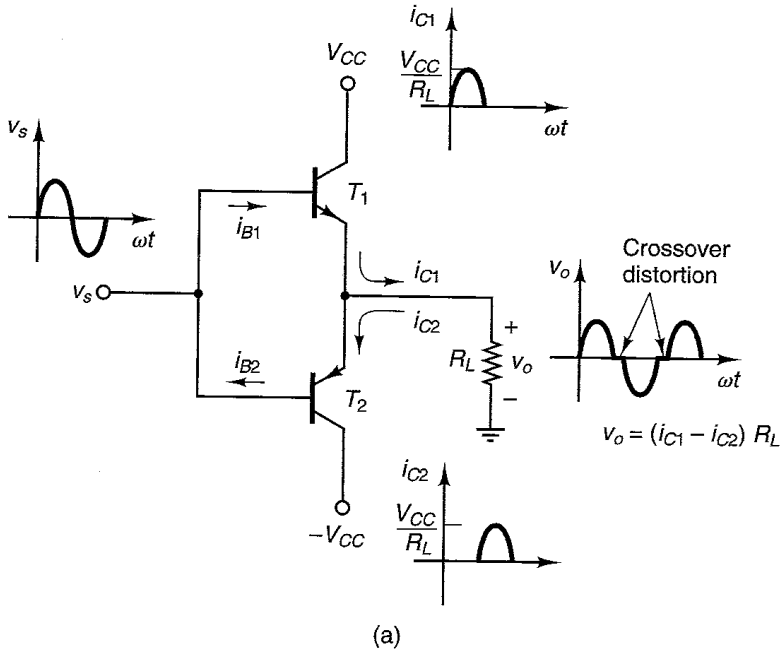


Figure 4.7.7 (a) A basic class-B complementary amplifier; (b) a basic class-AB complementary amplifier.

The amplifier shown in Fig. 4.7.7a suffers from crossover distortion since the base to emitter of each transistor must be forward biased before the transistor operates in its linear region. A type of operation called class AB is obtained if the transistors in Fig. 4.7.7a are biased at a Q point with $V_{BE} \approx 0.6$ V

so that the crossover distortion is eliminated. A class-AB complementary amplifier is shown in Fig. 4.7.7b.

Typical characterization of transistors fabricated to operate in class-B and class-C operation is at V_{CE} voltages of 12.5 V, 28 V, and 50 V. The 12.5-V amplifiers find applications in mobile transmitter equipment such as those used by police cars, trucks, and taxis. The 28-V and 50-V amplifiers find applications in high-power base-station transmitters and receivers.

In class-C the transistor is cut off until the ac signal between the base and emitter makes it conduct. Figure 4.7.8 illustrates a class-C amplifier. The emitter is grounded and the input RFC sets the quiescent value of the base to emitter voltage at zero. For the input ac signal, the RFC is an open circuit and the input signal applied between the base and emitter makes the transistor conduct. The conduction angle is less than 180° , about 140° for good efficiency and low harmonic content at the output.

The output matching network must have a high Q value in order to suppress the harmonics and pass the amplified fundamental signal. Efficiency is certainly better in class-C operation, but it is difficult to calculate.

In transistors made to operate in class-B and class-C amplifiers, the large-signal data provided by manufacturers are usually the input and output impedances of the transistor as a function of frequency for a given output power using 50- Ω source and load impedances. Therefore, lossless input and output matching networks must be designed to transform the 50- Ω source and load to the input and output impedances of the transistor, respectively. The output matching network must also provide the required Q in order to suppress the harmonics.

Power transistors are provided with flanges or studs for proper mounting and heat dissipation. The maximum junction temperature for a BJT is

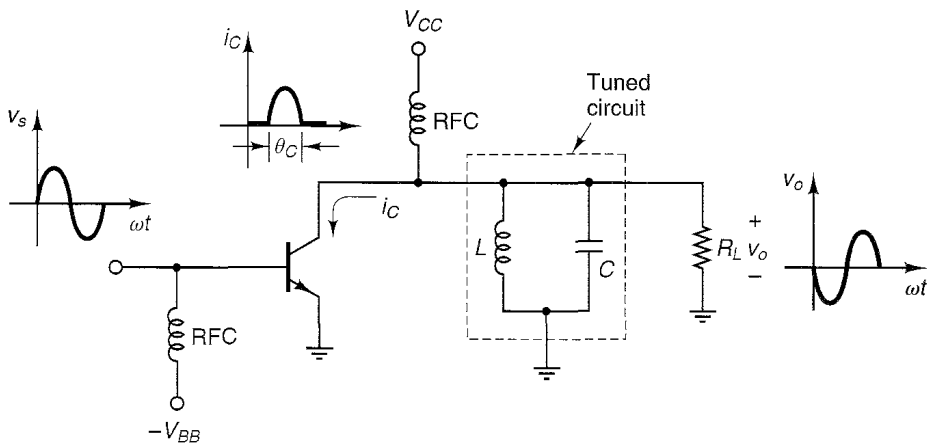


Figure 4.7.8 A basic class-C amplifier.

around 200°C, and the maximum channel temperature for a GaAs FET is around 175°C.

Intermodulation Distortion

A source of distortion in power amplifiers is that caused by intermodulation products. When two or more sinusoidal frequencies are applied to a nonlinear amplifier, the output contains additional frequency components called *intermodulation products*. For example, if two sinusoidal signals

$$v(t) = A \cos 2\pi f_1 t + A \cos 2\pi f_2 t \quad (4.7.6)$$

are applied to a nonlinear amplifier whose output voltage can be represented by the power series.

$$v_o(t) = \alpha_1 v(t) + \alpha_2 v^2(t) + \alpha_3 v^3(t) \quad (4.7.7)$$

the output signal will contain frequency components at dc, f_1 , f_2 , $2f_1$, $2f_2$, $3f_1$, $3f_2$, $f_1 \pm f_2$, $2f_1 \pm f_2$, and $2f_2 \pm f_1$. The frequencies $2f_1$ and $2f_2$ are the second harmonics, $3f_1$ and $3f_2$ are the third harmonics, $f_1 \pm f_2$ are the second-order intermodulation products (since the sum of the f_1 and f_2 coefficients is 2), and $2f_1 \pm f_2$ and $2f_2 \pm f_1$ are the third-order intermodulation products (since the sum of the f_1 and f_2 coefficients is 3). The input and output power spectra, from (4.7.6) and (4.7.7), are shown in Fig. 4.7.9.

Figure 4.7.9 shows that the third-order intermodulation products at $2f_1 - f_2$ and $2f_2 - f_1$ are very close to the fundamental frequencies f_1 and f_2 and fall within the amplifier bandwidth, producing distortion in the output.

If we measure the third-order intermodulation product output power ($P_{2f_1-f_2}$) versus the input power at f_1 (P_{f_1}), the graph shown in Fig. 4.7.10 results. The third-order intercept point (called P_{IP}) is defined as the point where P_{f_1} and $P_{2f_1-f_2}$ intercept, when the two-port is assumed to be linear. Observe that the slope of P_{f_1} is 1 and that of $P_{2f_1-f_2}$ is 3. This occurs because for the assumed $v_o(t)$ in (4.7.7) the power of the third-order intermodulation product is propor-

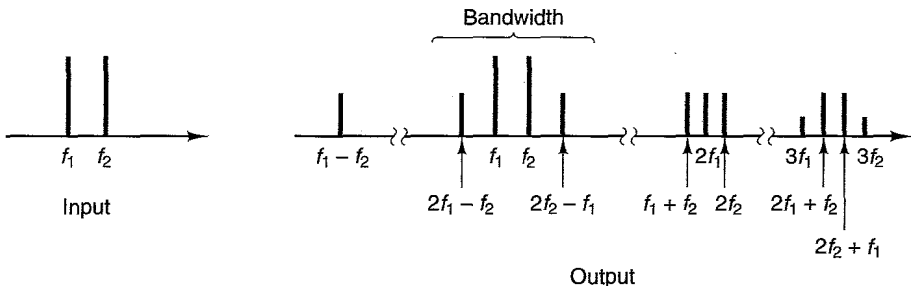


Figure 4.7.9 Input and output power spectrum.

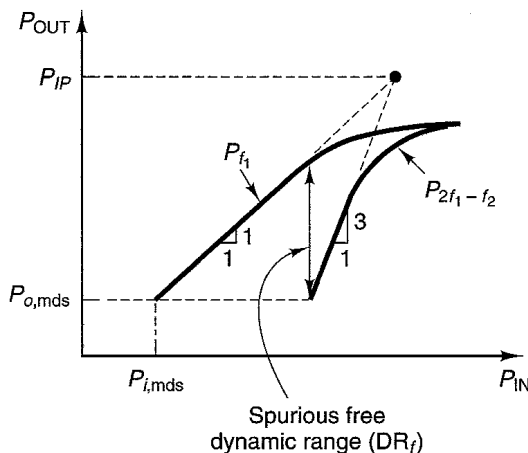


Figure 4.7.10 Third-order intercept point.

tional to the cube of the input signal amplitude A . The power P_{IP} is a theoretical level. However, it is a useful quantity to estimate the third-order intermodulation products at different power levels.

For the three-term series in (4.7.7), it can be shown analytically and experimentally that the third-order intercept point is approximately 10 dB above the 1-dB gain compression point. That is,

$$P_{IP}(\text{dBm}) = P_{1\text{ dB}}(\text{dBm}) + 10\text{ dB} \tag{4.7.8}$$

Also, it can be shown that

$$P_{2f_1-f_2} = 3P_{f_1} - 2P_{IP}$$

or

$$P_{f_1} - P_{2f_1-f_2} = \frac{2}{3}(P_{IP} - P_{2f_1-f_2}) \tag{4.7.9}$$

The spurious free dynamic range (DR_f) of an amplifier (see Fig. 4.7.10) is defined as the range $P_{f_1} - P_{2f_1-f_2}$, when $P_{2f_1-f_2}$ is equal to the minimum detectable output signal. Therefore, from (4.7.5) and (4.7.9),

$$\begin{aligned} DR_f &= \frac{2}{3}(P_{IP} - P_{o,mds}) \\ &= \frac{2}{3}[P_{IP} + 174\text{ dBm} - 10\log B - F(\text{dB}) - X(\text{dB}) - G_A(\text{dB})] \end{aligned}$$

Example 4.7.1

An amplifier has an available power gain of 40 dB, 500-MHz bandwidth, noise figure of 7 dB, and a 1-dB gain compression point of 25 dBm. Calculate DR and DR_f .

Solution. The minimum detectable input and output signals, from (4.7.4) and (4.7.5), assuming that $X = 3$ dB, are

$$P_{i,mds} = -174\text{ dBm} + 10\log(500 \times 10^6)\text{ dB} + 7\text{ dB} + 3\text{ dB} = -77\text{ dBm}$$

and

$$P_{o, \text{ mds}} = -77 \text{ dBm} + 40 \text{ dB} = -37 \text{ dBm}$$

Therefore,

$$\text{DR} = P_{1 \text{ dB}} - P_{o, \text{ mds}} = 25 \text{ dBm} + 37 \text{ dBm} = 62 \text{ dB}$$

The third-order intercept point, from (4.7.8), is

$$P_{IP} = 25 \text{ dBm} + 10 \text{ dB} = 35 \text{ dBm}$$

and

$$\text{DR}_f = \frac{2}{3} (35 \text{ dBm} + 37 \text{ dBm}) = 48 \text{ dB}$$

Another source of signal distortion is caused by a nonlinear phase characteristic. For a signal to be amplified with no distortion, the magnitude of the power gain transfer function must be constant as a function of frequency, and the phase must be a linear function of frequency. A linear phase shift produces a constant time delay to signal frequencies, and a nonlinear phase shift produces different time delays to different frequencies.

A phase distortion called *AM-to-PM conversion* occurs when an AM signal is transmitted through a power amplifier. The phase shift becomes a function of the instantaneous amplitude of the signal, and the output phase consists of a mean value with a small ripple. The AM-to-PM conversion is defined as the change in output phase for a 1-dB increment of the input power.

Power Combiners

When more power is required than can be provided by a single microwave transistor amplifier, power-combining techniques are used. One can use a method of paralleling several transistors, as shown in Fig. 4.7.11. However, this method is not recommended for several reasons:

1. The input and output impedance levels can be of the same order as the losses in the input and output matching networks. For example, a 0.1-nH

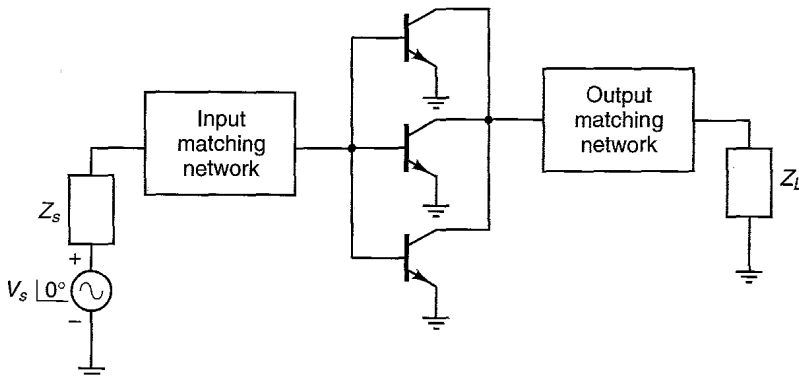


Figure 4.7.11 Method for paralleling transistors.

inductor having a Q of 150, at $f = 400$ MHz, has a resistance loss of $R = \omega L/Q = 1.6 \Omega$, which can be similar to the input resistance of several paralleled transistors. Therefore, the total power output that can be obtained from several paralleled transistors is less than the theoretical total output power because the efficiency decreases as the number of transistors increases.

2. If one transistor fails, the complete amplifier network fails.
3. All transistors must be well matched for power output and gain in order to obtain good load sharing.

A method that avoids the problem of paralleling power transistors is shown in Fig. 4.7.12. It uses a hybrid divider and a hybrid combiner to divide the input power equally to several amplifiers and to combine the output power of each amplifier. The failure of one amplifier does not cause failure of the complete unit. The complete unit will continue to operate with reduced output power. Many balance amplifiers use Lange couplers or Wilkinson couplers as dividers and combiners.

Figure 4.7.13 shows the block diagram of an n -way power combiner/divider. The insertion losses of the coupler limit the overall efficiency. The block diagram of an n -way amplifier is shown in Fig. 4.7.14.

Design Examples

Example 4.7.2

Design a power amplifier at 2 GHz using a BJT. The S parameters of the transistor and power characteristics at 2 GHz are

$$S_{11} = 0.64 \angle 153^\circ$$

$$S_{21} = 2.32 \angle 10^\circ$$

$$S_{12} = 0.07 \angle -8^\circ$$

$$S_{22} = 0.51 \angle -119^\circ$$

$$P_{1\text{dB}} = 29 \text{ dBm}$$

$$G_{1\text{dB}} = 11.5 \text{ dB}$$

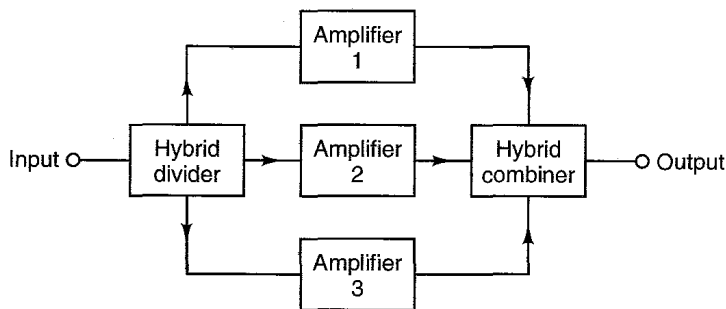


Figure 4.7.12 A hybrid combiner/divider.

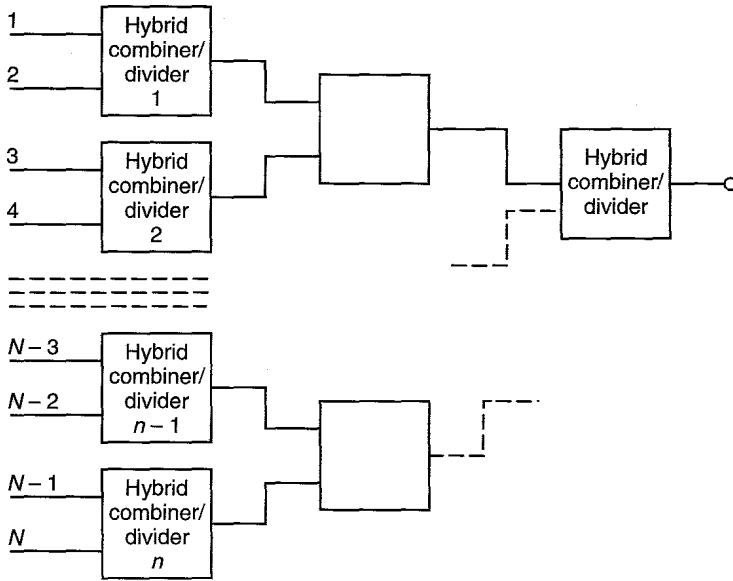


Figure 4.7.13 An n -way hybrid combiner/divider.

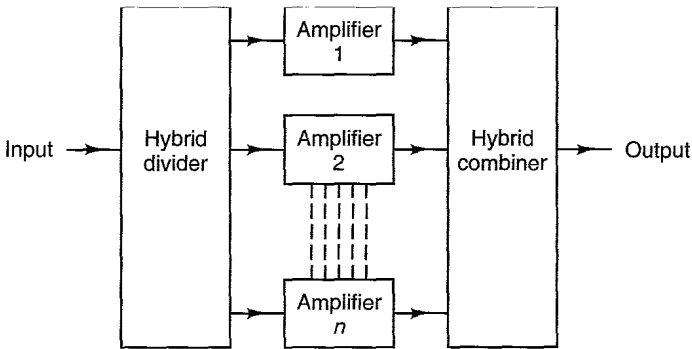


Figure 4.7.14 An n -way power amplifier.

Output power contours are shown in Fig. 4.7.15a. This figure shows the loci of equal $P_{1\text{ dB}}$ for different output loading. The input was conjugately matched at all times. The $P_{1\text{ dB}}$ point and the output conjugate match point were close. (This example is based on a design from Hewlett-Packard Application Note 972 [4.20].)

Solution. The transistor is unconditionally stable at 2 GHz since $K = 1.15$ and $\Delta = 0.207 \angle 58.5^\circ$. The output network is designed to provide the output power $P_{1\text{ dB}} = 29\text{ dBm}$. The output matching network design is shown in Fig. 4.7.15b. The $50\text{-}\Omega$ load was

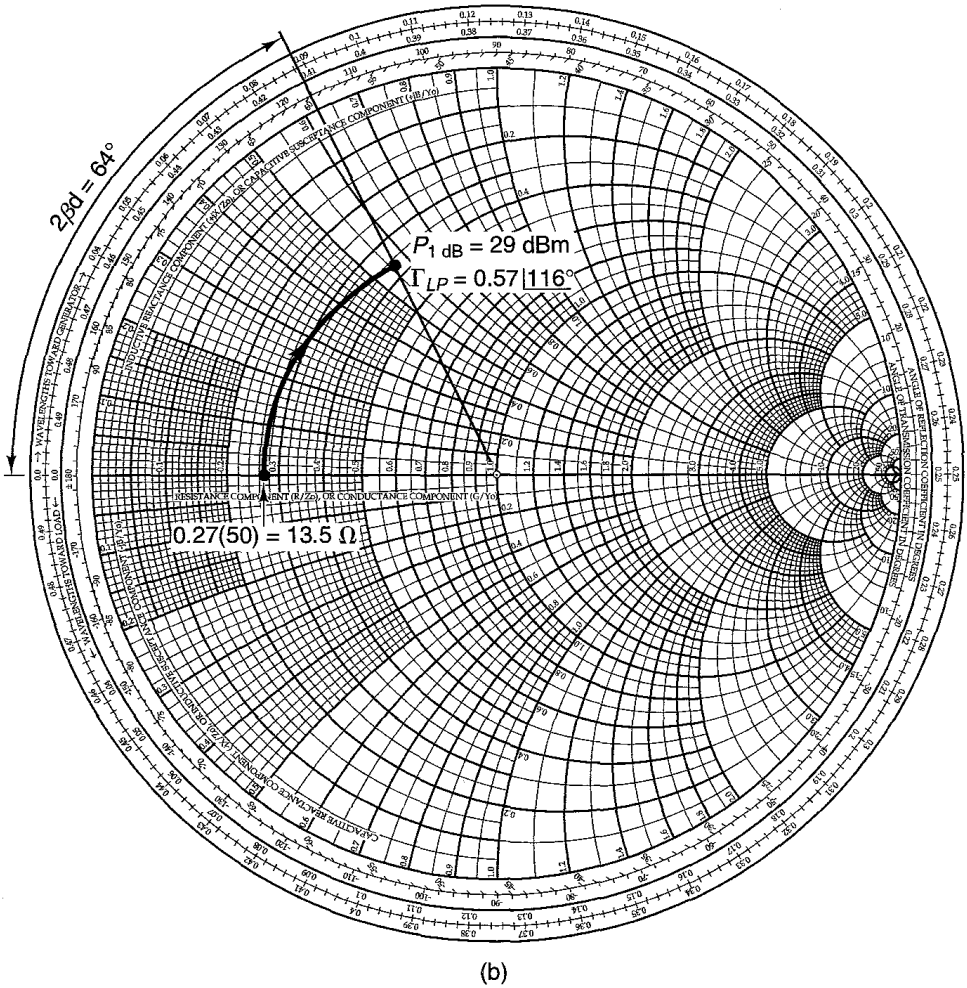
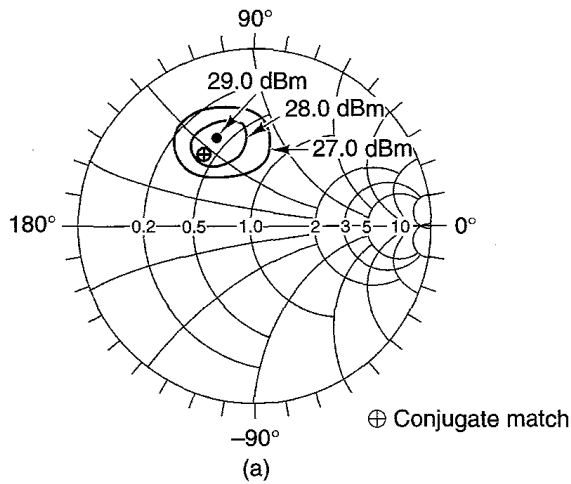


Figure 4.7.15 (a) Output power contours at 2 GHz, $V_{CE} = 18$ V, and $I_C = 110$ mA (From Ref. [4.20]; courtesy of Hewlett-Packard.); (b) design of the output matching network; (c) output network for the 2-GHz amplifier; (d) design of the input matching network; (e) schematic of the power amplifier.

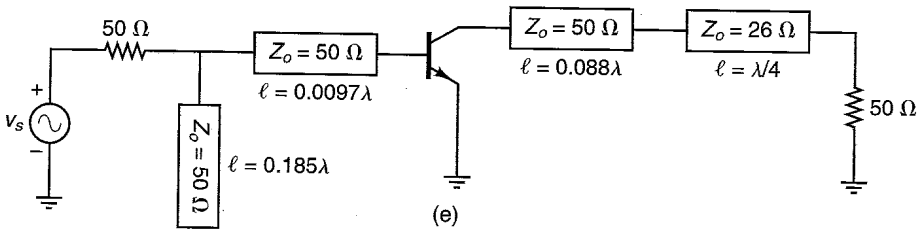
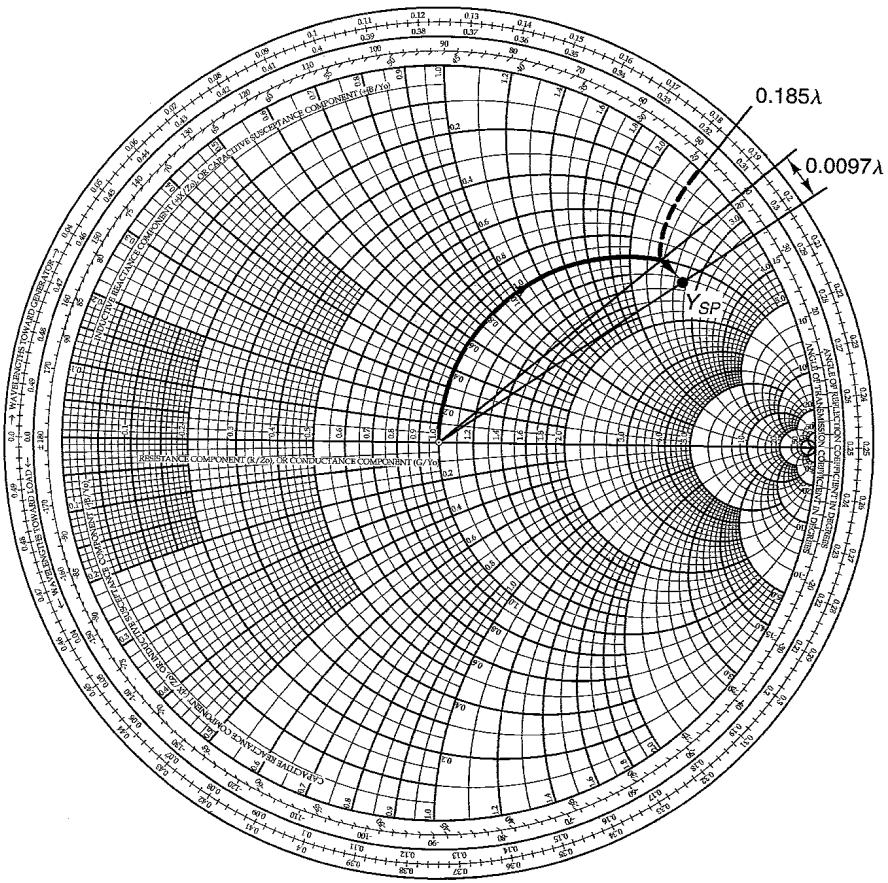
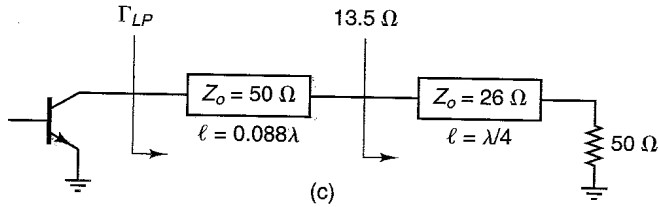


Figure 4.7.15 Continued

transformed to a resistance of 13.5Ω using a quarter-wave transformer with characteristic impedance Z_o given by

$$Z_o = \sqrt{50(13.5)} = 26 \Omega$$

A transmission line of length $\beta d = 32^\circ$ (i.e., 0.088λ) was used to complete the match. The output network schematic is shown in Fig. 4.7.15c.

To obtain an output power of 29 dBm, the input must be conjugately matched. The input conjugate match is calculated using (3.2.5)—namely,

$$\begin{aligned} \Gamma_{SP} = (\Gamma_{IN})^* &= \left[0.64 \angle 153^\circ + \frac{(0.07 \angle -8^\circ)(2.32 \angle 10^\circ)(0.57 \angle 116^\circ)}{1 - (0.51 \angle -119^\circ)(0.57 \angle 116^\circ)} \right]^* \\ &= 0.749 \angle -147.1^\circ \end{aligned}$$

The small-signal S parameters were used to calculate Γ_s since, for this transistor, at $P_{1\text{ dB}}$ the behavior can be assumed to be fairly linear.

The design of the input matching network is illustrated in Fig. 4.7.15d. An open-circuited shunt stub of length 0.185λ ($Z_o = 50 \Omega$), followed by a $50\text{-}\Omega$ series transmission line of length 3.5° (0.0097λ), were used to obtain the match. The complete ac schematic is shown in Fig. 4.7.15e.

Example 4.7.3

Design a 1-W (or 30-dBm) GaAs FET power amplifier for linear operation at 4 GHz. The input signal power is -5 dBm.

Solution. The required power gain of the power amplifier is

$$G_p(\text{dB}) = P_{\text{OUT}}(\text{dBm}) - P_{\text{IN}}(\text{dBm}) = 30 - (-5) = 35 \text{ dB}$$

For this design we selected the transistors from the *Hewlett-Packard Communications Components—GaAs & Silicon Products Designer's Catalog*. The transistors selected, with some pertinent data at 4 GHz, are listed in Fig. 4.7.16a. Figure 4.7.16a shows that the ATF44101 transistor can provide linear amplification with $G_p = 10$ dB and an output power of 1 W (or 30 dBm) at 4 GHz.

The required power gain of 35 dB can be obtained using three-stages, as shown in Fig. 4.7.16b. The gain and power levels of each stage are indicated in Fig. 4.7.16b.

The power gain of the three-stage amplifier in Fig. 4.7.16b is

$$G_p = G_{p1} + G_{p2} + G_{p3} = 14 + 11 + 10 = 35 \text{ dB}$$

Therefore, the output power is

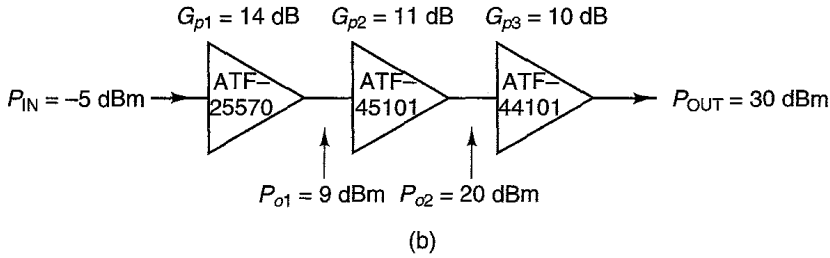
$$P_{\text{out}}(\text{dBm}) = P_{\text{in}}(\text{dBm}) + G_p = -5 + 35 = 30 \text{ dBm (or 1 W)}$$

Example 4.7.4

Design a 5-W linear amplifier to operate in the 470 MHz to 860 MHz band using the Motorola TPV593 transistor. (This example is based on Motorola Application Note AN1039.)

Transistor	Q point	G_p	$P_{1\text{ dB}}$	$G_{1\text{ dB}}$
ATF44101	9 V, 500 mA	10	32 dBm	9
ATF45101	9 V, 250 mA	11	29 dBm	10
ATF25570	5 V, 5 mA	14	20.5 dBm	13

(a)



(b)

Figure 4.7.16 (a) Transistors selected and some pertinent data at 4 GHz; (b) a 1-W, three-stage, linear power amplifier at 4 GHz.

Solution. The TPV593 is a transistor developed for linear class-A operation in TV amplifiers. Typical S parameters for the transistor at the recommended Q point of $V_{CE} = 25$ V and $I_C = 450$ mA are given in Fig. 4.7.17a. It is observed that the TPV593 transistor is unconditionally stable in the 470 MHz to 860 MHz band since $K > 1$ and $|\Delta| < 1$. The values of Γ_{Ms} and Γ_{ML} were calculated, as well as $G_{T,\max} = G_{p,\max} = G_{A,\max}$. The gain decreases by approximately 6 dB between 470 MHz and 860 MHz. Hence, if a constant gain is desired, the matching networks of the individual amplifiers must be designed to compensate for the gain slope (see Section 4.4). In Fig. 4.7.17a, the output power data and the intermodulation distortion (IMD) data provided by the manufacturer are also listed. The output power data show that a linear output power of 3 W is possible for this transistor.

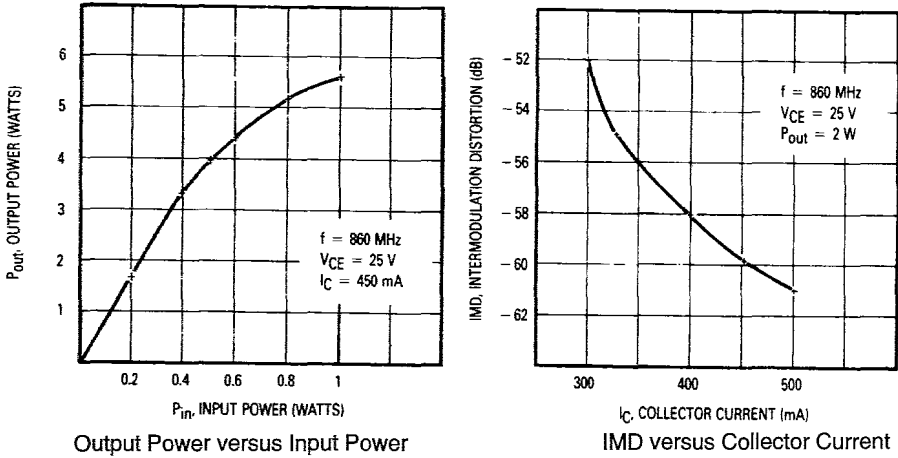
The desired output power of 5 W can be obtained by combining two identical amplifiers with an output power of 2.5 W with a 3-dB hybrid divider and a 3-dB hybrid combiner, as shown in Fig. 4.7.17b. Figure 4.7.17b shows the gains and power levels at various points in the circuit, neglecting the insertion loss of the 3-dB divider and of the 3-dB combiner. In practice, the 3-dB divider and 3-dB combiner introduce a certain insertion loss, and the power levels have to be adjusted accordingly to obtain $P_{OUT} = 5$ W. In the band of operation, the 3-dB divider and the 3-dB combiner can be constructed using parallel wire cable.

For further details, Motorola Application Note AN1039 gives a complete circuit schematic for the individual amplifiers, a practical board layout for the amplifier, and measurements on the performance of the amplifier. Also, a discussion of the design of the matching networks for an amplifier similar to that in Fig. 4.7.17b is given in Motorola Application Note AN1029.

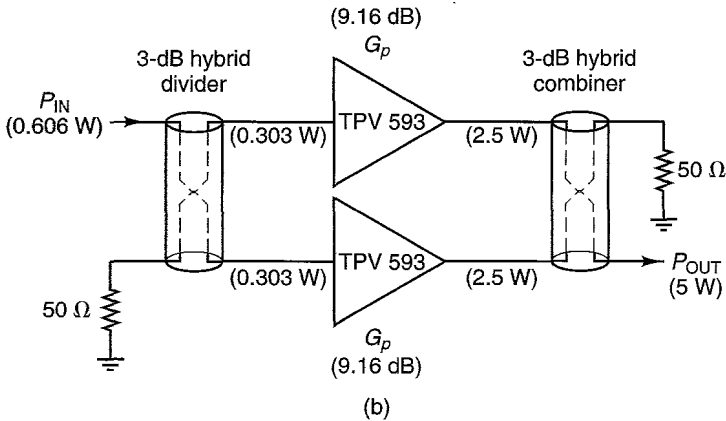
Example 4.7.5

Design a class-C amplifier to deliver 5 W to a 50- Ω load at 470 MHz using the Motorola MRF652 transistor.

f (MHz)	S_{11}	S_{12}	S_{21}	S_{22}	K	A	Γ_{Ms}	Γ_{ML}	$G_{p,max}$
470	0.927 170°	0.040 50°	1.50 63°	0.552 -166°	1.01	0.534 -2.1°	0.986 -173°	0.891 124°	15.1
650	0.926 165°	0.050 54°	1.06 50°	0.596 -169°	1.06	0.571 -9.1°	0.970 -168°	0.797 135°	11.7
860	0.918 162°	0.055 54°	0.79 38°	0.652 -169°	1.16	0.607 -11.1°	0.953 -165°	0.787 146°	9.18



(a)



(b)

Figure 4.7.17 (a) Data for the TPV593; (b) block diagram of the amplifier. (From *Motorola RF Device Data*, Vol. 1, 6th edition; Copyright of Motorola, used by permission.)

Solution. The Motorola MRF652 transistor is fabricated for operation from a 12.5-V supply (i.e., for mobile operation). The transistor large-signal impedance data are shown in Fig. 4.7.18a. These data are measured at an output power of 5 W to a 50- Ω load. The parameter Z_{OL}^* is simply the Z_{OUT} of the transistor. At 470 MHz, the required source and load impedances are

$$Z_s = Z_{IN}^* = 1.19 - j1.11$$

and

$$Z_L = Z_{OUT}^* = 7.6 + j5.1$$

The output matching network should be designed with a high Q (e.g., $Q > 10$) in order to provide suppression of the harmonics. A circuit diagram for the class-C amplifier is shown in Fig. 4.7.18b.

4.8 TWO-STAGE AMPLIFIER DESIGN

The configuration of a two-stage microwave transistor amplifier is shown in Fig. 4.8.1. The design of a two-stage amplifier usually consists of the optimization of one of the following requirements: (1) overall high gain, (2) overall low noise figure, or (3) overall high power. In a two-stage amplifier the stability of the individual stages, as well as the overall stability, must be checked.

In a design requiring overall high gain, the reflection coefficients are selected as follows:

$$\begin{aligned}\Gamma_s &= (\Gamma_{IN,1})^* \\ \Gamma_{IN,M} &= (\Gamma_{OUT,1})^* \\ \Gamma_{OUT,M} &= (\Gamma_{IN,2})^* \\ \Gamma_L &= (\Gamma_{OUT,2})^*\end{aligned}$$

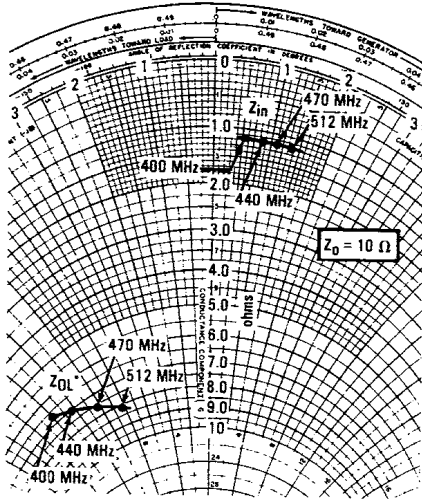
In a design requiring high power, the reflection coefficients are selected as follows:

$$\begin{aligned}\Gamma_s &= (\Gamma_{IN,1})^* \\ \Gamma_{IN,M} &= \Gamma_{LP,1} \\ \Gamma_{OUT,M} &= (\Gamma_{IN,2})^* \\ \Gamma_L &= \Gamma_{LP,2}\end{aligned}$$

where $\Gamma_{LP,1}$ and $\Gamma_{LP,2}$ are the large-signal load reflection coefficients of $T1$ and $T2$. In other words, the design of N_o results in $\Gamma_L = \Gamma_{LP,2}$ and the design of M is for a conjugate match at its output [i.e., $\Gamma_{OUT,M} = (\Gamma_{IN,2})^*$] and at its input $\Gamma_{IN,M} = \Gamma_{LP,1}$ (i.e., to present $\Gamma_{LP,1}$ to transistor $T1$). The network N_s presents a conjugate match at the input of transistor $T1$.

In a low-noise design, the reflection coefficients are selected as follows:

SERIES EQUIVALENT
INPUT/OUTPUT IMPEDANCE

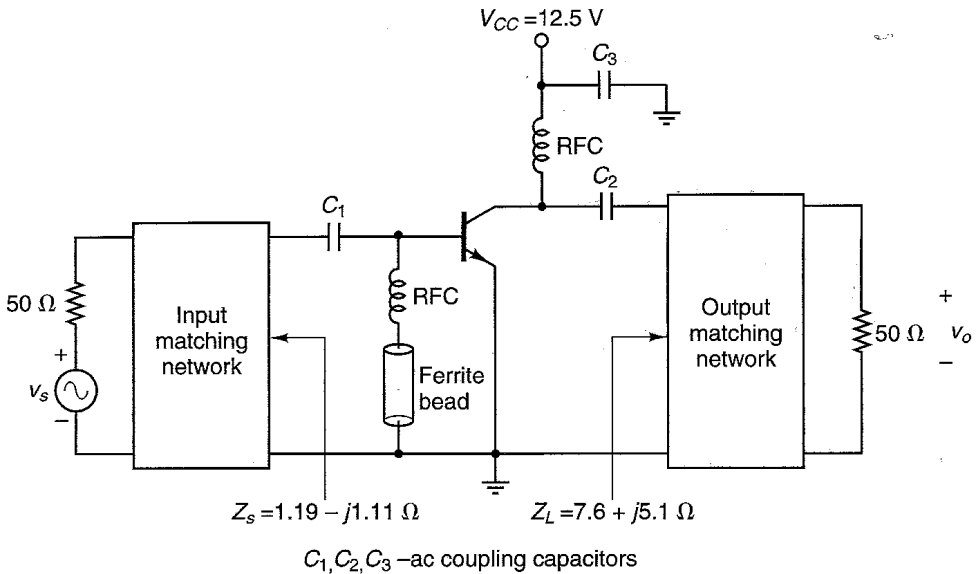


$V_{CC} = 12.5 \text{ Vdc}$
 $P_{out} = 5.0 \text{ W}$

f MHz	Z_{in} Ohms	Z_{OL}^* Ohms
400	$1.18 + j0.54$	$6.7 - j6.9$
440	$1.19 + j0.88$	$7.05 - j6.1$
470	$1.19 + j1.11$	$7.6 - j5.1$
512	$1.19 + j1.35$	$8.1 - j4.1$

Z_{OL}^* = Conjugate of the optimum load impedance into which the device operates at a given output power, voltage, and frequency.

(a)



(b)

Figure 4.7.18 (a) Large-signal impedances for the MRF652 transistor; (b) a class-C circuit diagram for the amplifier. (From *Motorola RF Device Data*, Vol. 1, 6th edition; Copyright of Motorola, used by permission.)

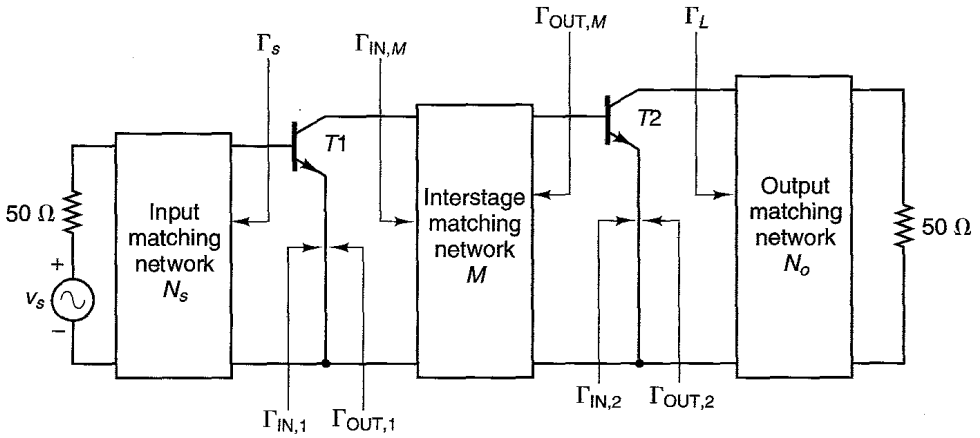


Figure 4.8.1 Diagram of a two-stage amplifier.

$$\begin{aligned} \Gamma_s &= \Gamma_{opt,1} \\ \Gamma_{IN,M} &= (\Gamma_{OUT,1})^* \\ \Gamma_{OUT,M} &= \Gamma_{opt,2} \\ \Gamma_L &= (\Gamma_{OUT,2})^* \end{aligned}$$

where $\Gamma_{opt,1}$ and $\Gamma_{opt,2}$ are the optimum noise source reflection coefficients for stages 1 and 2, respectively.

From (4.2.4), the overall noise figure of a two-stage amplifier depends on F_1, F_2 , and G_{A1} . The transistor of the first stage is usually selected to have a low noise figure, and a higher noise figure is permitted in the second stage. Although some trade-offs between noise figure and gain are possible, usually the optimum noise match with $\Gamma_{opt,1}$ and $\Gamma_{opt,2}$ is used.

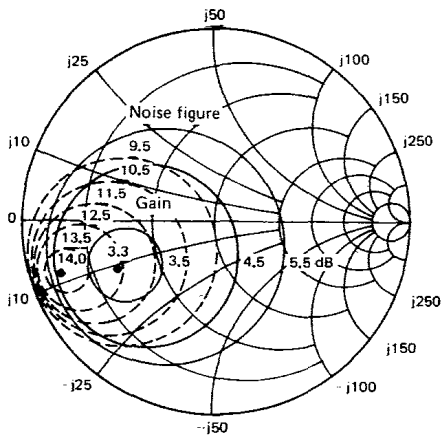
PROBLEMS

4.1. (a) Show that the noise figure for a three-stage amplifier is given by

$$F = F_1 + \frac{F_2 - 1}{G_{A1}} + \frac{F_3 - 1}{G_{A1}G_{A2}}$$

where F_1, F_2 and F_3 are the noise figures of the first, second, and third stages; and G_{A1} and G_{A2} are the available power gains of the first and second stages.

- (b) Two cascade amplifiers have noise figures of $F_1 = 1$ dB and $F_2 = 3$ dB, and a gain of $G_{A1} = 10$ dB and $G_{A2} = 16$ dB. Calculate the overall noise figure.
- 4.2 (a) A manufacturer provides the information shown in Fig. P4.2 for two micro-wave transistors. Evaluate the noise parameters for each transistor. Are the constant-gain circles given for G_T, G_A , or G_p ?
- (b) Verify the location of the $G_A = 10.7$ dB constant-gain circle in Fig. 4.3.4.

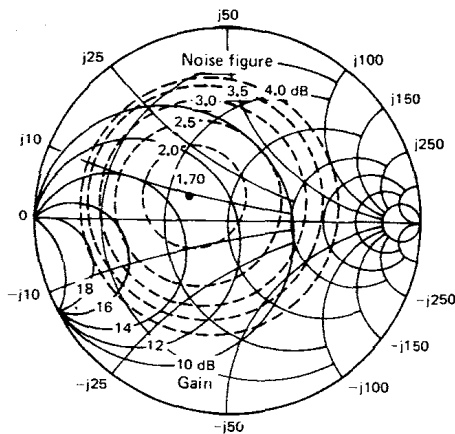


Frequency = 2 GHz, 10 V, 5 mA

$$S_{11} = 0.655 \angle 162.1^\circ \quad S_{21} = 2.286 \angle 45.8^\circ$$

$$S_{12} = 0.064 \angle 23.7^\circ \quad S_{22} = 0.569 \angle -54.6^\circ$$

(a)



Frequency = 2 GHz, 10 V, 5 mA

$$S_{11} = 0.646 \angle 172^\circ \quad S_{21} = 3.042 \angle 47.9^\circ$$

$$S_{12} = 0.051 \angle 13.5^\circ \quad S_{22} = 0.642 \angle -64^\circ$$

(b)

Figure P4.2 Two microwave transistors. (From Avantek Transistor Designers Catalog; courtesy of Avantek.)

4.3 (a) For the transistor in Fig. P4.2b, find a value of Γ_s that produces an available power gain of 14 dB and a noise figure of 2 dB.

(b) Find Γ_L for $(VSWR)_{out} = 1$ and determine $(VSWR)_{in}$.

4.4 The S parameters and the noise parameters of a transistor at 1 GHz are

$$S_{11} = 0.6 \angle -170^\circ \quad F_{min} = 2.5 \text{ dB}$$

$$S_{12} = 0.05 \angle 16^\circ \quad \Gamma_{opt} = 0.5 \angle 145^\circ$$

$$S_{21} = 2 \angle 30^\circ \quad R_n = 5 \Omega$$

$$S_{22} = 0.5 \angle -95^\circ$$

(a) Is the transistor unconditionally stable?

(b) Determine $G_{A,max}$.

(c) Draw the constant available power-gain circle which is 3 dB less than $G_{A,max}$.

(d) Draw the 3-dB and 4-dB constant noise figure circles.

(e) Determine the noise figure if the transistor is used in an amplifier designed for $G_{A,max}$.

4.5 Design a microwave transistor amplifier at 2 GHz to have a minimum noise figure using the transistor in Fig. P4.2a. Specify the resulting G_T , G_A , and G_p .

4.6 The scattering and noise parameters of a GaAs FET measured at a low-noise bias point ($V_{DS} = 5 \text{ V}$, $I_D = 15\% I_{DSS} = 10 \text{ mA}$) at $f = 12 \text{ GHz}$ are

$$\begin{aligned}
 S_{11} &= 0.75 \angle -116^\circ & F_{\min} &= 2.2 \text{ dB} \\
 S_{12} &= 0.01 \angle 67^\circ & \Gamma_{\text{opt}} &= 0.65 \angle 120^\circ \\
 S_{21} &= 3.5 \angle 64^\circ & R_n &= 10 \Omega \\
 S_{22} &= 0.77 \angle -65^\circ
 \end{aligned}$$

Design a microwave transistor amplifier to have a minimum noise figure.

- 4.7** The S parameters and the noise parameters of a BJT at $f = 2$ GHz, $V_{CE} = 8$ V, and $I_C = 10$ mA are

$$\begin{aligned}
 S_{11} &= 0.59 \angle 175^\circ & F_{\min} &= 1.6 \text{ dB} \\
 S_{12} &= 0.045 \angle 45^\circ & \Gamma_{\text{opt}} &= 0.2 \angle 155^\circ \\
 S_{21} &= 3.8 \angle 62^\circ & r_n &= 0.15 \Omega \\
 S_{22} &= 0.51 \angle -38^\circ
 \end{aligned}$$

Use the procedure in Example 4.3.2 to analyze the trade-offs between G_A , F , and $(\text{VSWR})_{\text{in}}$ as Γ_s varies between Γ_{Ms} and Γ_{opt} . Design the low-noise amplifier with $(\text{VSWR})_{\text{in}} \leq 2$. Draw a block diagram for the amplifier.

- 4.8** The scattering and noise parameters of a GaAs FET measured at a low-noise bias point ($V_{DS} = 3.5$ V, $I_D = 15\%$ $I_{DDs} = 12$ mA) at $f = 2$ GHz are

$$\begin{aligned}
 S_{11} &= 0.8 \angle -51.9^\circ & F_{\min} &= 1.25 \text{ dB} \\
 S_{12} &= 0.045 \angle 54.6^\circ & \Gamma_{\text{opt}} &= 0.73 \angle 60^\circ \\
 S_{21} &= 2.15 \angle 128.3^\circ & R_n &= 19.4 \Omega \\
 S_{22} &= 0.73 \angle -30.5^\circ
 \end{aligned}$$

Design a microwave transistor amplifier to have a minimum noise figure.

- 4.9** Design a microwave transistor amplifier at 2 GHz to have $F_i = 2$ dB using the transistor in Fig. P4.2b. Specify the resulting G_T , G_A , and G_p .
- 4.10** The S parameters and the noise parameters of two transistors are as follows:

<i>Transistor 1</i>		<i>Transistor 2</i>	
$S_{11} = 0.31 \angle -120.2^\circ$	$F_{\min} = 1.8 \text{ dB}$	$S_{11} = 0.6 \angle -190^\circ$	$F_{\min} = 1 \text{ dB}$
$S_{12} = 0.1 \angle 64.6^\circ$	$\Gamma_{\text{opt}} = 0.33 \angle 77^\circ$	$S_{12} = 0.05 \angle 50^\circ$	$\Gamma_{\text{opt}} = 0.42 \angle 32^\circ$
$S_{21} = 4.4 \angle 95.1^\circ$	$R_n = 14 \Omega$	$S_{21} = 9 \angle 120^\circ$	$R_n = 18 \Omega$
$S_{22} = 0.51 \angle -34.6^\circ$		$S_{22} = 0.7 \angle -35^\circ$	

For each transistor, follow a procedure similar to that in Example 4.3.4 to design a low-noise amplifier.

- 4.11** Use the GaAs FET in Example 4.3.4 to design a low-noise amplifier with $(\text{VSWR})_{\text{in}} \leq 2$. Follow a procedure similar to the one in Example 4.3.5 to design the amplifier.

4.12 The S parameters and the noise parameters of a transistor are

$$\begin{aligned}
 S_{11} &= 0.72 \angle -10^\circ & F_{\min} &= 1.9 \text{ dB} \\
 S_{12} &= 0.19 \angle 31^\circ & \Gamma_{\text{opt}} &= 0.6 \angle 71^\circ \\
 S_{21} &= 1.3 \angle 98^\circ & R_n &= 29 \ \Omega \\
 S_{22} &= 0.81 \angle -36^\circ
 \end{aligned}$$

Follow a procedure similar to the one in Example 4.3.5 to design a low-noise amplifier with $(\text{VSWR})_{\text{in}} \leq 1.5$.

4.13 Consider the LNB shown in Fig. P4.13. Calculate the total noise figure and the available gain.

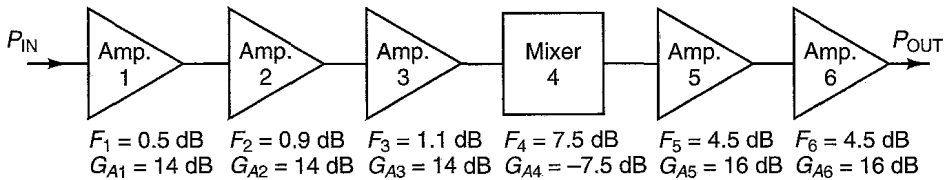


Figure P4.13

4.14 Design a broadband microwave BJT amplifier to have $G_{TV} = 12 \text{ dB}$ from 150 to 400 MHz. The transistor S parameters are as follows:

f (MHz)	S_{11}	S_{21}	S_{22}
150	$0.31 \angle -36^\circ$	5	$0.91 \angle -6^\circ$
250	$0.29 \angle -55^\circ$	4	$0.86 \angle -15^\circ$
400	$0.25 \angle -76^\circ$	2.82	$0.81 \angle -26^\circ$

(This problem is based on an example given in Ref. [4.21].)

Hint: G_s will be small and only G_L should be used to compensate for the variations of $|S_{21}|$ with frequency. G_s should be designed to provide a good VSWR at the input. The output matching network can be designed as in Fig. 4.4.4, or for a better match at the three frequencies an extra inductor in series with the 50- Ω load can be added.

4.15 Design a broadband microwave BJT amplifier with $G_{TV} = 10 \text{ dB}$ from 1 to 2 GHz with a noise figure of less than 4 dB. For this transistor, S_{12} can be neglected and the scattering and noise parameters are as follows:

f (GHz)	S_{11}	S_{21}	S_{22}	Γ_{opt}	R_n	F_{min} (dB)
1	0.64 \angle -98°	5.04 \angle 113°	0.79 \angle -30°	0.48 \angle 23°	23.3	1.45
1.5	0.60 \angle -127°	3.90 \angle 87°	0.76 \angle -35°	0.45 \angle 61°	15.6	1.49
2	0.59 \angle -149°	3.15 \angle 71°	0.75 \angle -43°	0.41 \angle 88°	15.7	1.61

In this problem, design the input and output matching networks so that $G_{TV} = 10$ dB at the band edges only, and calculate the resulting gain at 1.5 GHz. The noise figure over the band must be less than 4 dB.

- 4.16 (a)** The source and load impedance in the balance amplifier shown in Fig. 4.4.5 are 50Ω . The S parameters of the amplifiers A and B are identical and given by

$$S_{11} = 0.5 \angle 160^\circ$$

$$S_{12} = 0.08 \angle 60^\circ$$

$$S_{21} = 3.4 \angle 70^\circ$$

$$S_{22} = 0.4 \angle -45^\circ$$

Determine S_{11} , S_{22} , the input VSWR, the output VSWR, and the power gain.

- (b)** Consider the case where the S parameters of amplifier A are those in part (a) and the magnitude and phase of the S parameter of amplifier B are 5% higher. Determine S_{11} , S_{22} , the input VSWR, the output VSWR, and the power gain.
- 4.17 (a)** Show that K for the balance amplifier, using a 3-dB Lange coupler, is given by

$$K = \frac{1 + P^2}{2P}$$

where

$$P = |S_{21}S_{12}|$$

Show that K has a minimum value of 1 when $P = 1$ (i.e., when $|S_{21}S_{12}| = 1$) and $K > 1$ for all other values of P .

- (b)** The S parameters of a transistor at 2.1 GHz are

$$S_{11} = -0.699 - j0.348$$

$$S_{21} = -10.9 + j7.895$$

$$S_{22} = 0.309 + j0.459$$

$$S_{12} = 0.009 + j0.015$$

and the resulting K , $K = 0.48$, shows that the transistor is potentially unstable. If the transistor is used in a balanced amplifier configuration, calculate the resulting S parameters and K .

- 4.18** Verify (4.4.4), (4.4.5), and (4.4.6).

- 4.19** The BJT with shunt feedback in Fig. 4.4.10d at 100 MHz has S parameters given by

$$S_{11} = 0.97 \angle -8^\circ$$

$$S_{21} = 7.7 \angle 177^\circ$$

$$S_{22} = 0.97 \angle -7^\circ$$

Determine the value of R_2 in order to have $G_T = 10$ dB in a $50\text{-}\Omega$ system with $(VSWR)_{in} = (VSWR)_{out} \approx 1$.

- 4.20 (a)** The S parameters of the HXTR-3001 BJT transistor from 100 MHz to 1500 MHz are given in Fig. P4.20. Design a series-shunt feedback amplifier (see Fig. 4.4.10f) to have a constant transducer power gain of 10 dB in a $50\text{-}\Omega$ system.
- (b)** Use a CAD program to design input and output matching networks to provide a flat gain of 10 dB over the broadband of operation.

HXTR-3001 Typical common emitter S parameters ($V_{CE} = 15$ V, $I_C = 15$ mA)

Freq. (MHz)	S_{11}		S_{21}			S_{12}			S_{22}	
	Mag.	Ang.	(dB)	Mag.	Ang.	(dB)	Mag.	Ang.	Mag.	Ang.
100	0.651	-74	30.6	34.04	146	-37.2	0.014	59	0.851	-23
200	0.714	-113	27.8	24.66	125	-33.9	0.020	43	0.659	-33
300	0.741	-132	25.3	18.41	114	-32.9	0.023	36	0.539	-36
400	0.754	-143	23.2	14.46	107	-32.3	0.024	33	0.471	-36
500	0.761	-151	21.5	11.84	102	-32.0	0.025	31	0.429	-35
600	0.765	-155	20.0	10.00	98	-31.7	0.026	32	0.405	-34
700	0.767	-159	18.7	8.63	95	-31.5	0.027	32	0.389	-34
800	0.768	-162	17.6	7.59	93	-31.2	0.028	33	0.377	-34
900	0.769	-164	16.6	6.77	91	-31.0	0.028	34	0.370	-34
1000	0.770	-166	15.7	6.11	89	-30.7	0.029	35	0.365	-34
1500	0.770	-171	12.2	4.10	81	-29.3	0.034	41	0.358	-38

Figure P4.20

- 4.21 (a)** In the network shown in Fig. P4.21a, what is the best Γ_x that can be achieved in the frequency range 400 to 600 MHz?
- (b)** In the network shown in Fig. P4.21b, what is the best Γ_x that can be obtained in the range 6 to 12 GHz?
- 4.22** For the networks in Figs. 4.4.20b, c, and d, the gain-bandwidth restrictions are given by

$$\int_0^\infty \frac{1}{\omega^2} \ln \left| \frac{1}{\Gamma} \right| d\omega \leq \pi RC \quad (\text{for Fig. 4.4.20b})$$

$$\int_0^\infty \frac{1}{\omega^2} \ln \left| \frac{1}{\Gamma} \right| d\omega \leq \frac{\pi L}{R} \quad (\text{for Fig. 4.4.20c})$$

$$\int_0^\infty \ln \left| \frac{1}{\Gamma} \right| d\omega \leq \frac{\pi R}{L} \quad (\text{for Fig. 4.4.20d})$$

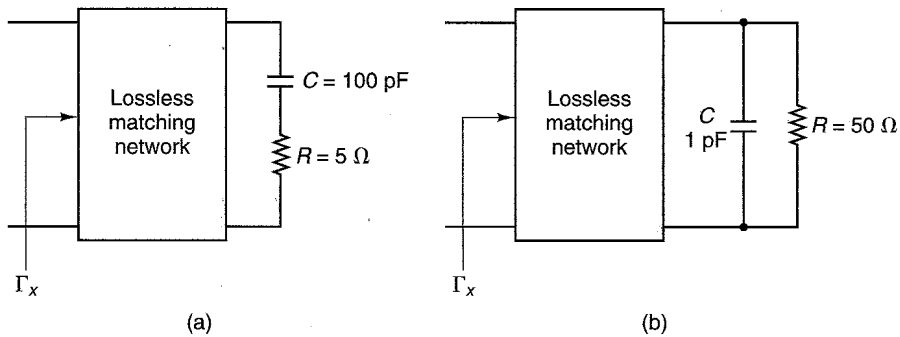


Figure P4.21

Show that Γ_x can be expressed in the form given in (4.4.16) when the appropriate definitions of Q_1 and Q_2 are used. These are given in Fig. 4.4.20.

- 4.23 (a) Verify the equation for δ_{IN} in (4.5.1).
 (b) Verify the relation between δ_{IN} and Γ_L in (4.5.2).
 (c) Derive a relation for δ_{OUT} .
- 4.24 The S parameters of a transistor at 8 GHz are

$$S_{11} = 0.75 \angle -100^\circ$$

$$S_{21} = 2.5 \angle 93^\circ$$

$$S_{12} = 0$$

$$S_{22} = 0.7 \angle -50^\circ$$

Determine

- (a) The terminations for $G_{TU,max}$.
 (b) The inherent bandwidths and Q of the input and output networks.
 (c) The additional elements (C or L) that must be added to the input and/or output networks to make the bandwidth 20% of the inherent bandwidth.
 (d) The optimum terminations for part (c) and the resulting G_{TU} .
- 4.25 In a microwave transistor amplifier, it is found that $\Gamma_{Ms} = 0.476 \angle 166^\circ$ and $\Gamma_{ML} = 0.846 \angle 72^\circ$ at $f = 4$ GHz. Calculate the amplifier input and output intrinsic bandwidths. If the bandwidth is to be limited to 400 MHz, find the value of C_{OUT} or L_{OUT} that must be added to the output network.
- 4.26 An amplifier has a transducer power gain of 30 dB, 800-MHz bandwidth, and a noise figure of 5 dB. The 1-dB gain compression point is given as 28 dBm. Calculate DR, DR_f , and the maximum output power for no third-order intermodulation distortion.
- 4.27 The specifications for two power GaAs FETs at a 4 GHz are as follows:

	P_1 dB (dBm)	G_1 dB (dB)	G_p (dB)
FET 1	25	6	7
FET 2	20	8	9

Show that the two-way power amplifier shown in Fig. P4.27 can be used to deliver $P_{OUT} = 27.7$ dBm, at 1 dB compression, with $P_{IN} = 6.3$ dBm. The loss of the two-

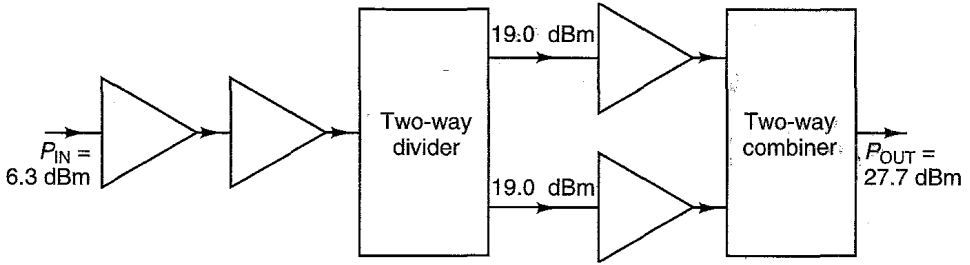


Figure P4.27

way combiner/divider is -0.3 dB. Specify the FET that must be used in each stage, and indicate the power and gain levels at all points. *Hint:* The power at the output of the divider is 19.0 dBm.

- 4.28 Design a power amplifier at 4 GHz using a BJT. The S parameters of the transistor and power characteristics at 4 GHz are

$$S_{11} = 0.32 \angle -145^\circ$$

$$S_{21} = 1.38 \angle -113^\circ$$

$$S_{12} = 0.08 \angle -98^\circ$$

$$S_{22} = 0.8 \angle -177^\circ$$

$$P_{1\text{dB}} = 27.5 \text{ dBm}$$

$$G_{1\text{dB}} = 7 \text{ dB}$$

$$\Gamma_{LP} = 0.1 \angle 0^\circ$$

- 4.29 A 4 GHz microwave amplifier consists of four stages, as shown in Fig. P4.29. The power gain of each stage is indicated and the input impedance of the first stage is 50Ω . Determine the input power (P_{IN}) and the output power (P_{OUT}) in dBm.

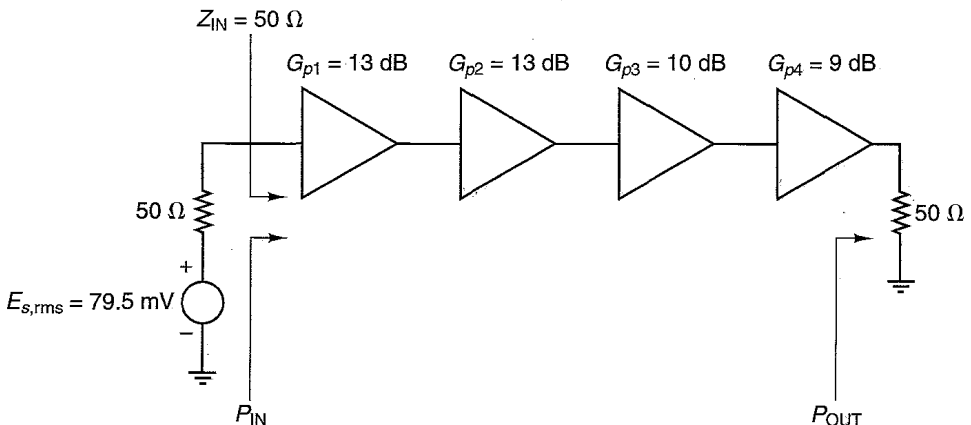


Figure P4.29

- 4.30 Show the block diagram of a 5-W class-C amplifier at 512 MHz using the Motorola MRF652 transistor whose large-signal data are given in Fig. 4.7.18a.
- 4.31 In the two-stage amplifier shown in Fig. 4.8.1, transistors T_1 and T_2 are potentially unstable. Can the overall amplifier be unconditionally stable?

REFERENCES

- [4.1] H. A. Haus (chairman), "Representation of Noise in Linear Two Ports," IRE Subcommittee 7.9 on Noise, *Proceedings of the IEEE*, January 1960.
- [4.2] "A Low Noise 4 GHz Transistor Amplifier Using the HXTR-6101 Silicon Bipolar Transistor," Hewlett-Packard Application Note 967, May 1975.
- [4.3] "A 6 GHz Amplifier Using the HFET-1101 GaAs FET," Hewlett-Packard Application Note 970, February 1978.
- [4.4] H. Fukui, "Available Power Gain, Noise Figure, and Noise Measure of Two-Ports and Their Graphical Representations," *IEEE Transactions on Circuit Theory*, June 1966.
- [4.5] C. R. Poole and D. K. Paul, "Optimum Noise Measure Terminations for Microwave Transistor Amplifiers," *IEEE Transactions on Microwave Theory and Techniques*, November 1985.
- [4.6] T. T. Ha, *Solid State Microwave Amplifier Design*, Wiley-Interscience, New York, 1981.
- [4.7] G. Matthaei, L. Young, and E. M. T. Jones, *Microwave Filters, Impedance-Matching Networks, and Coupling Structures*, Artech House, Inc., Dedham, Mass., 1980.
- [4.8] R. S. Elliot, *An Introduction to Guided Waves and Microwave Circuits*, Prentice Hall, 1993.
- [4.9] W. K. Chen, *Passive and Active Filters—Theory and Implementations*, John Wiley & Sons, 1986.
- [4.10] D. J. Mellor and J. G. Linvill, "Synthesis of Interstage Networks of Prescribed Gain versus Frequency Slopes," *IEEE Transactions on Microwave Theory and Techniques*, December 1975.
- [4.11] EAGLEWARE CORP., 1750 Mountain Glen, Stone Mountain, Ga., 30087.
- [4.12] S. E. Sussman-Fort, *Matchnet: Microwave Matching Network Synthesis*, Artech House, 1991.
- [4.13] R. W. Anderson, "S Parameter Techniques for Faster, More Accurate Network Design," Hewlett-Packard Application Note 95-1 (or *Hewlett-Packard Journal*), February 1967.
- [4.14] P. A. Rizzi, *Microwave Engineering—Passive Circuits*, Prentice Hall, 1988.
- [4.15] A. Presser, "Interdigitated Microstrip Coupler Design," *IEEE Transactions on Microwave Theory and Techniques*, October 1978.
- [4.16] J. Lange, "Integrated Stripline Quadrature Hybrids," *IEEE Transactions on Microwave Theory and Techniques*, December 1969.
- [4.17] I. Bahl and P. Bhartia, *Microwave Solid State Circuit Design*, Wiley Interscience, 1988.
- [4.18] L. Besser, "Microwave Circuit Design," *Electronic Engineering*, October 1980.

- [4.19] R. M. Fano, "Theoretical Limitations on the Broadband Matching of Arbitrary Impedances," *Journal of the Franklin Institute*, January 1950.
- [4.20] "Two Telecommunications Power Amplifiers for 2 and 4 GHz Using the HXTR-5102 Silicon Bipolar Power Transistor," Hewlett-Packard Application Note 972, 1980.
- [4.21] R. S. Carson, *High-Frequency Amplifiers*, Wiley-Interscience, New York, 1975.

5

MICROWAVE TRANSISTOR OSCILLATOR DESIGN

5.1 INTRODUCTION

In this chapter the analytical techniques that are used in the design of negative-resistance oscillators are discussed. The small- and large-signal S parameters provide all the information needed to design negative-resistance oscillators.

In a negative-resistance oscillator we refer to the matching networks at the two ports as the terminating and the load (or resonant) matching networks. The load-matching network is the network that determines the frequency of oscillation, and the terminating network is used to provide the proper matching.

The design of the terminating and load-matching networks must be done carefully. For example, the condition $|\Gamma_{IN}| > 1$ is necessary for oscillation. A short circuit at the terminating port can produce $|\Gamma_{IN}| > 1$. However, no power is delivered to a short-circuited termination.

Several negative-resistance oscillator configurations are discussed, including dielectric resonator oscillators and varactor-tuned oscillators.

5.2 OSCILLATION CONDITIONS

Feedback Oscillators

A basic feedback oscillator is shown in Fig. 5.2.1. The amplifier's voltage gain is $A_v(j\omega)$, and the voltage feedback network is described by the transfer function $\beta(j\omega)$. The amplifier gain $A_v(j\omega)$ is also called the open-loop gain since it is the gain between v_o and v_i when the path through $\beta(j\omega)$ is open.

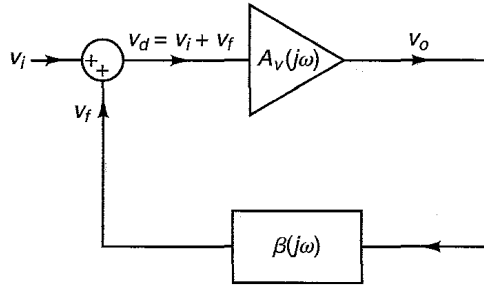


Figure 5.2.1 The basic feedback circuit.

The amplifier gain is, in general, a complex quantity. However, in many practical oscillators, at the frequency of oscillation, the amplifier is operating in its mid-band region where $A_v(j\omega)$ is a real constant. The constant $A_v(j\omega)$ is denoted by A_{vo} .

Negative feedback occurs when the feedback signal subtracts from the input signal. On the other hand, if v_f adds to v_i , the feedback is positive. The summing network in Fig. 5.2.1 shows the feedback signal added to v_i to suggest that the feedback is positive. Of course, the phase of v_f determines if v_f adds to or subtracts from v_i . The phase of v_f is determined by the closed-loop circuit in Fig. 5.2.1. If $A_v(j\omega) = A_{vo}$ and A_{vo} is a positive number, the phase shift through the amplifier is 0° , and for positive feedback the phase through $\beta(j\omega)$ should be 0° (or a multiple of 360°). If A_{vo} is a negative number, the phase shift through the amplifier is -180° (or 180°), and the phase through $\beta(j\omega)$ for positive feedback should be 180° (or 180° plus or minus a multiple of 360°). In other words, for positive feedback the total phase shift associated with the closed loop must be 0° or a multiple of 360° .

From Fig. 5.2.1 we can write

$$v_o = A_v(j\omega)v_d \tag{5.2.1}$$

$$v_f = \beta(j\omega)v_o \tag{5.2.2}$$

and

$$v_d = v_i + v_f \tag{5.2.3}$$

Thus, from (5.2.1) to (5.2.3), the closed-loop voltage gain $A_{vf}(j\omega)$ is given by

$$A_{vf}(j\omega) = \frac{v_o}{v_i} = \frac{A_v(j\omega)}{1 - \beta(j\omega)A_v(j\omega)} \tag{5.2.4}$$

For oscillations to occur, an output signal must exist with no input signal applied. With $v_i = 0$ in (5.2.4), it follows that a finite v_o is possible only when the denominator is zero. That is, when

$$1 - \beta(j\omega)A_v(j\omega) = 0$$

or

$$\beta(j\omega)A_v(j\omega) = 1 \tag{5.2.5}$$

Equation (5.2.5) expresses the fact that for oscillations to occur, the loop gain [i.e., $\beta(j\omega)A_v(j\omega)$] must be unity. This relation is known as the Barkhausen criterion. With $A_v(j\omega) = A_{vo}$ and letting

$$\beta(j\omega) = \beta_r(\omega) + j\beta_i(\omega)$$

where $\beta_r(\omega)$ and $\beta_i(\omega)$ are the real and imaginary parts of $\beta(j\omega)$, we can express (5.2.5) in the form

$$\beta_r(\omega)A_{vo} + j\beta_i(\omega)A_{vo} = 1$$

Equating the real and imaginary parts on both sides of the equation gives

$$\beta_r(\omega)A_{vo} = 1 \Rightarrow A_{vo} = \frac{1}{\beta_r(\omega)} \quad (5.2.6)$$

and

$$\beta_i(\omega)A_{vo} = 0 \Rightarrow \beta_i(\omega) = 0 \quad (5.2.7)$$

since $A_{vo} \neq 0$. The conditions in (5.2.6) and (5.2.7) are known as the Barkhausen criteria expressed in rectangular form.

The condition (5.2.6) is known as the gain condition, and (5.2.7) as the frequency of oscillation condition. The frequency of oscillation condition gives the frequency at which the phase shift around the closed loop is 0° or a multiple of 360° .

From the circuit theory we know that oscillation occurs when a network has a pair of complex conjugate poles on the imaginary axis. If the closed-loop gain in (5.2.4) has a pair of complex conjugate poles in the right-half plane, close to the imaginary axis, then, due to the ever-present noise voltage generated by thermal vibrations in the network (which can be represented by a superposition of input noise signals v_i), a growing sinusoidal output voltage appears. The characteristics of the sinusoidal signal are determined by the complex-conjugate poles in the right-half plane. As the amplitude of the noise-induced oscillation increases, the amplitude-limiting capabilities of the amplifier produce a change in the location of the poles. In the case of a transistor amplifier, as the amplitude of oscillation increases, its value of g_m decreases from its small-signal values. The changes are such that the complex-conjugate poles move toward the imaginary axis, and at some value of the oscillation amplitude the poles reach the imaginary axis. At this point, (5.2.6) and (5.2.7) are satisfied and the oscillation stabilizes at a constant amplitude value.

The previous discussion shows that for oscillations to start, the circuit must be unstable (i.e., the circuit must have poles in the right-half plane). The condition (5.2.5) does not predict if the circuit is unstable. However, if the circuit oscillates, the condition (5.2.5) must be satisfied at the frequency of oscillation. The stability of a circuit can be determined using the Nyquist stability test. In the Nyquist test, the complex function $\beta(j\omega)A_v(j\omega)$ is plotted versus frequency and the number of clockwise encirclements of the point $\beta(j\omega)A_v(j\omega) = 1$ de-

terminates the difference in the number of right-half plane zeroes and poles of the function $1 - \beta(j\omega)A_v(j\omega)$.

In a stable system, if there are no right-half plane poles of $\beta(j\omega)A_v(j\omega)$, the plot of $\beta(j\omega)A_v(j\omega)$ cannot encircle the point 1 in the complex $\beta(j\omega)A_v(j\omega)$ plane, in a clockwise direction. A clockwise encirclement of the point $\beta(j\omega)A_v(j\omega) = 1$ shows that the system is unstable. A peculiar situation can occur when the number of right-half plane poles is equal to the number of right-half plane zeroes. In this case, the system is unstable and the point $\beta(j\omega)A_v(j\omega) = 1$ is not encircled.

For a microwave circuit, a closed-loop gain function of the type in (5.2.5) can be developed as follows. Consider the circuit shown in Fig. 5.2.2a and its flow graph in Fig. 5.2.2b. The coefficient $\Gamma_L(j\omega)$ represents the load reflection coefficient and $\Gamma_{IN}(j\omega)$ the input reflection coefficient of an active device. The incident wave a_n represents a small noise signal generated in the circuit. From the flow graph in Fig. 5.2.2b, we can write

$$a_L = \frac{a_n \Gamma_{IN}(j\omega)}{1 - \Gamma_{IN}(j\omega) \Gamma_L(j\omega)} \tag{5.2.8}$$

Equation (5.2.8) is the closed-loop gain of the circuit in Fig. 5.2.2a. It is in the form of (5.2.4). From (5.2.8), we observe that the system is unstable when some noise produces a growing signal a_L . This occurs when the function $1 - \Gamma_{IN}(j\omega) \Gamma_L(j\omega)$ has right-half plane zeroes. The Nyquist test can be applied to analyze the function $1 - \Gamma_{IN}(j\omega) \Gamma_L(j\omega)$ by determining the encirclements of the point $\Gamma_{IN}(j\omega) \Gamma_L(j\omega) = 1$.

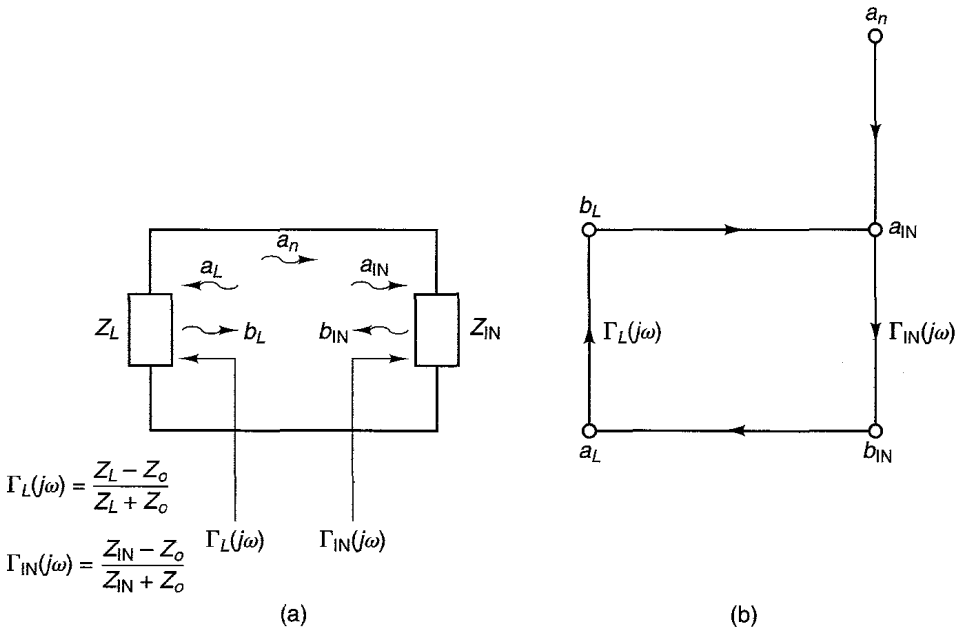


Figure 5.2.2 (a) A microwave circuit; (b) the flow graph.

Equation (5.2.8) shows that for oscillations to occur, the loop gain must be unity. That is,

$$\Gamma_{\text{IN}}(j\omega)\Gamma_L(j\omega) = 1 \quad (5.2.9)$$

The input impedance of the active device Z_{IN} is, in general, a function of the voltage (or current) amplitude and frequency, and we will show that for oscillations to occur, the real part of Z_{IN} must be negative.

One-Port Negative-Resistance Oscillators

A general schematic diagram for one-port negative-resistance oscillators is shown in Fig. 5.2.3. The negative-resistance device is represented by the amplitude and frequency-dependent impedance

$$Z_{\text{IN}}(A, \omega) = R_{\text{IN}}(A, \omega) + jX_{\text{IN}}(A, \omega) \quad (5.2.10)$$

where A is the amplitude of $i(t)$ and

$$R_{\text{IN}}(A, \omega) < 0$$

The oscillator is constructed by connecting the device to a passive load impedance, called

$$Z_L(\omega) = R_L(\omega) + jX_L(\omega) \quad (5.2.11)$$

The discussion in Section 3.3 showed that the one-port network in Fig. 5.2.3 is stable if

$$\text{Re}[Z_{\text{IN}}(A, \omega) + Z_L(\omega)] > 0$$

and from (5.2.9) the network will oscillate, at the amplitude $A = A_o$ and frequency $\omega = \omega_o$, when

$$\Gamma_{\text{IN}}(A_o, \omega_o)\Gamma_L(\omega_o) = 1 \quad (5.2.12)$$

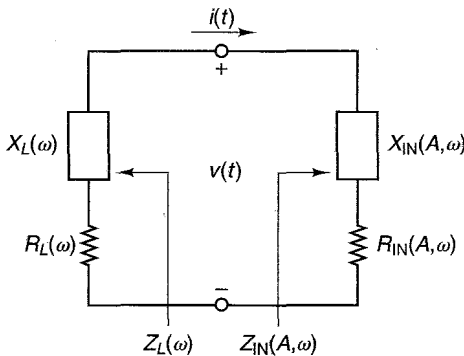


Figure 5.2.3 Schematic diagram for one-port negative-resistance oscillators.

The notation used in (5.2.12) is more suitable than the notation in (5.2.9) since it shows specifically the dependence of $\Gamma_{\text{IN}}(A, \omega)$ on the current amplitude and frequency. Since

$$\Gamma_{\text{IN}}(A_o, \omega_o) = \frac{Z_{\text{IN}}(A_o, \omega_o) - Z_o}{Z_{\text{IN}}(A_o, \omega_o) + Z_o} \quad (5.2.13)$$

and

$$\Gamma_L(\omega_o) = \frac{Z_L(\omega_o) - Z_o}{Z_L(\omega_o) + Z_o} \quad (5.2.14)$$

it follows that substituting (5.2.13) and (5.2.14) into (5.2.12), we can express (5.2.12) in the form

$$Z_{\text{IN}}(A_o, \omega_o) + Z_L(\omega_o) = 0 \quad (5.2.15)$$

Then, substituting (5.2.10) and (5.2.11) into (5.2.15) and equating the real and imaginary parts, the oscillation conditions can be written as

$$R_{\text{IN}}(A_o, \omega_o) + R_L(\omega_o) = 0 \quad (5.2.16)$$

and

$$X_{\text{IN}}(A_o, \omega_o) + X_L(\omega_o) = 0 \quad (5.2.17)$$

To be specific, the device is defined to be unstable over some frequency range $\omega_1 < \omega < \omega_2$ if $R_{\text{IN}}(A, \omega) < 0$. The one-port network is unstable for some ω in the range if the net resistance of the network is negative—that is, when

$$|R_{\text{IN}}(A, \omega)| > R_L(\omega) \quad (5.2.18)$$

Under proper conditions, a growing sinusoidal current will flow through the circuit. That is, at the start of oscillations, when the amplitude A is small, (5.2.18) must be satisfied. This is expressed in the form

$$|R_{\text{IN}}(0, \omega)| > R_L(\omega) \quad (5.2.19)$$

The oscillations will continue to build up as long as the loop resistance is negative, as required by (5.2.18). The amplitude of the current must eventually reach a steady-state value (i.e., at $A = A_o$ and $\omega = \omega_o$), which occurs when the loop resistance is zero. To satisfy the start of oscillation condition in (5.2.19), the build-up of oscillations, and the oscillation conditions in (5.2.16) and (5.2.17), the impedance $Z_{\text{IN}}(A, \omega)$ must be amplitude and frequency dependent.

The frequency of oscillation determined by (5.2.16) and (5.2.17) might not be stable since $Z_{\text{IN}}(A, \omega)$ is amplitude and frequency dependent. Therefore, it is necessary to find another condition to guarantee a stable oscillation. If the frequency dependence of $Z_{\text{IN}}(A, \omega)$ can be neglected for small variations around ω_o , Kurokawa [5.1] has shown that a stable oscillation is obtained when (5.2.16) and (5.2.17) are satisfied and the following condition is also satisfied:

$$\left. \frac{\partial R_{\text{IN}}(A)}{\partial A} \right|_{A=A_o} \left. \frac{dX_L(\omega)}{d\omega} \right|_{\omega=\omega_o} - \left. \frac{\partial X_{\text{IN}}(A)}{\partial A} \right|_{A=A_o} \left. \frac{dR_L(\omega)}{d\omega} \right|_{\omega=\omega_o} > 0 \quad (5.2.20)$$

The derivation of (5.2.20) is given in Appendix M.

In many cases,

$$\frac{dR_L(\omega)}{d\omega} = 0$$

(i.e., R_L is a constant) and (5.2.20) simplifies accordingly. Also, when R_L is constant, the term $R_L(\omega_o)$ in (5.2.16) is simply replaced by the constant value R_L .

In a given oscillator design, the input impedance of the active device is known for small-signal conditions. A practical way of designing R_L is to select the value of R_L for maximum oscillator power. If the magnitude of the negative resistance is a linearly decreasing function of A (see Fig. 5.2.4), we can express $R_{\text{IN}}(A)$ in the form

$$R_{\text{IN}}(A) = -R_0 \left(1 - \frac{A}{A_M} \right) \quad (5.2.21)$$

where $-R_0$ is the value of $R_{\text{IN}}(A)$ at $A = 0$, and A_M is the maximum value of A .

In Fig. 5.2.3, the power delivered to R_L by R_{IN} (for $A < A_M$) is

$$P = \frac{1}{2} \text{Re}[VI^*] = \frac{1}{2} |I|^2 |R_{\text{IN}}(A)| = \frac{1}{2} A^2 R_0 \left[1 - \frac{A}{A_M} \right]$$

Hence, the value of A that maximizes the oscillation power is found from

$$\frac{dP}{dA} = \frac{1}{2} R_0 \left[2A - \frac{3A^2}{A_M} \right] = 0$$

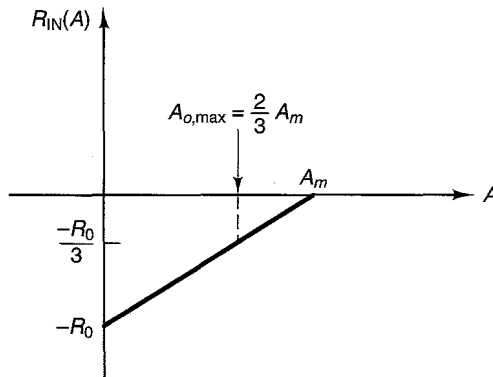


Figure 5.2.4 Linear variation of the negative resistance as a function of the current amplitude.

which gives the desired value of A , denoted by $A_{o,\max}$, that maximizes the power. That is,

$$A_{o,\max} = \frac{2}{3} A_M$$

At $A_{o,\max}$, the value of $R_{IN}(A_{o,\max})$ is

$$R_{IN}(A_{o,\max}) = -\frac{R_0}{3}$$

Hence a convenient value of R_L , which maximizes the oscillator power, is

$$R_L = \frac{R_0}{3} \tag{5.2.22}$$

Observe that (5.2.22) is valid when the negative input resistance varies linearly with amplitude. In practice, the selection of R_L according to (5.2.22) produces good results.

Example 5.2.1

(a) Determine the values of R_{IN} that make the circuit in Fig. 5.2.5a unstable. For simplicity in the analysis, choose $L = 1$ H and $C = 1$ F.

(b) Determine if a stable oscillation is possible, if $R_{IN}(A)$ is given by (5.2.21).

(c) Assume that $R_{IN}(A)$ is given by (5.2.21) with $R_0 = 45 \Omega$ and $A_M = 1$ ampere. Determine the value of R_L for maximum oscillator power.

Solution. (a) The location of Γ_{IN} and Γ_L can be selected arbitrarily. For the circuit in Fig. 5.2.5a, the input and load reflection coefficients were selected at the location indicated in the figure. That is,

$$Z_{IN} = R_{IN}$$

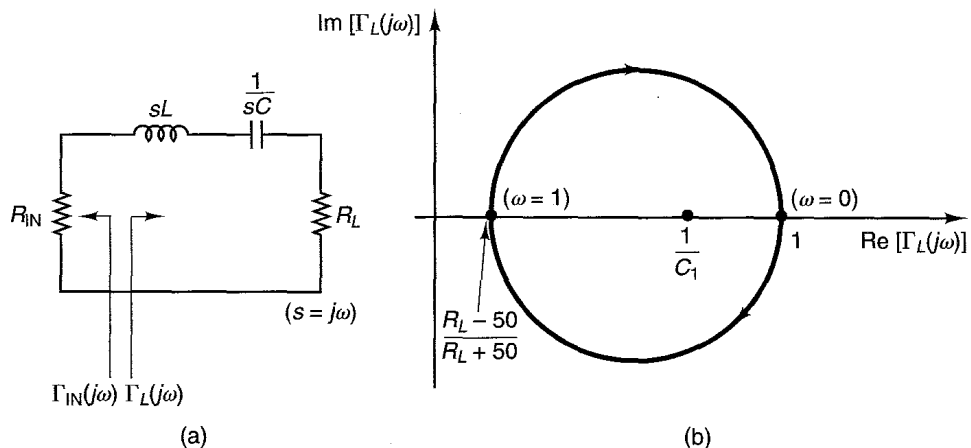


Figure 5.2.5 (a) Circuit for Example 5.2.1; (b) the Nyquist plot of $\Gamma_{IN}(j\omega)\Gamma_L(j\omega)$.

and

$$Z_L(s) = s + \frac{1}{s} + R_L = \frac{s^2 + R_L s + 1}{s}$$

where $s = j\omega$. Then, in a 50- Ω system,

$$\Gamma_{IN}(s) = \frac{R_{IN} - 50}{R_{IN} + 50} = C_1$$

and

$$\Gamma_L(s) = \frac{Z_L(s) - 50}{Z_L(s) + 50} = \frac{s^2 + s(R_L - 50) + 1}{s^2 + s(R_L + 50) + 1}$$

The selection of $Z_{IN} = R_{IN}$ made $\Gamma_{IN}(s)$ a constant, which is denoted by C_1 .

To apply the Nyquist test, we form

$$\Gamma_{IN}(j\omega)\Gamma_L(j\omega) = 1$$

or

$$\frac{(1 - \omega^2) + j\omega(R_L - 50)}{(1 - \omega^2) + j\omega(R_L + 50)} = \frac{1}{C_1} \quad (5.2.23)$$

The Nyquist plot of (5.2.23) is shown in Fig. 5.2.5b for positive values of C_1 (the plot for negative values of C_1 is quite similar). The Nyquist test applied to (5.2.23) shows that the circuit is unstable when the number of encirclements of the point $1/C_1$ is nonzero. Figure 5.2.5b shows that the circuit is unstable when

$$\frac{R_L - 50}{R_L + 50} < \frac{1}{C_1} < 1$$

Since $|C_1| > 1$, it follows that $1/C_1 < 1$; therefore, the circuit is unstable when

$$\frac{R_L - 50}{R_L + 50} < \frac{R_{IN} + 50}{R_{IN} - 50}$$

Since $R_{IN} < 0$, we can express the inequality in the form

$$(R_L - 50)(R_{IN} - 50) > (R_{IN} + 50)(R_L + 50)$$

which reduces to

$$R_L + R_{IN} < 0$$

or simply

$$R_{IN} < -R_L$$

which is the expected result for the circuit in Fig. 5.2.5a to be unstable.

(b) From (5.2.16), oscillations are possible when $R_{IN} + R_L = 0$, and from (5.2.17) (with $X_{IN} = 0$) the frequency of oscillation is given by

$$X_L(j\omega_o) = j\omega_o + \frac{1}{j\omega_o} = j\left(\omega_o - \frac{1}{\omega_o}\right) = 0$$

or

$$\omega_o = 1 \text{ rad/s}$$

For the circuit to maintain a stable oscillation at $\omega_o = 1 \text{ rad/s}$, the condition (5.2.20) must be satisfied. With R_{IN} given by (5.2.21), it follows that

$$\frac{\partial R_{IN}(A)}{\partial A} = \frac{R_0}{A_M}$$

Therefore, since $R_0 > 0$, we have that $\partial R_{IN}(A)/\partial A > 0$.

Also, with $jX_L = j(\omega - 1/\omega)$, it follows that

$$\frac{dX_L(\omega)}{d\omega} = 1 + \frac{1}{\omega^2}$$

Therefore,

$$\left. \frac{\partial R_{IN}(A)}{\partial A} \right|_{A=A_o} \left. \frac{dX_L(\omega)}{d\omega} \right|_{\omega=\omega_o} > 0$$

which shows that the oscillation is stable.

(c) From (5.2.21), the expression for $R_{IN}(A)$ is

$$R_{IN}(A) = -45(1 - A)$$

Using (5.2.22), the value of R_L that maximizes the oscillator power is

$$R_L = \frac{R_0}{3} = \frac{45}{3} = 15 \Omega$$

and the amplitude of A is

$$A_{o,\max} = \frac{2}{3} A_M = \frac{2}{3} (1) = \frac{2}{3} \text{ ampere}$$

In some cases it is more convenient to represent the one-port negative resistance oscillator using the parallel model shown in Fig. 5.2.6. The negative-resistance device is represented by the admittance

$$Y_{IN}(A', \omega) = G_{IN}(A', \omega) + jB_{IN}(A', \omega)$$

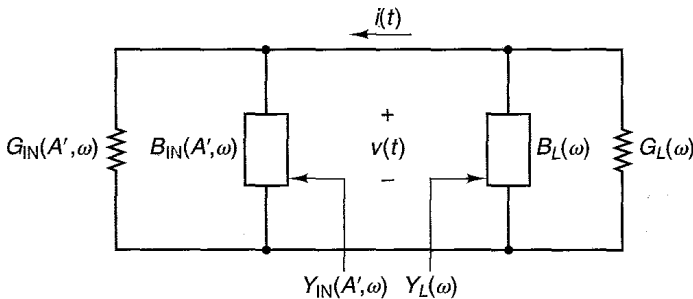


Figure 5.2.6 The parallel circuit model for the one-port negative-resistance oscillator.

where A' is the amplitude of $v(t)$, and $G_{IN}(A', \omega) < 0$.

The network in Fig. 5.2.6 will oscillate at the amplitude $A' = A'_o$ and frequency $\omega = \omega_o$ when

$$\Gamma_{IN}(A'_o, \omega_o) \Gamma_L(\omega_o) = 1 \quad (5.2.24)$$

where

$$\Gamma_{IN}(A'_o, \omega_o) = \frac{Y_o - Y_{IN}(A'_o, \omega_o)}{Y_o + Y_{IN}(A'_o, \omega_o)} \quad (5.2.25)$$

and

$$\Gamma_L(\omega_o) = \frac{Y_o - Y_L(\omega_o)}{Y_o + Y_L(\omega_o)} \quad (5.2.26)$$

Y_o is the normalized admittance.

Substituting (5.2.25) and (5.2.26) into (5.2.24), it follows that (5.2.24) can be expressed as

$$Y_{IN}(A'_o, \omega_o) + Y_L(\omega_o) = 0$$

or, in terms of the real and imaginary parts of the admittance, we have

$$G_{IN}(A'_o, \omega_o) + G_L(\omega_o) = 0 \quad (5.2.27)$$

and

$$B_{IN}(A'_o, \omega_o) + B_L(\omega_o) = 0 \quad (5.2.28)$$

The start of oscillation condition can be expressed in the form

$$|G_{IN}(0, \omega)| > G_L(\omega)$$

For stable oscillation, the Kurokawa condition in (5.2.20) must be satisfied. In terms of the circuit in Fig. 2.5.6, the condition reads

$$\left. \frac{\partial G_{IN}(A')}{\partial A'} \right|_{A'=A'_o} \left. \frac{dG_L(\omega)}{d\omega} \right|_{\omega=\omega_o} - \left. \frac{\partial B_{IN}(A')}{\partial A'} \right|_{A'=A'_o} \left. \frac{dB_L(\omega)}{d\omega} \right|_{\omega=\omega_o} > 0 \quad (5.2.29)$$

If the magnitude of $G_{IN}(A')$ decreases linearly with amplitude, we can express $G_{IN}(A')$ as

$$G_{IN}(A') = -G_0 \left(1 - \frac{A'}{A'_M} \right) \quad (5.2.30)$$

where $-G_0$ is the value of $G_{IN}(A')$ at $A' = 0$, and A'_M is the maximum value of A' . It follows that the value of G_L for maximum oscillation power is

$$G_L = \frac{G_0}{3} \quad (5.2.31)$$

Example 5.2.2

(a) Determine the values of G_{IN} that make the circuit in Fig. 5.2.7a unstable. For simplicity in the analysis, choose $L = 1$ H and $C = 1$ F.

(b) Determine if a stable oscillation is possible, if $G_{IN}(A')$ is given by (5.2.30).

(c) Assume that $G_{IN}(A')$ is given by (5.2.30) with $G_0 = 45$ mS and $A'_M = 1$ V. Determine the value of G_L for maximum oscillator power.

Solution. (a) For the circuit in Fig. 5.2.7a, the input and load reflection coefficients were selected at the location indicated in the figure. That is,

$$Y_{IN} = G_{IN}$$

and

$$Y_L(s) = s + \frac{1}{s} + G_L = \frac{s^2 + G_L s + 1}{s}$$

where $s = j\omega$. Then, in a 50- Ω system,

$$\Gamma_{IN}(s) = -\frac{G_{IN} - \left(\frac{1}{50}\right)}{G_{IN} + \left(\frac{1}{50}\right)} = -C'_1$$

and

$$\Gamma_L(s) = -\frac{Y_L(s) - \left(\frac{1}{50}\right)}{Y_L(s) + \left(\frac{1}{50}\right)} = -\frac{s^2 + s\left[G_L - \left(\frac{1}{50}\right)\right] + 1}{s^2 + s\left[G_L + \left(\frac{1}{50}\right)\right] + 1}$$

where C'_1 is a constant.

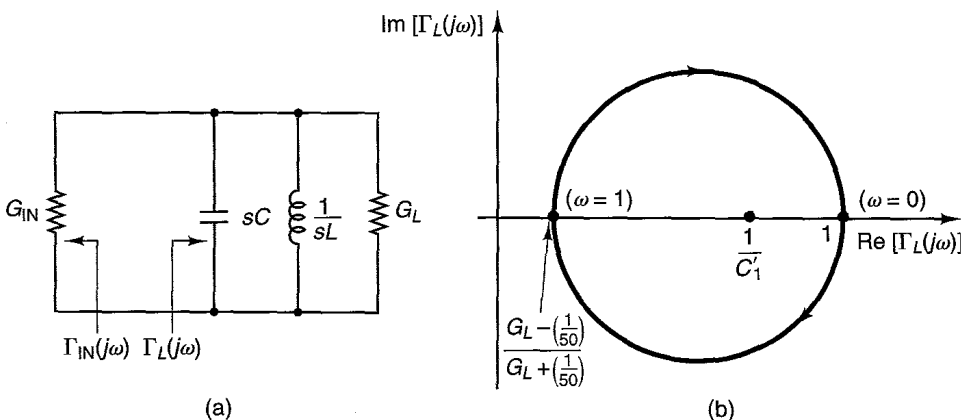


Figure 5.2.7 (a) Circuit for Example 5.2.2; (b) the Nyquist plot of $\Gamma_{IN}(j\omega)\Gamma_L(j\omega)$.

To apply the Nyquist test, we form

$$\Gamma_{\text{IN}}(j\omega)\Gamma_L(j\omega) = 1$$

or

$$\frac{(1 - \omega^2) + j\omega \left[G_L - \left(\frac{1}{50} \right) \right]}{(1 - \omega^2) + j\omega \left[G_L + \left(\frac{1}{50} \right) \right]} = \frac{1}{C'_1} \quad (5.2.32)$$

The Nyquist plot of (5.2.32) is shown in Fig. 5.2.7b for positive values of C'_1 (the plot for negative values of C'_1 is quite similar). The Nyquist test applied to (5.2.32) shows that the circuit is unstable when the number of encirclements of the point $1/C'_1$ is nonzero. Figure 5.2.7b shows that the circuit is unstable when

$$\frac{G_L - \left(\frac{1}{50} \right)}{G_L + \left(\frac{1}{50} \right)} < \frac{1}{C'_1} < 1$$

Since $|C'_1| > 1$, it follows that $1/C'_1 < 1$; therefore, the circuit is unstable when

$$\frac{G_L - \left(\frac{1}{50} \right)}{G_L + \left(\frac{1}{50} \right)} < \frac{G_{\text{IN}} + \left(\frac{1}{50} \right)}{G_{\text{IN}} - \left(\frac{1}{50} \right)}$$

Since $G_{\text{IN}} < 0$, we can express the inequality in the form

$$\left(G_L - \left(\frac{1}{50} \right) \right) \left(G_{\text{IN}} - \left(\frac{1}{50} \right) \right) > \left(G_{\text{IN}} + \left(\frac{1}{50} \right) \right) \left(G_L + \left(\frac{1}{50} \right) \right)$$

which reduces to

$$G_{\text{IN}} < -G_L$$

which is the expected result for the circuit in Fig. 5.2.7a to be unstable.

(b) From (5.2.27), oscillations are possible when $G_{\text{IN}} + G_L = 0$, and from (5.2.28) (with $B_{\text{IN}} = 0$) the frequency of oscillation is given by

$$B_L(j\omega_o) = j\omega_o + \frac{1}{j\omega_o} = j \left(\omega_o - \frac{1}{\omega_o} \right) = 0$$

or

$$\omega_o = 1 \text{ rad/s}$$

For the circuit to maintain a stable oscillation at $\omega_o = 1$ rad/s, the condition (5.2.29) must be satisfied. With G_{IN} given by (5.2.30), it follows that

$$\frac{\partial G_{\text{IN}}(A')}{\partial A'} = \frac{G_0}{A'_M}$$

Therefore, since $G_0 > 0$, we have that $\partial G_{\text{IN}}(A')/\partial A' > 0$.

Also, with $jB_L = j(\omega - 1/\omega)$, it follows that

$$\frac{dB_L(\omega)}{d\omega} = 1 + \frac{1}{\omega^2}$$

Therefore,

$$\left. \frac{\partial G_{\text{IN}}(A')}{\partial A'} \right|_{A'=A'_0} \left. \frac{dB_L(\omega)}{d\omega} \right|_{\omega=\omega_0} > 0$$

which shows that the oscillation is stable.

(c) From (5.2.30), the expression for $G_{\text{IN}}(A')$ is

$$G_{\text{IN}}(A') = -45(1 - A') \text{ mS}$$

Using (5.2.31), the value of G_L that maximizes the oscillator power is

$$G_L = \frac{G_0}{3} = \frac{45 \times 10^{-3}}{3} = 15 \text{ mS}$$

5.3 TWO-PORT NEGATIVE-RESISTANCE OSCILLATORS

The general block diagrams for two-port negative-resistance oscillators are shown in Figs. 5.3.1a and 5.3.1b. The transistor network is characterized by its S parameters, Z_T is the terminating network impedance, and Z_L is the load impedance. Observe the notation used in Figs. 5.3.1a and 5.3.1b, which shows that in an oscillator either port of the transistor can be used as the terminating port. Once the terminating port is selected, the other port is referred to as the input port. The load-matching network is connected to the input port, in agreement with the one-port notation used in Fig. 5.2.3.

When the two-port is potentially unstable, an appropriate Z_T permits the two-port to be represented as a one-port negative-resistance device with input impedance Z_{IN} , as shown in Fig. 5.2.3. The conditions for a stable oscillation are given by (5.2.16), (5.2.17), and (5.2.20). To start the oscillation, the value of R_L is selected according to (5.2.22) (i.e., $R_L = R_0/3$ or, in general, $R_L = |R_{\text{IN}}(0, \omega)|/3$).

When the input port is made to oscillate, the terminating port also oscillates. The fact that both ports are oscillating can be proved as follows.

The input port is oscillating when

$$\Gamma_{\text{IN}}\Gamma_L = 1 \quad (5.3.1)$$

and from (3.2.5) and (5.3.1),

$$\Gamma_L = \frac{1}{\Gamma_{\text{IN}}} = \frac{1 - S_{22}\Gamma_T}{S_{11} - \Delta\Gamma_T}$$

or

$$\Gamma_T = \frac{1 - S_{11}\Gamma_L}{S_{22} - \Delta\Gamma_L} \quad (5.3.2)$$

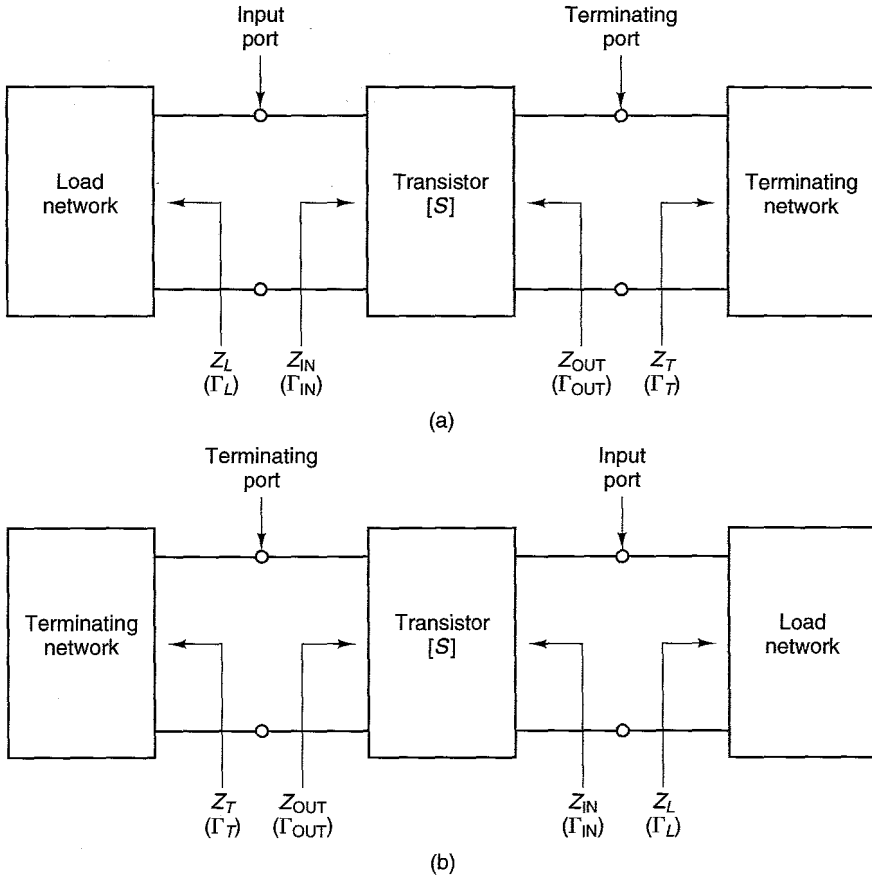


Figure 5.3.1 Two-port oscillator model.

Also, from (3.2.6),

$$\Gamma_{OUT} = \frac{S_{22} - \Delta\Gamma_L}{1 - S_{11}\Gamma_L} \tag{5.3.3}$$

and from (5.3.2) and (5.3.3) it follows that

$$\Gamma_{OUT}\Gamma_T = 1$$

which shows that the terminating port is also oscillating.

A design procedure for a two-port oscillator is as follows:

1. Use a potentially unstable transistor at the frequency of oscillation ω_o .
2. Design the terminating network to make $|\Gamma_{IN}| > 1$. Series or shunt feedback can be used to increase $|\Gamma_{IN}|$.

3. Design the load network to resonate Z_{IN} , and to satisfy the start of oscillation condition in (5.2.22). That is, let

$$X_L(\omega_o) = -X_{IN}(\omega_o) \quad (5.3.4)$$

and

$$R_L = \frac{R_0}{3} \quad \left(\text{or, in general, } R_L = \frac{|R_{IN}(0, \omega)|}{3} \right) \quad (5.3.5)$$

This design procedure is popular due to its high rate of success. However, the frequency of oscillation will shift somewhat from its designed value at ω_o . This occurs because the oscillation power increases until the negative resistance is equal to the load resistance and X_{IN} varies as a function of A (i.e., as a function of the oscillation power). Also, there is no assurance that the oscillator is providing optimum power.

Example 5.3.1

Design an 8-GHz GaAs FET oscillator using the reverse-channel configuration shown in Fig. 5.3.2a. The S parameters of the transistor, in the reverse-channel configuration, at 8 GHz are

$$S_{11} = 0.98 \angle 163^\circ$$

$$S_{21} = 0.675 \angle -161^\circ$$

$$S_{12} = 0.39 \angle -54^\circ$$

$$S_{22} = 0.465 \angle 120^\circ$$

(This example is based on a design from Refs. [5.2] and [5.3].)

Solution. The transistor is potentially unstable at 8 GHz (i.e., $K = 0.529$), and the stability circle at the gate-to-drain port is shown in Fig. 5.3.2b. In the notation of Fig. 5.3.1b, the gate-to-drain port is the terminating port.

As shown in Fig. 5.3.2b, any Γ_T in the shaded region produces $|\Gamma_{IN}| > 1$ (i.e., a negative resistance at the input port). Selecting Γ_T at point A in Fig. 5.3.2b (i.e., $\Gamma_T = 1 \angle -163^\circ$), the associated impedance is $Z_T = -j7.5 \Omega$. This reactance can be implemented by an open-circuited 50- Ω line of length 0.226λ . With Z_T connected, the input reflection coefficient is found to be $\Gamma_{IN} = 12.8 \angle -16.6^\circ$, and the associated impedance is $Z_{IN} = -58 - j2.6 \Omega$. The load matching network is designed using (5.3.4) and (5.3.5)—that is, $Z_L = 19 + j2.6 \Omega$ at $f_o = 8$ GHz.

As reported in Refs. [5.2] and [5.3], the oscillator was constructed and oscillated readily at frequencies between 7.5 and 7.8 GHz, with output power between 680 and 940 mW at $V_{DS} = 9$ V. Some tuning was necessary to move the oscillation frequency to 8 GHz.

Example 5.3.2

Design a 2.75-GHz oscillator using a BJT in a common-base configuration. The transistor S parameters at 2.75 GHz are

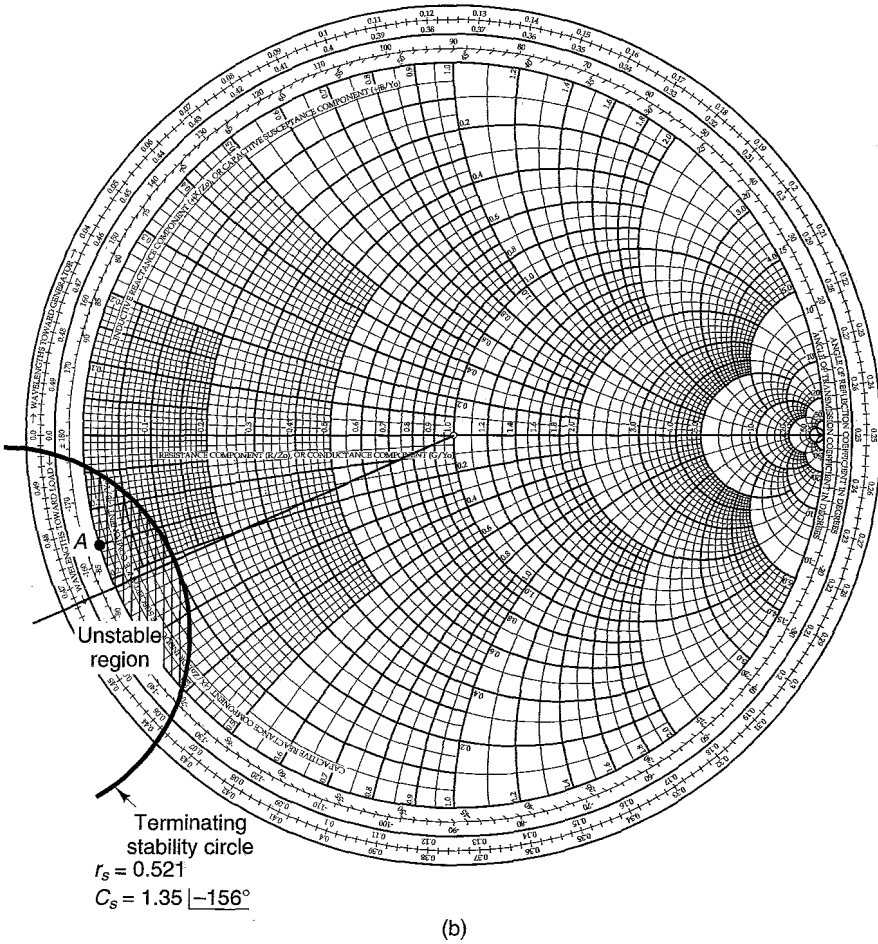
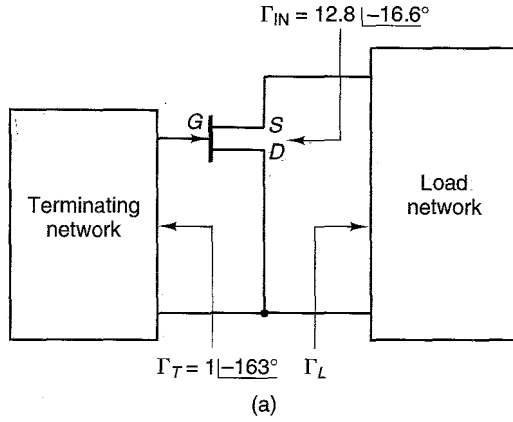


Figure 5.3.2 (a) Oscillator configuration; (b) terminating-port stability circle.

$$\begin{aligned} S_{11} &= 0.9 \angle 150^\circ \\ S_{21} &= 1.7 \angle -80^\circ \\ S_{12} &= 0.07 \angle 120^\circ \\ S_{22} &= 1.08 \angle -56^\circ \end{aligned}$$

(This example is based on a design from Ref. [5.4].)

Solution. The transistor is potentially unstable at 2.75 GHz ($K = -0.64$). The region of instability in the Smith chart can be increased using external feedback. For the common-base configuration, an inductor from base to ground (as shown in Fig. 5.3.3a) is commonly used.

The inductor provides series feedback, and its effect is to produce large values of $|S_{11}|$ and $|S_{22}|$. Of course, these values are obtained with 50- Ω terminations, and 50- Ω terminations are not necessarily used for the matching networks.

Varying L from 0.5 nH to 15 nH shows that the instability at the input and output is optimized with $L = 1.45$ nH. That is, with $L = 1.45$ nH the largest magnitudes of S_{11} and S_{22} were obtained; the resulting S parameters for the network in Fig. 5.3.3a are

$$\begin{aligned} S_{11} &= 1.72 \angle 100^\circ \\ S_{21} &= 2.08 \angle -136^\circ \\ S_{12} &= 0.712 \angle 94^\circ \\ S_{22} &= 1.16 \angle -102^\circ \end{aligned}$$

Either the input or the output ports can be used as the terminating port. In this design the emitter-to-ground port was selected for the load-matching network, and the collector-to-ground port for the terminating network. The terminating port stability circle is shown in Fig. 5.3.3b. This figure shows the large region of instability in the Smith chart. Observe that the center of the Smith chart is unstable. Hence, a 50- Ω resistor at the terminating port will ensure that $|\Gamma_{IN}| > 1$. However, a 50- Ω termination might not be the most suitable since for the associated value of Γ_{IN} the required value of Γ_L for the oscillator might be difficult to implement. In addition, some tuning capabilities are needed in the matching network as the desired frequency of oscillation is seldom reached with the exact designed values.

The values of Γ_T and Γ_{IN} are related by

$$\Gamma_{IN} = S_{11} + \frac{S_{12}S_{21}\Gamma_T}{1 - S_{22}\Gamma_T}$$

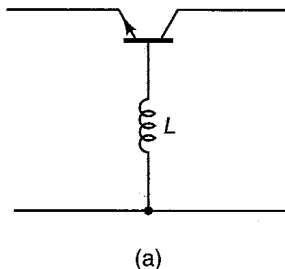


Figure 5.3.3 (a) BJT with external feedback to increase the region of instability; (b) terminating-port stability circle; (c) Γ_{IN} for various Γ_T ; (d) terminating network design.

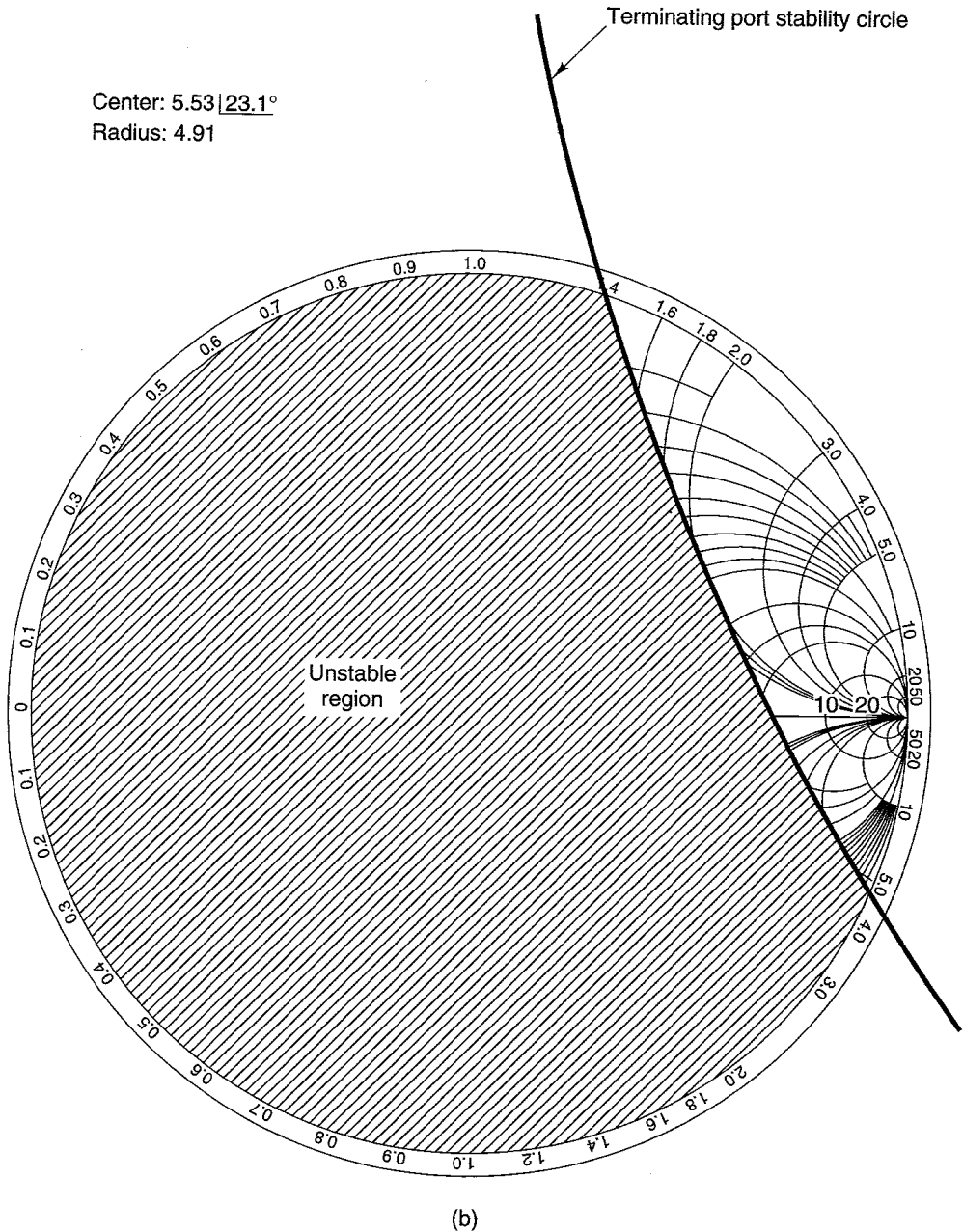
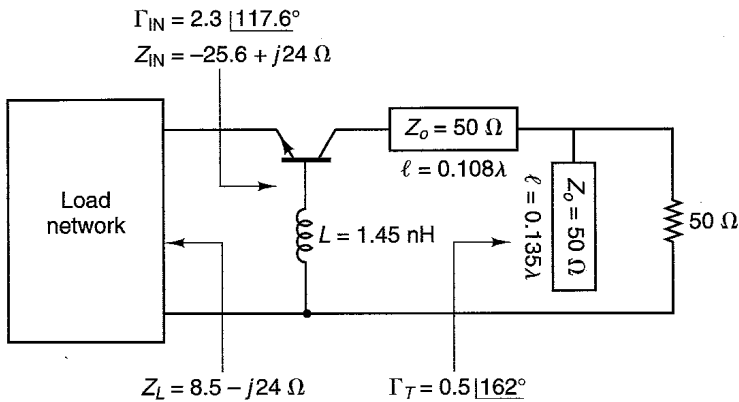


Figure 5.3.3 Continued

Figure 5.3.3c shows the value of Γ_{IN} as Γ_T is varied in the unstable region. The magnitude of Γ_T was set at 0.25, 0.5, 0.75, and 1, and the angle of Γ_T was varied from 90° to 270° in increments of 36° . From Fig. 5.3.3c it is seen that there are many convenient values of Γ_T that can be selected for this design. The value selected was $\Gamma_T = 0.5 \angle 162^\circ$, and it follows that $\Gamma_{IN} = 2.31 \angle 117.6^\circ$ ($Z_{IN} = -25.6 + j24 \Omega$). From (5.3.4) and (5.3.5), the impedance of the load-matching network should be $Z_L = 8.5 - j24 \Omega$.

Γ_T		Γ_{IN}	
Mag.	Phase	Mag.	Phase
1.00	90°	3.67	-67.1°
1.00	126°	3.79	154.5°
1.00	162°	2.24	137.3°
1.00	198°	1.78	130.5°
1.00	234°	1.52	125.9°
1.00	270°	1.33	121.7°
0.75	90°	4.68	18.5°
0.75	126°	4.13	127.1°
0.75	162°	2.35	128.7°
0.75	198°	1.84	125.6°
0.75	234°	1.57	122.2°
0.75	270°	1.38	118.3°
0.50	90°	2.80	67.0°
0.50	126°	3.11	104.8°
0.50	162°	2.31	117.6°
0.50	198°	1.88	118.9°
0.50	234°	1.62	117.2°
0.50	270°	1.44	113.9°
0.25	90°	2.05	87.8°
0.25	126°	2.21	98.5°
0.25	162°	2.07	106.8°
0.25	198°	1.86	110.2°
0.25	234°	1.68	110.2°
0.25	270°	1.55	108.1°

(c)



(d)

Figure 5.3.3 Continued

A design for the terminating network is illustrated in Fig. 5.3.3d. The power is delivered to the 50- Ω load in the terminating matching network.

5.4 OSCILLATOR DESIGN USING LARGE-SIGNAL MEASUREMENTS

The design method discussed in Section 5.3 provides good practical results. However, there is no assurance that the oscillator power is optimum. In this section, a method that optimizes the oscillator power, based on large-signal measurements, is developed. Basically, the method consists of designing the terminating network so that the two-port presents a negative resistance at the input port. The resulting one-port negative-resistance network can be placed in a nonoscillating circuit and the optimum load impedance as a function of power (i.e., large-signal measurements) can be measured.

The terminating network is designed so that Z_{IN} presents a negative impedance at the load port that has a real part with magnitude smaller than 50 Ω . This is necessary because the equipment used to measure the large-signal characteristics of the circuit has 50- Ω source impedance, and the total loop resistance must be positive in order to avoid oscillations during measurements. The one-port negative-resistance circuit at the load port can now be characterized by measuring the input impedance as a function of input power at the frequency ω_o . This is a large-signal characterization of the one-port network which is also called a *device-line characterization*.

It is a good idea, if possible, to place Γ_{IN} within the range shown with dots in Fig. 5.4.1. In this range the associated $|R_{IN}|$ is less than 50 Ω and X_{IN} can be tuned easily [i.e., $X_L = -X_{IN}$].

The large-signal characterization is achieved by measuring, in the circuit shown in Fig. 5.4.2, the current amplitude and the impedance $Z_{IN}(A, \omega_o)$, as V_s is varied. The measurements are made at the desired frequency of oscillation ω_o , and the source resistance is typically 50 Ω . With $|R_{IN}(A, \omega_o)| < 50 \Omega$, the circuit in Fig. 5.4.2 is stable.

In the circuit shown in Fig. 5.4.2, the current phasor $I(A, \omega_o)$ is given by

$$I(A, \omega_o) = \frac{V_s}{R_s + R_{IN}(A, \omega_o) + jX_{IN}(A, \omega_o)} \quad (5.4.1)$$

The power delivered by the negative resistance $R_{IN}(A, \omega_o)$ is

$$P_D(A, \omega_o) = \frac{1}{2} |I(A, \omega_o)|^2 |R_{IN}(A, \omega_o)|$$

The measurement of $P_D(A, \omega_o)$ versus $Z_{IN}(A, \omega_o)$ generates the large-signal characteristics of the one-port network. If the one-port is now terminated in the load impedance (see Fig. 5.2.3)

$$Z_L(\omega_o) = -Z_{IN}(A, \omega_o)$$

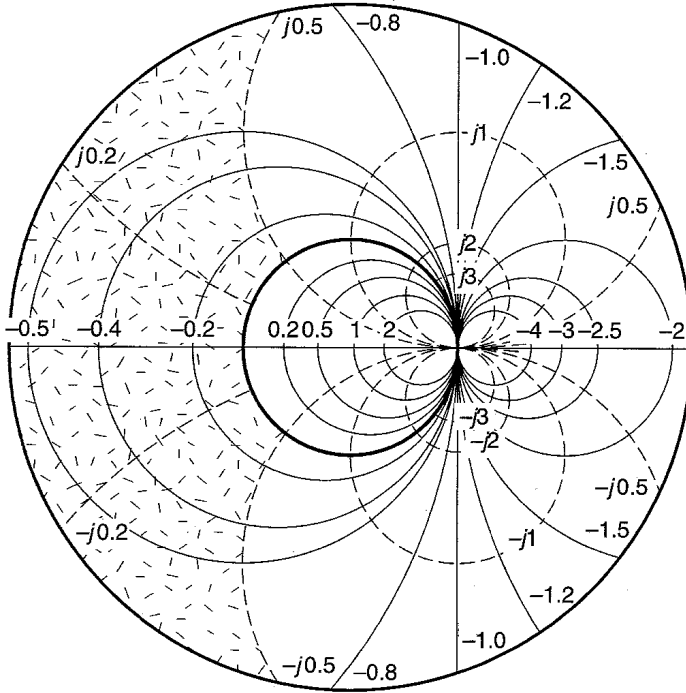


Figure 5.4.1 Best range for Γ_{IN} .

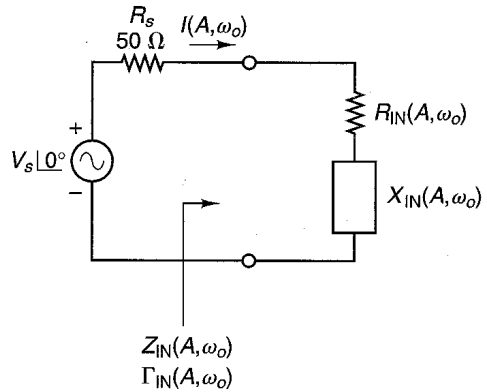


Figure 5.4.2 Large-signal measuring circuit.

the power delivered to Z_L is given by $P_L(A, \omega_o) = P_D(A, \omega_o)$.

Obviously, the measurement of $I(A, \omega_o)$ at microwave frequencies is difficult. Therefore, in practice the reflection coefficient $\Gamma_{IN}(A, \omega_o)$ as a function of the available power from the source is measured. The available power from the source is given by

$$P_{AVS} = \frac{V_s^2}{8R_s}$$

The power added P_{ADD} (i.e., the reflected minus the available input power) is given by

$$P_{\text{ADD}} = P_{\text{AVS}}(|\Gamma_{\text{IN}}|^2 - 1)$$

and for the circuit in Fig. 5.4.2, P_{ADD} can be expressed in the form

$$P_{\text{ADD}}(A, \omega_o) = \frac{V_s^2 |R_{\text{IN}}(A, \omega_o)|}{2[(R_{\text{IN}}(A, \omega_o) + R_s)^2 + X_{\text{IN}}^2]} \quad (5.4.2)$$

From (5.4.1) and (5.4.2) we can write

$$P_{\text{ADD}}(A, \omega_o) = \frac{1}{2} |I(A, \omega_o)|^2 |R_{\text{IN}}(A, \omega_o)|$$

which shows that the added power is the power that the one-port network will deliver to the load $Z_L(\omega_o) = -Z_{\text{IN}}(A, \omega_o)$.

The large-signal characterization of the one-port network is generated by measuring Γ_{IN} and P_{AVS} and calculating $P_{\text{ADD}}(A, \omega_o)$ versus $Z_{\text{IN}}(A, \omega_o)$. Typical large-signal characterization data are shown in Fig. 5.4.4c.

There are several ways of implementing the load impedance $Z_L(\omega_o)$ and, of course, not all of them will give us a stable oscillation. For a stable oscillation we have to check that $Z_L(\omega_o)$ satisfies the condition given in (5.2.20). This can be achieved easily since the amplitude dependence of $R_{\text{IN}}(A, \omega_o)$ can be obtained from the measured data, and the required impedance variation (i.e., $dX_L/d\omega \geq 0$) can be determined.

In conclusion, the design procedure uses the small-signal S parameters to establish the terminating impedance that results in a negative-resistance one-port network. Then the one-port oscillator performance is described by the measured large-signal characteristics.

A method for the design of Γ_T that produces the largest magnitude of Γ_{IN} , denoted by $\Gamma_{\text{IN,max}}$, can be developed. Of course, it is not necessary to design Γ_T for $\Gamma_{\text{IN,max}}$ in order to design an oscillator. In many cases the resulting $\Gamma_{\text{IN,max}}$ is not suitable for large-signal measurements or for an appropriate load-matching circuit.

From (3.2.5)

$$\Gamma_{\text{IN}} = \frac{S_{11} - \Delta\Gamma_T}{1 - S_{22}\Gamma_T} \quad (5.4.3)$$

This equation describes the mapping of the Γ_T plane into the Γ_{IN} plane. The mapping of the circle $|\Gamma_T| = 1$ into the Γ_{IN} plane gives information about the passive impedances at the terminating port (i.e., $|\Gamma_T| < 1$) that will make $|\Gamma_{\text{IN}}| > 1$. The mapping can be obtained using (J.2) and (J.3) in Appendix J. In the notation used in (J.2) and (J.3), the center and radius of the circle $|\Gamma_T| = 1$ are $C_{oo} = 0$ and $r_{oo} = 1$. Hence, the $|\Gamma_T| = 1$ circle maps onto a circle in the Γ_{IN} plane with center at

$$C_{\text{IN}} = \frac{S_{11} - \Delta S_{22}^*}{1 - |S_{22}|^2} \quad (5.4.4)$$

and radius of

$$r_{\text{IN}} = \frac{|S_{12}S_{21}|}{|1 - |S_{22}|^2|} \quad (5.4.5)$$

A typical mapping is shown in Fig. 5.4.3.

From Fig. 5.4.3 it is observed that the largest $|\Gamma_{\text{IN}}|$ is obtained when we select the value of Γ_{IN} on the $|\Gamma_T| = 1$ circle that has the same phase angle as C_{IN} . This value of Γ_{IN} , denoted by $\Gamma_{\text{IN,max}}$ is shown as point *a* in Fig. 5.4.3. The value of Γ_T associated with $\Gamma_{\text{IN,max}}$ produces the largest negative resistance for Z_{IN} , which can be realized using a passive terminating impedance. The magnitude of Γ_{IN} at point *a* is given by

$$|\Gamma_{\text{IN}}| = |C_{\text{IN}}| + r_{\text{IN}}$$

and the phase of Γ_{IN} at point *a* is

$$\angle \Gamma_{\text{IN}} = \angle C_{\text{IN}}$$

Hence, $\Gamma_{\text{IN,max}}$ can be expressed in the form

$$\Gamma_{\text{IN,max}} = (|C_{\text{IN}}| + r_{\text{IN}}) \underline{C_{\text{IN}}} \quad (5.4.6)$$

The value of Γ_T at point *a*, denoted by $\Gamma_{T,o}$, is obtained from (5.4.3)—namely,

$$\Gamma_{T,o} = \frac{\Gamma_{\text{IN,max}} - S_{11}}{\Gamma_{\text{IN,max}}S_{22} - \Delta} \quad (5.4.7)$$

The results that are obtained using (5.4.6) and (5.4.7) agree with those given by Wagner [5.5] (see Problem 5.9).

The value of $\Gamma_{T,o}$ in (5.4.7) produces the largest magnitude of Γ_{IN} (i.e., $\Gamma_{\text{IN,max}}$). In other words, the two-port network has been reduced to a negative-resistance one-port network by maximizing the magnitude of the small-signal input reflection coefficient. Observe that the small-signal S parameters of the transistor were used in the calculations. The large-signal measurements of the one-port network yields the desired data for the design of $Z_L(\omega_o)$.

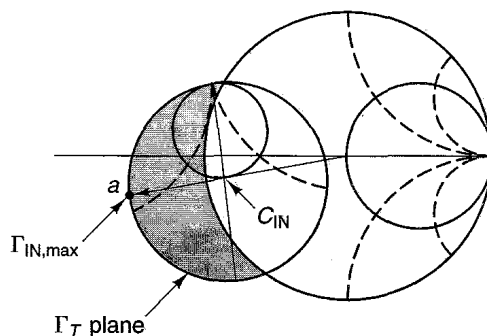


Figure 5.4.3 Typical mapping of the Γ_T plane into the Γ_{IN} plane.

Example 5.4.1

Design an oscillator using a GaAs FET whose S parameters at 10 GHz are

$$S_{11} = 0.9 \angle 180^\circ$$

$$S_{12} = 0.79 \angle -98^\circ$$

$$S_{21} = 0.89 \angle -163^\circ$$

$$S_{22} = 0.2 \angle 180^\circ$$

(This example is based on a design from Ref. [5.5].)

Solution. For this transistor, $K = 0.51$ and $\Delta = 0.753 \angle -67.34^\circ$, showing that the device is potentially unstable. From (5.4.4) and (5.4.5) it follows that $C_{IN} = 0.889 \angle -170.63^\circ$ and $r_{IN} = 0.732$. Hence, from (5.4.6) the value of $\Gamma_{IN,max}$ is

$$\Gamma_{IN,max} = (0.889 + 0.732) \angle -170.63^\circ = 1.62 \angle -170.63^\circ$$

The value of $\Gamma_{T,o}$ follows from (5.4.7). That is,

$$\Gamma_{T,o} = 1 \angle 113^\circ$$

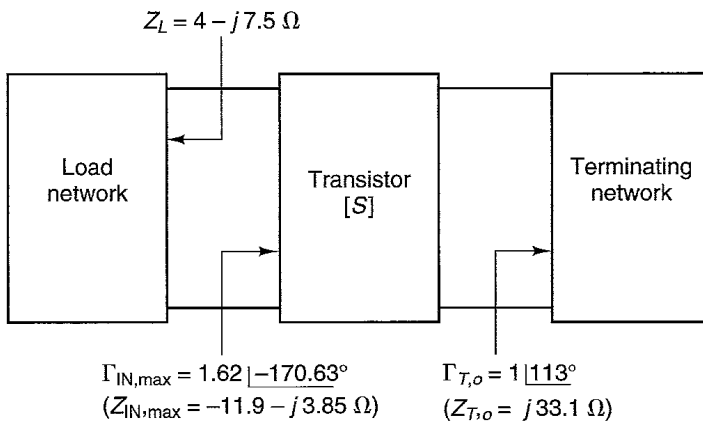
Then, the impedances associated with $\Gamma_{IN,max}$ and $\Gamma_{T,o}$ are

$$Z_{T,o} = Z_o \frac{1 + \Gamma_{T,o}}{1 - \Gamma_{T,o}} = 50(j0.662) = j33.1 \Omega$$

and

$$Z_{IN,max} = Z_o \frac{1 + \Gamma_{IN,max}}{1 - \Gamma_{IN,max}} = 50(-0.238 - j0.077) = -11.9 - j3.85 \Omega$$

The block diagram of the oscillator is shown in Fig. 5.4.4a. The complete mapping of the Γ_T plane into the Γ_{IN} plane is illustrated in Fig. 5.4.4b. Observe the locations of C_{IN} and $\Gamma_{IN,max}$.



(a)

Figure 5.4.4 (a) Block diagram of the oscillator; (b) mapping of the Γ_T plane into the Γ_{IN} plane; (c) large-signal characteristics at 10 GHz with $Z_{T,o} = j33.1 \Omega$ (Figs. 5.4.4b and 5.4.4c are from W. Wagner [5.5]; reproduced with permission of *Microwave Journal*.)

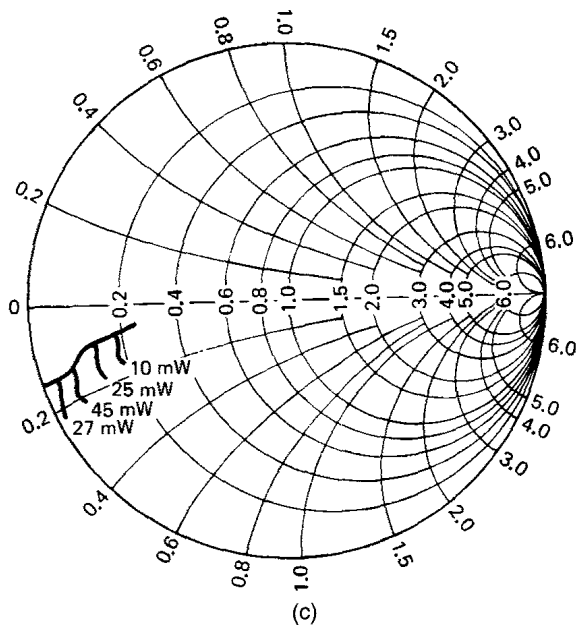
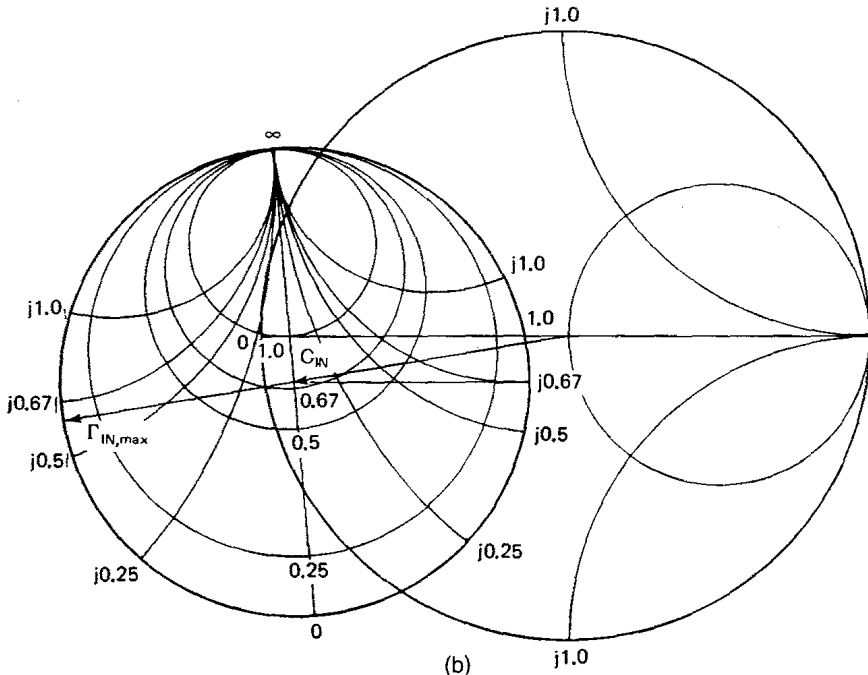


Figure 5.4 Continued

With the termination $Z_{T_o} = j33.1 \Omega$, the transistor large-signal characteristics are now measured. The results from the large-signal measurements are given in Fig. 5.4.4c. It is observed that the maximum power added is 45 mW when $Z_L = 4 - j7.5 \Omega$.

The following design procedure was suggested by Dr. Branko Avanic, who provided the drawing in Fig. 5.4.5. In some designs the load network consists of a resonator whose load impedance is known (i.e., Γ_L is known). The active device and the terminating-port network must be designed to provide an appropriate Γ_{IN} to the Γ_L of the resonator. This design method keeps the resonator intact in order not to degrade its Q . Γ_{IN} is selected so that the condition for oscillation, and the start of oscillation condition, are satisfied.

The procedure for obtaining Γ_T is illustrated in Fig. 5.4.5. Given the S parameters of a two-port network, the circle $|\Gamma_T| = 1$ is plotted in the Γ_{IN} plane using (5.4.4) and (5.4.5), as well as the value of Γ_{IN} that satisfies the oscillation conditions, and the start of oscillation condition. Let this value of Γ_{IN} have a magnitude denoted by k (where k is a constant greater than 1) and phase θ . If the value of Γ_{IN} intersects the $|\Gamma_T| = 1$ circle between the angles θ_1 and θ_2 , as shown in Fig. 5.4.5, then the value of Γ_T can be implemented. If not, another two-port network must be selected and the previous procedure repeated until Γ_T produces the desired Γ_{IN} .

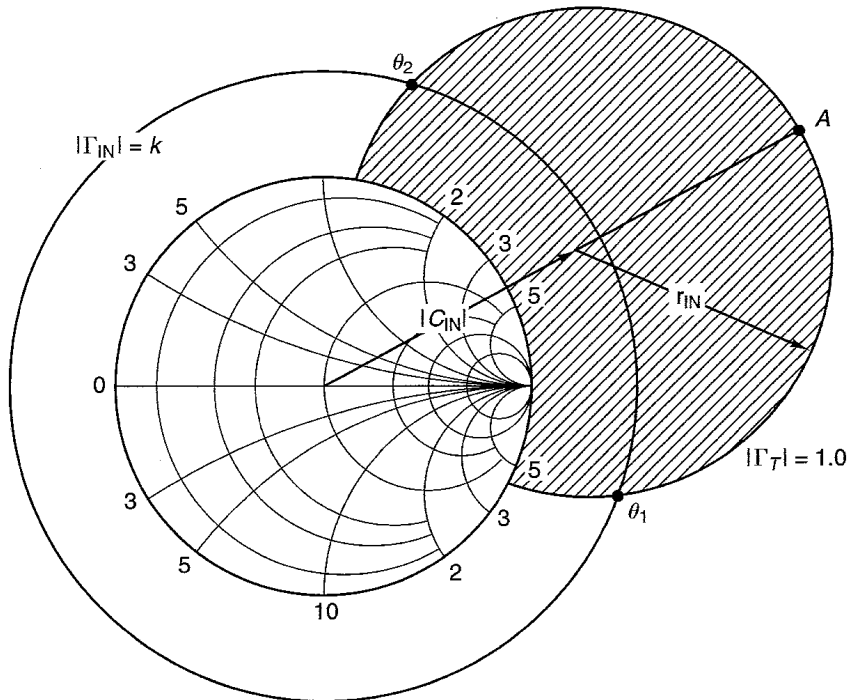


Figure 5.4.5 Mapping of $|\Gamma_T| = 1$ circle into the Γ_{IN} plane, and the circle $|\Gamma_{IN}| = k$ (k is a constant).

For the selected value of Γ_{IN} , the value of Γ_T is calculated using (5.4.3)—namely,

$$\Gamma_T = \frac{S_{11} - \Gamma_{IN}}{\Delta - S_{22}\Gamma_{IN}}$$

5.5 OSCILLATOR CONFIGURATIONS

At the low end of the microwave frequency range, lumped-element oscillators are commonly used. Three basic oscillator configurations used are the Colpitts, Hartley, and Clapp oscillators. They are shown in Fig. 5.5.1 in a common-base transistor configuration. The Colpitts network uses a capacitor voltage divider in the tuned circuit to provide the correct feedback. The Hartley network uses a tapped inductor tuned circuit, and the Clapp network is similar to the Colpitts network but with an extra capacitor in series with the inductor to improve the frequency stability.

The high- Q tapped inductor required in the Harley’s oscillator is difficult to build. Therefore, the Colpitts and Clapp oscillators are usually preferred.

Design methods for the tuned-circuit oscillators in Fig. 5.5.1 are usually presented using a feedback approach [i.e., using (5.2.6) and (5.2.7)]. In fact, whenever the feedback is obtained using external lumped elements, the feedback approach [based on (5.2.6) and (5.2.7)] is the method of choice. It is of theoretical interest to note that the oscillators in Fig. 5.5.1 can also be analyzed using a negative-resistance approach. For example, consider the FET Colpitts oscillator shown in Fig. 5.5.2a, and its small-signal ac model in Fig. 5.5.2b. Using (5.2.7), the frequency of oscillation is determined from

$$X_1 + X_2 + X_3 = -\frac{1}{\omega C_1} - \frac{1}{\omega C_2} + \omega L = 0 \tag{5.5.1}$$

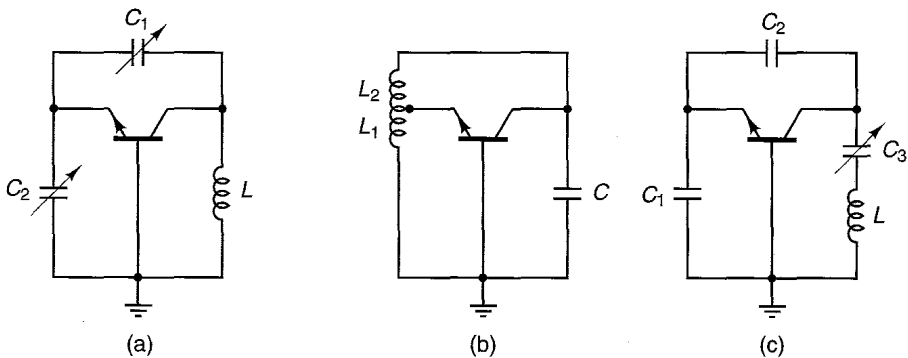


Figure 5.5.1 Three types of common-base transistor configurations: (a) Colpitts; (b) Hartley; (c) Clapp.

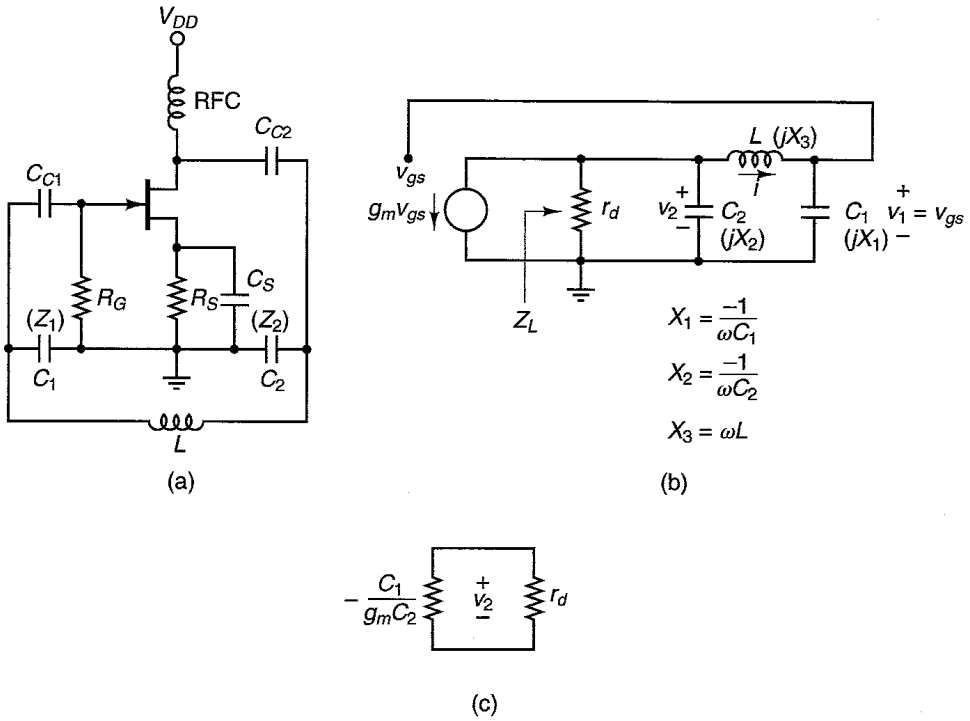


Figure 5.5.2 (a) The FET Colpitts oscillator configuration; (b) the ac model; (c) negative-resistance model at resonance.

or

$$\omega = \omega_o = \frac{1}{\sqrt{LC_T}}$$

where

$$C_T = \frac{C_1 C_2}{C_1 + C_2}$$

From Fig. 5.5.2b, the voltage feedback factor is

$$\beta(\omega) = \frac{v_1}{v_2} = \frac{v_{gs}}{v_2} = \frac{X_1}{X_1 + X_3}$$

Using (5.5.1), $\beta(j\omega)$ can be expressed as

$$\beta(\omega) = \frac{v_{gs}}{v_2} = -\frac{X_1}{X_2} = -\frac{C_2}{C_1}$$

Hence, the controlled current source in Fig. 5.5.2b can be expressed as

$$g_m v_{gs} = -\frac{g_m C_2}{C_1} v_2 \tag{5.5.2}$$

Equation (5.5.2) shows that the source $g_m v_{gs}$ can be replaced by a negative resistance given by $-C_1/g_m C_2$; and therefore, at resonance (i.e., at $\omega = \omega_o$), the model in Fig. 5.5.2c follows. For oscillation to occur, according to (5.2.16), the loop resistance must be zero. That is,

$$-\frac{C_1}{g_m C_2} + r_d = 0$$

or

$$g_m r_d = \frac{C_1}{C_2}$$

which is the well-known gain condition for the Colpitts oscillator.

At higher microwave frequencies (i.e., in the gigahertz range), the parasitic capacitances of the packaged transistors provide some or all the feedback needed for oscillation. In this range the negative-resistance design procedure is used, since the S parameters provide all the needed design information. The negative-resistance design procedure basically consists of selecting a transistor in an oscillator topology that provides the required output power. The transistor in the configuration selected must be potentially unstable at the desired frequency of oscillation. Feedback can be added to increase the negative resistance associated with Γ_{IN} or Γ_{OUT} . The terminating and load matching networks must be designed to provide the proper resonance conditions.

For a BJT negative-resistance oscillator the most effective network topology is the common-base configuration. This configuration, illustrated in Fig. 5.5.3, is used in low-power oscillator circuits, and it is easy to tune. The inductor feedback element is used to increase $|\Gamma_{IN}|$ and $|\Gamma_{OUT}|$. Common-emitter and common-collector configurations have also been used in microwave oscillators.

The two common network configurations for GaAs FETs oscillators are shown in Figs. 5.5.4a and 5.5.4b. The common-gate configuration is used in low-power oscillator circuits since it is easy to tune. A series inductive feedback is usually required to improve $|\Gamma_{IN}|$ and $|\Gamma_{OUT}|$. The common-source configuration is used for higher oscillator output power and the feedback network is usually a capacitor. The common-drain configuration is not popular because the oscillator implementation is difficult.

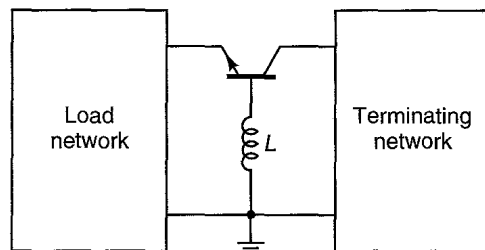


Figure 5.5.3 Common-base configuration.

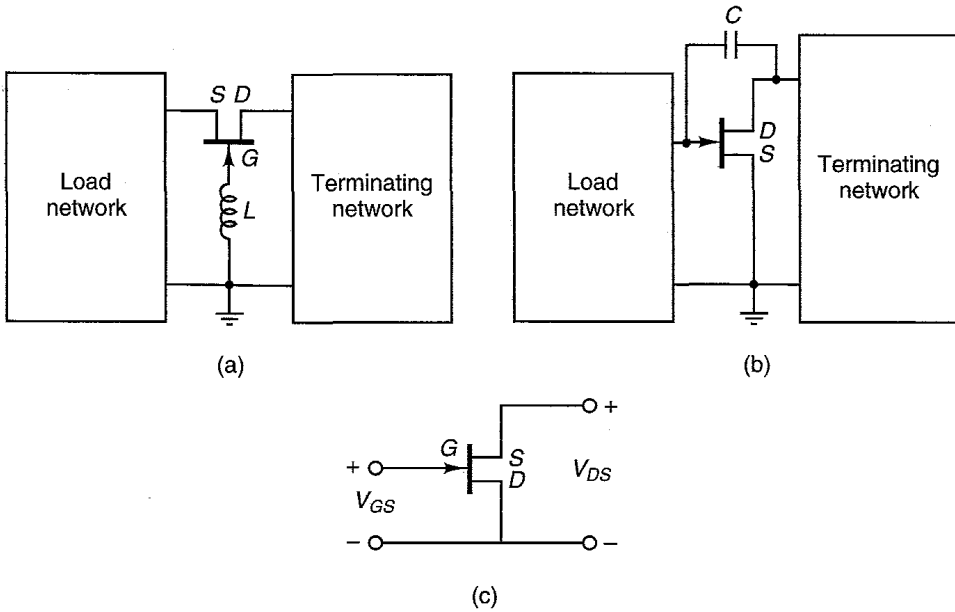


Figure 5.5.4 (a) Common-gate configuration; (b) common-source configuration; (c) reverse-channel GaAs FET.

A GaAs FET oscillator can also be built using the reverse-channel configuration shown in Fig. 5.5.4c. A reverse-channel configuration uses a symmetrical GaAs FET with a negative voltage applied to the drain terminal. The transistor becomes a noninverting device, making the common lead inductance regenerative. The S parameters in this reverse-channel configuration show that $|S_{12}|$ increases markedly with frequency and $|S_{11}|$ is greater than unity in a large frequency range.

The load-tuning elements are not limited to lossless or RLC networks. They can be designed using DRs (dielectric resonators), YIG (yttrium iron garnet) resonators, varactor diodes, etc. Two references that discuss a variety of oscillators are Vendelin, Pavo, and Rhode [5.6], and Vendelin [5.7].

Dielectric Resonator Oscillators

A dielectric resonator oscillator (DRO) is a high- Q , temperature-stable oscillator that is used in many practical applications at microwave frequencies. Transistor DROs are built using either BJTs or GaAs FETs. BJTs are used in DROs with oscillation frequencies up to about 15 GHz; with GaAs FETs, the frequency of oscillation of the DROs can be extended to about 35 GHz. Typical power levels of 10 to 15 dBm are possible.

Several compounds with dielectric constants between 20 and 80 are used in the construction of dielectric resonators (DRs). For microwave transistor oscillators, DRs having a solid cylindrical shape can cover the frequency range

from about 1 GHz to 40 GHz. In fact, they can operate up to 100 GHz. The problem with DRs at the lower frequencies is the large dimensions of the resonator. Dielectric resonators having a coaxial tubular shape (i.e., a hollow center) have been made for practical applications down to 500 MHz.

A good reference on DRs and applications is found in Kajfez and Guillon [5.8]. A dielectric resonator will resonate in several modes. The most commonly used mode in cylindrical resonators is a TE mode (specifically the $TE_{01\delta}$ mode). This mode can be easily coupled to a microstrip line. To understand the coupling of a dielectric resonator to a microstrip line, consider Fig. 5.5.5, which shows the field distribution of the $TE_{01\delta}$ mode. The electric field lines are concentric circles around the z axis, and there is no z component of the electric field. The magnetic field lines are also illustrated in Fig. 5.5.5.

Fig. 5.5.6 shows the dielectric resonator coupled to the microstrip line. The dielectric resonator is placed on top of the substrate at a distance d from the microstrip line. The distance d and the DR characteristics determine the coupling. Observe the magnetic coupling between the DR and the microstrip line. The metallic enclosure is used to minimize the radiation losses and, therefore, to increase the resonator Q . The $TE_{01\delta}$ is excited in the DR by the electromagnetic field produced by the microstrip line. In turn, the DR reflects RF energy at its resonant frequency, resulting in a high- Q resonator.

Figure 5.5.7a shows the DR coupled to a microstrip line with characteristic impedance Z_o and terminated in Z_o impedances (usually $Z_o = 50 \Omega$). The equivalent circuit of the DR coupled to the microstrip line is illustrated in Fig. 5.5.7b. It consists of a parallel tuned circuit placed in series, at the position XX' , with the transmission lines. The values of R , L , and C in the equivalent

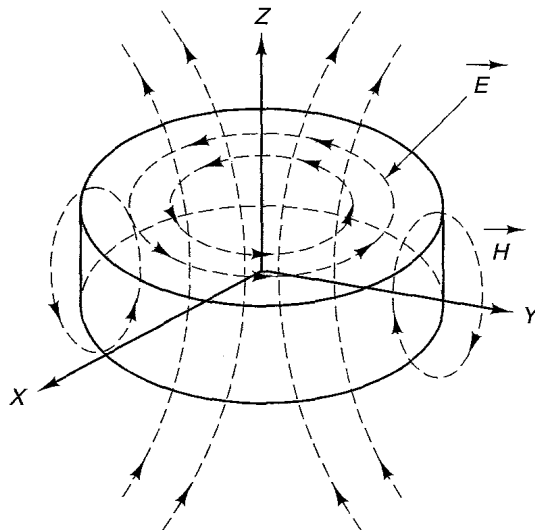


Figure 5.5.5 Field distribution of the $TE_{01\delta}$ mode in a cylindrical resonator.

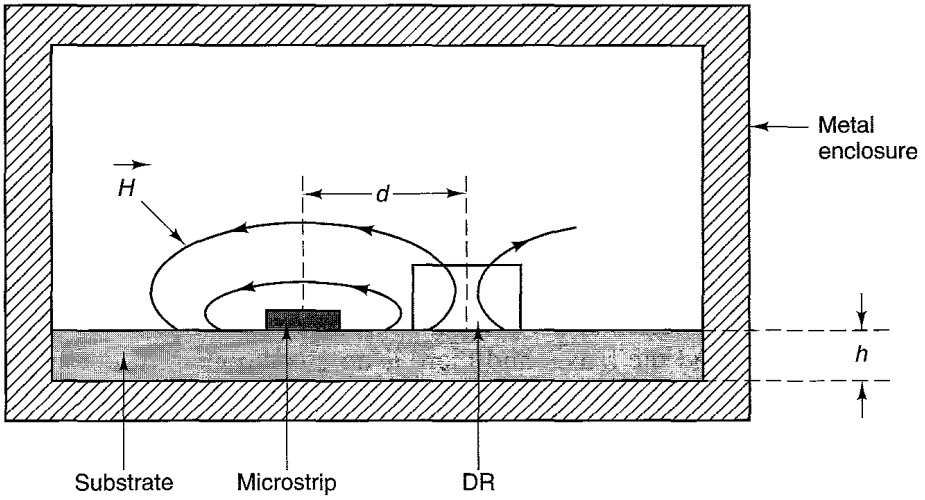


Figure 5.5.6 Coupling of a dielectric resonator to a microstrip line.

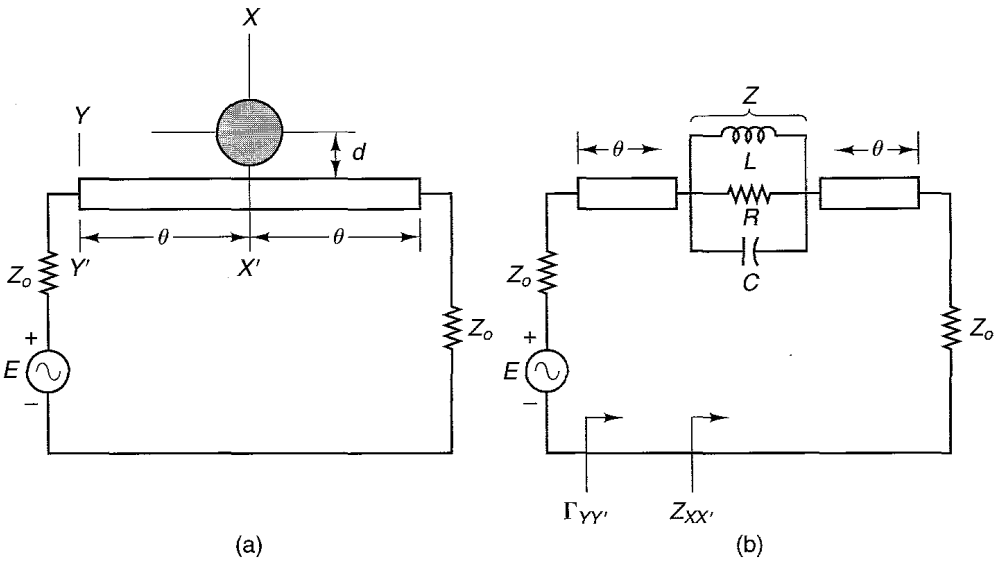


Figure 5.5.7 (a) Dielectric resonator coupled to a microstrip line; (b) equivalent circuit at the XX' plane.

circuit of the DR depend on the DR characteristics and the distance d . The impedance Z is given by

$$Z = \frac{1}{C} \frac{s}{s^2 + \frac{s}{RC} + \frac{1}{LC}} = \frac{1}{C} \frac{s}{s^2 + 2\alpha s + \omega_0^2} \tag{5.5.3}$$

where the bandwidth (BW) and resonant frequency are

$$\text{BW} = 2\alpha = \frac{1}{RC}$$

and

$$\omega_o = \frac{1}{\sqrt{LC}}$$

Letting $s = j\omega$, (5.5.3) can be expressed as

$$Z = \frac{R}{1 + jQ_u \frac{(\omega^2 - \omega_o^2)}{\omega\omega_o}} \quad (5.5.4)$$

where Q_u is the unloaded Q of the tuned circuit. That is,

$$Q_u = \frac{\omega_o}{2\alpha} = \omega_o RC = \frac{R}{\omega_o L} \quad (5.5.5)$$

Since the frequency of operation is very close to ω_o (i.e., $\omega + \omega_o \approx 2\omega$), we can approximate (5.5.4) by

$$Z = \frac{R}{1 + j2Q_u\delta} \quad (5.5.6)$$

where

$$\delta = \frac{\omega - \omega_o}{\omega_o}$$

At the reference plane XX' the input impedance is given by

$$Z_{XX'} = Z + Z_o$$

or

$$z_{XX'} = \frac{Z_{XX'}}{Z_o} = \frac{R/Z_o}{1 + j2Q_u\delta} + 1 \quad (5.5.7)$$

For convenience, a coupling coefficient β is defined as

$$\beta = \frac{R}{2Z_o} \quad (5.5.8)$$

Hence, in terms of β , we can write (5.5.7) as

$$z_{XX'} = \frac{2\beta}{1 + j2Q_u\delta} + 1$$

Observe that at $\omega = \omega_o$ (or $\delta = 0$), it follows that $z_{XX'} = 2\beta + 1$. Then the reflection coefficient at $\omega = \omega_o$, at the XX' plane, is

$$\Gamma_{XX'}(\omega_o) = \frac{z_{XX'} - 1}{z_{XX'} + 1} = \frac{\beta}{\beta + 1} \quad (5.5.9)$$

In general, the reflection coefficient at the XX' plane is given by

$$\Gamma_{XX'} = \frac{z_{XX'} - 1}{z_{XX'} + 1} = \frac{\beta}{\beta + 1 + j2Q_u\delta}$$

Hence, the reflection coefficient seen at the input of the line, denoted by $\Gamma_{YY'}$, is

$$\Gamma_{YY'} = \frac{\beta}{\sqrt{(\beta + 1)^2 + (2Q_u\delta)^2}} e^{-j\left(2\theta + \tan^{-1} \frac{2Q_u\delta}{\beta + 1}\right)} \quad (5.5.10)$$

At the resonant frequency (i.e., at $\omega = \omega_o$ or $\delta = 0$), (5.5.10) reduces to

$$\Gamma_{YY'}(\omega_o) = \Gamma_{XX'}(\omega_o)e^{-j2\theta} = \frac{\beta}{\beta + 1} e^{-j2\theta} \quad (5.5.11)$$

This relation shows that if β is a constant and the length of the line is varied from $\theta = 0^\circ$ to 360° , the values of $\Gamma_{YY'}$ lie on a circle in the Smith chart. Thus, with the appropriate selection of β the reflection coefficient $\Gamma_{YY'}$ can implement any passive impedance. Equation (5.5.11) is used to select the desired coupling and electrical length θ of the transmission line for a particular input impedance.

The previous discussion shows that the parameters β , ω_o , and Q_u describe the operation of the DR. These parameters are either measured or given by the manufacturer of the DR. Furthermore, the values of R , L , and C in Fig. 5.5.7b can be calculated in terms of β , ω_o , and Q_u . The value of R follows from (5.5.8), and the values of L and C from (5.5.5).

From Fig. 5.5.7b, at the resonant frequency ω_o , the S parameters of the tuned circuit (i.e., the DR coupled to the transmission line) are

$$[S(\omega_o)] = \begin{bmatrix} \frac{\beta}{\beta + 1} & \frac{1}{\beta + 1} \\ 1 & \frac{\beta}{\beta + 1} \\ \frac{\beta}{\beta + 1} & \frac{1}{\beta + 1} \end{bmatrix} \quad (5.5.12)$$

From (5.5.12), it follows that β can be expressed in terms of the $S_{11}(\omega_o)$ and $S_{21}(\omega_o)$ parameters. That is,

$$\beta = \frac{S_{11}(\omega_o)}{1 - S_{11}(\omega_o)} = \frac{1 - S_{21}(\omega_o)}{S_{21}(\omega_o)}$$

For a closely coupled resonator, typical values of β are from 2 to 20.

The value of Q_u can be found by measuring S_{21} . A typical plot of S_{21} in dB is shown in Fig. 5.5.8. The insertion loss L_o is given by

$$L_o(\text{dB}) = -20 \log|S_{21}(\omega_o)|$$

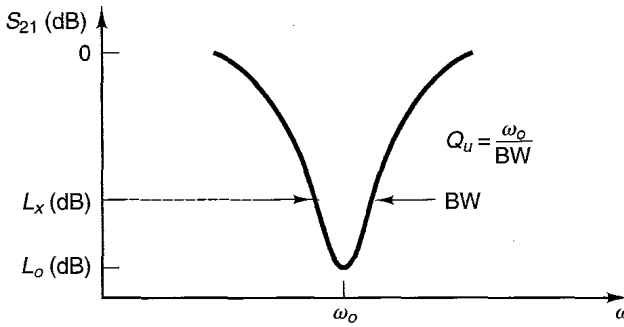


Figure 5.5.8 A typical plot of S_{21} (dB).

and the insertion loss L_x is given by

$$L_x(\text{dB}) = L_o(\text{dB}) - 3 + 10 \log(1 + 10^{-0.1L_o})$$

Hence, Q_u is found by dividing ω_o by the bandwidth where the insertion loss is L_x .

Some practical circuit configurations for DROs are shown in Fig. 5.5.9. In the configuration shown in Figs. 5.5.9a and 5.5.9b, the DR acts as a series feedback element resulting in a stable oscillation. The DR is connected to the terminating port, and the DR and transistor produce a negative resistance at the load port.

In the configuration shown in Fig. 5.5.9c, the DR acts as a parallel feedback element. The forward gain of the transistor compensates for the insertion loss of the DR. The DR is a high- Q tuned circuit and, therefore, oscillation will occur when the Barkhausen oscillation conditions are satisfied.

The series feedback configurations are simple to construct. The parallel configuration is somewhat more difficult to construct because of the coupling of the two lines. DROs constructed using BJTs have lower phase noise than those using GaAs FETs.

DROs can be tuned over a narrow range of frequencies using a metallic shield with a tuning screw, as shown in Fig. 5.5.10. The depth of the tuning screw increases the resonant frequency of the DR. The height h should be greater than 0.5 times the resonator height, in order not to decrease the Q of the resonator. Tuning bandwidths of the order of 0.1% to 1% of the resonant frequency are possible.

The DROs can also be tuned electrically. A varactor-tuned DRO is shown in Fig. 5.5.11. The varactor is coupled to the DR, resulting in two coupled circuits. The varactor's capacitance can be changed with an appropriate dc bias voltage, and this in turn changes the resonant frequency of the DR. The varactor can provide a resonant frequency tuning range of 1%. There are other ways of electrically tuning a DR [5.9].

The temperature stability of a DR is expressed in ppm/°C (parts per million per degree Centigrade). DRs with temperature coefficients ranging from

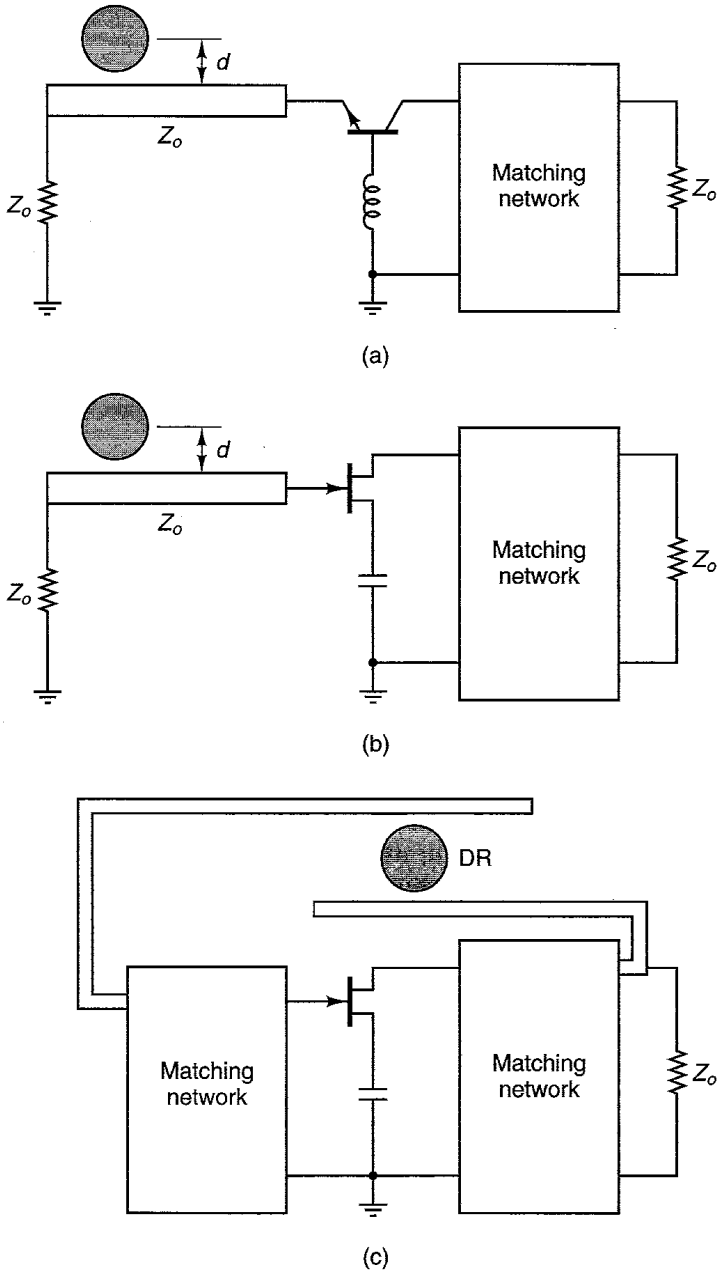


Figure 5.5.9 (a) A series feedback DRO using a BJT; (b) a series feedback DRO using a GaAs FET; (c) a parallel feedback DRO.

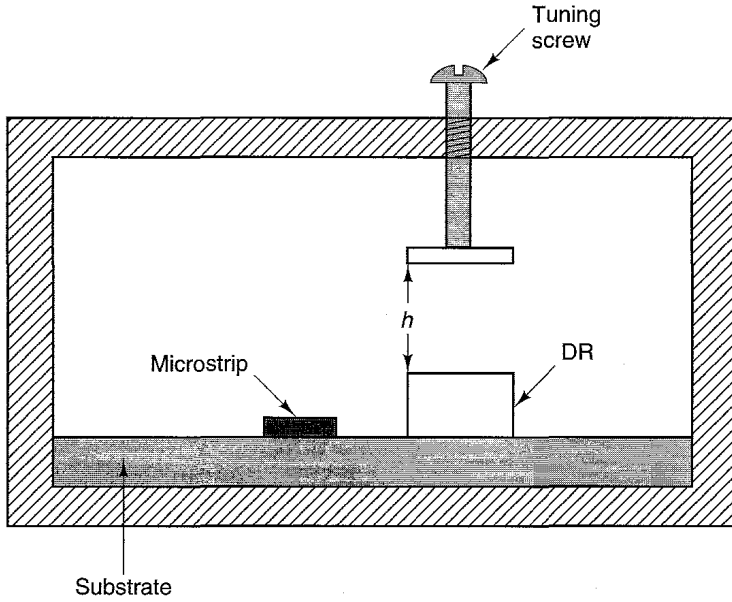


Figure 5.5.10 A mechanical tuning arrangement for DROs.

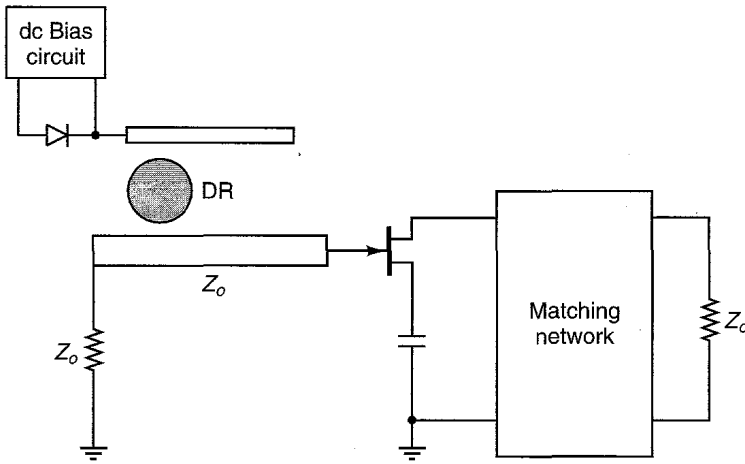


Figure 5.5.11 A varactor-tuned DRO.

–10 ppm/°C to 10 ppm/°C are available. For example, an 8-GHz DRO can be specified to have a frequency stability of 500 ppm over a temperature range of –50°C to 80°C. This requirement will fix the frequency drift to 4 MHz.

Example 5.5.1

Design a 10-GHz DRO using a GaAs FET whose *S* parameters (at 10 GHz) in a common source configuration are

$$S_{11} = 0.63 \angle 130^\circ$$

$$S_{12} = 0.15 \angle 6^\circ$$

$$S_{21} = 2.04 \angle 4^\circ$$

$$S_{22} = 0.19 \angle 134^\circ$$

The transistor power at the 1-dB compression point is $P_{1\text{dB}} = 15\text{ dBm}$.

Solution. The GaAs FET is unconditionally stable at 10 GHz since $K = 1.14$ and $\Delta = 0.358 \angle -151.3^\circ$. Using a series feedback capacitor having a series impedance of $Z = -j120\ \Omega$ (implemented as an open-circuited shunt stub in Fig. 5.5.12a) results in a potentially unstable configuration with the following S parameters:

$$S_{11} = 3.68 \angle -175.1^\circ$$

$$S_{12} = 3.86 \angle -38.26^\circ$$

$$S_{21} = 4 \angle 30.07^\circ$$

$$S_{22} = 2.77 \angle 176.17^\circ$$

The gate-to-ground port will be selected as the terminating port. The stability circle at the terminating port is drawn in Fig. 5.5.12b. Selecting β to have a value of 10, we obtain from (5.5.8) that

$$R = 10(2 \times 50) = 1000\ \Omega$$

and from (5.5.11)

$$\Gamma_T = \frac{10}{11} e^{-j2\theta} = 0.909 e^{-j2\theta}$$

The length l_1 of the transmission line is selected to place Γ_T in the unstable region. Selecting $l_1 = \lambda/4$ (i.e., $\theta = \pi/2$), it follows that the coefficient $\Gamma_T = 0.909 \angle -180^\circ$ is at point A in Fig. 5.5.12b. For this value of Γ_T the value of Γ_{IN} is $\Gamma_{\text{IN}} = 3.32 \angle -24.57^\circ$ (or $Z_{\text{IN}} = -83.75 - j23.1\ \Omega$). Hence, using (5.3.4) and (5.3.5), the load impedance can be selected to be $Z_L = 27.9 + j23.1\ \Omega$. The DRO circuit diagram is shown in Fig. 5.5.12c.

The expected output power of the oscillator will be a few dBs lower than the power at the 1-dB compression point (e.g., 10 dBm to 12 dBm).

YIG Oscillators

A YIG resonator consists of a ferrimagnetic material which can be modeled by a parallel RLC resonant circuit. The value of the elements depends on the magnetization, coupling, and resonance linewidth of the YIG sphere and on the applied dc magnetic field. The uniform dc magnetic field is applied with an electromagnet with a single gap. The gap design is important since a nonuniform dc magnetic field results in a tuning hysteresis and spurious responses. A common-gate GaAs FET oscillator using a YIG resonator is shown in Fig. 5.5.13.

The YIG sphere is strongly coupled to the transmission line that connects to the active device. Assuming that the YIG sphere is always magnetically

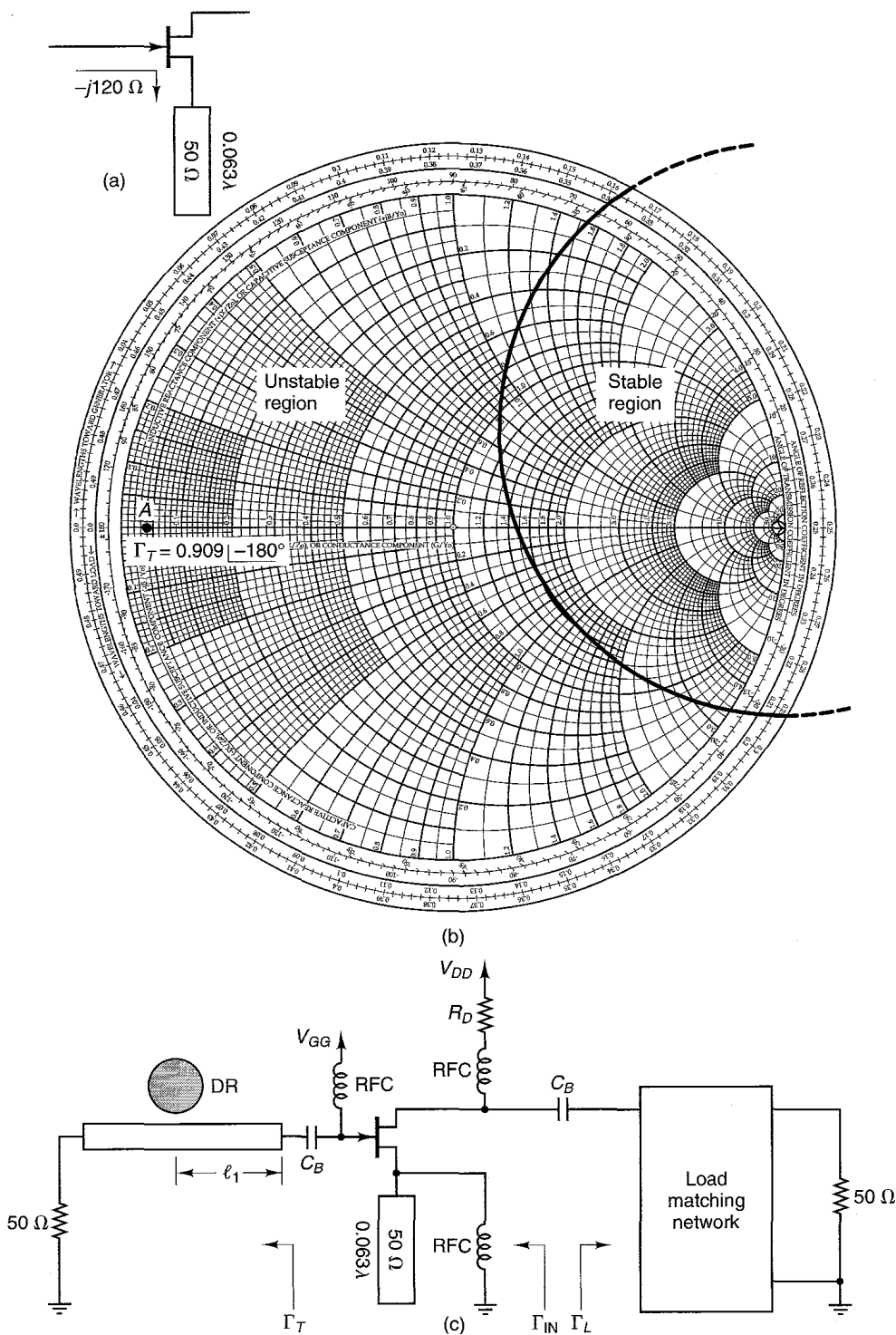


Figure 5.5.12 (a) GaAs FET with series feedback; (b) stability circle at the terminating port; (c) the DRO circuit.

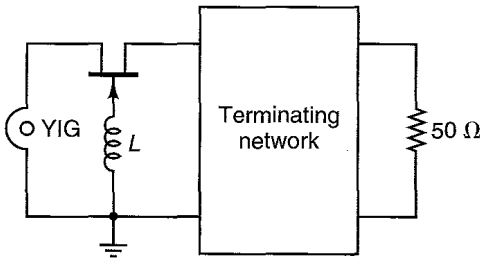


Figure 5.5.13 YIG-tuned oscillator.

saturated and that the sphere diameter is $\ll \lambda/4$, the YIG device can be modeled by a parallel resonant circuit, as shown in Fig. 5.5.14. The element values are given by [5.10, 5.11].

$$G_o = \frac{d^2}{\mu_o V \omega_m Q_U}$$

$$L_o = \frac{\mu_o V \omega_m}{\omega_o d^2}$$

$$C_o = \frac{1}{\omega_o^2 L_o}$$

where

$$\omega_m = \gamma 8\pi^2 M_s$$

$$Q_U = \frac{H_o - 4\pi M_s/3}{\Delta H}$$

Here $4\pi M_s$ is the saturation magnetization of the sphere, $\mu_o = 4\pi(10^{-7})$ Henrys per meter, V is the volume of the sphere, d is the coupling loop diameter, γ is the gyromagnetic ratio (2.8 MHz/Oe), H_o is the applied dc magnetic field, Q_u is the unloaded Q , ΔH is the resonance line width (approximately 0.2 Oe), and ω_o is the center frequency of resonance. The frequency ω_o can be expressed as

$$\omega_o = 2\pi\gamma H_o$$

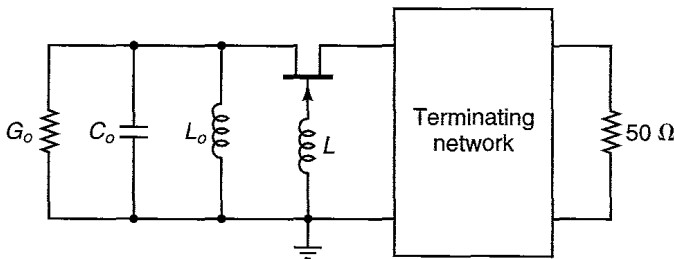


Figure 5.5.14 Equivalent network of a YIG sphere in a YIG-tuned oscillator.

Varactor-Tuned Oscillators

A varactor-tuned oscillator uses the voltage-controlled capacitance of a varactor diode to accomplish the electronic tuning. A basic schematic of a varactor-tuned oscillator is shown in Fig. 5.5.15. The capacitance of the varactor is determined by the voltage V , which is set by V^+ , R_1 , and R_2 .

Varactor diodes of different types having a wide range of capacitances are available. In the varactor circuit model shown in Fig. 5.5.16, the varactor diode capacitance (C_v), for Schottky-type devices, is given by the formula

$$C_v = \frac{C_0}{(1 + V/\phi)^{1/2}}$$

where C_0 is the value of capacitance at zero voltage, V the reverse bias voltage, and ϕ the junction contact potential ($\phi \approx 0.7$ V). The resistance R_s represents the series resistance of the diode, and the reverse diode resistance R_r is large and therefore can be neglected.

Example 5.5.2

Design a varactor-tuned oscillator to oscillate at 3 GHz.

Solution. The BJT configuration shown in Fig. 5.5.17a is used in the design. Assume that the S parameters of the BJT, at 3 GHz, with an inductor feedback are

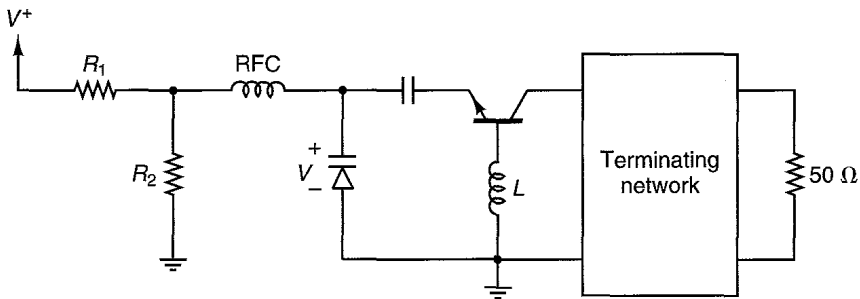


Figure 5.5.15 Varactor-tuned oscillator.

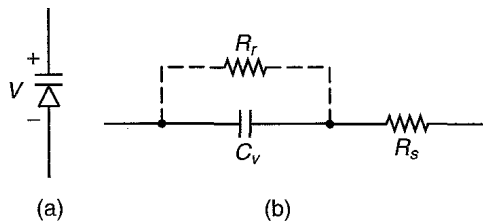


Figure 5.5.16 (a) Varactor diode circuit symbol; (b) model.

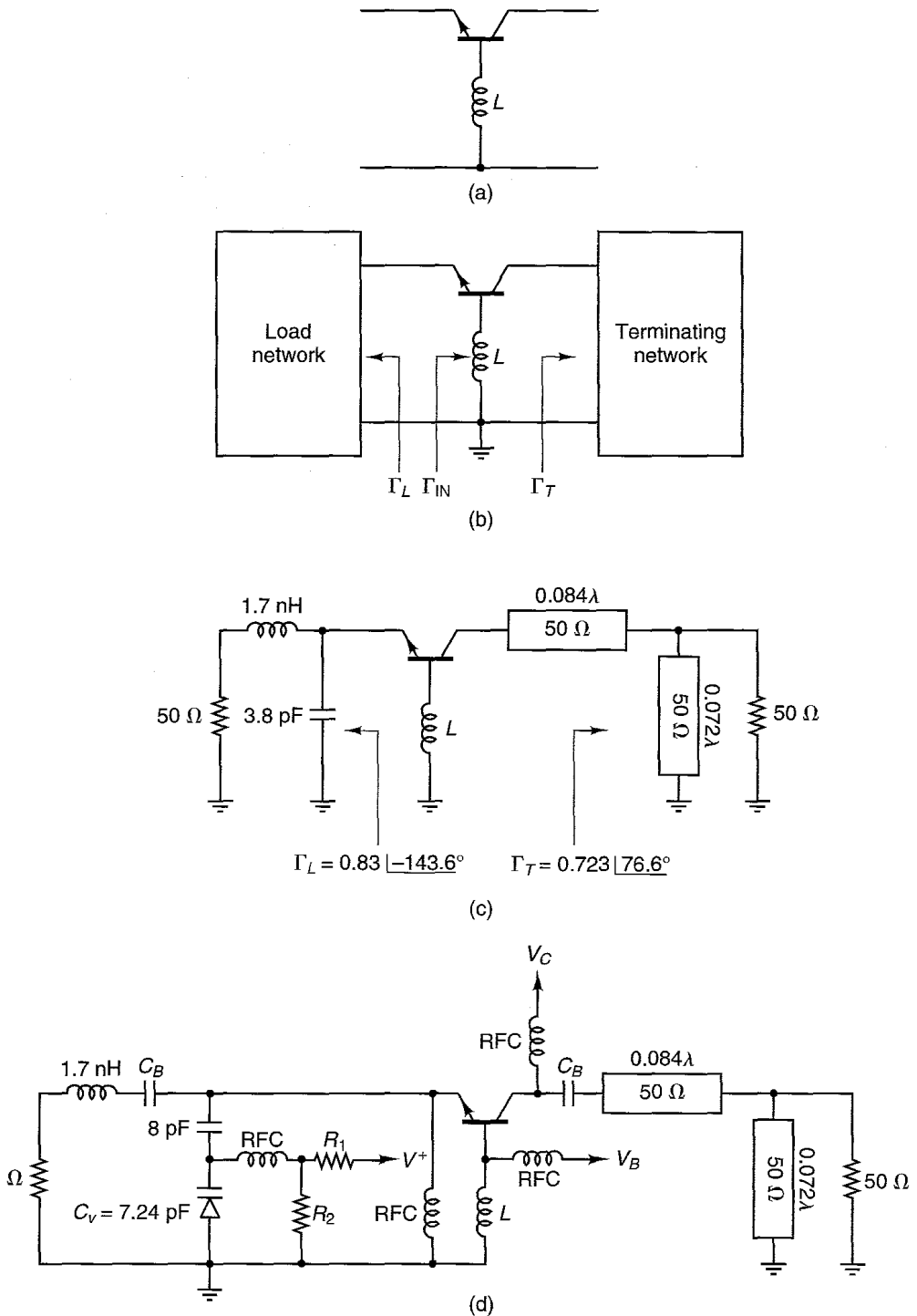


Figure 5.5.17 (a) BJT configuration for Example 5.5.2; (b) block diagram of the oscillator; (c) implementation of the load and termination circuit; (d) the oscillator circuit; (e) capacitance versus reverse voltage characteristics of the diode.

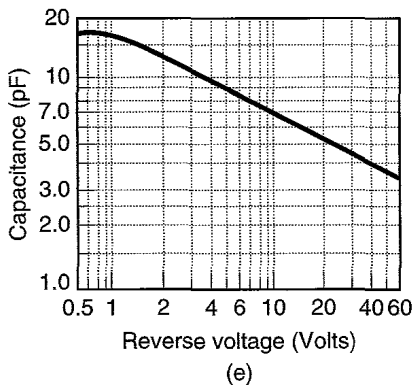


Figure 5.5.17 Continued

$$\begin{aligned}
 S_{11} &= 1.22 \angle 135^\circ \\
 S_{21} &= 1.69 \angle -80.4^\circ \\
 S_{12} &= 0.22 \angle 114^\circ \\
 S_{22} &= 1.0 \angle -50.2^\circ
 \end{aligned}$$

The design of the termination network in Fig. 5.5.17b involves the selection of Γ_T in the unstable region so that $|\Gamma_{IN}| > 1$. A CAD program was used to calculate Γ_{IN} as a function of Γ_T . A convenient value of Γ_T that places Γ_{IN} in the shaded region shown in Fig. 5.4.1 is $\Gamma_T = 0.723 \angle 76.6^\circ$. The resulting Γ_{IN} is $1.77 \angle 140.8^\circ$ (or $Z_{IN} = -15.5 + j16.3 \Omega$).

The load impedance was chosen according to (5.3.4) and (5.3.5)—namely,

$$R_L = \frac{|R_{IN}|}{3} = \frac{15.5}{3} = 5.17 \Omega$$

and

$$X_L = -X_{IN} = -j16.3 \Omega$$

Hence, $\Gamma_L = 0.83 \angle -143.6^\circ$.

The implementation of $\Gamma_T = 0.723 \angle 76.6^\circ$ and $\Gamma_L = 0.83 \angle -143.6^\circ$ is shown in Fig. 5.5.17c. Figure 5.5.17d shows the load circuit using a varactor diode to implement the 3.8-pF capacitor. The 3.8-pF capacitor is implemented using a fixed capacitor of 8 pF in series with a varactor capacitance of $C_v = 7.24$ pF. Figure 5.5.17e shows the capacitance versus voltage characteristics of the varactor diode selected. It is observed that for this varactor diode a bias voltage around 9 V produces the desired varactor's capacitance of 7.24 pF.

The frequency of oscillation can be set precisely by varying the varactor voltage (between 8V and 10 V) until the frequency is exactly 3 GHz. This type of oscillator can be used to implement a voltage-controlled oscillator (VCO), since changing the varactor capacitance changes the frequency of oscillation (within a certain range).

PROBLEMS

5.1 In Fig. 5.2.1 the gain of the amplifier is constant [i.e., $A_v(j\omega) = A_{vo}$] and

$$\beta(j\omega) = \frac{10^{-5}}{1 + j(\omega - 10^3)}$$

Use the Barkhausen criteria to determine the frequency of oscillation and the required value of A_{vo} .

5.2 In Fig. 5.2.5, $L = 50$ nH, $C = 10$ pF, and $R_{IN}(A) = -30(1 - A) \Omega$. Determine the frequency of oscillation and the value of R_L that maximizes the oscillator power.

5.3 In Fig. 5.2.7, $L = 25$ nH, $C = 5$ pF, and $G_{IN}(A') = -40(1 - A')$ mS. Determine the frequency of oscillation and the value of G_L that maximizes the oscillator power.

5.4 A negative-resistance device can be modeled by the parallel combination of a capacitor and a negative conductance, as shown in Fig. P5.4. The amplitude dependence of the negative conductance is given by (5.2.30).

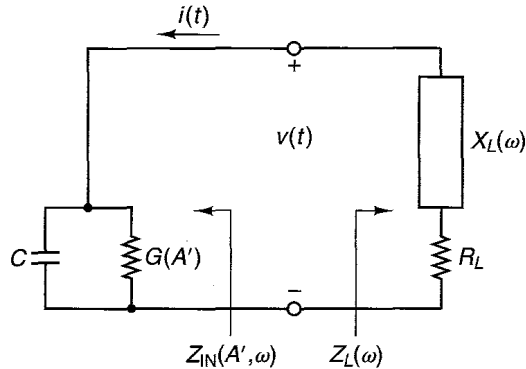


Figure P5.4

(a) Show that a stable oscillation at $\omega = \omega_o$ occurs when

$$R_L = \frac{-G(A')}{G^2(A') + \omega^2 C^2}$$

$$X_L(\omega_o) = \frac{\omega C}{G^2(A') + \omega^2 C^2}$$

and

$$\left. \frac{\partial R_{IN}}{\partial A'} \right|_{A'=A_o} \left. \frac{dX_L}{d\omega} \right|_{\omega=\omega_o} > 0$$

(b) Show that the oscillator power is a maximum when

$$G_L = \frac{G_0}{3}$$

where $Y_L(\omega) = G_L + jB_L(\omega)$.

- 5.5** Design a 10-GHz oscillator using a common-gate GaAs FET. The S parameters of the transistor at 10 GHz, $V_{DS} = 6$ V, $I_{DS} = 150$ mA are

$$S_{11} = 0.85 \angle -36^\circ$$

$$S_{21} = 0.53 \angle 96^\circ$$

$$S_{12} = 0.22 \angle -36^\circ$$

$$S_{22} = 1.125 \angle 171^\circ$$

Show the dc bias network.

- 5.6** Design the load-matching network for the oscillator in Example 5.3.1. Show the complete oscillator circuit.
- 5.7** Design a 2-GHz oscillator using a BJT with external feedback as shown in Fig. 5.3.3. The S parameters of the network at 2 GHz are as follows:

	$L = 0$ H	$L = 0.5$ nH
S_{11}	$0.94 \angle 174^\circ$	$1.04 \angle 173^\circ$
S_{21}	$1.90 \angle -28^\circ$	$2.00 \angle -30^\circ$
S_{12}	$0.013 \angle 98^\circ$	$0.043 \angle 153^\circ$
S_{22}	$1.01 \angle -17^\circ$	$1.05 \angle -18^\circ$

(This problem is based on a design from Ref. [5.7].)

- 5.8** Design an 8-GHz GaAs FET oscillator using the large-signal method discussed in Section 5.4. The S parameters of the transistor at 8 GHz are

$$S_{11} = 0.8 \angle 140^\circ$$

$$S_{12} = 0.2 \angle -70^\circ$$

$$S_{21} = 0.8 \angle 140^\circ$$

$$S_{22} = 0.9 \angle 170^\circ$$

The large-signal characteristics with the termination $Z_{T,o}$ are shown in Fig. P5.8.

- 5.9 (a)** Verify that (5.4.3) can be expressed in the form

$$\begin{aligned} \Gamma_{IN} &= \frac{S_{11} - \Delta S_{22}^*}{1 - |S_{22}|^2} + \frac{S_{12}S_{21}}{1 - |S_{22}|^2} \frac{\Gamma_T - S_{22}^*}{1 - S_{22}\Gamma_T} \\ &= \Gamma_{IN,o} + \alpha \Gamma_T' \end{aligned}$$

where

$$\begin{aligned} \Gamma_{IN,o} &= \frac{S_{11} - \Delta S_{22}^*}{1 - |S_{22}|^2} \\ \alpha &= \frac{S_{12}S_{21}}{1 - |S_{22}|^2} \frac{1 - S_{22}^*}{1 - S_{22}} \end{aligned}$$

and

$$\Gamma_T' = \frac{Z_T - Z_{22}^*}{Z_T + Z_{22}}$$

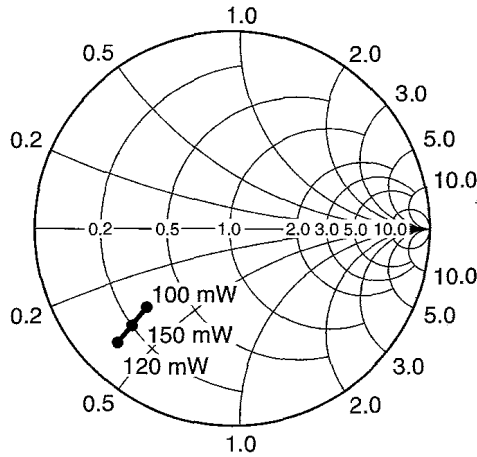


Figure P5.8

Then, show that $|\Gamma_{IN}|$ is a maximum when $|\Gamma_T| = 1$ and the phase of $\alpha|\Gamma_T|$ is equal to the phase of $\Gamma_{IN,o}$. That is,

$$\Gamma_{IN,max} = \Gamma_{IN,o} + |\alpha|\hat{u}_{\Gamma_{IN,o}}$$

where $\hat{u}_{\Gamma_{IN,o}}$ is a unit vector in the direction of $\Gamma_{IN,o}$.

(b) Show that the preceding expression for $\Gamma_{IN,max}$ is identical to (5.4.6).

(This problem is based on the paper by Wagner [5.5].)

5.10 Show that the S parameters of the DR in Fig. 5.5.7b, for frequencies close to the resonant frequency ω_o , are

$$[S] = \begin{bmatrix} \frac{\beta}{1 + \beta + j2Q_u\delta} & \frac{1 + j2Q_u\delta}{1 + \beta + j2Q_u\delta} \\ \frac{1 + j2Q_u\delta}{1 + \beta + j2Q_u\delta} & \frac{\beta}{1 + \beta + j2Q_u\delta} \end{bmatrix}$$

5.11 Use a design procedure similar to that in Example 5.5.1 to design a 12-GHz DRO. The S parameters of the GaAs FET, at 12 GHz, in a common-source configuration are

$$S_{11} = 0.67 \angle 107^\circ$$

$$S_{12} = 0.14 \angle -4^\circ$$

$$S_{21} = 1.65 \angle -19^\circ$$

$$S_{22} = 0.3 \angle 113^\circ$$

The transistor power at the 1-dB compression point is 13 dBm.

5.12 The conductance of a two-terminal negative-resistance device used in a YIG-tuned oscillator has a dependence on RF voltage amplitude A' given by (5.2.30). Assuming an equivalent circuit of the form shown in Fig. P5.12, determine the conditions for a stable oscillation.

5.13 Implement the input tuning network of Example 5.3.2 using a varactor diode. Specify the diode characteristics.

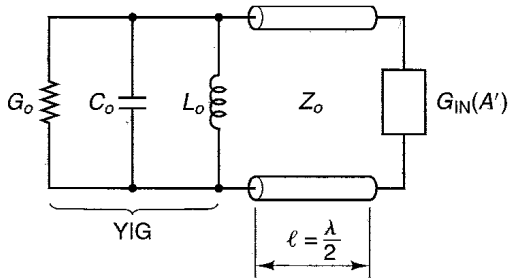


Figure P5.12

5.14 Assume that the S parameters of the BJT with an inductor feedback in Fig. 5.5.17a, at 3.5 GHz, are

$$S_{11} = 0.97 \angle -63.6^\circ$$

$$S_{12} = 0.3 \angle 104.2^\circ$$

$$S_{21} = 1.53 \angle -98.8^\circ$$

$$S_{22} = 1.26 \angle 123.5^\circ$$

Design a 3.5-GHz varactor-tuned oscillator.

5.15 (a) Johnson [5.12] shows that the output power of an oscillator can be approximated with the equation

$$P_{\text{OUT}} = P_{\text{sat}}(1 - e^{-G_o P_{\text{IN}}/P_{\text{sat}}})$$

where P_{sat} is the saturated output power of the amplifier, P_{IN} is the input power, and G_o is the small-signal power gain. Show that the maximum oscillator power [$P_{\text{osc(max)}}$] is given by

$$P_{\text{osc(max)}} = P_{\text{sat}} \left(1 - \frac{1}{G_o} - \frac{\ln G_o}{G_o} \right)$$

Hint: The maximum oscillator power occurs at the point of maximum $P_{\text{OUT}} - P_{\text{IN}}$, or where

$$\frac{\partial P_{\text{OUT}}}{\partial P_{\text{IN}}} = 1$$

(b) A GaAs FET has $G_o = 7.5$ dB with $P_{\text{sat}} = 1$ W. Calculate the maximum oscillator power.

(c) Draw a typical $P_{\text{osc}}/P_{\text{sat}}$ versus G_o plot.

REFERENCES

- [5.1] K. Kurokawa, "Some Basic Characteristics of Broadband Negative Resistance Oscillator Circuits," *The Bell System Technical Journal*, July 1969.
- [5.2] P. C. Wade, "Novel FET Power Oscillators," *Electronics Letters*, September 1978.
- [5.3] P. C. Wade, "Say Hello to Power FET Oscillators," *Microwaves*, April 1979.

- [5.4] COMPACT reference manual (1980), Compact Software, Inc., Paterson, N.J.
- [5.5] W. Wagner, "Oscillator Design by Device Line Measurement," *Microwave Journal*, February 1979.
- [5.6] G. Vendelin, A. Pavio, and U. L. Rhode, *Microwave Circuit Design Using Linear and Nonlinear Techniques*, Wiley-Interscience, 1990.
- [5.7] G. D. Vendelin, *Design of Amplifiers and Oscillators by the S Parameter Method*, Wiley-Interscience, New York, 1982.
- [5.8] D. Kajfez and P. Guillon, Editors, *Dielectric Resonators*, Artech House, 1986.
- [5.9] I. Bahl and P. Bhartia, *Microwave Solid State Circuit Design*, Wiley-Interscience, 1988.
- [5.10] D. V. Morgan and M. J. Howes, editors, *Microwave Solid State Devices and Applications*, Peter Peregrinus Ltd., New York, 1980.
- [5.11] P. M. Ollivier, "Microwave YIG-Tuned Transistor Oscillator Amplifier Design," *IEEE Journal of Solid-State Circuits*, February 1972.
- [5.12] K. M. Johnson, "Large Signal GaAs MESFET Oscillator Design," *IEEE Transactions on Microwave Theory and Techniques*, March 1979.

APPENDIX

COMPUTER-AIDED DESIGNS

There are many CAD programs available for microwave electronic applications that can perform a variety of tasks, varying from simple calculations to complex optimizations. A powerful CAD program is the Hewlett-Packard HP85150B Microwave and RF Design Systems (referred to as the HP MDS program). Another well-known company that offers powerful CAD programs is COMPACT SOFTWARE® [1].

It is not the purpose of this book to discuss how to use CAD programs and their many applications. In fact, many students of this book might not have access to one of these programs. However, this Appendix is included to illustrate some of the capabilities of a large-scale CAD program in the analysis, design, and optimization of various circuits.

As a microwave designer becomes more proficient in his or her profession, the use of a CAD program with analysis and optimization capabilities is of great importance. In some designs, straightforward calculations are a tedious process, and a CAD program is a must. In fact, powerful CAD methods are extremely valuable when used in conjunction with good engineering principles.

The program used in this Appendix is the HP MDS program. The HP MDS program provides analysis, optimization, modeling, schematic capture, and layout capabilities to take a preliminary design to a final production design, including its layout implementation.

The design capture system allows one to enter circuit schematics as easy as one would draw them on paper. After a circuit schematic is created, the simulations capabilities of the HP MDS program can perform linear and nonlinear simulations. The linear simulator predicts the performance of linear circuits, and the nonlinear simulator uses a harmonic balance technique to simulate the

steady-state characteristics of the circuit. The simulator performs a variety of calculations—namely, dc, ac, and S -parameter calculations; transient calculations; harmonic balance calculations; and Monte Carlo and yield analysis calculations.

The simulations can be optimized for certain goals. Then, the circuit can be updated using the optimized values for a final design or for further statistical simulations.

The HP MDS program allows the data to be presented in a variety of ways. Also, the program provides extensive documentation capabilities that allow the designer to produce a current and complete documentation of the design.

The purpose of the following examples is to illustrate some uses and capabilities of CAD methods in the design of microwave amplifiers.

EXAMPLE CAD.1 (REFER TO EXAMPLE 3.9.2b)

The program shown in Fig. CAD.1a calculates the operating point of the design in Example 3.9.2b and optimizes the circuit components for a more exact operating point location. The DC SIMULATION block requests a dc simulation of the circuit. With the original values of $R_1 = 19.25 \text{ k}\Omega$, $R_2 = 18.25 \text{ k}\Omega$, $R_3 = 1.75 \text{ k}\Omega$, and $R_4 = 350 \Omega$, the collector voltage of transistor Q_2 is $V_{C2} = 8.3 \text{ V}$, its collector current is $I_{C2} = 1.56 \text{ mA}$, and $I_3 = 3.83 \text{ mA}$.

One of the optimization GOALS is for the operating point of transistor Q_2 to be at $V_{C2} = 8 \text{ V}$ by specifying a BAD1 value of 7.99 V and a BAD2 value of 8.01 V. That is, try to keep V_{C2} in the range $7.99 \text{ V} < V_{C2} < 8.01 \text{ V}$. Similarly, the GOALS on I_{C2} and I_3 are to have $I_{C2} = 2 \text{ mA}$ and $I_3 = 4 \text{ mA}$. The variables that are varied in the optimization are the values of the resistors. The resistors can be varied by the optimization routine in the range shown in the figure. For example, the specification $R = 1.75 \text{ KOH}^*/10$ shows that the optimization can increase or decrease the value of the resistor by a factor of 10. The results of the optimization show that by changing the resistors as follows:

$$R_1 = 19.25 \text{ k}\Omega \text{ to } R_1 = 20.2 \text{ k}\Omega$$

$$R_2 = 18.25 \text{ k}\Omega \text{ to } R_2 = 17.8 \text{ k}\Omega$$

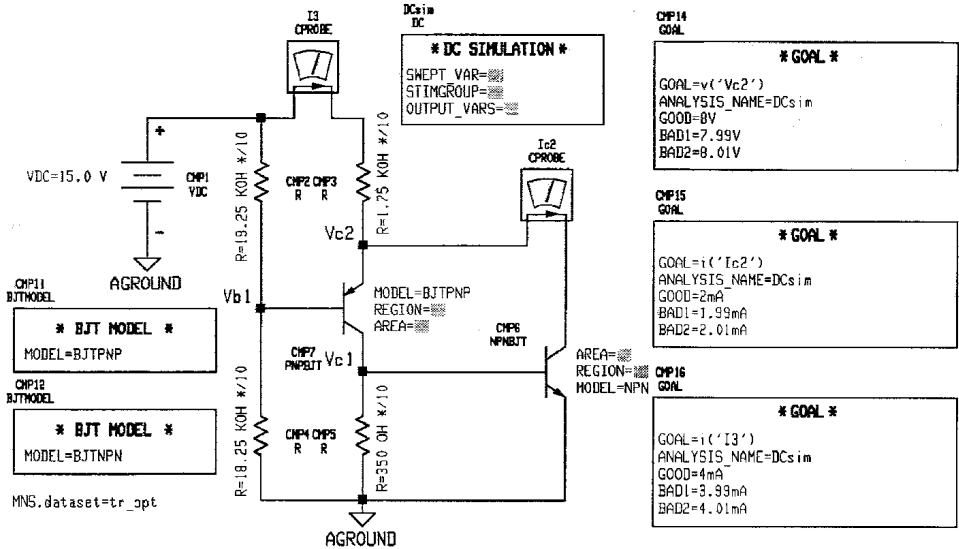
$$R_3 = 1.75 \text{ k}\Omega \text{ to } R_3 = 1.75 \text{ k}\Omega$$

$$R_4 = 350 \Omega \text{ to } R_4 = 401.4 \Omega$$

the following operating point is obtained: $V_{C2} = 8 \text{ V}$ and $I_{C2} = 1.99 \text{ mA}$ (see Fig. CAD.1b).

A stability analysis of the optimized circuit was performed by changing the beta of the transistors from 75 to 150. The following results were obtained:

β	V_{C2}	I_{C2}	I_3
75	8.05 V	1.96 mA	3.97 mA
150	7.95 V	2.04 mA	4.03 mA



Dataset=tr_opt

Qualifier=

Vc2
8.300

Ic2[I]
1.560E-03

I3
3.828E-03

Vc2-Vb1
0.790

Vc1
0.780

(a)

Dataset=tr_opt

Qualifier=

Vc2
8.000

Ic2
1.999E-03

I3
3.999E-03

Vc2-Vb1
0.787

Vc1
0.787

The operating point conditions for $B=100$, after optimization of parameters.

- $R_1 = 20.2 \text{ k}\Omega$
- $R_2 = 17.8 \text{ k}\Omega$
- $R_3 = 1.75 \text{ k}\Omega$
- $R_4 = 401.4 \text{ }\Omega$

(b)

Figure CAD.1 (a) The circuit program; (b) the results of the optimization.

These results show, as expected, that the circuit had good stability with respect to β variations.

EXAMPLE CAD.2 (REFER TO EXAMPLE 3.8.2)

The program shown in Fig. CAD.2a was used to design for the values of Γ_s and Γ_L that produce VSWR values lower than 1.5 in the design discussed in Example 3.8.2. When the impedance in PORT_SPAR is complex, the program calculates the generalized scattering parameters, using $Z_s = R_s + jX_s$ and $Z_L = R_L + jX_L$ as the normalizing impedances. From (2.8.11) and (2.8.12) (observing that $\Gamma_{p,IN} = S_{p11}$ and $\Gamma_{p,OUT} = S_{p22}$), it follows that

$$(\text{VSWR})_{\text{in}} = \frac{1 + |S_{p11}|}{1 - |S_{p11}|}$$

and

$$(\text{VSWR})_{\text{out}} = \frac{1 + |S_{p22}|}{1 - |S_{p22}|}$$

The first GOAL tries to keep $(\text{VSWR})_{\text{in}}$ below 1.5 by specifying a GOOD value for $|S_{p11}|$ of 0.15 [or $(\text{VSWR})_{\text{in}} = 1.35$] and a BAD1 value of 0.2 [or $(\text{VSWR})_{\text{in}} = 1.5$]. Similarly, the GOAL for $|S_{p22}|$ tries to keep $(\text{VSWR})_{\text{out}}$ below 1.5.

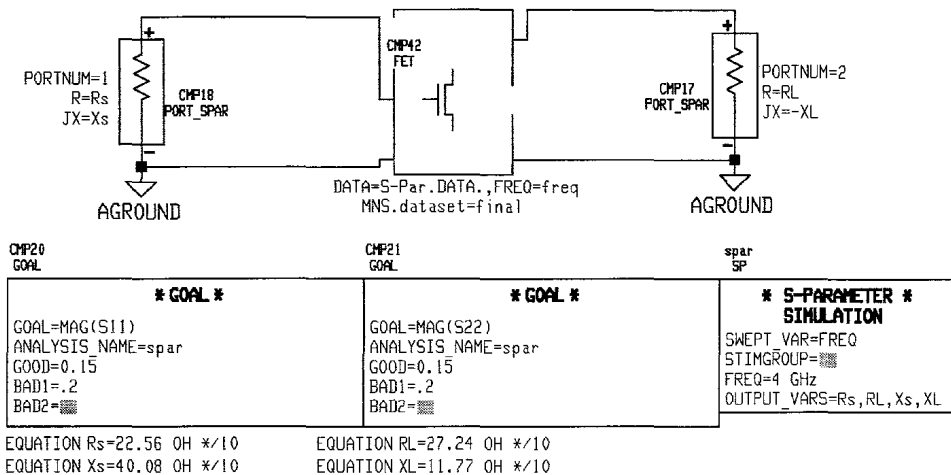
The original values of the source and load impedances are $Z_s = 22.56 + j40.08 \Omega$ (or $\Gamma_s = 0.586 \angle 95.48^\circ$) and $Z_L = 27.24 - j11.77 \Omega$ (or $\Gamma_L = 0.328 \angle -143.98^\circ$). These values, as shown in Fig. 3.8.3b, produce $(\text{VSWR})_{\text{in}} = 1.5$ and $(\text{VSWR})_{\text{out}} = 1.96$. The results of the optimization, shown in Fig. CAD.2b, show that with $\Gamma_s = 0.642 \angle 102.61^\circ$ and $\Gamma_L = 0.319 \angle -176.51^\circ$, a power gain of 12.7 dB can be obtained with $(\text{VSWR})_{\text{in}} = 1.52$ and $(\text{VSWR})_{\text{out}} = 1.58$.

A similar program was used to show that keeping Γ_L on the 12-dB power-gain circle at $\Gamma_L = 0.328 \angle -143.98^\circ$ (see point *b* in Fig. 3.8.3a) and varying Γ_s along the constant $(\text{VSWR})_{\text{in}} = 1.5$ circle, a minimum value of $(\text{VSWR})_{\text{out}} = 1.93$ is obtained when $\Gamma_s = 0.612 \angle 95.2^\circ$.

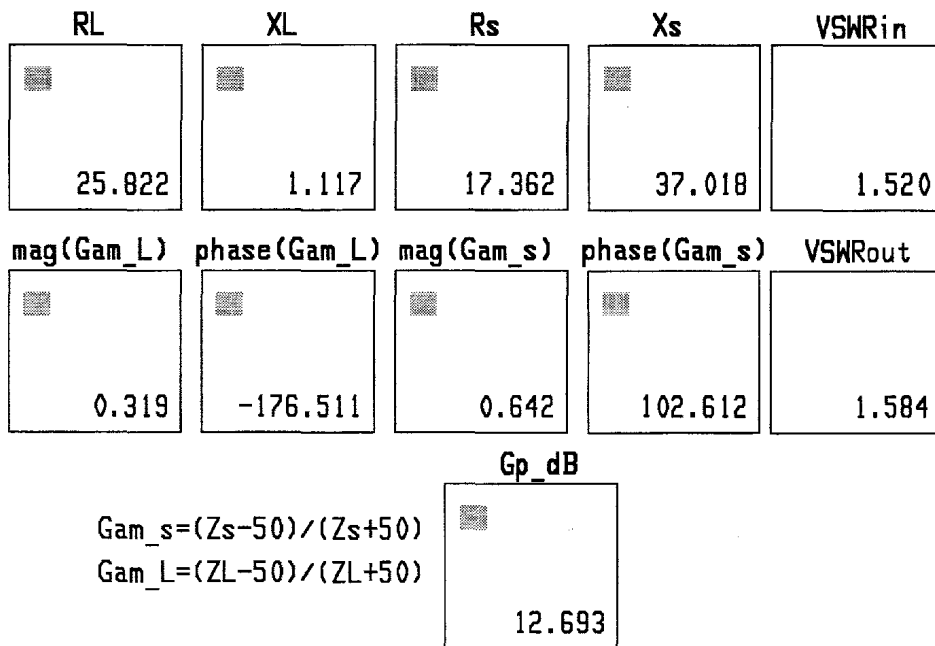
EXAMPLE CAD.3

This example involves the design of a flat-gain amplifier in the frequency range from 2.0 GHz to 2.2 GHz and an attempt to extend its flat-gain response to 2.4 GHz. The S parameters of the transistor selected are listed in Fig. CAD.3a.

Figure CAD.3a shows that the transistor is unconditionally stable in this range, and it calculates the values of $G_{T,\text{max}}$, Γ_{Ms} , and Γ_{ML} . We observe from this data that $G_{T,\text{max}}$ varies from 17.293 dB to 18.178 dB in the frequency range 2.0 GHz to 2.2 GHz. We can attempt to design the circuit to operate close to



(a)



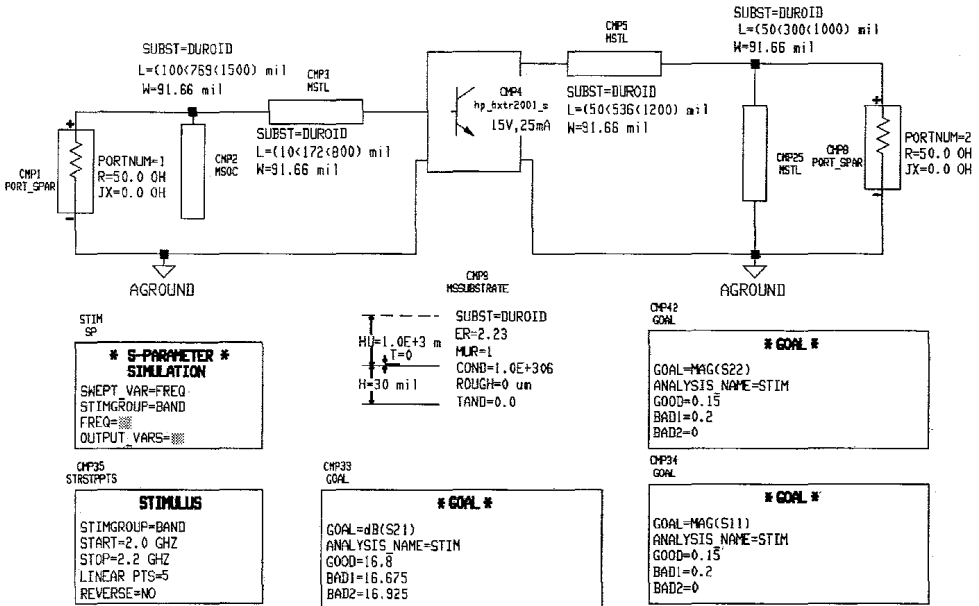
(b)

Figure CAD.2 (a) The circuit program; (b) the results of the optimization.

Freq	mag(S11)	phase(S11)	mag(S21)	phase(S21)	mag(S12)	phase(S12)	mag(S22)	phase(S22)
2.000E+09	0.770	-175.000	4.000	81.000	0.025	54.000	0.430	-20.000
2.050E+09	0.770	-175.170	3.905	80.602	0.025	54.458	0.430	-20.288
2.100E+09	0.770	-175.314	3.813	80.203	0.026	54.908	0.430	-20.581
2.150E+09	0.770	-175.436	3.725	79.803	0.026	55.350	0.430	-20.877
2.200E+09	0.770	-175.541	3.640	79.402	0.027	55.780	0.431	-21.176
2.250E+09	0.770	-175.631	3.558	79.001	0.027	56.196	0.431	-21.478
2.300E+09	0.770	-175.711	3.479	78.600	0.027	56.596	0.431	-21.781
2.350E+09	0.770	-175.784	3.404	78.199	0.028	56.979	0.430	-22.086
2.400E+09	0.770	-175.854	3.333	77.798	0.028	57.342	0.430	-22.391

Freq	GT_max	mag(G_MS)	phase(G_MS)	mag(G_ML)	phase(G_ML)	dB(S21)	K	abs(DELTA)
2.000E+09	18.178	0.859	176.852	0.669	29.049	12.041	1.422	0.250
2.050E+09	17.953	0.858	176.979	0.666	29.124	11.833	1.435	0.250
2.100E+09	17.730	0.857	177.082	0.664	29.215	11.626	1.448	0.250
2.150E+09	17.510	0.856	177.165	0.661	29.322	11.423	1.461	0.250
2.200E+09	17.293	0.855	177.232	0.659	29.443	11.222	1.474	0.250
2.250E+09	17.081	0.854	177.286	0.656	29.579	11.024	1.487	0.251
2.300E+09	16.875	0.853	177.332	0.654	29.729	10.830	1.499	0.251
2.350E+09	16.673	0.852	177.373	0.652	29.892	10.640	1.511	0.251
2.400E+09	16.478	0.851	177.414	0.650	30.069	10.456	1.521	0.251

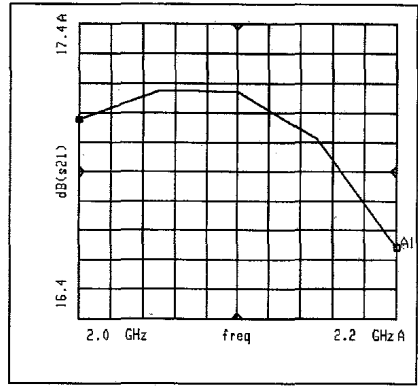
(a)



(b)

Figure CAD.3 (a) The S parameters of the transistor, and the values of $G_{T,max}$, Γ_{MS} , Γ_{ML} , K , and $|\Delta|$; (b) the circuit program; (c) the results of the optimization for the circuit in (b); (d) the circuit program using three-element matching networks; (e) the results of the optimization for the circuit in (d).

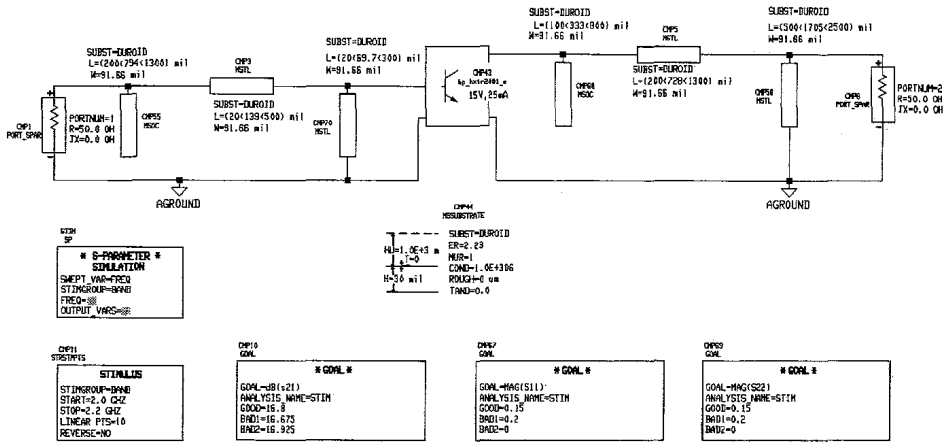
Freq	VSWR_in	VSWR_out	dB(s21)
2.000E+09	2.298	1.612	17.078
2.050E+09	1.868	1.534	17.177
2.100E+09	1.526	1.509	17.173
2.150E+09	1.378	1.539	17.015
2.200E+09	1.596	1.614	16.643



$$VSWR_{in} = (1 + \text{mag}(s11)) / (1 - \text{mag}(s11))$$

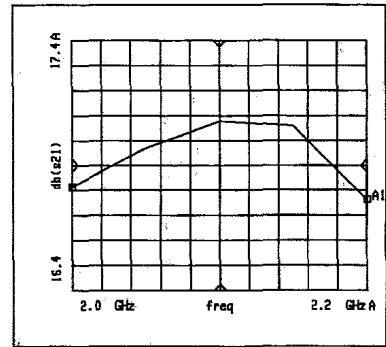
$$VSWR_{out} = (1 + \text{mag}(s22)) / (1 - \text{mag}(s22))$$

(c)



(d)

Freq	VSWR_in	VSWR_out	dB(s21)
2.000E+09	1.865	1.910	16.813
2.050E+09	1.708	1.707	16.969
2.100E+09	1.567	1.524	17.079
2.150E+09	1.501	1.460	17.060
2.200E+09	1.643	1.705	16.764



(e)

Figure CAD.3 Continued

$G_{T,\max}$ (e.g., at $G_T = 17$ dB) with an amplifier ripple of 0.25 dB. The preliminary design was done by simultaneously conjugate matching the transistor at 2.2 GHz (i.e., with $\Gamma_{Ms} = 0.855 \angle 177.2^\circ$ and $\Gamma_{ML} = 0.659 \angle 29.4^\circ$). The preliminary design is shown in Fig. CAD.3b. That is, the input matching network was designed with an open-circuited stub of length $L = 769$ mils, followed by a series microstrip line of length $L = 172$ mils. The substrate used was RT/Duroid® with $\epsilon_r = 2.23$, $W = 91.66$ mils, and $h = 30$ mils. Hence, the characteristic impedance is 50 Ω . The substrate specifications are described by the element MSSUBSTRATE.

The variables that are varied in the optimization are the lengths of the transmission lines. These lengths can be varied in the range shown. For example, the specification $L = (100 < 769 < 1500)$ mils in one of the microstrip lines shows that the optimization can vary the length of the line between 100 mils and 1500 mils.

The S-PARAMETER SIMULATION requests a simulation of the circuit in the frequency range specified by the STIMULUS (i.e., from 2 GHz to 2.2 GHz). One optimization GOAL is to keep G_T between 16.675 dB and 16.925 dB (i.e., a 0.25-dB gain ripple). The other GOALS try to keep the VSWRs below 1.5 by specifying a BAD1 value of 0.2 for $|S_{11}|$ and $|S_{22}|$. The GOALS might be a bit too ambitious because the bandwidth of this amplifier is close to 10%; hence, they are difficult to attain with two-element matching networks.

The results of the optimization are shown in Fig. CAD.3c. The optimizer changed the lengths of the microstrip lines as follows: the 769 mils to 730 mils, the 172 mils to 250 mils, the 536 mils to 474 mils, and the 300 mils to 505 mils. The results in Fig. CAD.3c show that the desired VSWRs were not obtained, and the gain ripple is 0.54 dB.

To improve the VSWRs and to lower the ripple, three-element matching networks were used, as shown in Fig. CAD.3d. The results of the optimization are shown in Fig. CAD.3e. This optimization changed the lengths of the microstrip lines as follows: the 794 mils to 708 mils, the 139 mils to 229 mils, the 69.7 mils to 151 mils, the 333 mils to 100 mils, the 728 mils to 1057 mils, and the 1705 mils to 1557 mils. The data show that $(VSWR)_{in}$ can be kept below 1.86, and $(VSWR)_{out}$ below 1.91. The gain ripple is 0.32 dB. These results are fairly good for this type of amplifier having a bandwidth close to 10%.

Finally, we attempted to extend the flat-gain response with the desired VSWRs to the frequency range 2.0 GHz to 2.4 GHz. The results of this optimization (not shown) produced a gain ripple of 0.85 dB with $(VSWR)_{in}$ lower than 2.29 and $(VSWR)_{out}$ lower than 2.5. Further improvements in the frequency response can be obtained by allowing the optimization to change the characteristic impedances of the microstrip lines.

EXAMPLE CAD.4

This example involves the design of a low-noise amplifier using the AFT-10136 GaAs FET at 4 GHz. The S parameters and the noise parameters of the

FET are given at $V_{DS} = 2$ V, $I_{DS} = 25$ mA, and $T_A = 25^\circ\text{C}$. The design specifications require a noise figure lower than 1 dB, with input and output VSWRs lower than 1.5.

$$\begin{aligned} S_{11} &= 0.54 \angle -120^\circ & F_{\min} &= 0.5 \text{ dB} \\ S_{12} &= 0.137 \angle 31^\circ & \Gamma_{\text{opt}} &= 0.39 \angle 126^\circ \\ S_{21} &= 3.6 \angle 61^\circ & r_n &= 0.36 \\ S_{22} &= 0.22 \angle -49^\circ \end{aligned}$$

The circuit program shown in Fig. CAD.4a is used to analyze the transistor performance at 4 GHz. Fig. CAD.4b shows the input stability circle, the 1-dB and 1.25-dB noise circles, and the 11-dB, 12-dB, and 13-dB available gain circles. These constant G_A circles correspond to 1 dB, 2 dB, and 3 dB less than G_{MSG} (which is approximately 14 dB).

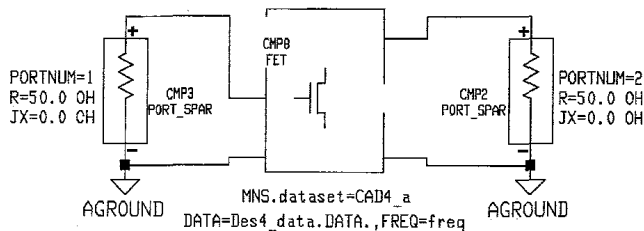
The preliminary design is done with $\Gamma_s = \Gamma_{\text{opt}} = 0.39 \angle 126^\circ$ (or $Z_s = 26.3 + j19.6 \Omega$) and $\Gamma_L = \Gamma_{\text{OUT}}^* = 0.324 \angle 97.6^\circ$ (or $Z_L = 37.6 + j26.9 \Omega$). Then the reflection coefficients Γ_s and Γ_L are varied (i.e., optimized) for the desired GOALS. The circuit program used is shown in Fig. CAD.4b. The GOAL on $\text{nf}[2]$ (which is the noise figure of the amplifier) is to keep the noise figure below 1 dB. Hence, a BAD1 value of 1 dB was specified. The GOALS on $|S_{11}|$ and $|S_{22}|$ are to keep the VSWRs below 1.5. Hence, a BAD1 value of 0.2 was specified for $|S_{11}|$ and $|S_{22}|$.

The results of the optimization and the final design are given in Fig. CAD.4d. That is, with $\Gamma_s = 0.528 \angle 125.9^\circ$ and $\Gamma_L = 0.267 \angle 101.6^\circ$, the low-noise amplifier has a noise figure of 0.9 dB with $(\text{VSWR})_{\text{in}} = 1.45$ and $(\text{VSWR})_{\text{out}} = 1.44$.

EXAMPLE CAD.5 (REFER TO EXAMPLE 4.4.3)

The CAD program used to optimize the feedback elements in Fig. 4.4.18a is shown in Fig. CAD.5a. The optimization GOAL is to vary R and L to have a G_T in the range $9.75 \text{ dB} < G_T < 10.25 \text{ dB}$. Observe that G_T in decibels is equal to the overall circuit S_{21} in decibels since $\text{dB}(S_{21}) = 20 \log|S_{21}| = 10 \log|S_{21}|^2$. This optimization produces the results given in Fig. CAD.5b, with R changed from 208Ω to 275.83Ω , and L changed from 28 nH to 13.9 nH .

The program used to optimize the complete amplifier is shown in Fig. CAD.5c. As discussed in Example 4.4.3, this circuit was obtained by using a simultaneous conjugate match at 1500 MHz. The GOAL on $G_T = \text{dB}(S_{21})$ is to have a gain in the range $9.9 \text{ dB} < G_T < 10.1 \text{ dB}$ (i.e., a 0.2-dB gain ripple). The GOALS on the VSWRs are to keep them below 1.5 (i.e., $|S_{11}|$ and $|S_{22}|$ less than 0.2). The results of the optimization are shown in Fig. CAD.5d. These results (discussed in Example 4.4.3) show that the amplifier exhibits an excellent gain flatness with $(\text{VSWR})_{\text{in}}$ less than 1.49 and $(\text{VSWR})_{\text{out}}$ less than 1.36.

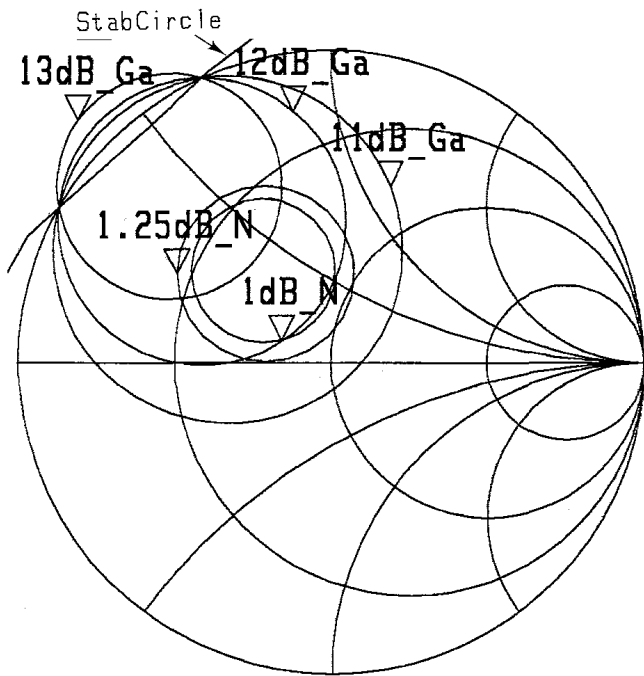


```

CMP4
NPORTNOISE
* N-PORT NOISE*
SIMULATION
SWEPT_VAR=FREQ
STIMGROUP=
FREQ=4 GHz
SAVE_S=YES
BANDWIDTH=1 HZ
OUTPUT_VARS=

```

(a)



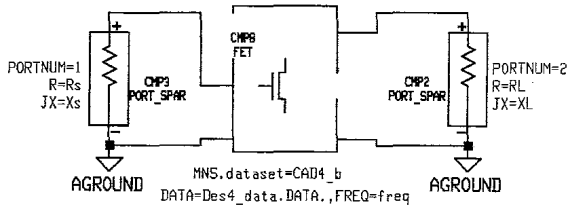
```

rnn=rn/50
Ga=GAcircle(S,11,1,3)
Stab_S=SrcStabCircle(S,1000)
Ns=NScircle(S,Sopt,rnn,nfmin,1,0.25,2,25)

```

(b)

Figure CAD.4 (a) The circuit program for the analysis of the transistor at 4 GHz; (b) the 1-dB and 1.25-dB noise circles and the 11-dB, 12-dB, and 13-dB available gain circles; (c) the circuit program for the optimization of the low-noise amplifier; (d) the results of the optimization.





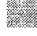
EQUATION Zs=Rs+j*Xs
 EQUATION ZL=RL+j*XL
 EQUATION Rs=26.3 OH */10
 EQUATION Xs=19.6 OH */10
 EQUATION RL=37.6 OH */10
 EQUATION XL=26.9 OH */10

*** N-PORT NOISE*
 SIMULATION**
 SWEPT_VAR=FREQ
 STIMGROUP=####
 FREQ=4 GHz
 SAVE_S=YES
 BANDWIDTH=1 HZ
 OUTPUT_VARS=####

CHP3 GOAL	CHP6 GOAL	CHP2 GOAL
* GOAL *	* GOAL *	* GOAL *
GOAL=MAG(S11) ANALYSIS_NAME=npnr GOOD=0.15 BAD1=0.2 BAD2=####	GOAL=MAG(S22) ANALYSIS_NAME=npnr GOOD=0.15 BAD1=0.2 BAD2=####	GOAL=nf[2] ANALYSIS_NAME=npnr GOOD=0.9 BAD1=1 BAD2=####

(c)

Rs=19.0 OH */10
 Xs=22.5 OH */10
 RL=39.4 OH */10
 XL=22.2 OH */10

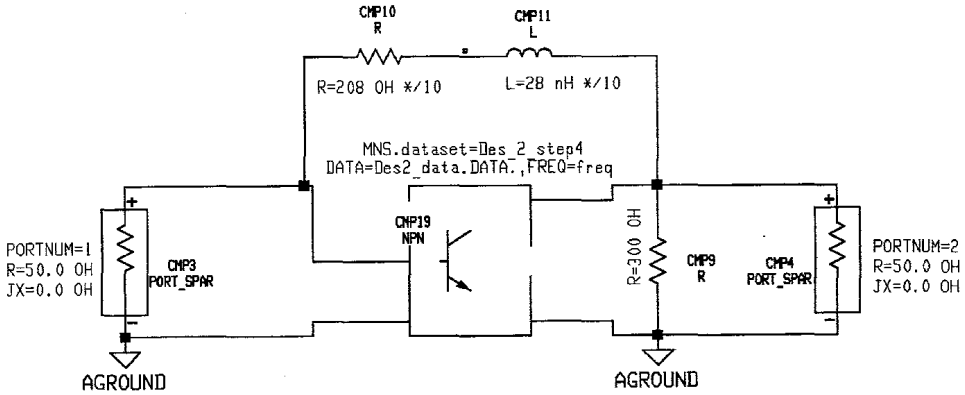
 VSWR_in 1.446	 VSWR_out 1.440	 nf[2] 0.909
---	--	---

(d)

Figure CAD.4 Continued

EXAMPLE CAD.6

The HP MDS program has a harmonic balance simulator which is suitable for a variety of large-signal applications. In this example, we use the harmonic balance simulator to design and determine the performance of a microwave oscillator at 3 GHz. The oscillator uses the BJT shown in Fig. CAD.6a. The transistor model (i.e., BJT MODEL) is specified, and three inductors were included at the emitter, base, and collector in order to improve the modeling of



```

Opt SP
* S-PARAMETER *
SIMULATION
SWEEP_VAR=FREQ
STIMGROUP=BAND
FREQ=
OUTPUT_VARS=

CHP8
POINTS
STIMULUS
STIMGROUP=BAND
POINT1=10 MHz
POINT2=100 MHz
POINT3=250 MHz
POINT4=500 MHz
POINT5=750 MHz
POINT6=1 GHz
POINT7=1.25 GHz
POINT8=1.5 GHz
POINT9=
POINT10=
REVERSE=NO
OTHER=

CHP13
GOAL
* GOAL *
GOAL=db(S21)
ANALYSIS_NAME=Opt
GOOD=10
BAD1=10.25
BAD2=9.75
    
```

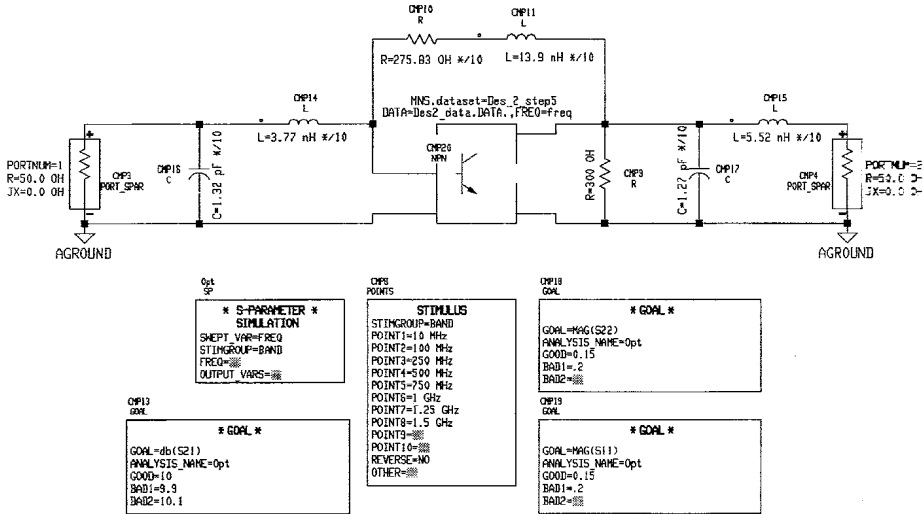
(a)

FREQ	mag(Tms2)	phase(Tms2)	mag(Tm12)	phase(Tm12)	K2	mag(Delta2)	dB(S21)
10000000.	0.213	-11.347	0.087	-130.243	1.215	0.516	9.969
100.0E+06	0.201	-5.113	0.075	-115.259	1.232	0.505	9.873
250.0E+06	0.186	5.472	0.106	-94.847	1.247	0.497	9.854
500.0E+06	0.163	24.015	0.163	-75.392	1.259	0.494	10.054
750.0E+06	0.142	73.196	0.164	-53.617	1.319	0.474	10.175
1.000E+09	0.175	110.099	0.194	-33.874	1.394	0.450	10.148
1.250E+09	0.195	123.903	0.282	-22.180	1.436	0.449	10.054
1.500E+09	0.236	130.251	0.365	-12.161	1.479	0.459	9.829

FREQ	mag(S11)	phase(S11)	mag(S12)	phase(S12)	mag(S21)	phase(S21)	mag(S22)	phase(S22)
10000000.	0.186	5.334	0.160	1.024	3.151	176.277	0.069	19.696
100.0E+06	0.179	-4.094	0.158	-1.979	3.117	173.034	0.080	32.324
250.0E+06	0.175	-21.408	0.155	-7.002	3.110	165.635	0.113	44.560
500.0E+06	0.178	-50.246	0.147	-14.387	3.182	153.345	0.178	49.273
750.0E+06	0.205	-85.453	0.133	-21.903	3.227	146.049	0.218	43.678
1.000E+09	0.253	-108.088	0.119	-27.470	3.217	137.642	0.264	35.595
1.250E+09	0.300	-118.916	0.108	-32.338	3.182	124.354	0.351	24.999
1.500E+09	0.364	-126.420	0.096	-37.121	3.100	109.469	0.441	14.035

(b)

Figure CAD.5 (a) The circuit program for the feedback design; (b) the results of the optimization in (a); (c) the complete broadband amplifier program; (d) the results of the optimization in (c).



(c)

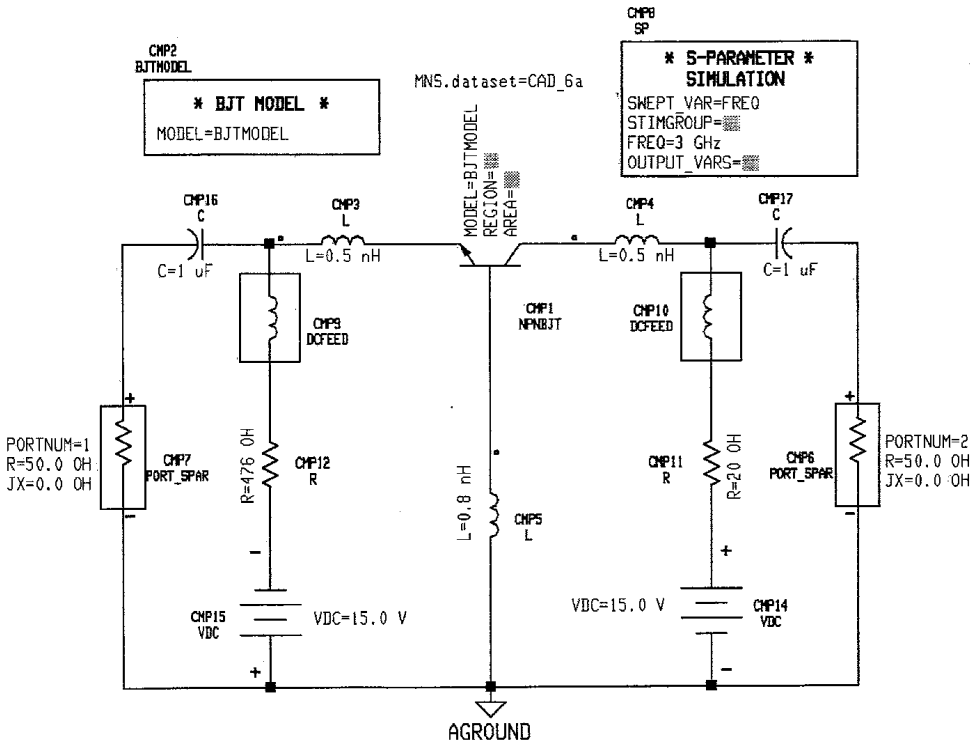
FREQ	mag(Tms4)	phase(Tms4)	mag(Tm14)	phase(Tm14)	K4	mag(Delta4)	dB(S21)	VSWRin2
10000000.	0.220	-10.311	0.065	-127.023	1.213	0.518	10.074	1.486
100.0E+06	0.206	1.346	0.076	-107.829	1.232	0.506	9.967	1.458
250.0E+06	0.187	20.890	0.108	-85.476	1.252	0.493	9.908	1.420
500.0E+06	0.152	54.169	0.155	-65.651	1.282	0.476	10.006	1.353
750.0E+06	0.123	119.704	0.124	-59.487	1.356	0.443	10.062	1.342
1.000E+09	0.139	178.292	0.095	-67.793	1.445	0.406	10.015	1.375
1.250E+09	0.145	-135.818	0.071	-81.072	1.514	0.379	9.997	1.357
1.500E+09	0.179	-97.875	0.105	-131.608	1.572	0.345	9.969	1.353

mag(S11)	phase(S11)	mag(S12)	phase(S12)	mag(S21)	phase(S21)	mag(S22)	phase(S22)	VSWRout2
0.195	4.353	0.158	0.532	3.189	175.679	0.077	17.214	1.167
0.186	-10.585	0.156	-6.817	3.150	167.174	0.086	26.338	1.189
0.174	-36.983	0.153	-19.045	3.129	151.056	0.112	35.652	1.251
0.150	-82.024	0.146	-38.320	3.165	125.063	0.152	38.746	1.359
0.146	-140.492	0.134	-58.093	3.185	102.751	0.147	38.859	1.343
0.158	169.122	0.123	-76.644	3.168	79.537	0.128	44.248	1.292
0.151	125.928	0.116	-85.155	3.161	51.061	0.096	47.007	1.213
0.150	89.992	0.110	-115.588	3.151	19.346	0.063	97.169	1.135

C = 1.32 pF to 1.08 pF
 L = 3.77 nH to 3.95 nH
 R = 275.83 Ω to 282.33 Ω
 L = 13.9 nH to 6.8 nH
 C = 1.27 pF to 1.27 pF
 L = 5.52 nH to 5.33 nH

(d)

Figure CAD.5 Continued



CMP13
BJTMODELFORM

```

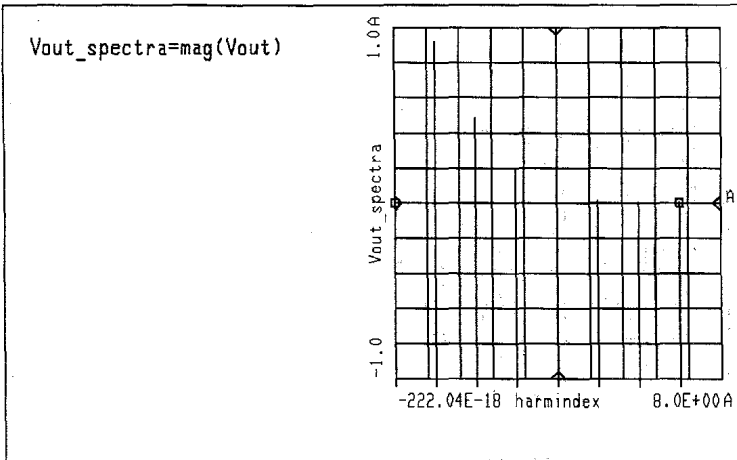
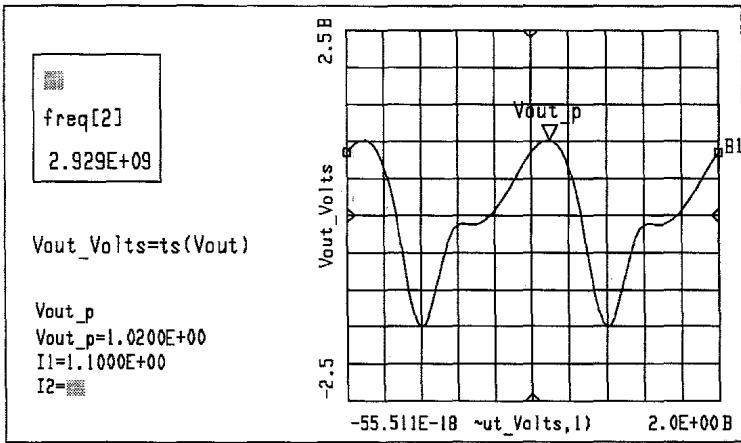
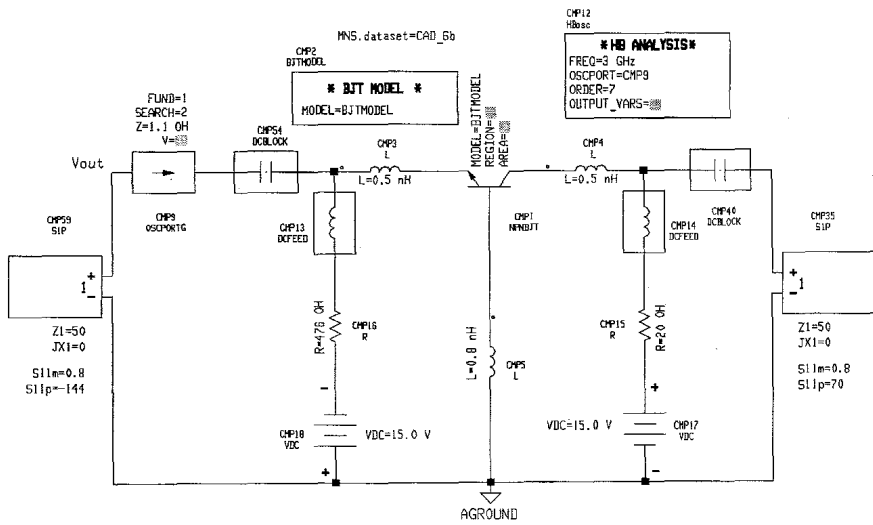
* BJT MODEL *
MODEL=BJTMODEL

NPN=yes
PNP=

Forward      Reverse      Diode and junction      Parasitics      Noise
BF=150       BR=1          EG=                      CJC=1.5 pF     RB=5           KF=
IKF=         IKR=          IS=2p                   VJC=.75       IRB=           AF=
ISF=         ISC=          IMAX=                   MJC=.5        RBM=           KB=
NE=          NC=          XT1=                     XCJC=         RE=1           AB=
VAF=75       VAR=         TNOM=                    FC=           RC=3           FB=
NF=          NR=          CJE=1.5 pF              VJE=.75
TF=30p       TR=75n       MJE=.5
XTF=
VTF=
ITF=
PTF=
XTB=
CJS=
VJS=
MJS=
    
```

(a)

Figure CAD.6 (a) Circuit program for the calculation of the S parameters of the BJT at 3 GHz with $V_{CE} = 15$ V and $I_C = 30$ mA; (b) circuit program for the harmonic balance analysis of the oscillator.



(b)

Figure CAD.6 Continued

the transistor. The bias circuit places the Q point at $V_{CE} = 15$ V and $I_C = 30$ mA. At this Q point, the *S*-PARAMETER SIMULATION calculates the following *S* parameters:

$$\begin{aligned} S_{11} &= 1.22 \angle 134.54^\circ & S_{12} &= 0.223 \angle 112.95^\circ \\ S_{21} &= 1.68 \angle -81.52^\circ & S_{22} &= 1 \angle -51.29^\circ \end{aligned}$$

Selecting the terminating port at the collector port of the transistor, the dependence of Γ_{IN} on Γ_T was analyzed at 3 GHz. It was found that a convenient value of Γ_T was $0.8 \angle 70^\circ$. This value of Γ_T produces $\Gamma_{IN} = 1.98 \angle 140^\circ$ (or $Z_{IN} = -18.4 + j16 \Omega$) at 3 GHz. The load matching network was designed as follows:

$$R_L = \frac{|R_{IN}|}{3} = \frac{18.4}{3} = 6.13 \Omega$$

and

$$X_L = -X_{IN} = -16 \Omega$$

The circuit program for the harmonic balance simulator is shown in Fig. CAD.6b with $\Gamma_T = 0.8 \angle 70^\circ$ and $\Gamma_L = 0.8 \angle -144^\circ$ (or $Z_L = 6.13 - j16 \Omega$), as well as the results of the optimization. The harmonic balance analysis shows that the circuit will have a fundamental frequency of oscillation at 2.929 GHz. The frequency spectrum of the oscillation signal is also shown. An optimization of the values of Γ_L and Γ_T can be performed to set the frequency of oscillation at exactly 3 GHz. In fact, with $\Gamma_L = 0.75 \angle -140^\circ$ and $\Gamma_T = 0.8 \angle 70^\circ$ the fundamental oscillation frequency is 3 GHz.

REFERENCE

- [1] COMPACT SOFTWARE, INC., 201 McLean Blvd, Paterson, N.J., 07504.

APPENDIX A

A.1 CIRCLE EQUATIONS: BILINEAR TRANSFORMATION

The distance between two complex points z and z_o is $|z - z_o|$. Therefore, it follows that the equation of a circle of radius r with center at z_o is given by

$$|z - z_o| = r \quad (\text{A.1})$$

Letting $z = x + jy$ and $z_o = x_o + jy_o$, (A.1) can be expressed in the form

$$|(x - x_o) + j(y - y_o)| = r$$

or

$$(x - x_o)^2 + (y - y_o)^2 = r^2 \quad (\text{A.2})$$

which is the well-known Cartesian representation of a circle centered at (x_o, y_o) with radius r .

Another representation of the circle equation is obtained by squaring (A.1)—namely,

$$\begin{aligned} |z - z_o|^2 &= r^2 \\ (z - z_o)(z - z_o)^* &= r^2 \\ (z - z_o)(z^* - z_o^*) &= r^2 \end{aligned}$$

Multiplying the left-hand side gives

$$|z|^2 - zz_o^* - z^*z_o + |z_o|^2 = r^2 \quad (\text{A.3})$$

The terms $zz_o^* + z^*z_o$ can also be written as $2\text{Re}[zz_o^*]$. Hence, another form of (A.3) is

$$|z|^2 - 2\text{Re}[zz_o^*] + |z_o|^2 = r^2$$

Several relations in this book involve algebraic manipulations that lead to circle equations. In fact, several relations are of the form

$$w = \frac{az + b}{cz + d} \quad (ad - bc \neq 0) \quad (\text{A.4})$$

which is recognized as the bilinear transformation. The bilinear transformation transforms (or maps) circles in the w plane into circles in the z plane, and vice versa.

For example, consider the transformation of the circle $|w| = \alpha$ into the z plane. From (A.4),

$$|w| = \alpha = \left| \frac{az + b}{cz + d} \right| \quad (\text{A.5})$$

Then

$$\alpha^2 = \left| \frac{az + b}{cz + d} \right|^2 = \left(\frac{az + b}{cz + d} \right) \left(\frac{az + b}{cz + d} \right)^*$$

which can be expanded as

$$\alpha^2[|cz|^2 + |d|^2 + czd^* + c^*z^*d] = |az|^2 + |b|^2 + azb^* + a^*z^*b$$

or

$$|z|^2[|a|^2 - \alpha^2|c|^2] - z[\alpha^2cd^* - ab^*] - z^*[\alpha^2c^*d - a^*b] + |b|^2 - \alpha^2|d|^2 = 0$$

Finally, we write the preceding expression in the form

$$|z|^2 - z \left[\frac{\alpha^2cd^* - ab^*}{|a|^2 - \alpha^2|c|^2} \right] - z^* \left[\frac{\alpha^2c^*d - a^*b}{|a|^2 - \alpha^2|c|^2} \right] + \frac{|b|^2 - \alpha^2|d|^2}{|a|^2 - \alpha^2|c|^2} = 0 \quad (\text{A.6})$$

Comparing (A.6) with (A.3), it follows that (A.6) is the equation of a circle centered at

$$z_o = \frac{\alpha^2c^*d - a^*b}{|a|^2 - \alpha^2|c|^2} \quad (\text{A.7})$$

and the radius of the circle is obtained from the relation

$$r^2 = |z_o|^2 - \frac{|b|^2 - \alpha^2|d|^2}{|a|^2 - \alpha^2|c|^2} \quad (\text{A.8})$$

Substituting (A.7) into (A.8) gives

$$r^2 = \left| \frac{\alpha^2c^*d - a^*b}{|a|^2 - \alpha^2|c|^2} \right|^2 - \frac{|b|^2 - \alpha^2|d|^2}{|a|^2 - \alpha^2|c|^2} = \frac{\alpha^2|ad - bc|^2}{||a|^2 - \alpha^2|c|^2|^2}$$

or

$$r = \frac{\alpha|ad - bc|}{\left||a|^2 - \alpha^2|c|^2\right|} \quad (\text{A.9})$$

Next we consider the transformation of a circle in the w -plane centered at w_o with radius α . That is, for $|w - w_o| = \alpha$ we write, from (A.4),

$$w - w_o = \frac{az + b}{cz + d} - w_o = \frac{(a - cw_o)z + (b - dw_o)}{cz + d}$$

Defining $a' = a - cw_o$ and $b' = b - dw_o$, we have

$$w - w_o = \frac{a'z + b'}{cz + d}$$

Then

$$|w - w_o| = \alpha = \left| \frac{a'z + b'}{cz + d} \right| \quad (\text{A.10})$$

and it follows that the center and radius of the circle in the z plane are given by (A.7) and (A.9), with a replaced by a' and b replaced by b' —namely,

$$z_o = \frac{\alpha^2 c^* d - (a')^* b'}{|a'|^2 - \alpha^2 |c|^2} \quad (\text{A.11})$$

and

$$r = \frac{\alpha^2 |a' d - b' c|}{\left||a'|^2 - \alpha^2 |c|^2\right|} \quad (\text{A.12})$$

A.2 DERIVATION OF THE INPUT AND OUTPUT STABILITY CIRCLES [EQUATIONS (3.3.5) AND (3.3.6)]

From (3.3.3), the values of Γ_L that produce $|\Gamma_{\text{IN}}| = 1$ are

$$|\Gamma_{\text{IN}}| = 1 = \left| S_{11} - \frac{S_{12} S_{21} \Gamma_L}{1 - S_{22} \Gamma_L} \right| = \left| \frac{S_{11} - \Delta \Gamma_L}{1 - S_{22} \Gamma_L} \right| \quad (\text{A.13})$$

which is recognized to be a bilinear transformation. Comparing (A.13) with (A.4) (with $\Gamma_L = z$ and $\Gamma_{\text{IN}} = w$), it follows that $a = -\Delta$, $b = S_{11}$, $c = -S_{22}$, and $d = 1$. The transformation (A.13) maps the circle $|\Gamma_{\text{IN}}| = 1$ into a circle in the Γ_L plane whose center and radius are given by (A.7) and (A.9), respectively. From (A.7), denoting the center by C_L , we obtain

$$C_L = \frac{c^* d - a^* b}{|a|^2 - |c|^2} = \frac{-S_{22}^* + \Delta^* S_{11}}{|\Delta|^2 - |S_{22}|^2} = \frac{(S_{22} - \Delta S_{11}^*)^*}{|S_{22}|^2 - |\Delta|^2}$$

and, from (A.9), denoting the radius by r_L , we obtain

$$r_L = \frac{|ad - bc|^2}{\left||a|^2 - |c|^2\right|^2} = \left| \frac{-\Delta + S_{11} S_{22}}{|\Delta|^2 - |S_{22}|^2} \right| = \left| \frac{S_{12} S_{21}}{|S_{22}|^2 - |\Delta|^2} \right|$$

The circle in the Γ_L plane is given by

$$|\Gamma_L - C_L| = r_L$$

which is recognized as (3.3.5). The derivation of (3.3.6) is similar.

APPENDIX B

STABILITY CONDITIONS

The necessary and sufficient conditions for a two-port network to be unconditionally stable can be derived from (3.3.1) to (3.3.4) (Kurokawa [B.1] and Ha [B.2]). An alternate derivation of the stability conditions begins with (3.3.11) and (3.3.12). Both derivations are now presented.

FIRST DERIVATION

The conditions for a two-port network to be unconditionally stable are given in (3.3.1) to (3.3.4)—namely,

$$|\Gamma_s| < 1 \quad (\text{B.1})$$

$$|\Gamma_L| < 1 \quad (\text{B.2})$$

$$|\Gamma_{\text{IN}}| = \left| S_{11} + \frac{S_{12}S_{21}\Gamma_L}{1 - S_{22}\Gamma_L} \right| < 1 \quad (\text{B.3})$$

and

$$|\Gamma_{\text{OUT}}| = \left| S_{22} + \frac{S_{12}S_{21}\Gamma_s}{1 - S_{11}\Gamma_s} \right| < 1 \quad (\text{B.4})$$

Equations (B.2) and (B.3) state that for all passive load impedances, the real part of the input impedance must be positive; while (B.1) and (B.4) state that for all passive source impedances, the real part of the output impedance must be positive.

Starting with (B.3), we can write the inequality in the form

$$\begin{aligned} \left| S_{11} + \frac{S_{12}S_{21}\Gamma_L}{1 - S_{22}\Gamma_L} \right| &= \left| \frac{S_{11} - \Delta\Gamma_L}{1 - S_{22}\Gamma_L} \right| = \left| \frac{\Delta - \Delta\Gamma_L S_{22} + S_{21}S_{12}}{S_{22}(1 - S_{22}\Gamma_L)} \right| \\ &= \left| \frac{1}{S_{22}} \left(\Delta + \frac{S_{12}S_{21}}{1 - S_{22}\Gamma_L} \right) \right| < 1 \end{aligned} \quad (\text{B.5})$$

where

$$\Delta = S_{11}S_{22} - S_{12}S_{21}$$

Hence, we need to determine the conditions that the S parameters must satisfy so that (B.5) holds for all values of Γ_L such that $|\Gamma_L| < 1$ [i.e., so that (B.2) is satisfied]. To this end, we write (B.5) as

$$|z| < 1 \quad (\text{B.6})$$

where

$$z = \frac{1}{S_{22}} \left(\Delta + \frac{S_{12}S_{21}}{1 - S_{22}\Gamma_L} \right) \quad (\text{B.7})$$

Next, we analyze the bilinear transformation in (B.7) to determine the mapping of the unit circle $|\Gamma_L| = 1$ on the z plane. The mapping of $|\Gamma_L| = 1$ on the z plane according to (B.7) can be viewed as a series of successive mappings. That is, let

$$z = \frac{1}{S_{22}} (\Delta + q) \quad (\text{B.8})$$

where

$$\begin{aligned} q &= \frac{S_{12}S_{21}}{1 - S_{22}\Gamma_L} = S_{12}S_{21}t \\ t &= \frac{1}{1 - S_{22}\Gamma_L} = \frac{1}{w} \end{aligned}$$

and

$$w = 1 - S_{22}\Gamma_L$$

The transformation $w = 1 - S_{22}\Gamma_L$ is a translation that maps the unit circle $|\Gamma_L| = 1$ onto the w plane as a circle, centered at 1 with radius $|S_{22}|$ (see Fig. B.1a). The inverse transformation

$$t = \frac{1}{w} = \frac{1}{1 - S_{22}\Gamma_L}$$

produces the mapping shown in Fig. B.1b. The center C_1 is located on the real axis at the midpoint between $1/(1 - |S_{22}|)$ and $1/(1 + |S_{22}|)$. That is,

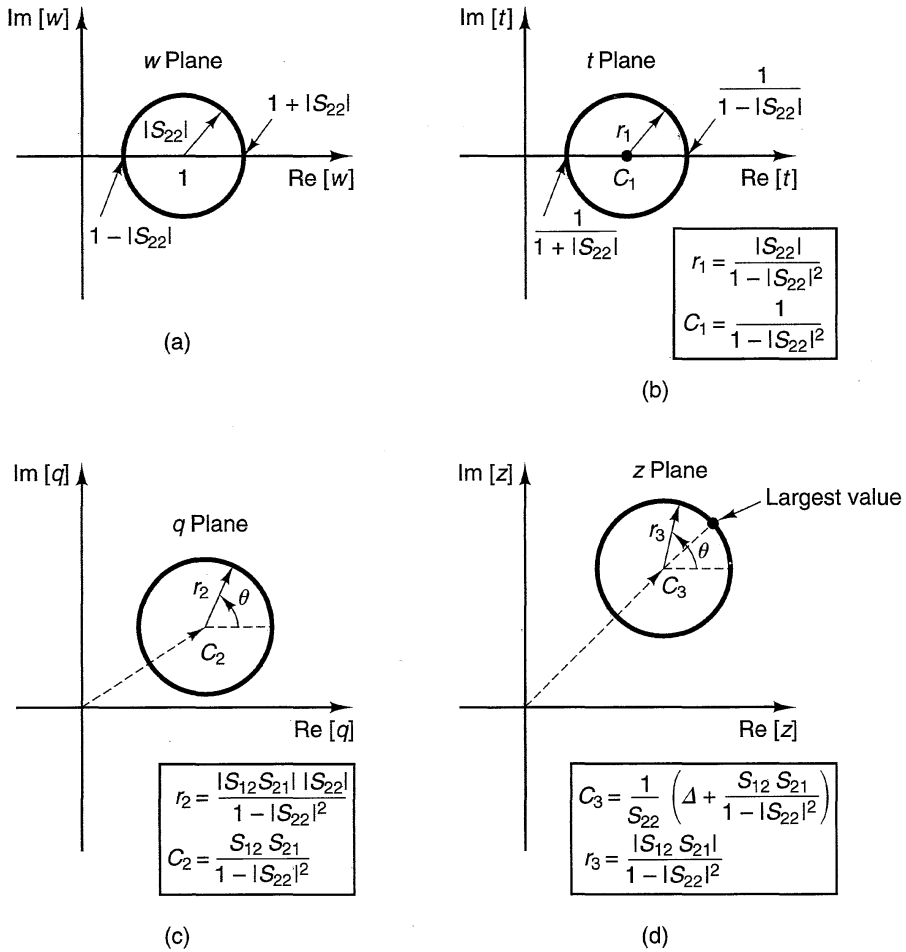


Figure B.1 (a) Mapping of $|\Gamma_L| = 1$ on the w plane, where $w = 1 - S_{22}\Gamma_L$; (b) mapping of $|\Gamma_L| = 1$ on the t plane, where $t = 1/w$; (c) mapping of the $|\Gamma_L| = 1$ plane on the q plane, where $q = S_{12}S_{21}t$; (d) mapping of the $|\Gamma_L| = 1$ plane on the z plane, where $z = 1/S_{22}(\Delta + q)$.

$$C_1 = \frac{1}{2} \left[\frac{1}{1 - |S_{22}|} + \frac{1}{1 + |S_{22}|} \right] = \frac{1}{1 - |S_{22}|^2}$$

The radius r_1 is given by

$$r_1 = \frac{1}{2} \left[\frac{1}{1 - |S_{22}|} - \frac{1}{1 + |S_{22}|} \right] = \frac{|S_{22}|}{1 - |S_{22}|^2}$$

Then, the transformation

$$q = S_{12}S_{21}t = \frac{S_{12}S_{21}}{1 - S_{22}\Gamma_L}$$

produces the mapping shown in Fig. B.1c. That is, the unit circle $|\Gamma_L| = 1$ maps into a circle in the q plane centered at

$$C_2 = \frac{S_{12}S_{21}}{1 - |S_{22}|^2}$$

with radius

$$r_2 = \frac{|S_{12}S_{21}S_{22}|}{1 - |S_{22}|^2}$$

The equation of the circle in the q plane can be expressed in the complex form

$$\begin{aligned} q &= C_2 + r_2 e^{j\theta} \\ &= \frac{S_{12}S_{21}}{1 - |S_{22}|^2} + \frac{|S_{12}S_{21}S_{22}|}{1 - |S_{22}|^2} e^{j\theta} \end{aligned} \quad (\text{B.9})$$

where θ varies from 0 to 2π .

Finally, from (B.9) and (B.8), we see that the unit circle $|\Gamma_L| = 1$ is mapped into a circle in the z plane, centered at C_3 with radius r_3 , given by

$$z = C_3 + r_3 e^{j\theta} \quad (\text{B.10})$$

where

$$C_3 = \frac{1}{S_{22}} \left(\Delta + \frac{S_{12}S_{21}}{1 - |S_{22}|^2} \right)$$

and

$$r_3 = \frac{|S_{12}S_{21}|}{1 - |S_{22}|^2}$$

The mapping is shown in Fig. B.1d.

From (B.10), we observe that $|z|$ has its largest value when θ is equal to the phase of the C_3 term. It follows that regardless of the value of θ , the inequality $|z| < 1$ [i.e., (B.6)] is satisfied when

$$\left| \frac{1}{S_{22}} \left(\Delta + \frac{S_{12}S_{21}}{1 - |S_{22}|^2} \right) \right| + \frac{|S_{12}S_{21}|}{1 - |S_{22}|^2} < 1 \quad (\text{B.11})$$

Since

$$\frac{1}{S_{22}} \left(\Delta + \frac{S_{12}S_{21}}{1 - |S_{22}|^2} \right) = \frac{S_{11} - \Delta S_{22}^*}{1 - |S_{22}|^2}$$

we can write (B.11) in the form

$$\left| \frac{S_{11} - \Delta S_{22}^*}{1 - |S_{22}|^2} \right| < 1 - \frac{|S_{12}S_{21}|}{1 - |S_{22}|^2} \quad (\text{B.12})$$

To further manipulate (B.12), we must square both sides of the inequality. However, we first observe that the left-hand side of the inequality is positive. Therefore, the right-hand side must also be positive. That is,

$$1 - \frac{|S_{12}S_{21}|}{1 - |S_{22}|^2} > 0$$

or

$$|S_{12}S_{21}| < 1 - |S_{22}|^2 \quad (\text{B.13})$$

Using the property that if $a < b$ with $a > 0$ and $b > 0$, then $a^2 < b^2$, we can write, from (B.12),

$$\left| \frac{S_{11} - \Delta S_{22}^*}{1 - |S_{22}|^2} \right|^2 < \left(1 - \frac{|S_{12}S_{21}|}{1 - |S_{22}|^2} \right)^2$$

or

$$|S_{11} - \Delta S_{22}^*|^2 < (1 - |S_{22}|^2 - |S_{12}S_{21}|)^2 \quad (\text{B.14})$$

The term in the left-hand side of (B.14) can be written in the form (see Problem 3.20)

$$|S_{11} - \Delta S_{22}^*|^2 = |S_{12}S_{21}|^2 + (1 - |S_{22}|^2)(|S_{11}|^2 - |\Delta|^2) \quad (\text{B.15})$$

Substituting (B.15) into (B.14) gives

$$|S_{12}S_{21}|^2 + (1 - |S_{22}|^2)(|S_{11}|^2 - |\Delta|^2) < (1 - |S_{22}|^2 - 2(1 - |S_{22}|^2)|S_{12}S_{21}| + |S_{12}S_{21}|^2)$$

Simplifying, we obtain

$$|S_{11}|^2 - |\Delta|^2 < 1 - |S_{22}|^2 - 2|S_{12}S_{21}|$$

which can be expressed in the form

$$K > 1$$

where K is

$$K = \frac{1 - |S_{11}|^2 - |S_{22}|^2 + |\Delta|^2}{2|S_{12}S_{21}|} \quad (\text{B.16})$$

Thus far, we have shown that (B.2) and (B.3) are satisfied when the S parameters satisfy (B.13) and (B.16). Starting with (B.1) and (B.4), the derivation is similar. In fact, it follows that the conditions for unconditional stability at the output port are simply obtained by interchanging S_{11} by S_{22} and S_{22} by S_{11} in (B.13) and (B.16)—that is, when

$$|S_{12}S_{21}| < 1 - |S_{11}|^2 \quad (\text{B.17})$$

and

$$K > 1$$

In conclusion, from (B.13), (B.16), and (B.17), the two-port network is unconditionally stable when

$$K = \frac{1 - |S_{11}|^2 - |S_{22}|^2 + |\Delta|^2}{2|S_{12}S_{21}|} > 1$$

$$|S_{12}S_{21}| < 1 - |S_{11}|^2$$

and

$$|S_{12}S_{21}| < 1 - |S_{22}|^2$$

SECOND DERIVATION

The conditions for a two-port network to be unconditionally stable can be expressed in the form given in (3.3.11) and (3.3.12)—namely,

$$|S_{11}| < 1 \quad (\text{B.18})$$

with

$$\begin{cases} |C_L| - r_L > 1 \\ \text{or} \\ r_L - |C_L| > 1 \end{cases} \quad (\text{B.19})$$

$$r_L - |C_L| > 1 \quad (\text{B.20})$$

and

$$|S_{22}| < 1 \quad (\text{B.21})$$

with

$$\begin{cases} |C_s| - r_s > 1 \\ \text{or} \\ r_s - |C_s| > 1 \end{cases} \quad (\text{B.22})$$

$$r_s - |C_s| > 1 \quad (\text{B.23})$$

where C_L , r_L , C_s , and r_s are given by (3.3.7) to (3.3.10).

Equation (B.19) states that the output stability circle is completely outside the Smith chart (see Fig. B.2a), and (B.20) states that the output stability circle completely encloses the Smith chart (see Fig. B.2b). Equation (B.18) makes the inside of the Smith chart the stable region (see Figs. B.2a and B.2b). Equations (B.21), (B.22), and (B.23) place similar conditions on the input stability circle.

Substituting (3.3.7) and (3.3.8) into (B.19) gives

$$\left| \frac{S_{22} - \Delta S_{11}^*}{|S_{22}|^2 - |\Delta|^2} \right| > 1 + \frac{|S_{12}S_{21}|}{|S_{22}|^2 - |\Delta|^2} \quad (\text{B.24})$$

In writing (B.24), we used the fact that when the origin is not enclosed by the output stability circle, it follows that $|S_{22}| > |\Delta|$ (see Problem 3.11). Therefore,

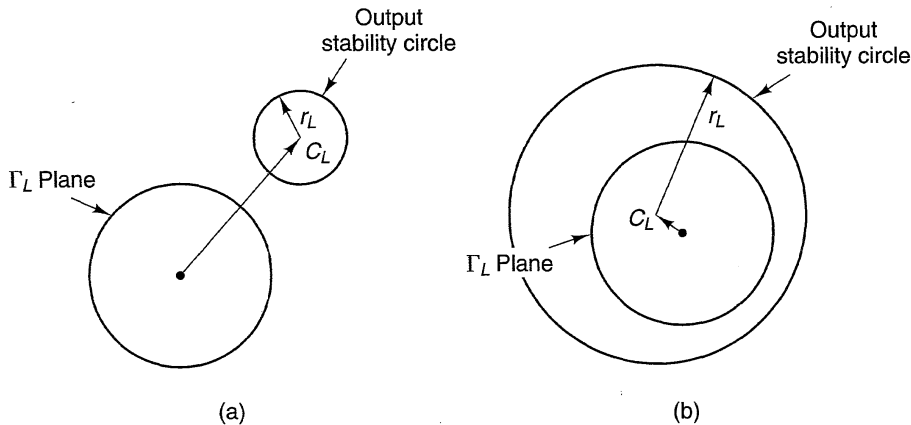


Figure B.2 (a) A typical output stability circle outside the Smith chart for unconditional stability; (b) a typical output stability circle enclosing the Smith chart for unconditional stability.

the term $|S_{12}S_{21}|/(|S_{22}|^2 - |\Delta|^2)$ (which is the expression for r_L) is positive. We can then square both sides of (B.24) to obtain

$$|S_{22} - \Delta S_{11}^*|^2 > (|S_{22}|^2 - |\Delta|^2 + |S_{12}S_{21}|)^2 \tag{B.25}$$

Using the identity (see Problem 3.20)

$$|S_{22} - \Delta S_{11}^*|^2 = |S_{12}S_{21}|^2 + (1 - |S_{11}|^2)(|S_{22}|^2 - |\Delta|^2) \tag{B.26}$$

we can write (B.25) in the form

$$|S_{12}S_{21}|^2 + (1 - |S_{11}|^2)(|S_{22}|^2 - |\Delta|^2) > (|S_{22}|^2 - |\Delta|^2)^2 + 2(|S_{22}|^2 - |\Delta|^2)|S_{12}S_{21}| + |S_{12}S_{21}|^2$$

Simplifying, we obtain

$$1 - |S_{11}|^2 > |S_{22}|^2 - |\Delta|^2 + 2|S_{12}S_{21}|$$

or simply

$$K = \frac{1 - |S_{11}|^2 - |S_{22}|^2 + |\Delta|^2}{2|S_{12}S_{21}|} > 1 \tag{B.27}$$

Next, substituting (3.3.7) and (3.3.8) into (B.20) gives

$$\left| \frac{S_{22} - \Delta S_{11}^*}{|S_{22}|^2 - |\Delta|^2} \right| < \frac{|S_{12}S_{21}|}{|\Delta|^2 - |S_{22}|^2} - 1 \tag{B.28}$$

In writing (B.28), we used the fact that when the origin is enclosed by the output stability circle, it follows that $|S_{22}| < |\Delta|$ (see Problem 3.11). Therefore, the term $|S_{12}S_{21}|/(|\Delta|^2 - |S_{22}|^2)$ (which is the expression for r_L) is positive. Since the left-hand side of (B.28) is positive, the right-hand side must also be positive. That is,

$$\frac{|S_{12}S_{21}|}{|\Delta|^2 - |S_{22}|^2} - 1 > 0$$

or

$$\frac{|\Delta|^2 - |S_{22}|^2}{|S_{12}S_{21}|} < 1 \quad (\text{B.29})$$

Using the property that if $a < b$ with $a > 0$ and $b > 0$, then $a^2 < b^2$, we can square (B.28) to obtain

$$|S_{22} - \Delta S_{11}^*|^2 < (|S_{12}S_{21}| - |\Delta|^2 + |S_{22}|^2)^2 \quad (\text{B.30})$$

Substituting (B.26) into (B.30) gives

$$\begin{aligned} |S_{12}S_{21}|^2 + (1 - |S_{11}|^2)(|S_{22}|^2 - |\Delta|^2) < |S_{12}S_{21}|^2 \\ - 2|S_{12}S_{21}|(|\Delta|^2 - |S_{22}|^2) + (|\Delta|^2 - |S_{22}|^2)^2 \end{aligned}$$

Simplifying, we obtain

$$-1 + |S_{11}|^2 < -2|S_{12}S_{21}| + |\Delta|^2 - |S_{22}|^2$$

or simply

$$K = \frac{1 - |S_{11}|^2 - |S_{22}|^2 + |\Delta|^2}{2|S_{12}S_{21}|} > 1$$

which is the same condition as (B.27). Thus far, we have shown that a two-port network is unconditionally stable when the conditions $K > 1$ and (B.29) are satisfied.

Next, we will show that the inequality (B.29) can be expressed as the inequality in (B.17). To show this, we write (B.27) in the form

$$2K = \frac{1 - |S_{11}|^2}{|S_{12}S_{21}|} + \frac{|\Delta|^2 - |S_{22}|^2}{|S_{12}S_{21}|} \quad (\text{B.31})$$

Since from (B.29) the last term in (B.31) is less than 1, we can write

$$\frac{|\Delta|^2 - |S_{22}|^2}{|S_{12}S_{21}|} = 1 - \alpha \quad (\text{B.32})$$

where α is a positive number smaller than 1. Substituting (B.32) into (B.31) gives

$$\frac{1 - |S_{11}|^2}{|S_{12}S_{21}|} = 2K - 1 + \alpha \quad (\text{B.33})$$

Since $K > 1$, we conclude from (B.33) that

$$\frac{1 - |S_{11}|^2}{|S_{12}S_{21}|} > 1$$

or

$$|S_{12}S_{21}| < 1 - |S_{11}|^2 \quad (\text{B.34})$$

We should also observe that since $|S_{12}S_{21}|$ is positive, the condition $|S_{11}| < 1$ is implied by (B.34).

Starting with (B.22) and (B.23), the derivation is similar, and we obtain the conditions

$$K > 1$$

and

$$\frac{|\Delta|^2 - |S_{11}|^2}{|S_{12}S_{21}|} < 1 \quad (\text{B.35})$$

Following similar steps to those in (B.31) and (B.34), the inequality (B.35) can be expressed as

$$|S_{12}S_{21}| < 1 - |S_{22}|^2 \quad (\text{B.36})$$

In conclusion, from (B.27), (B.34), and (B.36), the two-port network is unconditionally stable when

$$K > 1$$

$$|S_{12}S_{21}| < 1 - |S_{11}|^2$$

and

$$|S_{12}S_{21}| < 1 - |S_{22}|^2$$

OTHER DERIVATIONS

The stability criterion of active two-port networks has also been analyzed by other researchers working in active network theory. Their results are usually given in terms of z , y , or h parameters. For those who want to delve further into this topic the papers by Ku [B.3, B.4] and the textbook by Mitra [B.5] are recommended.

REFERENCES

- [B.1] K. Kurokawa, "Power Waves and the Scattering Matrix," *IEEE Transactions on Microwave Theory and Techniques*, March 1965.
- [B.2] T. T. Ha, *Solid State Microwave Amplifier Design*, Wiley Interscience, New York, 1981.
- [B.3] W. H. Ku, "Unilateral Gain and Stability Criterion of Active Two-Ports in Terms of Scattering Parameters," *Proceedings of the IEEE*, 1966.
- [B.4] W. H. Ku, "A Simple Derivation for the Stability Criterion of Linear Active Two-Ports," *Proceedings of the IEEE*, 1965.
- [B.5] S. K. Mitra, *Analysis and Synthesis of Linear Active Networks*, John Wiley & Sons, 1969.

APPENDIX C

UNCONDITIONAL STABILITY CONDITIONS: $K > 1$ AND $B_1 > 0$

From (3.3.17), we have

$$|\Delta| = |S_{11}S_{22} - S_{12}S_{21}| \leq |S_{11}S_{22}| + |S_{12}S_{21}|$$

and

$$|\Delta|^2 \leq |S_{11}S_{22}|^2 + 2|S_{11}S_{22}||S_{12}S_{21}| + |S_{12}S_{21}|^2$$

Then

$$\begin{aligned} B_1 &= 1 + |S_{11}|^2 - |S_{22}|^2 - |\Delta|^2 \\ &\geq 1 + |S_{11}|^2 - |S_{22}|^2 - |S_{11}S_{22}|^2 - 2|S_{11}S_{22}||S_{12}S_{21}| - |S_{12}S_{21}|^2 \end{aligned} \quad (C.1)$$

Using (3.3.15)—namely,

$$1 - |S_{22}|^2 > |S_{12}S_{21}|$$

we can express the inequality in (C.1) as

$$\begin{aligned} B_1 &> |S_{11}|^2 + |S_{12}S_{21}| - |S_{11}S_{22}|^2 - 2|S_{11}S_{22}||S_{12}S_{21}| - |S_{12}S_{21}|^2 \\ B_1 &> |S_{12}S_{21}|(1 - 2|S_{11}S_{22}| - |S_{12}S_{21}|) + |S_{11}|^2(1 - |S_{22}|^2) \\ B_1 &> |S_{12}S_{21}||1 - 2|S_{11}S_{22}| - (1 - |S_{22}|^2)| + |S_{11}|^2|S_{12}S_{21}| \\ B_1 &> |S_{12}S_{21}|(-2|S_{11}S_{22}| + |S_{22}|^2 + |S_{11}|^2) \end{aligned}$$

or

$$B_1 > |S_{12}S_{21}|(|S_{22}|^2 - |S_{11}|^2)^2 \quad (C.4)$$

The right-hand side of (C.4) is greater than zero. Hence,

$$B_1 > 0$$

Similarly, using (3.3.14), it follows that

$$B_2 = 1 + |S_{22}|^2 - |S_{11}|^2 - |A|^2 > 0$$

In Problem 3.13 it is shown that if $B_1 > 0$, then $B_2 > 0$, and vice versa. Hence the unconditional stability conditions in (3.3.13), (3.3.14), and (3.3.15) can be expressed as $K > 1$ and $B_1 > 0$, or as $K > 1$ and $B_2 > 0$.

APPENDIX D

DERIVATION OF THE UNILATERAL CONSTANT-GAIN CIRCLES [EQUATION (3.4.10)]

From (3.4.9),

$$g_i = \frac{1 - |\Gamma_i|^2}{|1 - S_{ii}\Gamma_i|^2} (1 - |S_{ii}|^2)$$

Then

$$g_i(1 + |S_{ii}\Gamma_i|^2 - S_{ii}\Gamma_i - S_{ii}^*\Gamma_i^*) = 1 - |\Gamma_i|^2 - |S_{ii}|^2 + |\Gamma_i|^2|S_{ii}|^2$$

Factoring $|\Gamma_i|^2$, we can write

$$|\Gamma_i|^2(1 - |S_{ii}|^2 + g_i|S_{ii}|^2) - g_i S_{ii}\Gamma_i - g_i S_{ii}^*\Gamma_i^* = 1 - g_i - |S_{ii}|^2$$

or

$$|\Gamma_i|^2 - \frac{g_i S_{ii}\Gamma_i}{1 - |S_{ii}|^2(1 - g_i)} - \frac{g_i S_{ii}^*\Gamma_i^*}{1 - |S_{ii}|^2(1 - g_i)} = \frac{1 - g_i - |S_{ii}|^2}{1 - |S_{ii}|^2(1 - g_i)} \quad (\text{D.1})$$

Comparing (D.1) with the circle equation (A.3), it follows that the center of the circle, denoted by C_{g_i} , is

$$C_{g_i} = \frac{g_i S_{ii}^*}{1 - |S_{ii}|^2(1 - g_i)} \quad (\text{D.2})$$

and the radius r_{g_i} follows from

$$r_{g_i}^2 - |C_{g_i}|^2 = \frac{1 - g_i - |S_{ii}|^2}{1 - |S_{ii}|^2(1 - g_i)} \quad (\text{D.3})$$

Substituting (D.2) into (D.3) and simplifying gives

$$r_{g_i} = \frac{\sqrt{1 - g_i}(1 - |S_{ii}|^2)}{1 - |S_{ii}|^2(1 - g_i)}$$

Hence, the constant-gain circles are given by

$$|\Gamma_i - C_{g_i}| = r_{g_i}$$

APPENDIX E

E.1 ANALYSIS OF (3.6.5) AND (3.6.6) FOR $|\Gamma_{Ms}| < 1$ AND $|\Gamma_{ML}| < 1$

Write (3.6.5) in the form

$$\Gamma_{Ms} = C_1^* \left\{ \frac{B_1 \pm \sqrt{B_1^2 - 4|C_1|^2}}{2|C_1|^2} \right\} = \frac{C_1^*}{|C_1|} \left\{ \frac{B_1}{2|C_1|} \pm \sqrt{\frac{B_1^2}{4|C_1|^2} - 1} \right\}$$

The magnitude of Γ_{Ms} is

$$|\Gamma_{Ms}| = \left| \frac{B_1}{2|C_1|} \pm \sqrt{\frac{B_1^2}{4|C_1|^2} - 1} \right| \quad (\text{E.1})$$

Letting

$$x = \frac{B_1}{2|C_1|} \quad (\text{E.2})$$

it follows that $|\Gamma_{Ms}| < 1$ when

$$|x \pm \sqrt{x^2 - 1}| < 1 \quad (\text{E.3})$$

The inequality in (E.3) can be analyzed using analytical methods. However, a simple way to analyze (E.3) is to plot the function $f_1(x) = x - \sqrt{x^2 - 1}$ and $f_2(x) = x + \sqrt{x^2 - 1}$ as a function of x and to determine the values of x that produce $|f_1(x)| < 1$ and $|f_2(x)| < 1$. The functions $f_1(x)$ and $f_2(x)$ are plotted in Fig. E.1.

From Fig. E.1a, it follows that $|f_1(x)| < 1$ when $x > 1$; and from Fig. E.1b, it follows that $|f_2(x)| < 1$ when $x < -1$. Hence, we conclude that the solution with the minus sign in (E.1) [see $f_1(x)$ in Fig. E.1a] produces $|\Gamma_{Ms}| < 1$ when

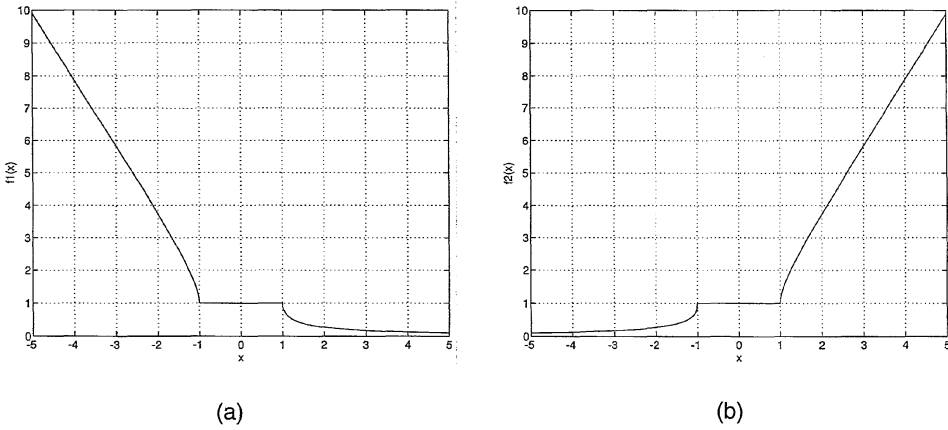


Figure E.1 (a) The function $f_1(x) = x - \sqrt{x^2 - 1}$ for $-5 < x < 5$; (b) the function $f_2(x) = x + \sqrt{x^2 - 1}$ for $-5 < x < 5$.

$|B_1/2C_1| > 1$ with $B_1 > 0$. Also, the solution with the plus sign in (E.1) [see $f_2(x)$ in Fig. E.1b] produces $|\Gamma_{Ms}| < 1$ when $|B_1/2C_1| > 1$ with $B_1 < 0$.

It is of interest to observe from Figs. E.1a and E.1b that for $|x| = |B_1/2C_1| < 1$, the magnitude of Γ_{Ms} is equal to 1. This is simple to verify since for $|x| < 1$, it follows that $x^2 < 1$ and from (E.1)

$$|x \pm \sqrt{x^2 - 1}| = |x \pm j\sqrt{1 - x^2}| = 1$$

The analysis of (3.6.6) is similar. Hence, the solution with the minus sign in (3.6.6) produces $|\Gamma_{ML}| < 1$ when $|B_2/2C_2| > 1$ with $B_2 > 0$; and the solution with the plus sign produces $|\Gamma_{ML}| < 1$ when $|B_2/2C_2| > 1$ with $B_2 < 0$.

E.2 CONDITION FOR A SIMULTANEOUS CONJUGATE MATCH

From $|B_1/2C_1|^2 > 1$, we can write

$$|B_1|^2 > 4|C_1|^2 \quad (\text{E.4})$$

From Problem 3.20, the quantity $|C_1|^2$ can be written as

$$|C_1|^2 = |S_{11} - \Delta S_{22}^*|^2 = |S_{12}S_{21}|^2 + (1 - |S_{22}|^2)(|S_{11}|^2 - |\Delta|^2) \quad (\text{E.5})$$

Substituting (3.6.7) and (E.5) into (E.4) gives

$$(1 + |S_{11}|^2 - |S_{22}|^2 - |\Delta|^2)^2 > 4[|S_{12}S_{21}|^2 + (1 - |S_{22}|^2)(|S_{11}|^2 - |\Delta|^2)]$$

or

$$[(1 - |S_{22}|^2) + (|S_{11}|^2 - |\Delta|^2)]^2 - 4(1 - |S_{22}|^2)(|S_{11}|^2 - |\Delta|^2) > 4|S_{12}S_{21}|^2 \quad (\text{E.6})$$

The left-hand side of the inequality is of the form $(a + b)^2 - 4ab$, which is equal to $(a - b)^2$. Hence, (E.6) can be simplified to read

$$[(1 - |S_{22}|^2) - (|S_{11}|^2 - |A|^2)]^2 > 4|S_{12}S_{21}|^2$$

or simply

$$K^2 > 1 \tag{E.7}$$

where

$$K = \frac{1 - |S_{11}|^2 - |S_{22}|^2 + |A|^2}{2|S_{12}S_{21}|}$$

From (E.4) and (E.7), it also follows that $|B_1/2C_1| > 1$ is similar to $|K| > 1$. A similar analysis shows that $|B_2/2C_2| > 1$ is similar to $|K| > 1$. Hence, a simultaneous conjugate match can be found when $K > 1$.

APPENDIX F

DERIVATION OF $G_{T,\max}$ [EQUATION (3.6.10)]

The starting point is (3.6.9)—namely,

$$G_{T,\max} = \frac{|S_{21}|^2(1 - |\Gamma_{ML}|^2)}{(1 - |\Gamma_{Ms}|^2)|1 - S_{22}\Gamma_{ML}|^2} \quad (\text{F.1})$$

Using (3.2.5) to express Γ_{Ms} in terms of Γ_{ML} , we obtain

$$\Gamma_{Ms} = \left(S_{11} + \frac{S_{12}S_{21}\Gamma_{ML}}{1 - S_{22}\Gamma_{ML}} \right)^* = \left(\frac{S_{11} - \Delta\Gamma_{ML}}{1 - S_{22}\Gamma_{ML}} \right)^*$$

Then

$$1 - |\Gamma_{Ms}|^2 = \frac{|1 - S_{22}\Gamma_{ML}|^2 - |S_{11} - \Delta\Gamma_{ML}|^2}{|1 - S_{22}\Gamma_{ML}|^2} \quad (\text{F.2})$$

Substituting (F.2) into (F.1) results in the expression

$$\begin{aligned} G_{T,\max} &= \frac{|S_{21}|^2(1 - |\Gamma_{ML}|^2)}{|1 - S_{22}\Gamma_{ML}|^2 - |S_{11} - \Delta\Gamma_{ML}|^2} \\ &= \frac{|S_{21}|^2(1 - |\Gamma_{ML}|^2)}{1 - |S_{11}|^2 + |\Gamma_{ML}|^2(|S_{22}|^2 - |\Delta|^2) - 2 \operatorname{Re}(\Gamma_{ML}C_2)} \end{aligned} \quad (\text{F.3})$$

where

$$C_2 = S_{22} - \Delta S_{11}^*$$

Next, we express the various terms in (F.3) in terms of K . To this end, we first develop a series of identities. From Problem 3.20, we have

$$|C_2|^2 = |S_{22} - \Delta S_{11}^*|^2 = |S_{12}S_{21}|^2 + (1 - |S_{11}|^2)(|S_{22}|^2 - |\Delta|^2) \quad (\text{F.4})$$

The term $1 - |S_{11}|^2$ can be written as

$$1 - |S_{11}|^2 = B_2 - (|S_{22}|^2 - |A|^2) \quad (\text{F.5})$$

where

$$B_2 = 1 + |S_{22}|^2 - |S_{11}|^2 - |A|^2$$

We can also express $1 - |S_{11}|^2$ in the form

$$1 - |S_{11}|^2 = 2K|S_{12}S_{21}| + (|S_{22}|^2 - |A|^2) \quad (\text{F.6})$$

Adding (F.5) and (F.6) gives

$$1 - |S_{11}|^2 = K|S_{12}S_{21}| + \frac{B_2}{2} \quad (\text{F.7})$$

Subtracting (F.6) from (F.5) produces the following identity:

$$|S_{22}|^2 - |A|^2 = \frac{B_2}{2} - K|S_{12}S_{21}| \quad (\text{F.8})$$

Substituting (F.7) and (F.8) into (F.4) gives

$$\begin{aligned} |C_2|^2 &= |S_{12}S_{21}|^2 + \left(K|S_{12}S_{21}| + \frac{B_2}{2} \right) \left(\frac{B_2}{2} - K|S_{12}S_{21}| \right) \\ &= |S_{12}S_{21}|^2(1 - K^2) + \frac{B_2^2}{4} \end{aligned} \quad (\text{F.9})$$

From (3.6.6), the expression for Γ_{ML} with the minus sign is

$$\Gamma_{ML} = \frac{B_2 - \sqrt{B_2^2 - 4|C_2|^2}}{2C_2} \quad (\text{F.10})$$

From (F.9),

$$B_2^2 - 4|C_2|^2 = 4|S_{12}S_{21}|^2(K^2 - 1) \quad (\text{F.11})$$

Substituting (F.11) into (F.10) gives

$$\Gamma_{ML} = \frac{B_2 - 2|S_{12}S_{21}|\sqrt{K^2 - 1}}{2C_2} \quad (\text{F.12})$$

Also,

$$2C_2\Gamma_{ML} = 2 \operatorname{Re}(\Gamma_{ML}C_2) = B_2 - 2|S_{12}S_{21}|\sqrt{K^2 - 1} \quad (\text{F.13})$$

is real, since the right-hand side is real.

Using (F.12), the term $1 - |\Gamma_{ML}|^2$ can be written as

$$1 - |\Gamma_{ML}|^2 = \frac{|C_2|^2 - \left(\frac{B_2^2}{4} \right) + |S_{12}S_{21}|B_2\sqrt{K^2 - 1} - |S_{12}S_{21}|^2(K^2 - 1)}{|C_2|^2} \quad (\text{F.14})$$

Substituting (F.9) into (F.14) gives

$$\begin{aligned}
 1 - |\Gamma_{ML}|^2 &= \frac{2|S_{12}S_{21}|\sqrt{K^2 - 1} \left(\frac{B_2}{2} - |S_{12}S_{21}|\sqrt{K^2 - 1} \right)}{\left(\frac{B_2}{2} \right)^2 - |S_{12}S_{21}|^2(K^2 - 1)} \\
 &= \frac{2|S_{12}S_{21}|\sqrt{K^2 - 1}}{\frac{B_2}{2} + |S_{12}S_{21}|\sqrt{K^2 - 1}} \quad (F.15)
 \end{aligned}$$

Using (F.7), (F.8), and (F.13), the denominator of (F.3) can be written as

$$\begin{aligned}
 \text{Denominator} &= K|S_{12}S_{21}| + \frac{B_2}{2} + |\Gamma_{ML}|^2 \left(\frac{B_2}{2} - K|S_{12}S_{21}| \right) \\
 &\quad - B_2 + 2|S_{12}S_{21}|\sqrt{K^2 - 1} \\
 &= (1 - |\Gamma_{ML}|^2) \left(K|S_{12}S_{21}| - \frac{B_2}{2} \right) + 2|S_{12}S_{21}|\sqrt{K^2 - 1} \\
 &= (1 - |\Gamma_{ML}|^2) \left[K|S_{12}S_{21}| - \frac{B_2}{2} + \frac{2|S_{12}S_{21}|\sqrt{K^2 - 1}}{1 - |\Gamma_{ML}|^2} \right] \quad (F.16)
 \end{aligned}$$

Substituting (F.16) into (F.3) gives

$$G_{T,\max} = \frac{|S_{21}|^2}{K|S_{12}S_{21}| - \frac{B_2}{2} + \frac{2|S_{12}S_{21}|\sqrt{K^2 - 1}}{1 - |\Gamma_{ML}|^2}} \quad (F.17)$$

Then, substituting (F.15) into (F.17) gives

$$\begin{aligned}
 G_{T,\max} &= \frac{|S_{21}|^2}{K|S_{12}S_{21}| - \frac{B_2}{2} + \frac{B_2}{2} + |S_{12}S_{21}|\sqrt{K^2 - 1}} \\
 &= \frac{|S_{21}|^2}{|S_{12}S_{21}|(K + \sqrt{K^2 - 1})} \\
 &= \frac{|S_{21}|}{|S_{12}|} (K - \sqrt{K^2 - 1})
 \end{aligned}$$

Similarly, for the solution of (3.6.6) with the plus sign, a minimum value of G_T is obtained. That is, for

$$\Gamma_{ML} = \frac{B_2 + \sqrt{B_2^2 - 4|C_2|^2}}{2C_2}$$

the minimum value of G_T is

$$G_{T,\min} = \frac{|S_{21}|}{|S_{12}|} (K + \sqrt{K^2 - 1})$$

APPENDIX G

DERIVATION OF THE CONSTANT OPERATING POWER-GAIN CIRCLES

Starting with (3.7.2)—namely,

$$g_p = \frac{1 - |\Gamma_L|^2}{1 - |S_{11}|^2 + |\Gamma_L|^2(|S_{22}|^2 - |A|^2) - 2 \operatorname{Re}(\Gamma_L C_2)}$$

it follows that

$$|\Gamma_L|^2[1 + g_p(|S_{22}|^2 - |A|^2)] - 2g_p \operatorname{Re}(\Gamma_L C_2) = 1 - g_p(1 - |S_{11}|^2)$$

Then, we can write

$$|\Gamma_L|^2 - \frac{g_p C_2 \Gamma_L}{1 + g_p(|S_{22}|^2 - |A|^2)} - \frac{g_p C_2^* \Gamma_L^*}{1 + g_p(|S_{22}|^2 - |A|^2)} = \frac{1 - g_p(1 - |S_{11}|^2)}{1 + g_p(|S_{22}|^2 - |A|^2)} \quad (\text{G.1})$$

Comparing (G.1) with the circle equation in (A.3), it follows that the center of the circle, denoted by C_p , is

$$C_p = \frac{g_p C_2^*}{1 + g_p(|S_{22}|^2 - |A|^2)} \quad (\text{G.2})$$

and the radius r_p follows from

$$r_p^2 - |C_p|^2 = \frac{1 - g_p(1 - |S_{11}|^2)}{1 + g_p(|S_{22}|^2 - |A|^2)} \quad (\text{G.3})$$

Substituting (G.2) into (G.3) and simplifying gives

$$r_p = \frac{[1 - 2K|S_{12}S_{21}|g_p + |S_{12}S_{21}|^2g_p^2]^{1/2}}{|1 + g_p(|S_{22}|^2 - |A|^2)|}$$

Hence, the constant operating power-gain circles are given by

$$|\Gamma_L - C_p| = r_p$$

APPENDIX H

EXPRESSIONS FOR Γ_{ML}

In this Appendix we show that for an unconditionally stable two-port network, the expression (3.6.6) (using the minus sign) is equivalent to (3.7.9). Starting with (3.6.6), we write

$$\Gamma_{ML} = \frac{B_2 - \sqrt{B_2^2 - 4|C_2|^2}}{2C_2} = C_2^* \left[\frac{B_2 - \sqrt{B_2^2 - 4|C_2|^2}}{2|C_2|^2} \right] \quad (\text{H.1})$$

Using (F.9) and (F.11), we can write (H.1) in the form

$$\begin{aligned} \Gamma_{ML} &= 2C_2^* \left[\frac{B_2 - 2|S_{12}S_{21}|\sqrt{K^2 - 1}}{B_2^2 - 4|S_{12}S_{21}|(K^2 - 1)} \right] \\ &= C_2^* \left[\frac{1}{\frac{B_2}{2} + |S_{12}S_{21}|\sqrt{K^2 - 1}} \right] \end{aligned} \quad (\text{H.2})$$

Using (F.8) in (H.2), we obtain

$$\begin{aligned} \Gamma_{ML} &= C_2^* \left[\frac{1}{K|S_{12}S_{21}| + (|S_{22}|^2 - |A|^2) + |S_{12}S_{21}|\sqrt{K^2 - 1}} \right] \\ &= \frac{C_2^*}{|S_{12}S_{21}|(K + \sqrt{K^2 - 1}) + (|S_{22}|^2 - |A|^2)} \end{aligned}$$

which can be expressed in the form

$$\Gamma_{ML} = \frac{C_2^* g_{p,\max}}{1 + g_{p,\max}(|S_{22}|^2 - |A|^2)}$$

where

$$g_{p,\max} = \frac{1}{|S_{12}S_{21}|} \frac{1}{(K + \sqrt{K^2 - 1})} = \frac{1}{|S_{12}S_{21}|} (K - \sqrt{K^2 - 1})$$

APPENDIX I

CONSTANT VSWR CIRCLES

Starting with (3.8.1) and (3.8.2),

$$(\text{VSWR})_{\text{in}} = \frac{1 + |\Gamma_a|}{1 - |\Gamma_a|}$$

where

$$|\Gamma_a| = \left| \frac{\Gamma_{\text{IN}} - \Gamma_s^*}{1 - \Gamma_{\text{IN}}\Gamma_s} \right| = \left| \frac{\Gamma_{\text{IN}}^* - \Gamma_s}{1 - \Gamma_{\text{IN}}\Gamma_s} \right| \quad (\text{I.1})$$

Hence, a constant $(\text{VSWR})_{\text{in}}$ value fixes the value of $|\Gamma_a|$.

From (I.1), for a given Γ_{IN} , the reflection coefficients Γ_a and Γ_s are related by a bilinear transformation. Comparing (I.1) to (A.5) (i.e., with $a = -1$, $b = \Gamma_{\text{IN}}^*$, $c = -\Gamma_{\text{IN}}$, and $d = 1$), it follows that a constant $|\Gamma_a|$ circle maps into a circle in the Γ_s plane given by

$$|\Gamma_s - C_{V_i}| = r_{V_i}$$

where the center of the circle C_{V_i} is given by [see (A.7)]

$$C_{V_i} = \frac{\Gamma_{\text{IN}}^*(1 - |\Gamma_a|^2)}{1 - |\Gamma_a\Gamma_{\text{IN}}|^2}$$

and the radius by [see (A.9)]

$$r_{V_i} = \frac{|\Gamma_a| |1 - |\Gamma_{\text{IN}}|^2|}{|1 - |\Gamma_a\Gamma_{\text{IN}}|^2|} \quad (\text{I.2})$$

Since $|\Gamma_a|$ and $|\Gamma_{\text{IN}}|$ are both less than one, we can express (I.2) in the form

$$r_{V_i} = \frac{|\Gamma_a|(1 - |\Gamma_{IN}|^2)}{1 - |\Gamma_a\Gamma_{IN}|^2}$$

Similarly, a constant value of $(VSWR)_{out}$ fixes the value of $|\Gamma_b|$ according to (3.8.6)—namely,

$$|\Gamma_b| = \left| \frac{\Gamma_{OUT} - \Gamma_L^*}{1 - \Gamma_{OUT}\Gamma_L} \right| = \left| \frac{\Gamma_{OUT}^* - \Gamma_L}{1 - \Gamma_{OUT}\Gamma_L} \right|$$

Therefore, for a given Γ_{OUT} , a constant $|\Gamma_b|$ circle maps into a circle in the Γ_L plane given by

$$|\Gamma_L - C_{V_o}| = r_{V_o}$$

where the center C_{V_o} is given by

$$C_{V_o} = \frac{\Gamma_{OUT}^*(1 - |\Gamma_b|^2)}{1 - |\Gamma_b\Gamma_{OUT}|^2}$$

and the radius r_{V_o} is

$$r_{V_o} = \frac{|\Gamma_b|(1 - |\Gamma_{OUT}|^2)}{1 - |\Gamma_b\Gamma_{OUT}|^2}$$

APPENDIX J

MAPPING OF CIRCLES IN THE Γ_s AND Γ_L PLANES

The values of Γ_s and Γ_{OUT} are related by the bilinear transformation (3.2.6)—namely,

$$\Gamma_{\text{OUT}} = \frac{S_{22} - \Delta\Gamma_s}{1 - S_{11}\Gamma_s}$$

or

$$\Gamma_s = \frac{S_{22} - \Gamma_{\text{OUT}}}{\Delta - S_{11}\Gamma_{\text{OUT}}} \quad (\text{J.1})$$

Comparing (J.1) with (A.4) (i.e., with $a = -1$, $b = S_{22}$, $c = -S_{11}$, and $d = \Delta$) and referring to (A.10) (i.e., with $w_o = C_{ii}$ and $\alpha = r_{ii}$), it follows that a circle in the Γ_s plane given by

$$|\Gamma_s - C_{ii}| = r_{ii}$$

maps into a circle in the Γ_{OUT} plane given by

$$|\Gamma_{\text{OUT}} - C_{\text{OUT}}| = r_{\text{OUT}}$$

where the center of the circle is given by [see (A.11)]

$$C_{\text{OUT}} = \frac{(1 - S_{11}C_{ii})^*(S_{22} - \Delta C_{ii}) - r_{ii}^2 \Delta S_{11}^*}{|1 - S_{11}C_{ii}|^2 - r_{ii}^2 |S_{11}|^2}$$

and the radius is [see (A.12)]

$$r_{\text{OUT}} = \frac{r_{ii} |S_{12} S_{21}|}{|1 - S_{11}C_{ii}|^2 - r_{ii}^2 |S_{11}|^2}$$

Hence, in the Γ_L plane, the circle $\Gamma_L = \Gamma_{\text{OUT}}^*$ is given by

$$|\Gamma_L - C_o| = r_o$$

where

$$C_o = C_{\text{OUT}}^*$$

and

$$r_o = r_{\text{OUT}}$$

Similarly, from (3.2.5), we can write

$$\Gamma_L = \frac{S_{11} - \Gamma_{\text{IN}}}{\Delta - S_{22}\Gamma_{\text{IN}}}$$

and it follows that a circle in the Γ_L plane given by

$$|\Gamma_L - C_{oo}| = r_{oo}$$

maps into a circle in the Γ_{IN} plane given by

$$|\Gamma_{\text{IN}} - C_{\text{IN}}| = r_{\text{IN}}$$

where

$$C_{\text{IN}} = \frac{(1 - S_{22}C_{oo})^*(S_{11} - \Delta C_{oo}) - r_{oo}^2 \Delta S_{22}^*}{|1 - S_{22}C_{oo}|^2 - r_{oo}^2 |S_{22}|^2} \quad (\text{J.2})$$

and

$$r_{\text{IN}} = \frac{r_{oo} |S_{12} S_{21}|}{\|1 - S_{22}C_{oo}\|^2 - r_{oo}^2 |S_{22}|^2} \quad (\text{J.3})$$

Hence, in the Γ_s plane, the circle $\Gamma_s = \Gamma_{\text{IN}}^*$ is given by

$$|\Gamma_s - C_i| = r_i$$

where

$$C_i = C_{\text{IN}}^*$$

and

$$r_i = r_{\text{IN}}$$

APPENDIX K

NOISE CONCEPTS

If the noise voltage (v_n) produced by several identical circuits is measured over a period of time, it is usually found that the measurements at any instant of time, as well as over any time interval, are all different and not related. However, there are some statistical properties that can be measured. It is found that the mean value of such noise is zero. That is,

$$\overline{v_n} = \lim_{T \rightarrow \infty} \frac{1}{T} \int_{t_1}^{t_1+T} v_n(t) dt = 0$$

We also find that the mean-square value of v_n has a constant value. That is,

$$\overline{v_n^2} = \lim_{T \rightarrow \infty} \frac{1}{T} \int_{t_1}^{t_1+T} [v_n(t)]^2 dt = \text{constant}$$

The root-mean-square value of v_n is given by

$$v_{n,\text{rms}} = \sqrt{\overline{v_n^2}}$$

or

$$v_{n,\text{rms}}^2 = \overline{v_n^2}$$

If the frequency spectrum of v_n is flat, the noise is called white noise. If the frequency spectrum is flat but limited to a certain band, the noise is called band-limited white noise.

There are several types of noise produced by microwave devices. The most important is thermal noise. Thermal noise is produced by the random motion of thermally agitated electrons in a conductor.

Johnson (from Bell Telephone Labs) made the first observation of thermal noise at the output of an amplifier. Thermal noise is also known as *Johnson noise*. Nyquist showed that the rms value of the thermal noise voltage produced by a resistor R is given by

$$v_{n,\text{rms}} = \sqrt{v_n^2} = \sqrt{4kTRB} \quad (\text{K.1})$$

This expression is valid at room temperature for frequencies up to approximately 1000 GHz. Hence, it is certainly usable in the microwave range.

Figure K.1 shows the equivalent noise models of a noisy resistor. The model in Fig. K.1a consists of a noiseless resistor R in series with a noise source given by (K.1). An alternate model is shown in Fig. K.1b. Noise sources are usually drawn without the standard polarity symbols. This convention is used to make a distinction between the standard voltage and current sources and noise sources. In the literature, we also find that noise sources are sometimes labeled as $\overline{v_n^2}$ and $v_{n,\text{rms}}$ (or i_n^2 and $i_{n,\text{rms}}$) without the polarity symbols.

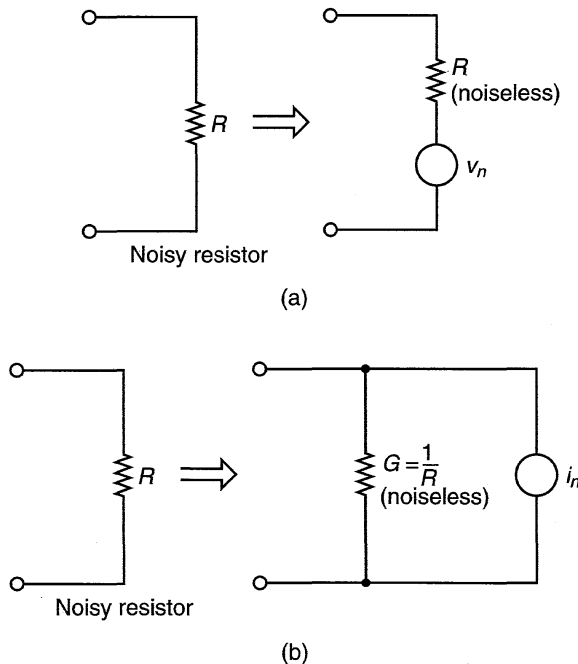


Figure K.1 (a) Model of a noisy resistor; (b) an alternate model of a noisy resistor.

The maximum noise power that a noisy resistor can deliver to a network is

$$P_N = \frac{V_{n,rms}^2}{4R} = kTB$$

This power is known as the available noise power from R .

Consider the noisy network shown in Fig. K.2a, where P_a is the available noise power at its terminals. The network can be modeled by a noisy resistor at a temperature T_s such that it produces a noise power equal to P_a . That is, let

$$T_s = \frac{P_a}{kB} \tag{K.2}$$

The temperature T_s is known as the noise temperature. Figure K.2b shows the resistor R at the noise temperature T_s producing the available noise power P_a .

Next, we consider the noise characterization of a two-port network. A two-port network is shown in Fig. K.3a, where the available input noise power from the resistor R_s at temperature T_s is $P_{Ni} = kT_sB$. This input noise power gets amplified by the available gain of the two-port network (G_A) and appears at the output. In addition, the noisy two-port network contributes a certain

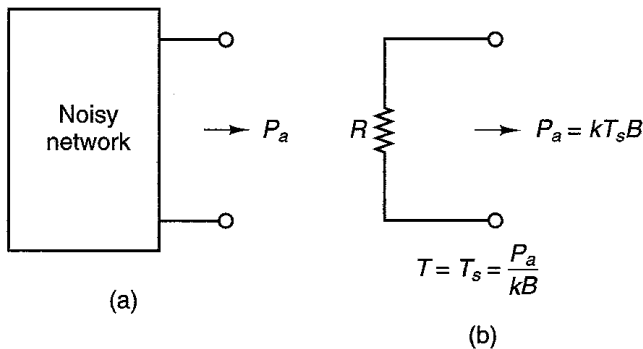


Figure K.2 (a) Noisy network producing the available power P_a ; (b) noise model of the network.

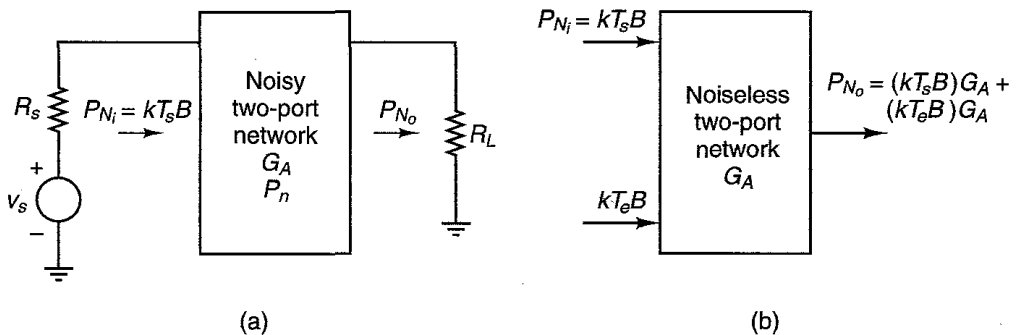


Figure K.3 (a) Noisy two-port network; (b) noiseless two-port representation.

amount of noise power to the output, shown as P_n in Fig. K.3a. The total available noise power at the output is

$$P_{N_o} = G_A P_{N_i} + P_n = G_A kT_s B + P_n$$

Associated with P_n , we can define an effective input noise temperature T_e such that

$$T_e = \frac{P_n}{kB G_A}$$

Then, the noisy two-port network can be modeled by a noiseless two-port with two noise power inputs, as shown in Fig. K.3b. One input represents the noise from the source ($kT_s B$) and the other input the noise from the internal sources ($kT_e B$). From Fig. K.3b, we can write

$$P_{N_o} = kT_s B G_A + kT_e B G_A = kT_s \left(1 + \frac{T_e}{T_s} \right) B G_A$$

or

$$1 + \frac{T_e}{T_s} = \frac{P_{N_o}}{kT_s B G_A} = \frac{P_{N_o}}{P_{N_i} G_A} \quad (\text{K.3})$$

G_A can be expressed in the form

$$G_A = \frac{P_{S_o}}{P_{S_i}} \quad (\text{K.4})$$

where P_{S_o} is the available signal power at the output and P_{S_i} is the available signal power at the input. Substituting (K.4) into (K.3), we obtain

$$1 + \frac{T_e}{T_s} = \frac{P_{S_i}/P_{N_i}}{P_{S_o}/P_{N_o}} \quad (\text{K.5})$$

which expresses the fact that the quantity $1 + T_e/T_s$ represents the ratio of the available signal-to-noise power ratio at the input to the available signal-to-noise power ratio at the output.

The noise figure F of a two-port network at a specific signal frequency is defined as

$$F = \frac{P_{N_o}}{P_{N_i} G_A} = \frac{P_{S_i}/P_{N_i}}{P_{S_o}/P_{N_o}} \quad (\text{K.6})$$

and it follows from (K.5) that F can be expressed in the form

$$F = 1 + \frac{T_e}{T_s} \quad (\text{K.7})$$

The measurement of the noise figure according to its definition in (K.6) [see also (K.7)] requires that a reference temperature be used for the source. The temperature 290°K is known as the standard temperature T_o (i.e., $T_o = 290^\circ\text{K}$). The reference temperature is set at 290°K (i.e., $T_s = T_o = 290^\circ\text{K}$). The representation of the noisy two-port network in terms of the noise figure F is shown in Fig. K.4a. Alternative, Fig. K.4b shows that F is a measure of the degradation in the signal-to-noise ratio between the input and output ports.

Both the effective input noise temperature T_e and the noise figure F can be used to characterize the noise performance of two-port networks. For microwave applications, the noise figure characterization is the more convenient. In Fig. K.3 or Fig. K.4, the noise contribution from the two-port network is represented by P_n . Researchers interested in the design and fabrication of low-noise microwave transistors have developed detailed noise models of the various microwave transistors. These models are beyond the scope of this book. Their development requires the analysis of the thermal noise, the shot noise, and the flicker noise of the device. Shot noise is due to the discrete nature of the charge carriers as they move across the pn junction. Flicker noise (also known as $1/f$ noise) is a low-frequency phenomenon.

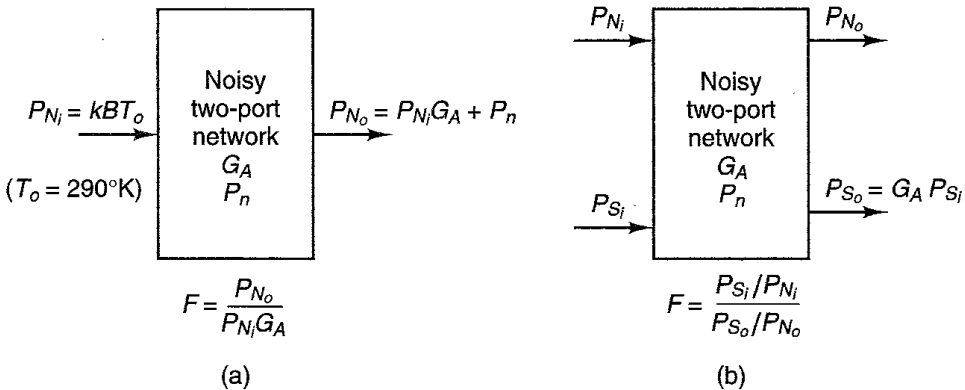


Figure K.4 (a) Noisy two-port network and its noise figure, (b) the noise figure.

APPENDIX L

NOISE FIGURE OF AN AMPLIFIER

There are two methods for analyzing the effect of noise in electronic devices and circuits. The first method consists of using equivalent noise sources at the appropriate physical location in the small-signal model of the device. For example, consider the noise produced by two resistors in series, as shown in Fig. L.1a. Using the noise model of a resistor, the noise model shown in Fig. L.1b is obtained. The mean-square value of the open circuit voltage is

$$\overline{v_{no}^2} = \overline{(v_{n1} + v_{n2})^2} = \overline{v_{n1}^2} + 2\overline{v_{n1}v_{n2}} + \overline{v_{n2}^2} \quad (\text{L.1})$$

However, since v_{n1} and v_{n2} are statistically independent (i.e., uncorrelated), the mean value of the product term in (L.1) is zero. Therefore,

$$\overline{v_{no}^2} = \overline{v_{n1}^2} + \overline{v_{n2}^2} = 4kT(R_1 + R_2)B$$

The preceding result shows that superposition can be used to calculate the total mean-square noise voltage when the noise sources are uncorrelated.

The second method for analyzing the effect of noise in a circuit is based on the fact that a noisy circuit can be modeled by a noiseless circuit with external noise sources. For example, a noisy two-port network that contains internal noise sources is shown in Fig. L.2a. The effect of the internal noise sources can be represented by the external noise voltage sources v_{n1} and v_{n2} placed in series with the input and output terminals, respectively, as shown in Fig. L.2b. These sources must produce the same noise voltages at the circuit terminals as the internal noise sources. The values of v_{n1} and v_{n2} are calculated as follows. Representing the noise-free two-port network in Fig. L.2b by its z parameters, we can write

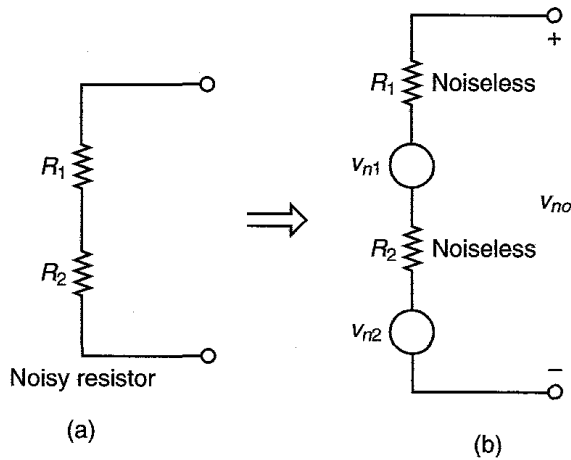


Figure L.1 The total noise voltage produced by two resistors in series.

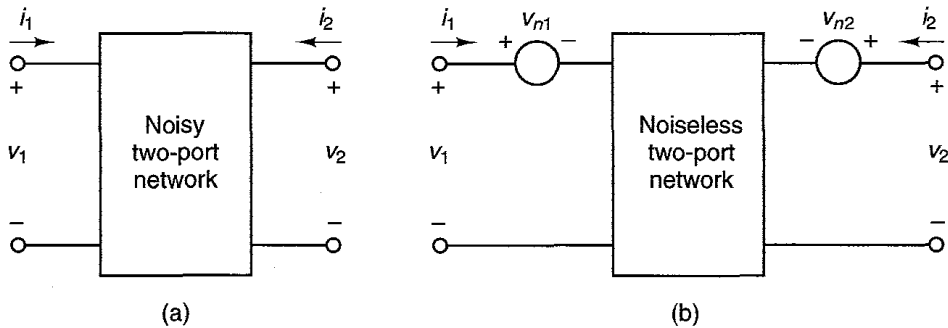


Figure L.2 (a) A noisy two-port network; (b) representation of the noisy two-port network in terms of a noise-free two-port network with external noise voltage sources v_{n1} and v_{n2} .

$$v_1 = z_{11}i_1 + z_{12}i_2 + v_{n1} \quad (\text{L.2})$$

and

$$v_2 = z_{21}i_1 + z_{22}i_2 + v_{n2} \quad (\text{L.3})$$

Equations (L.2) and (L.3) show that the values of v_{n1} and v_{n2} can be determined from open-circuit measurements in the noisy two-port network. From (L.2) and (L.3), it follows that when the input and output terminals are open (i.e., for $i_1 = i_2 = 0$), then

$$v_{n1} = v_1|_{i_1=i_2=0}$$

and

$$v_{n2} = v_2|_{i_1=i_2=0}$$

In other words, v_{n1} and v_{n2} are equal to the resulting open-circuit voltages.

Example L.1

A noisy two-port is shown in Fig. L.3a, where the noise voltage produced by the resistors is shown as e_{n1} , e_{n2} , and e_{n3} . Determine the values of v_{n1} and v_{n2} in the equivalent noise-free representation of the network, shown in Fig. L.3b.

Solution. The loop equations for the network in Fig. L.3a are

$$v_1 = (R_1 + R_3)i_1 + R_3i_2 + (e_{n1} + e_{n3}) \quad (\text{L.4})$$

and

$$v_2 = R_3i_1 + (R_2 + R_3)i_2 + (e_{n2} + e_{n3}) \quad (\text{L.5})$$

A comparison of (L.2) and (L.3) with (L.4) and (L.5) shows that the equivalent noise sources at the input and output are

$$v_{n1} = e_{n1} + e_{n3}$$

and

$$v_{n2} = e_{n2} + e_{n3}$$

Hence, the equivalent network with external noise sources shown in Fig. L.3b follows.

In general, the external sources v_{n1} and v_{n2} are not independent. In this example, v_{n1} and v_{n2} are functions of e_{n3} .

An alternate representation of the noisy two-port network is shown in Fig. L.4. In this case, the external sources are the current noise sources i_{n1} and i_{n2} and

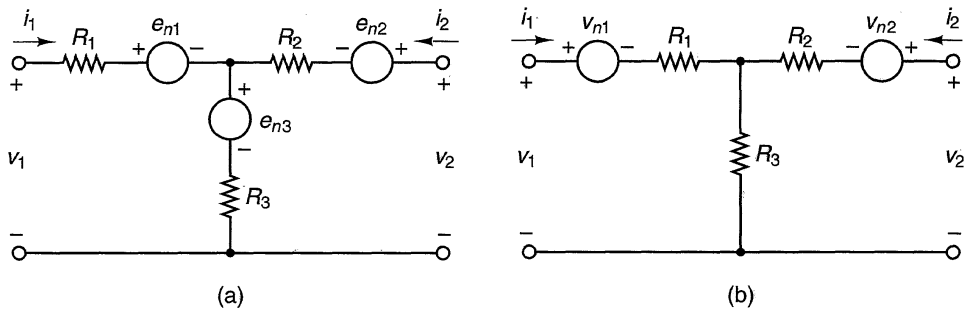
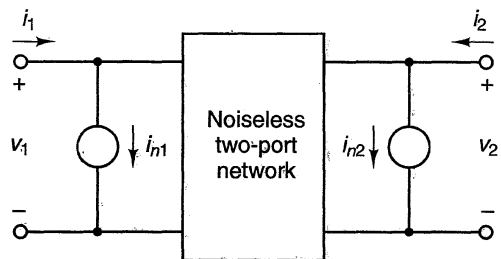


Figure L.3 Noisy two-port for Example L.3.

Figure L.4 Representation of a noisy two-port network in terms of a noise-free two-port network with external noise current sources i_{n1} and i_{n2} .



i_{n2} . Representing the noise-free two-port network in Fig. L.4 by its y parameters, we can write

$$i_1 = y_{11}v_1 + y_{12}v_2 + i_{n1}$$

and

$$i_2 = y_{21}v_1 + y_{22}v_2 + i_{n2}$$

The values of i_{n1} and i_{n2} in Fig. L.4 follow from the short-circuit measurements taken in the noisy two-port network. That is,

$$i_{n1} = i_1|_{v_1=v_2=0}$$

and

$$i_{n2} = i_2|_{v_1=v_2=0}$$

In addition to the representation in Figs. L.2b and L.4, there are other representations that can be derived for a noisy two-port. A convenient representation for noise analysis is to have the noise sources at the input of the network, as shown in Fig. L.5. Representing the noise-free two-port network in Fig. L.5 by its $ABCD$ parameters, we can write

$$v_1 = Av_2 + B(-i_2) + v_n$$

and

$$i_1 = Cv_2 + D(-i_2) + i_n$$

The previous equations show that there is no simple way of evaluating v_n and i_n in Fig. L.5 using short-circuit and open-circuit measurements. From a practical point of view, the values of v_n and i_n in Fig. L.5 can be determined in terms of the noise voltages v_{n1} and v_{n2} in Fig. L.2b (which only require open-circuit measurements). The relations between the noise sources v_n and i_n in Fig. L.5 and the noise sources v_{n1} and v_{n2} in Fig. L.2b are derived as follows. Using z parameters to represent the noise-free two-port network in Fig. L.5, we can write

$$v_1 = z_{11}(i_1 - i_n) + z_{12}i_2 + v_n = z_{11}i_1 + z_{12}i_2 + (v_n - z_{11}i_n) \quad (\text{L.6})$$

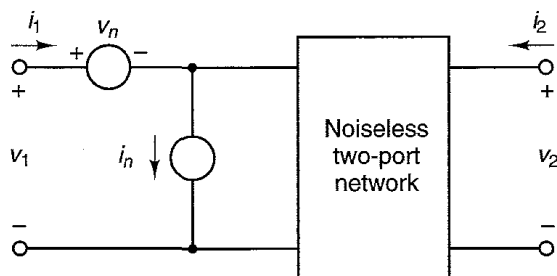


Figure L.5 Representation of a noisy two-port network in terms of a noise-free two-port network with external noise sources v_n and i_n at the input.

and

$$v_2 = z_{21}(i_1 - i_n) + z_{22}i_2 = z_{21}i_1 + z_{22}i_2 - z_{21}i_n \quad (\text{L.7})$$

Comparing (L.2) and (L.3) with (L.6) and (L.7), it follows that

$$v_{n1} = v_n - i_n z_{11} \quad (\text{L.8})$$

and

$$v_{n2} = -i_n z_{21} \quad (\text{L.9})$$

Hence, solving (L.8) and (L.9) for v_n and i_n gives

$$v_n = v_{n1} - \left(\frac{z_{11}}{z_{21}} \right) v_{n2}$$

and

$$i_n = -\frac{v_{n2}}{z_{21}}$$

An alternate method for determining v_n and i_n would have been to relate them to the noise sources i_{n1} and i_{n2} in Fig. L.4. It is easy to show that the relations in this case are

$$v_n = -\frac{i_{n2}}{y_{21}} \quad (\text{L.10})$$

and

$$i_n = i_{n1} - \left(\frac{y_{11}}{y_{21}} \right) i_{n2} \quad (\text{L.11})$$

A source connected to the noisy two-port network is shown in Fig. L.6. The source is represented by a current source with admittance Y_s . We also assume that the noise from the source and the noise from the two-port network are uncorrelated. The noise figure F of the circuit in Fig. L.6 is now derived.

The total output noise power is proportional to the mean square of the short-circuit current (denoted by i_{sc}^2) at the input port of the noise-free amplifier,

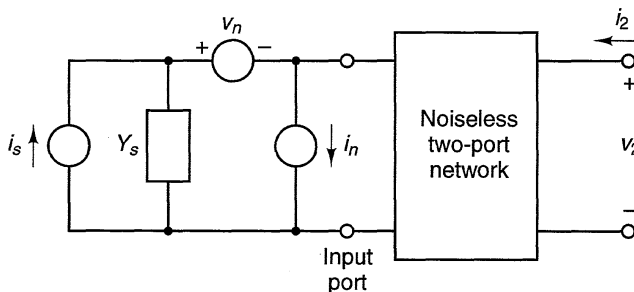


Figure L.6 Noise model for calculation of the amplifier noise figure.

while the noise power due to the source alone is proportional to the mean square of the source current (i.e., $\overline{i_s^2}$). Hence, the noise figure F is given by

$$F = \frac{\overline{i_{sc}^2}}{\overline{i_s^2}} \quad (\text{L.12})$$

Since

$$i_{sc} = -i_s + i_n + v_n Y_s$$

it follows that the mean square of i_{sc} is given by

$$\overline{i_{sc}^2} = \overline{(-i_s + i_n + v_n Y_s)^2} = \overline{i_s^2} + \overline{(i_n + v_n Y_s)^2} - 2\overline{i_s(i_n + v_n Y_s)} \quad (\text{L.13})$$

Since the noise from the source and the noise from the two-port network are uncorrelated, we have

$$\overline{i_s(i_n + v_n Y_s)} = 0$$

and (L.13) reduces to

$$\overline{i_{sc}^2} = \overline{i_s^2} + \overline{(i_n + v_n Y_s)^2} \quad (\text{L.14})$$

Substituting (L.14) into (L.12) gives

$$F = 1 + \frac{\overline{(i_n + v_n Y_s)^2}}{\overline{i_s^2}} \quad (\text{L.15})$$

There is some correlation between the external sources v_n and i_n . Hence, we can write i_n in terms of two parts; one part is uncorrelated to v_n (called i_{nu}), and the other part is correlated to v_n (called i_{nc}). Thus,

$$i_n = i_{nu} + i_{nc} \quad (\text{L.16})$$

Furthermore, we can define the relation between i_{nc} and v_n in terms of a correlation admittance Y_c —namely,

$$i_{nc} = Y_c v_n \quad (\text{L.17})$$

Y_c is not an actual admittance in the circuit. In fact, Y_c is defined by (L.17) and can be calculated as follows. From (L.16),

$$i_n = i_{nu} + Y_c v_n \quad (\text{L.18})$$

Multiplying (L.18) by v_n^* , taking the mean, and observing that $\overline{i_{nu} v_n^*} = 0$, we obtain

$$\overline{v_n^* i_n} = Y_c \overline{v_n^2}$$

or

$$Y_c = \frac{\overline{v_n^* i_n}}{\overline{v_n^2}}$$

Substituting (L.18) into (L.15) results in the following expression for F :

$$F = 1 + \frac{\overline{(inu + (Y_c + Y_s)v_n)^2}}{\overline{i_s^2}} \quad (\text{L.19})$$

The noise produced by the source is related to the source conductance by

$$\overline{i_s^2} = 4kT_o G_s B \quad (\text{L.20})$$

where $G_s = \text{Re}[Y_s]$. The noise voltage can be expressed in terms of an equivalent noise resistance R_n as

$$\overline{v_n^2} = 4kT_o R_n B \quad (\text{L.21})$$

and the uncorrelated noise current can be expressed in terms of an equivalent noise conductance G_u —namely,

$$\overline{i_{nu}^2} = 4kT_o G_u B \quad (\text{L.22})$$

Substituting (L.20), (L.21), and (L.22) into (L.19), and letting $Y_c = G_c + jB_c$ and $Y_s = G_s + jB_s$ gives

$$\begin{aligned} F &= 1 + \frac{4kT_o G_u B + |G_s + jB_s + G_c + jB_c|^2 4kT_o R_n B}{4kT_o G_s B} \\ &= 1 + \frac{G_u}{G_s} + \frac{R_n}{G_s} [(G_s + G_c)^2 + (B_s + B_c)^2] \end{aligned} \quad (\text{L.23})$$

The noise factor can be minimized by the proper selection of Y_s . From (L.23), F is decreased by selecting

$$B_s = -B_c \quad (\text{L.24})$$

Hence, from (L.23),

$$F|_{B_s=-B_c} = 1 + \frac{G_u}{G_s} + \frac{R_n}{G_s} (G_s + G_c)^2 \quad (\text{L.25})$$

The dependence of the expression in (L.25) on G_s can be minimized by setting

$$\frac{dF|_{B_s=-B_c}}{dG_s} = 0$$

which gives

$$\frac{dF|_{B_s=-B_c}}{dG_s} = -\frac{G_u}{G_s^2} + R_n \left(\frac{2G_s(G_s + G_c) - (G_s + G_c)^2}{G_s^2} \right) = 0$$

Solving for G_s , we obtain

$$G_s = \sqrt{G_c^2 + \frac{G_u}{R_n}} \quad (\text{L.26})$$

The values of G_s and B_s in (L.26) and (L.24) give the source admittance, which results in the minimum noise figure. This optimum value of the source admittance is commonly denoted by $Y_{\text{opt}} = G_{\text{opt}} + jB_{\text{opt}}$. That is,

$$Y_{\text{opt}} = G_{\text{opt}} + jB_{\text{opt}} = \sqrt{G_c^2 + \frac{G_u}{R_n}} - jB_c \quad (\text{L.27})$$

From (L.25), the minimum noise figure F_{min} is

$$F_{\text{min}} = F|_{Y_s=Y_{\text{opt}}} = 1 + \frac{G_u}{G_{\text{opt}}} + \frac{R_n}{G_{\text{opt}}} (G_{\text{opt}} + G_c)^2 \quad (\text{L.28})$$

Solving (L.26) for G_u/G_{opt} and substituting into (L.28) gives

$$\begin{aligned} F_{\text{min}} &= 1 + R_n \left(G_{\text{opt}} - \frac{G_c^2}{G_{\text{opt}}} \right) + \frac{R_n}{G_{\text{opt}}} (G_{\text{opt}}^2 + 2G_{\text{opt}}G_c + G_c^2) \\ &= 1 + 2R_n(G_{\text{opt}} + G_c) \end{aligned} \quad (\text{L.29})$$

Using (L.29), we can write (L.23) in the form

$$F = F_{\text{min}} - 2R_n(G_c + G_{\text{opt}}) + \frac{G_u}{G_s} + \frac{R_n}{G_s} [(G_s + G_c)^2 + (B_s - B_{\text{opt}})^2] \quad (\text{L.30})$$

Solving (L.26) for G_u and substituting into (L.30), the expression for F can be simplified to read

$$F = F_{\text{min}} + \frac{R_n}{G_s} [(G_s - G_{\text{opt}})^2 + (B_s - B_{\text{opt}})^2] \quad (\text{L.31})$$

Equation (L.31) shows that F depends on $Y_{\text{opt}} = G_{\text{opt}} + jB_{\text{opt}}$, R_n , and F_{min} . Once these quantities are specified, the value of F can be determined for any source admittance Y_s . Equation (L.31) can also be expressed in the form

$$F = F_{\text{min}} + \frac{r_n}{g_s} |y_s - y_{\text{opt}}|^2$$

where $r_n = R_n/Z_o$ is the normalized noise resistance, y_s is the normalized source admittance,

$$y_s = \frac{Y_s}{Y_o} = \frac{G_s + jB_s}{Y_o} = g_s + jb_s$$

and y_{opt} is the normalized value of the optimum source admittance,

$$y_{\text{opt}} = \frac{Y_{\text{opt}}}{Y_o} = \frac{G_{\text{opt}} + jB_{\text{opt}}}{Y_o} = g_{\text{opt}} + jb_{\text{opt}}$$

APPENDIX M

CONDITIONS FOR A STABLE OSCILLATION

Consider the one-port network shown in Fig. M.1. Over a narrowband range of frequencies around the frequency of oscillation, we assume that the input resistance $R_{\text{IN}}(A, \omega)$ [where $R_{\text{IN}}(A, \omega) < 0$] and the input reactance $X_{\text{IN}}(A, \omega)$ of the active device are only a function of the amplitude of $i(t)$. That is,

$$Z_{\text{IN}}(A, \omega) \approx Z_{\text{IN}}(A) = R_{\text{IN}}(A) + jX_{\text{IN}}(A)$$

where $R_{\text{IN}}(A) < 0$.

The current $i(t)$ can be written as

$$i(t) = A(t) \cos[\omega t + \theta(t)] = \text{Re}[A(t)e^{j[\omega t + \theta(t)]}] \quad (\text{M.1})$$

where the time-dependent amplitude $A(t)$ and phase $\theta(t)$ are slowly varying functions of time. At steady state, $A(t)$ and $\theta(t)$ are constants and $i(t)$ becomes a sinusoidal signal with constant amplitude and phase.

Using (M.1), the voltage $v(t)$ is given by

$$\begin{aligned} v(t) &= \text{Re}[A(t)e^{j[\omega t + \theta(t)]}Z_{\text{IN}}(A)] \\ &= A(t)R_{\text{IN}}(A)\cos[\omega t + \theta(t)] - A(t)X_{\text{IN}}(A)\sin[\omega t + \theta(t)] \end{aligned} \quad (\text{M.2})$$

The voltage $v(t)$ can also be expressed in terms of $Z_L(\omega)$. This is a little more difficult to determine since $i(t)$ is not an exact periodic function, and a question arises as to the value of the frequency used to evaluate $Z_L(\omega)$. This frequency should be the instantaneous frequency of $i(t)$, denoted by ω_i . Since $A(t)$ and $\theta(t)$ are slowly varying functions of time, we can approximately express $v(t)$ in terms of $Z_L(\omega_i)$ as

$$v(t) \approx -\text{Re}[A(t)e^{j[\omega t + \theta(t)]}Z_L(\omega_i)] \quad (\text{M.3})$$

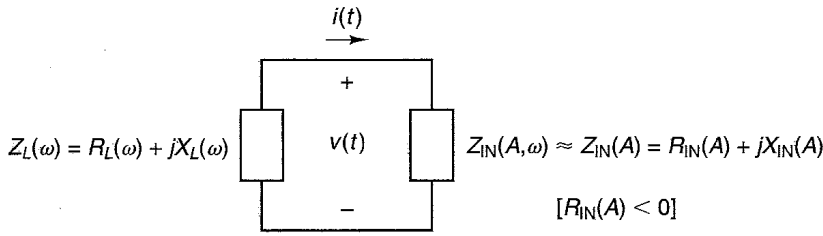


Figure M.1 One-port model of a negative-resistance oscillator.

where ω_i is the instantaneous frequency of $i(t)$.

To find the instantaneous frequency of $i(t)$, we calculate

$$\begin{aligned}
 \frac{di(t)}{dt} &= \frac{d}{dt} \{\text{Re}[A(t)e^{j[\omega t + \theta(t)]}]\} \\
 &= \text{Re} \left\{ \left[j \left(\omega + \frac{d\theta(t)}{dt} \right) + \frac{1}{A(t)} \frac{dA(t)}{dt} \right] A(t) e^{j[\omega t + \theta(t)]} \right\} \\
 &= \text{Re} \left\{ \left[j \left[\omega + \frac{d\theta(t)}{dt} - j \frac{1}{A(t)} \frac{dA(t)}{dt} \right] A(t) e^{j[\omega t + \theta(t)]} \right\} \quad (\text{M.4})
 \end{aligned}$$

From (M.4), it follows that the instantaneous frequency ω_i is complex and given by

$$\omega_i = \omega + \frac{d\theta(t)}{dt} - j \frac{1}{A(t)} \frac{dA(t)}{dt}$$

The value of $Z_L(\omega_i)$ is given by

$$\begin{aligned}
 Z_L(\omega_i) &= Z_L \left(\omega + \frac{d\theta(t)}{dt} - j \frac{1}{A(t)} \frac{dA(t)}{dt} \right) \\
 &= R_L \left(\omega + \frac{d\theta(t)}{dt} - j \frac{1}{A(t)} \frac{dA(t)}{dt} \right) + jX_L \left(\omega + \frac{d\theta(t)}{dt} - j \frac{1}{A(t)} \frac{dA(t)}{dt} \right) \quad (\text{M.5})
 \end{aligned}$$

Since $A(t)$ and $\theta(t)$ are slowly varying functions of time, we have

$$\omega \gg \frac{d\theta(t)}{dt}$$

and

$$\omega \gg \frac{1}{A(t)} \frac{dA(t)}{dt}$$

Hence, (M.5) can be approximated using the first two terms of its Taylor's expansion about ω —namely,

$$\begin{aligned}
Z_L(\omega_i) &\approx Z_L(\omega) + \frac{dZ_L(\omega)}{d\omega} \left(\frac{d\theta(t)}{dt} - j \frac{1}{A(t)} \frac{dA(t)}{dt} \right) \\
&= R_L(\omega) + \frac{dR_L(\omega)}{d\omega} \left(\frac{d\theta(t)}{dt} - j \frac{1}{A(t)} \frac{dA(t)}{dt} \right) \\
&\quad + jX_L(\omega) + j \frac{dX_L(\omega)}{d\omega} \left(\frac{d\theta(t)}{dt} - j \frac{1}{A(t)} \frac{dA(t)}{dt} \right) \\
&= R_L(\omega) + \frac{dR_L(\omega)}{d\omega} \frac{d\theta(t)}{dt} + \frac{dX_L(\omega)}{d\omega} \frac{1}{A(t)} \frac{dA(t)}{dt} \\
&\quad + j \left[X_L(\omega) + \frac{dX_L(\omega)}{d\omega} \frac{d\theta(t)}{dt} - \frac{dR_L(\omega)}{d\omega} \frac{1}{A(t)} \frac{dA(t)}{dt} \right] \quad (M.6)
\end{aligned}$$

Substituting (M.6) into (M.3) gives

$$\begin{aligned}
v(t) &= - \left[R_L(\omega) + \frac{dR_L(\omega)}{d\omega} \frac{d\theta(t)}{dt} + \frac{dX_L(\omega)}{d\omega} \frac{1}{A(t)} \frac{dA(t)}{dt} \right] A(t) \cos[\omega t + \theta(t)] \\
&\quad + \left[X_L(\omega) + \frac{dX_L(\omega)}{d\omega} \frac{d\theta(t)}{dt} - \frac{dR_L(\omega)}{d\omega} \frac{1}{A(t)} \frac{dA(t)}{dt} \right] A(t) \sin[\omega t + \theta(t)] \quad (M.7)
\end{aligned}$$

Equating (M.2) to (M.7) produces the relation

$$R_L(\omega) + \frac{dR_L(\omega)}{d\omega} \frac{d\theta(t)}{dt} + \frac{dX_L(\omega)}{d\omega} \frac{1}{A(t)} \frac{dA(t)}{dt} = -R_{IN}(A) \quad (M.8)$$

and

$$X_L(\omega) + \frac{dX_L(\omega)}{d\omega} \frac{d\theta(t)}{dt} - \frac{dR_L(\omega)}{d\omega} \frac{1}{A(t)} \frac{dA(t)}{dt} = -X_{IN}(A) \quad (M.9)$$

These coupled equations can be solved for $dA(t)/dt$ and $d\theta(t)/dt$. Multiplying (M.8) by $dX_L(\omega)/d\omega$ and (M.9) by $-dR_L(\omega)/d\omega$, and adding the resulting equations, gives

$$\begin{aligned}
[R_L(\omega) + R_{IN}(A)] \frac{dX_L(\omega)}{d\omega} - [X_L(\omega) + X_{IN}(A)] \frac{dR_L(\omega)}{d\omega} \\
+ \left| \frac{dZ_L(\omega)}{d\omega} \right|^2 \frac{1}{A(t)} \frac{dA(t)}{dt} = 0 \quad (M.10)
\end{aligned}$$

Similarly, multiplying (M.8) by $dR_L(\omega)/d\omega$ and (M.9) by $dX_L(\omega)/d\omega$ and adding the resulting equations, gives

$$\begin{aligned}
[R_L(\omega) + R_{IN}(A)] \frac{dR_L(\omega)}{d\omega} + [X_L(\omega) + X_{IN}(A)] \frac{dX_L(\omega)}{d\omega} \\
+ \left| \frac{dZ_L(\omega)}{d\omega} \right|^2 \frac{d\theta(t)}{dt} = 0 \quad (M.11)
\end{aligned}$$

At steady state, the oscillator voltage $v(t)$ is such that $dA(t)/dt = 0$ and $d\theta(t)/dt = 0$. Hence, the steady-state solutions of (M.10) and (M.11), at which $A = A_o$ and $\omega = \omega_o$, are obtained when

$$[R_L(\omega_o) + R_{IN}(A_o)] \left. \frac{dX_L(\omega)}{d\omega} \right|_{\omega=\omega_o} + [X_L(\omega_o) + X_{IN}(A_o)] \left. \frac{dR_L(\omega)}{d\omega} \right|_{\omega=\omega_o} = 0$$

and

$$[R_L(\omega_o) + R_{IN}(A_o)] \left. \frac{dR_L(\omega)}{d\omega} \right|_{\omega=\omega_o} + [X_L(\omega_o) + X_{IN}(A_o)] \left. \frac{dX_L(\omega)}{d\omega} \right|_{\omega=\omega_o} = 0$$

These equations show that at steady state the oscillator must satisfy the following conditions:

$$R_L(\omega_o) + R_{IN}(A_o) = 0 \quad (\text{M.12})$$

and

$$X_L(\omega_o) + X_{IN}(A_o) = 0 \quad (\text{M.13})$$

or simply when

$$Z_L(\omega_o) + Z_{IN}(A_o) = 0$$

or equivalently when

$$\Gamma_{IN}(A_o)\Gamma_L(\omega_o) = 1$$

The oscillations might not reach the steady-state conditions described by (M.12) and (M.13) when a small variation in the amplitude produces an oscillation with increasing amplitude. Let A_o be the steady-state value of A . A small variation ΔA in the amplitude is given by $A = A_o + \Delta A$. Then a Taylor expansion of $R_{IN}(A)$ and $X_{IN}(A)$ about A_o is

$$R_{IN}(A) = R_{IN}(A_o + \Delta A) \approx R_{IN}(A_o) + \left. \frac{\partial R_{IN}(A)}{\partial A} \right|_{A=A_o} \Delta A \quad (\text{M.14})$$

and

$$X_{IN}(A) = X_{IN}(A_o + \Delta A) \approx X_{IN}(A_o) + \left. \frac{\partial X_{IN}(A)}{\partial A} \right|_{A=A_o} \Delta A \quad (\text{M.15})$$

Substituting (M.12) and (M.13) into (M.14) and (M.15) gives

$$R_{IN}(A) = R_{IN}(A_o + \Delta A) \approx -R_L(\omega_o) + \left. \frac{\partial R_{IN}(A)}{\partial A} \right|_{A=A_o} \Delta A \quad (\text{M.16})$$

and

$$X_{IN}(A) = X_{IN}(A_o + \Delta A) \approx -X_L(\omega_o) + \left. \frac{\partial X_{IN}(A)}{\partial A} \right|_{A=A_o} \Delta A \quad (\text{M.17})$$

Then, substituting (M.16) and (M.17) into (M.10) gives

$$\Delta A \left[\frac{\partial R_{\text{IN}}(A)}{\partial A} \Big|_{A=A_o} \frac{dX_L(\omega)}{d\omega} \Big|_{\omega=\omega_o} - \frac{\partial X_{\text{IN}}(A)}{\partial A} \Big|_{A=A_o} \frac{dR_L(\omega)}{d\omega} \Big|_{\omega=\omega_o} \right] + \left| \frac{dZ_L(\omega)}{d\omega} \right|^2 \Big|_{\omega=\omega_o} \frac{1}{A_o} \frac{d(\Delta A)}{dt} = 0$$

which can be conveniently written as

$$\frac{d(\Delta A)}{dt} + \beta(\Delta A) = 0 \quad (\text{M.18})$$

where

$$\beta = \frac{A_o}{\left| \frac{dZ_L(\omega)}{d\omega} \right|^2 \Big|_{\omega=\omega_o}} \left(\frac{\partial R_{\text{IN}}(A)}{\partial A} \Big|_{A=A_o} \frac{dX_L(\omega)}{d\omega} \Big|_{\omega=\omega_o} - \frac{\partial X_{\text{IN}}(A)}{\partial A} \Big|_{A=A_o} \frac{dR_L(\omega)}{d\omega} \Big|_{\omega=\omega_o} \right)$$

The solution of (M.18) is of the form $e^{-\beta t}$. This solution shows that the disturbance ΔA decays with time when $\beta > 0$. Since A_o and

$$\left| \frac{dZ_L(\omega)}{d\omega} \right|^2 \Big|_{\omega=\omega_o}$$

are both positive quantities, it follows that a stable oscillation requires that

$$\frac{\partial R_{\text{IN}}(A)}{\partial A} \Big|_{A=A_o} \frac{dX_L(\omega)}{d\omega} \Big|_{\omega=\omega_o} - \frac{\partial X_{\text{IN}}(A)}{\partial A} \Big|_{A=A_o} \frac{dR_L(\omega)}{d\omega} \Big|_{\omega=\omega_o} > 0$$

INDEX

A

ABCD parameters, 2–4, 61–63
matrix, 2–4
Active bias:
 BJT, 277–280
 GaAs FET, 283
Added power, 406
Admittance coordinates Smith chart
 (*see* Smith chart)
Admittance parameters, 1–3, 61–63
matrix, 2, 334
AM to PM conversion, 364
Amplifier:
 balanced, 327–333
 bandwidth, 307, 348–52
 broadband, 323–47
 class A, 352–56
 class AB, 352, 360–61
 class B, 352, 356–61
 class C, 352, 356–61, 370–73
 feedback, 333–44, 441, 444
 high-gain, 240–47, 372
 high-power, 352–74
 low-noise, 295–322, 372–74,
 440–42

 low VSWR, 240, 254, 257, 262–73,
 307–20, 436, 440–41
 n-way, 365–66
 simultaneous conjugate match,
 240–47
 stability (*see* Stability)
 tuning, 348
 two-stage, 372–74
Attenuation constant, 20
Available noise power, 295, 482–83
Available power (*see* Power available)
Available power gain (*see* Power gain)
Average power, 29

B

Balanced amplifier, 327–33
Balanced shunt stubs, 164–68
Bandwidth:
 analysis, 125–129, 348–52
 inherent, 349–50
 reduction factor, 352
Barkhausen criteria, 386
Beta cutoff frequency, 70, 78–79

Bias circuit (*see* dc bias)
 Bilinear transformation, 218, 449–51, 476, 478
 BJT:
 bias (*see* dc bias)
 characteristics, 71–79
 figure of merit, 78
 junction temperature, 361
 model, 71–78
 typical performances, 72
 Boltzman constant, 295
 Branch-line coupler, 327–28
 Broadband design, 327–28

C

CAD, 273, 280, 342, 433–48
 Capacitor:
 bypass, 273, 277
 chip, 164
 coupling, 164
 Cascade, 3–4, 25–26
 Chain parameters, 2
 matrix, 2
 Chain scattering parameters, 25
 matrix, 22, 25–26
 Characteristic impedance:
 complex, 21
 definition, 9
 microstrip, 143–48
 real, 9
 transmission line, 9–22
 Chip, 66, 70, 78, 81–82, 109–10, 164
 Circles:
 constant-conductance, 97, 113–25, 137, 156–57, 175
 constant-gain (*see* Constant-gain circles)
 constant-gamma, 101, 103, 157, 169, 173
 constant-reactance, 95–98, 137
 constant-resistance, 95–98, 108, 113–21, 137
 constant-susceptance, 97, 137
 constant VSWR (*see* VSWR)
 equations, 449–452
 mapping, 266–67, 406–07, 450, 454–56, 476–79
 Class:
 A operation, 352–56
 AB operation, 352, 360–61
 B operation, 352, 356–61
 C operation, 352, 356–61, 370–73
 Compensated matching networks, 323–24
 Complex propagation constant, 20
 Compressed Smith chart (*see* Smith chart)
 Compression point (*see* Gain compression point)
 Computer-aided design (*see* CAD)
 Conduction loss, 149–51
 Conjugate match:
 maximum gain, 241
 minimum gain, 242
 simultaneous (*see* Simultaneous conjugate match)
 Constant-conductance circles (*see* Circles)
 Constant-gain circles:
 available power gain, 257–60, 262–67, 302–04, 313–16
 potentially unstable, 260
 unconditionally stable, 257–60
 operation power gain, 247–57, 266–67, 316–18, 472–73
 potentially unstable, 252–57
 unconditionally stable, 247–52
 transducer power gain, 228–47
 bilateral case, 240–47
 potentially unstable, 242, 246–47
 unconditionally stable, 241–47
 unilateral case, 228–38, 464–65
 potentially unstable, 234–38
 unconditionally stable, 231–34
 Constant-reactance circles (*see* Circles)
 Constant-resistance circles (*see* Circles)
 Constant-susceptance circles (*see* Circles)
 Constant VSWR circles (*see* VSWR)
 Contact potential, 425
 Contact resistance, 110
 Conversions of parameters, 60–63, 193
 Coupler, 327–33
 branch-line, 327–28
 Lange, 327–28, 365
 Wilkinson, 332–34, 365
 3-dB coupler, 327–34

Coupling coefficient, 329
 Coupling coefficient in DRO, 417–18,
 422

D

dc bias:
 active (*see* Active bias)
 BJT, 273–80
 GaAs FET, 280–83
 networks, 273–83
 operating point, 278, 282
 stability, 275–77, 279–80
 Device-line characterization, 404
 Dielectric constant:
 effective, 143–49
 relative, 143–47
 Dielectric loss, 149–51
 Dielectric resonator oscillator (*see*
 DRO)
 Dielectric substrate, 143, 146, 149, 151
 Directional coupler, 61–66
 Dispersion, 148–49
 Distortion, 360–64
 Divider/Combiner (*see* Hybrid com-
 biner/divider)
 Dynamic range, 354, 363–64
 free spurious, 363–64

E

Electrical length, 12
 Electron transit time, 84
 Ell matching sections, 113–30

F

Fano, 344
 Feedback:
 negative (*see* Negative feedback)
 series, 334–40
 shunt, 334–40
 Figure of merit, 78

Flow graph (*see* Signal flow graphs)

G

GaAs FET:
 bias (*see* dc bias)
 characteristics, 79–85
 junction temperature, 362
 model, 79–85
 typical performances, 82
 GaAs MESFET (*see* GaAs FET)
 Gain-bandwidth, 78–79, 84, 342, 346
 Gain circles (*see* Constant-gain circles)
 Gain compression point, 353–54
 Gate length, 85
 Generalized scattering parameters, 45,
 50–55, 58, 192–94
 Gyromagnetic ratio, 424

H

h parameters (*see* Hybrid parameters)
 h_{FE} , 78, 81, 274–75
 HBJT, 79
 HEMT, 85
 Heterojunction bipolar transistor (*see*
 HBJT)
 High electron mobility transistor (*see*
 HEMT)
 HP MDS program, 433–48
 Hybrid combiner/divider, 365–66
 Hybrid coupler, 327
 Hybrid parameters, 2, 4, 62
 matrix, 2
 Hybrid- π model, 71–77

I

Impedance coordinates Smith chart (*see*
 Smith chart)
 Impedance matching networks (*see*
 Matching)

Impedance matching networks (*see* Matching)

Impedance parameters, 1–4, 62
matrix, 2

Incident:

current, 48–49, 54
power, 29–31
voltage, 22–23, 28–29, 48–49, 54, 61, 64
wave, 12, 21, 22–24, 29–31, 45–48, 177, 329–30

Incoming wave, 12

Indefinite scattering matrix, 44

Input reflection coefficient (*see* Reflection coefficient)

Input stability circle, 218, 451

Interdigitated, 71, 81

Intermodulation distortion:
products, 362–63
third-order, 362–63

Interstage design, 324, 374

K

Kuroda's identities, 323

L

Lange coupler, 327–28, 365

Large signal:

characterization, 404–10
measurements, 356, 359, 404–10
parameters, 352–356

Low-noise amplifier (*see* Amplifier)

Low-noise amplifier (LNA), 320–22

Low-noise block (LNB), 320–22

M

Mason's rule, 175, 179–85

Matched:

line, 15–16, 30, 32–35

load, 182

termination, 24

Matching:

microstrip, 141, 152–75

network, 112–141

network design, 112–41

Maximum available gain (*see* Power gain)

Maximum available noise power, 482

Maximum frequency of oscillation (f_{\max}), 78–79, 84–85

Maximum stable gain, 242, 267, 313

Measurements:

reflection coefficient, 65

scattering parameters, 61–66

Metal semiconductor field-effect transistor (*see* GaAs FET)

Microstrip:

attenuation, 149–50

capacitance, 143

characteristic impedance, 143–48

definition, 142

dispersion, 148–49

effective dielectric, 143–44

effective width, 146–48

field configuration, 143

geometry, 143

losses, 149–52

matching network design, 141, 152–75

phase velocity, 143

quality factor, 151

radiation factor, 151

wavelength, 143–48

Microwave amplifier:

block diagram, 113

signal flow graph, 179–80

Microwave transistor:

BJT, 71–79

GaAs FET, 79–85

HBJT, 79

HETM, 85

MODFET, 85

Minimum noise figure (*see* Noise)

Mismatch factor:

source, 188, 190–92, 195–200, 215–16

load, 190–92, 196–200, 216

MODFET, 85

Modulation doped field effect transistor (*see* MODFET)

N

Negative feedback, 333–40, 385
 Negative resistance, 98–100, 384, 388–97, 413
 Negative resistance oscillators (*see* Oscillators)
 Nepers, 20
 Network analyzer, 61–66
 Noise:
 bandwidth, 295–96
 concepts, 480–84
 extrinsic, 85
 figure, 296–02, 321, 483–92
 figure circles, 299–304
 figure parameter, 299
 flicker, 79, 85, 484
 intrinsic, 85
 Johnson, 295, 481
 measure, 298, 317–19
 measurement, 299
 minimum, 299–304, 492
 parameters, 299, 302, 307, 308
 power, 295, 482–83
 resistance, 299, 491–92
 resistor, 295, 482
 shot, 79, 85
 temperature, 295, 482
 thermal, 295, 481
 two-stage amplifier, 296–98
 voltage, 295, 481, 485–89
 white, 295, 480
 Normalizing impedance, 29–30, 32, 36–38, 44, 50, 52
 admittance, 97
 Z_o system, 35–36, 52
 n -port network, 42–44, 52–55
 n -way amplifier, 365–66
 n -way hybrid combiner/divider, 365–66
 Nyquist test, 386–87, 392, 395–96

O

Open-circuited line, 16, 103
 shunt stub, 152–72

Operating point (*see de bias*)
 Operating power gain (*see* Power gain)
 circles (*see* Constant-gain circles)
 Optimization, 433–48
 Optimum:
 noise figure, 299
 terminations, 231, 234
 Oscillation conditions, 384–97
 Oscillators:
 BJT, 399–404, 413–14, 419–20, 425–27
 Clapps, 411
 Colpitts, 411–13
 configurations, 411–14
 design procedure, 398–404
 frequency of oscillation, 386–89, 392, 396, 411–12
 GaAs FET, 399, 408, 413–14, 419–24
 gain condition, 386, 413
 Hartley, 411
 large-signal measurement, 404–11
 maximum power, 390–397, 404
 negative resistance, 384, 388–404, 407, 413, 494
 one-port, 388–97
 reverse channel, 399, 414
 stable oscillation, 389–94, 396–97, 493–97
 start of oscillation condition, 389, 394, 399
 terminating network, 397–404, 406–11
 two-port, 397–404
 varactor tuned, 425–27
 YIG tuned, 422–24
 Outgoing wave, 12
 Output reflection coefficient (*see* Reflection coefficient)
 Output stability circle, 218, 451

P

Packaged, 66–73, 76–78, 83–84
 Packaged capacitance, 76–78
 inductance, 76–78, 83
 Paralleling, 364–65

Parameters conversions, 60–63, 193
 Parasitics, 76–78, 83
 Period, 10
 Phase velocity, 12, 143
 Phasor, 7–8, 28
 Pi network, 130–34
 Potentially unstable:
 bilateral, 252–57, 260
 unilateral, 234–38
 Power amplifier, 352–74
 Power available;
 from the network, 184, 189–90,
 213, 216
 from the source, 31–35, 42, 45–46,
 52, 182–84, 188–93, 213, 216,
 405–06
 Power combiners and dividers:
 hybrid, 327, 365–66
 Lange, 327–328, 365
 n -way, 365–66
 paralleling, 364–65
 Wilkinson, 332–34, 365
 Power delivered to the load, 20, 32, 34,
 39, 42, 46, 52, 55–58
 Power gain:
 available, 184, 191, 193, 213–16,
 257–60, 262–66, 302–21
 maximum operating, 242, 248–51
 maximum stable, 242, 253, 267
 maximum transducer, 241–43,
 469–71
 maximum unilateral transducer,
 229–34
 minimum operating, 252, 256–57
 minimum transducer, 242, 471
 operating, 183–84, 190, 193, 213–16,
 247–57
 transducer, 34–35, 52, 182–83, 190–91,
 194, 213–16, 238–47, 256, 340–42,
 469–71
 unilateral transducer, 228–38
 Power waves, 45–60
 for one port, 45–49
 for two ports, 50–52, 58–60
 for n -ports, 52–54
 reflected, 45–47
 reflection coefficient, 47–48
 Propagation constant, 9

Q

Q point, 24, 61, 64, 273–83, 360, 370
 Quality factor (*see* *Que*)
 Quarter-wave line or transformer, 15,
 16–17, 157–60
 Quasi-TEM, 143–44
 Que (Q)
 constant contour, 131–34
 loaded, 125–30
 of matching networks, 125–30
 node, 125–37
 unloaded, 417
 Quiescent point (*see* Q point)

R

Radiation quality factor, 151
 Radio frequency coil or choke (RFC),
 61, 277
 Reference
 impedance, 51, 54–55
 plane, 26–27
 Reflected:
 current, 48–49
 power, 29–32, 46–47
 voltage, 22–23, 28–29, 48–49, 61, 64
 wave, 12, 21–24, 30, 40–41, 45–48,
 55–58, 177
 Reflection coefficient:
 current, 48–50
 definition, 13, 21–22, 47–50
 input, 24, 101, 180–81, 186, 214–15
 load, 13–16, 18, 101
 output, 24, 181, 187, 214–15
 plane, 93
 power, 47–50, 198–200, 354–56
 simultaneous conjugate match,
 240–47
 transmission line, 13–22
 two-stage design, 372–74
 voltage, 48–50
 Resonance line width, 424
 Reverse channel, 399, 414

Reverse current I_{CBO} , 273–75
 Richard's transformation, 323

S

S parameters:

conversions, 60–62, 193, 334–35
 definitions, 23–24
 generalized, 50–55, 58, 192–94
 indefinite, 44
 large-signal, 352, 384, 404–06
 matrix, 23–24
 measurement, 61–66
n-port, 42–44
 properties, 28–36
 transistors, 66–71, 109–12
 two-port network, 23–24, 32–38, 72

Saturation drift velocity, 85

Scattering matrix, 4, 23–24

Scattering parameters (see *S*

voltage source, 177–78

Simultaneous conjugate match, 240–47,
 466–68, 474–75

Small-signal conditions, 24, 61, 72, 294,
 352–53, 406

Smith chart:

admittance or *Y* chart, 95–97, 103–04,
 154–62, 173

compressed, 98–100

gain circles (*see* Constant-gain
 circles)

impedance calculation, 99–103, 108

impedance or *Z* chart, 93–101, 169–72

negative resistance, 98–100

network characteristics, 108–12

normalized impedance and admit-
 tance or *ZY* chart, 105–08, 113–24,
 137, 175

theory, 93–98, 105–08

wavelength scale, 101

Stability:

analysis, 217–226, 453–61

circles, 218, 220, 222, 24

Thévenin, 33–35, 188–89
 Third-order intercept point, 363–64
 Three-port, 44
 Transconductance, 74, 337–39
 Transducer cutoff frequency, 70
 Transducer power gain, 34, 35, 52,
 182–83, 190–91, 213–16, 228–30, 238–47
 Transfer or T parameters (*see* Chain
 scattering parameters)
 Transmission coefficient:
 forward, 24, 34
 reverse, 24
 Transmission line, 4–22
 input admittance, 103
 input impedance, 14–15, 18, 22, 40,
 101–03
 lossless, 6, 9, 28, 30
 lossy, 20–22
 matched, 15–16
 microstrip (*see* Microstrip)
 model, 4–6
 open-circuited, 16, 103, 152–72
 quarter-wave, 16–17
 short-circuited, 16, 38–39, 103, 152–72
 uniform, 5
 Traveling waves, 10–12, 24, 27, 45, 48, 50,
 56–58, 185–87
 Tuning factor, 348
 Two-port network:
 cascade, 3, 25–26
 noise, 299, 485–92
 parameters conversions, 60–63, 193
 representations, 1–4, 24, 28, 50
 Two-stage amplifier:
 design, 372–374
 high-gain, 372
 high-power, 372
 low-noise, 296–98, 372–74

U

Unconditionally stable (*see* Stability)
 Unilateral figure of merit, 238–39
 Unilateral transducer power gain (*see*
 Power gain)
 Unit diagonal matrix, 61

Unstable two-port (*see* Stability)

V

Varactor diode, 173, 425–27
 Vector voltmeter, 61–64, 240, 243,
 251–54, 267–73, 307–20
 Voltage gain, 184
 Voltage standing-wave ratio (*see*
 VSWR)
 VSWR, 15–16, 18, 39, 42, 101, 194–200,
 252
 constant circles, 260–73, 476–77
 input, 194–200, 216, 240, 243, 253–54,
 257, 260–61, 307–20
 output, 195–96, 200, 216, 241, 243,
 251–54, 257, 261–62, 314–20

W

Wave functions, 10
 Waves (*see* Power waves and Traveling
 waves)
 Wavelength, 10, 143–44
 Wilkinson's coupler, 332–34, 365

Y

y parameters (*see* Admittance
 parameters)
 YIG sphere, 422

Z

z parameters (*see* Impedance
 parameters)
 Z_o system (*see* Normalizing impedance)